



**HAL**  
open science

# Bis-vanillin substrates as source of $\pi$ -conjugated polymers for organic electronic

Lauriane Giraud

► **To cite this version:**

Lauriane Giraud. Bis-vanillin substrates as source of  $\pi$ -conjugated polymers for organic electronic. Polymers. Université de Bordeaux, 2019. English. NNT : 2019BORD0404 . tel-03132303

**HAL Id: tel-03132303**

**<https://theses.hal.science/tel-03132303>**

Submitted on 5 Feb 2021

**HAL** is a multi-disciplinary open access archive for the deposit and dissemination of scientific research documents, whether they are published or not. The documents may come from teaching and research institutions in France or abroad, or from public or private research centers.

L'archive ouverte pluridisciplinaire **HAL**, est destinée au dépôt et à la diffusion de documents scientifiques de niveau recherche, publiés ou non, émanant des établissements d'enseignement et de recherche français ou étrangers, des laboratoires publics ou privés.

THÈSE PRÉSENTÉE  
POUR OBTENIR LE GRADE DE  
**DOCTEUR DE**  
**L'UNIVERSITÉ DE BORDEAUX**

ÉCOLE DOCTORALE DES SCIENCES CHIMIQUES  
SPÉCIALITÉ POLYMERES

Par Lauriane GIRAUD

**Dérivés de la vanilline pour la synthèse de polymères  
 $\pi$ -conjugués biosourcés : application en électronique  
organique**

Bis-vanillin substrates as source of  $\pi$ -conjugated polymers for organic electronic

Sous la direction de : Pr. Henri CRAMAIL et Dr. Cyril BROCHON  
Co-encadrants : Pr. Stéphane GRELIER, Dr. Etienne GRAU, Dr. Éric CLOUTET,  
Dr. Laurent GAREL

Soutenue le 16/12/2019

Membres du jury :

Mme FICHET, Odile, Professeure, Université de Cergy-Pontoise  
M. HIORNS, Roger, Directeur de Recherche, CNRS  
Mme VIGNAU, Laurence, Professeure, Université de Bordeaux  
M. GAREL, Laurent, Ingénieur-Docteur, Solvay GBU-Aroma Performance  
M. BROCHON, Cyril, Maître de Conférence, Université de Bordeaux  
M. CRAMAIL, Henri, Professeur, Université de Bordeaux

Rapporteur  
Rapporteur  
Présidente  
Examineur  
Co-directeur de thèse  
Directeur de thèse



A mes parents et à mon frère



« Un problème sans solution est un problème mal posé. »  
Albert Einstein



## Remerciements

Voici maintenant la partie que j'avais le plus hâte d'écrire quand j'étais plongée dans les affres de la rédaction – il est enfin temps de remercier les gens qui ont participé, de loin ou de près à cette thèse :

Tout d'abord je remercie le jury pour avoir accepté d'évaluer ces travaux de thèse, pour être venus pour la soutenance (malgré la grève) et pour la qualité des discussions qui ont suivi. Je remercie donc ainsi Pr. Laurence Vignau, Pr. Odile Fichet, Dr. Roger Hiorns et Dr. Laurent Garel.

Je remercie également Solvay et la région Nouvelle Aquitaine pour avoir financé ce projet de thèse, le chef du laboratoire, les chefs des équipes 2 et 4 du LCPO ainsi que tout le personnel du LCPO, que cela soit le personnel administratif, les ingénieurs et techniciens m'ayant aidée durant ces années.

Je remercie mes (nombreux) encadrants, Henri Cramail, Cyril Brochon, Etienne Grau, Stéphane Grelier, Eric Cloutet et Laurent Garel pour m'avoir fait confiance et encadrée sur ce projet. Je remercie particulièrement Cyril pour sa disponibilité, Henri pour son efficacité et sa rapidité qui m'ont été particulièrement précieuses lors de la rédaction, et Laurent Garel pour m'avoir permis de visiter le site de Solvay à Saint-Fons.

Je remercie Dario Bassani pour son aide précieuse sur les complexes à transfert de charge.

Je remercie également tous les B8ers, présents et passés, qui m'ont accueillie/formée/accompagnée pendant ces 3 ans. En particulier, et de façon relativement chronologique :

Je remercie Olga : merci pour ta gentillesse, ta bonne humeur, et ta disponibilité – toi qui étais prête à lâcher tout ce que tu faisais dès que j'avais un problème, c'est grâce à toi que j'ai pu maîtriser la Flash ! Merci également à Guillaume (Garbay) pour avoir eu l'idée qui a permis de lancer mon projet de thèse, et pour avoir pris du temps pour me former alors que tu étais occupé par ta soutenance.

Rim, ma co-bureau (et commère) préférée : merci pour les discussions (ragots) avec le thé tôt le matin, le thé du dimanche aprèm, pour tes bons conseils sur à peu près tout, et merci d'être venue à ma soutenance ❤️ (et vive les chouquettes !). A Alizée, merci pour ton aide au labo et pour tous ces bons moments : le yoga, les concerts, les spectacles, les ateliers ... Je garde précieusement le gâteau que tu m'as magnifiquement plié.

Yanid, la sportive de l'extrême et reine des choux, merci pour ces discussions sur la pâtisserie le matin autour d'un thé – rendez-vous aux Meilleurs Pâtissiers pour la dixième année ! Guillaume (Kevin), ton humour et tes memes « limite limite » vont me manquer – courage, bientôt la fin ! Évite de trop mélanger tes vials et tout va bien se passer ... Merci Mumtaz pour m'avoir donné ton avis éclairé sur différents protocoles expérimentaux un peu exotiques et les distillations – sans toi je n'aurais jamais réussi ma première formylation. Merci à Mickaël pour ton aide précieuse sur les OLED ; merci aussi à Mélanie pour m'avoir formée sur les SEC et m'avoir fait confiance pendant ton congé mat'. Je tiens également à remercier Eunkyung, ma coach ! Merci de m'avoir motivée (et surveillée) pendant la rédaction – sans toi, ça serait allé moins vite ... Micah, merci pour ton aide avec Origin et l'atelier peinture - bon courage pour la suite, que tes données soient cohérentes (et bonnes tant qu'à faire).

Je tiens également à remercier les autres B8ers : Nicoletta, pour ton énergie, ta bonne humeur et ton rire de petit cochon (mignon le cochon), Florian (quitte à en payer le prix, j'aurais mieux fait de t'amener à l'aquagym), Gilles pour ton aide à l'évap' et avec le réacteur micro-onde, Daniele, Emin, Lorenzo, Silvia, Cindy, Solène, Florent, Cian, Tommaso, Siham, Alex, Antoine, Benjamin, Shekhar, Muriel, Naser, Alberto, Anirudh, Quentin S., Siham, Maël, Ariana ...

Ma thèse s'est déroulée avec deux équipes du LCPO, je tiens donc à remercier toute l'équipe 2 et plus particulièrement Fiona, my aussie mate (et PhD mate, après tout on a commencé le même jour) – merci pour tous ces bons moments en Australie, ça a été un plaisir de te connaître :). Merci également à Anne-Laure pour les analyses RMN et la formation approfondie, Etienne Sav' pour la formation à la



divanilline, Hélène pour ta gentillesse, Quentin P., Pauline, Christopher et les « nouveaux », Jeremy, Nicolas, Léa, Perroline, Jessie, Jaimie, Anderson, ...

Hors LCPO, merci à Clara pour ton soutien à distance et les voyages : deux en 3 mois ça reste notre record !

Je tiens enfin à remercier ma famille : Maouchat, Tonton Zinou ; et Tatie Françoise et Tonton Jean-Marc, merci d'être venus à la soutenance. J'ai une pensée particulière pour mes grands-parents : Papi Zoom, Mamie Zoom et Papi Tounet, qui j'en suis sûre, seraient très fiers de moi.

Et enfin, merci à mon frère pour ses encouragements et à mes parents pour leur soutien et leur amour inconditionnels – je vous aime.

---

# General Table of Contents

|                                    |    |
|------------------------------------|----|
| <b>List of Abbreviations</b> ..... | 1  |
| <b>Résumé en français</b> .....    | 5  |
| <b>General Introduction</b> .....  | 17 |

## Chapter 1

|  |    |
|--|----|
| <b>1. Introduction</b> .....   | 25 |
| <b>2. Building blocks from biomass</b> .....   | 25 |
| 2.1 Lignocellulose: brief description .....  | 25 |
| 2.2. Aromatic molecules from lignin .....  | 27 |
| 2.3. Furan and its derivatives .....   | 29 |
| 2.4. Lignocellulosic biomass: conclusion .....   | 30 |
| <b>3. Synthesis of <math>\pi</math>-conjugated polymers via more sustainable pathways</b> .....    | 31 |
| 3.1. Direct Hetero Arylation Polymerization.....   | 31 |
| 3.2. One step further: transition-metal free syntheses .....                                       | 33 |
| 3.2.1. Conjugated polymers synthesized with halogen.....   | 33 |
| 3.2.1.1. Bromine-catalyzed reaction .....  | 33 |
| 3.2.1.2. Synthesis of conjugated polymers by oxidative homocoupling of bis-Grignard reagents ..... | 34 |
| 3.2.2. Synthesis of conjugated polymers without halogen <i>via</i> condensation reaction .....     | 34 |
| 3.2.2.1. Synthesis of polyazomethines.....   | 34 |
| 3.2.2.2. Knoevenagel reaction .....  | 35 |
| 3.2.2.3. Horner-Wadsworth-Emmons reaction.....   | 36 |
| 3.2.2.4. Condensation of squaric acid.....   | 37 |
| 3.2.2.5. Aldol condensation .....  | 38 |
| 3.3. Transition metal-free syntheses: conclusion.....  | 39 |
| <b>4. Synthesis of conjugated polymers with bio-based monomers</b> .....                           | 40 |
| 4.1. From a micro-organism: 3-amino-4-hydroxybenzoic acid.....                                     | 40 |
| 4.2. From lignocellulosic biomass: Furan and difuran .....   | 41 |
| 4.3. From lignocellulosic biomass: vanillin.....   | 43 |
| 4.4. Bio-based monomers for the synthesis of conjugated polymers: conclusion.....                  | 44 |
| <b>5. General conclusion</b> .....   | 45 |
| <b>6. References</b> .....   | 46 |

## Chapter 2

|   |    |
|---|----|
| <b>1. Introduction</b> .....  | 59 |
| <b>2. Divanillin-based polyazomethines</b> .....  | 60 |
| 2.1. Synthesis of polyazomethines.....  | 60 |
| 2.1.1 Monomer synthesis: enzymatic coupling of vanillin and acetovanillone.....             | 60 |
| 2.1.2. Polyazomethines synthesis and physical characterization.....                         | 62 |
| 2.1.2.1. Polymerization of bisvanillin-based compounds and diamines.....                    | 62 |
| 2.1.2.2. Reproducibility of the polymerization reaction.....                                | 66 |
| 2.1.2.3. Syntheses of random copolymers with various amount of meta-phenylene diamine ..... | 68 |
| 2.1.3. Improvement of the polymerization experimental conditions.....                       | 69 |
| 2.1.4. Stability of divanillin-based polyazomethines.....                                   | 74 |
| 2.1.2. Conclusion for polyazomethine synthesis .....  | 76 |
| 2.2.1. Optical characterization of divanillin-based polyazomethines.....                    | 77 |
| 2.2.2. Optical properties of divanillin-based polyazomethines: conclusion.....              | 81 |
| <b>3. Model compounds of divanillin-based polyazomethines</b> .....                         | 82 |
| 3.1. Synthesis of model compounds .....   | 82 |
| 3.2. X-Ray Diffraction characterization of model compounds.....                             | 85 |
| 3.3. Optical characterization of vanillin-based model compounds.....                        | 88 |
| 3.4. General conclusion for model compounds .....   | 92 |
| <b>4. General conclusion</b> .....  | 94 |
| <b>5. References</b> .....  | 97 |
| <b>6. Experimental Part</b> .....   | 99 |

## Chapter 3

|  |     |
|--|-----|
| <b>1. Introduction</b> .....   | 139 |
| <b>2. Synthesis of new bio-based monomers by enzymatic coupling</b> .....  | 140 |
| 2.1. Enzymatic coupling of ortho-vanillin .....  | 140 |
| 2.2. Enzymatic coupling of iso-vanillin.....   | 142 |
| 2.3. Conclusion .....  | 144 |
| <b>3.2. Synthesis and characterization of para-divanillin monomer</b> .....  | 145 |
| 3.2.1. Literature overview of metalation.....  | 145 |
| 3.2.2. Synthesis of para-divanillin monomer <i>via</i> formylation by metalation .....                               | 146 |
| 3.2.3. Conclusion .....  | 149 |
| <b>4. Polyazomethines with para-divanillin-based monomer</b> .....   | 150 |
| 4.1. Polyazomethine synthesis, physical characterizations and comparison with divanillin-based polyazomethines ..... | 150 |

|  |     |
|--|-----|
| 4.2. Conclusion on the synthesis and thermal characterizations of polyazomethines from para-divanillin ..... | 152 |
| 4.3. Optical properties of polyazomethines from para-divanillin .....  | 152 |
| 4.4. Conclusion on optical properties .....  | 154 |
| <b>5. Model compounds of para-divanillin-based polyazomethines</b> .....                                     | 155 |
| 5.1. Synthesis and purification of model compounds .....   | 155 |
| 5.2. X-Ray Diffraction analysis .....  | 157 |
| 5.3. Brief conclusion on synthesis and X-Ray Diffraction characterization .....                              | 158 |
| 5.4. Optical characterization .....  | 159 |
| 5.5. General conclusion on para-divanillin-based model compounds .....                                       | 163 |
| <b>6. General conclusion</b> .....   | 164 |
| <b>7. References</b> .....   | 166 |
| <b>8. Experimental part</b> .....  | 168 |

## Chapter 4

|   |     |
|---|-----|
| <b>1. Introduction</b> .....  | 187 |
| <b>2. Literature overview of polybenzobisthiazoles and polythiazolothiazoles</b> .....                | 188 |
| <b>3. Synthesis and characterization of polymers with benzobisthiazole and thiazolothiazole</b> ..... | 190 |
| 3.1. Synthesis and physical characterization .....  | 190 |
| 3.2. Optical characterization .....   | 194 |
| 3.3. Divanillin-based polybenzobisthiazoles and polythiazolothiazoles: conclusion .....               | 196 |
| <b>4. Model compounds of divanillin-based polybenzobisthiazoles</b> .....                             | 197 |
| 4.1. Synthesis and purification of model compounds .....  | 197 |
| 4.2. X-Ray Diffraction characterization of model compounds .....                                      | 199 |
| 4.2. Optical properties of model compounds .....  | 201 |
| 4.3. Model compounds with benzothiazole and benzobisthiazole: conclusion .....                        | 206 |
| <b>5. Toward Organic Light Emitting Diode</b> .....   | 206 |
| <b>6. General conclusion</b> .....  | 209 |
| <b>7. References</b> .....  | 211 |
| <b>8. Experimental part</b> .....   | 213 |
| <b>General Conclusion and Perspectives</b> .....  | 221 |

## General Table of Contents

---

---

## List of Abbreviations

|                 |  |
|-----------------|--|
| 3,4-AHBA        | 3-Amino-4-HydroxyBenzoic Acid  |
| 5-HMF           | 5-HydroxyMethylFurfural  |
| Ar              | Aromatic   |
| ATR-FTIR        | Attenuated Total Reflectance - Fourier Transform Infrared Spectroscopy |
| BBTz            | BenzoBisThiazole   |
| BTz             | BenzoThiazole  |
| CPS             | Count Per Second   |
| CT              | Charge Transfer  |
| CV              | Cyclic Voltammetry   |
| Đ               | Dispersity   |
| DABCO           | 1,4-DiAzaBiCyclo[2.2.2]Octane  |
| DAcV            | DiAcetoVanillon  |
| DAcVEH          | DiAcetoVanillon 2-EthylHexylated                                       |
| DAcVM           | DiAcetoVanillon Methylated   |
| DHAP            | Direct Hetero Arylation Polymerization                                 |
| DMF             | N, N-DiMethylFormamide   |
| DMG             | Directed Metalation group  |
| DMSO            | DiMethylSulfOxyde  |
| DOM             | Directed Ortho-Metalation (reaction)                                   |
| DP <sub>n</sub> | Degree of Polymerization   |
| DV              | DiVanillin   |
| DVEH            | DiVANillin 2-EthylHexylated  |
| DVM             | DiVanillin Methylated  |
| DSC             | Diferential Scanning Calorimetry                                       |
| E <sup>+</sup>  | Electrophile   |
| ECL             | Effective Conjugation Length   |
| EDOT            | 3,4-EthyleneDiOxyThiophene   |
| ELSD            | Evaporative Light Scattering Detector                                  |
| Eq              | Equivalent   |
| EQE             | External Quantum Efficiency  |
| ESI             | Electron Spray Ionization  |

## List of Abbreviations

---

|       |   |
|-------|---|
| FDCA  | Furan-2,5-DiCarboxylic Acid                           |
| Fc    | Ferrocene   |
| GRIM  | Grignard Metathesis Methods                           |
| HOMO  | Highest Occupied Molecular Orbital                    |
| HSQC  | Heteronuclear Single Quantum Coherence (spectroscopy) |
| HTL   | Hole Transport Layer                                  |
| HWE   | Horner-Wadsworth-Emmons                               |
| IUPAC | International Union of Pure and Applied Chemistry     |
| LE    | Locally Excited (state)                               |
| LUMO  | Lowest Occupied Molecular Orbital                     |
| nBuLi | n-Buthyl Lithium                                      |
| Mn    | Number Average Molar Mass                             |
| mPD   | meta Phenylene Diamine                                |
| Mw    | Mass Average Molar Mass                               |
| NMR   | Nuclear Magnetic Resonance (spectroscopy)             |
| NMRP  | Nitroxide-Mediated Radical Polymerization             |
| OFET  | Organic Field Effect Transistor                       |
| OLED  | Organic Light Emitting Diode                          |
| OPV   | Organic PhotoVoltaic                                  |
| oVEH  | ortho-Vanillin 2-EthylHexylated                       |
| oVM   | ortho-Vanillin Methylated                             |
| PANi  | Poly(aniline)   |
| PBBTz | Poly(BenzoBisThiazole)                                |
| pDVEH | paraDiVanillin 2-EthylHexylated                       |
| pDVM  | paraDiVanillin Methylated                             |
| PLED  | Polymer Light Emitting Diode                          |
| pPD   | para-Phenylene Diamine                                |
| PPV   | Poly(PhenyleneVinylene)                               |
| PS    | Poly(Styrene)   |
| PTSA  | Para Toluene Sulfonic Acid                            |
| PTTz  | Poly(ThiazoloThiazole)                                |
| QY    | Quantum Yield   |
| RI    | Refractive Index                                      |
| RT    | Room Temperature                                      |

## List of Abbreviations

---

|                    |  |
|--------------------|--|
| SEC                | Size Exclusion Chromatography                                  |
| TBAPF <sub>6</sub> | TetraButylAmmonium HexaFluoroPhosphate                         |
| TEA                | TriEthylAmine  |
| TGA                | ThermoGravimetric Analysis                                     |
| THF                | TetraHydroFuran  |
| TICT               | Twisted Intramolecular Charge Transfer                         |
| TMEDA              | N,N,N',N'-TetraMethylEthyleneDiAmine                           |
| TTz                | ThiazoloThiazole   |
| UV-Vis             | UltraViolet-Visible (spectroscopy)                             |
| VEH                | Vanillin 2-EthylHexylated                                      |
| VM                 | Vanillin Methylated  |
| XPS/UPS            | UV X-ray Photoelectron Spectroscopy/Photoelectron Spectroscopy |
| X-RD               | X-Ray Diffraction  |



## List of Abbreviations

---

## Résumé de la thèse

### Introduction

L'électronique organique est une branche de l'électronique générale qui se base sur les propriétés semi-conductrices de polymères ou petites molécules « organiques », c'est-à-dire à base de carbone. L'électronique organique est souvent opposée à l'électronique « inorganique », majoritairement à base de silicium. Cette dernière, bien qu'efficace et industrialisée, présente néanmoins des inconvénients car l'extraction et la mise en forme du silicium sont des étapes difficiles, pour lesquelles de grandes puretés sont nécessaires. En comparaison, l'électronique organique permet l'utilisation de composés qui peuvent être mis en solution et donc facilement mis en forme, par exemple par impression, tournette, raclage, etc. Cela permet de les intégrer dans des dispositifs flexibles notamment, comme illustré en **Figure 1**.

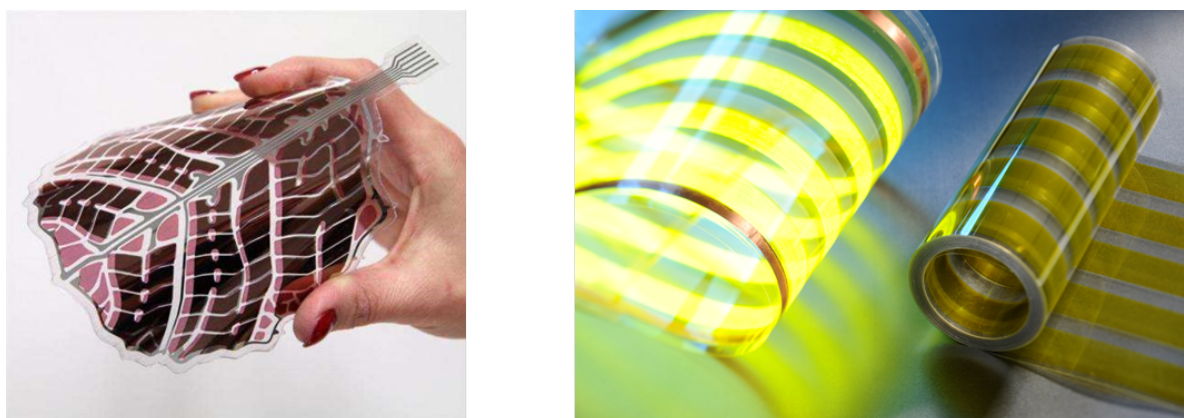


**Figure 1** : Exemples de dispositifs flexibles

Shirakawa *et al.* ont été les premiers à rapporter les propriétés conductrices d'un polymère, le polyacétylène.<sup>1</sup> Depuis, de nombreux autres polymères ont été synthétisés. En choisissant les monomères, il est possible d'ajuster les propriétés des polymères finaux. Les méthodes les plus utilisées pour la synthèse de polymères  $\pi$ -conjugués requièrent des catalyseurs à base de métaux de transition, notamment le palladium. De plus, certaines réactions de couplage nécessitent également l'utilisation de monomères toxiques et produisent ainsi, en quantité stœchiométrique, des sous-produits dangereux (à base d'étain notamment pour le couplage de Stille). Les métaux de transition, mais aussi les halogènes ont un impact sur les propriétés des polymères finaux : il faut donc purifier ces derniers, ce qui demande du temps et de l'énergie.<sup>2</sup> De plus, les monomères sont majoritairement pétrosourcés, ce qui génère des problèmes environnementaux mais aussi une faible diversité structurale.

Dans ce contexte, l'objectif de cette thèse est de synthétiser des polymères conjugués pour l'électronique organique en utilisant des monomères bio-sourcés et des procédés plus « verts ». Le monomère de base choisi est la vanilline, car celle-ci peut être facilement obtenue à partir de la biomasse lignocellulosique. Des travaux récemment conduits au Laboratoire ont également démontré que la vanilline peut être dimérisée de façon efficace et régiosélective par voie enzymatique.<sup>3,4</sup>

Trois familles de polymères ont été synthétisées et étudiées dans cette thèse et correspondent donc aux trois parties de ce résumé. Tout d'abord les polyazométhines à base de divanilline, puis les polyazométhines à base de « para-divanilline » et enfin les polythiazolothiazoles à base de divanilline. A chaque fois, les polymères ont été synthétisés et caractérisés, sur le plan de leurs propriétés physiques mais aussi optiques. Des molécules modèles mimant leur structure ont également été synthétisées et caractérisées au plan structural par diffraction des rayons X.

## I/ Polyazométhines à base de divanilline

La divanilline a été obtenue par couplage enzymatique avec la Laccase *Trametes Versicolor*.<sup>4</sup> Ce couplage se fait à température ambiante et sans solvants dangereux. Tout d'abord la vanilline est dissoute dans un mélange eau/acétone, auquel est ajouté l'enzyme. Le milieu est ensuite saturé en oxygène permettant la formation de la divanilline qui précipite et est récupérée par simple filtration. La solution contenant l'enzyme peut être réutilisée en rajoutant de la vanilline : il est ainsi possible de faire des cycles, comme illustré dans la **Figure 2**.

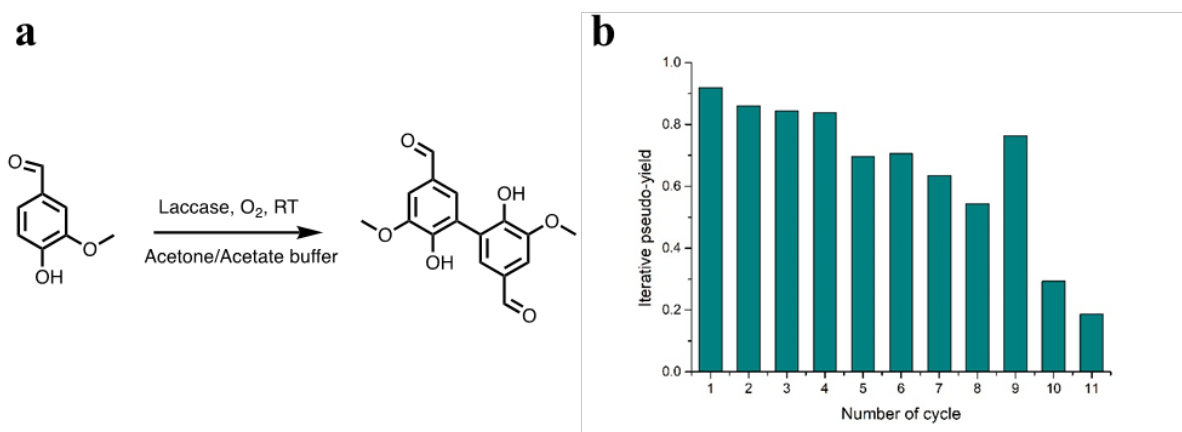


**Figure 2a** : Dimérisation de la vanilline par voie enzymatique. **b** : Pseudo-rendement lors du couplage de la vanilline, pour chaque cycle effectué

Ce protocole expérimental a également été appliqué à l'acétovanillone, permettant d'obtenir la diacétovanillone avec un bon rendement (85%). La diacétovanillone et la divanilline ont ensuite été alkylées *via* leurs fonctions hydroxyle avec deux types de groupements alkyle : méthyl ou 2-éthylhexyl. Ces composés ont ensuite été utilisés pour la synthèse de polyazométhines, comme représenté dans le **Schéma 1**.

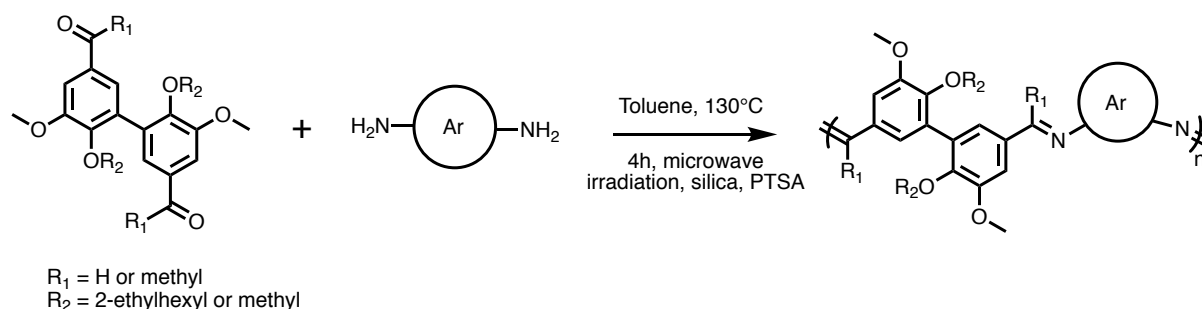
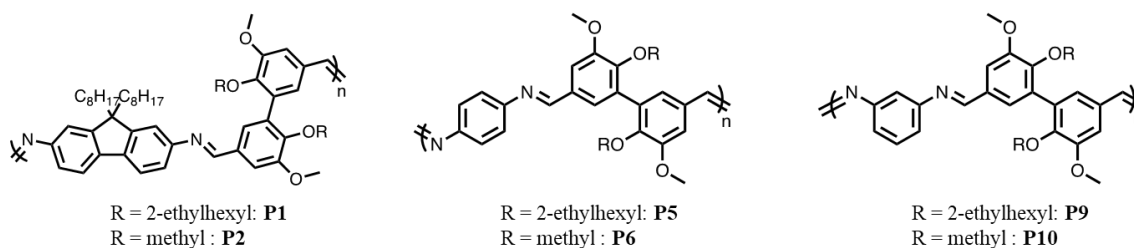


**Schéma 1** : Schéma réactionnel général pour la synthèse de polyazométhines à base de divanilline ou diacétovanillone

La spectroscopie RMN et la chromatographie par exclusion stérique (SEC) ont confirmé la formation de polyazométhines à base de divanilline ; en revanche, aucun polyazométhine à base de diacétovanillone n'a été obtenu, mais seulement des mélanges d'oligomères. La diacétovanillone a donc été mise de côté pour se concentrer sur les polymères à base de divanilline. La réaction de polycondensation se fait sans aucun catalyseur de type métal de transition, ni composés halogénés, le seul sous-produit étant l'eau. La réaction se fait sous irradiation au micro-onde avec le toluène comme solvant et la silice comme desséchant et catalyseur acide. Les masses molaires déterminées par SEC sont données dans le **Tableau 1**. Tous les polymères sont solubles, sauf **P9** qui n'a donc pas pu être analysé. De manière générale, les polymères ont une dispersité proche de 2, ce qui était attendu pour une réaction de polycondensation.



| Name | $\bar{M}_n^a$ (g/mol) | $\bar{M}_w^a$ (g/mol) | $\bar{D}^a$ | $T_d^b$ (°C) |
|------|-----------------------|-----------------------|-------------|--------------|
| P1   | 21 100                | 45 500                | 2.2         | 387          |
| P2   | 10 900                | 26 100                | 2.4         | 379          |
| P5   | 10 600                | 21 900                | 2.1         | 374          |
| P6   | 3 300                 | 9 100                 | 2.8         | 349          |
| P9   | -                     | -                     | -           | 375          |
| P10  | 2 200                 | 15 600                | 7.1         | 165          |

**Tableau 1 :** Caractéristiques des polyazométhines à base de divanilline. (<sup>a</sup> Déterminé par SEC dans le THF, calculé par rapport aux standards polystyrène. <sup>b</sup> Température de décomposition correspondant à 10% de perte en masse - déterminée par ATG sous argon à 10°C/min.

Le protocole expérimental a été amélioré pour ne plus utiliser la silice, car cette dernière impacte négativement les polyazométhines. En effet, soit elle les dégrade par hydrolyse, soit elle fausse les mesures de fluorescence. La synthèse se fait donc désormais en seulement 5 minutes sans silice avec pour étape 'clé', l'étape de « récupération » du polymère. Lors de cette étape, le polymère brut est dissous dans un minimum de dichlorométhane puis du méthanol est ajouté. Les solvants sont ensuite retirés avec un évaporateur rotatif, ce qui permet de continuer la polymérisation et d'augmenter nettement les masses molaires, comme illustré en **Figure 3**.

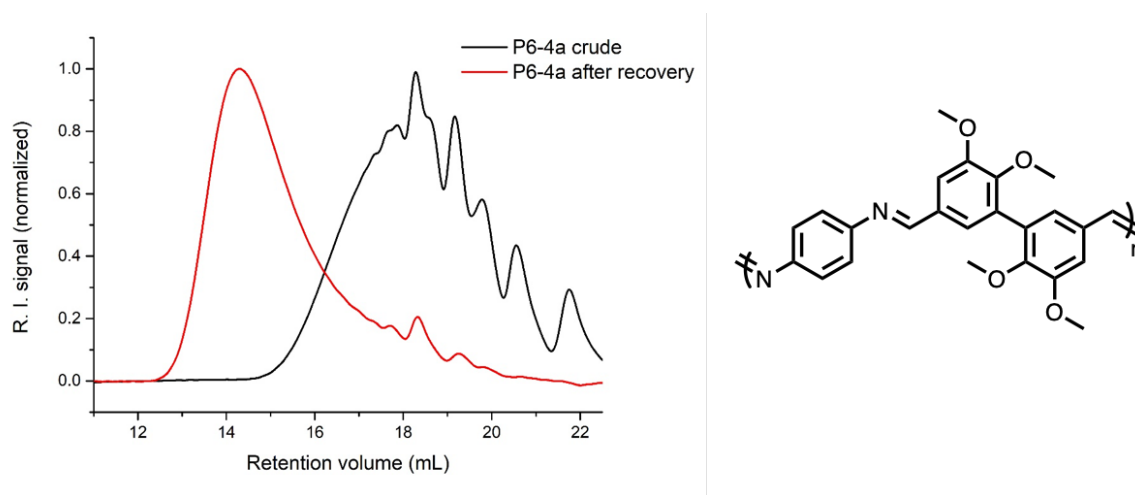


**Figure 3 :** Chromatogrammes d'exclusion stérique d'un polyazométhine brut et après « récupération » (dans le THF), avec sa structure

Les polyazométhines ont également été caractérisés par spectroscopie optique : les spectres d'absorbance sont donnés en **Figure 4**.

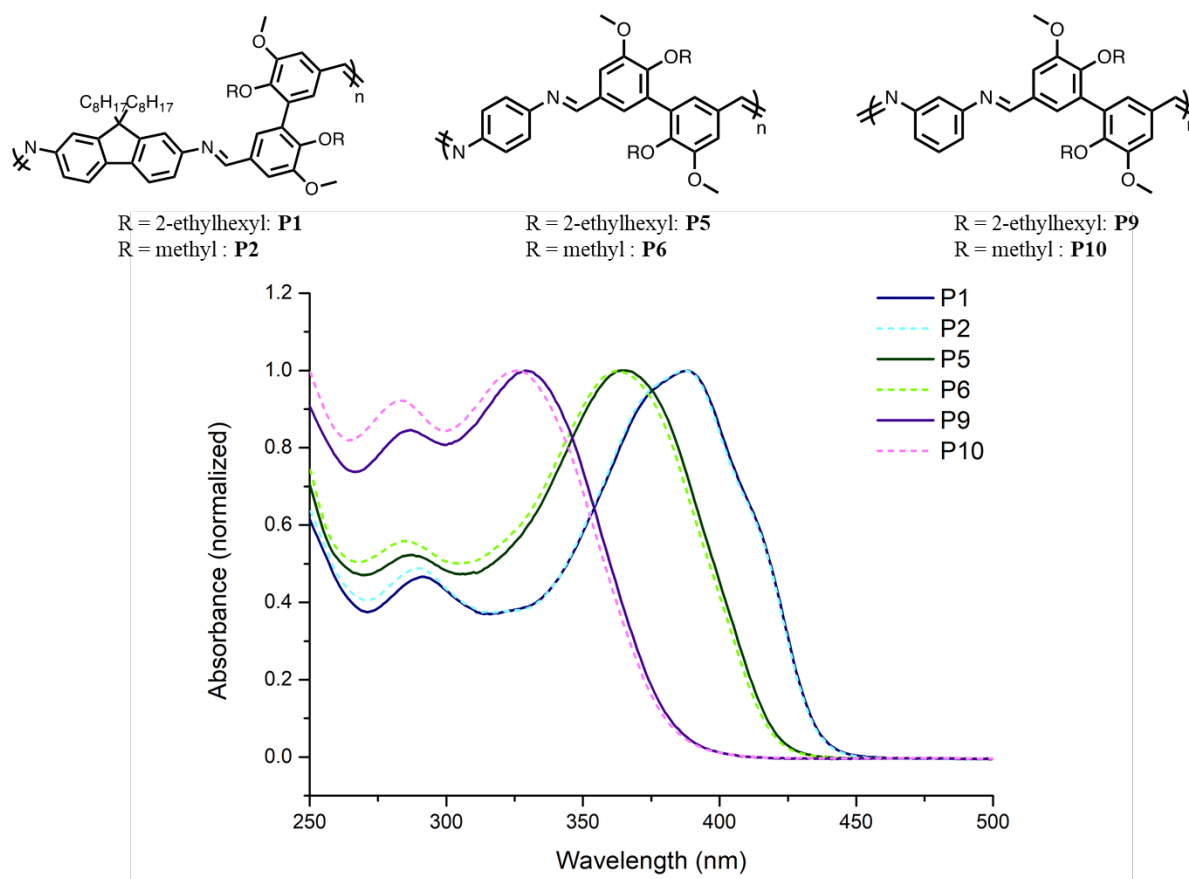


**Figure 4** : Spectres d'absorbance des polyazométhines à base de divanilline (en solution, dichlorométhane,  $10^{-2}$  g/L)

De manière générale, les spectres ont le même aspect : tout d'abord un maximum local vers les faibles longueurs d'onde qui correspond certainement aux transitions  $n-\sigma^*$ , puis un maximum global vers les plus grandes longueurs d'onde, probablement correspondant aux transitions  $\pi-\pi^*$ . Les polyazométhines avec le fluorène diamine (**P1** et **P2**) présentent également un épaulement vers les grandes longueurs d'onde, potentiellement dû à des interactions  $n-\pi^*$  ou bien à des agrégats. **P1** et **P2** ont le maximum d'absorbance le plus élevé : en effet ces polyazométhines ont un chemin de conjugaison plus étendu et plus plan, ce qui entraîne donc un décalage du maximum d'absorbance vers les grandes longueurs d'onde (et donc les plus faibles énergies). Les polyazométhines issus de la para-phénylène diamine sont légèrement décalés vers les plus faibles longueurs d'onde, car leur chemin de conjugaison est plus court, et les polyazométhines avec la para-phénylène diamine sont ceux avec le maximum d'absorbance le plus faible.

Pour mieux comprendre les propriétés de ces polyazométhines, des molécules modèles ont été synthétisées et caractérisées, par absorbance notamment mais aussi diffraction des rayons X (DRX) car elles ont pu être recristallisées. Les spectres d'absorbance du polyazométhine **P6** et de molécules modèles reproduisant sa structure sont donnés en **Figure 5**.

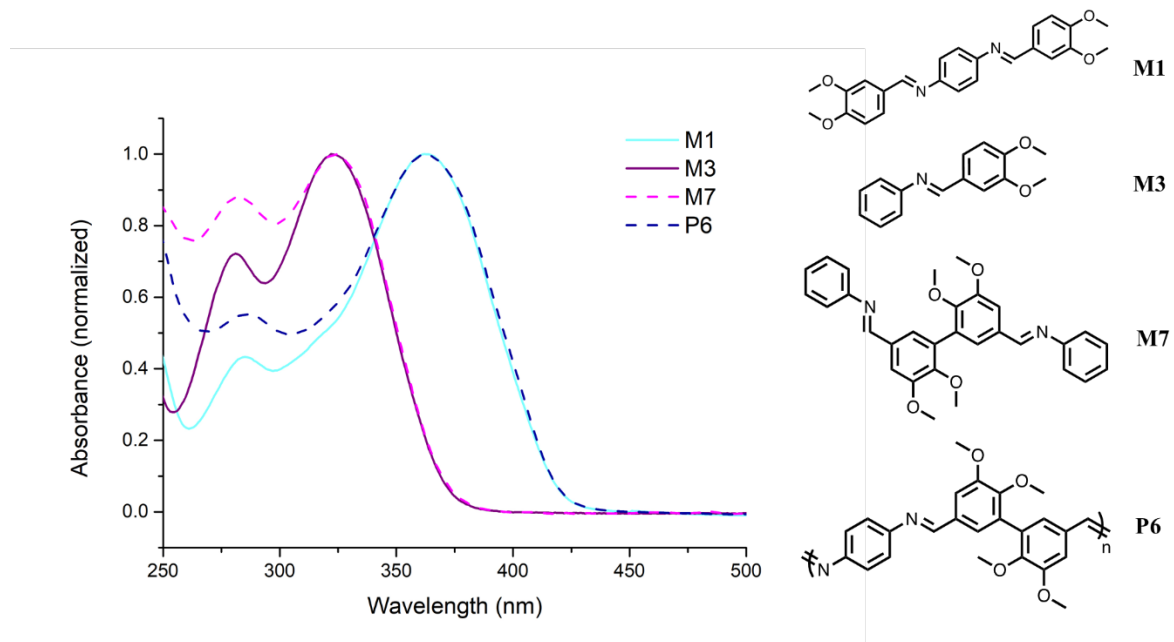


**Figure 5 :** Spectres d'absorbance de **P6** et de plusieurs molécules modèles (en solution, dichlorométhane,  $10^{-2}$  g/L)

Le résultat marquant dans cette figure est que le polymère **P6** a le même maximum d'absorbance qu'une molécule modèle – un décalage bathochromique était attendu, car **P6** est sensé avoir un chemin de conjugaison plus long que des petites molécules modèles. Ce n'est cependant pas le cas, à cause du lien entre les cycles aromatiques de la divanilline, qui est en méta par rapport aux fonctions azométhine. Cela entraîne une rupture de la conjugaison, expliquant pourquoi **M3** et **M7** (voir **Figure 5**) ont le même maximum d'absorbance. Le polyazométhine **P6** a donc le même maximum d'absorbance que **M1**, car ce dernier représente le chemin de conjugaison le plus long qu'il soit possible de parcourir dans le polymère sans rencontrer le lien en méta de la divanilline.

L'analyse des molécules modèles par DRX a également permis d'observer les différents angles au sein des molécules et de mieux comprendre le comportement des polyazométhines : en effet, un potentiel comportement type transfert de charge avait été observé en émission. Ce dernier pourrait être dû à l'agencement des molécules de la divanilline dans l'espace, comme illustré en **Figure 6**. En effet des interactions entre l'atome d'azote du lien azométhine et les hydrogènes de la divanilline peuvent être observées. L'angle de torsion entre les cycles aromatiques de la divanilline peut également être mesuré : il est de  $126.9^\circ$ .

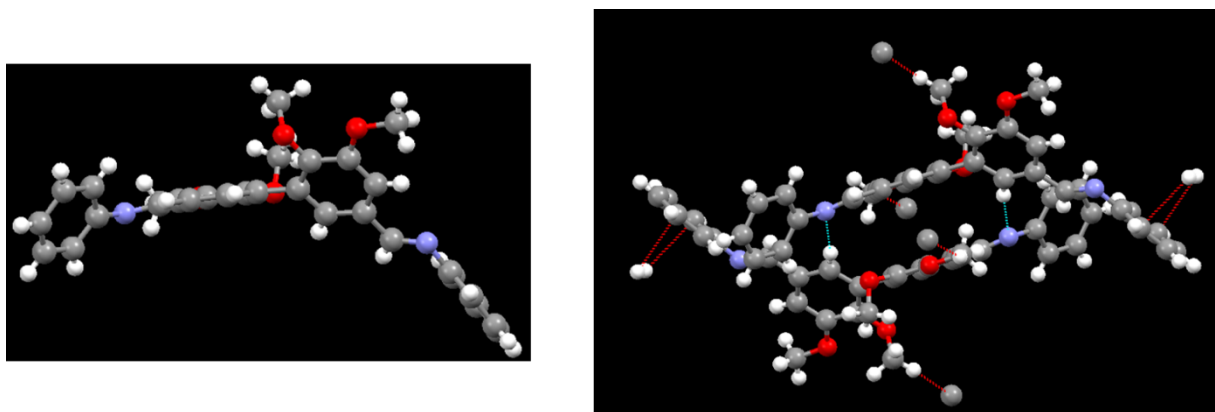


**Figure 6 :** Structure de la molécule modèle **M7** donnée par DRX, vue de profil et vue de deux molécules et de leurs interactions

## II/ Polyazométhines à base de para-divanilline

Pour améliorer le court chemin de conjugaison de la divanilline, une nouvelle molécule a été synthétisée : la para-divanilline. Cette dernière est obtenue en trois étapes, comme représenté en **Schéma 2**.

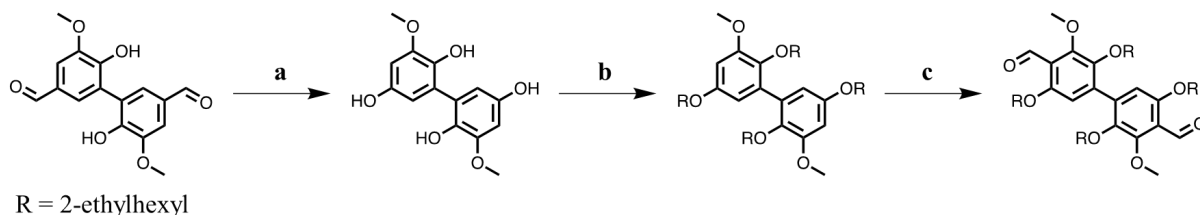


**Schéma 2** : Synthèse de para-divanilline (a : Oxydation de Dakin, b : Alkylation, c : Formylation par métallation)

La para-divanilline a donc les fonctions aldéhyde en position para par rapport à la liaison entre les deux cycles aromatiques, ce qui devrait la rendre complètement conjuguée. La para-divanilline est obtenue notamment *via* formylation par métallation : cette technique polyvalente peut être utilisée pour ajouter différents groupements.<sup>5</sup> Il serait donc possible d'utiliser cette stratégie pour synthétiser des molécules type para-divanilline, mais avec des fonctions amine à la place des aldéhydes par exemple.

La para-divanilline a été polymérisée avec différentes diamines : fluorène diamine et para-phénylène diamine. Les polyazométhines obtenus sont partiellement solubles dans les solvants usuels, ce qui empêche de les caractériser totalement en SEC. Ces polyazométhines sont également moins stables thermiquement que leurs homologues à base de divanilline avec des températures de dégradation plus basses de 67°.

En revanche ces polyazométhines ont un maximum d'absorbance plus élevé que leurs équivalents à base de divanilline, comme représenté en **Figure 7**. En effet, un décalage de 18 nm entre **P1** et **P15**, et de 11 nm entre **P5** et **P16** est à noter.

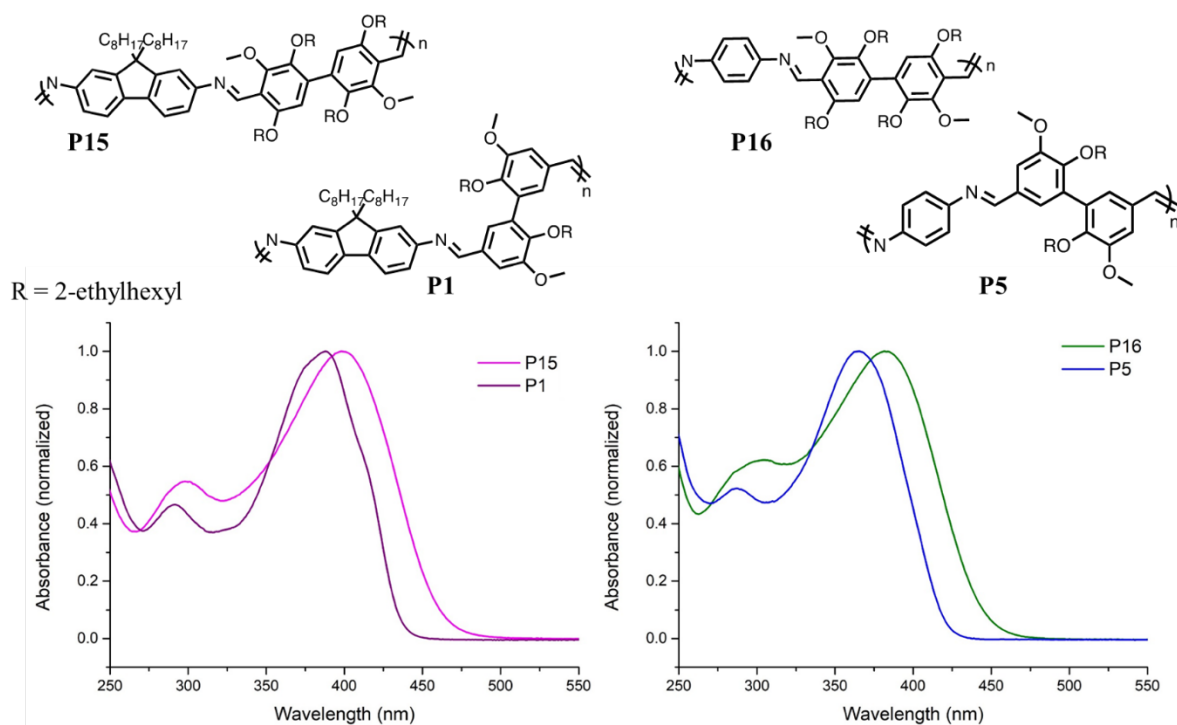


**Figure 7** : Structures et spectres d'absorbance de polyazométhines à base de divanilline et de para-divanilline

Cependant des valeurs plus élevées étaient attendues pour ces décalages bathochromiques : en effet, passer de polyazométhines à court chemin de conjugaison (**P1** et **P5**) à des polyazométhines

complètement conjugués (**P15** et **P16**), devraient permettre d'atteindre des valeurs d'absorbance bien plus élevées, ce qui n'est pas le cas.

L'analyse de molécules modèles a permis d'éclaircir ce point ; en effet, la para-divanilline n'est pas plus conjuguée que la divanilline. Les deux cycles aromatiques de la para-divanilline sont quasiment perpendiculaires, comme illustré en **Figure 8**.

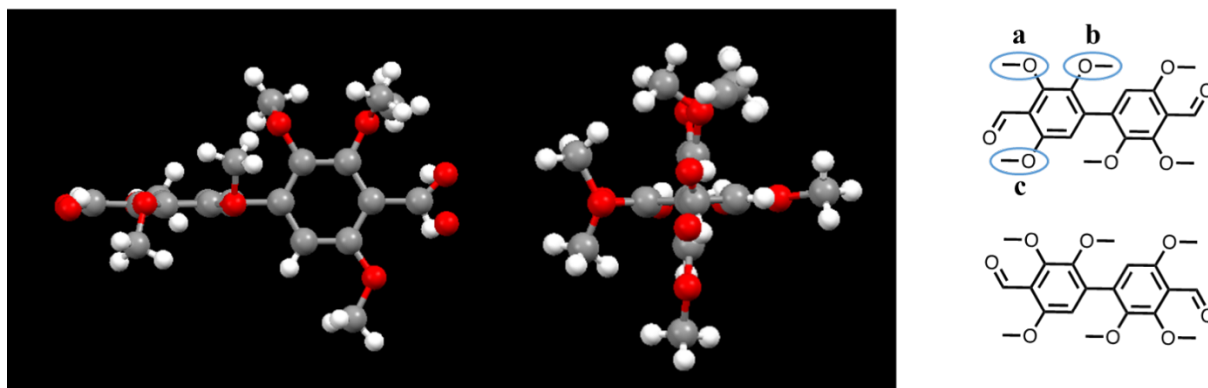


**Figure 8** : Structure de la para-divanilline méthylée donnée par DRX

Cette torsion est probablement due à de la gêne stérique entre les groupements notés **b** – elle empêche le recouvrement orbitalaire et entraîne donc une coupure de la conjugaison. Le décalage bathochromique observé entre **P1** et **P15**, mais aussi **P5** et **P16** est en fait lié à la présence d'un groupement supplémentaire sur la para-divanilline par rapport à la divanilline (noté **c** sur la **Figure 8**).

Cette molécule pourrait donc être utilisée pour rompre la conjugaison de façon contrôlée, mais aussi pour l'optique non linéaire.

### III/ Polythiazolothiazole

Le court chemin de conjugaison de la divanilline a été utilisé dans l'optique d'améliorer la solubilité de polymères rigides, type benzobisthiazole et thiazolothiazole (**Figure 9**).



Benzobisthiazole (BBTz)

Thiazolothiazole (TTz)

**Figure 9** : Structure des motifs benzobisthiazole et thiazolothiazole

En effet, ces polymères présentent des propriétés intéressantes pour l'électronique organique (cristallinité et fluorescence par exemple), mais sont aussi utilisés pour leurs excellentes propriétés mécaniques et leur stabilité thermique. La solubilité est donc un enjeu majeur lors de la synthèse de PBBTz et PTTz.<sup>6,7</sup> Après plusieurs essais avec divers protocoles expérimentaux, aucun PBBTz à base de divanilline n'a pu être obtenu : les composés étant des oligomères de faibles masses molaires ou insolubles. En revanche un PTTz à base de divanilline a pu être obtenu, comme représenté en **Schéma 3**. La synthèse se fait en 40 heures par chauffage conventionnel, sans aucun catalyseur métallique. Le polymère final (noté **P21**) a une masse molaire de 4 700 g/mol et une dispersité égale à 2.1, ce qui était attendu pour une polycondensation.



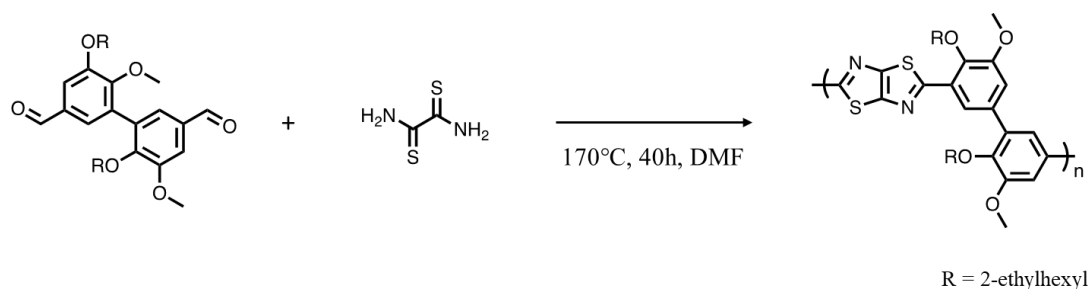


**Schéma 3** : Synthèse de PTTz à base de divanilline

Les spectres d'absorbance et d'émission de **P21** en film et en solution sont donnés en **Figure 10**.

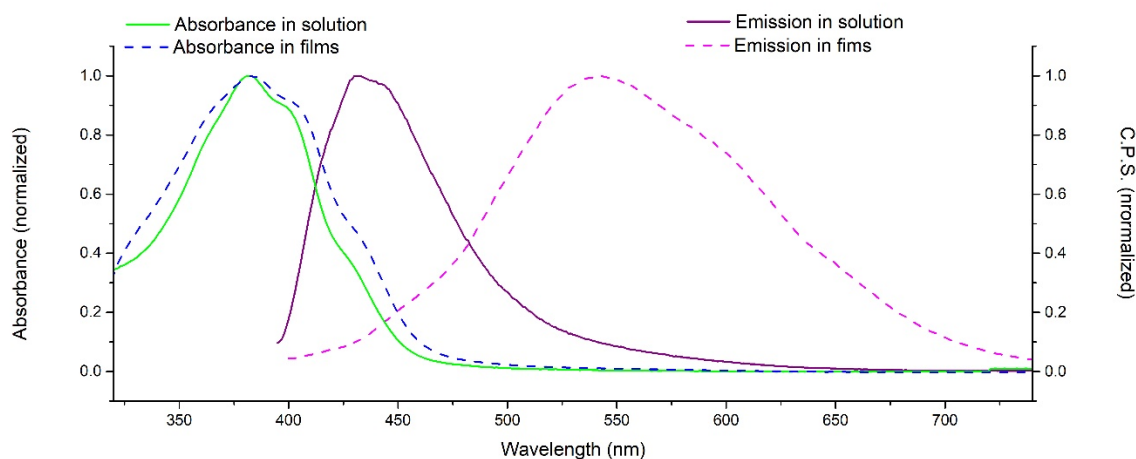


**Figure 10** : Spectres d'absorbance et d'émission de **P21** (en film : réalisé par « drop casting » sur lame de quartz. En solution, dans du dichlorométhane : à  $10^{-2}$  g/L pour l'absorbance, à  $10^{-5}$  g/L pour l'émission

**P21** a des spectres d'absorbance en solution et en film bien structurés, avec les différents pics des structures vibroniques bien visibles : cela signifie que le polymère a une structure rigide et bien ordonnée, phénomène courant pour les PTTz.<sup>8,9,10</sup> Le spectre d'émission en solution est relativement fin, et correspond à une émission dans le bleu. En revanche l'émission en film est beaucoup plus large et décalée vers les longueurs d'onde plus élevées : elle correspond à une émission dans le jaune. Il y a donc un déplacement de Stokes de 157 nm entre les maxima d'absorbance et d'émission en film, ce qui pourrait être très utile pour une intégration dans des OLED. En effet ce large déplacement de Stokes devrait permettre de limiter le phénomène de réabsorption. En revanche **P21** a un faible rendement quantique, seulement 2%, attribué à la formation d'agrégats qui entraineraient une auto-extinction de fluorescence.<sup>11</sup>

De nombreuses molécules modèles ont été synthétisées mais seules deux ont pu être purifiées et sont représentées en **Figure 11**.

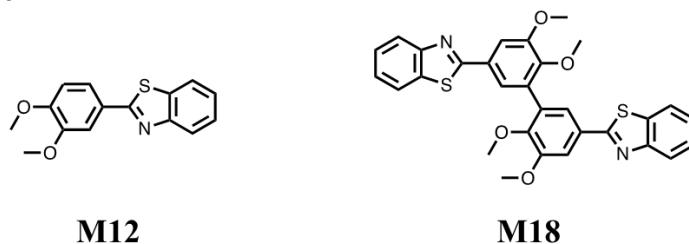


**Figure 11** : Structures de molécules modèles à base de benzothiazole et de vanilline ou divanilline

Les spectres d'absorbance et d'émission en solution de ces deux molécules sont donnés en **Figure 12**.

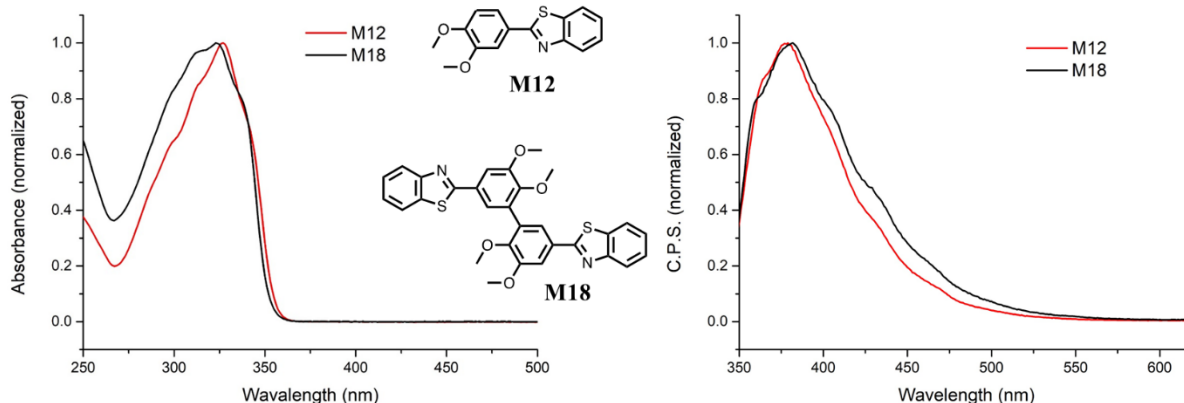


**Figure 12** : Spectres d'absorbance (à gauche) et d'émission (à droite) en solution de **M12** et **M18** (dans du dichlorométhane : à  $10^{-2}$  g/L pour l'absorbance, à  $10^{-5}$  g/L pour l'émission)

**M12** et **M18** ont des maxima d'absorbance proches – **M12** est légèrement plus décalée vers les grandes longueurs d'onde. Dans le cas de **M18**, la gêne stérique ou bien la présence du cycle aromatique supplémentaire pourrait expliquer ce léger décalage hypsochromique. Les deux molécules modèles ont une fluorescence dans le début du spectre visible (violet) avec un rendement quantique prometteur de 20% : ce dernier, associé à un déplacement de Stokes de 50 nm, pourrait permettre d'intégrer **M12** et **M18** dans des OLED – il faudrait cependant les rendre plus solubles et donc plus facilement mises en forme, en les alkylant avec des groupements aliphatiques plus longs du type 2-éthylhexyl.

**M18** pourrait également être intégrée dans des dispositifs se basant sur le transfert de charge : en effet l'analyse de **M18** par DRX a révélé que cette dernière présentait un empilement  $\pi$ , comme représenté en **Figure 13**.

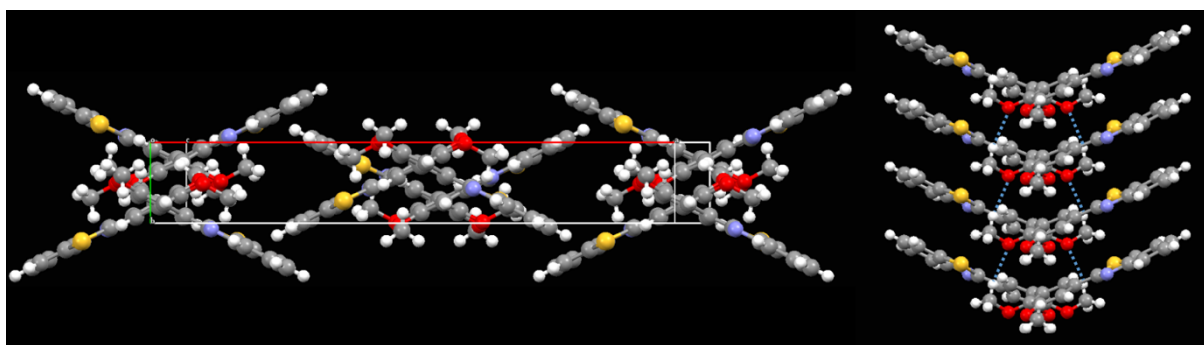


**Figure 13** : Structure de **M18** donnée par DRX, vue suivant l'axe b et empilement  $\pi$  de 4 molécules de **M18**

Cet empilement correspond à une distance entre molécule de 3.92 Å, avec un motif de type « chevrons ». En effet l'empilement  $\pi$  ne se fait pas le long de toute la molécule de façon ininterrompue à cause de l'angle de torsion entre les deux cycles aromatiques de la divanilline.

## Conclusion

L'objectif de cette thèse était de synthétiser des polymères biosourcés et  $\pi$ -conjugués, valorisables en électronique organique. La brique de base choisie pour synthétiser les polymères est la vanilline, car elle peut être facilement obtenue à partir de la biomasse lignocellulosique et sa dimérisation est bien maîtrisée.

Tout d'abord, des polyazométhines à base de divanilline ont été synthétisés (**Figure 14**). Le protocole expérimental a été amélioré et la synthèse se fait en seulement 5 minutes sous irradiation micro-ondes. L'étape clé est en fait l'étape de « récupération » après la synthèse pendant laquelle la polymérisation continue, ce qui permet d'accroître les masses molaires.

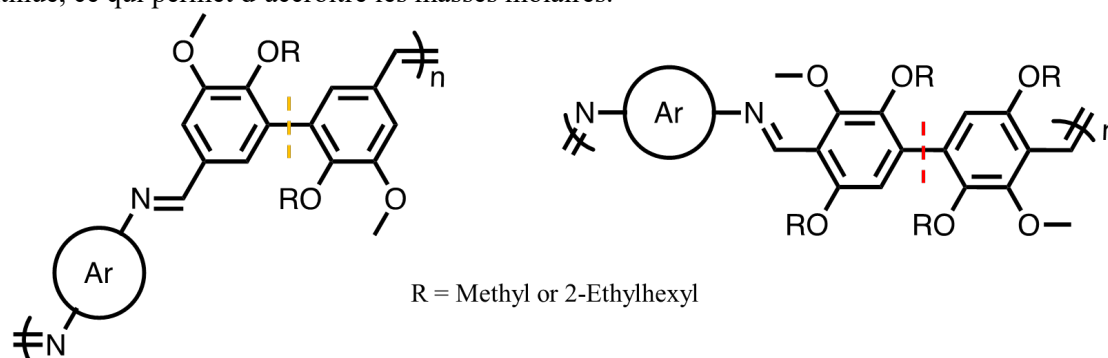
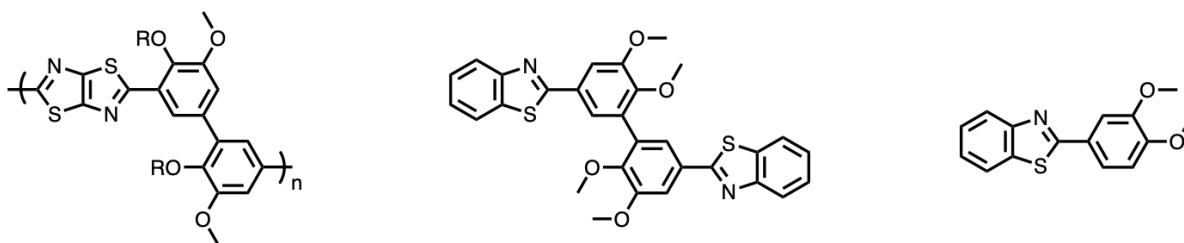


**Figure 14** : Structures de polyazométhines à base de divanilline et para-divanilline, avec représentation schématique de la rupture de conjugaison

Les maxima d'absorbance sont compris entre 325 et 388 nm, suivant la diamine choisie. En revanche ces polyazométhines ont un chemin de conjugaison très court, comme l'a révélé l'analyse de molécules modèles. En effet les fonctions aldéhyde de la divanilline sont en position méta par rapport à la liaison entre les deux cycles aromatiques, ce qui entraîne une rupture de la conjugaison. Pour allonger ce chemin de conjugaison, une nouvelle molécule a été synthétisée à partir de la divanilline. Cette molécule, nommée para-divanilline a les fonctions aldéhyde en position para par rapport au lien entre les deux cycles aromatiques, laissant entrevoir des polymères complètement conjugués (**Figure 14**). Ce n'est en fait pas le cas : en effet, l'analyse de molécules modèles a révélé que les deux cycles aromatiques de la para-divanilline sont quasiment perpendiculaires (sous forme cristalline) à cause de la gêne stérique entre groupements. Cela entraîne un mauvais recouvrement orbitalaire et donc une rupture de conjugaison. Cette molécule pourrait donc être utilisée pour rompre la conjugaison d'un polymère conjugué à des endroits précis.

Enfin, un polythiazolothiazole (PTTz) à base de divanilline a été synthétisé. Ce dernier est soluble dans les solvants usuels, probablement grâce à la divanilline qui coupe le chemin de conjugaison et empêche d'avoir un polymère trop rigide. Bien qu'ayant des propriétés d'absorbance et d'émission intéressantes, ce PPTz a un faible rendement quantique de seulement 2%.

Des molécules modèles à base de benzothiazole ont également été synthétisées (**Figure 15**), avec cette fois-ci un rendement quantique en fluorescence de 20%. La molécule modèle à base de divanilline et benzothiazole présente également un empilement  $\pi$  avec un motif « chevrons ». Ces deux molécules pourraient donc être intégrées dans des dispositifs type OLED ou photovoltaïque.



R = 2-Ethylhexyl

Figure 15 : Structures de PTTZ à base de divanilline et de molécules modèles à base de benzothiazole

## Références

1. Shirakawa, H., Louis, E. J., MacDiarmid, A. G., Chiang, C. K. & Heeger, A. J. Synthesis of electrically conducting organic polymers: Halogen derivatives of polyacetylene,  $(\text{CH})_x$ . *J. Chem. Soc. Chem. Commun.* 578–580 (1977). doi:10.1039/C39770000578
2. Usluer, Ö. *et al.* Metal residues in semiconducting polymers: Impact on the performance of organic electronic devices. *ACS Macro Lett.* **3**, 1134–1138 (2014).
3. Llevot, A. Resinic acid and lignin derivative dimers: new precursors for the synthesis of biobased polymers. (Université de Bordeaux, 2014).
4. Llevot, A., Grau, E., Carlotti, S., Grelier, S. & Cramail, H. Selective laccase-catalyzed dimerization of phenolic compounds derived from lignin: Towards original symmetrical bio-based (bis) aromatic monomers. *J. Mol. Catal. B Enzym.* **125**, 34–41 (2016).
5. Snieckus, V. Directed Ortho Metalation. Tertiary Amide and O-Carbamate Directors in Synthetic Strategies for Polysubstituted Aromatics. *Chem. Rev.* **90**, 879–933 (1990).
6. Ahmed, E., Subramaniyan, S., Kim, F. S., Xin, H. & Jenekhe, S. A. Benzobisthiazole-based donor-acceptor copolymer semiconductors for photovoltaic cells and highly stable field-effect transistors. *Macromolecules* **44**, 7207–7219 (2011).
7. Osaheni, J. A. & Jenekhe, S. A. New Red Light-Emitting Conjugated Rigid-Rod Polymer: Poly (benzobisthiazole-1,4-phenylenebisvinylene). *Macromolecules* **26**, 4726–4728 (1993).
8. Peng, Q., Peng, J. B., Kang, E. T., Neoh, K. G. & Cao, Y. Synthesis and electroluminescent properties of copolymers based on fluorene and 2,5-Di(2-hexyloxyphenyl)thiazolothiazole. *Macromolecules* **38**, 7292–7298 (2005).
9. Ahmed, E., Kim, F. S., Xin, H. & Jenekhe, S. A. Benzobisthiazole - Thiophene copolymer semiconductors: synthesis, enhanced stability, field-effect transistors, and efficient solar cells. *Macromolecules* **42**, 8615–8618 (2009).
10. Subramaniyan, S. *et al.* Thiazolothiazole donor-acceptor conjugated polymer semiconductors for photovoltaic applications. *Macromolecules* **47**, 4199–4209 (2014).
11. Pinto, M. R., Takahata, Y. & Atvars, T. D. Z. Photophysical properties of 2,5-diphenyl-thiazolo[5,4-d]thiazole. *J. Photochem. Photobiol. A Chem.* **143**, 119–127 (2001).



## General Introduction

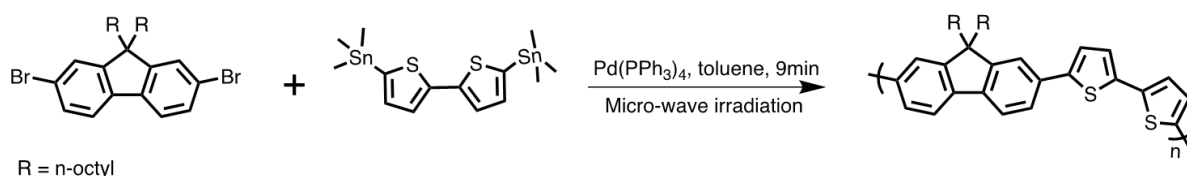
Electronic organic is an ever-expanding field that uses the properties of semi-conductive polymers or small molecules in various devices: OLEDs (Organic Light Emitting Diode), OFETs (Organic Field Effect Transistor), solar cells, etc. Electronic organic is usually opposed to “inorganic electronic”, which relies mostly on silicon and other inorganic materials. Inorganic semiconductors were successfully integrated in various devices, such as solar panels for example, with high efficiency and a large-scale production. However inorganic electronic has drawbacks too, mainly linked to the extraction and processing of silicon as high purities are required.<sup>1,2</sup>

While organic electronic cannot (yet?) compete with silicon-based technologies, it is more easily processed than the latter. Indeed, polymers and small molecules either can be dissolved or dispersed and therefore processed *via* many current technologies: Doctor Blade, spin coating, printing, etc. These techniques can lead to light and flexible devices with a relatively low production cost, as illustrated in **Figure 1**.<sup>3,4</sup>



**Figure 1:** Examples of flexible devices: solar cells (left) and OLED (right) (Source: VTT, Technical Research Centre of Finland)

Hideki Shirakawa *et al.* reported the electric conductivity of polyacetylene in 1977, giving rise to organic electronic.<sup>5</sup> Since then, a wide family of polymers have been synthesized, with tunable properties and multiple applications. Most polymers are synthesized using transition-metal catalyzed coupling, such as Stille and Suzuki couplings. Despite their efficiency and reliability, these coupling reactions also have some issues. Indeed, the latter require transition metal as catalyst (the most used being palladium), but also hazardous monomers, leading to the production of stoichiometric amounts of toxic by-products such as tin-based compounds in the case of Stille coupling (**Scheme 1**).<sup>6,7</sup>



**Scheme 1:** Synthesis of fluorene-based polymer using Stille coupling under microwave irradiation. Reaction time using conventional heating: 72h (adapted from <sup>6</sup>)

While efforts were made to improve such coupling reactions by reducing the reaction time (**Scheme 1**) or by using less toxic solvents,<sup>8</sup> there are still metallic impurities in the final polymer. The latter impurities have an impact on the ensuing device’s performances, as they can act as charge traps.<sup>9</sup>

Consequently tedious purification processes have to be carried out, requiring solvent and energy. In addition, the diversity of monomers, all coming from oil resource, is rather limited.

In this context, this PhD aims at synthesizing conjugated polymers with original properties for OLED or OPV (Organic Photovoltaics) applications, using divanillin-based monomers and other conjugated monomers. In order to better understand the polymers' properties, model compounds mimicking their backbones were synthesized and characterized.

This manuscript is organized in four chapters: the first one will briefly review the synthesis of conjugated polymers without metal, and the integration of bio-based monomers in conjugated polymers. The second chapter is dedicated to the synthesis of divanillin-based polyazomethines: their synthesis, characterization and model compounds will be presented and analyzed. The third chapter is about the synthesis of new bio-based monomers and their integration in polyazomethines as well as the characterization of the latter polymers. The fourth and final chapter will discuss the synthesis and characterization of divanillin-based polybenzobisthiazoles and polythiazolothiazoles, and their corresponding model compounds.

---

**References**

1. Xakalashé, B. S. & Tangstad, M. Silicon processing: from quartz to crystalline silicon solar cells. *South. African Pyrometallurgy Int. Conf.* 1–18 (2011).
2. Mohammad Bagher, A. Comparison of Organic Solar Cells and Inorganic Solar Cells. *Int. J. Renew. Sustain. Energy* **3**, 53 (2014).
3. Chochos, C. L. & Choulis, S. A. How the structural deviations on the backbone of conjugated polymers influence their optoelectronic properties and photovoltaic performance. *Prog. Polym. Sci.* **36**, 1326–1414 (2011).
4. Brunetti, F. G., Kumar, R. & Wudl, F. Organic electronics from perylene to organic photovoltaics: Painting a brief history with a broad brush. *J. Mater. Chem.* **20**, 2934–2948 (2010).
5. Shirakawa, H., Louis, E. J., MacDiarmid, A. G., Chiang, C. K. & Heeger, A. J. Synthesis of electrically conducting organic polymers: Halogen derivatives of polyacetylene, (CH)<sub>x</sub>. *J. Chem. Soc. Chem. Commun.* 578–580 (1977). doi:10.1039/C39770000578
6. Nehls, B. S. *et al.* Semiconducting polymers via microwave-assisted Suzuki and Stille cross-coupling reactions. *Adv. Funct. Mater.* **14**, 352–356 (2004).
7. Milstein, D. & Stille, J. K. A General, Selective, and Facile Method for Ketone Synthesis from Acid Chlorides and Organotin Compounds Catalyzed by Palladium. *J. Am. Chem. Soc.* **100**, 3636–3638 (1978).
8. Marrocchi, A., Facchetti, A., Lanari, D., Petrucci, C. & Vaccaro, L. Current methodologies for a sustainable approach to  $\pi$ -conjugated organic semiconductors. *Energy Environ. Sci.* **9**, 763–786 (2016).
9. Usluer, Ö. *et al.* Metal residues in semiconducting polymers: Impact on the performance of organic electronic devices. *ACS Macro Lett.* **3**, 1134–1138 (2014).





# **Chapter 1: Design of $\pi$ -conjugated polymers *via* metal-free and bio-sourced routes**



## Table of Contents

|  |    |
|--|----|
| <b>1. Introduction</b> .....   | 25 |
| <b>2. Building blocks from biomass</b> .....   | 25 |
| 2.1 Lignocellulose: brief description .....  | 25 |
| 2.2. Aromatic molecules from lignin .....  | 27 |
| 2.3. Furan and its derivatives .....   | 29 |
| 2.4. Lignocellulosic biomass: conclusion .....   | 30 |
| <b>3. Synthesis of <math>\pi</math>-conjugated polymers <i>via</i> more sustainable pathways</b> ..... | 31 |
| 3.1. Direct Hetero Arylation Polymerization .....  | 31 |
| 3.2. One step further: transition metal-free syntheses.....  | 33 |
| 3.2.1. Conjugated polymers synthesized with halogen.....   | 33 |
| 3.2.1.1. Bromine-catalyzed reaction .....  | 33 |
| 3.2.1.2. Synthesis of conjugated polymers by oxidative homocoupling of bis-Grignard reagents .....     | 34 |
| 3.2.2. Synthesis of conjugated polymers without halogen <i>via</i> condensation reaction.....          | 34 |
| 3.2.2.1. Synthesis of polyazomethines .....  | 34 |
| 3.2.2.2. Knoevenagel reaction.....   | 35 |
| 3.2.2.3. Horner-Wadsworth-Emmons reaction .....  | 36 |
| 3.2.2.4. Condensation of squaric acid .....  | 37 |
| 3.2.2.5. Aldol condensation .....  | 38 |
| 3.3. Transition metal-free syntheses: conclusion .....   | 39 |
| <b>4. Synthesis of conjugated polymers with bio-based monomers</b> .....                               | 40 |
| 4.1. From a micro-organism: 3-amino-4-hydroxybenzoic acid .....  | 40 |
| 4.2. From lignocellulosic biomass: Furan and difuran.....  | 41 |
| 4.3. From lignocellulosic biomass: vanillin .....  | 43 |
| 4.4. Bio-based monomers for the synthesis of conjugated polymers: conclusion .....                     | 44 |
| <b>5. General conclusion</b> .....   | 45 |
| <b>6. References</b> .....   | 46 |



## 1. Introduction

While unavoidable, chemistry is facing today big challenges. The era of petroleum reaches some limits, as concerns about sustainability logically arise more drastically. Indeed, the petroleum resources are finite and require millions of years to be renewed. Moreover, in the minds of people, chemistry is associated with pollution, plastic wastes, climate warming, etc.

One alternative to petroleum resources is biomass. Biomass is a “Material produced by the growth of micro-organisms, plants or animals” (definition from IUPAC<sup>1</sup>). Therefore, there is not “one” biomass, but rather multiple biomasses, each with its own characteristics. One promising biomass is the lignocellulose: the latter has a rather short production cycle (from 1 to 50 years) and does not compete with food production, as opposed to crop biomass, for example. Lignocellulosic biomass can be used for energy production and has the potential to provide a large palette of molecules.<sup>2,3,4</sup>

As seen in the general introduction, organic electronic has also challenges to face and would greatly benefit both from the use of bio-based monomers and the development of synthetic pathways avoiding the use of toxic metals. Indeed, the latter are often used as catalysts or are sometimes embedded in the structure of monomers.

First, the obtention of bio-based derivatives from lignocellulosic biomass will be briefly described. The synthesis of conjugated polymers *via* sustainable coupling reactions will be then discussed and, finally, some examples of bio-based conjugated polymers will be detailed.

## 2. Building blocks from biomass

### 2.1 Lignocellulose: brief description

Lignocellulosic biomass corresponds to forestry biomass, crops and crop residues. The latter biomass is mainly composed of lignin, cellulose and hemicelluloses, with various percentages depending on the vegetal species (**Figure 1a**).<sup>5</sup> Cellulose is the most abundant biopolymer in Nature; it is composed of cellobiose repeating units,<sup>6</sup> as shown in **Figure 1b**.

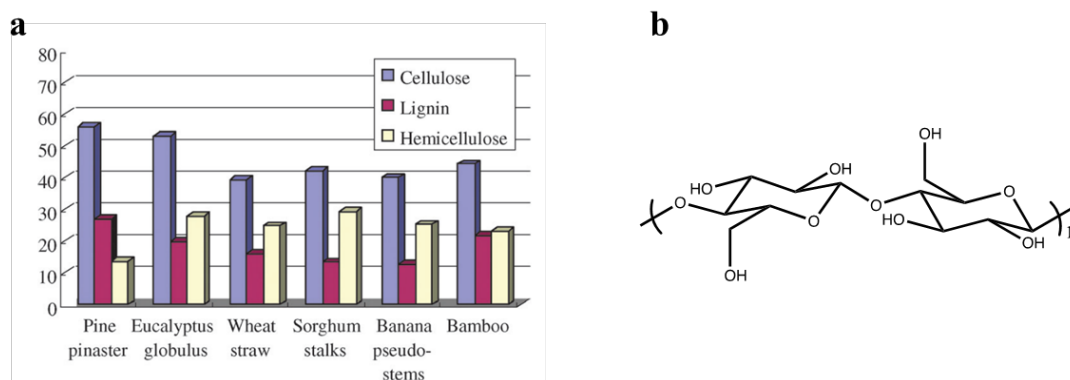


**Figure 1a:** Weight percentages of cellulose, hemicelluloses and lignin in various plants (Source: <sup>7</sup>) **b:** Structure of cellulose (Adapted from <sup>6</sup>)

Cellulose has a crystalline structure, which enables to maintain the structure of the plant. On the contrary, hemicelluloses are branched polysaccharides with an amorphous morphology, the composition

of which depending on the vegetal species.<sup>8</sup> Finally, lignin is an aromatic polymer with a complex structure that also depends on the plant species. Example of lignin in poplar is given in **Figure 2**.

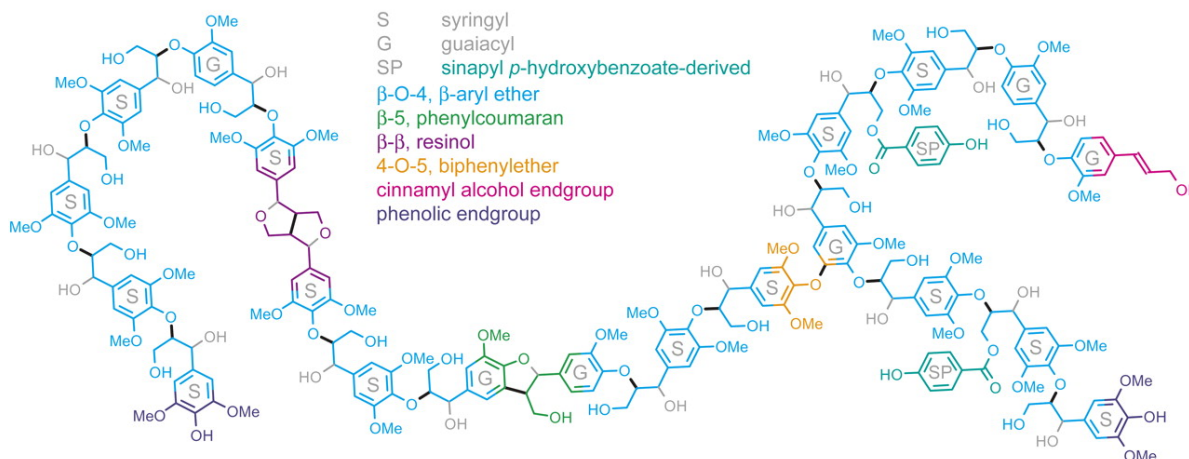


**Figure 2:** Representation of lignin from poplar, as predicted by NMR spectroscopy (Source: <sup>9,10</sup>)

Hemicelluloses act as a glue that binds cellulose and lignin together and the hydrophobicity of lignin and its phenolic structure protect the wood against external aggressions.<sup>11</sup>

Cellulose and hemicelluloses have various applications, mostly for the paper industry (500 million tons of paper estimated to be produced in 2020<sup>12</sup>), and can also be used as biofuels. However, the latter industry still has many challenges to overpass as it is facing higher prices than anticipated for the raw materials, and a lowering of investment. Many biofuels start-ups have either failed or are actually using lignocellulosic biomass to synthesize specialty molecules.<sup>13</sup>

Apart from these two main applications, cellulose and hemicellulose can also be used in opto-electronic devices (**Figure 3**). Karakawa *et al.* grafted fluorescent units on the available hydroxyl functions of cellulose, leading to a compound that was successfully integrated into an OLED. This grafted cellulose acts as an host material for the emissive layer of the device.<sup>14</sup> Cellulose was also used as a substrate for various opto-electronic applications, to replace plastic. Thanks to its flexibility and transmittance in visible range, cellulose was integrated as a substrate for flexible OLED leading to efficient and promising devices with high brightness and efficiency.<sup>15,16</sup>

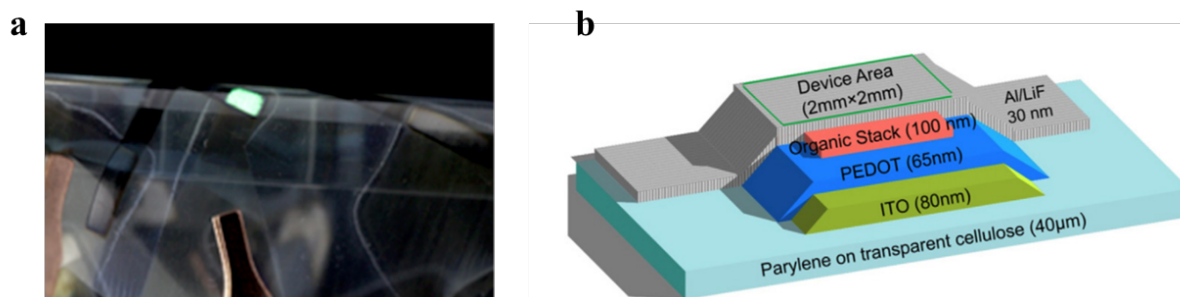


**Figure 3:** Photo and structure of flexible OLED using cellulose as substrate (source: <sup>15</sup>)

Qian *et al.* reported the fabrication of an OFET using cellulose as a flexible and biodegradable substrate, coated with chitosan, another bio-based polymer that can be obtained from shrimp shells.<sup>17</sup> Chitosan acted as a smoothing layer, as the roughness of cellulosic paper can be an impediment to the use of paper as substrate for opto-electronic applications.<sup>18</sup>

As for lignin, the latter is mainly burnt to produce energy for the paper plant. However, it is estimated that 30-75 millions tons of lignin per day could be produced by the kraft pulp plants without affecting their energy needs (estimated for a plant that produces 0.5 billion of oven dried wood pulp (odw) annually<sup>19</sup>). When not burnt, lignin can be used as a cement dispersant, optimizing the latter properties.<sup>20,21</sup> Lignin can also be depolymerized and used to produce various organic molecules, as will be exemplified in the next section.

## 2.2. Aromatic molecules from lignin

Two main industrial processes are used to produce lignin: (i) Kraft process and (ii) bisulfite process. The Kraft process is used by the paper industry to obtain pulp but also resins and terpenes.<sup>22</sup> As mentioned previously, the lignin obtained as a black liquor is most of the time burnt to produce energy. In the bisulfite process, cellulose of higher purity can be obtained and lignin is once more a by-product obtained as liginosulfonates. Borregaard Lignotech (Norway) and Rayonier (USA) are the main producers of liginosulfonates.

Both of these chemical processes break chemical bonds of lignin, but they also create new ones. Subsequently other methods were tested to depolymerize lignin in a more controlled way and avoid unwanted bond formations or impurities. Amongst them, Organosolv process is the most industrially advanced,<sup>23</sup> but others are also tested, like the enzymatic way.<sup>24,25</sup> Once the lignin is isolated, it can be decomposed to obtain aromatic synthons. Two ways can be followed: (i) oxidation or (ii) reduction pathways. The reduction pathway can lead to benzene, toluene and xylene platform,<sup>26</sup> while the oxidation route can lead to various other aromatic compounds,<sup>27</sup> as represented in **Figure 4**.

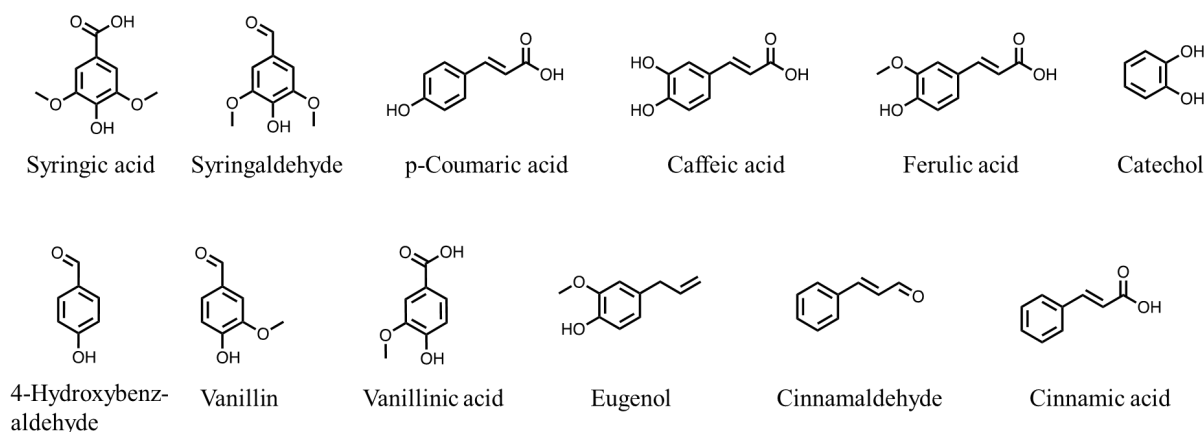
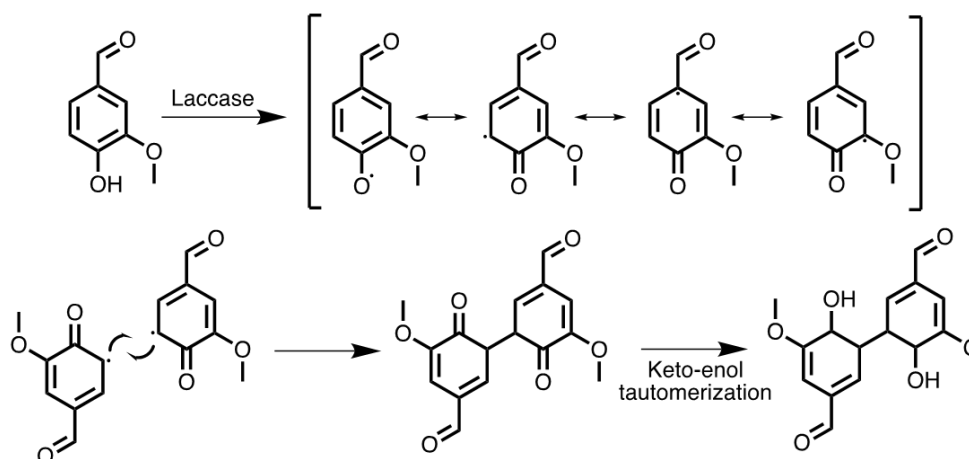


**Figure 4:** Structures of aromatic molecules that can be obtained from lignin (source: <sup>27,28,29,30</sup>)

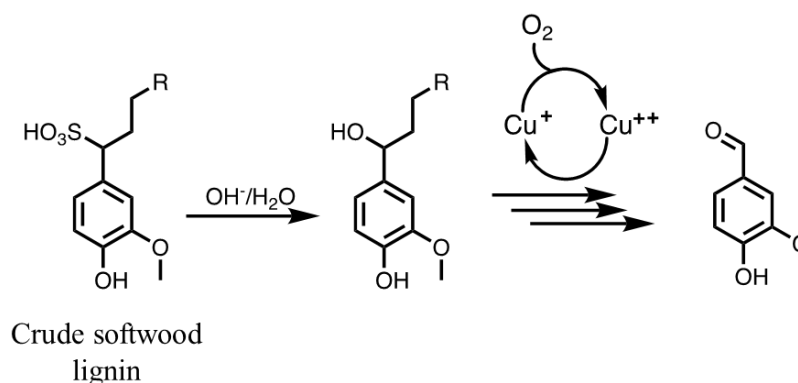
To consider such molecules as potential monomers, they have to be at least bi-functional. One way to bring this bifunctionality is to make dimers from C-C coupling. Caillol *et al.* recently reviewed the various ways to create such bonds.<sup>3</sup> Following an enzymatic coupling strategy, Grelier and coll. developed a platform of vanillin dimers as promising building blocks for opto-electronic applications.<sup>31,32,33,34</sup> The dimerization of vanillin is given in **Scheme 1**.





**Scheme 1:** Laccase-catalyzed vanillin dimerization

This procedure requires nonhazardous solvents (water/acetone) and is done at room temperature. Divanillin is produced as the only product in high yield, and this reaction can be performed on a 6-gram scale.<sup>35,31</sup> Vanillin is naturally synthesized in Nature by a climbing orchid and can be recovered after curing the pods. However, this process is long, slow and tedious, with a very low yield: 500 kg of vanilla pods are required to produce 1 kg of vanillin.<sup>36</sup> Therefore natural vanillin is expensive and in 2019, its cost was around 500\$ per kg.<sup>37</sup> Another way to obtain vanillin is to derivatize petroleum-based guaiacol,<sup>38</sup> but more environmental-friendly and bio-sourced ways are available. Indeed, vanillin can be obtained from eugenol<sup>39</sup> but also from liginosulfonates. The main producer of vanillin starting from liginosulfonates is Borregaard (Norway); their experimental protocol is represented in **Scheme 2**.



**Scheme 2:** Borregaard process to obtain vanillin from lignin (adapted from <sup>40</sup>)

Solvay also produces vanillin by bioconversion of ferulic acid from rice bran (Rhovanil<sup>41</sup>). In both cases, the obtained vanillin is used as a flavoring agent for the food industry. But vanillin was also widely developed as polymer precursor.<sup>42,43</sup> Llevot *et al.* notably demonstrated that dimers of vanillin can easily undergo polymerization, leading polyesters,<sup>35</sup> polyepoxides,<sup>44</sup> etc. Subsequently, it was chosen as a monomer in this PhD project, for the synthesis of conjugated polymers.

## 2.3. Furan and its derivatives

Furan and its derivatives also gained massive interests as bio-based compounds. Indeed, the furan moiety is reported to yield polymers with high thermal stability<sup>45</sup> and has promising properties for opto-electronic applications. The latter is structurally close to thiophene, one of the main building blocks for organic electronic.<sup>46</sup> The furan moiety is believed to have superior properties than thiophene, as its oxygen atom is smaller than the sulfur one of thiophene. This size difference is expected to bring better planarity and therefore more efficient  $\pi$ -stacking and charge transport; the furan moiety also enables strong fluorescence.<sup>47</sup>

Furfural can be obtained by dehydration of xylose, which can be derivatized from hemicellulose. 5-HydroxyMethylFurfural (5-HMF) is another furan-based compound that can be obtained by dehydration of sugars - it is also easily found in food products,<sup>48</sup> and can be derivatized in 2,5-Dimethylfuran, a promising biofuel.<sup>49</sup> By dehydrating 5-carbon sugars or derivatizing furfural or 5-HMF, various compounds are accessible: some are represented in **Figure 5**.

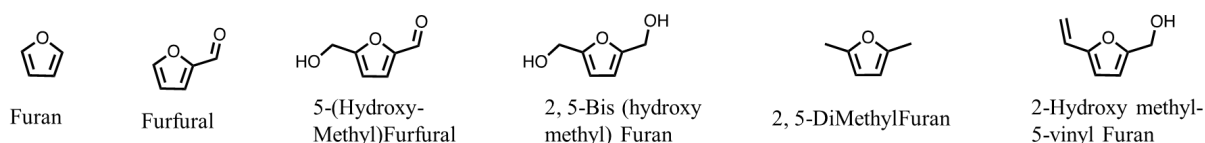


**Figure 5:** Examples of furan-based compounds that can be obtained from bio-based resources<sup>5</sup>

These compounds can be used as monomers: 2, 5-Bishydroxymethylfuran was used as such in the course of polymerization, leading to self-healing polymer.<sup>50</sup> Furan-based polymers can also be obtained by polymerizing a methacrylate furan-based compound, leading to polymers with furan as a pendant group.<sup>51</sup> 5-HMF can be derivatized as a dicarboxylic furan (Furan-2,5-DiCarboxylic Acid, FDCA, in **Figure 6**);<sup>52</sup> the latter led to various polyesters with promising properties that rival those of petroleum-based plastics.<sup>53,54,55</sup> However, in these examples the conjugated structure of furan is not fully exploited. Furan-based monomers that could lead to conjugated polymers are represented in **Figure 6**.

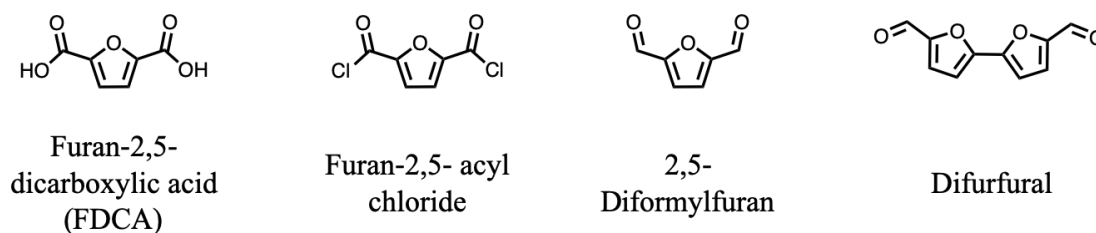
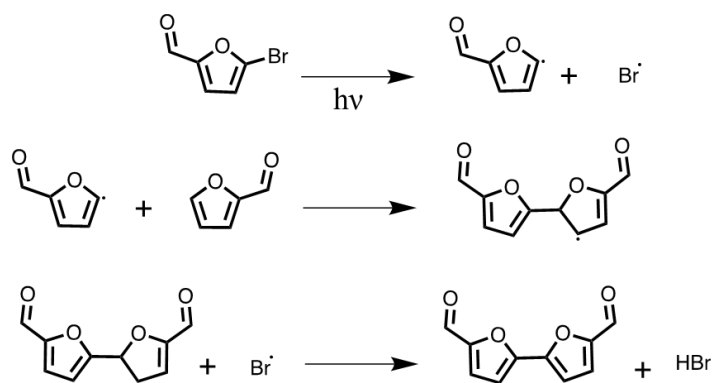


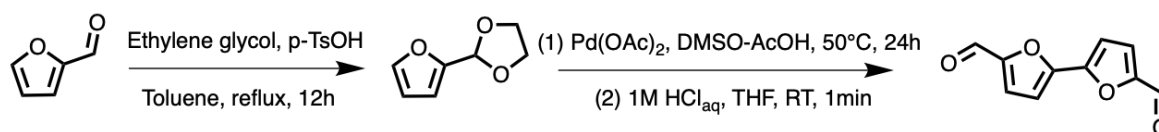
**Figure 6:** Structure of difunctional furan-based monomers

Furan-2,5-diacyl chloride can easily be obtained by derivatization of FDCA, in a single and solvent-free step.<sup>56</sup> 2,5-diformylfuran can be obtained by selective oxidation of 5-HMF, but also in one step by derivatizing fructose.<sup>57,58</sup> Finally, difurfural can be obtained by dimerization of bromofurfural under photoirradiation. The latter experimental protocol was improved by using bromofurfural as a photosensitive initiator, and furfural as the main reagent. The dimerization takes place between furfural molecules, leading to difurfural in good yield - subsequently this process was scaled-up. A reaction mechanism was proposed by the authors, and is represented in **Scheme 3**.<sup>59</sup>



**Scheme 3:** Synthesis of difurfural *via* photochemistry (adapted from <sup>59</sup>)

This experimental procedure was published in 2000 and surprisingly no development could be found afterwards. Nowadays, reports on difurfural synthesis actually describe a longer experimental protocol, with a protection/deprotection step but also the use of a palladium-based catalyst,<sup>60</sup> as shown in **Scheme 4**.



**Scheme 4:** Experimental protocol to obtain difurfural from furfural (Adapted from <sup>60,61</sup>)

#### 2.4. Lignocellulosic biomass: conclusion

Lignocellulosic biomass can provide a wide range of molecules, from phenol- to furan-based compounds but many others, with different structures are potentially available.<sup>2</sup> Bio-based molecules can then undergo polymerization, leading to various polymers with different properties and applications. We chose to focus on the compounds that could be used for organic electronic, namely with moieties that could bring conjugation: aromatic and furan-based molecules. Vanillin is an interesting compound, as it can be easily dimerized by an environmental friendly reaction.<sup>31</sup> Another type of promising molecules for organic electronic is furan-based compounds - they could be comparable to thiophene and may even be better than the latter, thanks to their efficient  $\pi$ -stacking and strong fluorescence. In **Figure 7**, the simulation of HOMO and LUMO of difurfural shows how planar it can be, heralding promising opto-electronic properties.<sup>62</sup>

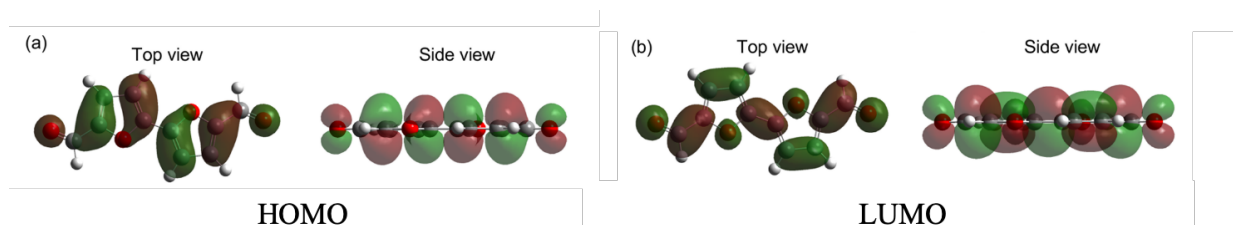


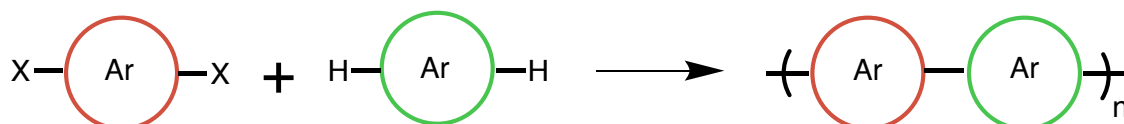
**Figure 7:** Optimized structure of electronic orbitals of difurfural (a. HOMO, b. LUMO) (Source: <sup>60,62</sup>)

In the next section, the synthesis of  $\pi$ -conjugated polymers using sustainable methodologies will be briefly reviewed, and finally the incorporation of bio-based monomers will be discussed.

### 3. Synthesis of $\pi$ -conjugated polymers *via* more sustainable pathways

#### 3.1. Direct Hetero Arylation Polymerization

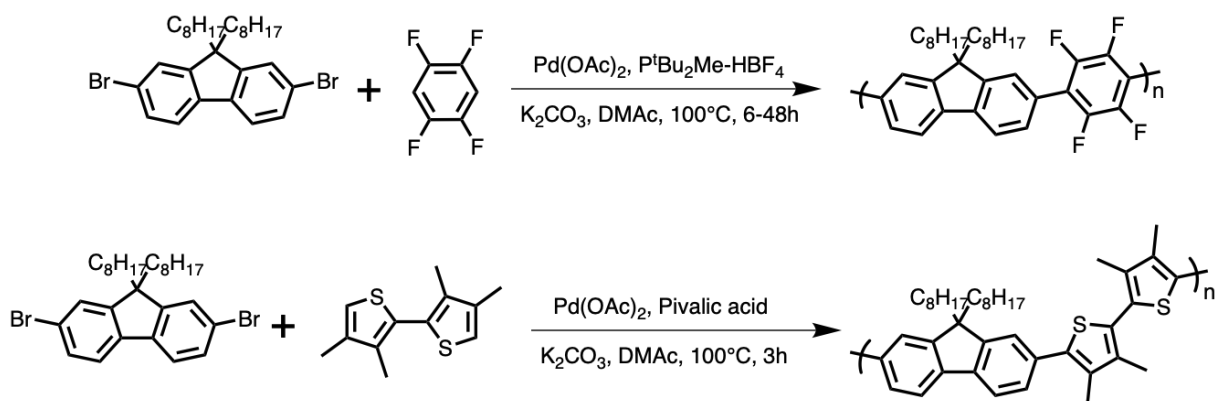
Despite their reliability and efficiency, common methodologies used to synthesize  $\pi$ -conjugated polymers have several drawbacks. One of them is the use of hazardous monomers and subsequently the production of hazardous by-products, as discussed in the introduction. For instance, the Stille reaction requires trialkylstannane monomers and leads to the production of stoichiometric amounts of tin-based by-products.<sup>63</sup> Direct Hetero Arylation Polymerization, or DHAP, is a relatively recent method that enables the synthesis of conjugated polymers while generating fewer wastes and using “simpler” and less hazardous monomers. Indeed, DHAP is a metal-catalyzed coupling reaction between an arene and an aryl halide (see **Scheme 5**).



**Scheme 5:** General reaction scheme of DHAP (X = halogen)

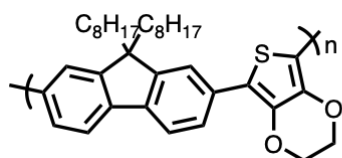
DHAP was first investigated by Lemaire and coll. to synthesize poly(alkylthiophenes).<sup>64</sup> This reaction has since then been used to synthesize various conjugated polymers. Indeed, DHAP has multiple advantages, the main one being that it is done on easily accessible monomers: arene and aryl halide. DHAP also allows the use of monomers bearing various substituents.<sup>65</sup> The latter coupling reaction is performed with a metal-based catalyst: rhodium (III/IV) can be used but palladium-based catalysts are more frequently investigated. Palladium acetate is the most employed, as it was reported to improve deprotonation of the arene.<sup>66</sup> Two other reagents are used to perform DHAP: a Brønsted base which neutralizes the hydrogen halides formed during the reaction and a phosphine ligand. The latter's role is still investigated and the phosphine ligand is chosen on a case-by-case basis. Some phosphine-free systems were reported to reduce the amount of impurities in the final polymers.<sup>67,68</sup>

Despite its various applications and promising results, DHAP also has drawbacks: as stated above, it relies on palladium-based catalyst and, depending on the targeted polymer, phosphine ligand can be used. The latter catalysts lead to the formation of impurities in the final polymers, affecting their properties.<sup>69</sup> DHAP also has the disadvantages of not controlling the regioselectivity and of enabling homocoupling. These latter both induce structural defects in the final polymers leading to poor optoelectronic properties. Homocoupling can be avoided by a careful choice of experimental conditions, such as the use of phosphine ligand or relatively low temperature.<sup>70</sup> The lack of regioselectivity and branching reactions can be avoided by tuning the experimental conditions (choice of solvent and catalyst), and also by blocking the other positions. Kanbara and coll. investigated the latter strategy, as represented in **Scheme 6**.



**Scheme 6:** Synthesis of polymers *via* DHAP using monomers with blocked positions (Top: adapted from <sup>71</sup>, Bottom: adapted from <sup>68</sup>)

DHAP allows the synthesis of polymers that cannot or can hardly be synthesized by “traditional” coupling. DHAP also enables to synthesize polymers with similar or even better properties than polymers synthesized with Stille or Suzuki couplings for example. For instance, Kanbara *et al.* synthesized a polymer through various experimental protocols, as summed up in **Figure 8**.

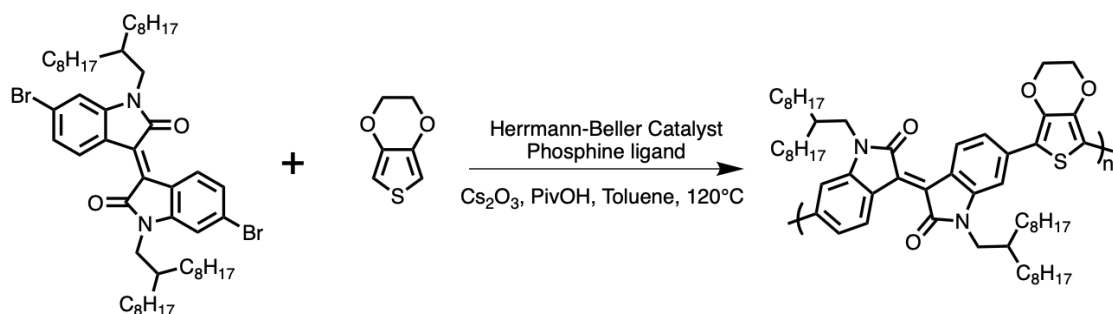


**H-PEDOTF:** DHAP, conventional heating  
**L-PEDOTF:** DHAP, micro-wave irradiation  
**S-PEDOTF:** Suzuki, conventional heating

**Figure 8:** Structure of PEDOTF, synthesized *via* various ways: DHAP and Suzuki coupling (Adapted from: <sup>72</sup>)

DHAP using conventional heating yielded the highest average molar mass (147 000 g/mol) with a dispersity around 3. Comparatively, **S-PEDOTF** (obtained by Suzuki coupling) has an average molar mass of 47 500 g/mol and a lower dispersity (2). The authors investigated the remaining quantities of palladium in the final polymers: this value is 1590 and 2300 ppm for **H-PEDOTF** and **L-PEDOTF** respectively and 4390 ppm for **S-PEDOTF**. This doubled value for **S-PEDOTF** can be explained by a higher quantity of catalyst required for Suzuki coupling (5%mol, opposed to 1%mol for the DHAP). The aforementioned polymers were then integrated in OFET and photovoltaic devices: in both cases, **H-PEDOTF** gave the best results. According to the authors, the high molar masses and good purity of **H-PEDOTF** explained the improved properties of the OFET and solar cells.<sup>72</sup>

Kanbara’s team has extensively worked on DHAP, aiming at testing new monomers or experimental conditions (e.g. use of micro-wave reaction to reduce reaction time<sup>72</sup>). The team of Leclerc has also worked extensively on DHAP.<sup>73,74,75</sup> The authors notably synthesized a polymer by DHAP in batch but also following continuous flow process, which would lower the price of the synthesis - the reaction scheme is given in **Scheme 7**.



**Scheme 7:** Synthesis of PiEDOT by DHAP (Adapted from <sup>76</sup>)

The obtained polymer has an average molar mass around 30 000 g/mol, and the synthesis is quite reproducible - however the dispersity is rather high under continuous flow ( $\sim 2$  in batch, but  $\sim 3$  under continuous flow). The isoindigo-based polymer obtained has promising properties for OFET and solar cells (NB: isoindigo, while being an isomer of indigo, is not bio-based<sup>77</sup>).

### 3.2. One step further: transition metal-free syntheses

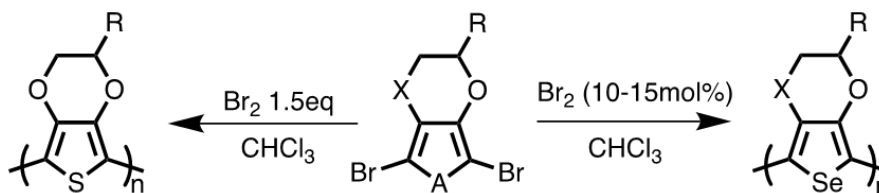
Usluer *et al.* showed that polymer's properties were greatly improved after removing metal traces.<sup>69</sup> Indeed, the latter act as charge traps and extensive purification is needed to remove them. The best OFET and OPV performances were obtained for a polymer purified with a Soxhlet apparatus and metal complexing agents. The latter purification techniques require time, energy and solvents.

Kanbara and coll. investigated the role of terminal halogen atoms on polymers' properties and concluded that the presence of terminal bromide had a bigger impact on opto-electronic properties than residual palladium.<sup>78</sup> Therefore limiting the use of not only transition metals but also halogens is crucial, to avoid long and tedious purification but also additional steps to remove the final halogen, and improve the polymers' properties. The next section first lists reactions leading to conjugated polymers without the use of transition metals but with halogen atoms. Then, reactions with neither halogen atoms nor transition metals are summed up. The aim of this section is not to provide an exhaustive list of transition metal-free syntheses, but rather to identify key reactions leading to promising polymers for organic electronic applications and/or reactions that could be applied to bio-based monomers.

#### 3.2.1. Conjugated polymers synthesized with halogen

##### 3.2.1.1. Bromine-catalyzed reaction

Patra *et al.* investigated the synthesis of PEDOT and PEDOS using bromine as a catalyst, as is represented in **Scheme 8**.



**Scheme 8:** Synthesis of PEDOT and PEDOS derivatives (adapted from <sup>79</sup>)

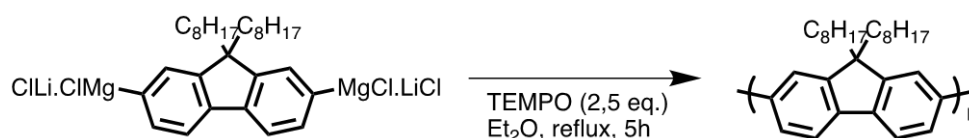
The authors hypothesized that the polymerization starts by the oxidation of the monomers by  $\text{Br}_2$  to form a radical cation. The latter then attacks the monomer, resulting in the formation of a dimer and elimination of bromine. The dimer species is more reactive than the monomer and subsequently reacts with the latter, leading to the polymer growth. This process works well to synthesize PEDOS, a type of polymer hardly synthesized by other methods. Yet these experimental conditions are poorly adapted to the synthesis of PEDOT, even with an excess of bromine. Indeed, neither soluble PEDOT nor PEDOT's analogues were obtained using the bromine-catalyzed coupling. Moreover, the insoluble recovered polymer had a low conductivity.

However, this coupling is well-adapted for the synthesis of PEDOS, yielding polymers with molar mass of 4000 - 5000 g/mol with dispersity of 2.1-2.3, and promising properties for applications as hole transport layers.<sup>79</sup> Nevertheless the authors do not comment on the regioregularity of the obtained PEDOS. Heeney *et al.* reported the synthesis of regioregular PEDOS but using a transition metal catalyzed coupling.<sup>80</sup> To remove the remaining bromine at the end of the reaction, Patra and coll.

reported the use of hydrazine hydrate and extraction with a Soxhlet system to “de-dope” the polymers after synthesis; a rather long and tedious purification - the authors also did not comment on the amount of bromine left after purification.

### 3.2.1.2. Synthesis of conjugated polymers by oxidative homocoupling of bis-Grignard reagents

A Nitroxide-Mediated Radical Polymerization (NMRP) approach was successfully applied to the synthesis of conjugated polymers. This homocoupling of Grignard reagent does not require any transition metal, but halogen, magnesium and lithium-bearing species are needed to perform this polymerization. Studer *et al.* investigated the synthesis of polyfluorene using this approach, with TEMPO as a catalyst (Scheme 9).<sup>81</sup> The latter can be regenerated after treatment with air, which is interesting both from economical and sustainable points.



**Scheme 9:** Synthesis of polyfluorene by oxidative homocoupling of Grignard reagent (adapted from <sup>81</sup>)

Polyfluorene was obtained in good yield (more than 90%) with average molar mass lower than the ones obtained by GRIM synthesis (9 000 g/mol *vs* 62 000 g/mol) but higher dispersity (2.0-2.2 *vs* 1.5).<sup>82</sup> The homocoupling of Grignard reagents also leads to fewer residual transition metals in the final impurities: 1-15 ppm of nickel were detected in polyfluorene synthesized through this method, compared to 840-1560 ppm for a polyfluorene synthesized with GRIM polymerization. Studer and coll. also investigated the synthesis of other fluorene-based conjugated polymers using the NMRP approach, as represented in Figure 9.

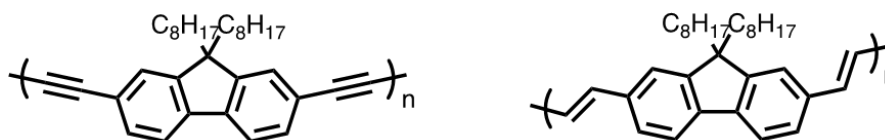


**Figure 9:** Structure of fluorene-based polymers obtained by oxidative homocoupling of Grignard reagent (adapted from <sup>81</sup>)

The fluorene-based polyvinylene could be integrated in OLED for example, as it has a strong fluorescence (quantum yield of 0.5).<sup>83</sup>

However, the oxidative homocoupling of Grignard reagent has also some drawbacks: some bromide atoms are located at the chain ends affecting the final properties and the synthesis of the bis-Grignard monomer is long and tedious. Indeed, the latter has to be obtained with high purity to perform the polymerization afterwards.<sup>81</sup>

## 3.2.2. Synthesis of conjugated polymers without halogen *via* condensation reaction

### 3.2.2.1. Synthesis of polyazomethines

Polyazomethines have been widely investigated, as they have multiple applications for optoelectronics.<sup>84,85,86</sup> Their main advantage is their easy synthesis and recovery: indeed, they can be obtained from the condensation of a diamine and a dialdehyde, without any catalyst and with only water as a by-product. Subsequently a wide range of polymers can be obtained, with various properties by changing

the monomers.<sup>87,88</sup> Skene and coll. investigated extensively the synthesis of fluorene-based azomethines; the authors successfully synthesized all fluorene-based polyazomethines, as represented in **Figure 10**.

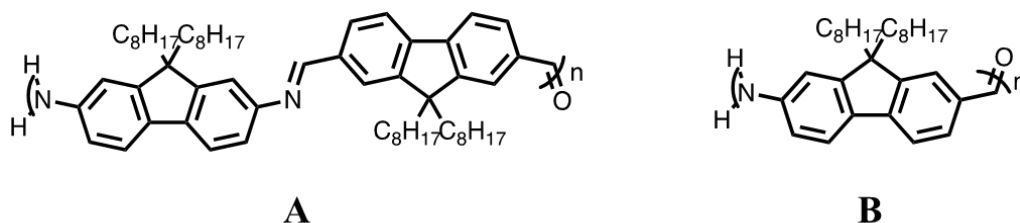


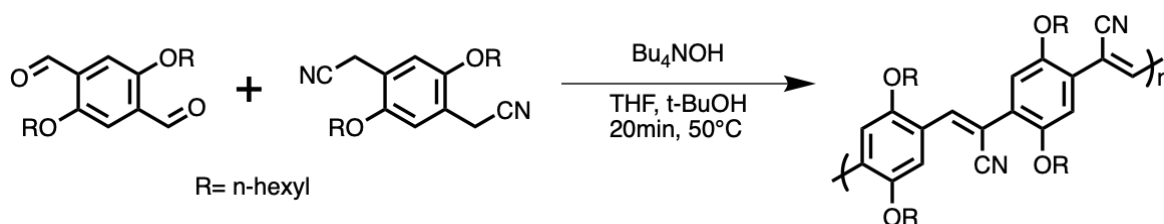
**Figure 10:** Fluorene-based polyazomethines (Adapted from <sup>89,90</sup>)

The polyazomethine noted **A** has promising properties, such as fluorescence (quantum yield (QY) of 0.19) and electrochromism. High molar masses could be obtained, up to 145 800 g/mol after few days of polymerization (performed in a pressure tube).<sup>89</sup> Polyazomethine **B** was obtained by self-condensation of a monomer bearing both amine and aldehyde functions. However, the reaction required additional metallic catalyst ( $\text{TiCl}_4$ ). Additionally, the molar mass is low: only 2 180 g/mol after one week of reaction. Yet this polyazomethine has promising properties, as it is highly fluorescent (QY of 0.48); the authors also investigated its use as detector for explosive.<sup>90</sup>

Polyazomethines will be further discussed in **Chapter 2**, which will focus on the synthesis of vanillin-based polyazomethines.

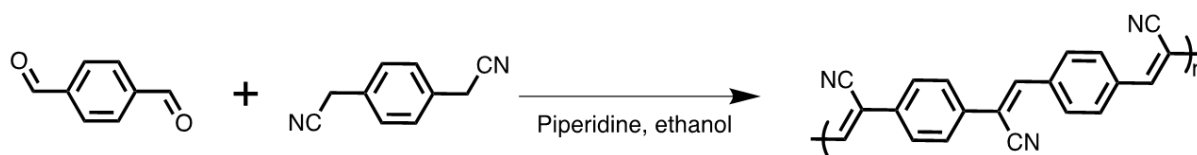
### 3.2.2.2. Knoevenagel reaction

The Knoevenagel reaction can yield conjugated polymers bearing a pendant cyano group. The latter can improve electron affinity, therefore leading to better properties for the polymers. Greenham *et al.* investigated the synthesis of a PPV-like polymer, as represented in **Scheme 10**.



**Scheme 10:** Synthesis of conjugated polymer *via* Knoevenagel reaction (Adapted from <sup>91</sup>)

The polymer obtained was successfully integrated into OLED showing promising properties.<sup>91</sup> However, the Knoevenagel reaction does not allow a good control of the final polymer's regioselectivity, leading to structural defect with adverse effects on opto-electronic properties.<sup>92</sup> Another type of PPV-like polymer was obtained by a Knoevenagel reaction by Cao *et al.* as represented in **Scheme 11**.



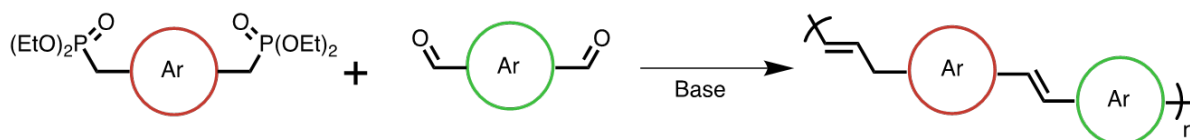
**Scheme 11:** Synthesis of PPV like polymer *via* Knoevenagel reaction (adapted from <sup>93</sup>)

The polymer obtained showed promising applications for hydrogen production, but low quantum yield (0.03). This could be due to self-quenching, a phenomenon frequently reported for aggregates.<sup>94</sup> Moreover, the polymer is poorly soluble, which makes it harder to process.<sup>93</sup>



## 3.2.2.3. Horner-Wadsworth-Emmons reaction

The Horner-Wadsworth-Emmons (HWE) reaction is an alternative to the Wittig reaction and enables well-controlled polymerization. Indeed, the HWE reaction allows for a better control of regioselectivity, as it leads primarily to double bonds with *trans* configuration - this is not the case for the Wittig reaction, which also leads to *cis* configuration. The general scheme of the HWE reaction is given in **Scheme 12**.



**Scheme 12:** General scheme of the Horner-Wadsworth-Emmons reaction (adapted from <sup>92</sup>)

Liao and coll. synthesized various polymers and model compound mimicking their backbone using the HWE reaction (**Figure 11**).

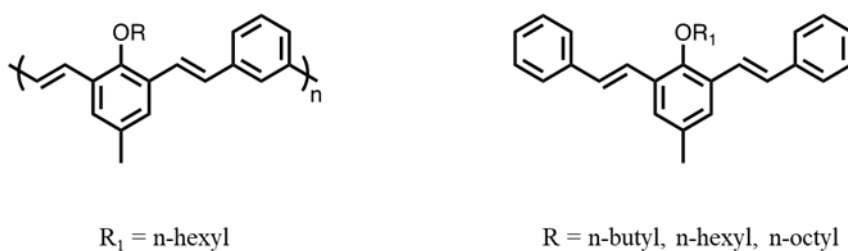
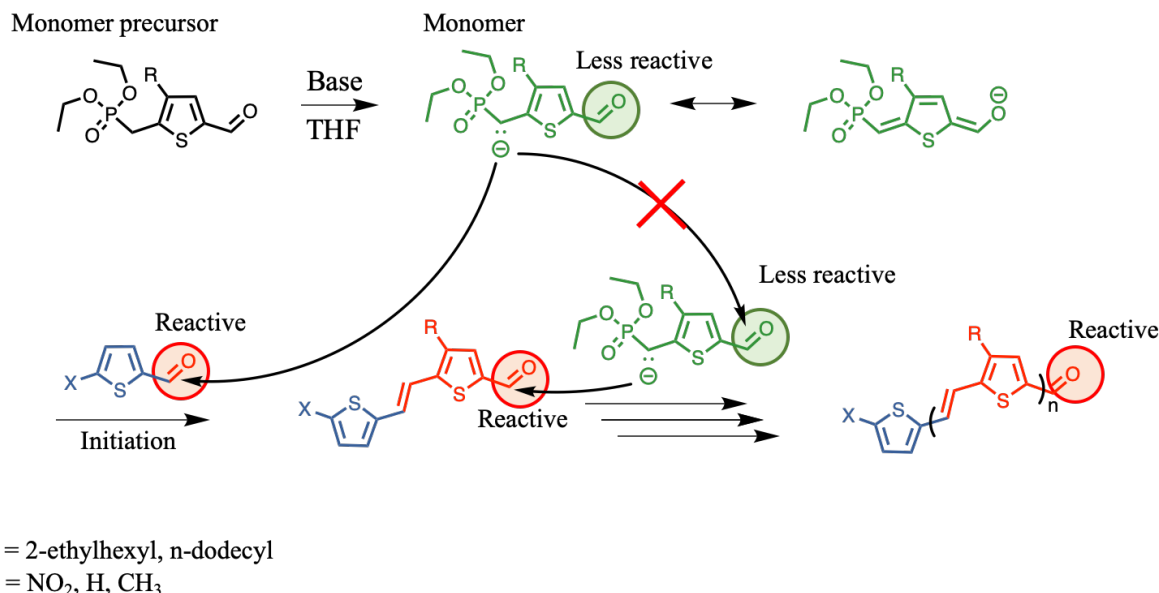


**Figure 11:** Polymer and model compound mimicking its backbone, all synthesized with HWE reaction (adapted from <sup>95,96</sup>)

Only the polymer bearing an *n*-hexyl group was characterized by SEC and NMR, suggesting that the others were not soluble in common solvents. The latter soluble polymer has a molar mass of 4 000 g/mol, and a dispersity of 2.1. All polymers showed intense fluorescence (QY from 0.4 to 0.55), while the corresponding model compound has a quantum yield of 0.68.<sup>95</sup> This increased quantum yield is most likely due to self-quenching of the polymers, a phenomenon that does not affect the smaller model compound.<sup>94</sup> The polymers were integrated in OLEDs emitting in the blue range.

Van de Wetering and coll. used the HWE reaction to synthesize poly(thienylenevinylene). The latter corresponded to one block of a low bandgap polymer, with the objective of using the latter for photovoltaic application.<sup>97</sup> The HWE reaction was also used on a monomer bearing both an aldehyde function and a phosphonic acid function. Yet the authors tried to avoid self-condensation to control the polymerization and achieve chain-growth polymerization (**Scheme 13**).

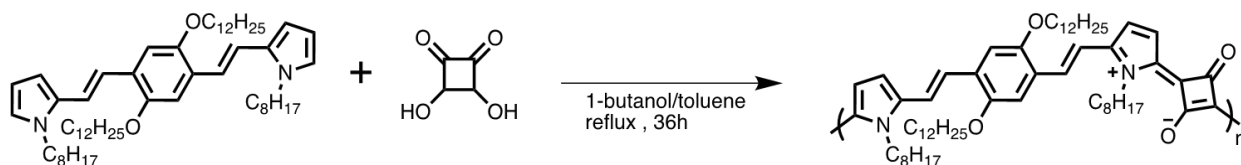


**Scheme 13:** Synthesis of thiophene-based conjugated polymer *via* HWE reaction (Adapted from <sup>98</sup>)

Crown ethers were used to capture the potassium cation, leading to improved molar masses: up to 7 600 g/mol, with a dispersity of 1.2. When targeting molar masses higher than 10 000 g/mol, precipitation was observed, most likely due to strong  $\pi$ - $\pi$  interactions leading to aggregations, as suggested by the authors.<sup>98</sup> The main drawback of the HWE reaction is the production of phosphorus-based wastes.

#### 3.2.2.4. Condensation of squaric acid

Polysquaraines are characterized by a low band gap and absorption in the near infrared range. The latter can be obtained by reacting squaric acid and an electron rich moiety,<sup>99</sup> which can be aromatic or heterocyclic, as represented in **Scheme 14**.



**Scheme 14:** Synthesis of polysquaraine (adapted from <sup>100</sup>)

The polymer obtained in **Scheme 14** was successfully integrated in OFET with promising properties and in solar cells with high power conversion efficiency (0.86%).<sup>100</sup> The polysquaraines represented in **Figure 12** were synthesized by Stille/Suzuki coupling and by condensation of squaric acid. Interestingly, the metal-free approach led to higher molar masses. These two polysquaraines exhibited a low band gap (1.6-1.7 eV) and promising properties for their future integration in bulk heterojunction solar cells.<sup>101</sup>

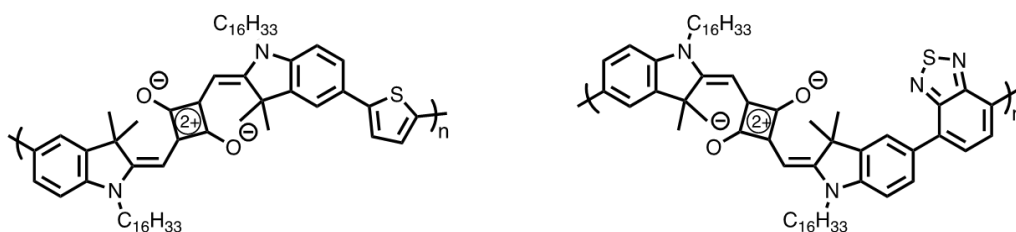


**Figure 12:** Structure of polysquaraines synthesized by either Stille/Suzuki coupling or condensation of squaric acid (adapted from <sup>101</sup>)

By changing the comonomer, various polysquaraines can be obtained, as illustrated in **Figure 13**.

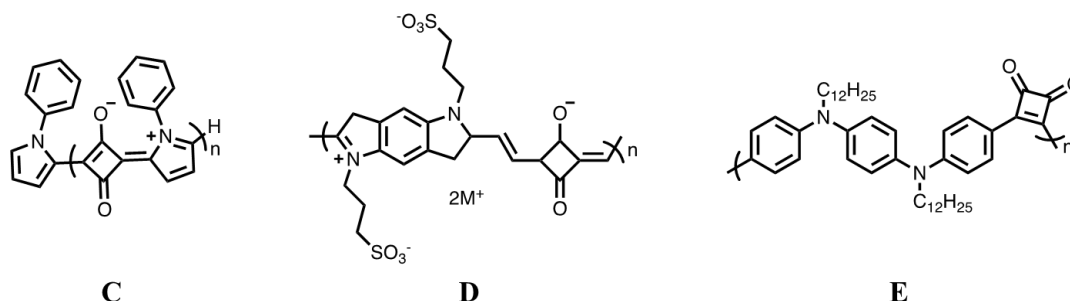
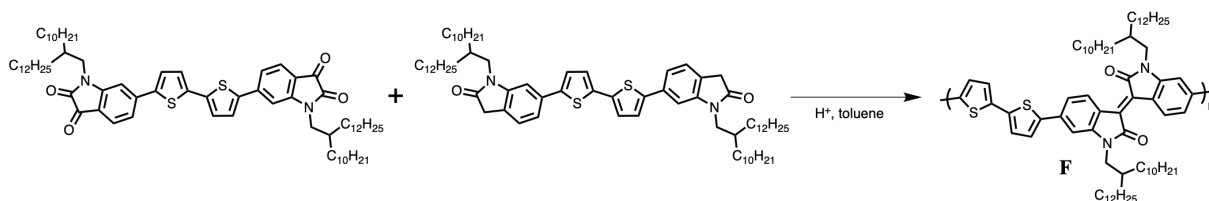


**Figure 13:** Structure of polysquaraines (adapted from <sup>102,103,104</sup>)

The polymer **C** was used as a sensor for humidity for breath monitoring, with short response time (less than a second). The latter polymer is most likely poorly soluble and was used to decorate silver particles.<sup>102</sup> On the contrary the polymer **D** is water-soluble, a promising property for bio-imaging.<sup>103</sup> Various derivatives of the polymer **E** were synthesized, as solvent (1,3-propane diol) can be integrated in the polymer chains, allowing to tune the optical properties. This type of polymer was integrated in OLED giving promising properties (almost white emission). However, the molar masses are rather low (3 700 g/mol at most) and the absorbance in the visible range, while the near infrared was expected. In addition, the polysquaraines were obtained by first chlorinating the squaric acid through the alcohol functions, meaning that traces of halogens in the polymers may remain as impurities.<sup>104</sup>

### 3.2.2.5. Aldol condensation

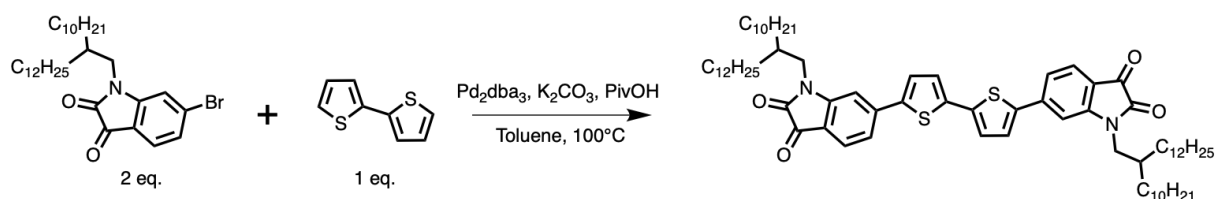
Zhang and coll. investigated the synthesis of an isoindigo-based polymer using aldol condensation,<sup>105</sup> as represented in **Scheme 15**.



**Scheme 15:** Aldol condensation of isoindigo-based polymer (adapted from <sup>105</sup>)

Aldol condensation is primarily used to synthesize small dyes<sup>106</sup> - the authors claimed they were the first to use it to prepare conjugated polymers. This method allows the synthesis of the polymer **F** without the use of any metallic catalyst with a good regioselectivity (no branching). The latter polymer has been extensively studied and was also synthesized by transition metal-based coupling, such as Stille coupling (noted Polymer **F-S**).<sup>107,108,109</sup> Polymer **F** and polymer **F-S** have similar absorbance properties. Surprisingly, OFET-based on polymer **F** showed lower properties than the one with polymer **F-S**. The

contrary was expected, as polymer **F** is supposed to contain less transition metal impurities than polymer **F-S**. Yet polymer **F** is not completely metal-free as a palladium-based catalyst was used to obtain the monomers by DHAP, as illustrated in **Scheme 16**.



**Scheme 16:** Synthesis of isoindigo-based monomer *via* DHAP (adapted from <sup>105</sup>)

Zhang *et al.* claimed that the lower properties of polymer **F**-based OFET are due to small molar masses, or because the device is not improved enough. Still, polymer **F** showed promising properties, and polymer **F-S** was successfully integrated in solar cells with high power conversion efficiency (up to 6.3%).<sup>107</sup> Aldol condensation is a promising reaction pathway that could be used to obtain various donor-acceptor conjugated polymers and possibly thieno-isoindigo-based polymers (**Figure 14**). Indeed, the link between the two halves of the thieno-isoindigo moiety is obtained by aldol condensation - then the polymer is obtained by Stille coupling. Thieno-isoindigo-based polymers exhibit a low band gap, absorbance in the near infrared and promising properties for photovoltaics or OFET.<sup>110,111</sup>

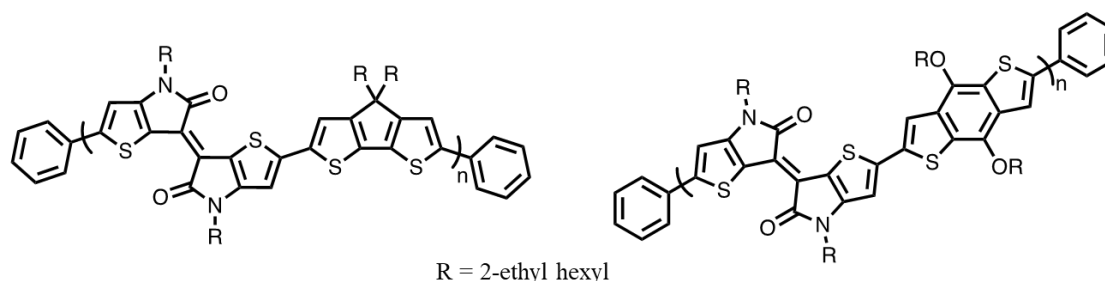


**Figure 14:** Thieno-isoindigo-based polymers (adapted from <sup>110,111</sup>)

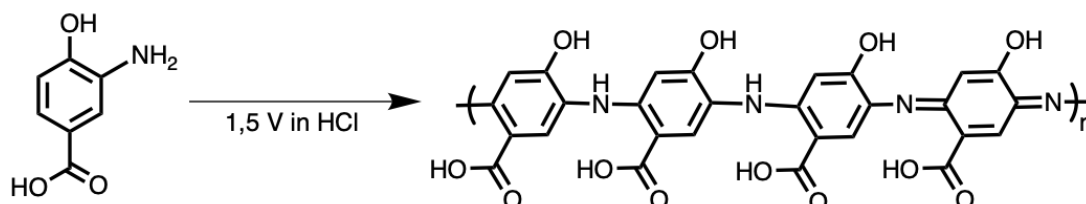
### 3.3. Transition metal-free syntheses: conclusion

To avoid transition metal catalyst, various other coupling strategies are available, with and without halogen atoms, the latter leading to the least impurities in the final polymers. These coupling reactions are not as developed as Stille or Suzuki reactions - but they allow the syntheses of various original polymer structures sometimes not available by other coupling reactions. Another way to avoid transition metal catalysts is to drastically change the experimental conditions and to perform polymerization *via* electropolymerization<sup>112,113</sup> or vapor deposition<sup>114</sup> for example. Metal-free coupling may have their drawbacks and be not as efficient as “traditional” coupling reactions but are definitely more sustainable. To reinforce the sustainable criteria, the use of bio-based monomers including 3-amino-4-hydroxybenzoic acid (3,4-AHBA), furan and its derivatives as well as vanillin can be considered as it is discussed in the next part.

#### 4. Synthesis of conjugated polymers with bio-based monomers

##### 4.1. From a micro-organism: 3-amino-4-hydroxybenzoic acid

3-amino-4-hydroxybenzoic acid, noted 3,4-AHBA, can be easily obtained by *Streptomyces griseus*, a microorganism found in sandy grounds.<sup>115</sup> By implementing the correct DNA sequence, other microorganisms can also carry out the synthesis of 3,4-AHBA.<sup>116</sup> The latter is a versatile monomer that can be easily polymerized through electropolymerization (**Scheme 17**). This method relies on a potential difference between two electrodes - the polymerization can occur either on the anode or the cathode, depending on the monomer.<sup>113,117</sup>



**Scheme 17:** Electropolymerization of 3,4-AHBA (adapted from <sup>118</sup>)

The polymer obtained bears strong similarities with polyaniline (PANI), an intensively studied conducting polymer. The latter exhibits strong conductivity and stability and can easily be doped/dedoped under acidic/basic conditions. For example PANi can be used for biomedical applications<sup>119</sup>, but also as nanofibers.<sup>120,121</sup> However PANi is poorly soluble in common solvents, which makes it harder to process. On the contrary, poly(3,4-AHBA) is more soluble and its molar mass was determined by SEC in THF (5 500 g/mol, dispersity  $\sim 1$ ). Poly(3,4-AHBA) showed a behavior similar to PANi's, with halochromism but also solvatochromism.<sup>118</sup> Another team synthesized poly(3,4-AHBA) *via* electropolymerization and obtained nanoparticles, by using different experimental conditions. The latter nanoparticles exhibit good pH sensitivity, even better than PANi's, thanks to the two additional pH-sensitive function on the monomer units: hydroxy and carboxylic acid. These nanoparticles could be used for electrochemical sensors and biosensors.<sup>122</sup>

3,4-AHBA can also be polymerized to form polybenzoxazoles. These polymers are mostly used for their high tensile strength, Young modulus and excellent thermal stability. Zylon (poly(p-phenylene-2,6-benzobisoxazole) was used as ballistic vest for example.<sup>123</sup> The synthesis of polybenzoxazoles from 3,4-AHBA was patented with the objective to use the polymer for its mechanical properties.<sup>124</sup> Yet polybenzoxazoles are also promising conjugated polymers. Indeed, the polymer represented in **Figure 15a** was successfully used for fluorescent imaging and fluorescent patterning (synthesis performed *via* Suzuki coupling).<sup>125</sup> Moreover benzoxazoles are well-known dyes, with bright fluorescence even in the solid state.<sup>126,127</sup> An example of synthesis is given in **Figure 15b**.

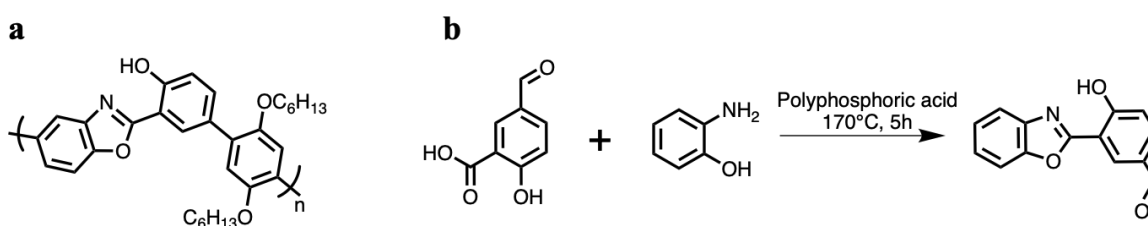
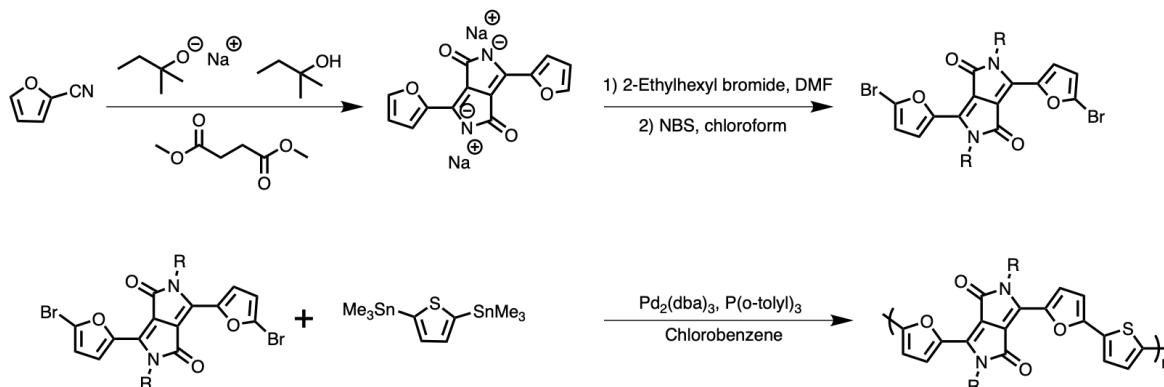


**Figure 15a:** Polybenzoxazole used for fluorescent imaging and patterning (adapted from <sup>125</sup>). **b:** Synthesis of benzoxazole dye (adapted from <sup>127</sup>)

3,4-AHBA could also be used to synthesize polybenzobisthiazoles and polythiazolothiazoles, a family of polymers that will be discussed in **Chapter 4**. Therefore 3,4-AHBA could be used as a building block for conjugated polymers. Moreover, its available hydroxy function could be alkylated to improve the ensuing polymer's solubility.

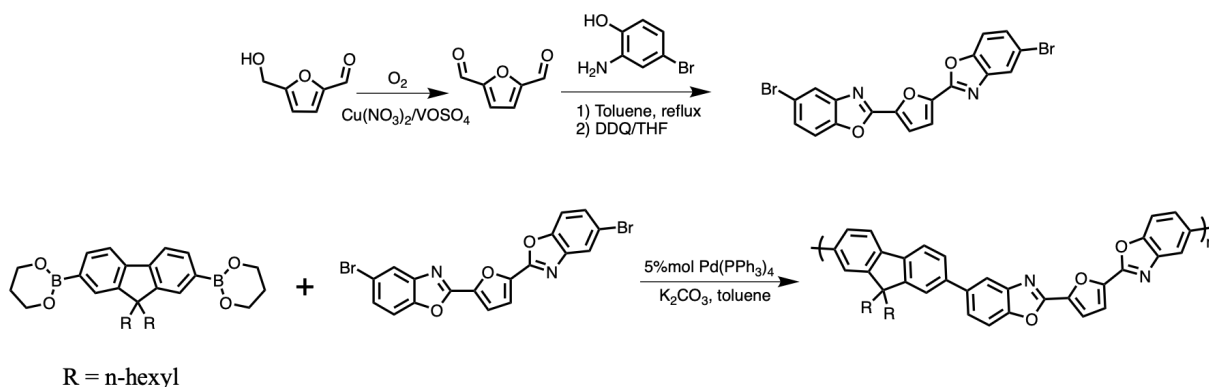
#### 4.2. From lignocellulosic biomass: Furan and difuran

As mentioned previously, furan is a promising building block for the synthesis of conjugated polymers.<sup>128,129</sup> Indeed, furan can exhibit similar and even superior properties to thiophene.<sup>47</sup> One promising furan-based monomer is represented in **Scheme 18**, along with its ensuing polymer.



**Scheme 18:** Synthesis of furan-based monomer and ensuing polymerization *via* Stille coupling (adapted from <sup>130</sup>)

This monomer can be obtained from cyano furan and the polymer is synthesized *via* Stille coupling. The latter polymer has a low band gap and was integrated in efficient OFET<sup>131,132</sup> and solar cells.<sup>130,133</sup> Ma and coll. also synthesized a furan-based polymer,<sup>134</sup> starting from bio-based 5-HMF as represented in **Scheme 19**.

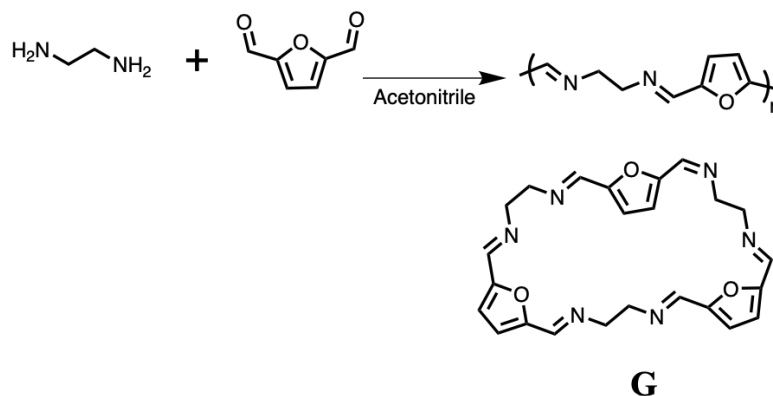


**Scheme 19:** Synthesis of furan-based monomer and polymer thereof *via* Suzuki coupling (adapted from <sup>134</sup>)

Interestingly, the benzoxazole-based monomer could be obtained from 3,4-AHBA. The polymer has a relatively low molar mass (3900 g/mol, i.e. 6 units) but has a strong blue fluorescence, with a quantum yield of 0,57.<sup>134</sup>

Even if efforts were made to make the polymer's integration in devices<sup>132</sup> or monomer's synthesis more sustainable,<sup>134</sup> the coupling reactions still induce the presence of transition metal impurities in the polymer, as well as the production of hazardous wastes. To avoid these issues, another way to obtain furan-based conjugated polymers is to synthesize polyazomethines.<sup>135</sup>

Xiang and coll. synthesized various furan-based polyazomethines, by using aromatic and aliphatic diamines, as represented in **Scheme 20**.



**Scheme 20:** Synthesis of furan-based polyazomethines and cyclic specie obtained during polymerization (adapted from <sup>136</sup>)

The polymerization was performed at room temperature without any catalysts. The polymer represented in **Scheme 20** precipitated during polymerization, while the cyclic species **G** remained in solution. The structure of the latter was confirmed by mass spectroscopy. Solubility was an issue for the various polymers synthesized and subsequently the molar masses were determined by mass spectroscopy. The latter masses are rather low (6 units), as the polymerization reaction is limited due to the precipitation of the polymers and the formation of cyclic species. A polyazomethine with aromatic diamines also exhibited low molar masses and its optical properties were not extensively studied. Moreover, the latter is not fully conjugated - yet it has an absorbance maxima close to the visible range, heralding promising properties for a fully conjugated polyazomethine (**Figure 16**).<sup>136</sup>

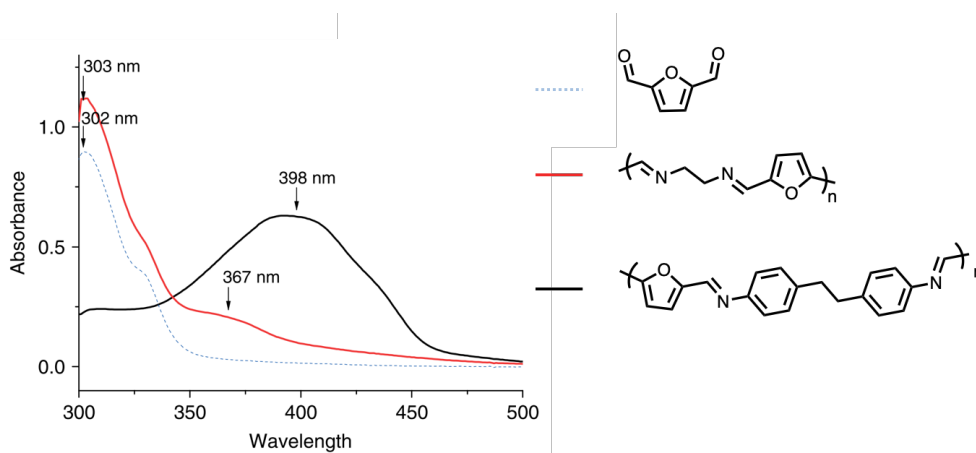
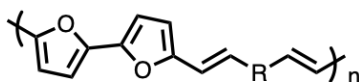


**Figure 16:** Absorbance spectra of dialdehyde furan and furan-based polyazomethines (in *m*-cresol) (adapted from <sup>136</sup>)

Tachibana *et al.* investigated the synthesis of difurfural-based polyazomethines. The authors synthesized difurfural through a palladium-based coupling (**Scheme 3**) and then reacted it with various diamines, as represented in **Figure 17**. The polymerization was performed in *m*-cresol or in bulk but in both cases without any catalysts.



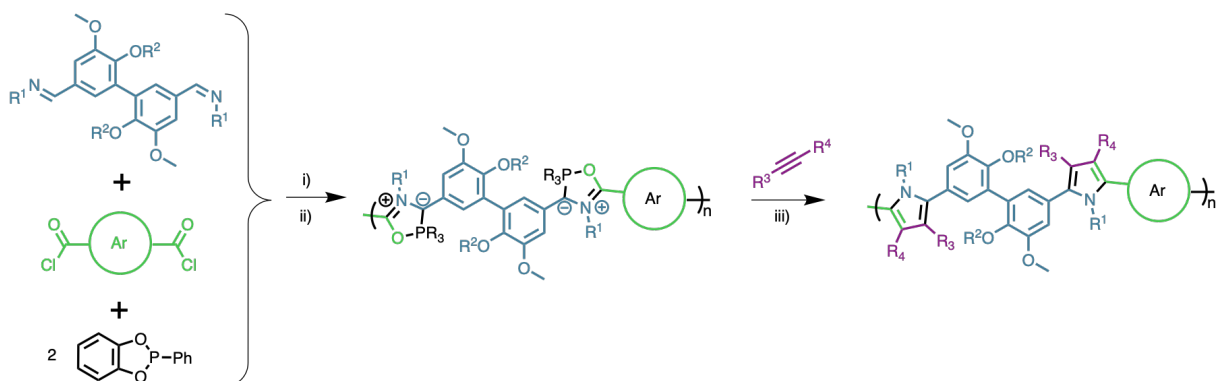
R = n-ethyl (H), n-propyl (I), n-butyl (J), n-pentyl (K), n-hexyl (L), phenyl (M)

**Figure 17:** General structure of difurfural-based polyazomethines (adapted from <sup>60</sup>)

While not clearly measured, the molar masses of the polymers are ranging from 1 000 to 10 000 g/mol depending on the diamine. Interestingly, the formation of cyclics was also observed in this polymerization. Polymer **M** has an absorbance maximum at 442 nm - the authors did not optically characterize further these polyazomethines, as they were interested in their mechanical properties.<sup>60</sup>

#### 4.3. From lignocellulosic biomass: vanillin

As stated previously, vanillin can easily be dimerized *via* enzymatic coupling.<sup>31</sup> The team of Arndtsen investigated the synthesis of cross-conjugated polymers *via* multi-components synthesis, and applied it with divanillin as a starting monomer. They improved the synthetic protocol, from palladium-catalyzed<sup>137</sup> to transition metal-free,<sup>33</sup> as illustrated in **Scheme 21**.



**Scheme 21:** Multi-components synthesis of divanillin-based polypyrrole (i) Dichloromethane, 45°C, 24h, ii) DBU, RT, 15 minutes, iii) RT, 18 hours) (adapted from <sup>33</sup>)

First divanillin was reacted with an amine and integrated in a one-pot synthesis with an aromatic acid chloride and catechyl (PPh). Then a substituted alkene was added to finally yield the polymer. This multi-component synthesis enables high step-economy; its drawback would be the use of acyl chloride moiety. By modulating the acyl chloride moiety and the various substituents ( $R^1$ ,  $R^2$ ,  $R^3$ , and  $R^4$ ), a whole range of cross-conjugated polymers were obtained, with tunable optical properties. The most promising polymers are represented in **Figure 18**.



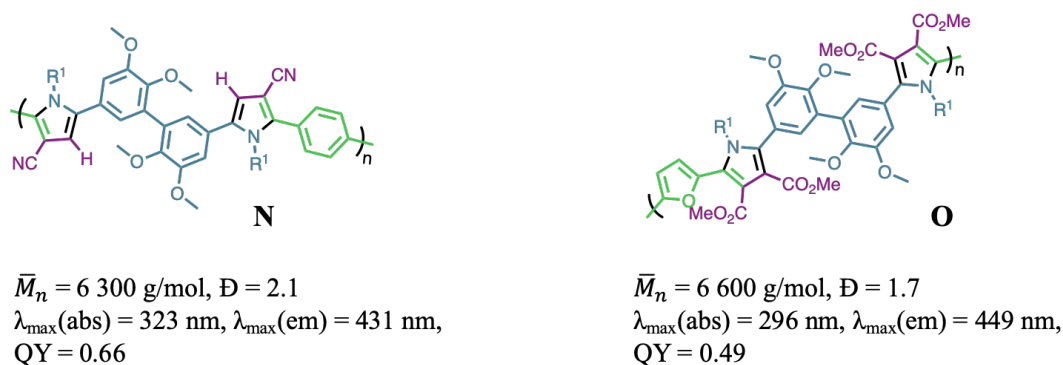
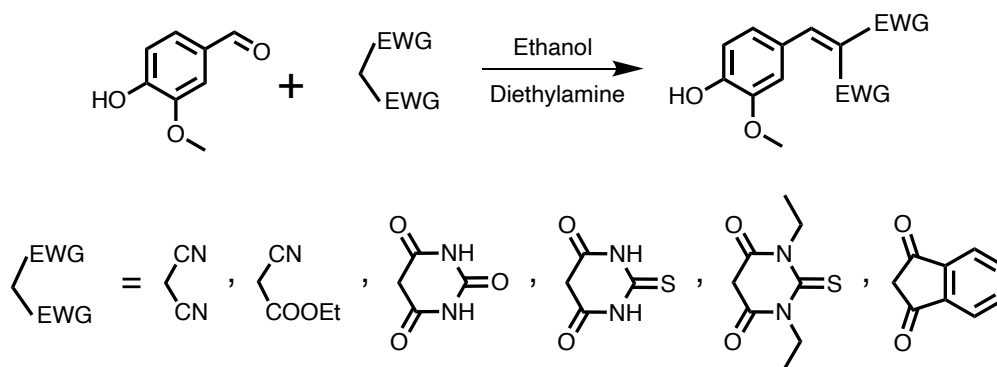


**Figure 18:** Structure and characteristics of divanillin-based cross-conjugated polymers (molar masses determined by SEC in THF, and optical properties determined in chloroform, QY determined versus an anthracene standard) (adapted from <sup>33</sup>)

Their absorbance maxima are rather low (in the near-UV range), but both polymers exhibited a strong fluorescence with a high quantum yield, heralding promising properties for ensuing OLED.<sup>138</sup> Notably polymer **O** was synthesized using FDCA, which can be obtained from 5-HMF (Section 2.3), paving the way towards fully bio-based conjugated polymers.

Other reactions are possible, for example by transposing the synthesis of vanillin-based small dyes to the synthesis of divanillin-based polymer, as illustrated in Scheme 22 with a Knoevenagel condensation.



**Scheme 22:** Synthesis of vanillin-based dyes *via* Knoevenagel condensation (adapted from <sup>139</sup>)

The obtained dyes were used as sensors for volatile amines.<sup>139</sup> Another type of coupling using vanillin is the formation of Schiff base.<sup>140,141</sup> The latter compounds have been intensively studied, but mostly for their antibacterial properties<sup>142</sup> or as complexes.<sup>143</sup> The synthesis of divanillin-based polyazomethines will be the subject of Chapter 2.

#### 4.4. Bio-based monomers for the synthesis of conjugated polymers: conclusion

The synthesis of conjugated polymers using three different bio-based monomers was summed up. The latter were 3,4-AHBA, a molecule synthesized by a microorganism and two substrates obtained from lignocellulosic biomass: furan and its derivatives and vanillin. All three were integrated in conjugated polymers which exhibit various properties and potential applications (OLED, OFET). The conjugated polymers were obtained by different reactions, such as Stille and Suzuki couplings but also multi-components reactions and electropolymerization. The multi-components reaction yielded polymers with high quantum yield, heralding promising properties for their integration in OLED.<sup>33</sup> The most sustainable pathway appears to be the condensation of dialdehyde and diamine, to form polyazomethines. Indeed, this reaction does not require any metallic catalyst, only produces water as a

by-product and dialdehyde can easily be obtained from biomass, without extensive derivatization. Yet the synthesis of efficient polyazomethines requires a careful choice of monomers to obtain the desired properties and notably to prevent poor quantum yield for example.<sup>88</sup>

## 5. General conclusion

Lignocellulosic biomass can be the source of a wide platform of substrates with various structures (aromatic, heterocyclic, linear, etc.) and functionalities (aldehyde, hydroxy and methoxy for example). In this PhD work, we selected bio-based substrates having a good potential in the field of organic electronic, i.e. vanillin as well as furan and its derivatives. Indeed, both were used as promising monomers for the synthesis of various polymers (e.g. vanillin-based<sup>144,43</sup> and furan-based polyesters<sup>53</sup>) and are also promising building blocks for organic electronic.<sup>47</sup>

Organic electronic relies heavily on “traditional” reaction couplings, which implies the pollution of the conjugated polymers with transition metal. Other coupling reactions are accessible to avoid these metal impurities and some were discussed in this chapter. Firstly, it is possible to avoid hazardous monomers *via* DHAP. This coupling, based on palladium catalyst, allows the formation of a C-C bond between an aryl halide and an arene. Some transition metal-free coupling can be performed to synthesize conjugated polymers, such as bromine-catalyzed coupling<sup>79</sup> and NMRP-mediated approach.<sup>81</sup> Amongst others, the formation of azomethine bonds<sup>86</sup> and the Knoevenagel reaction<sup>93</sup> enable the synthesis of conjugated polymers without neither transition metal nor halogen impurities. It is also possible to integrate bio-based compounds in conjugated polymers, leading to promising properties such as high quantum yield, as exemplified in **Figure 19** with a vanillin and furan-based polymer.<sup>33</sup>

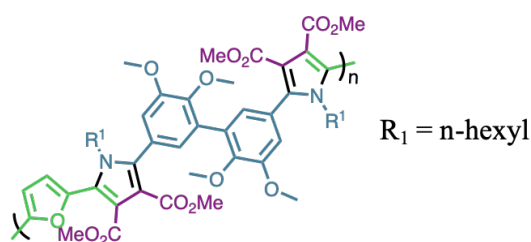


**Figure 19:** Vanillin and furan-based cross-conjugated polymer obtained by multi-components reaction (adapted from<sup>33</sup>)

However, some of these promising polymers were synthesized with either transition metal catalyst or with a halogen containing monomer. As a consequence, there are still many challenges to tackle with the aim to design organic electronic materials more sustainably, which includes sustainable bio-based monomers, metal-free coupling reactions, greener processes, etc. all this to provide conjugated polymers with improved properties in comparison to existing systems.

## 6. References

1. Nagel, B., Dellweg, H. & Gierasch, L. M. Glossary for chemists of terms used in biotechnology. *Pure Appl. Chem.* **64**, 143–168 (1992).
2. Isikgor, F. H. & Becer, C. R. Lignocellulosic Biomass: A Sustainable Platform for Production of Bio-Based Chemicals and Polymers. *Polym. Chem.* 34–50 (2015). doi:10.1016/B978-1-84569-741-9.50002-1
3. Decostanzi, M., Auvergne, R., Boutevin, B. & Caillol, S. Biobased phenol and furan derivative coupling for the synthesis of functional monomers. *Green Chem.* **21**, 724–747 (2019).
4. Bozell, J. J. & Petersen, G. R. Technology development for the production of biobased products from biorefinery carbohydrates - The US Department of Energy's 'top 10' revisited. *Green Chem.* **12**, 539–554 (2010).
5. Isikgor, F. H. & Becer, C. R. Lignocellulosic biomass: a sustainable platform for the production of bio-based chemicals and polymers. *Polym. Chem.* **6**, 4497–4559 (2015).
6. O'Sullivan, A. C. Cellulose: the structure slowly unravels. *Cellulose* **4**, 173–207 (1997).
7. Zhou, C. H., Xia, X., Lin, C. X., Tong, D. S. & Beltramini, J. Catalytic conversion of lignocellulosic biomass to fine chemicals and fuels. *Chem. Soc. Rev.* **40**, 5588–5617 (2011).
8. Puls, J. Chemistry and biochemistry of hemicelluloses: Relationship between hemicellulose structure and enzymes required for hydrolysis. *Macromol. Symp.* **120**, 183–196 (1997).
9. Stewart, J. J., Akiyama, T., Chapple, C., Ralph, J. & Mansfield, S. D. The effects on lignin structure of overexpression of ferulate 5-hydroxylase in hybrid poplar 1[W]. *Plant Physiol.* **150**, 621–635 (2009).
10. Vanholme, R., Demedts, B., Morreel, K., Ralph, J. & Boerjan, W. Lignin biosynthesis and structure. *Plant Physiol.* **153**, 895–905 (2010).
11. Ithal, N. *et al.* Developmental transcript profiling of cyst nematode feeding cells in soybean roots. *Mol. Plant-Microbe Interact.* **20**, 510–525 (2007).
12. Gopal, P. M., Sivaram, N. M. & Barik, D. *Paper Industry Wastes and Energy Generation From Wastes. Energy from Toxic Organic Waste for Heat and Power Generation* (Elsevier Ltd., 2019). doi:10.1016/b978-0-08-102528-4.00007-9
13. Lynd, L. R. The grand challenge of cellulosic biofuels. *Nat. Biotechnol.* **35**, 912–915 (2017).
14. Karakawa, M. *et al.* Organic light-emitting diode application of fluorescent cellulose as a natural polymer. *Macromol. Chem. Phys.* **208**, 2000–2006 (2007).
15. Purandare, S., Gomez, E. F. & Steckl, A. J. High brightness phosphorescent organic light emitting diodes on transparent and flexible cellulose films. *Nanotechnology* **25**, (2014).
16. Min, S. H., Kim, C. K., Lee, H. N. & Moon, D. G. An OLED using cellulose paper as a flexible substrate. *Mol. Cryst. Liq. Cryst.* **563**, 159–165 (2012).
17. Qian, C., Sun, J., Yang, J. & Gao, Y. Flexible organic field-effect transistors on biodegradable cellulose paper with efficient reusable ion gel dielectrics. *RSC Adv.* **5**, 14567–14574 (2015).
18. Kurra, N., Dutta, D. & Kulkarni, G. U. Field effect transistors and RC filters from pencil-trace on paper. *Phys. Chem. Chem. Phys.* **15**, 8367–8372 (2013).
19. Berlin, A. & Balakshin, M. *Industrial Lignins: Analysis, Properties, and Applications. Bioenergy Research: Advances and Applications* (Elsevier, 2014). doi:10.1016/B978-0-444-59561-

4.00018-8

20. Sengupta, Ashoke K., Gargulak, J., Bushar, L. & Zajakowski, V. Low retarding, high fluidity producing lignin dispersant for concrete. (2001).
21. Otani, S., Fukuoka, K., Fukuoka, Y., Igarashi, B. & Sasaki, T. Method for Producing Carbonized Lignin Fiber. (1969).
22. Chakar, F. S. & Ragauskas, A. J. Review of current and future softwood kraft lignin process chemistry. *Ind. Crops Prod.* **20**, 131–141 (2004).
23. Muurinen, E. S. A. Organosolv Pulping A review and distillation study related to peroxyacid pulping. (University of Oulu, 2000).
24. Rakotoveloa, A. Fragmentation enzymatique de la lignine pour l'obtention de synthons phénoliques. (Université de Bordeaux, 2016).
25. Hämäläinen, V. *et al.* Enzymatic processes to unlock the lignin value. *Front. Bioeng. Biotechnol.* **6**, 1–10 (2018).
26. Huber, G. W., Iborra, S. & Corma, A. Synthesis of transportation fuels from biomass: Chemistry, catalysts, and engineering. *Chem. Rev.* **106**, 4044–4098 (2006).
27. Lange, H., Decina, S. & Crestini, C. Oxidative upgrade of lignin - Recent routes reviewed. *Eur. Polym. J.* **49**, 1151–1173 (2013).
28. van Haveren, J., Scott, E. L. & Sanders, J. Bulk chemicals from biomass. *Biofuels, Bioprod. Biorefining* **2**, 41–57 (2008).
29. Rahimi, A., Ulbrich, A., Coon, J. J. & Stahl, S. S. Formic-acid-induced depolymerization of oxidized lignin to aromatics. *Nature* **515**, 249–252 (2014).
30. Arevalo-Gallegos, A., Ahmad, Z., Asgher, M., Parra-Saldivar, R. & Iqbal, H. M. N. Lignocellulose: A sustainable material to produce value-added products with a zero waste approach—A review. *Int. J. Biol. Macromol.* **99**, 308–318 (2017).
31. Llevot, A., Grau, E., Carlotti, S., Grelier, S. & Cramail, H. Selective laccase-catalyzed dimerization of phenolic compounds derived from lignin: Towards original symmetrical bio-based (bis) aromatic monomers. *J. Mol. Catal. B Enzym.* **125**, 34–41 (2016).
32. Chithambarathanu, T., Vanaja, K. & Magdaline, J. D. Molecular structure, spectroscopic studies, HOMO-LUMO profile and NBO analysis of 3-Ethoxy-4-hydroxy benzaldehyde. *Rasayan J. Chem.* **8**, 490–508 (2015).
33. Kayser, L. V., Hartigan, E. M. & Arndtsen, B. A. Multicomponent Coupling Approach to Cross-Conjugated Polymers from Vanillin-Based Monomers. *ACS Sustain. Chem. Eng.* acssuschemeng.6b02302 (2016). doi:10.1021/acssuschemeng.6b02302
34. Andraud, C. *et al.* Theoretical and experimental investigations of the nonlinear optical properties of vanillin, polyenovanillin, and bisvanillin derivatives. *J. Am. Chem. Soc.* **116**, 2094–2102 (1994).
35. Llevot, A. Resinic acid and lignin derivative dimers: new precursors for the synthesis of biobased polymers. (Université de Bordeaux, 2014).
36. Gallage, N. J. *et al.* Vanillin formation from ferulic acid in *Vanilla planifolia* is catalysed by a single enzyme. *Nat. Commun.* **5**, (2014).
37. Gelski, J. Vanilla prices slowly drop as crop quality improves. *Food Business News* **1**, 27–28 (2019).

38. Reimer, K. Ueber eine neue Bildungsweise aromatischer Aldehyde. *Berichte der Dtsch. Chem. Gesellschaft* **9**, 423–424 (1876).
39. Hocking, M. B. Vanillin: Synthetic flavoring from spent sulfite liquor. *J. Chem. Educ.* **74**, 1055–1059 (1997).
40. Bjørsvik, H. R. & Minisci, F. Fine chemicals from lignosulfonates. 1. Synthesis of vanillin by oxidation of lignosulfonates. *Org. Process Res. Dev.* **3**, 330–340 (1999).
41. Solvay. Rhovanil® Natural CW | Solvay.
42. Fache, M. *et al.* Vanillin, a promising biobased building-block for monomer synthesis. *Green Chem.* **16**, 1987–1998 (2014).
43. Fache, M., Boutevin, B. & Caillol, S. Vanillin, a key-intermediate of biobased polymers. *Eur. Polym. J.* **68**, 488–502 (2015).
44. Savonnet, E., Grau, E., Grelier, S., Defoort, B. & Cramail, H. Divanillin-Based Epoxy Precursors as DGEBA Substitutes for Biobased Epoxy Thermosets. *ACS Sustain. Chem. Eng.* **6**, 11008–11017 (2018).
45. Vasiliou, A. G., Nimlos, M. R., Daily, J. W. & Ellison, G. B. Thermal decomposition of furan generates propargyl radicals. *J. Phys. Chem. A* **113**, 8540–8547 (2009).
46. Perepichka, I. F., Perepichka, D. F. & Meng, H. *Handbook of Thiophene-Based Materials: Applications in Organic Electronics and Photonics*. (2009). doi:10.1002/9780470745533.ch19
47. Zhao, Z. *et al.* Furan Is Superior to Thiophene: A Furan-Cored AIEgen with Remarkable Chromism and OLED Performance. *Adv. Sci.* **4**, 1–8 (2017).
48. Shapla, U. M., Solayman, M., Alam, N., Khalil, M. I. & Gan, S. H. 5-Hydroxymethylfurfural (HMF) levels in honey and other food products: effects on bees and human health. *Chem. Cent. J.* **12**, 1–18 (2018).
49. Eldeeb, M. A. & Akih-Kumgeh, B. Recent trends in the production, combustion and modeling of furan-based fuels. *Energies* **11**, 1–47 (2018).
50. Zeng, C., Seino, H., Ren, J., Hatanaka, K. & Yoshie, N. Bio-based furan polymers with self-healing ability. *Macromolecules* **46**, 1794–1802 (2013).
51. He, J., Zhang, Y. & Chen, E. Y. X. Anionic polymerization of biomass-derived furfuryl methacrylate: Controlling polymer tacticity and thermoreversibility. *J. Polym. Sci. Part A Polym. Chem.* **51**, 2793–2803 (2013).
52. Sajid, M., Zhao, X. & Liu, D. Production of 2,5-furandicarboxylic acid (FDCA) from 5-hydroxymethylfurfural (HMF): Recent progress focusing on the chemical-catalytic routes. *Green Chem.* **20**, 5427–5453 (2018).
53. Sousa, A. F. *et al.* Biobased polyesters and other polymers from 2,5-furandicarboxylic acid: A tribute to furan excellency. *Polym. Chem.* **6**, 5961–5983 (2015).
54. De Jong, E., Dam, M. A., Sipos, L. & Gruter, G. J. M. Furandicarboxylic acid (FDCA), A versatile building block for a very interesting class of polyesters. *ACS Symp. Ser.* **1105**, 1–13 (2012).
55. E4tech (UK) for LBNet. *UK Top Bio-based Chemicals Opportunities*. (2017).
56. Dutta, S., Wu, L. & Mascal, M. Production of 5-(chloromethyl)furan-2-carbonyl chloride and furan-2,5-dicarbonyl chloride from biomass-derived 5-(chloromethyl)furfural (CMF). *Green Chem.* **17**, 3737–3739 (2015).

57. Zhou, C. *et al.* One-Step Approach to 2,5-Diformylfuran from Fructose over Molybdenum Oxides Supported on Carbon Spheres. *ACS Sustain. Chem. Eng.* **7**, 315–323 (2019).
58. 27. Furan dialdehyde. *Sugar Ser.* **13**, 210–213 (2000).
59. 20. Difurfural (5,5'-diformyl-2,2'-difuran). *Sugar Ser.* **13**, 164–169 (2000).
60. Tachibana, Y., Hayashi, S. & Kasuya, K. I. Biobased Poly(Schiff-Base) Composed of Bifurfural. *ACS Omega* **3**, 5336–5345 (2018).
61. Masui, K., Ikegami, H. & Mori, A. Palladium-Catalyzed C-H Homocoupling of Thiophenes: Facile Construction of Bithiophene Structure. *J. Am. Chem. Soc.* **126**, 5074–5075 (2004).
62. Bloom, J. W. G. & Wheeler, S. E. Benchmark torsional potentials of building blocks for conjugated materials: Bifuran, bithiophene, and biselenophene. *J. Chem. Theory Comput.* **10**, 3647–3655 (2014).
63. Milstein, D. & Stille, J. K. A General, Selective, and Facile Method for Ketone Synthesis from Acid Chlorides and Organotin Compounds Catalyzed by Palladium. *J. Am. Chem. Soc.* **100**, 3636–3638 (1978).
64. Sévignon, M., Papillon, J., Schulz, E. & Lemaire, M. New synthetic method for the polymerization of alkylthiophenes. *Tetrahedron Lett.* **40**, 5873–5876 (1999).
65. Iizuka, E., Wakioka, M. & Ozawa, F. Mixed-ligand approach to palladium-catalyzed direct arylation polymerization: Synthesis of donor-acceptor polymers with dithienosilole (DTS) and thienopyrroledione (TPD) units. *Macromolecules* **48**, 2989–2993 (2015).
66. Biswas, B., Sugimoto, M. & Sakaki, S. C-H Bond Activation of Benzene and Methane by M( $\eta^2$ -O<sub>2</sub>CH)<sub>2</sub> (M = Pd or Pt). A Theoretical Study. *Organometallics* **19**, 3895–3908 (2000AD).
67. Morin, P. O. *et al.* Conjugated polymers à la carte from time-controlled direct (hetero)arylation polymerization. *ACS Macro Lett.* **4**, 21–24 (2015).
68. Fujinami, Y., Kuwabara, J., Lu, W., Hayashi, H. & Kanbara, T. Synthesis of thiophene- and bithiophene-based alternating copolymers via Pd-catalyzed direct C-H arylation. *ACS Macro Lett.* **1**, 67–70 (2012).
69. Usluer, Ö. *et al.* Metal residues in semiconducting polymers: Impact on the performance of organic electronic devices. *ACS Macro Lett.* **3**, 1134–1138 (2014).
70. Lombeck, F., Komber, H., Gorelsky, S. I. & Sommer, M. Identifying homocouplings as critical side reactions in direct arylation polycondensation. *ACS Macro Lett.* **3**, 819–823 (2014).
71. Lu, W., Kuwabara, J. & Kanbara, T. Polycondensation of dibromofluorene analogues with tetrafluorobenzene via direct arylation. *Macromolecules* **44**, 1252–1255 (2011).
72. Kuwabara, J. *et al.* Direct arylation polycondensation: A promising method for the synthesis of highly pure, high-molecular-weight conjugated polymers needed for improving the performance of organic photovoltaics. *Adv. Funct. Mater.* **24**, 3226–3233 (2014).
73. Robitaille, A., Jenekhe, S. A. & Leclerc, M. Poly(naphthalene diimide- alt-bithiophene) Prepared by Direct (Hetero)arylation Polymerization for Efficient All-Polymer Solar Cells. *Chem. Mater.* **30**, 5353–5361 (2018).
74. Leclerc, M., Brassard, S. & Beaupré, S. Direct (hetero)arylation polymerization: toward defect-free conjugated polymers. *Polym. J.* (2019). doi:10.1038/s41428-019-0245-9
75. Bura, T. *et al.* Direct heteroarylation polymerization: Guidelines for defect-free conjugated polymers. *Chem. Sci.* **8**, 3913–3925 (2017).

76. Grenier, F. *et al.* Electroactive and photoactive poly[isoidigo-alt-EDOT] synthesized using direct (hetero)arylation polymerization in batch and in continuous flow. *Chem. Mater.* **27**, 2137–2143 (2015).
77. Mei, J., Graham, K. R., Stalder, R. & Reynolds, J. R. Synthesis of isoidigo-based oligothiophenes for molecular bulk heterojunction solar cells. *Org. Lett.* **12**, 660–663 (2010).
78. Kuwabara, J., Yasuda, T., Takase, N. & Kanbara, T. Effects of the Terminal Structure, Purity, and Molecular Weight of an Amorphous Conjugated Polymer on Its Photovoltaic Characteristics. *ACS Appl. Mater. Interfaces* **8**, 1752–1758 (2016).
79. Patra, A. *et al.* Metal Free Conducting PEDOS, PEDOT, and Their Analogues via an Unusual Bromine-Catalyzed Polymerization. *Macromolecules* **48**, 8760–8764 (2015).
80. Heeney, M. *et al.* Regioregular poly(3-hexyl)selenophene: A low band gap organic hole transporting polymer. *Chem. Commun.* 5061–5063 (2007). doi:10.1039/b712398a
81. Maji, M. S., Pfeifer, T. & Studer, A. Transition-metal-free synthesis of conjugated polymers from bis-grignard reagents by using TEMPO as Oxidant. *Chem. - A Eur. J.* **16**, 5872–5875 (2010).
82. Huang, L., Wu, S., Qu, Y., Geng, Y. & Wang, F. Grignard Metathesis Chain-Growth Polymerization for Polyfluorene. *Macromolecules* **41**, 8944–8947 (2008).
83. Mallet, C., Bolduc, A., Bishop, S., Gautier, Y. & Skene, W. G. Unusually high fluorescence quantum yield of a homopolyfluorenylazomethine – towards a universal fluorophore. *Phys. Chem. Chem. Phys.* **16**, 24382–24390 (2014).
84. Grankowska Ciechanowicz, S. *et al.* Toward Better Efficiency of Air-Stable Polyazomethine-Based Organic Solar Cells Using Time-Resolved Photoluminescence and Light-Induced Electron Spin Resonance as Verification Methods. *J. Phys. Chem. C* **120**, 11415–11425 (2016).
85. Gawlinska, K. *et al.* Searching of new, cheap, air- and thermally stable hole transporting materials for perovskite solar cells. *Opto-electronics Rev.* **25**, 274–284 (2017).
86. Bolduc, A., Mallet, C. & Skene, W. G. Survey of recent advances of in the field of  $\pi$ -conjugated heterocyclic azomethines as materials with tuneable properties. *Sci. China Chem.* **56**, 3–23 (2013).
87. Yang, C. J. & Jenekhe, S. A. Conjugated Aromatic Poly(azomethines). 1. Characterization of Structure, Electronic Spectra, and Processing of Thin Films from Soluble Complexes. *Chem. Mater.* **3**, 878–887 (1991).
88. Barik, S., Bletzacker, T. & Skene, W. G.  $\pi$ -Conjugated fluorescent azomethine copolymers: Opto-electronic, halochromic, and doping properties. *Macromolecules* **45**, 1165–1173 (2012).
89. Barik, S. & Skene, W. G. A fluorescent all-fluorene polyazomethine—towards soluble conjugated polymers exhibiting high fluorescence and electrochromic properties. *Polym. Chem.* **2**, 1091–1097 (2011).
90. Mallet, C., Le Borgne, M., Starck, M. & Skene, W. G. Unparalleled fluorescence of a polyazomethine prepared from the self-condensation of an automer and its potential use as a fluorimetric sensor for explosive detection. *Polym. Chem.* **4**, 250–254 (2013).
91. Greenham, N. C., Moratti, S. C., Bradley, D. D. C., Friend, R. H. & Holmes, A. B. Efficient light-emitting diodes based on polymers with high electron affinities. *Nature* **365**, 628–630 (1993).
92. *Design and Synthesis of Conjugated Polymers.* (2010).
93. Cao, X. *et al.* A fluorescent conjugated polymer photocatalyst based on Knoevenagel

- polycondensation for hydrogen production. *New J. Chem.* **43**, 7093–7098 (2019).
94. Jakubiak, R., Collison, C. J., Chou, W. A., Rothberg, L. J. & Hsieh, B. R. Aggregation quenching of luminescence in electroluminescent conjugated polymers. *J. Phys. Chem. A* **103**, 2394–2398 (1999).
  95. Liao, L., Pang, Y., Ding, L. & Karasz, F. E. Blue-emitting soluble poly(m-phenylenevinylene) derivatives. *Macromolecules* **34**, 7300–7305 (2001).
  96. Liao, L. *et al.* Synthesis and luminescence of yellow/orange-emitting poly[tris(2,5-dihexyloxy-1,4-phenylenevinylene)-alt-(1,3-phenylenevinylene)]s. *J. Polym. Sci. Part A Polym. Chem.* **42**, 5853–5862 (2004).
  97. Van De Wetering, K., Brochon, C., Ngov, C. & Hadziioannou, G. Design and synthesis of a low band gap conjugated macroinitiator: Toward rod-coil donor-acceptor block copolymers. *Macromolecules* **39**, 4289–4297 (2006).
  98. Goto, E., Ochiai, Y., Ueda, M. & Higashihara, T. Transition-metal-free and halogen-free controlled synthesis of poly(3-alkylthiophenylene vinylene): Via the Horner-Wadsworth-Emmons condensation reaction. *Polym. Chem.* **9**, 1996–2001 (2018).
  99. Ajayaghosh, A. Chemistry of squaraine-derived materials: Near-IR dyes, low band gap systems, and cation sensors. *Acc. Chem. Res.* **38**, 449–459 (2005).
  100. Broggi, A. *et al.* Squaraine-Based Polymers: Toward Optimized Structures for Optoelectronic Devices. *Macromol. Chem. Phys.* **218**, 1–9 (2017).
  101. Oriou, J. *et al.* Synthesis of squaraine-based alternated  $\pi$ -conjugated copolymers: From conventional cross-coupling reactions to metal-free polycondensation. *Polym. Chem.* **5**, 7100–7108 (2014).
  102. Zhou, J. *et al.* Surface modification of polysquaraines to sense humidity within a second for breath monitoring. *Sensors Actuators, B Chem.* **271**, 137–146 (2018).
  103. Havinga, E. E., Pomp, A., ten Hoeve, W. & Wynberg, H. Water-soluble polysquaraines and polycroconaines. *Synth. Met.* **69**, 581–582 (1995).
  104. Garbay, G. *et al.* Triaryl-1,4-diamine-based polysquaraines: Effect of co-solvent and monomer insertion on optoelectronic properties. *Polym. Chem.* **9**, 1288–1292 (2018).
  105. Zhang, G. *et al.* Facile green synthesis of isoindigo-based conjugated polymers using aldol polycondensation. *Polym. Chem.* **8**, 3448–3456 (2017).
  106. Mei, J., Graham, K. R., Stalder, R. & Reynolds, J. R. Synthesis of isoindigo-based oligothiophenes for molecular bulk heterojunction solar cells. *Org. Lett.* **12**, 660–663 (2010).
  107. Wang, E. *et al.* An Easily Accessible Isoindigo-Based Polymer for High-Performance Polymer Solar Cells. **133**, 14244–14247 (2011).
  108. Stalder, R., Mei, J., Graham, K. R., Estrada, L. A. & Reynolds, J. R. Isoindigo, a versatile electron-deficient unit for high-performance organic electronics. *Chem. Mater.* **26**, 664–678 (2014).
  109. Guo, C., Sun, B., Quinn, J., Yan, Z. & Li, Y. Synthesis and properties of indigo based donor – acceptor conjugated polymers †. 4289–4296 (2014). doi:10.1039/c3tc32276a
  110. Koizumi, Y. *et al.* Thienoisindigo-based low-band gap polymers for organic electronic devices. *Polym. Chem.* **4**, 484 (2013).
  111. Ide, M. *et al.* Near-infrared absorbing thienoisindigo-based copolymers for organic photovoltaics. *J. Phys. Chem. C* **117**, 26859–26870 (2013).



112. Konkol, K. L., Schwiderski, R. L. & Rasmussen, S. C. Synthesis, characterization, and electropolymerization of extended fused-ring thieno[3,4-b]pyrazine-based terthienyls. *Materials (Basel)*. **9**, (2016).
113. Sayyah, S. M., El-Rabiey, M. M., Abd El-Rehim, S. S. & Azooz, R. E. Electropolymerization kinetics of o-aminophenol and characterization of the obtained polymer films. *J. Appl. Polym. Sci.* **99**, 3093–3109 (2006).
114. Bilger, D., Homayounfar, S. Z. & Andrew, T. L. A critical review of reactive vapor deposition for conjugated polymer synthesis. *J. Mater. Chem. C* **7**, 7159–7174 (2019).
115. Antony-Babu, S. & Goodfellow, M. Biosystematics of alkaliphilic streptomycetes isolated from seven locations across a beach and dune sand system. *Antonie van Leeuwenhoek, Int. J. Gen. Mol. Microbiol.* **94**, 581–591 (2008).
116. Suzuki, H., Ohnishi, Y., Furusho, Y., Sakuda, S. & Horinouchi, S. Novel benzene ring biosynthesis from C3 and C4 primary metabolites by two enzymes. *J. Biol. Chem.* **281**, 36944–36951 (2006).
117. Utley, J. H. P. & Gruber, J. Electrochemical synthesis of poly(p-xylylenes) (PPXs) and poly(p-phenylenevinylene)s (PPVs) and the study of xylylene (quinodimethane) intermediates; an underrated approach. *J. Mater. Chem.* **12**, 1613–1624 (2002).
118. Kan, K., Yamamoto, H., Kaneko, D., Tateyama, S. & Kaneko, T. Novel  $\pi$ -conjugated bio-based polymer, poly(3-amino-4-hydroxybenzoic acid), and its solvatochromism. *Pure Appl. Chem.* **86**, 685–690 (2014).
119. Zare, E. N. *et al.* Progress in Conductive Polyaniline-Based Nanocomposites for Biomedical Applications: A Review. *J. Med. Chem.* (2019). doi:10.1021/acs.jmedchem.9b00803
120. Dan, L. I., Huang, J. & Kaner, R. B. Polyaniline nanofibers: a unique polymer nanostructure for versatile applications. *Acc. Chem. Res.* **42**, 135–145 (2009).
121. Huang, J. Syntheses and applications of conducting polymer polyaniline nanofibers. *Pure Appl. Chem.* **78**, 15–27 (2006).
122. Chen, C., Hong, X. & Gao, Y. Electrosynthesis of poly(3-amino-4-hydroxybenzoic acid) nanoparticles with electroactivity even in highly alkaline solutions. *J. Appl. Polym. Sci.* **132**, 1–10 (2015).
123. Dan Tompkins. *Body Armor Safety Initiative. NIJ Journal* (2006).
124. Suzuki, M. (Kawasaki), Yokoyama, K. (Kawasaki) & Kikuchi, Y. (Kawasaki). METHOD FOR PRODUCING AN AMINOHYDROXYBENZOIC ACID-TYPE COMPOUND (75). (2012).
125. Lee, J. K. *et al.* A new synthetic approach for polybenzoxazole and light-induced fluorescent patterning on its film. *Macromolecules* **38**, 9427–9433 (2005).
126. Carayon, C. & Fery-Forgues, S. 2-Phenylbenzoxazole derivatives: A family of robust emitters of solid-state fluorescence. *Photochem. Photobiol. Sci.* **16**, 1020–1035 (2017).
127. Affeldt, R. F., De Amorim Borges, A. C., Russowsky, D. & Severo Rodembusch, F. Synthesis and fluorescence properties of benzoxazole-1,4-dihydropyridine dyads achieved by a multicomponent reaction. *New J. Chem.* **38**, 4607–4614 (2014).
128. Pyo, S. M. *et al.* Synthesis and characterization of a new blue-light-emitting polyimide. *Macromolecules* **31**, 4777–4781 (1998).
129. Park, H. K. & Ree, M. Blue-light-emitting polymers prepared from a new monomer having a well-defined conjugation length. *Synth. Met.* **117**, 197–198 (2001).

130. Woo, C. H., Beaujuge, P. M., Holcombe, T. W., Lee, O. P. & Fréchet, J. M. J. Incorporation of furan into low band-gap polymers for efficient solar cells. *J. Am. Chem. Soc.* **132**, 15547–15549 (2010).
131. Sonar, P., Foong, T. R. B., Singh, S. P., Li, Y. & Dodabalapur, A. A furan-containing conjugated polymer for high mobility ambipolar organic thin film transistors. *Chem. Commun.* **48**, 8383–8385 (2012).
132. Lee, S. M. *et al.* High-Performance Furan-Containing Conjugated Polymer for Environmentally Benign Solution Processing. *ACS Appl. Mater. Interfaces* **9**, 15652–15661 (2017).
133. Yiu, A. T. *et al.* Side-chain tunability of furan-containing low-band-gap polymers provides control of structural order in efficient solar cells. *J. Am. Chem. Soc.* **134**, 2180–2185 (2012).
134. Ma, J., Du, Z., Xu, J., Chu, Q. & Pang, Y. Efficient aerobic oxidation of 5-hydroxymethylfurfural to 2,5-diformylfuran, and synthesis of a fluorescent material. *ChemSusChem* **4**, 51–54 (2011).
135. Hui, Z. & Gandini, A. POLYMERIC SCHIFF BASES BEARING FURAN MOIETIES. *Eur. Polym. J.* **28**, 1461–1469 (1992).
136. Xiang, T. *et al.* Schiff base polymers derived from 2,5-diformylfuran. *Polym. Int.* **62**, 1517–1523 (2013).
137. Leitch, D. C. *et al.* A palladium-catalysed multicomponent coupling approach to conjugated poly(1,3-dipoles) and polyheterocycles. *Nat. Commun.* **6**, 1–8 (2015).
138. Camurlu, P. Polypyrrole derivatives for electrochromic applications. *RSC Adv.* **4**, 55832–55845 (2014).
139. Asiri, A., Baghaffar, G., Al-Harby, A. & Zayed, M.-A. Synthesis of Some Vanillin Derivatives and their Use as an Optical Sensor for the Detection of Volatile Organic Compounds. *J. King Abdulaziz Univ.* **21**, 117–128 (2009).
140. E. A. Dikumar, V. I. P. N. G. K. and A. P. Y. Synthesis of N,N'-bis-[3-alkoxy-4-(hydroxy, alkoxy, acyloxy)-phenylmethylene- and -Phenylmethyl]-1,3-phenylenediamines. *J. Pept. Sci.* **60**, 58–60 (2001).
141. Dikumar, E. A., Kozlov, N. G., Potkin, V. I., Azarko, V. A. & Yuvchenko, A. P. Synthesis, film-forming properties, and thermal and light sensitivity of N,N'-bis[4-hydroxy(alkoxy, acyloxy)-3-alkoxyphenylmethylidene]benzene-1,4- diamines. *Russ. J. Gen. Chem.* **78**, 281–285 (2008).
142. Petrović, Z. D., Orović, J., Simijonović, D., Petrović, V. P. & Marković, Z. Experimental and theoretical study of antioxidative properties of some salicylaldehyde and vanillic Schiff bases. *RSC Adv.* **5**, 24094–24100 (2015).
143. Laye, R. H. Syntheses and photophysical properties of a series of [2:2] silver(I) metallocycles. *Inorganica Chim. Acta* **360**, 439–447 (2007).
144. Llevot, A., Grau, E., Carlotti, S., Grelier, S. & Cramail, H. Renewable (semi)aromatic polyesters from symmetrical vanillin-based dimers. *Polym. Chem.* **6**, 6058–6066 (2015).



## **Chapter 2: Synthesis of divanillin-based polyazomethines: optical and physical characterisation, model compounds**



## Table of contents

|  |    |
|--|----|
| <b>1. Introduction</b> .....   | 59 |
| <b>2. Divanillin-based polyazomethines</b> .....   | 60 |
| 2.1. Synthesis of polyazomethines.....   | 60 |
| 2.1.1 Monomer synthesis: enzymatic coupling of vanillin and acetovanillone.....            | 60 |
| 2.1.2. Polyazomethines synthesis and physical characterization.....                        | 62 |
| 2.1.2.1. Polymerization of divanillin-based compounds and diamines .....                   | 62 |
| 2.1.2.2. Reproducibility of the polymerization reaction .....                              | 66 |
| 2.1.2.3. Syntheses of random copolymers with various amount of meta-phenylene diamine..... | 68 |
| 2.1.3. Improvement of the polymerization experimental conditions.....                      | 69 |
| 2.1.4. Stability of divanillin-based polyazomethines.....                                  | 74 |
| 2.1.2. Conclusion for polyazomethine synthesis.....  | 76 |
| 2.2.1. Optical characterization of divanillin-based polyazomethines .....                  | 77 |
| 2.2.2. Optical properties of divanillin-based polyazomethines: conclusion .....            | 81 |
| <b>3. Model compounds of divanillin-based polyazomethines</b> .....                        | 82 |
| 3.1. Synthesis of model compounds.....   | 82 |
| 3.2. X-Ray Diffraction characterization of model compounds.....                            | 85 |
| 3.3. Optical characterization of vanillin-based model compounds.....                       | 88 |
| 3.4. General conclusion for model compounds.....   | 92 |
| <b>4. General conclusion</b> .....   | 94 |
| <b>5. References</b> .....   | 97 |
| <b>6. Experimental Part</b> .....  | 99 |



## 1. Introduction

Azomethines, also known as imines or Schiff bases, are characterized by the presence in their structure of a  $-C=N-$  bond. Azomethines and polyazomethines can be synthesized by polycondensation of a diamine with a bisaldehyde releasing water as the only by-product. This straightforward method enables the formation of polymers without extensive purification. Conjugated polyazomethines have applications in various fields, such as photovoltaics<sup>1,2,3</sup> and liquid crystals.<sup>4</sup> They were also used as dynamers by Lehn *et al.*, with stimuli-dependent properties.<sup>5</sup>

Adams *et al.* first reported the synthesis of polyazomethines in 1923, with the production of infusible and insoluble polymer.<sup>6</sup> Until the end of the 80's, the polyazomethines synthesized were poorly soluble and used as high stretch fibers.<sup>7</sup> The insertion of an alkyl side moiety significantly improved the solubility of conjugated polyazomethines, allowing better characterization.<sup>8</sup>

Another breakthrough happened in 2008 when Kim *et al.*<sup>9</sup> first showed that protonation could induce fluorescence in conjugated polyazomethines. Since then, a large palette of polyazomethines has been synthesized, with various motives.

Fluorescence in polyazomethines is a major challenge, as it is essential for various applications and can be extremely weak for these polymers. Indeed, the azomethine bond is reported to quench most fluorophores<sup>10</sup>. This issue can be overcome by protonation and lowering the temperature to improve the fluorescent yield<sup>11</sup> or by a careful choice of the chemical structures to make fluorescent copolymers. Fluorene is one of these interesting groups, as it can give polyazomethines with high fluorescence quantum yield. Skene's team investigated these types of conjugated polyazomethines, by synthesizing both fluorene and EDOT-based polyazomethines, as is illustrated in **Figure 1**.

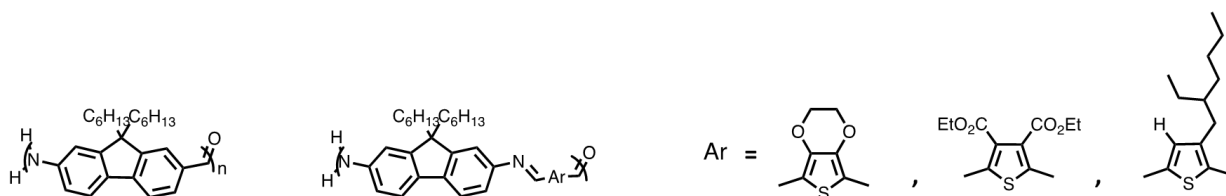


**Figure 1:** Structures of  $\pi$ -conjugated polyazomethines synthesized by Skene's team with fluorene and other EDOT based moieties. (Adapted from <sup>12,13</sup>)

The all-fluorene polyazomethine has a quantum yield of 0.48 in solution without doping at room temperature, which is quite high for polyazomethines. In comparison, the other polyazomethines represented in **Figure 1** have quantum yields ranging from 0.13 to 0.26. By changing the co-monomer of the fluorene-based polyazomethine, polyazomethines can be obtained with a large range of HOMO-LUMO gaps and therefore a large range of optical properties, which is promising for further applications.

Polyazomethines are believed to be rather unstable and prone to hydrolysis; however, Jenekhe *et al.* prepared a polyazomethine and its vinylene counterpart, and the polyazomethine was the more stable of the two under ambient conditions.<sup>14</sup> This enhanced stability is due in part to its larger band gap and higher oxidation potential. Mallet and coll. showed that a small conjugated EDOT-based azomethine molecule was resistant to hydrolysis and reduction, even after a few hours under reflux with reducing agents.<sup>15</sup>

The objective of the present work is to obtain bio-based conjugated polymers with interesting properties such as broad emission, to incorporate them into devices like OLED. In this chapter, the synthesis and characterization of divanillin-based polyazomethines will be described. Firstly, monomers from vanillin and vanillin derivatives were synthesized and then polymerized with different diamines. These



polyazomethines were then characterized in terms of physical and optical properties. Secondly, model compounds of the previously synthesized polyazomethines were synthesized and purified. These model compounds were then characterized optically and by X-Ray Diffraction.

## 2. Divanillin-based polyazomethines

### 2.1. Synthesis of polyazomethines

#### 2.1.1 Monomer synthesis: enzymatic coupling of vanillin and acetovanillone

Divanillin can be synthesized *via* chemical methods, like phenol oxidative coupling. This can be done using iron sulfate giving divanillin with high yield, up to 95%.<sup>16</sup> Another possible way to couple two rings through the carbons 5 and 5' is to use enzymatic coupling. Different types of enzymes can be used, like horse radish peroxidase, which is the enzyme used in the patent for production of divanillin.<sup>17</sup> Other enzymes can form this dimer, notably Laccase.<sup>18,19</sup> Laccase from *Trametes Versicolor* was used previously to develop a new and efficient method to dimerize vanillin.<sup>20</sup> This procedure requires nonhazardous solvents, is done at room temperature and produces divanillin in high yield as the only product. First, vanillin was dissolved in a buffer medium containing acetone and acetic acid, and Laccase from *Trametes Versicolor* was added; finally, the medium was saturated with oxygen (cf. **Figure 2a**).

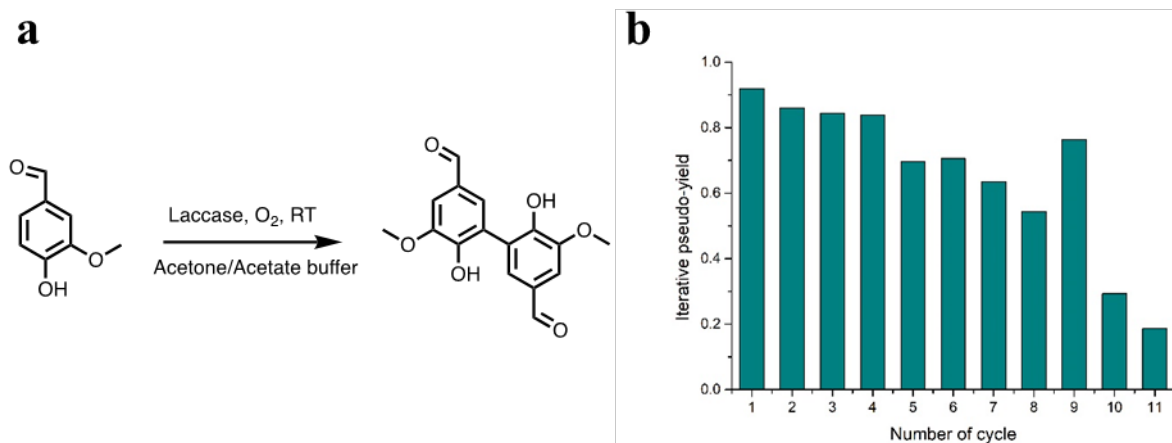


**Figure 2a:** Enzyme-catalyzed vanillin dimerization. **b:** Pseudo-yield for vanillin coupling for each batch

As the divanillin is formed in the medium, its concentration will exceed the solubility limit and divanillin will precipitate. Therefore, it is easily recovered by simple filtration and the filtrate can be re-used by adding vanillin continuously. In **Figure 2b**, the iterative yield is indicated for each batch made, the reaction being done on a 6-gram scale. The yield generally goes down, which might be because for every batch, there was an addition of acetone to rinse the divanillin which may change the concentration of the buffer.

The purity of the divanillin was determined by <sup>1</sup>H-NMR analysis: a peak at 7 ppm is characteristic of the aromatic proton of vanillin that disappeared during the coupling. By integrating this peak a purity can be obtained, it is on average 86 % (cf. **Figure 3**). Divanillin can be purified further by precipitation in ethanol, to obtain a final purity of 98 % on average.

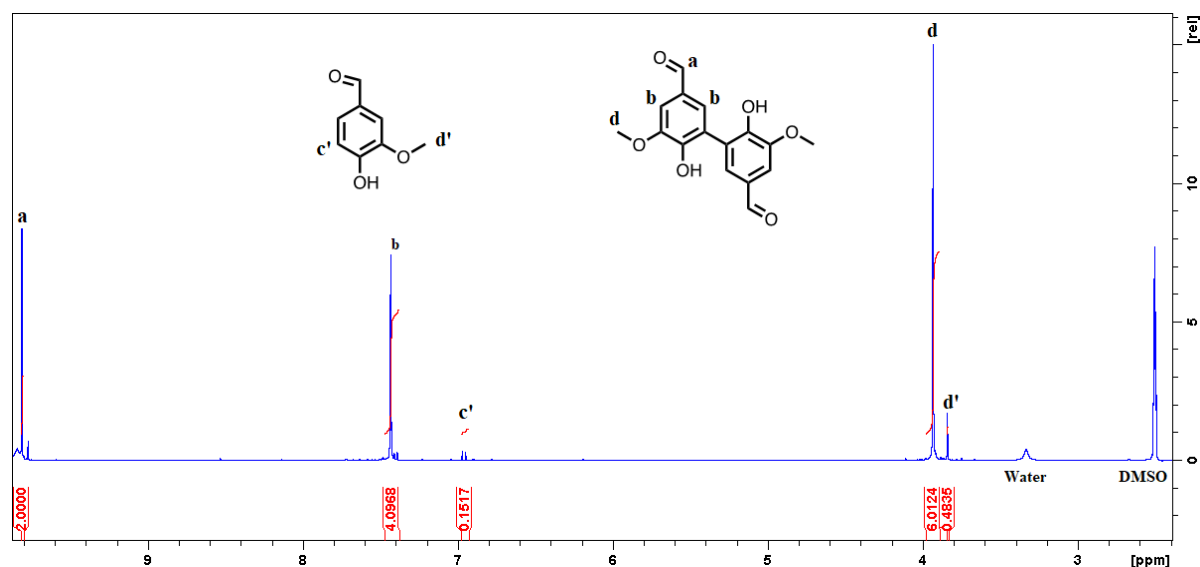


**Figure 3:**  $^1\text{H-NMR}$  spectrum of crude divanillin (in  $\text{DMSO-d}_6$ )

Another vanillin-based monomer was prepared, diacetovanillone, by enzymatic coupling of acetovanillone. Acetovanillone, or apocynin, is like vanillin a lignin derivatives that can be found in various plants and has interesting pharmacological properties.<sup>21</sup> The protocol for acetovanillone dimerization is the same as the one developed for divanillin (cf. **Figure 4a**), and the iterative pseudo-yield can be found in **Figure 4b**, with the same observations as divanillin.

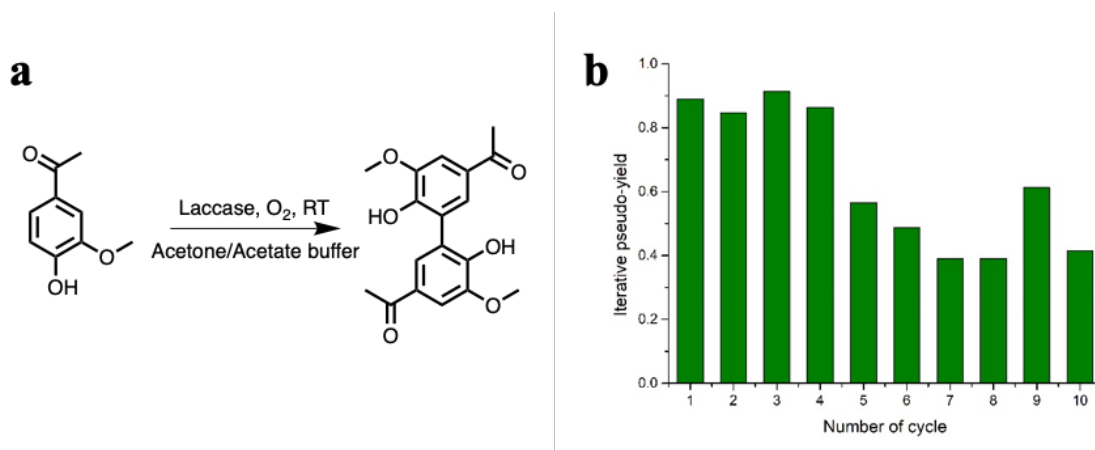
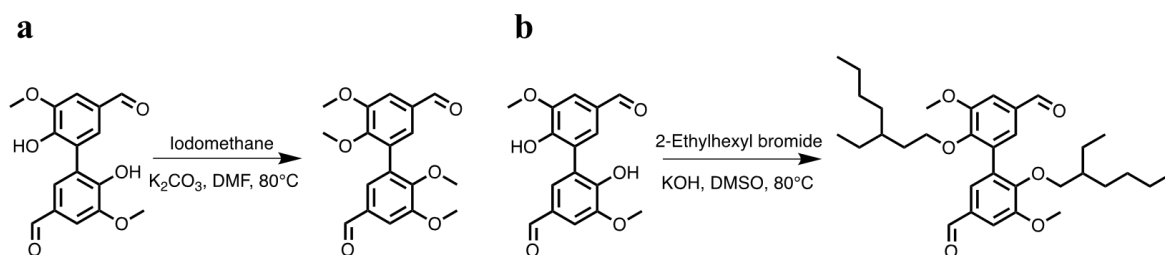


**Figure 4a:** Enzyme catalyzed acetovanillone dimerization. **b:** Pseudo-yield for acetovanillone coupling, for every batch made.

The purity was estimated by  $^1\text{H-NMR}$  analysis, by integrating the peak characteristic of the disappearing proton, like for the divanillin. The purity is 89% on average, the impurity being unreacted acetovanillone. The diacetovanillone was used as such for the next alkylation step.

To improve the solubility of the final polyazomethines, the vanillin and acetovanillone based-monomers were alkylated with either methyl or 2-ethylhexyl alkyl moieties. For the methylation, the same protocol as the one described in literature<sup>22</sup> was used (cf. **Scheme 1a**). The reacting mixture was poured into water and the product that precipitates out of the solution can be recovered by filtration, as a beige powder that requires no further purification. For the 2-ethylhexylation, another protocol was used<sup>23</sup> (cf. **Scheme 1b**). The final product was purified by flash chromatography. All monomers were stored at low temperature to prevent any potential degradation of the aldehyde function.



**Scheme 1a:** Alkylation of divanillin with a methyl group. **b:** Alkylation of divanillin with a 2-ethylhexyl group

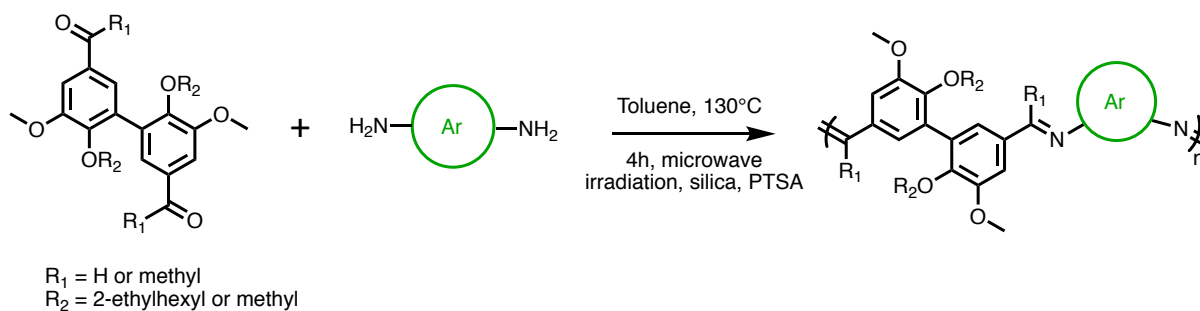
$^1\text{H-NMR}$  analysis confirmed that both alkylations worked correctly, with correct integrations and apparition of protons of alkyl groups. Diacetovanillone was also alkylated successfully on both phenol functions, with the same alkyl substituents as divanillin (See **Experimental part** for characterizations). Divanillin bearing a methyl moiety will henceforth be referred to as **DVM** (short for DiVanillin Methylated), and Divanillin bearing a 2-ethylhexyl chain will be referred to as **DVEH** (DiVanillin 2-EthylHexylated).

To conclude, two symmetric bisaldehyde dimers were obtained using enzymatic coupling, with an efficient method giving high yield (90%) and no by-products. They were alkylated with two different alkyl groups to improve the solubility of the final polyazomethines and see the influence of the alkyl group length.

## 2.1.2. Polyazomethines synthesis and physical characterization

### 2.1.2.1. Polymerization of divanillin-based compounds and diamines

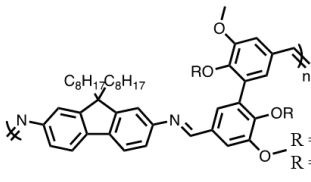
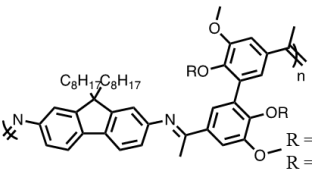
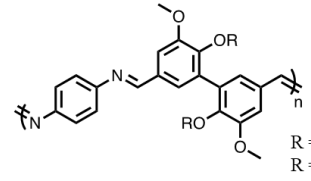
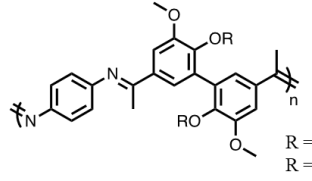
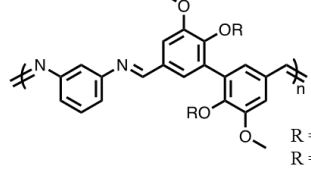
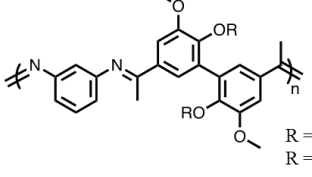
The previously synthesized monomers were then used for polymerization with different diamines. The general reaction scheme is shown in **Scheme 2**.



**Scheme 2:** General reaction scheme for the synthesis of polyazomethines

The reaction was done using a stoichiometric amount of monomer under microwave irradiation, which is usually faster than conventional heating.<sup>24,25</sup> Toluene was used as a solvent as it is one in which the final polyazomethines were almost all soluble – the temperature reaction is above its boiling point as the microwave reactor enables doing reactions under pressure. PTSA is a catalyst and silica acts as a desiccant, to remove water from the medium and move the equilibrium towards the formation of the polyazomethines. These experimental conditions do not require any metallic catalysts, and the only by-product is water.

For the monomers, the different divanillin and diacetovanillone synthesized previously were used. As for the diamines, three different ones were chosen: fluorene diamine, and para and meta phenylene diamines to see the impact of the position of the substituent on the properties of the polyazomethines. **Table 1** summarizes the different polyazomethines synthesized, along with their given names.

|                | Divanillin derivatives  | Diacetovanillon derivatives   |
|----------------|---|---|
| Fluorene       |  <p>R = 2-ethylhexyl : <b>P1</b><br/>R = methyl : <b>P2</b></p>  |  <p>R = 2-ethylhexyl : <b>P3</b><br/>R = methyl : <b>P4</b></p>   |
| Para-phenylene |  <p>R = 2-ethylhexyl : <b>P5</b><br/>R = methyl : <b>P6</b></p>  |  <p>R = 2-ethylhexyl : <b>P7</b><br/>R = methyl : <b>P8</b></p>   |
| Meta-phenylene |  <p>R = 2-ethylhexyl : <b>P9</b><br/>R = methyl : <b>P10</b></p> |  <p>R = 2-ethylhexyl : <b>P11</b><br/>R = methyl : <b>P12</b></p> |

**Table 1:** Sum up of the different polyazomethines synthesized

The polyazomethines are all soluble in common solvents (chloroform, THF, methylene chloride, toluene), except **P9**, the polyazomethine with **DVEH** and the meta-phenylene moiety. This could be explained by the position of the different substituents on the phenylene ring: the meta position might give a polymer with a highly twisted chain, making it poorly soluble. For the polyazomethines bearing divanillin derivatives, the reaction was assessed with  $^1\text{H-NMR}$  analysis and the appearance of the characteristic peak of azomethines around 8.4 ppm (see **Figure 5** for an example). ATR-FTIR and SEC in THF also confirmed the formation of polyazomethines (See **Experimental part** for ATR-FTIR,  $^1\text{H-NMR}$  spectra and SEC traces).

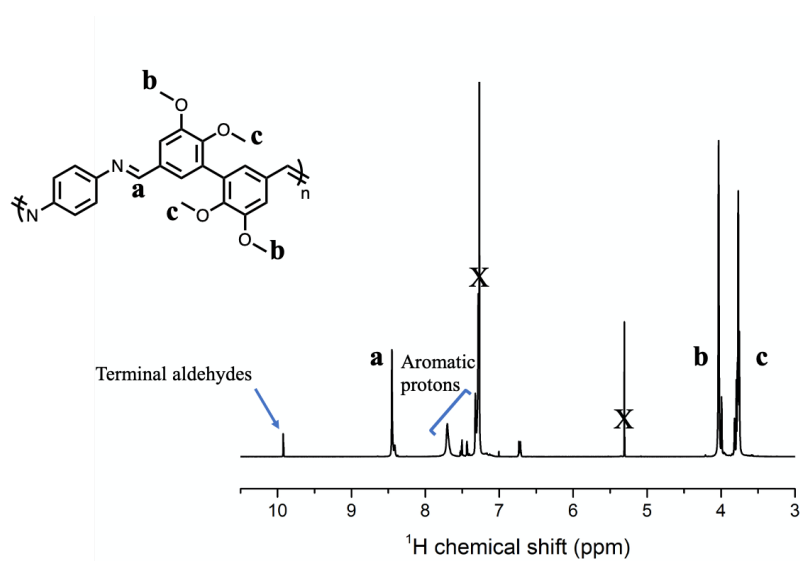


**Figure 5:**  $^1\text{H-NMR}$  spectrum of polyazomethine **P6** in  $\text{CDCl}_3$  (128 scans)

However, for the polymers synthesized with diacetovanillone derivatives, the compounds obtained still have the peak of the ketone protons, around 2.5 ppm. If the polymerization really occurred, this peak should be shifted toward 1 ppm, with only residual ketone protons left at 2.5 ppm. However this was not observed, nor were any signs of polycondensation in SEC analysis (see **Annexes** for  $^1\text{H-NMR}$  spectra). As is illustrated in **Figure 6**, the SEC trace of **P3** corresponds to a mixture of oligomers, confirming that the monomers did not polymerize completely. To compare, the SEC chromatogram of **P1**, its equivalent with **DVEH** and fluorene diamine, is also given in **Figure 6**.

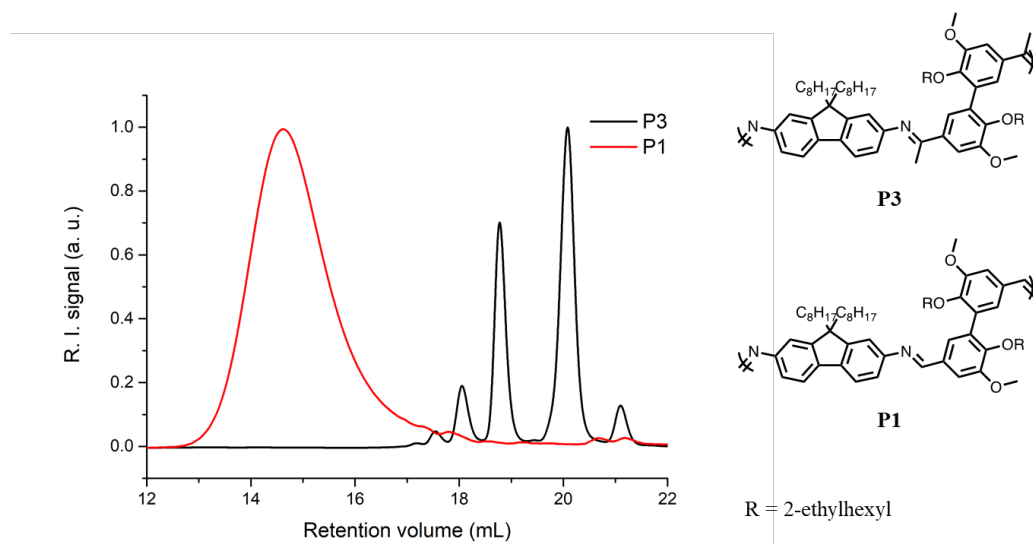
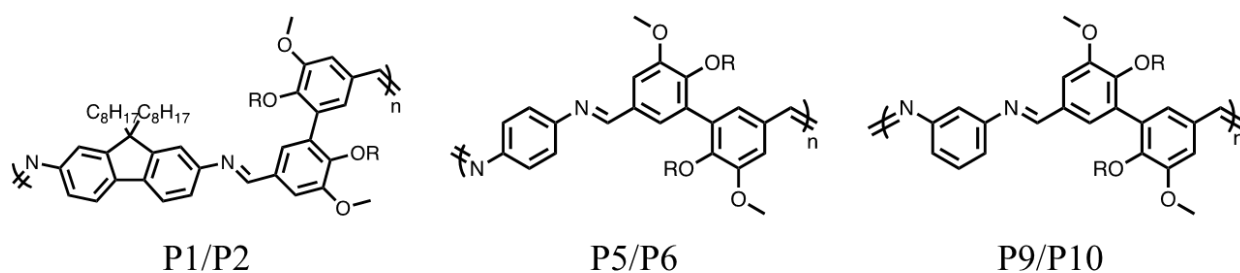


**Figure 6:** SEC traces of **P3** and **P1** in THF, R.I. detection

These lower molar masses could be explained by the diminished reactivity induced by the presence of the ketone moiety as opposed to the aldehyde. This leads to the formation of oligomers rather than polymer – for this reason, the polymers with diacetovanillone are set aside, to focus on the polyazomethines synthesized with the divanillin moiety.

In **Table 2**, the different characterizations of the polyazomethines are detailed, along with their structure.



| Name | $\bar{M}_n^a$ (g/mol) | $\bar{M}_w^a$ (g/mol) | $\bar{D}^a$ | $\bar{DP}_n^a$ | $\bar{DP}_{n,NMR}^b$ | Alkyl chain  | $T_d^c$ (°C) |
|------|-----------------------|-----------------------|-------------|----------------|----------------------|--------------|--------------|
| P1   | 21 100                | 45 500                | 2.2         | 23             | 23                   | 2-Ethylhexyl | 387          |
| P2   | 10 900                | 26 100                | 2.4         | 15             | 15                   | Methyl       | 379          |
| P5   | 10 600                | 21 900                | 2.1         | 18             | 42                   | 2-Ethylhexyl | 374          |
| P6   | 3 300                 | 9 100                 | 2.8         | 8              | 11                   | Methyl       | 349          |
| P9   | -                     | -                     | -           | -              | -                    | 2-Ethylhexyl | 375          |
| P10  | 2 200                 | 15 600                | 7.1         | 5              | -                    | Methyl       | 165          |

**Table 2:** Structures of divanillin-based polyazomethines and table summing up their properties. <sup>a</sup> Determined by Size Exclusion Chromatography (SEC) relative to polystyrene standards in THF at 30°C. <sup>b</sup> Determined by <sup>1</sup>H-NMR analysis in CDCl<sub>3</sub>, 128 scans. <sup>c</sup> Decomposition temperature at 10 % weight loss, evaluated under N<sub>2</sub> at a heating rate of 10 °C/min by TGA.

These polyazomethines exhibit molar masses going up to 21 100 g/mol for **P1**. They all have a dispersity close to 2, which is coherent with a polycondensation (see **Equation 1** in the case of complete conversion), except for **P10**. The SEC trace of this polyazomethine reveals the presence of low molar masses, but also a shoulder for high molar masses that could be the sign of aggregates.

$$\frac{\bar{M}_w}{\bar{M}_n} = 1 + p$$

**Equation 1:** Equation obtained by developing Carothers equation ( $p$  = monomer conversion)

What is worth noticing is that when compared two-by-two, polyazomethines with the same structure but bearing 2-ethylhexyl groups have higher degree of polymerization than the ones bearing a methyl group. As an example, **P1**, which has a 2-ethylhexyl moiety, is 23-unit long, while **P2**, which has a methyl pendant group, is 15-unit long. This can also be observed for **P5** and **P6**. For **P9** and **P10**, as **P9** is not soluble in THF, it could not be analyzed – however it might have a high molar mass. This high molar mass combined with its twisted behavior induced by the meta-bond of the phenylene could explain its poor solubility. This difference between polyazomethines with methyl and 2-ethylhexyl alkyl groups could be explained by the difference of solubility during the reaction. A polyazomethine bearing

2-ethylhexyl moiety will be more soluble and therefore will stay longer in solution, giving way to higher molar masses as compared to their methyl group-bearing homologues.

The molar masses could also be obtained by  $^1\text{H-NMR}$  analysis, by calculating the ratio between aldehyde protons as chain ends and azomethine protons. The hypothesis is that there is one aldehyde per chain. This gives  $\overline{\text{DP}}_n$  in good correlation with SEC results for **P1**, and **P2**, and slightly less close for **P6** but still relatively coherent. This shows that the hydrodynamic radius of the polyazomethine is close to the one of PS, as SEC analyses give results in good agreement with NMR spectroscopy. However, for **P5** the  $\overline{\text{DP}}_n$  given by NMR analysis is more than double the one given by SEC; this will be more detailed in the next section.

The polyazomethines have a good thermal stability, with degradation temperatures above  $350^\circ\text{C}$ , and even close to  $400^\circ\text{C}$  for **P1**. For **P10**, its comparatively low degradation temperature at 10% could be explained by the presence of oligomers with small molar masses and remaining monomers in the sample: these latter will be degraded before the longer chains, giving this low  $T_d$ . The degradation temperature at 20% is  $349^\circ\text{C}$  and could correspond to these longer chains (see **Experimental part** for TGA analyses and SEC traces).

### 2.1.2.2. Reproducibility of the polymerization reaction

Polymer synthesis being performed at a relatively small scale (150 mg) and knowing that polycondensation is highly sensitive to stoichiometry, several replicates were performed to see if the syntheses were reproducible, using the same conditions as before on **P5** and **P6**. In **Figure 7** a column graph of the different molar masses obtained is shown for **P5**, with its structure.

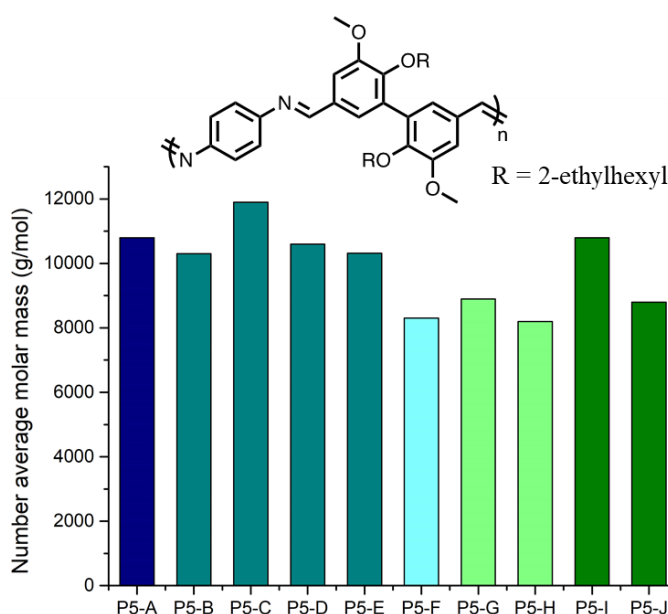


**Figure 7:** Column graph of the number average molar mass of different syntheses of **P5**, with different batches of **DVEH** (each colour corresponds to a batch of **DVEH** – molar masses determined by SEC in THF relative to PS standards, R.I. detection)

Each column corresponds to one experiment, and columns with the same colour were synthesized using the same batch of **DVEH**. The average for  $\overline{M}_n$  is  $9\,900\text{ g/mol}$  (16 motives) with a standard deviation of  $1\,250\text{ g/mol}$  (two motives). This shows that the synthesis of **P5** is quite reproducible. The slight drop in  $\overline{M}_n$  for **P5-F**, **P5-G** and **P5-H** could be explained by a lower purity of **DVEH**. Indeed, traces of solvent can affect the weighting of monomers and therefore change the ratio, giving way to lower molar masses.

Some of the batches were characterized by  $^1\text{H-NMR}$  spectroscopy, and their molar mass obtained using the same hypothesis as in the previous section. The results are summed up in **Table 3**.

| Name | $\overline{\text{DP}}_n^a$ (SEC) | $\overline{\text{DP}}_n^b$ (NMR) | Ratio $\overline{\text{DP}}_n^{\text{RMN}}/\overline{\text{DP}}_n^{\text{SEC}}$ |
|------|----------------------------------|----------------------------------|---|
| P5-C | 20                               | 50                               | 2.5   |
| P5-D | 18                               | 40                               | 2.2   |
| P5-E | 17                               | 53                               | 3.1   |
| P5-F | 14                               | 30                               | 2.1   |
| P5-G | 13                               | 25                               | 1.9   |
| P5-I | 20                               | 29                               | 1.5   |
| P5-J | 15                               | 13                               | 0.9   |

**Table 3:** Comparison of the molar masses of **P5** determined <sup>a</sup> by SEC in THF relative to PS standards and <sup>b</sup> by  $^1\text{H-NMR}$  analysis in  $\text{CDCl}_3$ , 128 scans

The  $\overline{\text{DP}}_n$  obtained by  $^1\text{H-NMR}$  analysis are all higher than the ones obtained by SEC, except for **P5-J**. Furthermore, there is no real logic between the different batches of **P5**, as can be seen when comparing the ratio  $\overline{\text{DP}}_n^{\text{SEC}}/\overline{\text{DP}}_n^{\text{NMR}}$ . The relaxation time was optimized and the analysis repeated, but the obtained  $\overline{\text{DP}}_n$  is still much higher than the SEC  $\overline{\text{DP}}_n$  (43 units for **P5-G**). Another factor that could explain the SEC/NMR difference is the use of PS standard for SEC analysis. Indeed, if the polymer has a refractive index increment ( $dn/dc$ ) different than the one of PS, its molar mass will be wrongly determined.<sup>26</sup> For this reason, the  $dn/dc$  of **P5** was measured using universal calibration, and its molar mass calculated. **P5-D** has a  $\overline{\text{DP}}_n$  of 11 calculated by universal calibration, which is smaller than the one obtained by conventional calibration. The difference between NMR analysis and SEC could be explained by the use of a wrong hypothesis for the calculations: maybe there is not one aldehyde as chain end in average. As this was only observed for **P5** and not for the other polyazomethine, SEC will still be used to give molar mass.

A reproducibility test was also done with **P6**, which was synthesized several times. The SEC traces of the different syntheses are shown in **Figure 8**.

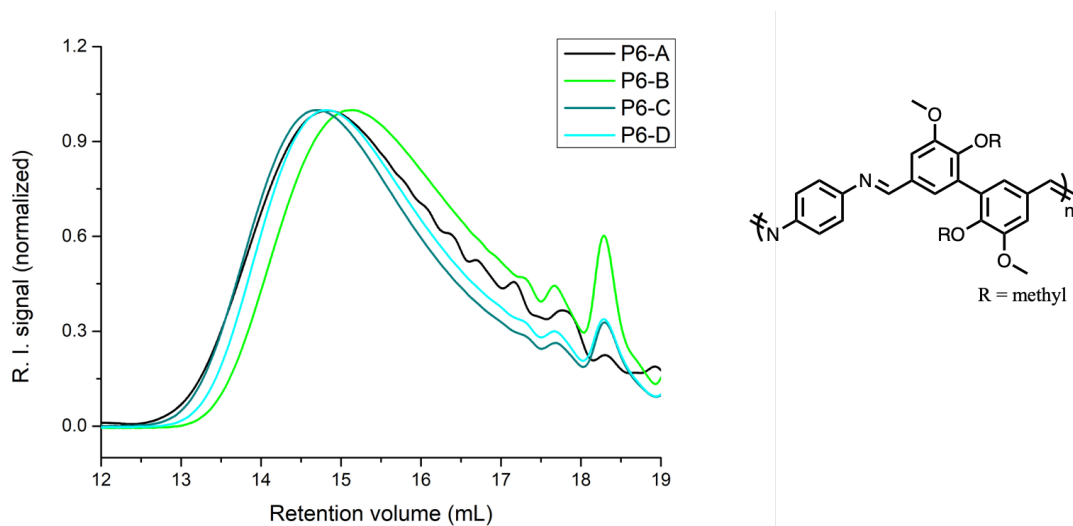


**Figure 8:** SEC traces in THF of different **P6** samples, R.I. detection



**P6-B**, **P6-C** and **P6-D** were synthesized using the same batch of **DVM**. **P6-B** was synthesized first, and then the batch of **DVM** used was oven dried under vacuum, and used to synthesize **P6-C** and **P6-D**. This highlights the importance of a dry and pure monomer, as **P6-C** and **P6-D** both have higher molar masses than **P6-B**. The same monomer, if dried correctly, can yield polyazomethines with higher molar masses. The average  $\bar{M}_n$  for the different **P6** is 3 300 g/mol (8 motives) with a standard deviation of 600 g/mol (1.5 motive).

To conclude this section, the experimental conditions used for the synthesis of polyazomethines are reproducible, as long as the monomers are pure and dry enough.

### 2.1.2.3. Syntheses of random copolymers with various amount of meta-phenylene diamine

**P9**, the polyazomethine bearing a meta-phenylene (mPD) moiety and **DVEH** is insoluble, while its homologue with para-phenylene (**P5**) is completely soluble in common solvents. To see if the solubility could be improved, some random copolymers were prepared with different ratios of meta and para-phenylene diamine. In **Figure 9** their structure and theoretical composition are indicated, as well as their SEC traces. The different random copolymers are all poorly soluble in THF but could be analyzed by SEC in chloroform with TriEthylAmine (TEA), as TEA improves separation on the columns (around 75% of the sample could be dissolved and analyzed).

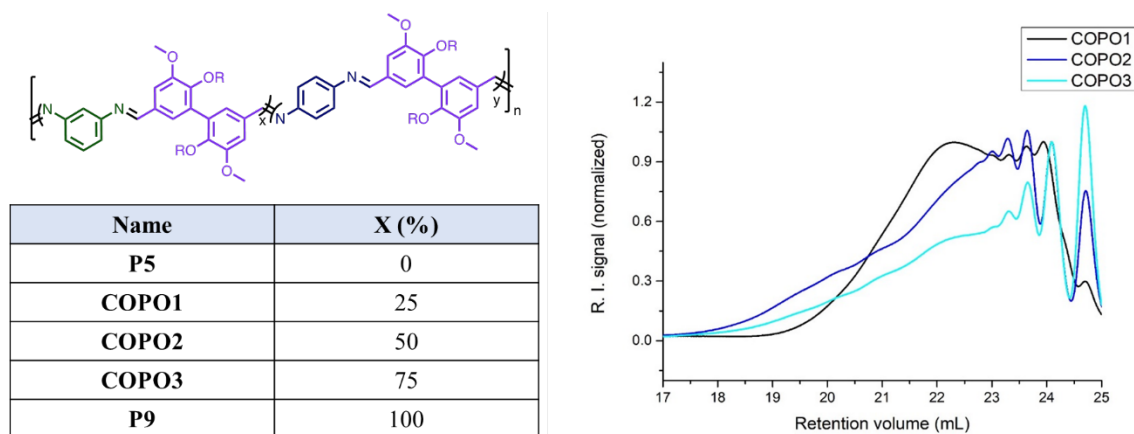


**Figure 9:** Structure of **DVEH**-based random copolymers different amounts of meta and para-phenylene diamine and table summing up their theoretical composition (left) and SEC traces of the different random copolymers in chloroform +1 %TEA, R.I. detection.

**COPO1**, the one containing less meta-phenylene diamine, has a typical polymer SEC trace, but also multiple peaks at higher retention volumes, indicating the presence of various oligomers and remaining monomers. Whereas for **COPO2** and **COPO3**, these latter exhibit a broad distribution, with a higher amount of oligomers in comparison to **COPO1**, but also a shoulder toward higher molar masses. There are multiple possibilities to explain these differences between copolymers, like the presence of aggregates or even the lower reactivity of meta-phenylene diamine. There could also be chain populations with different compositions. However, it is difficult to conclude definitely, as the copolymers are not fully soluble.

## 2.1.3. Improvement of the polymerization experimental conditions

To better analyze the polymerization and to improve the experimental conditions, some kinetic experiments were performed. Indeed, while the polymerizations were realized during four hours of reaction, some literature data report similar syntheses through microwave irradiation in few minutes.<sup>27</sup> Moreover, the objective of this PhD work is to obtain polymers without any metallic catalysts that can affect opto-electronic properties. However, it appeared that silica can be a pollutant for the final polyazomethines and is still present within the polymers after polymerization, even after filtration. Silica can then affect XPS/UPS measurements, but also emission measurements. For all these reasons, **P6** syntheses were performed to improve first the experimental conditions but also to remove silica. **P6** was chosen as the monomers are powders, which are easier to weight than oily monomer like **DVEH**.

In **Table 4**, the names and experiment conditions of the different **P6** polyazomethines synthesized are indicated.

| Name  | Time of reaction | Silica | Shape of SEC trace for the crude <sup>a</sup> |
|-------|------------------|--------|---|
| P6-1a | 30min            | Yes    | Multiple peaks                                |
| P6-1b | 30min            | Yes    | Monomodal                                     |
| P6-2a | 1h               | Yes    | Monomodal                                     |
| P6-2b | 1h               | Yes    | Multiple peaks                                |
| P6-3a | 2h               | Yes    | Multiple peaks                                |
| P6-3b | 2h               | Yes    | Multiple peaks                                |
| P6-4a | 30min            | No     | Multiple peaks                                |
| P6-4b | 30min            | No     | Multiple peaks                                |
| P6-5a | 1h               | No     | Multiple peaks                                |
| P6-5b | 1h               | No     | Monomodal                                     |
| P6-6a | 2h               | No     | Multiple peaks                                |
| P6-6b | 2h               | No     | Multiple peaks                                |

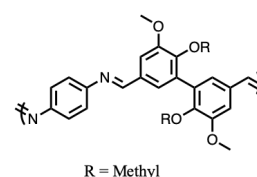


**Table 4:** Sum up of the different synthesis done for **P6**. <sup>a</sup> Determined by SEC in THF, R.I. detection

As the reaction was performed under pressure inside the microwave reactor and the medium heterogeneous, it was not possible to take aliquots during the reaction. For this reason, a series of **P6** syntheses were performed at different reaction times in the presence (or not) of silica. The syntheses were done twice, to check their reproducibility. Once the crude obtained, it was filtered to remove silica (if used), dried and analyzed by SEC. In **Table 4**, the shape of the SEC trace of the crude is indicated for each synthesis. As a general trend, oligomers were formed, except for **P6-1b**, **P6-2a** and **P6-5b** as higher molar mass polymers were obtained. However, these latter conditions were not found reproducible.

The samples were recovered by dissolving them in a minimum amount of methylene chloride, then adding methanol and finally evaporating the solvents using a rotary evaporator. After this step, all the **P6** batches have a typical polymer SEC trace (monomodal) without any drop in yield (around 80 %). They also have roughly the same molar mass apart from a few exceptions, as is shown in **Figure 10**:

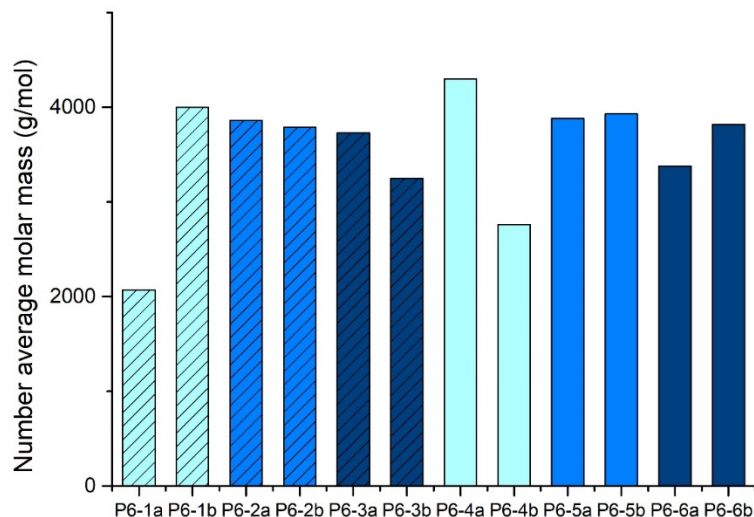


**Figure 10:** Column graph of the number average molar mass (determined by SEC in THF, relative to PS standards) of the different batches of **P6**, synthesized with different experimental conditions. (From light to dark blue: 30min, 1h and 2h of reaction, all done twice (with patten: with silica))

The reaction time does not seem to matter, as the polyazomethines formed after 30 minutes have the same molar mass as the ones synthesized in two hours. Silica does not have an impact on the molar mass either. What governs the final polyazomethine molar mass is the mode of recovery. In **Figure 11**, the SEC chromatogram of **P6-4a** is given, for the crude and after recovery.

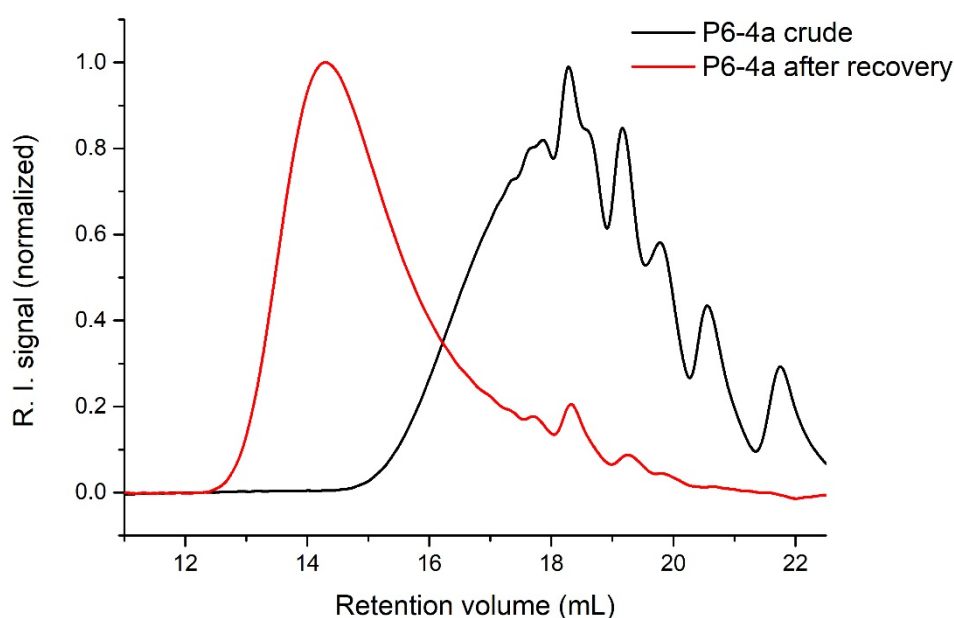


**Figure 11:** SEC traces of **P6-4a** in THF, before and after recovery (R.I. detection)

The SEC trace changed dramatically, without any loss of matter (final yield at 75%). This change means that the polymerization continues during the recovery step. The recovery was done by dissolving the crude in a minimum amount of methylene chloride, and then adding methanol. At this stage, the solution turned turbid but there is no evident precipitation due to the presence of oligomers, which are still soluble enough. The solvents were then removed using a rotary evaporator, to obtain a yellow powder. This powder was rinsed with methanol, to give the final polyazomethine. As water is removed along with the

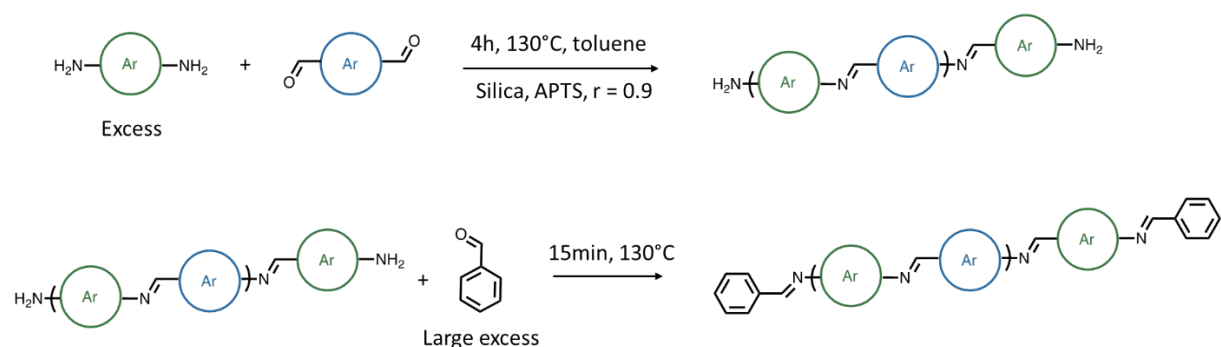
solvents through the rotary evaporator, it moves the equilibrium towards the formation of polyazomethines.

A test to end-cap the polyazomethines chains before the recovery stage was undertaken. The polyazomethines were synthesized with a ratio of 0.9 and an excess of diamine. According to Carothers equation (see **Equation 2**), this ratio should give polymer chains with 19 units as an average.

$$\overline{DP}_n = \frac{1 + R}{1 - R}$$

**Equation 2:** Simplified Carothers equation (in the case of full monomers conversion)

At the end of the reaction, the chains should all be ended with an amine function. Benzaldehyde was then added, to react with the amine terminal functions. The steps are summed up in **Scheme 3**:



**Scheme 3:** Synthesis of polyazomethines with  $[CHO]/[NH_2] = 0.9$ , end-capped with benzaldehyde

After recovery, the different polyazomethines obtained were analyzed by SEC, and they are all composed of a mixture of oligomers, like **P6-4a crude** in **Figure 11**. As expected, these similarities between crude and recovered polyazomethines are due to the end-capping step during the synthesis. Indeed, at the end of the reaction, the oligomers have a non-reactive benzaldehyde moiety as both chain ends, preventing any chain extension.

As the polymerization time does not affect the final molar mass after recovery, it was reduced to five minutes, giving molar masses similar and even higher than what was obtained before, as is highlighted in **Figure 12**.

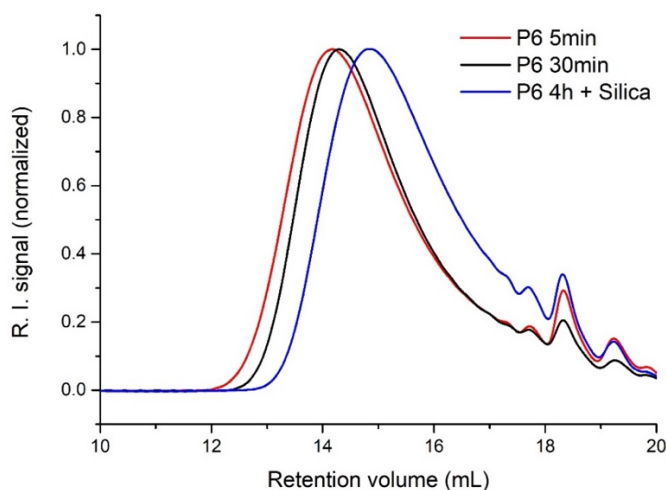


**Figure 12:** SEC traces of **P6** in THF for different reaction times (R.I. detection)

The recovery step is done by evaporating methanol using a rotary evaporator, but it was also tested with toluene instead, as it is used for the microwave irradiation step. Two polyazomethines, **P1** and **P5**, were synthesized, and their crude split in two fractions. One half was recovered using methanol, and the other with toluene – all were analyzed by SEC and the chromatograms are given in **Figure 13**:

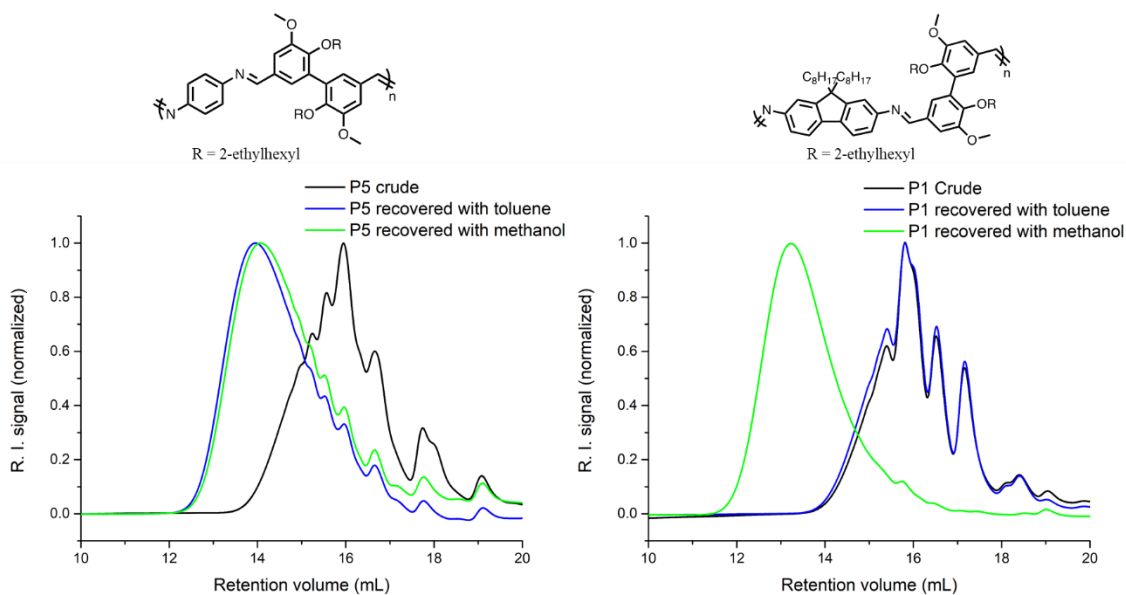


**Figure 13:** SEC traces of **P1** and **P5** in THF as crude, and after recovery with methanol or toluene (R.I. detection)

For **P5**, the crude is a mixture of oligomers, and the two fractions recovered have the SEC trace of a polymer. There is a slight difference between the fraction recovered with methanol and the one with toluene, the latter exhibiting a slightly higher molar mass. However, this difference is negligible, and does not allow concluding clearly on the effect of toluene or methanol in the recovery step. For **P1**, the crude and the fraction recovered using toluene have the same SEC trace, exhibiting mixture of oligomers. It appears that toluene does not allow the reaction to continue, as the SEC chromatogram remains the same after recovery with toluene in this case. Whereas with methanol, the SEC trace shifts towards higher molar masses. This phenomenon was also observed with **P2**, the equivalent of **P1** but with methyl substituents.

Toluene can form a heteroazeotrope with water, but at higher water quantities than the ones in this synthesis. Furthermore, as the reaction is done at reduced pressure the azeotrope is modified. On the contrary, methanol does not form any azeotrope with water, but these solvents are fully miscible in any proportions. Therefore, a methanol/water mixture can be evaporated like a perfect binary mixture according to Raoult's Law. The solubility might also have an impact: oligomers and polymers are both soluble in toluene, while oligomers are partially soluble in methanol, and polyazomethines are insoluble in methanol.

Since the polymerization continues during the recovery step, a test was done to see if it would be possible to do the polymerization during this step, using only a rotary evaporator. The monomers were put into a flask with a minimum amount of methylene chloride, catalytic quantities of PTSA and methanol, and then evaporated using a rotary evaporator. After each cycle, solvent was added again, and an aliquot collected to be analyzed by SEC. The different chromatograms are given in **Figure 14**:

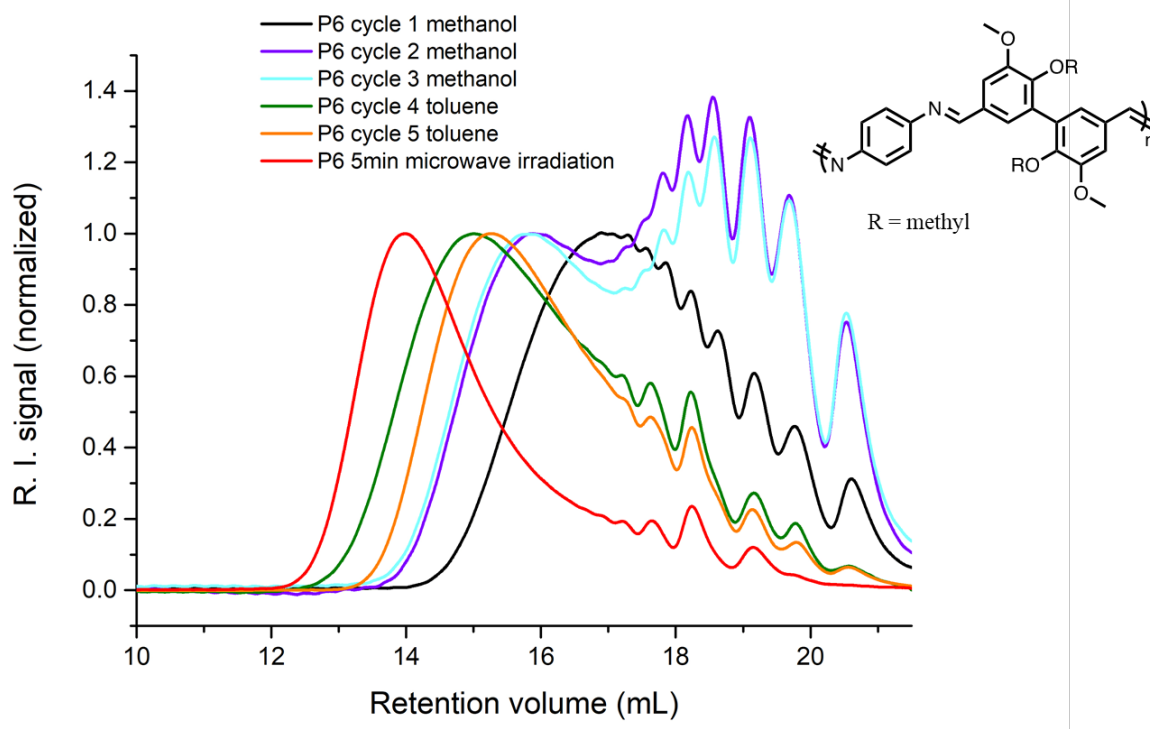


**Figure 14:** SEC traces of P6 in THF synthesized using a rotary evaporator, after different cycles (R.I. detection)

After one cycle, the product obtained exhibits a SEC trace typical of polymer obtained by polycondensation. This proves that the polymerization can happen *in situ*, using only a rotary evaporator. Two more cycles were done, adding and evaporating methanol, to give higher molar masses. However, after these two cycles the molar mass remains similar, with remaining oligomers.

These oligomers were removed by filtration, and toluene was added and evaporated. After this new cycle, the molar mass starts increasing again. This is most likely the effect of filtration. Indeed, as the oligomers with low molar masses are removed from the medium, it enables more reactions between longer chains, leading to the formation of higher molar masses. The slight decrease of molar mass after the final cycle could be due to the reversal of equilibrium, toward the formation of monomer instead of polyazomethines – however, this would imply the presence of water in the reaction medium.

As an example, the SEC trace of a polyazomethine synthesized in five minutes under microwave irradiation and then recovered is shown too in **Figure 14**. Its molar mass is higher than the polyazomethines synthesized using only rotary evaporator, even after multiple cycles. This first step with microwave irradiation forms oligomers that will react more efficiently in the rotary evaporator, giving way to higher molar masses. For these reasons, the new protocol for polyazomethine synthesis is to use microwave irradiation for only five minutes to produce reactive oligomers followed by a recovery step using methanol, leading to chain extension by solvent removal with a rotary evaporator.

## 2.1.4. Stability of divanillin-based polyazomethines

As seen in the previous section, polyazomethines have a good thermal stability, with a degradation temperature above 350°C and even close to 400°C depending on the diamine used. However, polyazomethines can be degraded by other means, as the carbon-nitrogen double bond can be cleaved by hydrolysis,<sup>28</sup> even if some works report stable azomethine compounds.<sup>15</sup> One of the previously synthesized polyazomethines, **P1**, was monitored in terms of absorbance, SEC and <sup>1</sup>H-NMR analysis. This polyazomethine was synthesized without silica. The follow up of **P1** absorbance and its structure are given in **Figure 15**:

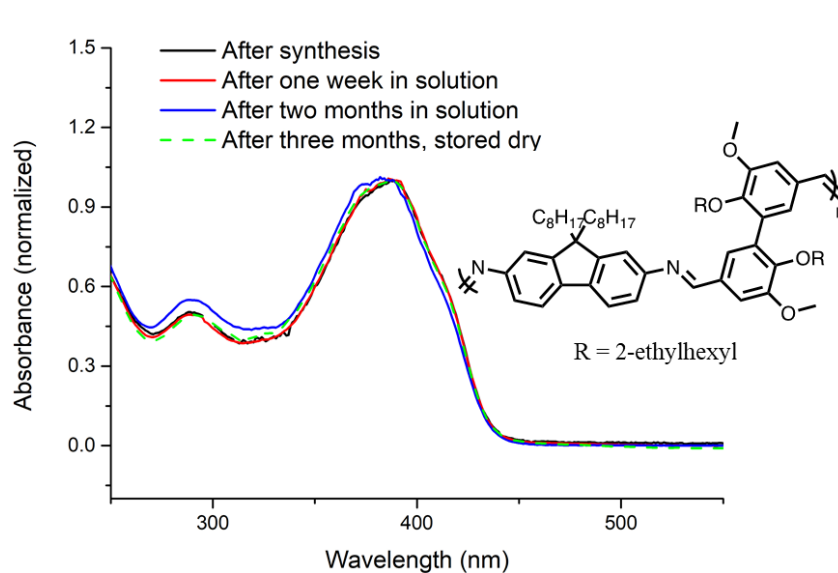


**Figure 15:** Follow up of **P1** absorbance in methylene chloride (10<sup>-2</sup> g/L)

**P1** was kept in solution in methylene chloride, and its absorbance spectrum recorded at different times. After one week kept in solution at RT, the absorbance spectrum remains the same. However, after two months kept in solution in methylene chloride the spectrum shifts slightly towards smaller wavelength. This hypsochromic shift indicates a loss of conjugation, which could be due to hydrolysis. When stored dry, the polyazomethine still has the same absorbance spectrum three months after, even at room temperature.

The SEC trace was also recorded at different times for a **P1** sample kept in solution in THF and compared to one kept dry in the fridge. The SEC chromatograms are compared in **Figure 16** – the chromatograms for the three-month old samples are given separately from the others, as they were analyzed on a different set of columns.

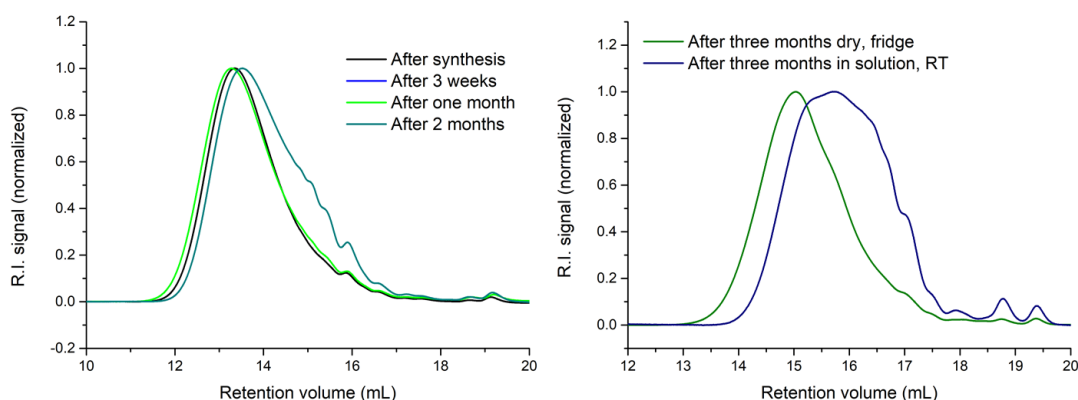


**Figure 16:** Follow up of P1 SEC traces in THF at different times and stored in different conditions (left, all stored in solution; R.I. detection)

After one month, the SEC trace remains the same; there is even a small shift towards higher molar masses. However, after two months the trace shifts towards smaller molar masses, indicating that the polyazomethine starts to degrade, maybe because of hydrolysis. Moreover, the way the polyazomethines are stored is crucial. If kept dry in the fridge the polyazomethine will stay with the same molar mass, even after three months. However, if kept at RT in solution there will be a shift towards smaller molar masses, as is illustrated in **Figure 16**.

As for the NMR analysis, the different spectra are given in **Figure 17**:

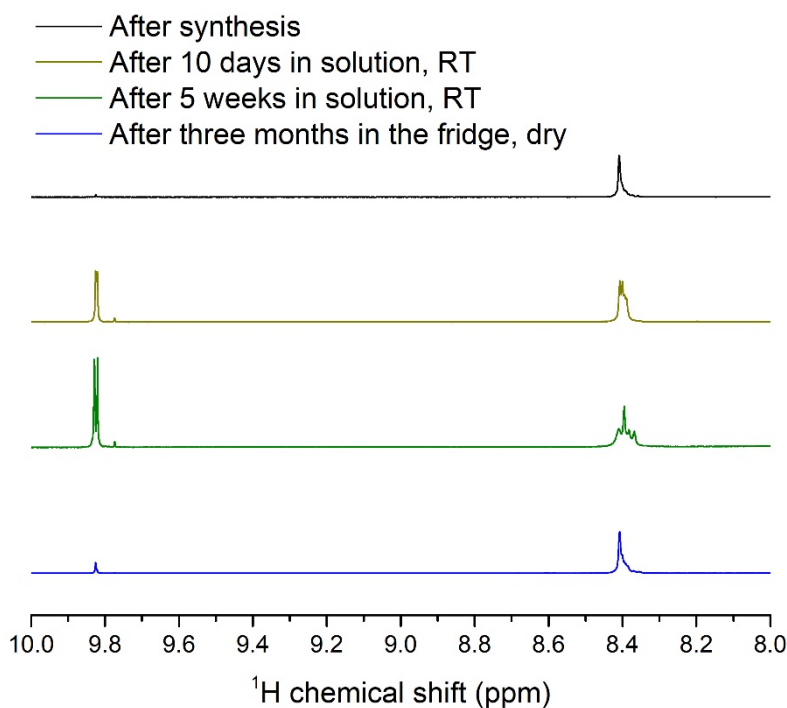


**Figure 17:** Follow up of P1 <sup>1</sup>H-NMR spectrum at different times and stored in different conditions (in CDCl<sub>3</sub>, 128 scans)

After only one week in solution, the azomethine peak starts to get broader and multimodal, while the aldehyde peak gets more intense. These degradations signs get even more obvious after five weeks in solution, as the aldehyde peak gets even more intense. This shows that the chains are degraded after one



week in solution. The same polyazomethine, kept dry in the fridge, has a spectrum slightly different than the one right after the synthesis. The aldehyde peak gets faintly more intense and the azomethine peak a bit broader. Even with those changes, this spectrum is still similar to the one done right after synthesis.

These characterizations showed that the polyazomethine chains could be modified in solution, even after one week, as noticed from  $^1\text{H-NMR}$  analysis. However, the SEC trace does not change significantly after only one week, suggesting that the degradation phenomenon affects the azomethine bond but does not cleave the polymer chains. Furthermore, the polyazomethines stored dried in the fridge keep their absorbance properties, even if after three months the  $^1\text{H-NMR}$  spectrum starts to change. For this reason, the polyazomethines were kept dry at low temperature, and used and analyzed within three months before they were synthesized again. This weak stability for polyazomethines does not necessarily mean that the final OLEDs will be poorly stable too. In this type of devices, the polymers are exposed to different conditions than the ones investigated here, as they are in solid state, stacked between different layers of other active components and with no traces of water.

### 2.1.2. Conclusion for polyazomethine synthesis

Vanillin and acetovanillone were dimerized by enzymatic coupling. This efficient process can be done on a six-gram scale. Divanillin and diacetovanillone were alkylated on their phenol functions with either a methyl or a 2-ethylhexyl moiety. These alkyl groups will give a better solubility to the final polyazomethines. The alkylated monomers were then reacted with various diamines: fluorene diamine, para and meta-phenylene diamine. Syntheses with diacetovanillone did not yield polyazomethines, but rather a mixture of oligomers – this could be due to a lower reactivity compared to divanillin, the latter bringing an aldehyde function instead of a ketone one. Therefore, diacetovanillone was set aside as a monomer, to focus on divanillin. All the divanillin-based polyazomethines are soluble in common solvents, except the one bearing **DVEH** and meta-phenylene diamine. SEC,  $^1\text{H-NMR}$  spectroscopy and ATR-FTIR, confirmed the formation of polymers bearing an azomethine moiety. The polyazomethines have also a high thermal stability, with a degradation temperature above  $350^\circ\text{C}$ . However, the azomethine bond can be derivatized, after only one week in solution, even if the polyazomethine's molar mass remains the same according to SEC analysis. The polyazomethines were kept dry at low temperature, as this seems to slow down the degradation process. They were used within three months and then synthesized again.

The syntheses were done using microwave irradiation for four hours and silica to remove water from the medium. The effect of silica could be observed on the polyazomethine molar masses: polyazomethines bearing **DVEH** have higher molar masses than their counterpart with **DVM**. This could be explained by a change of solubility during synthesis: polyazomethines with longer alkyl group (2-ethylhexyl) are more soluble and will stay longer in solution, whereas polyazomethines with short alkyl group (methyl) will precipitate more easily on silica, stopping the reaction thus yielding lower molar masses.

The protocol was improved, going from four hours of microwave irradiation with silica to five minutes without silica. The key step of the synthesis is actually the recovery, done by dissolving the polyazomethine in dichloromethane and methanol and by evaporating the solvents using a rotary evaporator: the molar mass increases dramatically during this step. It is even possible to obtain polyazomethines by doing only this recovery step. However, the molar masses are higher with five minutes of microwave irradiation before the recovery step, which is why this protocol was preferred to synthesize polyazomethines with relatively high molar masses (up to  $21\,000\text{ g/mol}$ ) and good solubility. These polyazomethines were then characterized in terms of optical properties, as is discussed in the next section.

## 2.2.1. Optical characterization of divanillin-based polyazomethines

The polyazomethines previously synthesized were characterized by absorbance spectroscopy, in methylene chloride. Their spectra are compared in **Figure 18**.

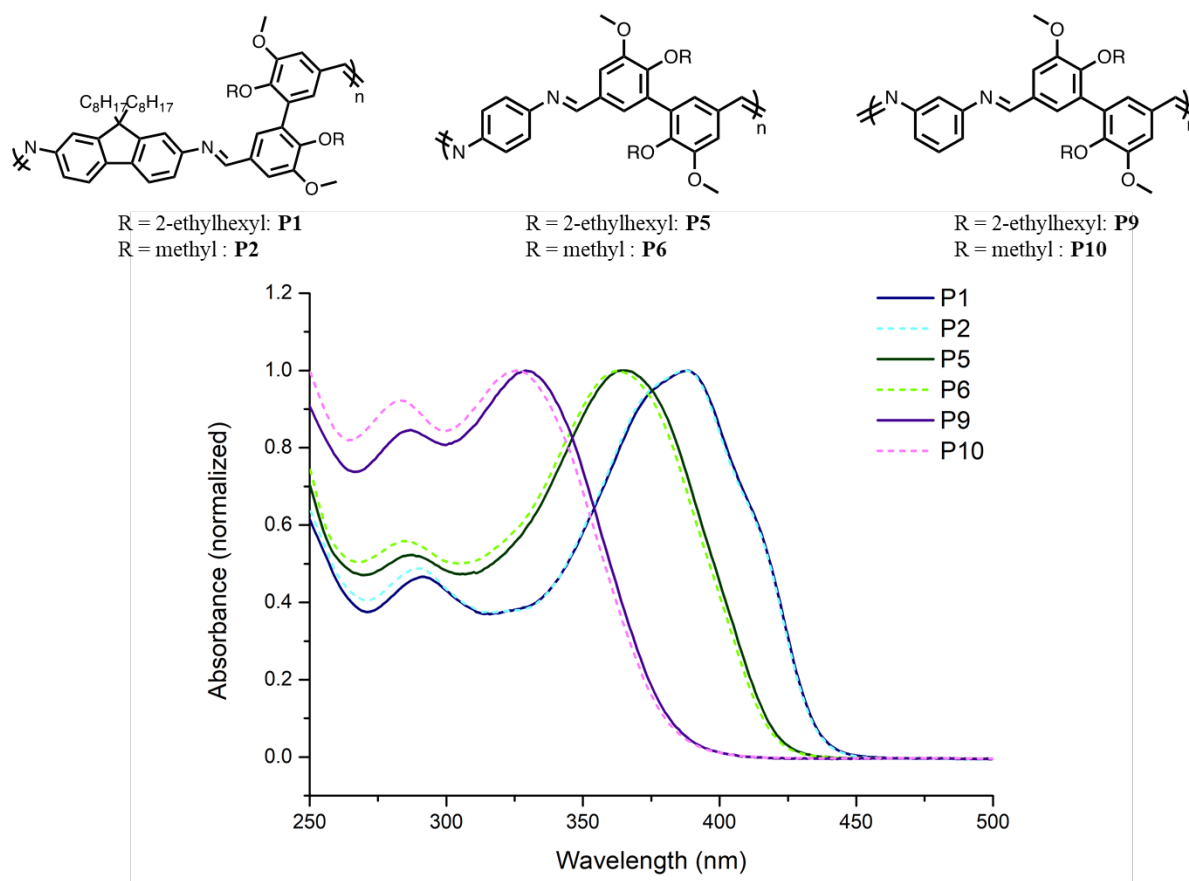


**Figure 18:** Absorbance spectra of polyazomethines in methylene chloride and their structure ( $10^{-2}$  g/L, soluble fraction for **P9**)

All the **DVEH**-based polyazomethines have the same type of absorbance spectrum: first one peak, which could be due to  $\pi$ - $\pi^*$  transition, and then another one at lower wavelength, which could correspond to  $n$ - $\sigma^*$  transitions. **P1** and **P2** also have a slight shoulder towards higher wavelengths. It could be linked to  $n$ - $\pi^*$  transitions, as there are heteroatoms with non-covalent bonds in the polyazomethine (N and O). This shoulder could also be due to aggregates. **P5** and **P6** have similar spectra, but slightly more red-shifted in the case of **P5**, which bears 2-ethylhexyl groups on the side compared to methyl groups for **P6**. **P9** also is slightly more red-shifted than **P10**. This shift toward higher wavelength for polyazomethines bearing 2-ethylhexyl moiety is due to the effect of the pendant alkyl group, and was also observed for the monomers. Indeed, **DVEH** is slightly more red-shifted than **DVM** (see **Experimental part** for spectra). The pendant 2-ethylhexyl group might force the backbone into a more planar conformation, making it more red-shifted. Maybe the branched alkyl segment enables better interdigitation between the polymer chains, leading once again to more planarity and therefore a bathochromic shift.<sup>29</sup> This effect is less detectable with **P1** and **P2**, as there is already two long alkyl groups on the fluorene moiety affecting the planarity: therefore, the presence of a 2-ethylhexyl or a methyl group does not have a detectable effect. Polyazomethines bearing a fluorene moiety (**P1** and **P2**) are the most red-shifted. As the fluorene moiety bears three attached rings, it brings more planarity and a longer conjugation pathway to the polyazomethines, leading to a bathochromic shift. The second most red-shifted polyazomethines are the ones with a para-phenylene moiety (**P5** and **P6**). Besides divanillin,

these latter have only one aromatic ring, meaning the conjugation pathway is shorter. The most blue-shifted of the polyazomethines are the ones with meta-phenylene diamine moiety (**P9** and **P10**); this is due to the meta bond, which interrupts conjugation and leads to a twist in the backbone.

The emission of the polyazomethines was also characterized. As mentioned in the previous section, silica is a pollutant for the polyazomethines: at relatively high concentrations, the acidity of silica unravels the polyazomethine chains as it causes hydrolysis. Moreover, in dilute solutions silica emits in the emission range spectra of the polyazomethines, even if it does not affect the absorbance spectrum. Silica might also dope the polyazomethines by protonation. In **Figure 19**, **P1**'s absorbance and emission spectra are shown with different amount of silica – all solutions were filtered before analysis.

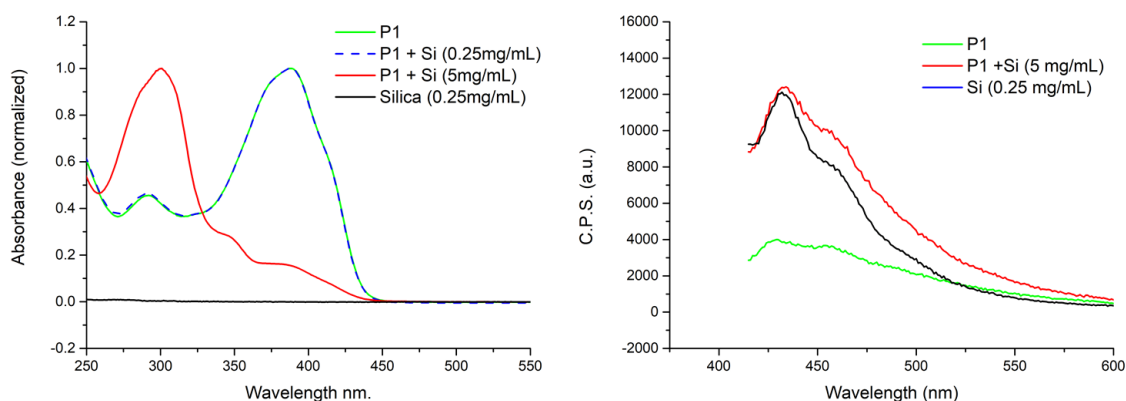


**Figure 19:** Absorbance spectra of **P1** in methylene chloride (10<sup>-2</sup> g/L) with different amount of silica and emission spectra of **P1** (10<sup>-3</sup> g/L, excitation at 360 nm) with and without silica. All solutions were filtered before analysis.

At relatively low concentrations (0.25 mg/mL), silica does not affect the absorbance spectrum of the polyazomethine – however at higher concentrations (5 mg/mL), the absorbance spectrum is dramatically affected. This change is due to hydrolysis: the acidity of silica cleaves the polyazomethines chains and forms monomers again. In addition, the polyazomethines also tend to precipitate on silica (which is removed before analysis), while the monomers do not. All this leads to a new absorbance spectrum with a blue shift.

Emission spectra were recorded with an excitation at 365 nm, to avoid the solvent Raman peak, as the fluorescence quantum yields are quite low. The emission spectra of silica and **P1** with silica (5mg/mL) are similar, with two well-defined peaks at 430 and 460 nm. However, the spectrum of **P1** is actually broad and not well structured, as expected for a polymer. This proves that silica affects the emission spectra, even if it does not absorb in the range used. Even traces of silica on glassware and cuvettes are enough to bias the emission spectra of polyazomethines.

For these reasons, only the spectra of polyazomethines synthesized without silica will be discussed. To improve the quality of the spectra, these latter were recorded with higher concentrations to get a more intense signal and the excitation was done at lower wavelength than the absorbance maximum. This enables shifting slightly the Raman peak of the solvent, to better see the emission of the polyazomethines.

The spectra of the polyazomethines are shown in **Figure 20**:

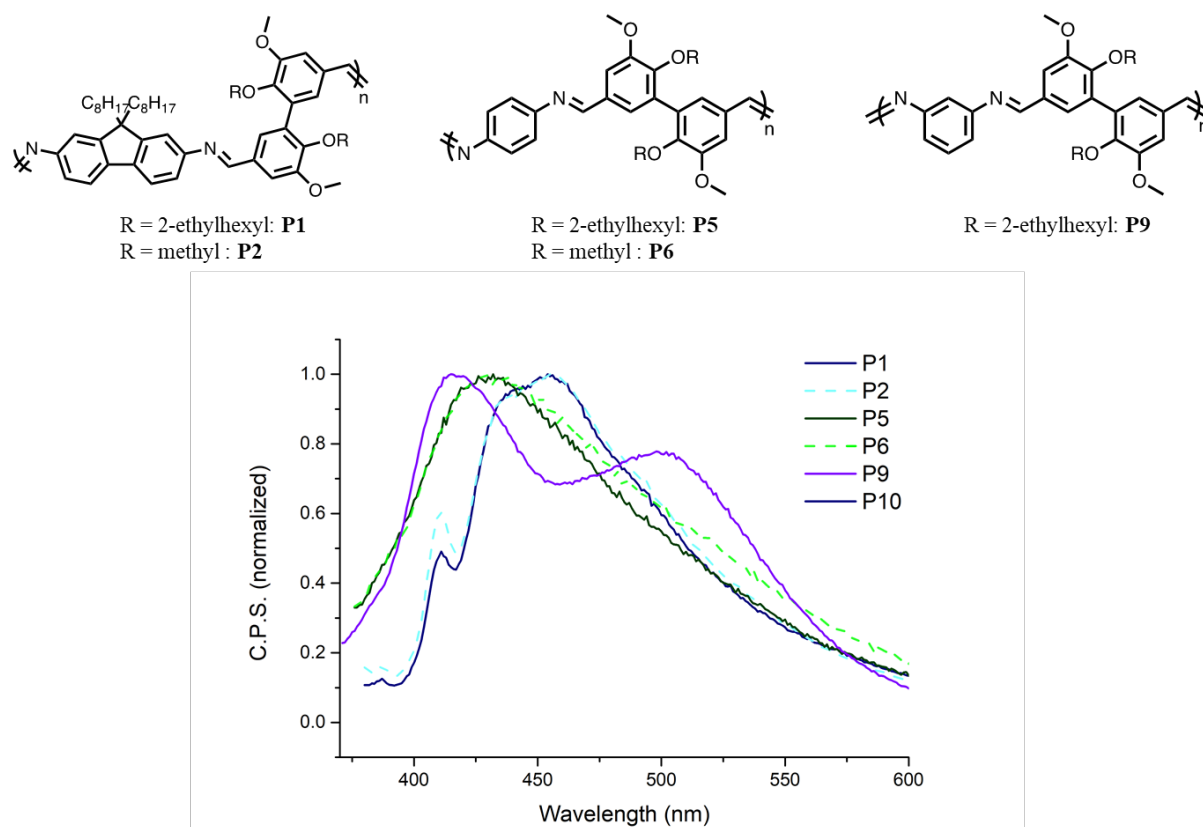
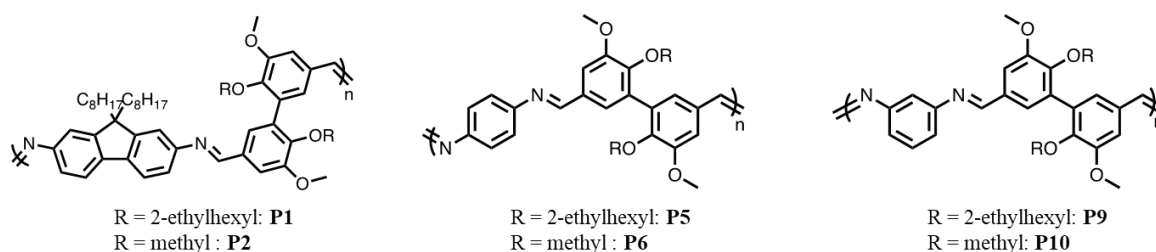


**Figure 20:** Emission spectra of polyazomethines in methylene chloride and their structure ( $10^{-2}$  g/L, soluble fraction for **P9**, integration time: 0.5s)

**P1** and **P2** have the same emission spectrum demonstrating that pendant alkyl moieties do not affect their emission properties. **P5** and **P6** have also similar spectra, even if **P6** exhibits a slight shoulder towards higher wavelength, probably due to the formation of aggregates. For **P9**, the spectrum has two peaks, the first one corresponding to the fluorophore emitting at the maximum of absorbance (325 nm) and the second one to the spectrum obtained when the polyazomethine is excited at 400 nm, a wavelength at which the polyazomethine barely absorbs. As the solution is quite concentrated, this additional peak could also be due to aggregates, excimer or charge transfer complexes. In the case of **P10**, the spectrum is very broad, which could be explained by the superposition of two peaks, as for **P9**. For clarity, the spectrum of **P10** was not added to **Figure 20** but can be found in the **Experimental part**.

The absorbance and emission properties of the polyazomethines were also characterized in films, and are summed up in **Table 5** with the data for polyazomethines in solution:



| Name | Absorbance                      |                                  | Emission                        |                                  |
|------|---------------------------------|----------------------------------|---------------------------------|----------------------------------|
|      | $\lambda_{\max}^{\text{sol a}}$ | $\lambda_{\max}^{\text{film b}}$ | $\lambda_{\max}^{\text{sol a}}$ | $\lambda_{\max}^{\text{film b}}$ |
| P1   | 388                             | 392                              | 455                             | 470 - 560                        |
| P2   | 388                             | 395                              | 455                             | 470 - 515                        |
| P5   | 365                             | 371                              | 432                             | 460 - 510                        |
| P6   | 363                             | 371                              | 432                             | 465 - 525                        |
| P9   | 330                             | 342                              | 415 - 500                       | 500                              |
| P10  | 326                             | 336                              | 390 - 488                       | 490                              |

**Table 5:** Sum up of the polyazomethines optical properties, in solution and in film <sup>a</sup> In methylene chloride,  $10^{-2}$  g/L <sup>b</sup> Films prepared by drop-casting on quartz plate

The maximum of absorbance is red-shifted in films compared to the absorbance in solution. This bathochromic shift is due to a rearrangement of the polyazomethine chains in films, as the chains can get more planar than in solution. It appears that the alkyl side groups have an effect on this bathochromic shift: in film, **P2** is more red-shifted than **P1**; but **P9** is more red-shifted than **P10**. The methyl pendant group might get **P2** more planar than **P1**. Maybe the 2-ethylhexyl moiety on **P1**, combined with the alkyl groups of the fluorene moiety create more constraint. For **P5** and **P6**, the pendant alkyl groups do not have an impact on the absorbance maximum in films. However, **P9** is red-shifted compared to **P10**, which could be due to more constraint for **P10**. Another factor to take into account is the thickness and homogeneity of the films, which can affect the optical properties observed.

With respect to emission properties, all the polyazomethines present a charge transfer-like behavior in films. Indeed, their most intense emission is obtained when exciting them at a wavelength at which they barely absorb, which is typical of charge-transfer (CT) like behavior. When an electron donor/acceptor molecule is excited, it can form a locally excited state (LE) or an excited state with a larger dipole moment, which will be called CT state.<sup>30</sup>

A CT state has a low overlap with the ground state, which is why it has a low absorption – it also has a different geometry from the ground state, which gives a broad and structure-less emission spectrum. For a locally excited state, the maximum of emission is obtained when exciting the compound at the most intense absorbance wavelength. However, for a charge transfer state the maximum of emission is obtained when exciting at a higher wavelength than the maximum of absorbance, as illustrated in **Figure 21**.

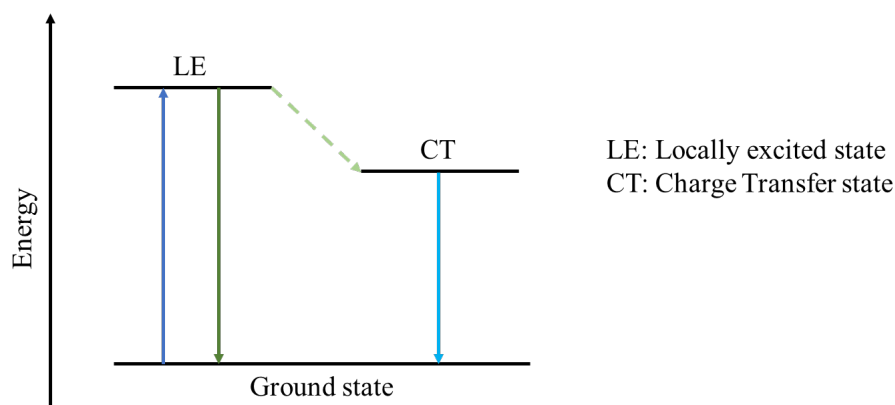


**Figure 21:** Schematic energy diagram of LE and CT states

This CT-like behavior is extremely potent for **P9** and **P10**, as this is the only phenomenon that can be observed in films, overpowering the emission of the locally excited state. For the other polyazomethines, it can be also observed, with some shift depending on the alkyl group. As already discussed, the thickness of the film or its homogeneity could explain this feature. Emission in films is exemplified in **Figure 22** for **P1**:

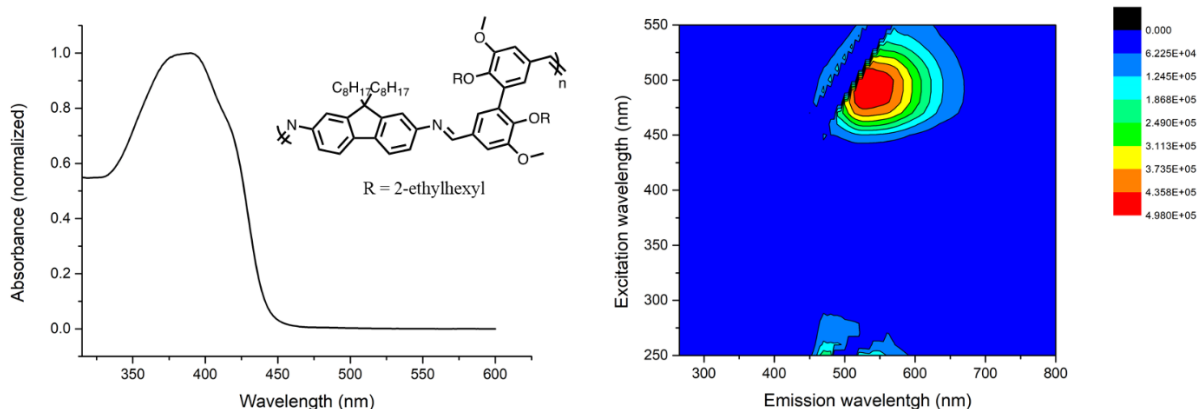


**Figure 22:** Absorbance spectrum and emission-excitation spectra of **P1** in film (drop-casted on quartz)

**P1** has a maximum of emission when excited around 500 nm, a wavelength at which it barely absorbs anymore. This could be due to charge-transfer that is more potent on film, as the chains can arrange and stack themselves more closely.

### 2.2.2. Optical properties of divanillin-based polyazomethines: conclusion

The polyazomethines synthesized have absorbance maxima ranging from 325 nm to 390 nm, depending on the diamine used. The ones with the fluorene moiety are the most red-shifted, as they have the longest conjugation pathway. The pendant alkyl group has also an impact on the absorbance maxima, also depending on the diamine used. The pendant alkyl moiety of divanillin does not affect the polyazomethines' properties when combined with fluorene moiety, while the other polyazomethines with meta or para-phenylene diamines are slightly more red-shifted when they contain divanillin with 2-ethylhexyl moiety instead of methyl group.

The polyazomethines emit in the visible range, from 400 to 600 nm. They emit weakly in solution, in agreement with literature data.<sup>15</sup> Due to the conditions used to obtain the spectra (relatively high

concentrations) quantum yield could not be measured properly. The polyazomethines have also a potential charge transfer-like behavior, especially in films. Indeed, they emit intensely when excited at a wavelength at which they barely absorb. To better understand this unexpected emission behavior, some model compounds were synthesized and characterised and will be discussed in the next section.

### 3. Model compounds of divanillin-based polyazomethines

#### 3.1. Synthesis of model compounds

To better understand the optical and physical properties of the vanillin-based polyazomethines, model compounds were designed. Vanillin and divanillin derivatives, bearing either a methyl or a 2-ethylhexyl group were synthesized to see the influence of the alkyl group on the opto-electronic properties. In addition, the impact of the position of these substituents was also investigated, by synthesizing model compounds based on ortho-vanillin. These vanillin derivatives were then reacted with a diamine or a mono-amine, to prepare dimers or trimers as models of the polyazomethine backbone (**Figure 23**).

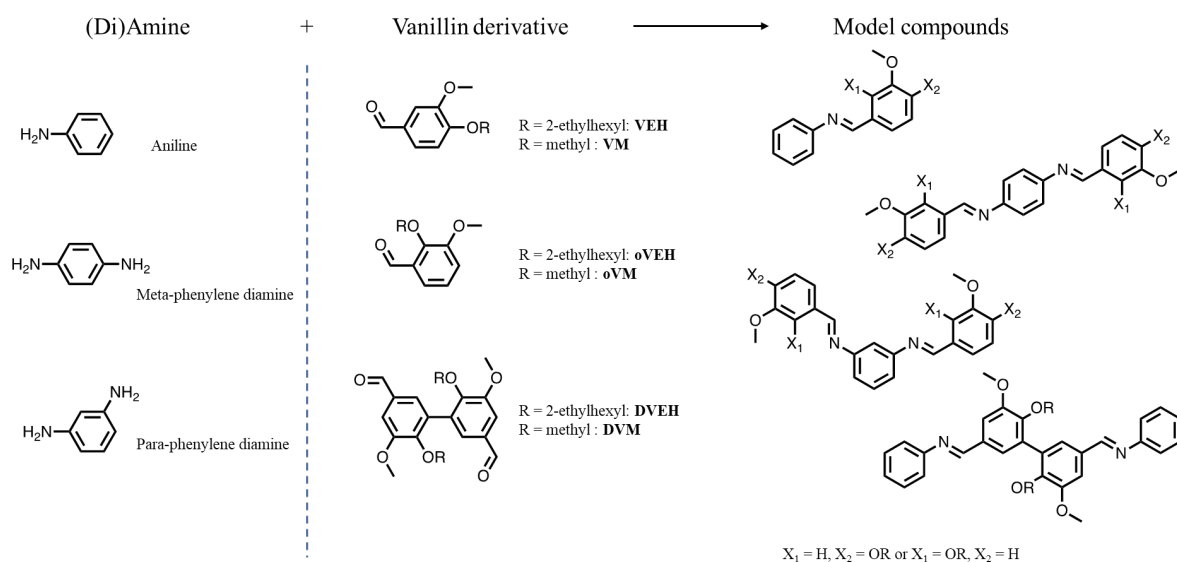


**Figure 23:** Structures of the model compounds of vanillin-based polyazomethines

The vanillin derivatives were alkylated using the same protocol as previously described. The model compounds were synthesized following different experimental conditions: four hours at 130°C in toluene under microwave irradiation or conventional heating. These latter compounds were then recovered as a mixture of isomers as the azomethine bond can either be cis or trans. This leads to the presence of two peaks at 8.43 and 8.39 ppm on the <sup>1</sup>H-NMR spectrum, as exemplified in **Figure 24** in the case of VM and para-phenylene diamine.

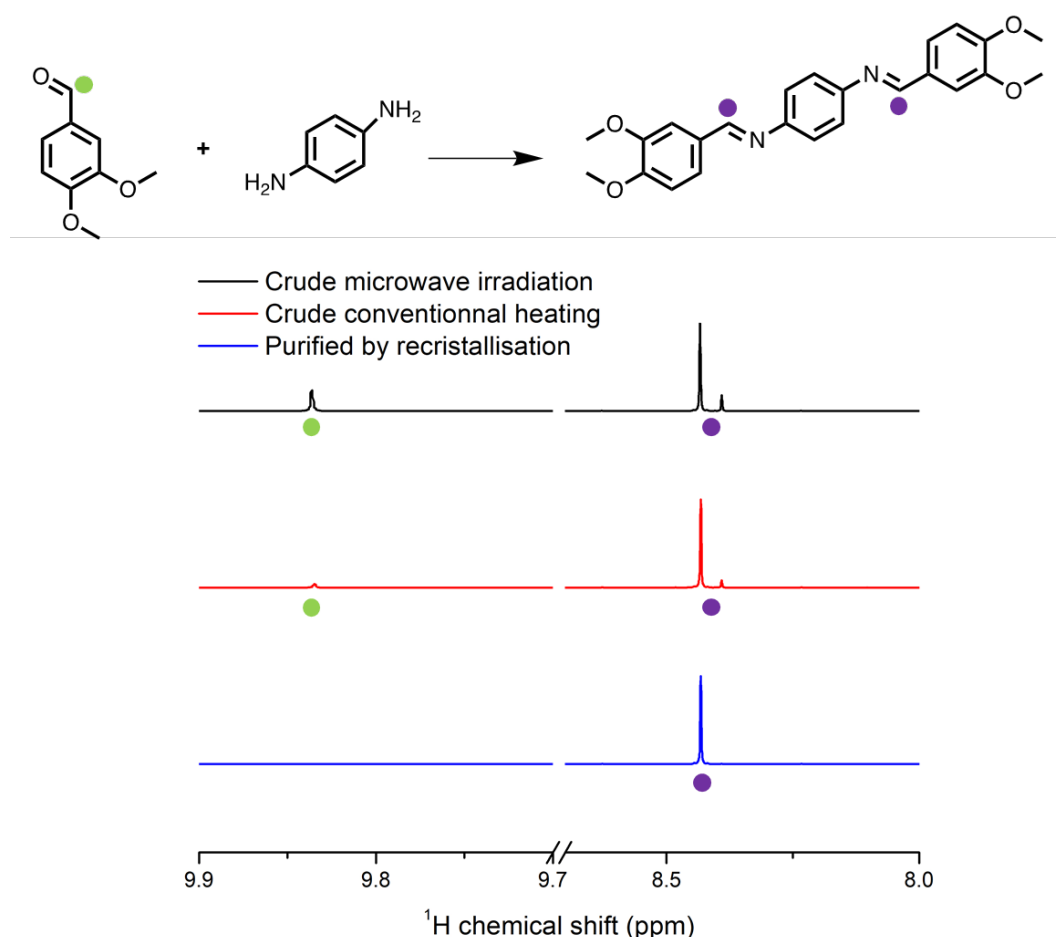


**Figure 24:** Scheme and  $^1\text{H}$ -NMR spectra of a model compound with VM and para-phenylene diamine, with different experimental conditions ( $\text{CDCl}_3$ )

The (E, E) structure represented in **Figure 24** is theoretically the main one as it is the most thermodynamically stable,<sup>31</sup> but there are also other isomers in the crude: E, Z and Z, Z. To remove residual reactants and isolate the main isomer, the model compounds were purified. At first, they were separated by flash chromatography using a silica column and methylene chloride/methanol as eluent. Unfortunately, these conditions led to the degradation of the compounds, most likely due to the acidity of the silica coupled with methanol. Precipitation was also tested as a way to purify the model compounds, but this process was not selective enough.

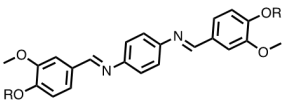
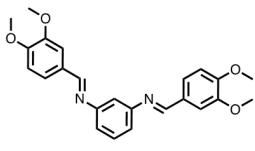
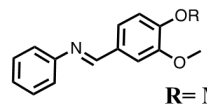
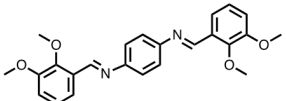
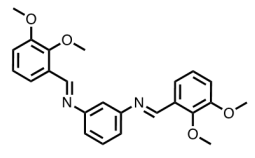
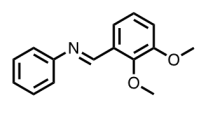
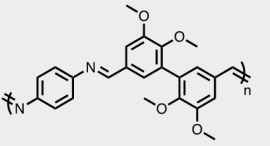
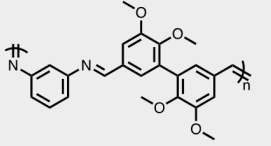
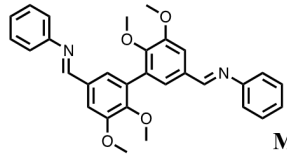
To obtain pure model compounds, the experimental conditions were changed: going from four hours in toluene using microwave irradiation to 30 minutes using conventional heating and methanol at the reflux.<sup>31</sup> This change of experimental conditions synthesis enables us improving the yield, going from 87% to 97%, as is highlighted in **Figure 24**. The purification method chosen was recrystallization: it enables to recover the desired product with high purity to be characterized by single-crystal X-Ray Diffraction (X-RD). As is apparent in **Figure 24**, after purification by recrystallization, there is no remaining aldehyde, and only one azomethine peak meaning that there is only one isomer isolated, the E, E one.

The method of recrystallization required two solvents, methylene chloride and methanol respectively: one in which the molecule is soluble at various temperatures, and the other at which it is soluble only at relatively high temperature. The mixture of isomers was first dispersed in the bad solvent (methanol), at low temperature. The solution was then warmed up close to the boiling point of methanol, and the good solvent (methylene chloride) was added dropwise. As soon as the solution was completely limpid,



the solution was filtered and then left to cool down to room temperature slowly. If the cooling down is too harsh, the compound might precipitate or form crystals too small for X-RD. The model compounds with 2-ethylhexyl groups were set aside to focus on the ones bearing a methyl substituent, more prone to recrystallize.

In **Table 6**, a sum up of the model compounds that were synthesized and recrystallized is given with their names, yields and E/Z ratio in the crude.

|  | Para-phenylene diamine  | Meta-phenylene diamine  | Aniline   |
|--|---|---|---|
| <b>VM</b>                              | <br>R = Me: <b>M1</b><br>R = H: <b>M1'</b> | <br><b>M2</b>    | <br>R = Me: <b>M3</b><br>R = H: <b>M3'</b> |
| Conversion (E/Z in crude) <sup>a</sup> | <b>M1: 95% (E/Z : 92/8).</b><br><b>M1': 85% (E/Z : 85/15)</b>   | <b>96% (E/Z : 95/5)</b>   | <b>M3: 94% (E/Z : 100/0)</b><br><b>M3': 95% (E/Z : 100/0)</b>   |
| <b>oVM</b>                             | <br><b>M4</b>                              | <br><b>M5</b>    | <br><b>M6</b>                              |
| Conversion (E/Z in crude) <sup>a</sup> | <b>95% (E/Z : 90/10)</b>  | <b>80% (E/Z : 75/25)</b>  | <b>84% (E/Z : 100/0)</b>  |
| <b>DVM</b>                             | <br><b>P6</b>                            | <br><b>P10</b> | <br><b>M7</b>                             |
| Conversion (E/Z in crude) <sup>a</sup> |   |   | <b>98% (E/Z : ND)</b>   |

**Table 6:** Sum up of the model compounds of vanillin-based polyazomethines synthesized and recrystallized  
<sup>a</sup> Determined by <sup>1</sup>H-NMR analysis of the crude molecule in CDCl<sub>3</sub>

All the model compounds are soluble in common solvents (THF, toluene, chloroform, methylene chloride), except the two synthesized with non-methylated vanillin and divanillin (**M1'** and **M3'**); these latter are soluble in DMSO and were recrystallized using cyclohexane and methylene chloride. This highlights the importance of the alkyl substituents, which help in the solubilisation. Without these substituents, even a small molecule like **M3'** is poorly soluble. This implies that a polyazomethine chain like **P6** synthesized without alkylating first the divanillin would also be poorly soluble. As will be discussed in the next section, the E configuration is the one that was isolated after recrystallization – this was confirmed by X-RD. It is possible to calculate a ratio of E/Z azomethine bond using <sup>1</sup>H-NMR spectrum on the crude. As a general trend, the E isomer is the most present in the crude and is even the only isomer for molecules with only one azomethine bond (**M3**, **M3'** and **M6**). However, there are comparatively much more Z isomer for **M5** and **M1'**. This could be due to interactions between the nitrogen of the azomethine bond and the substituent in ortho position, or to hydrogen bonding. Interestingly, this increase of Z isomers is accompanied with a lower yield.

The structures were confirmed by <sup>1</sup>H- and <sup>13</sup>C-NMR spectroscopy, and the spectra can be found in the **Experimental part**. The model compounds were also analyzed by X-RD, as will be discussed in the next section.

## 3.2. X-Ray Diffraction characterization of model compounds

The model compounds were resolved by X-RD; for all of them, the E isomer was solved. Aside from this unequivocal isomer determination, X-RD also enables determining the angle for the azomethine bond with the phenyl ring bearing the nitrogen atom as can be seen in **Figure 25**.

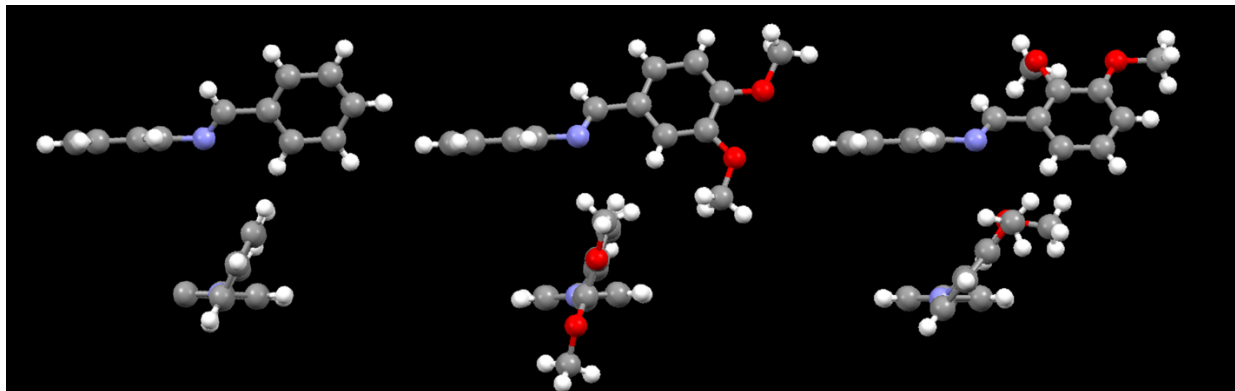


**Figure 25:** Face and side view of the X-RD structure of (E)-N-benzylideneaniline, **M1**, and **M3**

Burgi *et al.*<sup>32</sup> solved the structure of benzylideneaniline – the angle between the plan of the phenyl ring and the one of the aniline moiety (noted  $\theta_1$ ) is  $65.5^\circ$  for this molecule without any substituents. This twist is due to the interactions between the azomethine bond and the substituents on the phenyl group, in this case the protons. Comparatively, the vinylenes counterparts of azomethines are coplanar.<sup>33</sup> For **M1** the angle between azomethine bond and phenyl is  $69.1^\circ$ , while for **M3** it goes down to  $51.8^\circ$ . This is due to the interactions between the methoxy at the ortho positions and the azomethine bond, which help enhancing the planarity. This angle is even lower for **M1'**, which is the equivalent of **M1** but with a non-methylated vanillin. For this model compound, there are two types of molecule in the lattice, linked together by interaction between the phenol of one molecule and the azomethine bond of the other one. This leads to more planarity, as one molecule has a  $\theta_1$  of  $39.7^\circ$  and the other of  $15.7^\circ$  (see **Figure 26**).

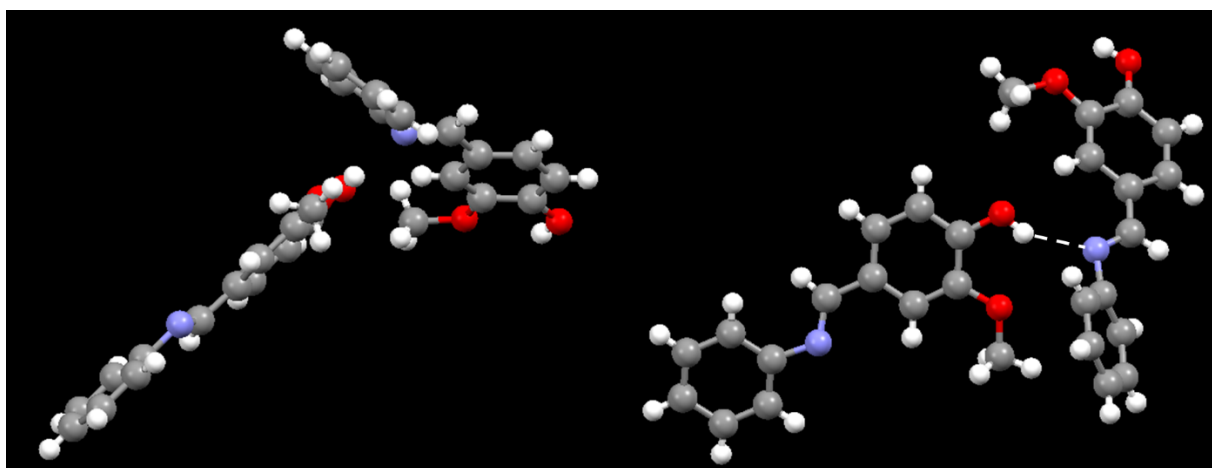


**Figure 26:** X-RD structure of the two molecules present in the lattice of **M1'**, with drawn hydrogen bond

**M2**, which has a meta-phenylene moiety, has also low  $\theta_1$ ,  $26.2^\circ$  and  $20.9^\circ$  for the two azomethine bonds respectively. However even if they appear more planar, the molecules in the lattice seem to twist around each other, as is shown in **Figure 27**. This could explain the poor solubility of the corresponding polymer, as chains might twist around each other helicoidally.

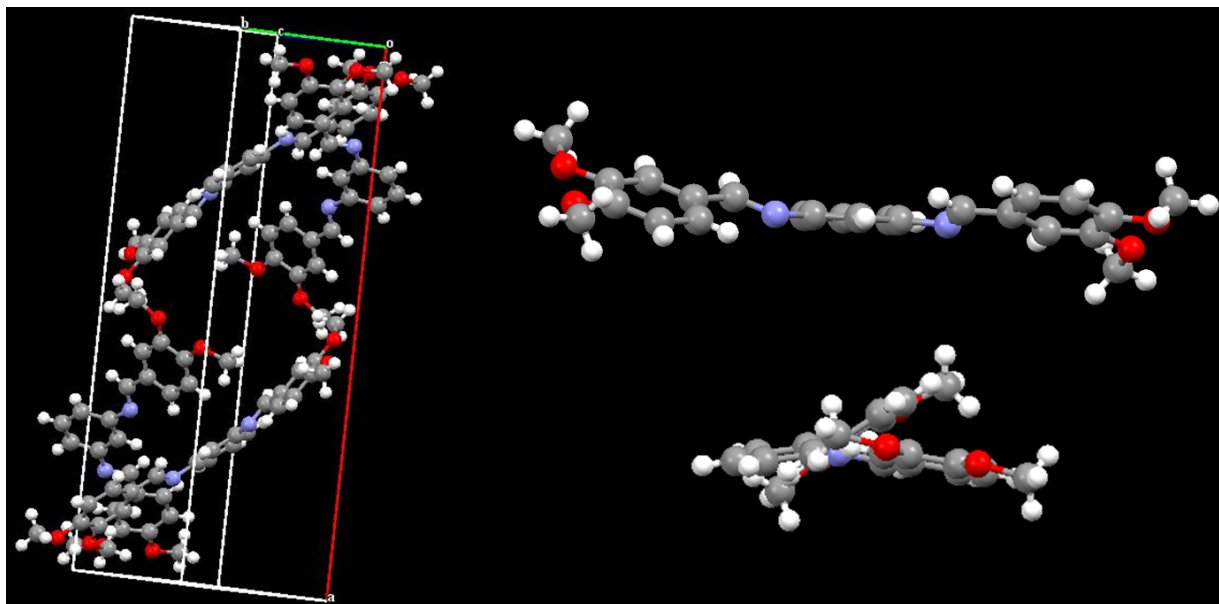


Figure 27: X-RD structure of **M2** in lattice (left) and face and side view (right)

Comparatively, **M1** has  $\theta_1$  of  $42.4^\circ$ . The molecules go two by two in the lattice and are linked to each other on the side by interactions between the oxygen and hydrogen of the vanillin rings. Therefore, the vanillin rings are nearly parallel or coplanar with each other. Moreover, with its relative planarity and symmetry, **M1** can achieve  $\pi$  stacking, as two molecules can stack neatly on top of each other (See Figure 28).

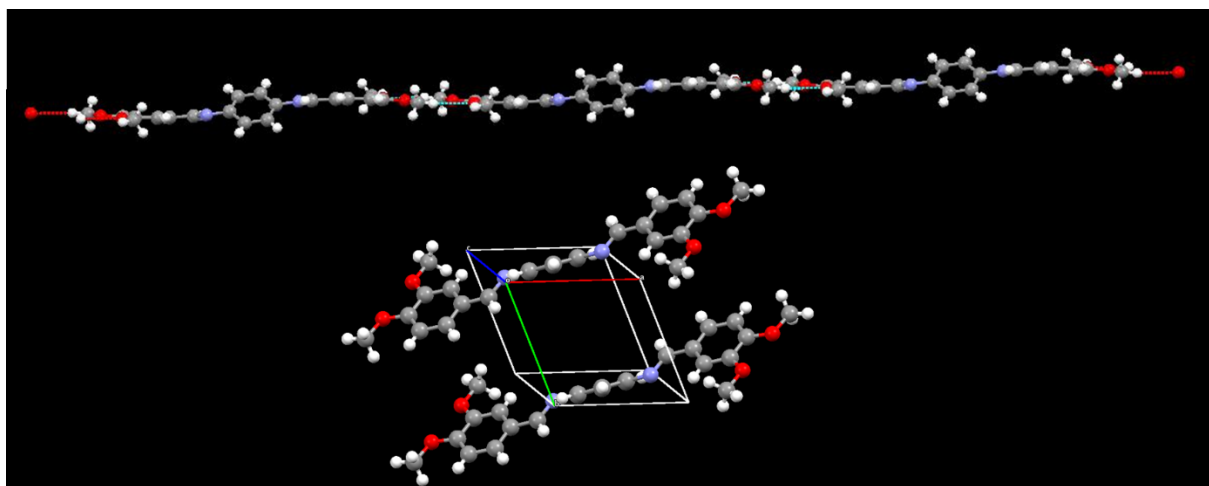


Figure 28: X-RD structure of three molecules of **M1** face view, with short interactions represented (top), and in lattice (bottom)

**M4**, which also has two para bonds but bears ortho-vanillin moieties, cannot achieve  $\pi$  stacking, even if it has relatively low  $\theta_1$  ( $47.2^\circ$ ). This absence of  $\pi$  stacking could be due to steric hindrance and interactions between the oxygen and hydrogen of methoxy moieties, as is illustrated in Figure 29.

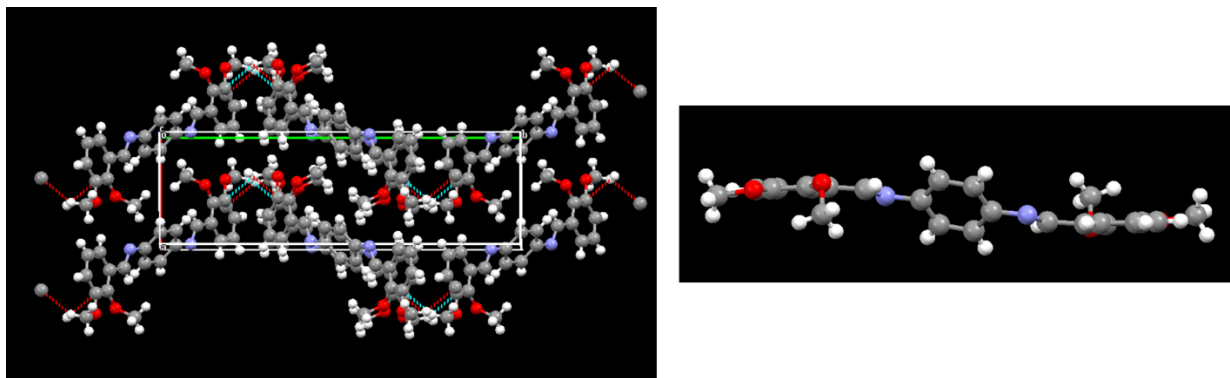


Figure 29: X-RD structure of M4 in lattice (left, short contact represented) and face view (right)

M5, the counterpart of M4 but with meta bonds, does not present the same short contact interaction as M4, neither does it achieve  $\pi$  stacking. The molecules also do not twist around each other as opposed to M2, as is shown in Figure 30.

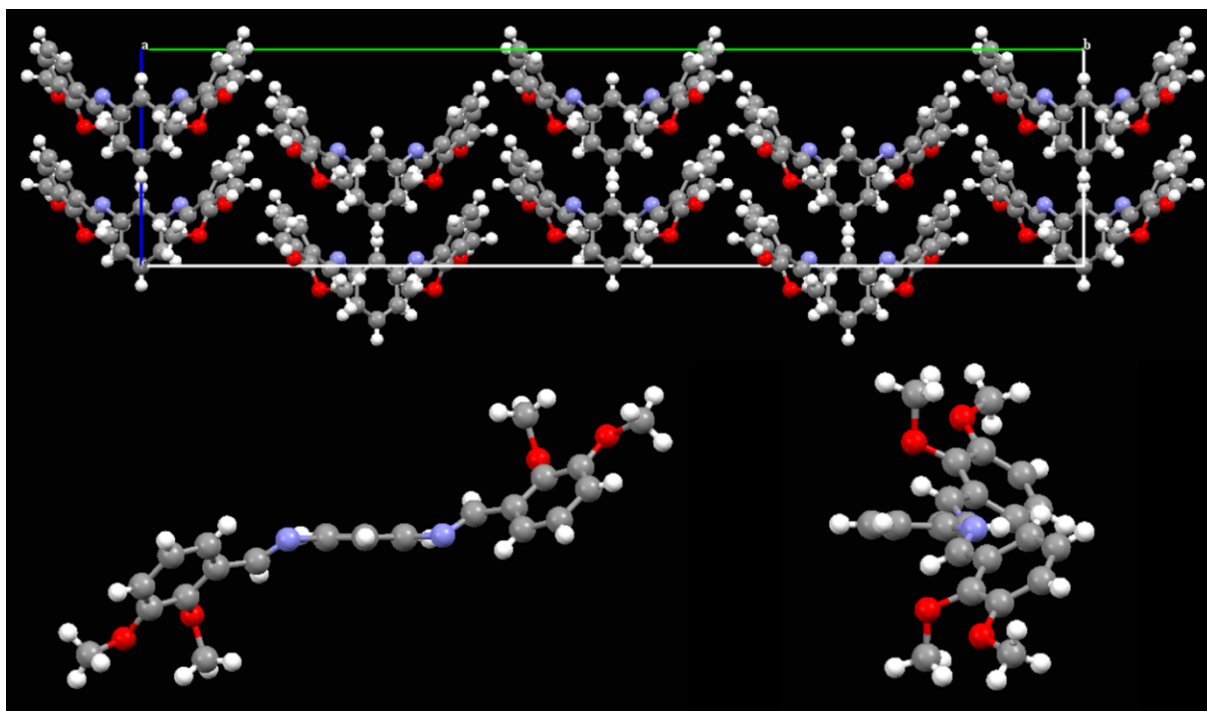
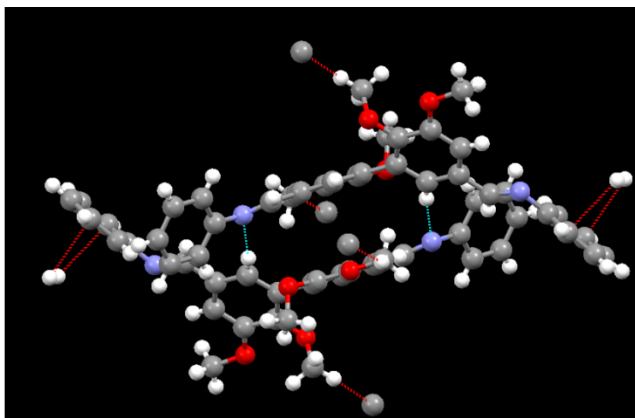
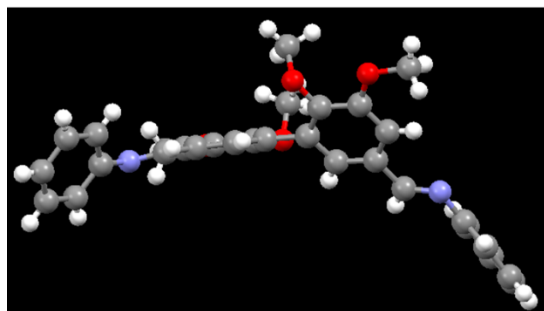


Figure 30: X-RD structure of M5, in lattice (top), face and side view (bottom)

The model compound **M7** has a **DVM** moiety between two phenylimino moieties – its structure solved by X-RD is given in **Figure 31**:



**Figure 31:** X-RD structure of a single molecule of **M7**

The twist between the two aromatic rings of the divanillin can be observed: it is a torsion angle of  $126.9^\circ$ . **M7** has  $\theta_1$  of  $57.1^\circ$  and  $54.7^\circ$  for each azomethine bond. In **Figure 31**, one molecule in the lattice is also represented with another one, with the short contact interactions between them. These molecules also twist around each other. Moreover, there are some interactions between the nitrogen of the azomethine bond and the hydrogen on the rings of the divanillin. These interactions suggest the formation of charge transfer complex, between the two molecules. Indeed, these interactions can create a dipole in the molecule, with the nitrogen of the azomethine acting as an acceptor and the electron rich ring of the divanillin acting as a donor.

### 3.3. Optical characterization of vanillin-based model compounds

The model compounds were also characterized in terms of absorbance: the absorbance spectra of **M1**, **M3**, **M7** and **P6** are shown in **Figure 32** with their structure:

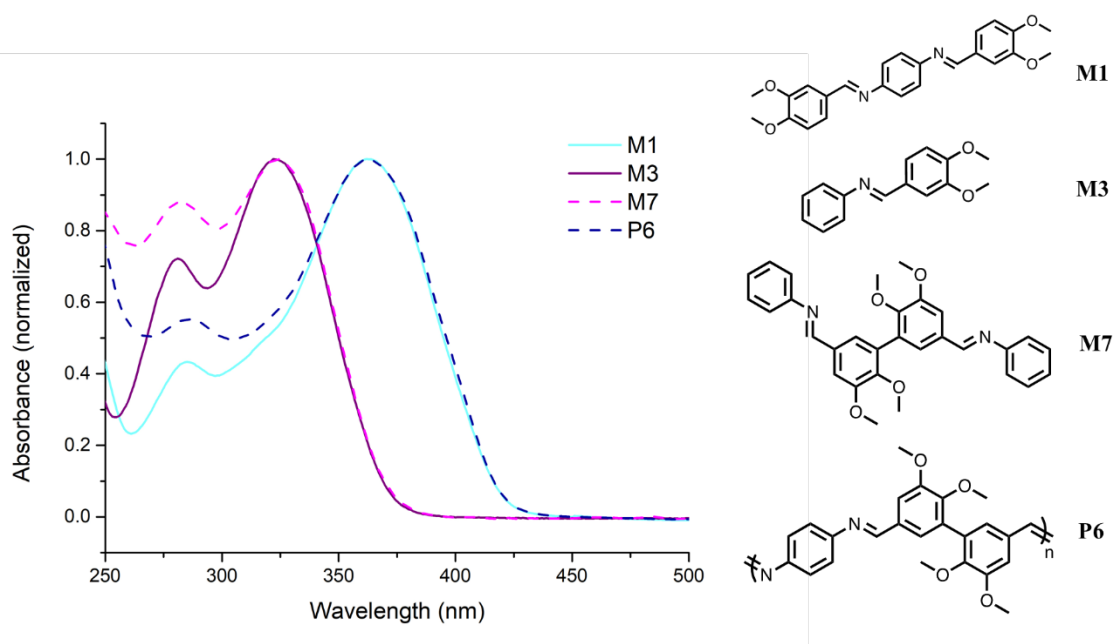


**Figure 32:** Absorbance spectra of **M1**, **M3**, **M7** and **P6** in methylene chloride ( $10^{-2}$  g/L)

**M1** is more red-shifted than **M3**, which is expected, as **M1** has a longer conjugation pathway than **M3**, with its three aromatic rings. However, **M3** and **M7** have the same absorbance maximum: **M7** should be at least slightly shifted, as it corresponds to twice **M3** – yet this is not the case. There is actually a slight change on the second peak of the absorbance spectrum, at 280 nm – this peak is comparatively more intense for **M7** than for **M3**. **M1** also has the same absorbance maximum as **P6** – **P6** should be more red-shifted, as it corresponds to a polymer chain, which should have a longer conjugation pathway, and yet this is once more not the case. The identical absorbance spectra of **M1** and **P6** are due to the bond between the aromatic rings of the divanillin, which is in meta with respect to the azomethine bonds. This meta bond marks the end of the conjugation pathway in the polyazomethine, but also in the model compound. This is the reason why **M3** and **M7** have the same absorbance maximum: even if **M7** is twice longer than **M3**, the two halves are linked by a meta bond, which dramatically lowers, and even breaks conjugation. This is also true for **P6** – the length of the conjugation pathway is dictated by the meta bond of divanillin. **P6** has the same absorbance as **M1**, the latter having the longest possible length along the polymer chain without encountering a meta bond.

**Figure 33** compares the absorbance of model compounds with meta-phenylene diamine. **M2** and **P10** have nearly the same absorbance maximum, as **M2** is slightly more red-shifted than **P10**. This could be due to constraints and hindrance along the polymer chains that are not present in the corresponding model compound. **M3** is blue shifted compared to the two others: this is most likely due to the presence of only one azomethine bond on the central phenyl ring and not due to an extension of conjugation.

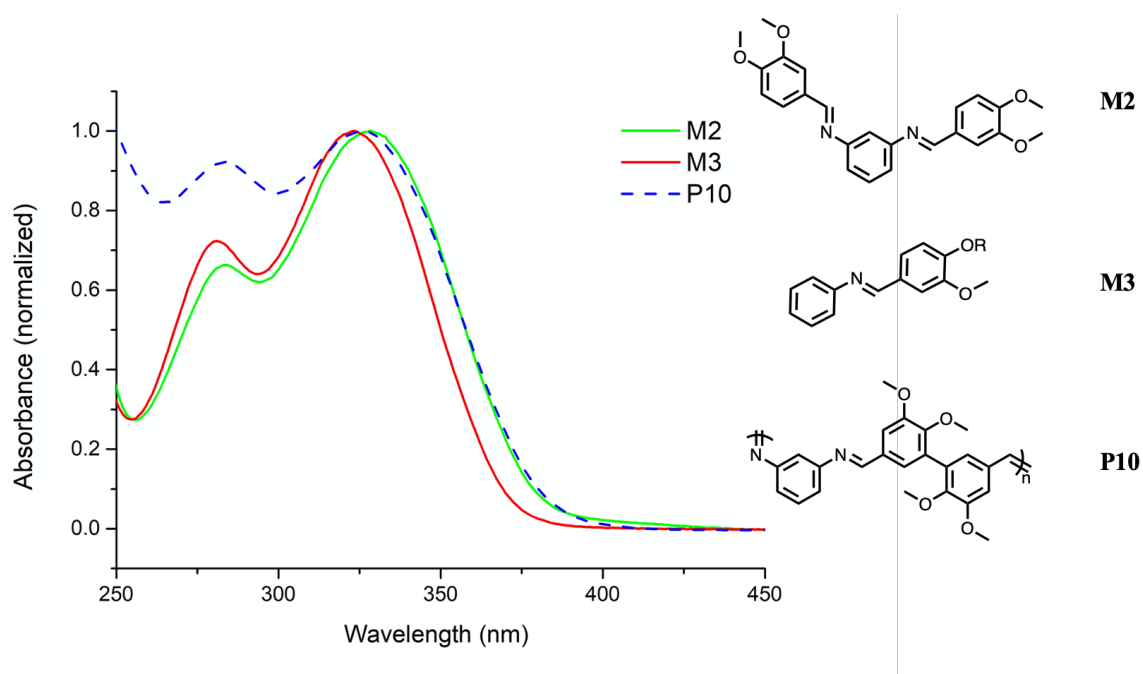


**Figure 33:** Absorbance spectra of **M2**, **M3** and **P10** in methylene chloride ( $10^{-2}$  g/L)

The absorbance spectra of the model compounds based on **oVM** are given in **Figure 34**:

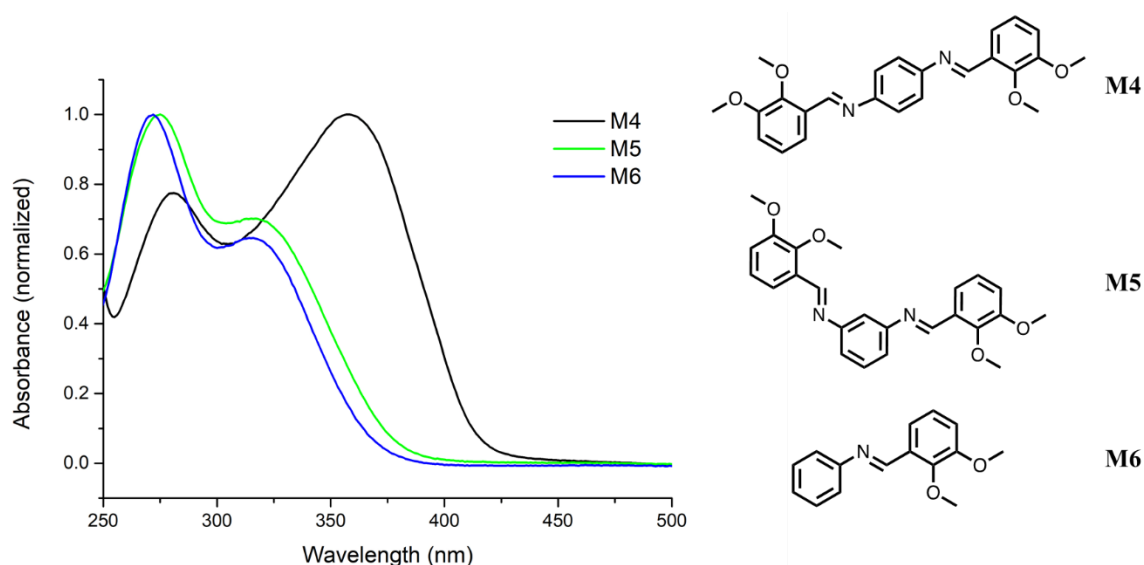


**Figure 34:** Absorbance spectra of **M4**, **M5** and **M6** in methylene chloride (10<sup>-2</sup> g/L)

The most red-shifted of the three is **M4**, which has the longest conjugation pathway, without any meta bond. **M5** and **M6** have nearly the same absorbance maximum, but slightly more red-shifted and relatively more intense for **M5**. Moreover, the shape of these two spectra is different from the other spectra observed until now: in this case, the most intense peak is the one toward 270 nm, and not the one around 320 nm. The peaks at 320 nm correspond to  $\pi$ - $\pi^*$  interactions – in these molecules, the interactions between  $\pi$  orbitals might be affected and weakened by the closeness of the methoxy group in ortho position to the azomethine bond. This proximity could lead to a weaker signal, while the peak around 270 nm is less affected.

The absorbance characterizations are summed up in **Table 7**.

|     |     |     | Name    | Absorbance maximum <sup>a</sup> | $\epsilon$ toluene <sup>b</sup><br>( $\text{cm}^{-1} \cdot \text{mol}^{-1} \cdot \text{L}^{-1}$ ) | $\epsilon$ dichloromethane <sup>a</sup><br>( $\text{cm}^{-1} \cdot \text{mol}^{-1} \cdot \text{L}^{-1}$ ) |
|-----|-----|-----|---------|---------------------------------|---|---|
| VM  | M1  |     |         | 363 - 285                       | 40 700  | 34 400  |
|     |     | M2  |         | 328 - 284                       | 29 100  | 29 600  |
|     |     |     | M3      | 323 - 283                       | 18 800  | 22 700  |
| oVM | M4  |     |         | 358 - 281                       | 25 200  | 26 400  |
|     |     | M5  |         | 317 - 275                       | 18 800  | 17 900  |
|     |     |     | M6      | 316 - 272                       | 10 600  | 10 400  |
| DVM | P6  |     |         | 363 - 286                       | ND  | 293 000   |
|     |     | P10 |         | 326 - 284                       | ND  | 139 000   |
|     |     |     | M7      | 323 - 281                       | 30 600  | 44 000  |
|     | pPD | mPD | aniline |                                 |   |   |

**Table 7:** Absorbance characterizations of model compounds and corresponding polymers. <sup>a</sup> Determined in methylene chloride,  $10^{-2}$  g/L <sup>b</sup> Measured in toluene by using a range of concentrations (pPD: para-Phenylene Diamine. mPD: meta-Phenylene Diamine)

The effect of the ortho-vanillin can also be observed – **M1** is more red-shifted than its homologue with **oVM**, **M4**. The molar extinction coefficients ( $\epsilon$ ) were measured precisely in toluene using multiple concentrations. They are also indicated in methylene chloride to give an order of magnitude, but were not measured precisely, as methylene chloride tends to evaporate quickly. When comparing  $\epsilon$  values, the effect of the meta bond is not as potent as when comparing absorbance maximum: indeed, in this case **M7** has a  $\epsilon$  higher than **M3**, by 60 %. The  $\epsilon$  for **P6** is much higher than the one of **P10**, which is most likely due to the presence of meta-phenylene diamine in the motive of **P10**.

The model compounds were also characterized in terms of emission. They exhibit a weak fluorescence, and like for the polymers, the experimental conditions were adapted to improve the quality of the spectra: use of more concentrated solutions (absorbance of 1 instead of 0.1 usually), excitation at lower wavelength to move the Raman peak of the solvent, and increase of the integration time. The emission spectra are given in **Figure 35**:



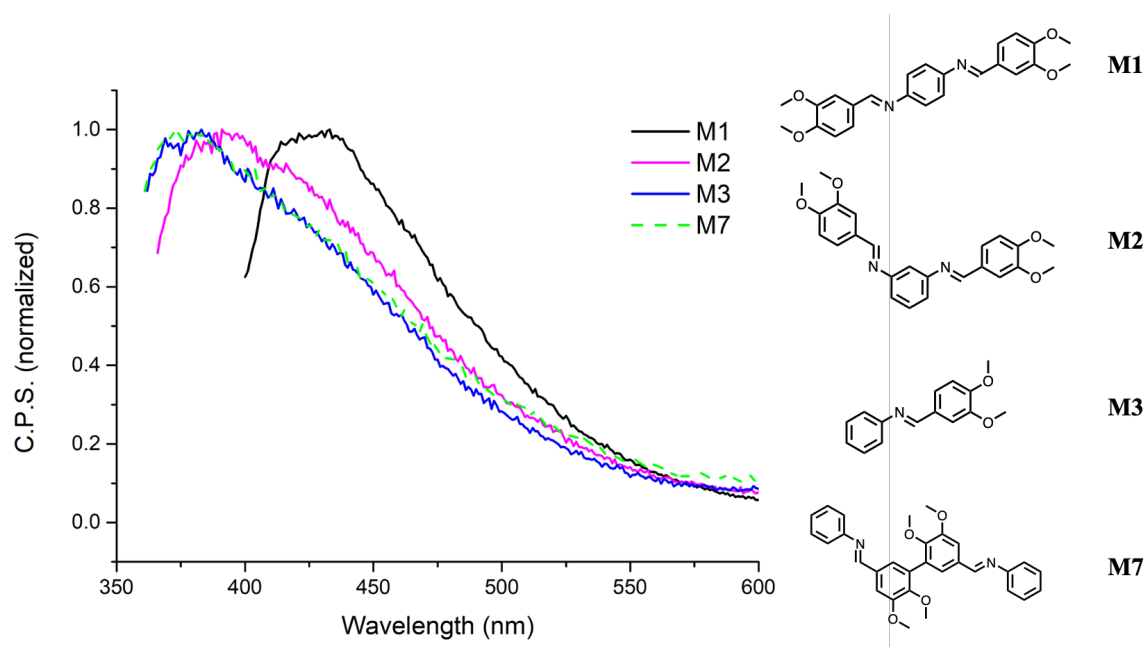


**Figure 35:** Emission spectra of **M1**, **M2**, **M3** and **M7** in methylene chloride ( $10^{-2}$  g/L)

The emission spectrum of **M1** is the most red-shifted, as it corresponds to a model compound with the longest conjugation pathway. **M3** and **M7** have the same spectrum, which shows the influence of the meta-bond of divanillin, that nearly breaks conjugation. **M3** is slightly more red-shifted than **M3** and **M7**, but this could be due to the effect of the substituent on the central phenyl ring rather than the effect of the meta-bond. No charge-transfer behavior was observed in solution for the model compounds.

#### 3.4. General conclusion for model compounds

A series of model compounds was synthesized, to better understand the behavior of the previously synthesized polyazomethines. Model compounds bearing vanillin and ortho-vanillin moiety were synthesized, with different amine or diamines: aniline, para and meta-phenylene diamine. They were at first synthesized using vanillin and ortho-vanillin with either a 2-ethylhexyl or a methyl alkyl moiety. However, there were some issues with respect to the purification step, as the model compounds are degraded onto silica column (flash chromatography) and do not precipitate selectively. Recrystallization was required to purify the model compounds, allowing X-Ray Diffraction (X-RD) measurements. Model compounds with methyl substituents were selected as they crystallize more easily than their ethyl hexyl group-bearing counterparts do.

The model compounds were recrystallized and the structures confirmed by NMR analysis. X-RD confirmed that the azomethine bonds of all model compounds was trans (E), even if some cis (Z) could be observed in the crude. The angle of the azomethine was also measured and can be affected by the presence of substituent in ortho position, as was observed with model compounds with ortho-vanillin. The angle between the two phenyl rings of the divanillin was also measured; it is a torsion angle of  $126.9^\circ$ .

The model compounds were also characterized in terms of absorbance and emission. The key result is the impact of the bond between the two rings of divanillin which is in meta position with respect to the aldehyde functions and breaks conjugation. Indeed, one of the model compounds synthesized has the same absorbance maximum as the corresponding polyazomethine, as summed up in **Figure 36**:

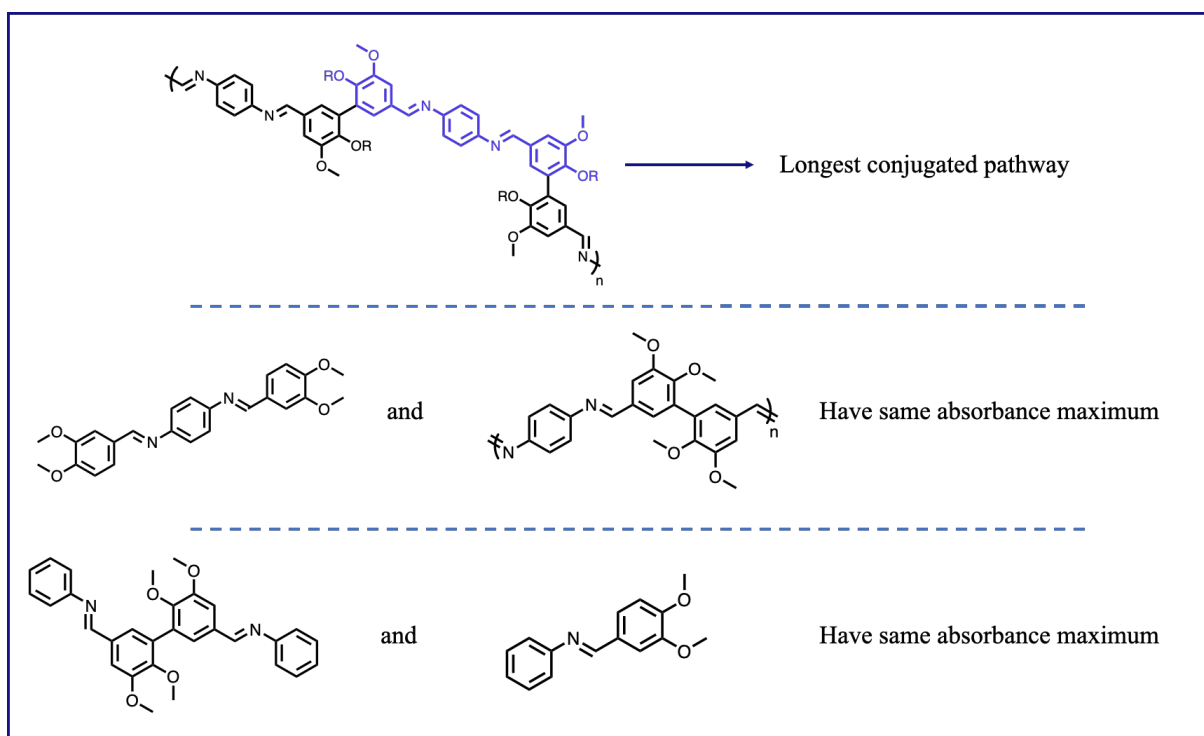


**Figure 36:** Sum up of the influence of the bond between rings of divanillin on the absorbance maximum of the model compounds and corresponding polymer

For conjugated polymers, the conjugation pathway is not infinite. Even in the case of perfectly planar and defect-free conjugated polymers, there is a limit after which adding one more unit does not change the opto-electronic properties. This limit is called Effective Conjugation Length (ECL) and governs the opto-electronic properties. The usual ECL is around ten-units long – after this limit, the delocalization of electrons is not as effective. In the case of **DVEH**-based polyazomethines, there is a break of conjugation after only one unit. This short conjugation pathway is not necessarily a problem, as polymers can make homogeneous films easily, and have interesting optical properties, such as CT behavior in emission and near visible absorbance.

#### 4. General conclusion

Divanillin and diacetovanillone were synthesized by enzymatic coupling, using an efficient experimental protocol that produces the dimers in high yield and purity. These latter vanillin and acetovanillone derivatives were alkylated to improve the solubility of the final polymers and polymerized with various diamines. The selected diamines are the fluorene diamine, and the meta and para phenylene diamines. This choice allowed us evaluating the influence of the position of the substituents.

Diacetovanillone did not yield any polymers but rather mixture of oligomers and was therefore set aside. Syntheses with alkylated divanillin yielded polyazomethines, which are recalled in **Figure 37**.

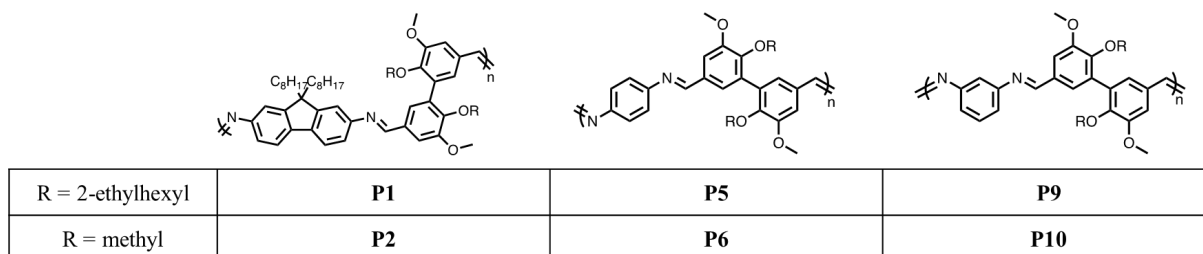


**Figure 37:** Sum up of the divanillin-based polyazomethines synthesized

The polymerization was performed using microwave irradiation, in toluene as a solvent for 4 hours in the presence of silica as a desiccant and acidic catalyst. <sup>1</sup>H-NMR analysis confirmed the formation of the azomethine bond and the polyazomethines were analyzed by SEC – all are soluble in common solvents except **P9**. The highest molar mass obtained was 21 100 g/mol for **P1**. The type of alkyl moiety has an impact on the molar mass: indeed, polyazomethines with 2-ethylhexyl moieties have higher molar masses than their homologues bearing methyl groups. This feature could be due to solubility issues: during the polymerization, polymer chains with 2-ethylhexyl moiety remain soluble over longer reaction time thus leading to higher molar masses. Contrarily, polyazomethines bearing shorter alkyl groups (methyl) are much less soluble when their molar masses increase and precipitate rapidly.

The syntheses are quite reproducible: **P5** and **P6** were synthesized multiple times, leading to polyazomethines with  $16 \pm 2$  and  $8 \pm 1.5$  repeating units, respectively. The experimental protocol was improved, going from 4 hours with silica to 5 minutes without silica. This improvement is fundamental for further applications, as silica degrades the polymers at high concentrations and at low concentrations it distorts the emission spectra.

The key step during the synthesis is actually the recovery step, during which molar masses are greatly improved. This step is done by dissolving the crude polyazomethine in a minimum amount of methylene chloride, then adding methanol and evaporating both solvents using a rotary evaporator. This technique is exemplified in **Figure 38** for **P1**.

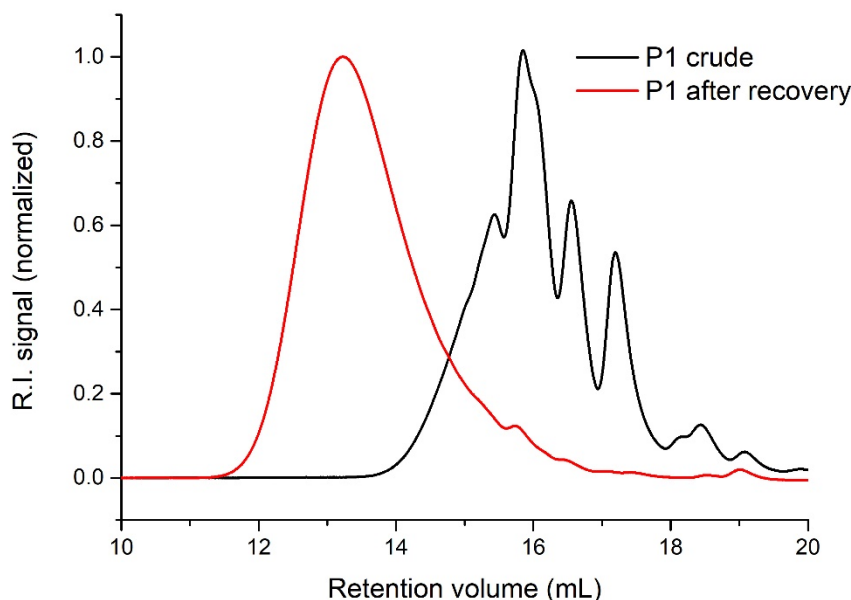


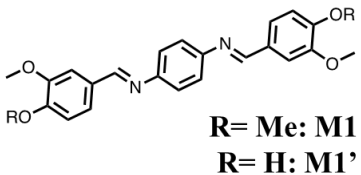
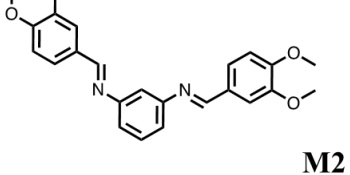
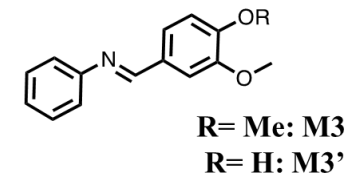
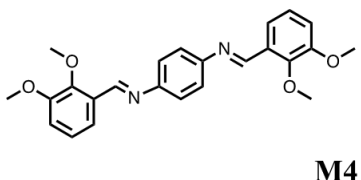
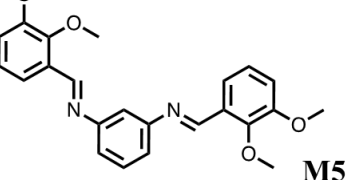
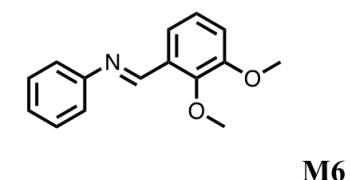
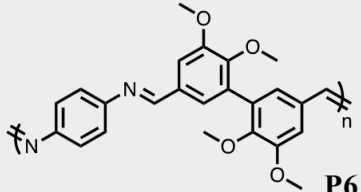
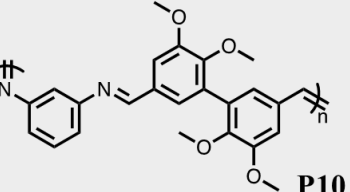
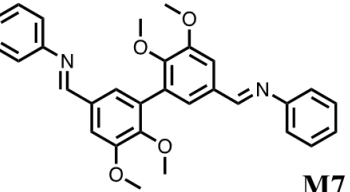
**Figure 38:** SEC profiles of **P1** before and after a recovery step

The removal of solvents during the recovery step leads to a dramatic increase of the molar masses – it is also possible to synthesize polyazomethines by using only this technique.

As a general trend, the divanillin-based polyazomethines have a good thermal stability, with degradation temperature up to 387°C for **P1**. The stability of **P1** was evaluated by monitoring regularly its absorbance spectrum, its SEC profile and its  $^1\text{H-NMR}$  spectrum. When stored dry in the fridge, **P1** has the same absorbance spectrum and SEC profile up to 3 months after synthesis. However, its  $^1\text{H-NMR}$  spectrum starts to change after this time, possibly because of hydrolysis. For this reason, the polyazomethines were kept dry at low temperature and synthesized again regularly.

The divanillin-based polyazomethines were also characterized in terms of absorbance and emission. These latter have absorbance maxima ranging from 326 to 388 nm, depending on the diamine used. The most red-shifted are the polyazomethines with fluorene, as this moiety corresponds to a longer conjugation pathway compared to the others. The polyazomethines with meta-phenylene are the most blue-shifted as the latter moiety leads to twisted chains, possibly the reason of the low solubility of **P9**. The polyazomethines have a weak emission, as expected for this type of polymers – indeed, the azomethine bond is reported to quench fluorescence.<sup>10</sup> Fluorescence can be improved by lowering the temperature or by protonation using an acid.<sup>13</sup> The divanillin-based polyazomethines exhibit a charge transfer like behavior in emission, particularly potent in films, as the latter completely hides the locally excited state emission.

Model compounds were designed for structure-properties studies, with methylated vanillin derivatives – this allows to recrystallize the compounds, enabling X-RD analysis on the compounds. A series of vanillin, ortho-vanillin and divanillin azomethine derivatives were synthesized and recrystallized (**Figure 39**).

|            | Para-phenylene diamine   | Meta-phenylene diamine   | Aniline  |
|------------|--|--|--|
| <b>VM</b>  |  <p><b>R= Me: M1</b><br/><b>R= H: M1'</b></p> |  <p><b>M2</b></p>  |  <p><b>R= Me: M3</b><br/><b>R= H: M3'</b></p> |
| <b>oVM</b> |  <p><b>M4</b></p>                             |  <p><b>M5</b></p>  |  <p><b>M6</b></p>                             |
| <b>DVM</b> |  <p><b>P6</b></p>                             |  <p><b>P10</b></p> |  <p><b>M7</b></p>                             |

**Figure 39:** Sum up of the model compounds synthesized and analysed by X-RD

X-RD proved without any ambiguity that the E isomer is the main one for all molecules. X-RD also gave some insights on the angle between azomethine bond and surrounding aromatic rings, and the effect of substituents position on this angle. The twist between the two aromatic rings of divanillin was also observed: it is a torsion angle of 126.9°.

Just like the corresponding polyazomethines, the model compounds have weak emission. What is remarkable is their absorbance spectra: indeed, **M7** and **M3** have the same absorbance maxima and **M1** has the same absorbance maxima as **P6**. These observations highlight the effect of the nature of the link between the aromatic rings of divanillin, which is in meta with respect to the azomethine bond. This meta position induces a break of conjugation, explaining why a polymer has the same absorbance as a model compound mimicking its backbone.

However, these divanillin-based polyazomethines also have interesting emission properties, such as a broad emission in films due to a CT-like behavior. Therefore, these latter could be used for opto-electronic applications. Moreover, by mixing the various polymers obtained it would be possible to adjust the color of the OLED obtained. Further characterizations are needed, and doping could be a solution to improve fluorescence.

## 5. References

1. Grankowska Ciechanowicz, S. *et al.* Toward Better Efficiency of Air-Stable Polyazomethine-Based Organic Solar Cells Using Time-Resolved Photoluminescence and Light-Induced Electron Spin Resonance as Verification Methods. *J. Phys. Chem. C* **120**, 11415–11425 (2016).
2. Gawlinska, K. *et al.* Searching of new, cheap, air- and thermally stable hole transporting materials for perovskite solar cells. *Opto-electronics Rev.* **25**, 274–284 (2017).
3. Petrus, M. L. *et al.* Conjugated poly(azomethine)s via simple one-step polycondensation chemistry: synthesis, thermal and optoelectronic properties. *Polym. Chem.* **4**, 4182 (2013).
4. Hussein, M. A., Abdel-Rahman, M. A., Asiri, A. M., Alamry, K. A. & Aly, K. I. Review on: Liquid crystalline Polyazomethines polymers. Basics, syntheses and characterization. *Des. Monomers Polym.* **15**, 431–463 (2012).
5. Giuseppone, N., Fuks, G. & Lehn, J. M. Tunable fluorene-based dynamers through constitutional dynamic chemistry. *Chem. - A Eur. J.* **12**, 1723–1735 (2006).
6. Adams, R., Bullock, J. E. & Wilson, W. C. Contribution to the structure of benzidine. *J. Am. Chem. Soc.* **45**, 521–527 (1923).
7. Wojtkowski, P. W. Aromatic—Aliphatic Azomethine Ether Polymers And Fibers. *Macromolecules* **20**, 740–748 (1987).
8. Lee, K.-S., Won, J. C. & Jung, J. C. Synthesis and characterization of processable conducting polyazomethines. *Die Makromol. Chemie* **190**, 1547–1552 (1989).
9. Kim, H. J., Lee, J. H., Lee, M. & Lee, T. S. Optical switching and anion-induced chromogenic application in conjugated polyazomethine derivatives. *React. Funct. Polym.* **68**, 1696–1703 (2008).
10. Skene, W. G. & Pérez Guarín, S. A. Spectral characterization of thiophene acylhydrazides. *J. Fluoresc.* **17**, 540–546 (2007).
11. Barik, S. & Skene, W. G. A fluorescent all-fluorene polyazomethine—towards soluble conjugated polymers exhibiting high fluorescence and electrochromic properties. *Polym. Chem.* **2**, 1091–1097 (2011).
12. Mallet, C., Le Borgne, M., Starck, M. & Skene, W. G. Unparalleled fluorescence of a polyazomethine prepared from the self-condensation of an automer and its potential use as a fluorimetric sensor for explosive detection. *Polym. Chem.* **4**, 250–254 (2013).
13. Barik, S., Bletzacker, T. & Skene, W. G.  $\pi$ -Conjugated fluorescent azomethine copolymers: Opto-electronic, halochromic, and doping properties. *Macromolecules* **45**, 1165–1173 (2012).
14. Yang, C. J. & Jenekhe, S. A. Conjugated Aromatic Poly(azomethines). 1. Characterization of Structure, Electronic Spectra, and Processing of Thin Films from Soluble Complexes. *Chem. Mater.* **3**, 878–887 (1991).
15. Bolduc, A., Mallet, C. & Skene, W. G. Survey of recent advances of in the field of  $\pi$ -conjugated heterocyclic azomethines as materials with tuneable properties. *Sci. China Chem.* **56**, 3–23 (2013).
16. Delomenède, M. *et al.* Development of novel antiatherogenic biaryls: Design, synthesis, and reactivity. *J. Med. Chem.* **51**, 3171–3181 (2008).
17. I. Reiss, L. I. Gatfield, G. Krammer, A. Clerc, G. K. US 2006/0286237 A1. (2006).
18. Nishimura, R. T., Giammanco, C. H. & Vosburg, D. A. Green, enzymatic syntheses of divanillin

- and diapocynin for the organic, biochemistry, or advanced general chemistry laboratory. *J. Chem. Educ.* **87**, 526–527 (2010).
19. Krings, U., Esparan, V. & Berger, R. G. The taste enhancer divanillin: A review on sources and enzymatic generation. *Flavour Fragr. J.* **30**, 362–365 (2015).
  20. Llevot, A., Grau, E., Carlotti, S., Grelier, S. & Cramail, H. Selective laccase-catalyzed dimerization of phenolic compounds derived from lignin: Towards original symmetrical bio-based (bis) aromatic monomers. *J. Mol. Catal. B Enzym.* **125**, 34–41 (2016).
  21. 't Hart, B. A., Copray, S. & Philippens, I. Apocynin, a Low Molecular Oral Treatment for Neurodegenerative Disease. *Biomed Res. Int.* **2014**, 1–6 (2014).
  22. Llevot, A., Grau, E., Carlotti, S., Grelier, S. & Cramail, H. Renewable (semi)aromatic polyesters from symmetrical vanillin-based dimers. *Polym. Chem.* **6**, 6058–6066 (2015).
  23. Garbay, G. Original metal-free synthesis routes of semi-conducting oligomers and (co)polymers for organic electronics. (Université de Bordeaux, 2016).
  24. Gedye, R. *et al.* The use of microwave ovens for rapid organic synthesis. *Tetrahedron Lett.* **27**, 279–282 (1986).
  25. Nayak, S. N., Bhasin, C. P. & Nayak, M. G. A review on microwave-assisted transesterification processes using various catalytic and non-catalytic systems. *Renew. Energy* **143**, 1366–1387 (2019).
  26. Wang, D., Yuan, Y., Mardiyati, Y., Bubeck, C. & Koynov, K. From single chains to aggregates, how conjugated polymers behave in dilute solutions. *Macromolecules* **46**, 6217–6224 (2013).
  27. Roberts, B. A. & Strauss, C. R. Toward rapid, 'green', predictable microwave-assisted synthesis. *Acc. Chem. Res.* **38**, 653–661 (2005).
  28. Cordes, E. H. & Jencks, W. P. On the Mechanism of Schiff Base Formation and Hydrolysis. *J. Am. Chem. Soc.* **84**, 832–837 (1962).
  29. Mei, J. & Bao, Z. Side chain engineering in solution-processable conjugated polymers. *Chem. Mater.* **26**, 604–615 (2014).
  30. Yoshihara, T., Druzhinin, S. I. & Zachariasse, K. A. Fast intramolecular charge transfer with a planar rigidized electron donor/acceptor molecule. *J. Am. Chem. Soc.* **126**, 8535–8539 (2004).
  31. Dikumar, E. A., Kozlov, N. G., Potkin, V. I., Azarko, V. A. & Yuvchenko, A. P. Synthesis, film-forming properties, and thermal and light sensitivity of N,N'-bis[4-hydroxy(alkoxy, acyloxy)-3-alkoxyphenylmethylidene]benzene-1,4- diamines. *Russ. J. Gen. Chem.* **78**, 281–285 (2008).
  32. Burgi, H. B. & Dunitz, D. Crystal and Molecular Structures of Benzylideneaniline, Benzylideneaniline -p-carboxylic acid and p -Methylbenzylidene -p -nitroaniline. *Helv. Chim. Acta* **53**, 1747–1764 (1970).
  33. Bernstein, J., Bar, I. & Christensen, A. Molecular conformation and electronic structure. IV. p - ( N -Methylbenzylidene)- p -methylaniline (form III) . *Acta Crystallogr. Sect. B Struct. Crystallogr. Cryst. Chem.* **32**, 1609–1611 (1976).

**6. Experimental Part**

|  |     |
|--|-----|
| <b>6.1. General</b> .....  | 100 |
| <b>6.2. Characterization</b> .....   | 100 |
| <b>6.3. Synthesis and characterization of monomers</b> .....                             | 101 |
| 6.3.1. Synthesis and characterization of <b>DV</b> .....                                 | 101 |
| 6.3.2. Synthesis and characterization of <b>DAcV</b> .....                               | 103 |
| <b>6.4. General procedure for the alkylation with methyl group</b> .....                 | 104 |
| 6.4.1 Characterization of <b>DVM</b> .....   | 104 |
| 6.4.2. Characterization of <b>DAcVM</b> .....  | 106 |
| <b>6.5. General procedure for alkylation with 2-ethylhexyl group</b> .....               | 107 |
| 6.5.1. Characterization of <b>DVEH</b> .....   | 107 |
| 6.5.2. Characterization of <b>DAcVEH</b> .....   | 109 |
| 6.5.3. Dimerization of ortho-vanillin and iso-vanillin.....                              | 110 |
| <b>6.6. Synthesis and characterization of polyazomethines</b> .....                      | 111 |
| 6.6.1. General protocol for polymerization.....  | 111 |
| 6.6.2. Characterization of <b>P1</b> .....   | 111 |
| 6.6.3. Characterization of <b>P2</b> .....   | 112 |
| 6.6.4. Characterization of <b>P3</b> .....   | 114 |
| 6.6.5. Characterization of <b>P4</b> .....   | 115 |
| 6.6.6. Characterization of <b>P5</b> .....   | 116 |
| 6.6.7. Characterization of <b>P6</b> .....   | 117 |
| 6.6.8. Characterization of <b>P7</b> .....   | 118 |
| 6.6.9. Characterization of <b>P8</b> .....   | 119 |
| 6.6.10. Characterization of <b>P9</b> .....  | 120 |
| 6.6.11. Characterization of <b>P10</b> .....   | 121 |
| 6.6.12. Characterization of <b>P11</b> and <b>P12</b> .....                              | 123 |
| <b>6.7. Synthesis and characterization of model compounds and their precursors</b> ..... | 123 |
| 6.7.1. Characterization of <b>VM</b> .....   | 123 |
| 6.7.2. Characterization of <b>oVM</b> .....  | 124 |
| <b>6.8. General protocol for the synthesis of model compounds</b> .....                  | 125 |
| 6.8.1. Synthesis and purification of <b>M1</b> .....                                     | 125 |
| 6.8.2. Synthesis and purification of <b>M1'</b> .....                                    | 126 |
| 6.8.3. Synthesis and purification of <b>M2</b> .....                                     | 127 |
| 6.8.4. Synthesis and purification of <b>M3</b> .....                                     | 128 |
| 6.8.5. Synthesis and purification of <b>M3'</b> .....                                    | 129 |
| 6.8.6. Synthesis and purification of <b>M4</b> .....                                     | 130 |



|  |     |
|--|-----|
| 6.8.7. Synthesis and purification of <b>M5</b> ..... | 131 |
| 6.8.8. Synthesis and purification of <b>M6</b> ..... | 132 |
| 6.8.9. Synthesis and purification of <b>M7</b> ..... | 133 |

## 6.1. General

Ethyl-vanillin and ortho-vanillin were graciously provided by Solvay. Vanillin (>97 %), Laccase from *Trametes Versicolor*, 2-ethylhexyl bromide (95 %), potassium carbonate, para and meta phenylene diamine were obtained from Sigma-Aldrich. Acetovanillone was obtained from Alfa Aesar. Paratoluene sulfonic acid (PTSA, 99 %) and 2, 7-diamino-9, 9-di-n-octylfluorene were purchased from TCI. Silica gel (pore size 60 Å, 230-400 mesh particle size, particle size 40-63 µm) was obtained from Honeywell Fluka. Potassium hydroxide, and iodomethane were obtained from Fischer. Aniline was obtained from Acros Organics. All products and solvents (reagent grade) were used as received except otherwise mentioned. The solvents were of reagent grade quality and were purified whenever necessary according to the methods reported in the literature. For the emission and absorbance measurements, methylene chloride with spectroscopy grade from Sigma was used. Flash chromatography was performed on a Grace Reveleris apparatus, employing silica cartridges from Grace. Cyclohexane: ethyl acetate gradients and methylene chloride were used as eluents. The detection was performed through ELSD and UV detectors at 254 nm and 280 nm. The reactions under microwave irradiation were performed on a Discover-SP from CEM, with the temperature measured by infrared; the power of the apparatus is constantly adjusted to reach and then stay at the set temperature.

## 6.2. Characterization

<sup>1</sup>H, <sup>13</sup>C and <sup>1</sup>H-<sup>13</sup>C HSQC NMR measurements were performed with a Bruker Avance 400 spectrometer (400.20 MHz and 100.7 MHz for <sup>1</sup>H and <sup>13</sup>C, respectively) at room temperature using deuterated solvent.

IR spectra were recorded with Bruker Tensor 27 spectrometer using a 0.6 mm-diameter beam. Samples were analyzed with the attenuated total reflection (ATR) method.

Mass spectra were performed by the CESAMO (Bordeaux, France) on a Qexactive mass spectrometer (Thermo). The instrument is equipped with an ESI source and spectra were recorded in the positive mode. The spray voltage was maintained at 3200 V and capillary temperature set at 320°C. Samples were introduced by injection through a 20 µL sample loop into a 300 µL/min flow of methanol from the LC pump.

Optical absorption spectra were obtained with a UV-visible spectrophotometer (UV-3600, Shimadzu). Fluorescence spectra were obtained from a spectrofluorometer (Fluoromax-4, Horiba Scientific). In both cases, solvents of spectroscopic grade were used (from Sigma), and quartz cells were used.

Molar masses of polymers were determined by size exclusion chromatography (SEC) using a three-columns set of Resipore Agilent: one guard column Resipore Agilent PL1113-1300, then two columns Resipore Agilent PL1113-6300, connected in series, and calibrated with narrow polystyrene standards from polymer Laboratories using both refractometric (GPS 2155) and UV detectors (Viscotek). THF was used as eluent (0.8 mL/min) and trichlorobenzene as a flow marker (0.15 %) at 30°C.

For the molar masses of polymers samples measured by SEC in chloroform, chloroform with TCB as flow-marker (0.15%) and 1% of TEA was used as eluent (0.8 mL/min). The analyses were done at 30°C using a four-columns set from Agilent: one PLGel 5µm Guard (PL1110-1520) and three Mixed C PLGel 5µm (PL1110-6500) connected in series, calibrated with narrow polystyrene standards from polymer Laboratories using both refractometric (GPS 2155) and UV detectors (Viscotek).

TGA have been performed on a TA-Q50, from 25°C to 600 - 700 °C with a heating of 10°C/min under nitrogen flow.

Diffraction data from a single crystal of the different model compounds were measured by the IECB (Bordeaux, France) on a 3 kW microfocus Rigaku FRX rotating anode. The source is equipped with high flux Osmic Varimax HF mirrors and a hybrid Dectris Pilatus 200 K detector. The source is operating at the copper  $\text{K}\alpha$  wavelength with a partial chi goniometer that decreases blind areas and enables automatic axial adjustment. Data were processed with the CrysAlisPro suite version 1.171.38.43.<sup>1</sup> Empirical absorption correction using spherical harmonics, implemented in SCALE3 ABSPACK scaling algorithm was used.

The structure was solved with Shelxt<sup>2</sup> and refined by full-matrix least-squares method on F2 with Shelxl-2014<sup>2</sup> within Olex2.<sup>3</sup> For all atoms, anisotropic atomic parameters were used. Hydrogen atoms were placed at idealized position and refined as riding of their carriers with  $\text{Uiso}(\text{H}) = 1.2 \text{ Ueq}$  (CH, CH<sub>2</sub>, NH) and  $\text{Uiso}(\text{H}) = 1.5 \text{ Ueq}$  (CH<sub>3</sub>). DFIX and AFIX instructions were used to improve the geometry of molecules and RIGU to model atomic displacement parameters. Disordered solvent molecules were removed using the SQUEEZE procedure from the PLATON suite.<sup>4</sup> For search and analysis of solvent accessible voids in the structures default parameters were utilized: grid 0.20 Å, probe radius 1.2 Å and NStep 6. Calculated total potential solvent accessible void volumes and electron counts per unit cell are given in the CIF files that were checked using IUCR's checkcif algorithm. Due to the characteristics of some of the crystals, i.e. large volume fractions of disordered solvent molecules, weak diffraction intensity and moderate resolution, few A -level and B -level alerts remain in the check cif file. These alerts are inherent to the data and refinement procedures and do not reflect errors on the model refined.

<sup>1</sup> CrysAlisPRO : CrysAlisPRO, Oxford Diffraction /Agilent Technologies UK Ltd, Yarnton, England.

<sup>2</sup> Sheldrick, G. M. (2015). Acta Cryst. A71, 3-8.

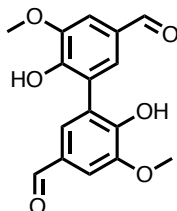
<sup>3</sup> OLEX2: O. V. Dolomanov, L. J. Bourhis, R. J. Gildea, J. A. K. Howard and H. Puschmann. J. Appl. Cryst. (2009). 42, 339-341.

<sup>4</sup> Spek, A. L. (2009). Acta Cryst. D65, 148-155.

### 6.3. Synthesis and characterization of monomers

#### 6.3.1. Synthesis and characterization of DV

##### 6,6'-Dihydroxy-5,5'-dimethoxy-[1,1'-biphenyl]-3,3'-dicarboxaldehyde



5.6g of sodium acetate and 1.75 mL of acetic acid were dissolved in 1L of water to give the buffer. In an appropriate vessel, 6g of vanillin were dissolved in 80mL of acetone, afterwards 720 mL of the previously prepared buffer were added. 49.6mg of Laccase from Trametes Versicolor were finally added, and the medium was saturated with oxygen. After 24 h at 25°C under constant and light stirring, the medium was filtrated to give crude divanillin as a brown powder – the filtrate was charged again in vanillin and saturated in oxygen to start a new cycle. To purify it further, 6g of crude divanillin were completely dissolved in 100 mL of a 0.5 M solution of NaOH. This solution is then poured in 600 mL of ethanol, which is then acidified with fuming HCl until divanillin spontaneously precipitates. It is then recovered by simple filtration and rinsed with water and acetone. Yield: 85 %

<sup>1</sup>H-NMR (400.20 MHz, DMSO-d<sub>6</sub>, ppm): d 9.81 (s, 2H); 7.44-7.42 (m, 4H); 3.93 (s, 6H).  
<sup>13</sup>C-NMR (100.70 MHz, DMSO-d<sub>6</sub>, ppm): 191.2; 150.6; 148.3; 128.2; 127.8; 124.6; 109.2; 56.1.  
 FT-IR (ATR, cm<sup>-1</sup>):  $\nu = 3192; 2967; 2941; 1667; 1583; 1455; 1421; 1399; 1353; 1310; 1280; 1255; 1180; 1132; 1078; 1045; 969; 919; 882; 846; 771; 759; 742; 717; 664; 633; 603; 587; 555; 432; 417.$

Aspect: dark beige powder

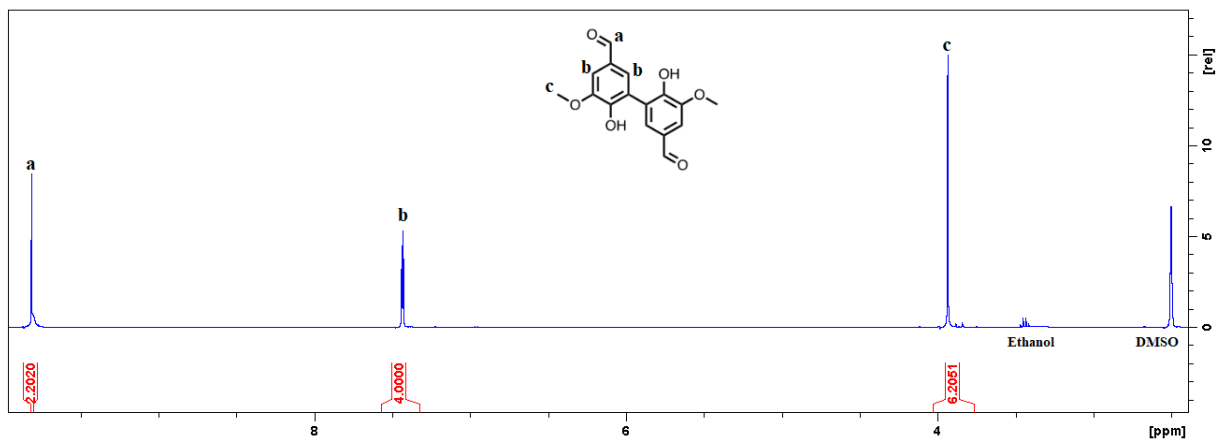


Figure 40:  $^1\text{H-NMR}$  spectrum of purified DV (400.20 MHz, in DMSO-d6)

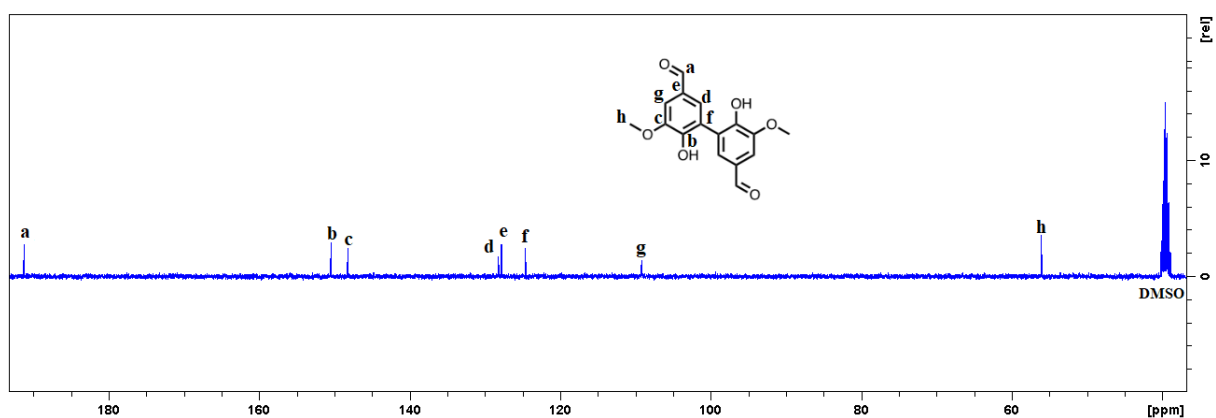


Figure 41:  $^{13}\text{C-NMR}$  spectrum of purified DV (100.70 MHz, in DMSO-d6)

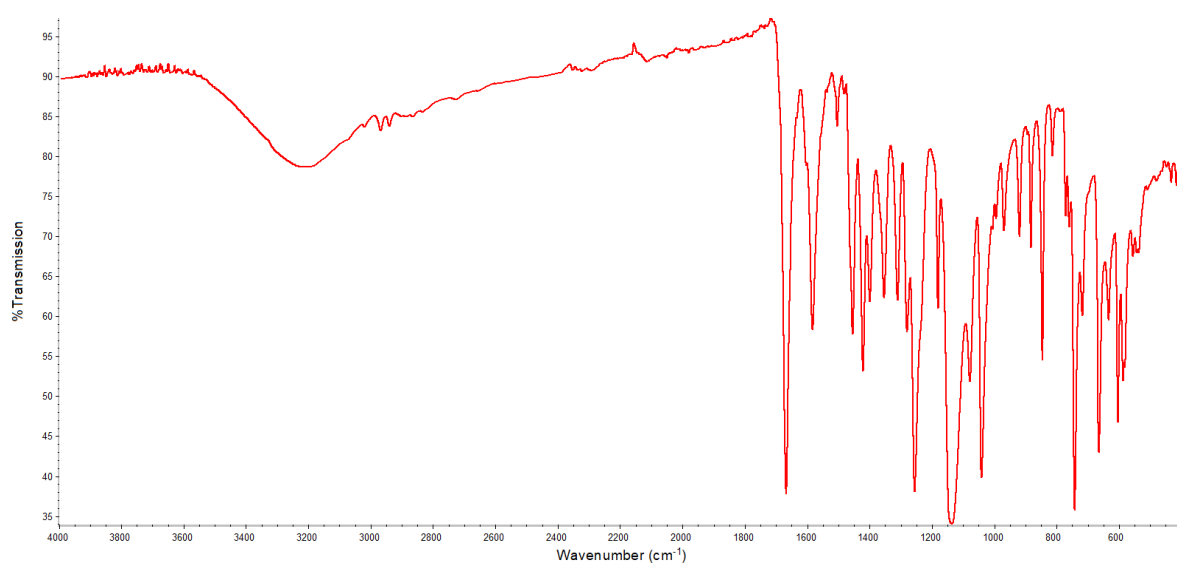
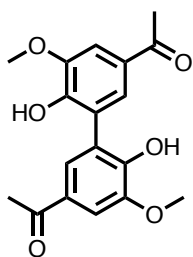


Figure 42: ATR-FTIR spectrum of DV

6.3.2. Synthesis and characterization of **DAcV**

## 6,6'-Dihydroxy-5,5'-dimethoxy-[1,1'-biphenyl]-3,3'-diethanone



5.6g of sodium acetate and 1.75 mL of acetic acid were dissolved in 1L of water to give the buffer. In an appropriate vessel, 1.5g of acetovanillone were dissolved in 20 mL of acetone, afterwards 180 mL of the previously prepared buffer were added. 12.4 mg of Laccase from *Trametes Versicolor* were finally added, and the medium was saturated with oxygen. After 24 h at 25°C under constant and light stirring, the medium was filtrated to give crude divanillin as a brown powder – the filtrate was charged again in acetovanillone and saturated in oxygen to start a new cycle. Yield: 85 %

$^1\text{H-NMR}$  (400.20 MHz, DMSO- $d_6$ , ppm): 9.5 (s, 2H); 7.48-7.46 (m, 4H); 3.91 (s, 6H); 2.51 (s, 6H).  $^{13}\text{C-NMR}$  (100.70 MHz, DMSO- $d_6$ , ppm): 196.2; 149.5; 147.6; 127.8; 125.3; 124.6; 109.7; 56.1; 26.3. FT-IR (ATR,  $\text{cm}^{-1}$ ):  $\nu$ = 3321.07; 3013; 1667; 1590; 1462; 1453; 1408; 1368; 1309; 1288; 1243; 1209; 1183; 1127; 1085; 1035; 909; 890; 845; 804; 687; 639; 597; 566; 433; 415.

Aspect: fine beige powder

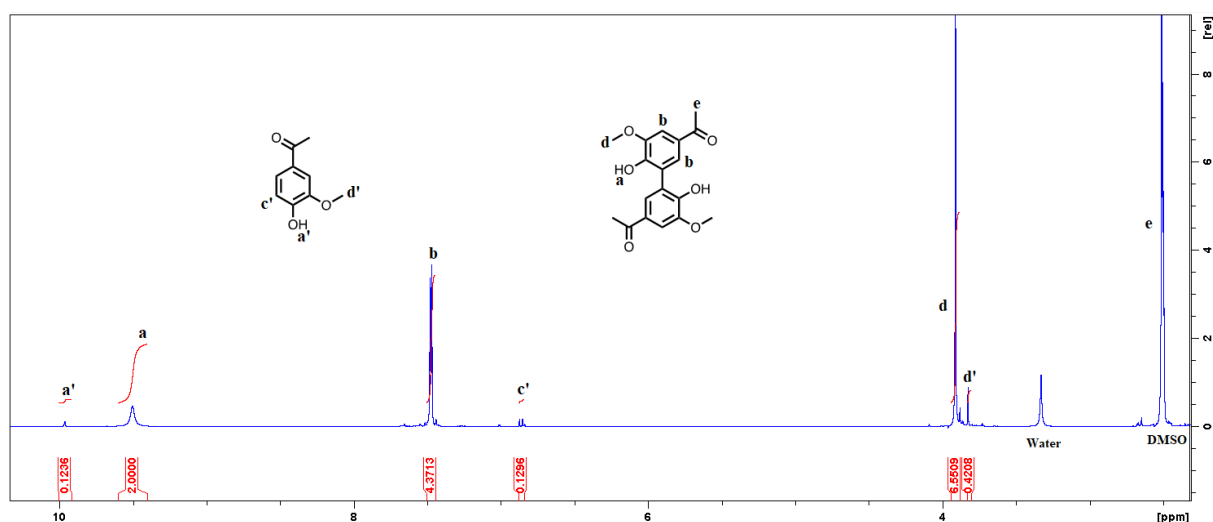


**Figure 43:**  $^1\text{H-NMR}$  spectrum of crude **DAcV** (400.20 MHz, in DMSO- $d_6$ )

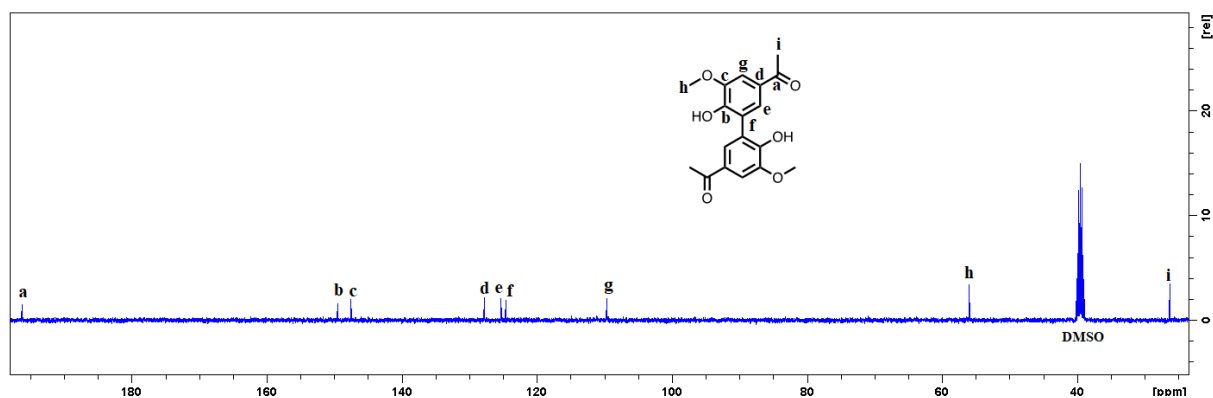


**Figure 44:**  $^{13}\text{C-NMR}$  spectrum of crude **DAcV** (100.70 MHz, in DMSO- $d_6$ )

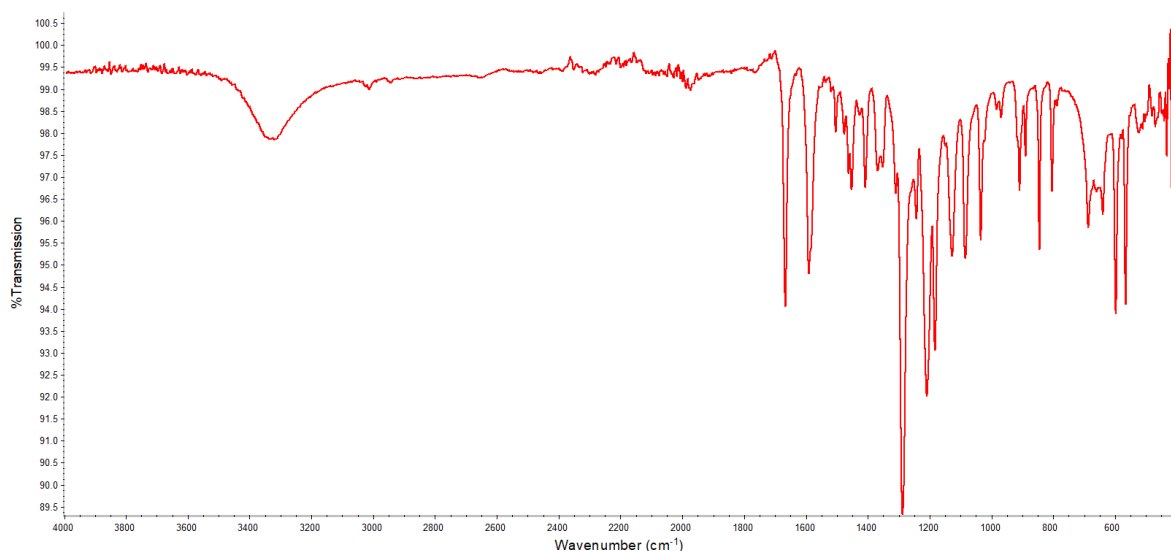


**Figure 45:** ATR-FTIR spectrum of **DAcV**

#### 6.4. General procedure for the alkylation with methyl group

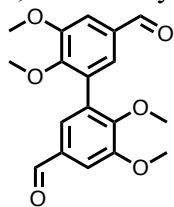
In a flame-dried and nitrogen flushed 100 mL glassware equipped with a condenser, the bisphenol of interest (divanillin or diacetovanillone, 6.6 mmol) was solubilized in 40 mL of previously dried DMF. Then  $K_2CO_3$  (3.8 g, 27.5 mmol) was added to the reaction mixture, which was heated at 80°C for 2 hours. Then, 2.45 mL of iodomethane (39.5 mmol) were added slowly to the reaction mixture and it was left 16 more hours at 80°C.

Afterwards, the reaction mixture was poured into 300 mL of water and left 5 minutes until it completely precipitated. The final product was then recovered after simple filtration and extensively dried before use without further purification.

Yield: 90 %

##### 6.4.1 Characterization of **DVM**

###### 6,6'-Methoxy-5,5'-dimethoxy-[1,1'-biphenyl]-3,3'-dicarboxaldehyde



$^1H$ -NMR (400.20 MHz,  $CDCl_3$ , ppm): 9.84 (s, 2H); 7.44-7.43 (d,  $J = 4$ Hz, 2H); 7.33-7.32 (d,  $J = 4$ Hz, 2H); 3.91 (s, 6H); 3.70 (s, 6H).  $^{13}C$ -NMR (100.70 MHz,  $CDCl_3$ , ppm): 191.1; 153.5; 152.5; 132.3; 131.9; 127.7; 110.6; 61.1; 56.2. FT-IR (ATR,  $cm^{-1}$ ):  $\nu = 2942$ ; 2836; 1690; 1576; 1463; 1448; 1413; 1386; 1361; 1263; 1242; 1203; 1177; 1134; 1047; 996; 878; 847; 798; 791; 763; 738; 701; 650; 604; 591; 551; 543.

Aspect: beige powder – fluffy crystals obtained by recrystallization from a warm mixture of cyclohexane and ethyl acetate.

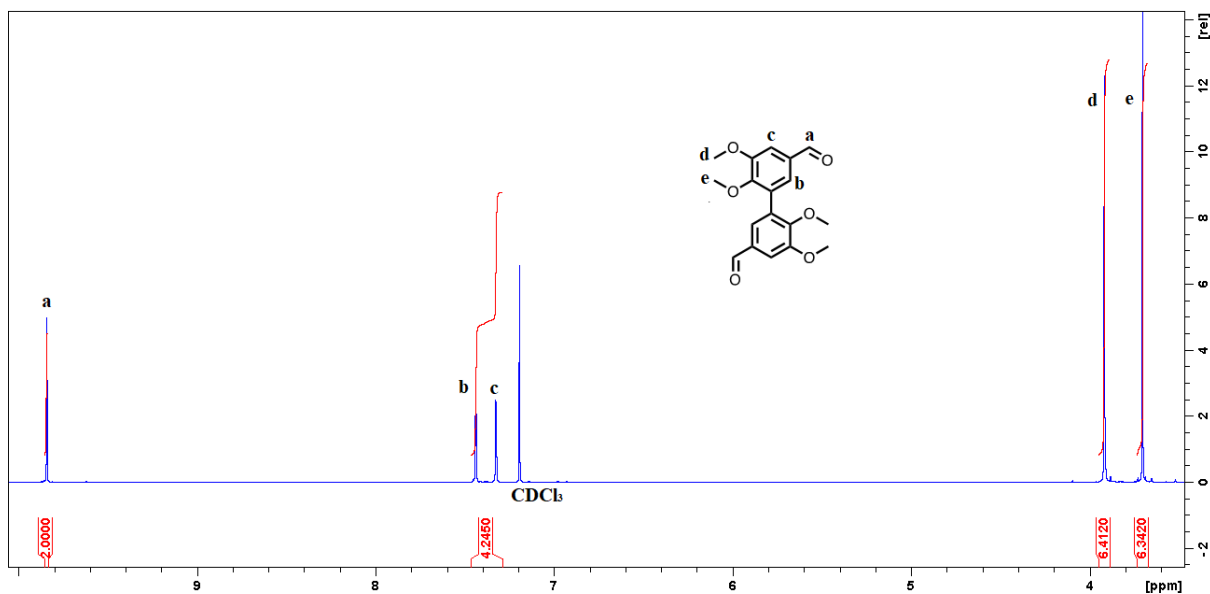


Figure 46:  $^1\text{H-NMR}$  spectrum of DVM (400.20 MHz, in  $\text{CDCl}_3$ )

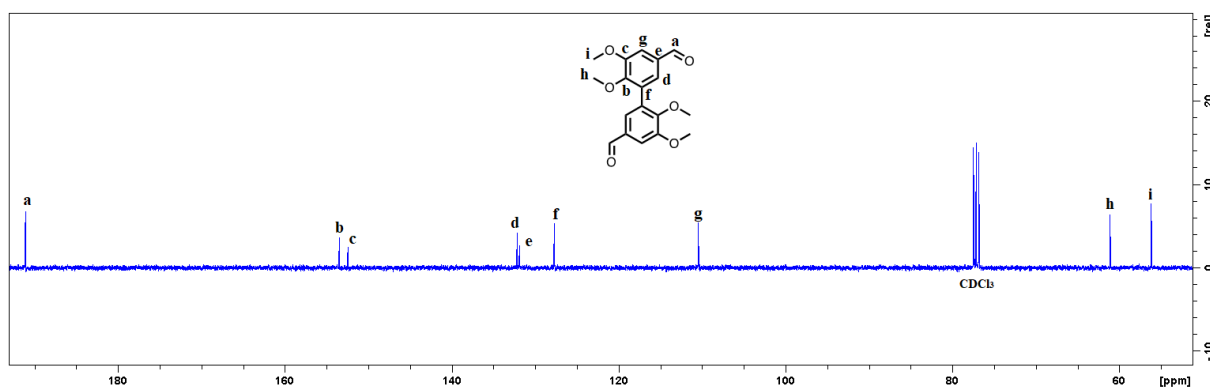


Figure 47:  $^{13}\text{C-NMR}$  spectrum of DVM (100.70 MHz, in  $\text{CDCl}_3$ )

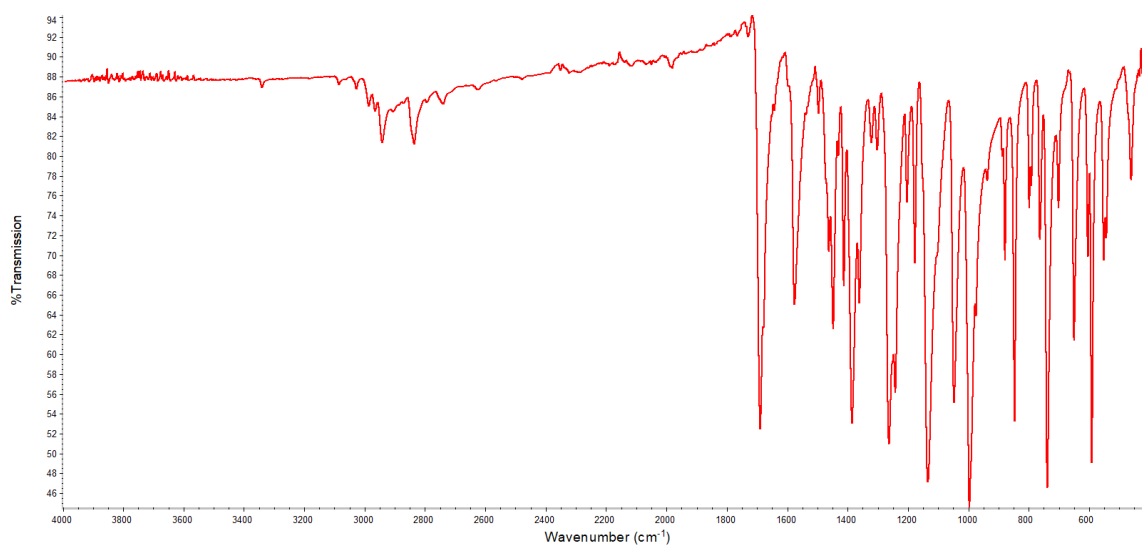
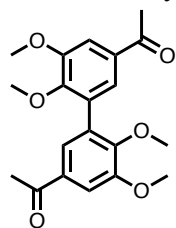


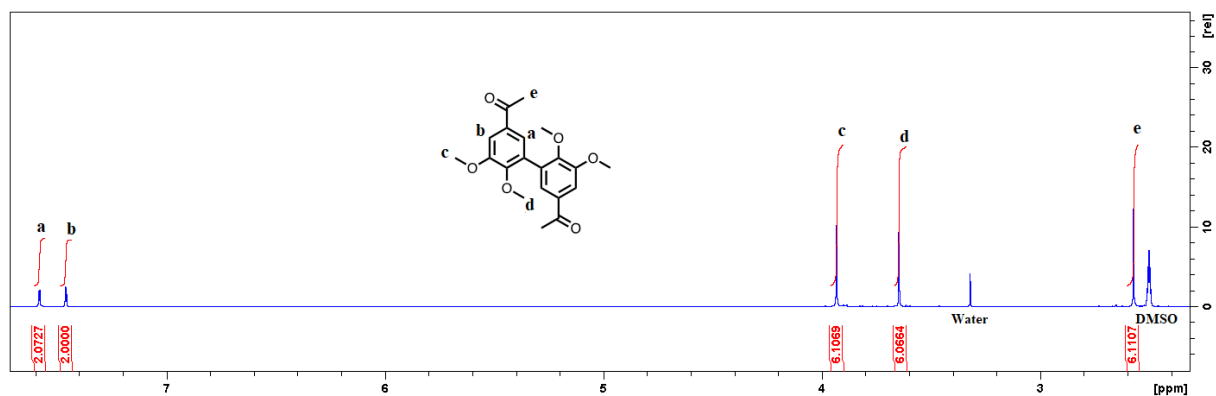
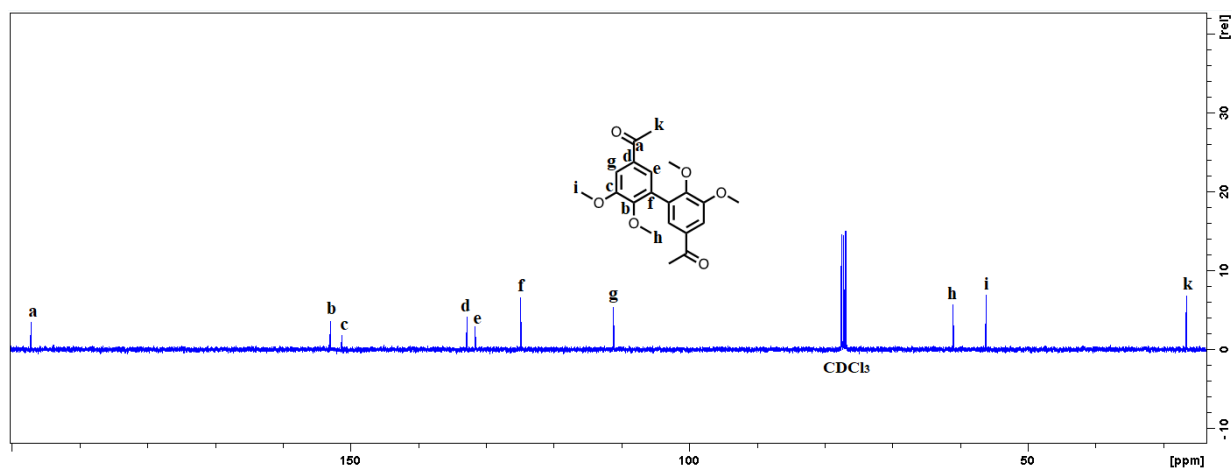
Figure 48: ATR-FTIR spectrum of DVM

6.4.2. Characterization of **DAcVM**

6,6'- methoxy-5,5'-dimethoxy-[1,1'-biphenyl]-3,3'-diethanone



$^1\text{H-NMR}$  (400.20 MHz, DMSO- $d_6$ , ppm): 9.82 (s, 2H); 7.58-7.57 (d,  $J = 4\text{Hz}$ , 2H); 7.46-7.45 (d,  $J = 4\text{Hz}$ , 2H) 3.93 (s, 6H); 3.65 (s, 6H); 2.57 (s, 6H).  $^{13}\text{C-NMR}$  (100.70 MHz,  $\text{CDCl}_3$ , ppm): 197.1; 153.0; 151.2; 132.8; 131.6; 124.9; 11.2; 61.1; 56.2; 26.6. FT-IR (ATR,  $\text{cm}^{-1}$ ):  $\nu = 3014$ ; 2969; 2941; 2841; 1686; 1578; 1494; 1457; 1446; 1421; 1397; 1370; 1352; 1317; 1279; 1244; 1225; 1199; 1157; 1087; 1037; 1004; 973; 932; 899; 877; 866; 783; 761; 685; 647; 635; 594; 572.

Aspect: white powderFigure 49:  $^1\text{H-NMR}$  spectrum of **DAcVM** (400.20 MHz, in DMSO- $d_6$ )Figure 50:  $^{13}\text{C-NMR}$  spectrum of **DAcVM** (100.70 MHz, in  $\text{CDCl}_3$ )

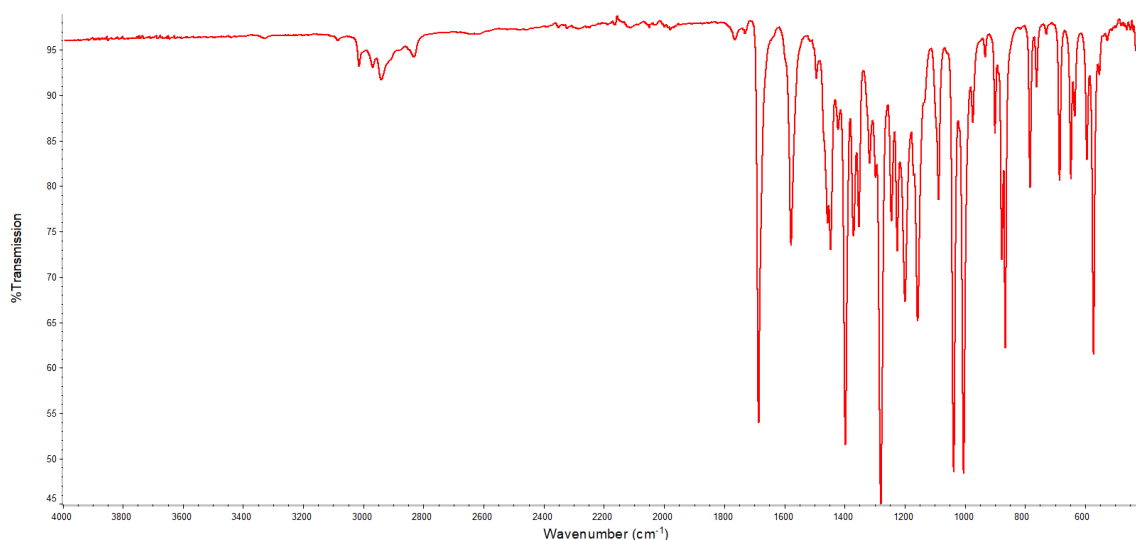


**Figure 51:** ATR-FTIR spectrum of **DAcVM**

### 6.5. General procedure for alkylation with 2-ethylhexyl group

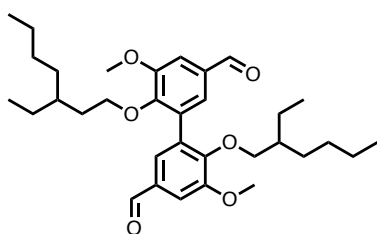
In a flame-dried and nitrogen flushed 100 mL glassware equipped with a condenser, the bisphenol of interest (divanillin or diacetovanillone, 6.6 mmol) was solubilized in 20 mL of previously dried DMSO. Then KOH (0.89 g, 15.9 mmol) was added to the reaction mixture, which was heated at 80°C for 2 hours. Then, 2.2 equivalent of 2-ethylhexyl bromide were added to the reaction mixture and it was left 16 more hours at 80°C.

Afterwards, the reaction mixture was poured into 300 mL of water and extracted with 100 mL of ethyl acetate three times. The organic phase was dried on MgSO<sub>4</sub> and the solvent removed using a rotary evaporator. This dried crude was then purified by flash chromatography on a silica column (80g) using cyclohexane and ethyl acetate as eluents (85/15).

Yield: 40-55 %

#### 6.5.1. Characterization of **DVEH**

##### 6,6'-2-ethylhexoxy-5,5'-dimethoxy-[1,1'-biphenyl]-3,3'-dicarboxaldehyde



<sup>1</sup>H-NMR (400.20 MHz, (CDCl<sub>3</sub>, ppm): 9.82 (s, 2H); 7.4-7.38 (d, J = 8Hz, 4H); 3.88 (s, 6H); 3.78-3.69 (m, 4H); 1.33-0.89 (m, 19H), 0.73 (t, J = 8Hz, 6H); 0.62 (t, J = 8Hz, 6H). <sup>13</sup>C-NMR (100.70 MHz, (CDCl<sub>3</sub>, ppm): 191.1; 153.6; 152.1; 132.0; 131.6; 128.6; 109.7; 75.2; 55.9; 40.4; 30.3; 29.0; 23.5; 22.9; 14.1; 11.0. FT-IR (ATR, cm<sup>-1</sup>): ν = 2956; 2928; 2872; 1691; 1577; 1457; 1417; 1379; 1351; 1269; 1225; 1135; 1090; 1046; 1000; 956; 862; 771; 741; 618; 592.

Aspect: pale yellow oil



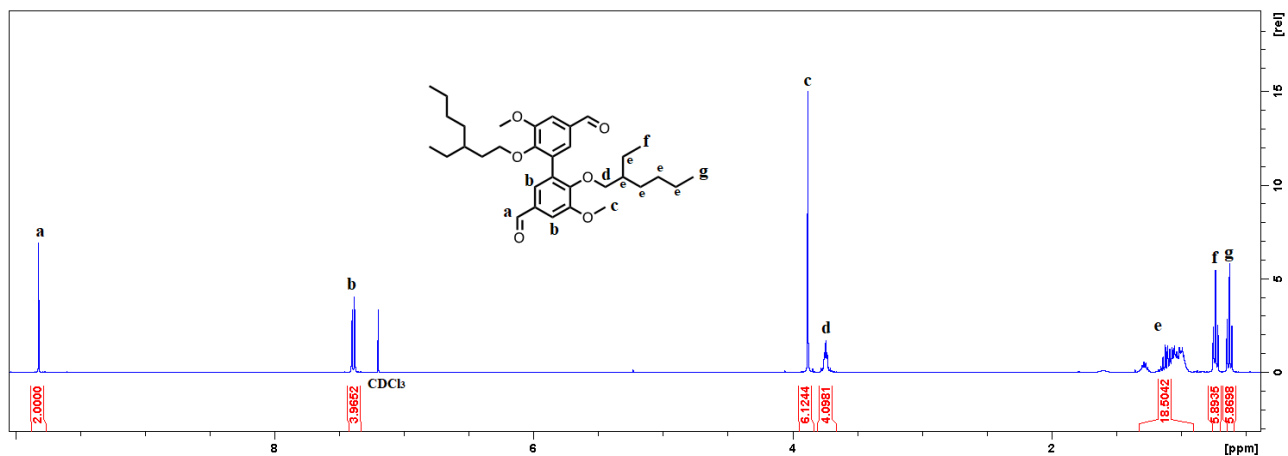


Figure 52:  $^1\text{H-NMR}$  spectrum of DVEH (400.20 MHz, in  $\text{CDCl}_3$ )

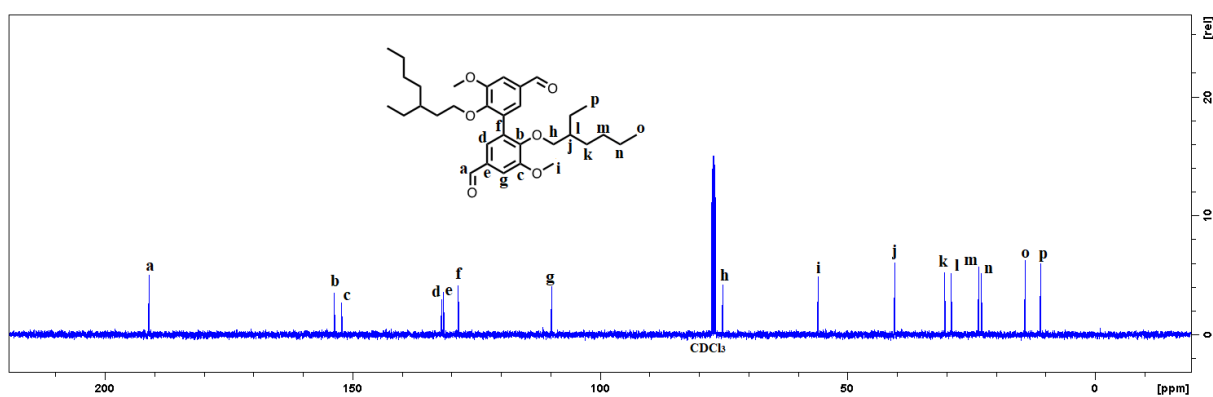


Figure 53:  $^{13}\text{C-NMR}$  spectrum of DVEH (100.70 MHz, in  $\text{CDCl}_3$ )

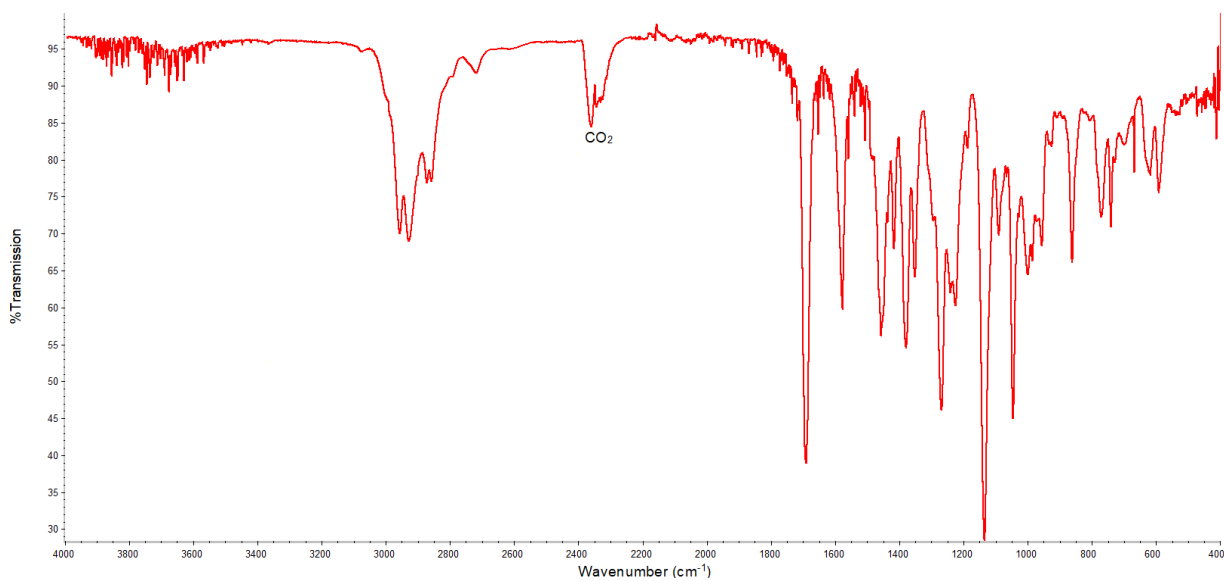
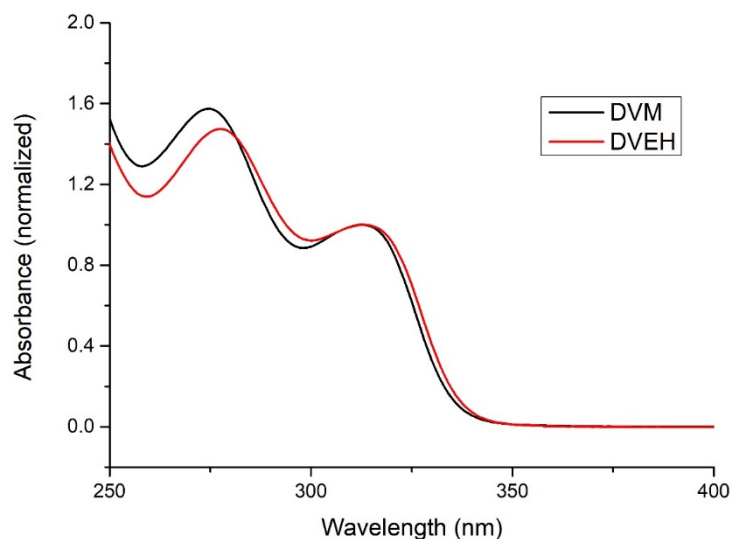


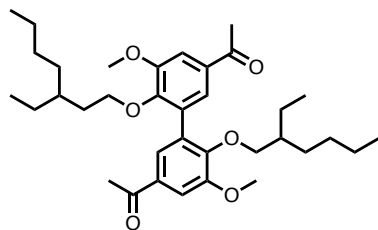
Figure 54: ATR-FTIR spectrum of DVEH



**Figure 55:** Absorbance spectra of **DVEH** and **DVM** in methylene chloride,  $10^{-2}$  g/L

### 6.5.2. Characterization of **DAcVEH**

#### 6,6'- 2-ethylhexoxy-5,5'-dimethoxy-[1,1'-biphenyl]-3,3'-diethanone



$^1\text{H-NMR}$  (400.20 MHz, DMSO- $d_6$ , ppm): 7.56-7.55 (d,  $J = 4\text{Hz}$ , 2H); 7.51-7.50 (d,  $J = 4\text{Hz}$ , 2H); 3.89 (s, 6H); 3.78-3.68 (m, 4H); 2.55 (s, 6H); 1.33-0.92 (m, 20H), 0.75 (t,  $J = 8\text{Hz}$ , 6H); 0.62 (td,  $J = 8\text{Hz}$ ,  $J = 4\text{Hz}$ , 6H).  $^{13}\text{C-NMR}$  (100.70 MHz,  $\text{CDCl}_3$ , ppm): 197.2; 153.2; 150.9; 132.2; 131.6; 125.9; 110.5; 75.3; 56.1; 40.5; 30.8; 29.3; 26.5; 23.6; 23.1; 14.3; 11.2. FT-IR (ATR,  $\text{cm}^{-1}$ ):  $\nu = 2955$ ; 2927; 2871; 1675; 1574; 1456; 1402; 1367; 1278; 1224; 1214; 1191; 1180; 1169; 1088; 1039; 1006; 980; 958; 892; 869; 827; 693; 648;

601; 571.

Aspect: white oil, solid at RT

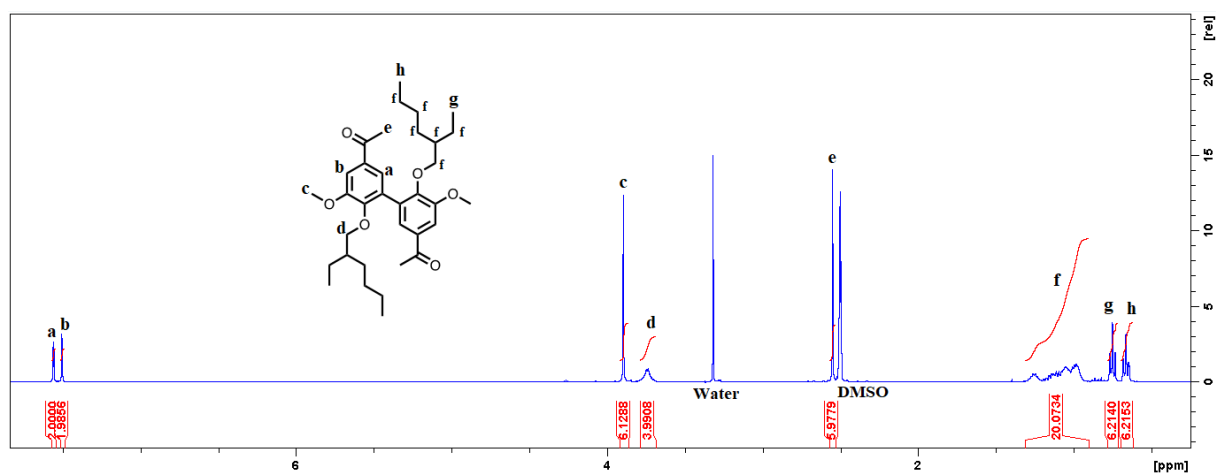


**Figure 56:**  $^1\text{H-NMR}$  spectrum of **DAcVEH** (400.20 MHz, in DMSO- $d_6$ )

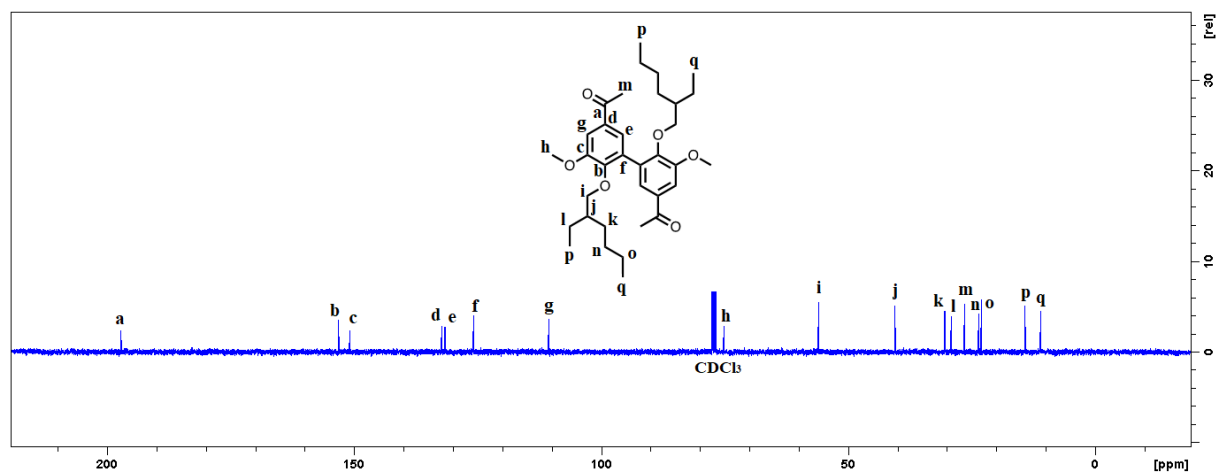


Figure 57:  $^{13}\text{C}$ -NMR spectrum of DAcVEH (100.70 MHz, in  $\text{CDCl}_3$ )

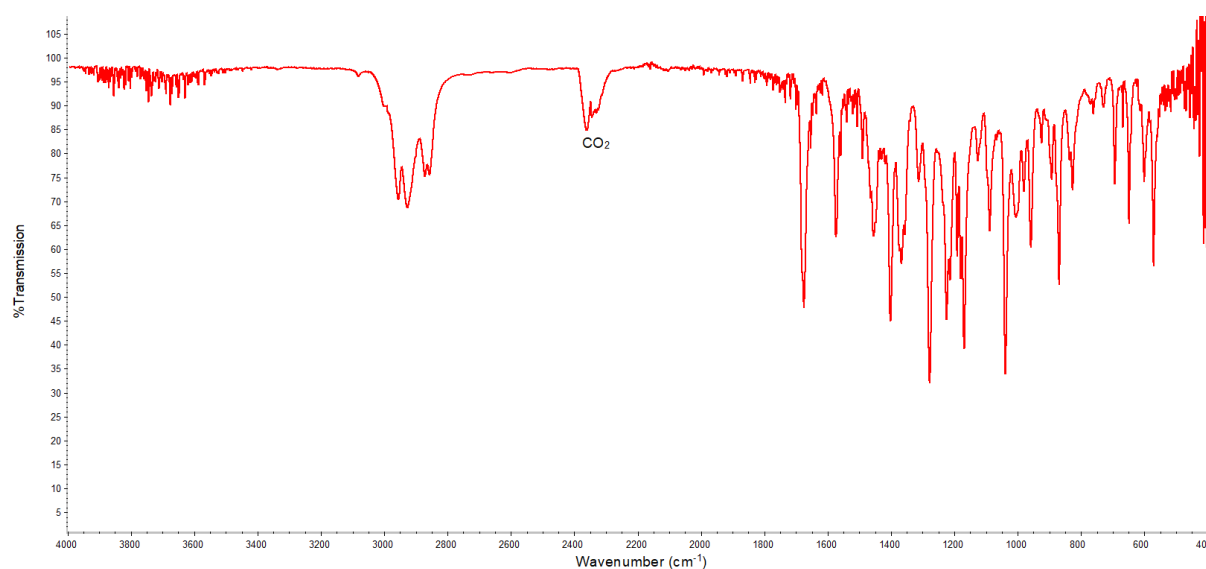


Figure 58: ATR-FTIR spectrum of DAcVEH

### 6.5.3. Dimerization of ortho-vanillin and iso-vanillin

5.6g of sodium acetate and 1.75 mL of acetic acid were dissolved in 1 L of water to give the buffer. In an appropriate vessel, 1.5 g of ortho or iso-vanillin were dissolved in 20 mL of acetone, afterwards 180mL of the previously prepared buffer were added. 12.4 mg of Laccase from *Trametes Versicolor* were finally added, and the medium was saturated with oxygen. After 24 h at  $25^\circ\text{C}$  under constant and light stirring, the medium was filtrated to give a brown or beige powder for ortho and iso-vanillin respectively. The filtrate was extracted three times with methylene chloride. Afterwards the organic and aqueous phase were both dried separately to give two final fractions.

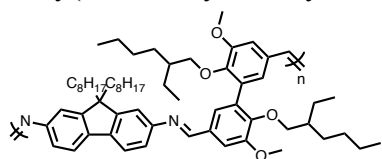
## 6.6. Synthesis and characterization of polyazomethines

### 6.6.1. General protocol for polymerization

In a 10 mL microwave dedicated glassware, a stoichiometric amount of *p*-phenylenediamine or 2,7-diaminocarbazole and of divanillin or diacétovanillone derivative is put in suspension in 5 mL of toluene. Silica (300 mg) was then added with catalytic amount of PTSA and the reaction heated at 130°C for 4 hours using microwave irradiation. The crude polymer was then solubilized in a minimum amount of methylene chloride, and 100 mL of methanol are added. The solution turns cloudy. The solvents are then evaporated using rotary evaporator, to obtain a powder which is rinsed with methanol, to give the final polymer.

### 6.6.2. Characterization of P1

Poly(6,6'-2-ethylhexoxy-5,5'-dimethoxy-[1,1'-biphenyl] – 3,3'-methylidene- (9,9 dioctyl n,n, fluorenylamine



<sup>1</sup>H-NMR (400.2 MHz, CDCl<sub>3</sub>): 9.89 (s, 0.043H); 8.48 (s, 2H); 7.69 (m, 3.9H); 7.41 (m, 1.78H); 7.21 (s, 4.67H); 4.00 (s, 5.67H); 3.80-3.79 (d, J = 4Hz, 3.9H); 2.10-1.69 (m, 11H); 1.49-0.93 (m, 44H); 0.85-0.72 (m, 19H). FT-IR (ATR, cm<sup>-1</sup>): ν = 2954; 2924; 2854; 1623; 1572; 1461; 1408; 1374; 1265; 1224; 1140; 1092; 1049; 1001; 962; 863; 819.

Aspect: yellow/orange film

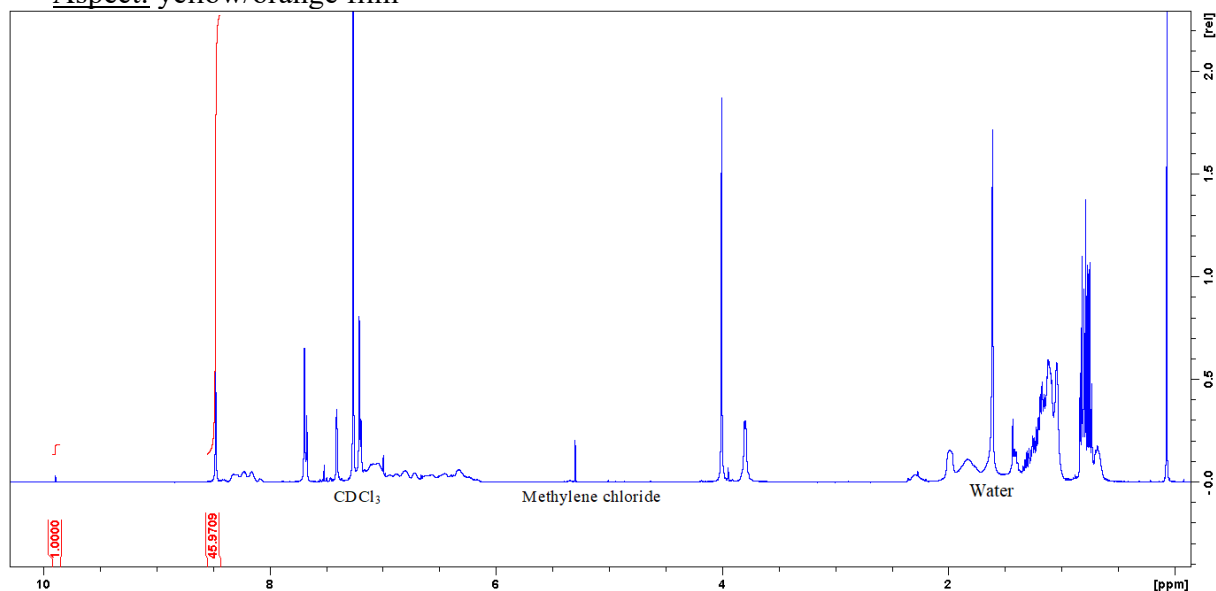
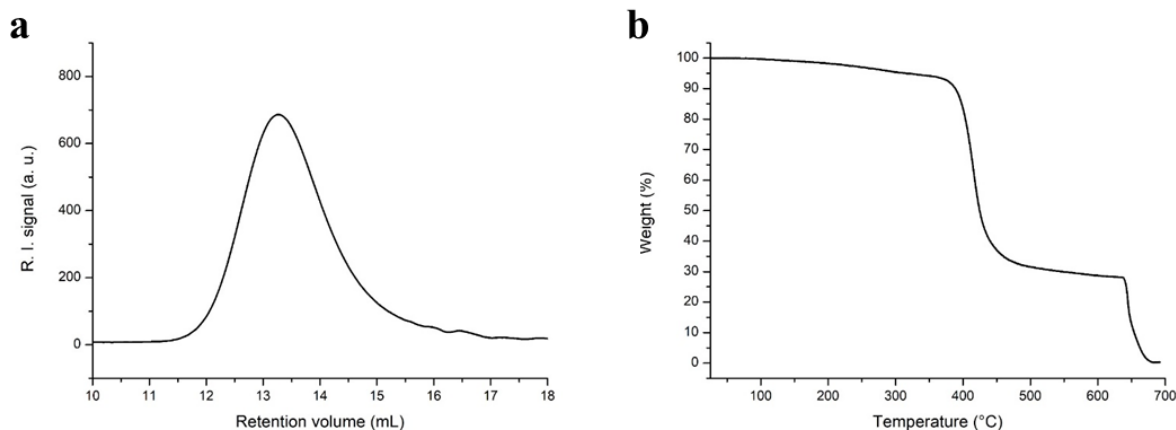
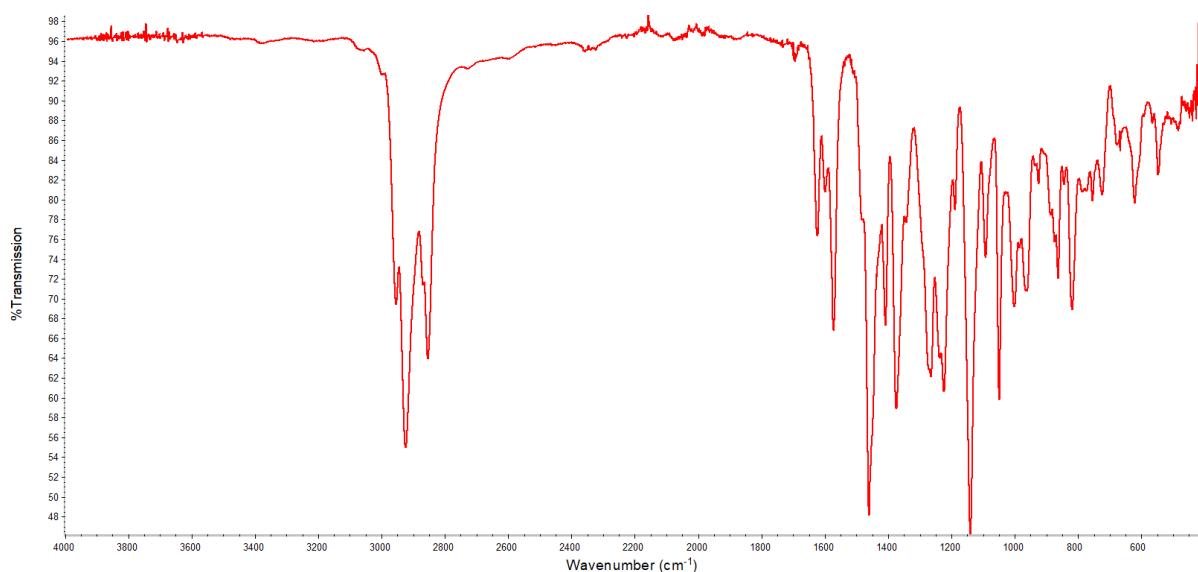


Figure 59: <sup>1</sup>H-NMR spectrum of P1 (400.20 MHz, in CDCl<sub>3</sub>, 128 scans)



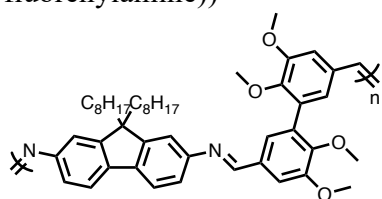
**Figure 60a:** SEC trace of **P1** in THF, R. I. detection. **b:** TGA curve of **P1** at 10°C/min under N<sub>2</sub> until 650°C, then under air



**Figure 61:** ATR-FTIR spectrum of **P1**

### 6.6.3. Characterization of **P2**

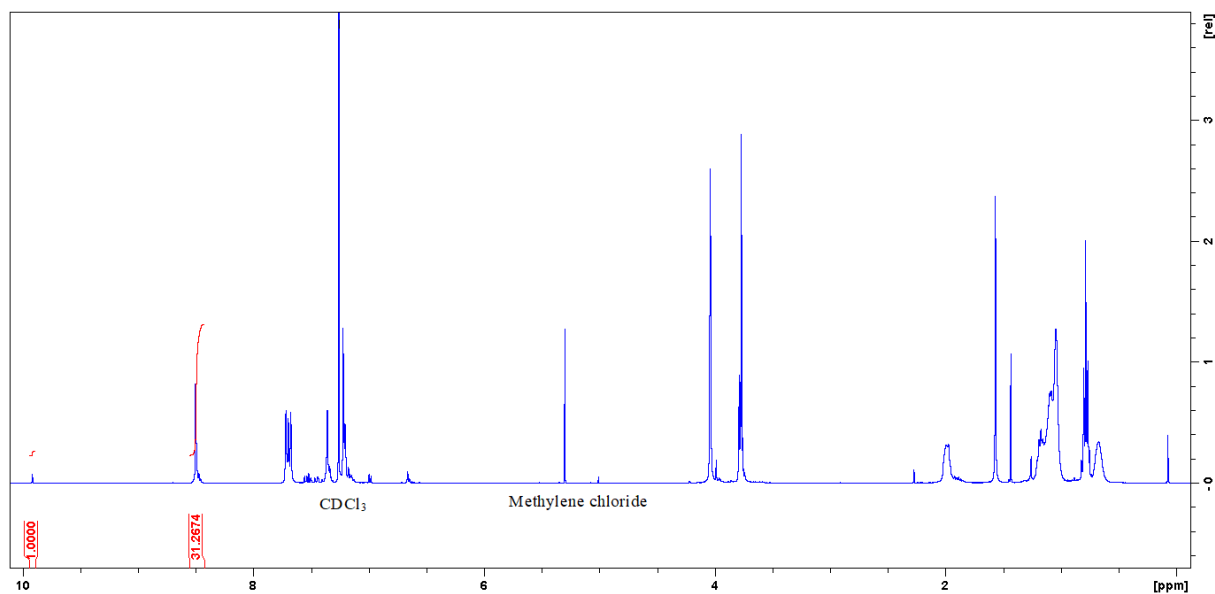
Poly(6,6'-methoxy-5,5'-dimethoxy-[1,1'-biphenyl] - 3,3'-methylidene- (9,9 dioctyl n,n, fluorenylamine))



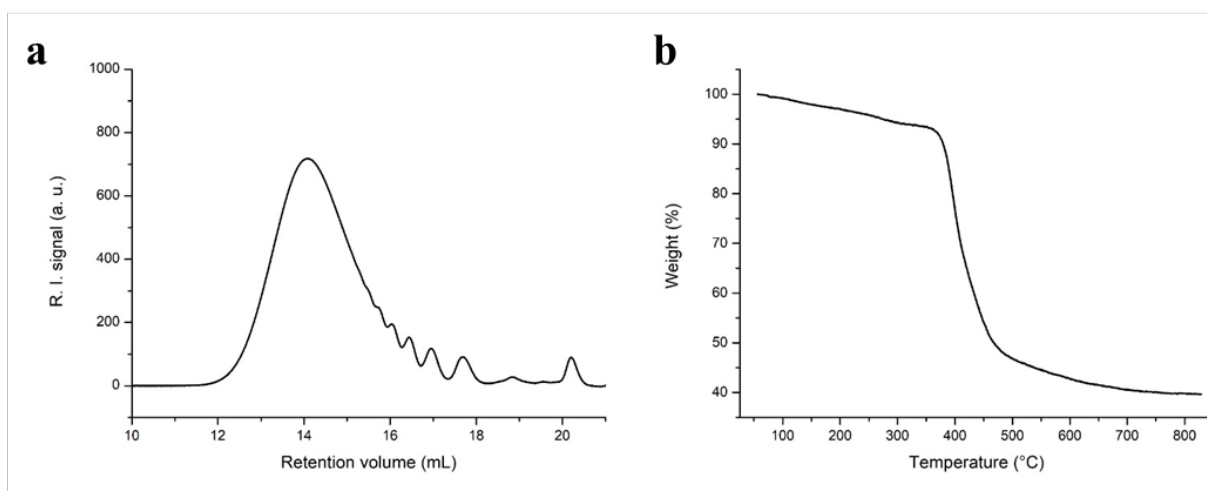
<sup>1</sup>H-NMR (400.2 Hz, CDCl<sub>3</sub>): 9.92 (s, 0.064H); 8.50 (s, 2H); 7.72-7.67 (m, 3.8H); 7.36 (m, 1.78H); 7.22 (s, 3.4H); 4.04 (s, 5.8H); 3.77 (s, 6.2H); 2.05 -1.9 (m, 3.8H); 1.27-0.98 (m, 23.2H); (d, J = 4Hz, 3.9H); 2.10-1.69 (m, 11H); 1.49-0.93 (m, 44H); 0.85-0.57 (m, 11.3H). FT-IR (ATR, cm<sup>-1</sup>): ν= 2922; 2850; 1623; 1575; 1482; 1460; 1408; 1375; 1340; 1274; 1232; 1189; 1136; 1091; 1048; 1003; 968; 862; 820; 753; 720; 668; 621; 567; 546;

509.

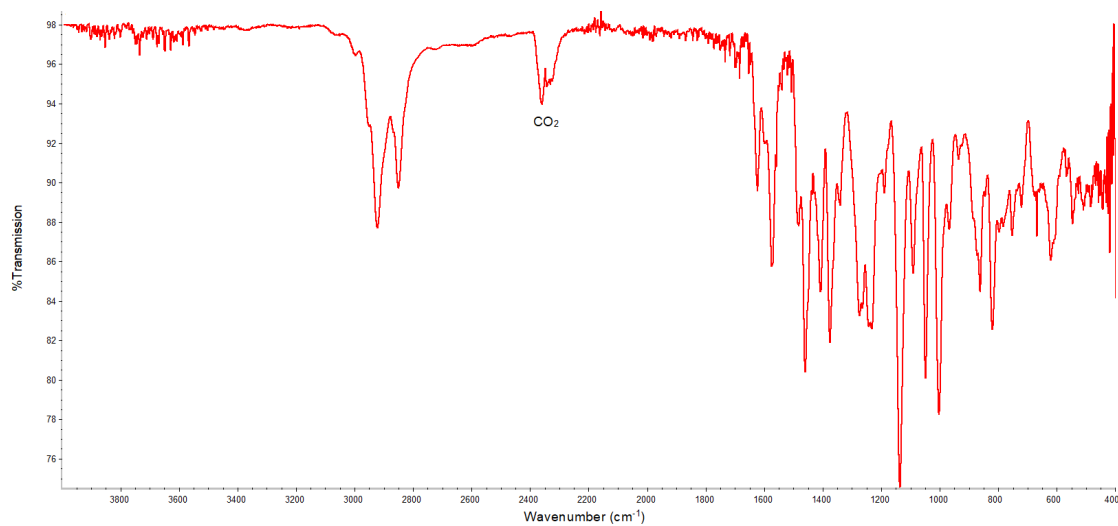
Aspect: yellow film



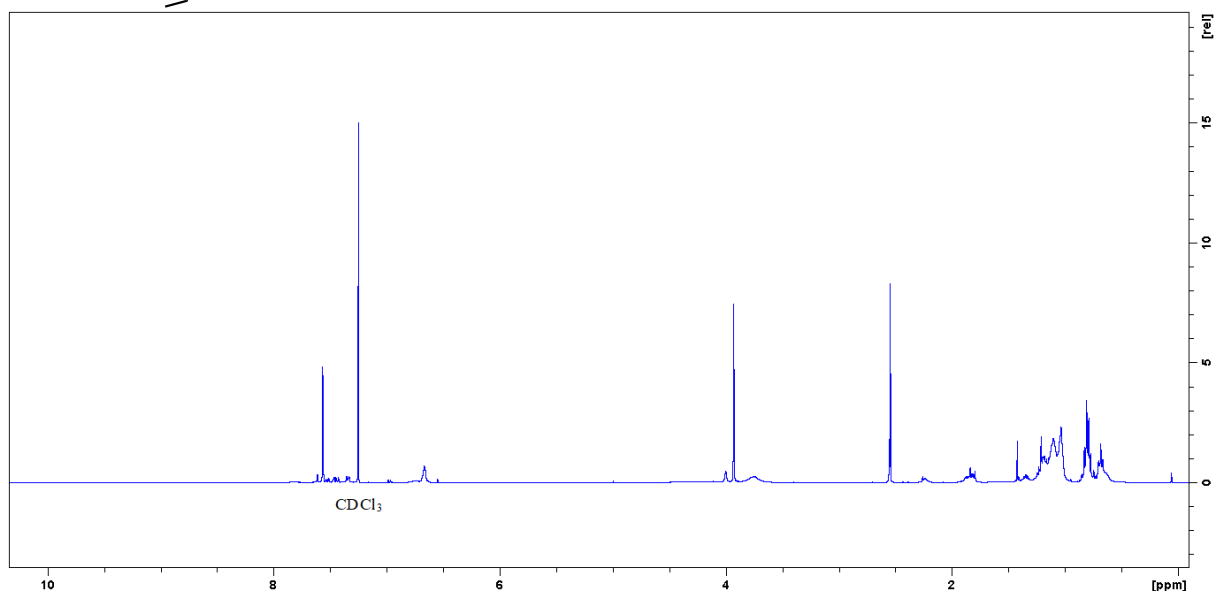
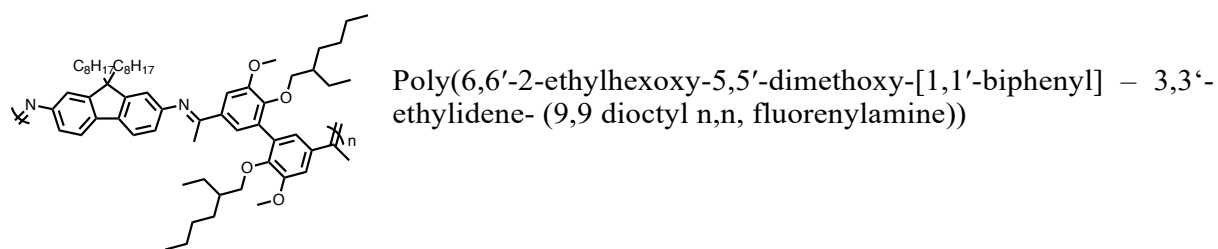
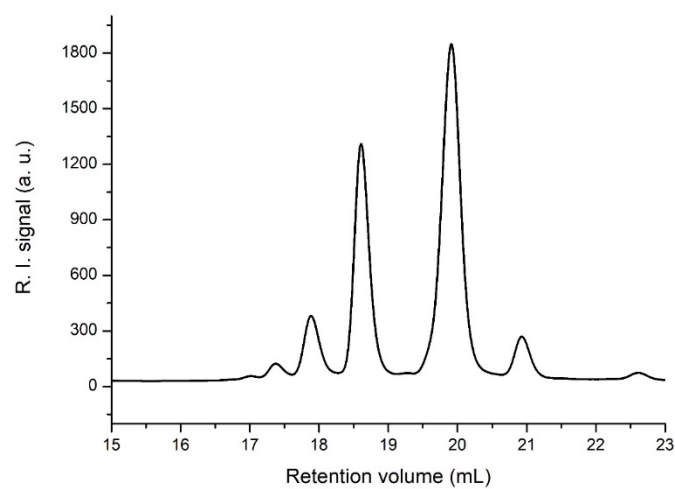
**Figure 62:**  $^1\text{H-NMR}$  spectrum of **P2** (400.20 MHz, in  $\text{CDCl}_3$ , 128 scans)

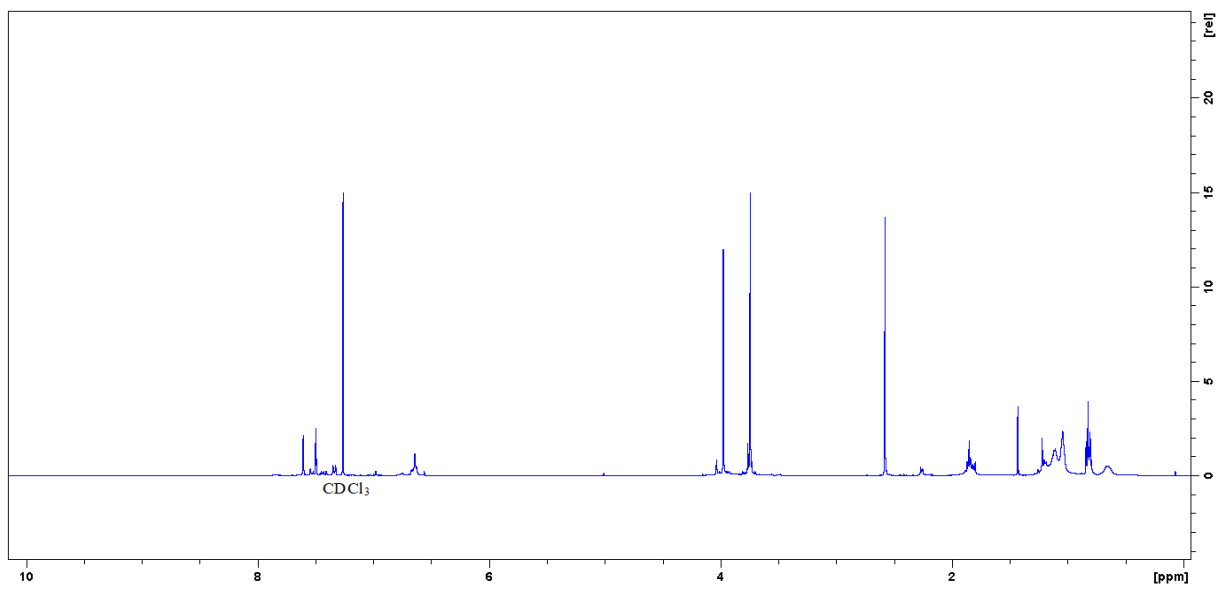
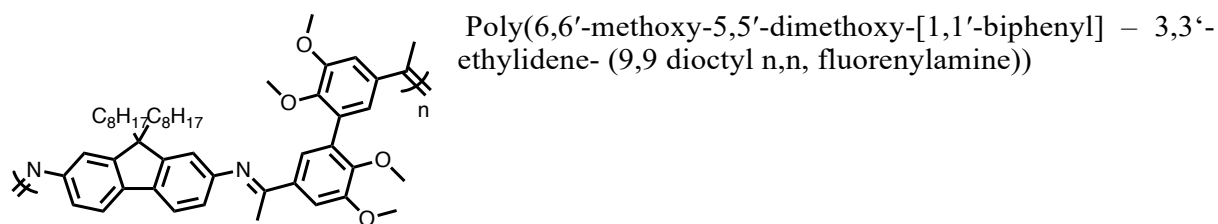


**Figure 63a:** SEC trace of **P2** in THF, R. I. detection. **b:** TGA curve of **P2** at  $10^{\circ}\text{C}/\text{min}$  under  $\text{N}_2$



**Figure 64:** ATR-FTIR spectrum of **P2**

6.6.4. Characterization of **P3****Figure 65:** <sup>1</sup>H-NMR spectrum of **P3** (400.20 MHz, in CDCl<sub>3</sub>)**Figure 66:** SEC trace of **P3** in THF, R.I. detection

6.6.5. Characterization of **P4**

**Figure 67:** <sup>1</sup>H-NMR spectrum of **P4** (400.20 MHz, in CDCl<sub>3</sub>)

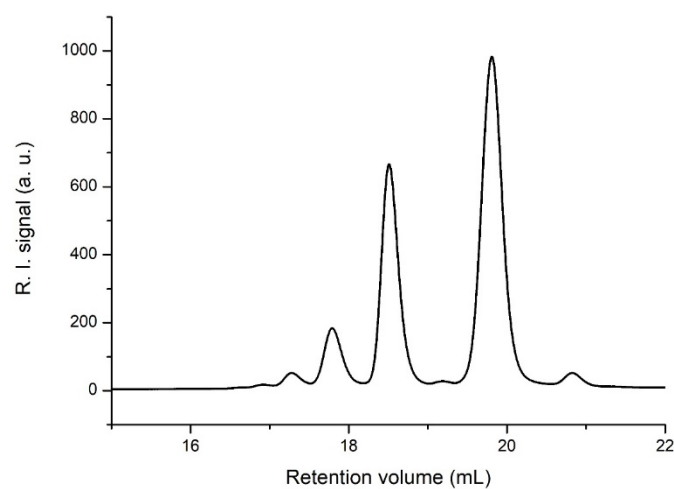
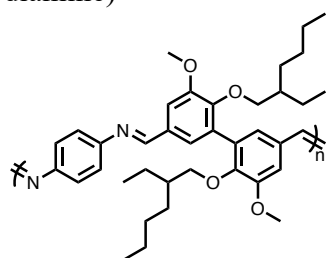


**Figure 68:** SEC trace of **P4** in THF, R.I. detection



6.6.6. Characterization of **P5**

Poly(6,6'-2-ethylhexoxy-5,5'-dimethoxy-[1,1'-biphenyl]-3,3'-methylidene-(1,4-benzene diamine))



$^1\text{H-NMR}$  (400.2 MHz,  $\text{CDCl}_3$ ): 9.89 (s, 0.024H); 8.42 (s, 2H); 7.67 (m, 1.9H); 7.36 (m, 1.6H); 3.99 (s, 6.4H); 3.77 (s, 4H); 1.58 (s, 1.5H); 1.45-1.01 (m, 20H); 0.81 (t,  $J = 8\text{Hz}$ , 6.2H); 0.73 (t,  $J = 8\text{Hz}$ , 6.2H). (NB: the four protons of the phenylene moiety are superposed with the solvent peak). FT-IR (ATR,  $\text{cm}^{-1}$ ):  $\nu = 2954$ ; 2925; 2857; 1617; 1570; 1497; 1448; 1406; 1364; 1268; 1217; 1190; 1141; 1046; 999; 969; 865; 821; 770; 742; 728; 625; 580; 539; 505.

Aspect: dark yellow film

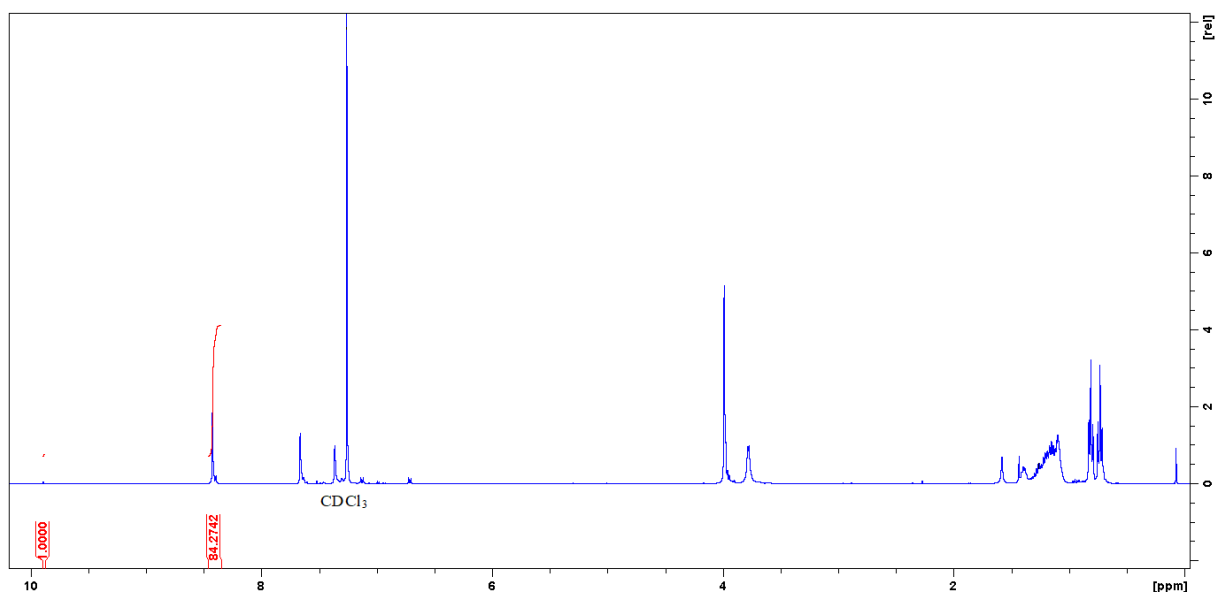


**Figure 69:**  $^1\text{H-NMR}$  spectrum of **P5** (400.20 MHz, in  $\text{CDCl}_3$ , 128 scans)

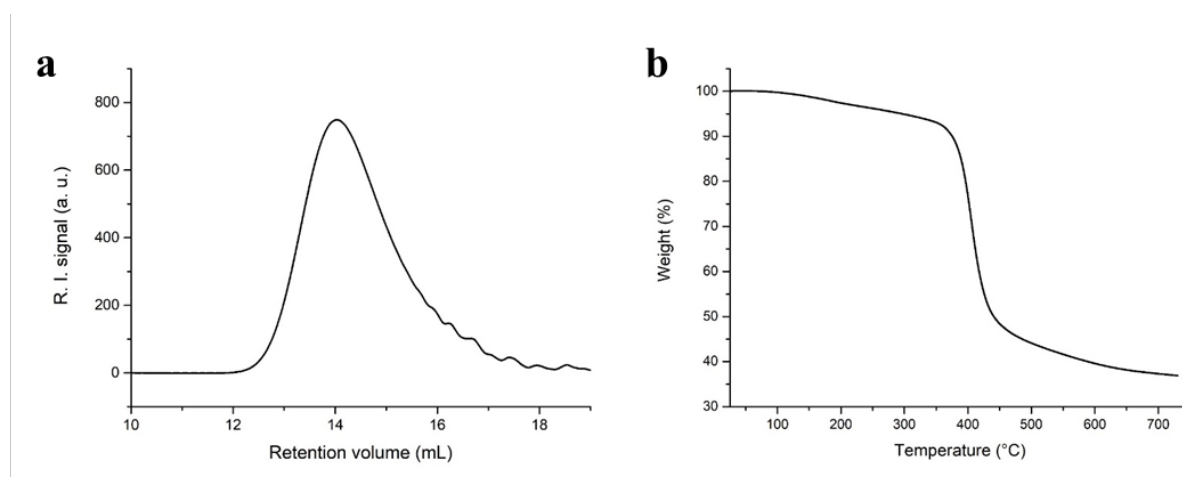


**Figure 70a:** SEC trace of **P5** in THF, R. I. detection. **b:** TGA curve of **P5** at  $10^\circ\text{C}/\text{min}$  under  $\text{N}_2$

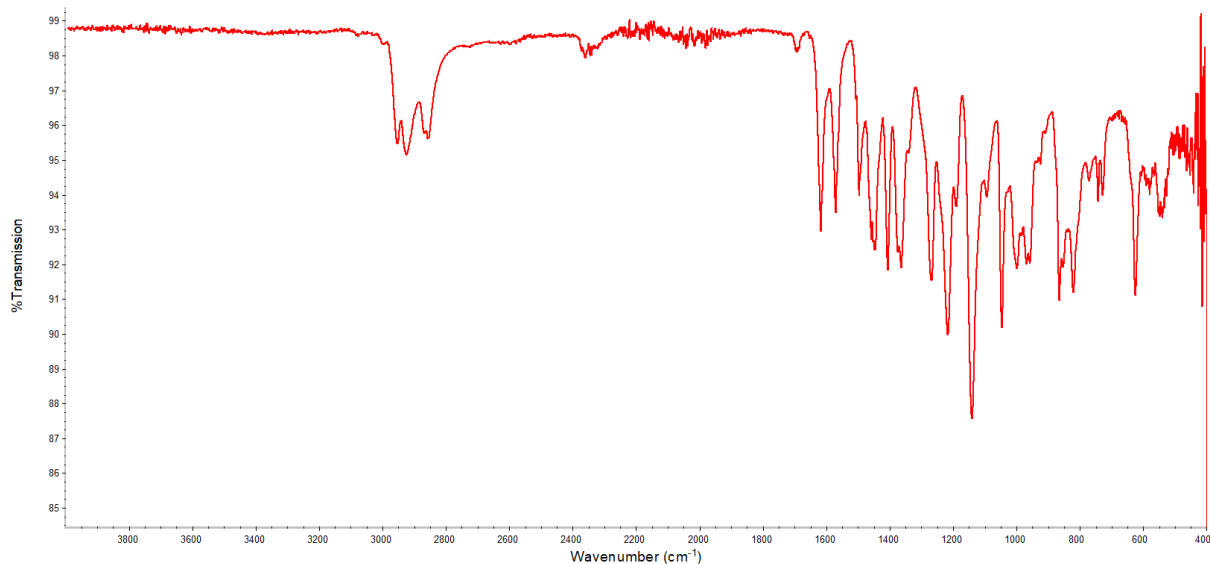
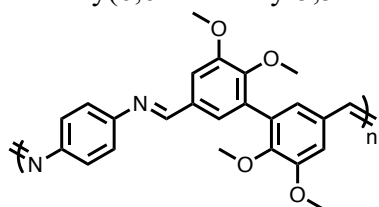


Figure 71: ATR-FTIR spectrum of P5

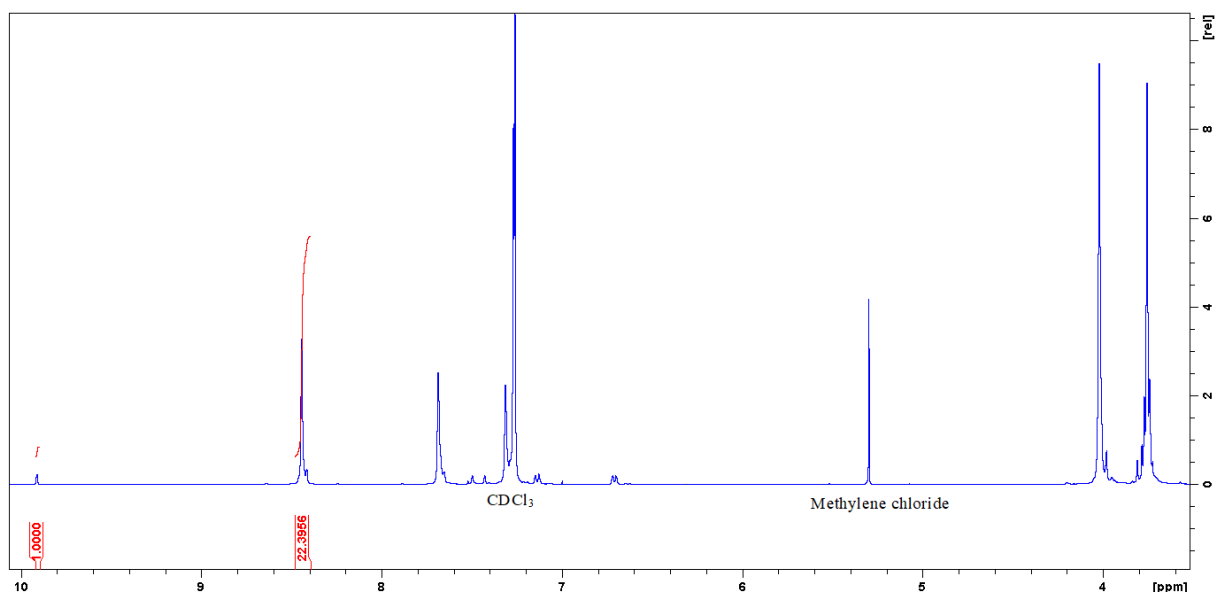
## 6.6.7. Characterization of P6

Poly(6,6'-methoxy-5,5'-dimethoxy-[1,1'-biphenyl]-3,3'-methylidene-(1,4-benzene diamine)



$^1\text{H-NMR}$  (400.2 MHz,  $\text{CDCl}_3$ ): 9.91 (s, 0.092H); 8.44 (s, 2H);  
7.68 (s, 1.9H); 7.31 (m, 1.6H); 4.02 (s, 6.2H); 3.75 (s, 6.5H).  
FT-IR (ATR,  $\text{cm}^{-1}$ ):  $\nu =$  2934; 1617; 1576; 1570; 1559; 1507;  
1496; 1490; 1472; 1457; 1405; 1374; 1339; 1273; 1231; 1133;  
1089; 1046, 998; 854; 783; 730; 668; 622; 585; 546; 526; 517.

Aspect: dark yellow powder

Figure 72:  $^1\text{H-NMR}$  spectrum of P6 (400.20 MHz, in  $\text{CDCl}_3$ , 128 scans)

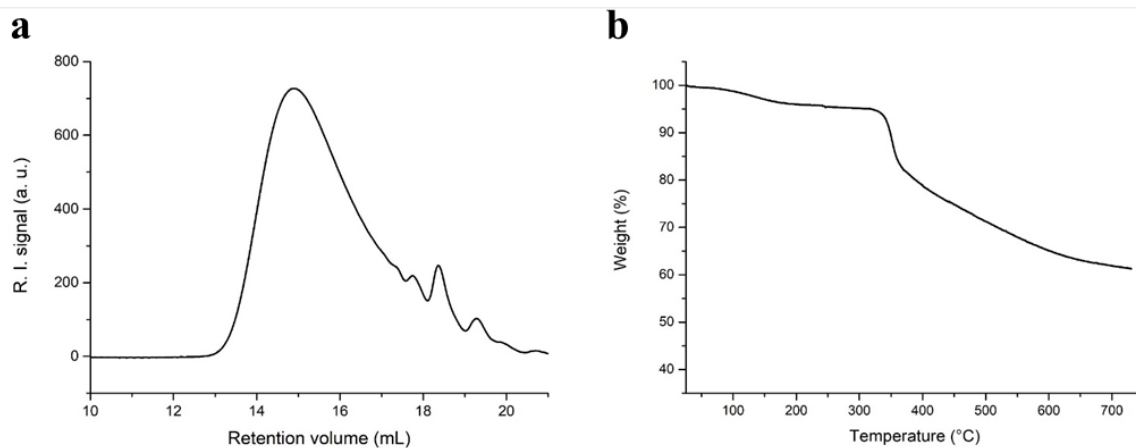


**Figure 73a:** SEC trace of **P6** in THF, R. I. detection. **b:** TGA curve of **P6** at 10°C/min under N<sub>2</sub>

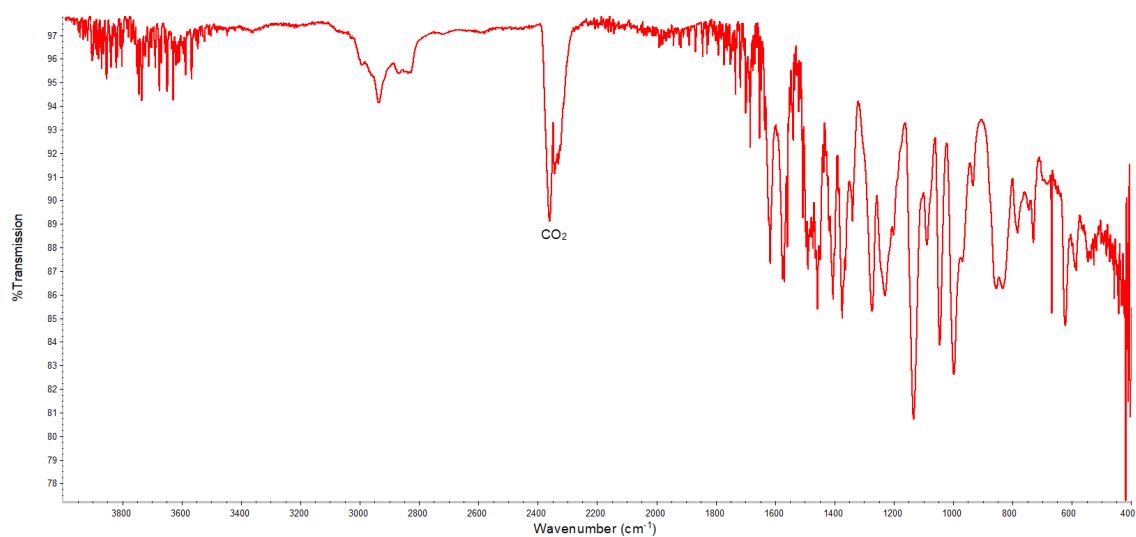
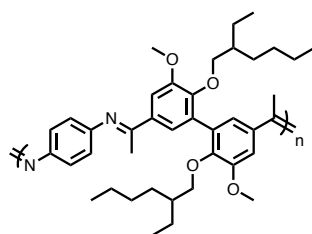


**Figure 74:** ATR-FTIR spectrum of **P6**

#### 6.6.8. Characterization of **P7**



Poly(6,6'-2-ethylhexoxy-5,5'-dimethoxy-[1,1'-biphenyl]-3,3'-ethylidene-(1,4-benzene diamine))

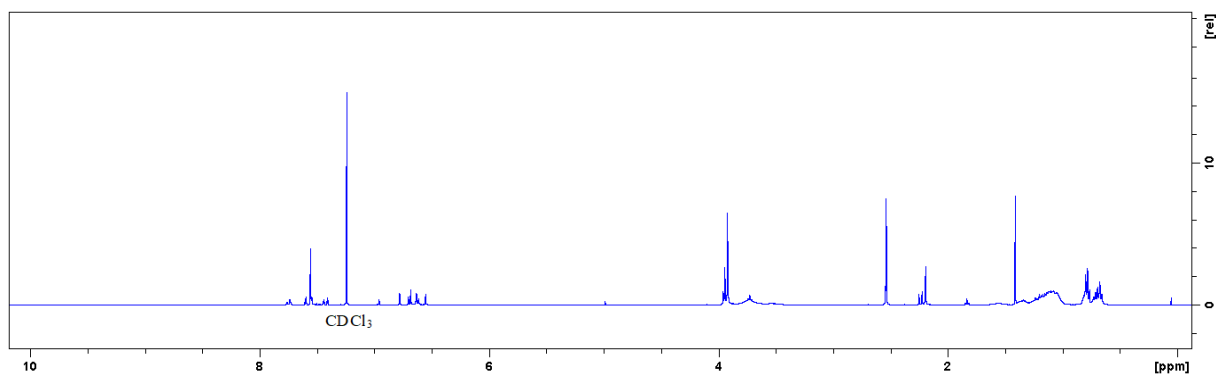


**Figure 75:**  $^1\text{H-NMR}$  spectrum of **P7** (400.20 MHz, in  $\text{CDCl}_3$ )

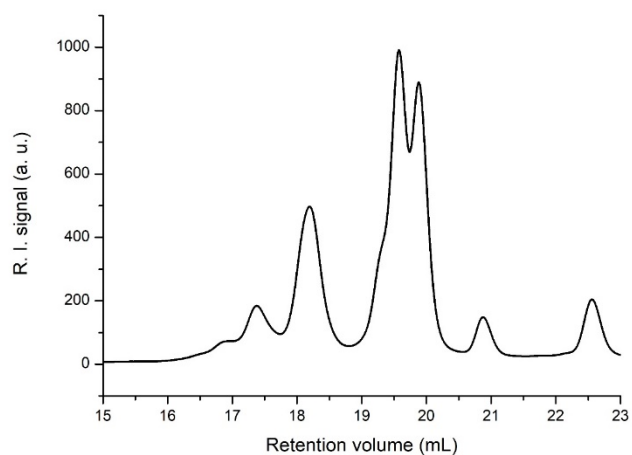
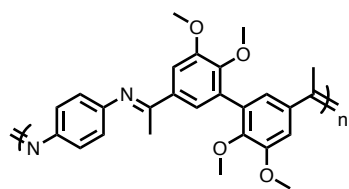


**Figure 76:** SEC trace of **P7** in THF, R.I. detection

#### 6.6.9. Characterization of **P8**



Poly(6,6'-methoxy-5,5'-dimethoxy-[1,1'-biphenyl]-3,3'-methylidene-(1,4-benzene diamine))

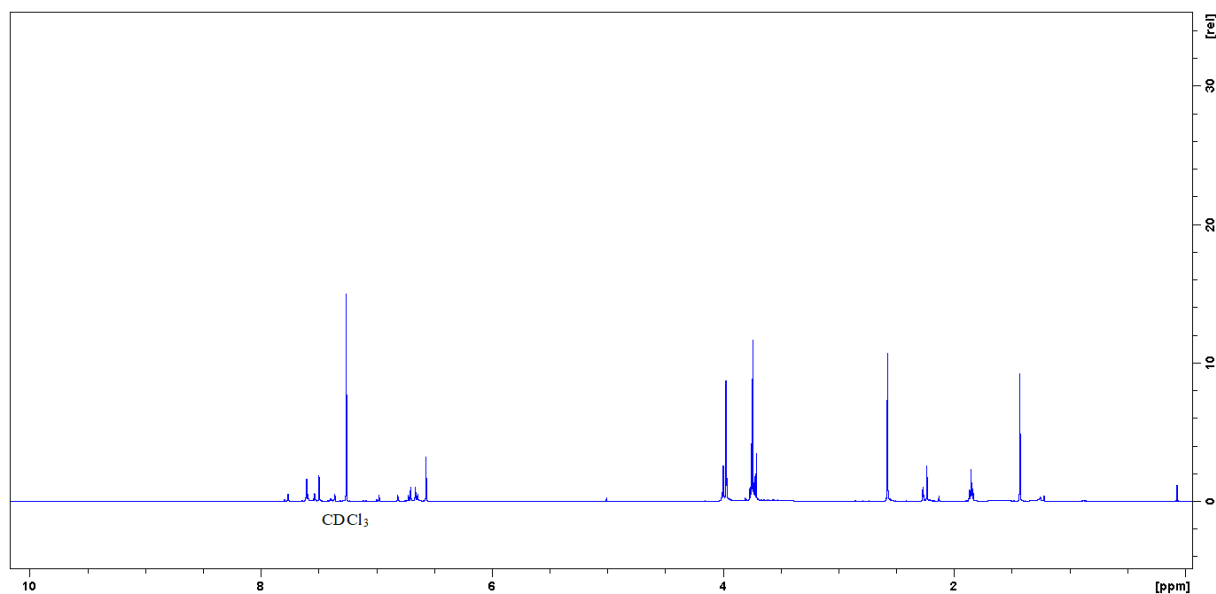


**Figure 77:**  $^1\text{H-NMR}$  spectrum of **P8** (400.20 MHz, in  $\text{CDCl}_3$ )

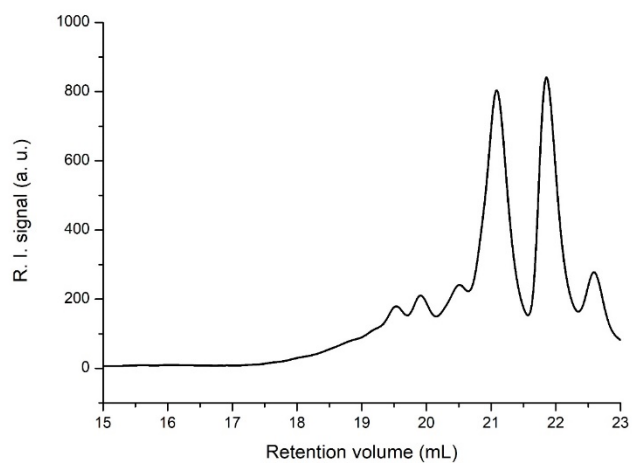
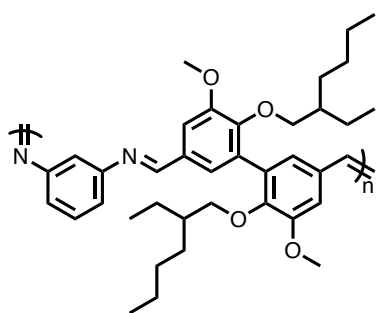


**Figure 78:** SEC trace of **P8** in THF, R.I. detection

#### 6.6.10. Characterization of **P9**



Poly(6,6'-2-ethylhexoxy-5,5'-dimethoxy-[1,1'-biphenyl]-3,3'-methylidene-(1,3-benzene diamine)  
 FT-IR (ATR,  $\text{cm}^{-1}$ ):  $\nu=$  2954, 2926, 2857, 1625, 1572, 1449, 1407, 1372, 1269, 1223, 1188, 1135, 1090, 1048, 998, 954, 863, 773, 691, 621, 543, 458.

Aspect: yellow “fibers”, insoluble



**Figure 79:** ATR-FTIR spectrum of **P9**

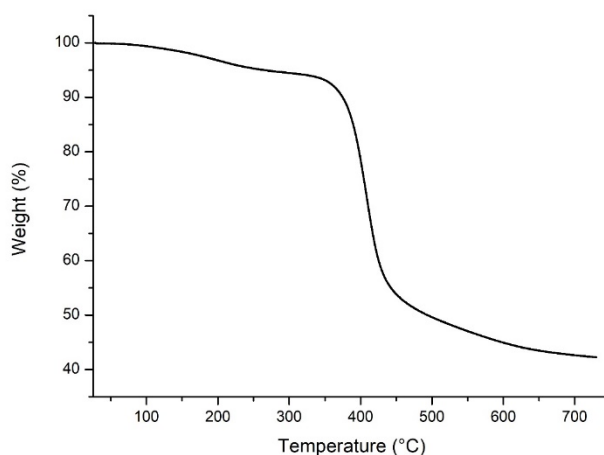
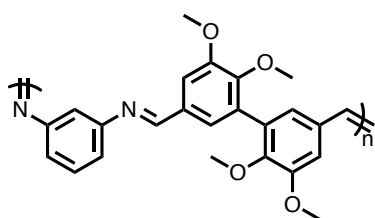


**Figure 80:** TGA curve of **P9** at 10°C/min under N<sub>2</sub>

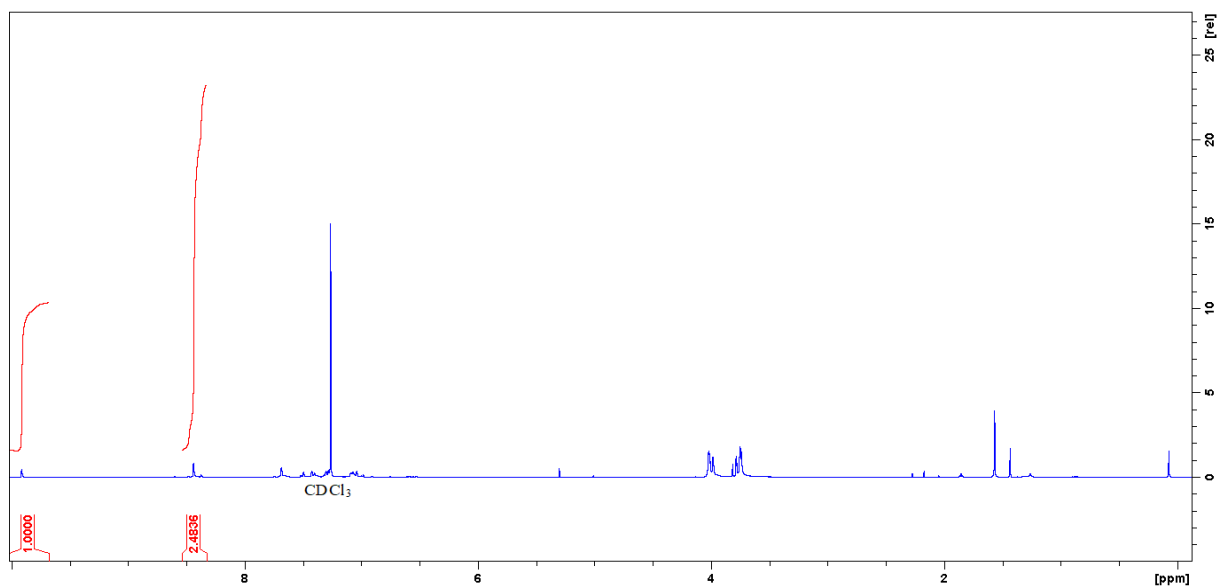
#### 6.6.11. Characterization of **P10**



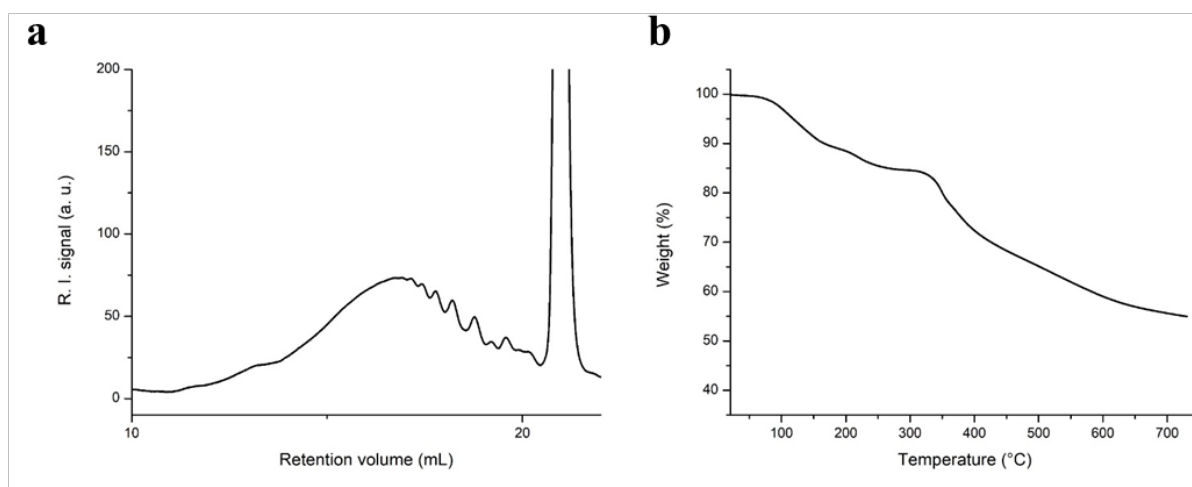
Poly (6, 6'- methoxy- 5,5'- dimethoxy - [1,1'- biphenyl] - 3,3'-methylidene -(1,3benzene diamine)

<sup>1</sup>H-NMR (400.2 Hz, CDCl<sub>3</sub>): 9.91 (s, 1H); 8.44 (s, 2.45H); 7.68 (s, 2.45H); 7.49 (m, 1.1H); 7.43-7.36 (m, 2.42H); 7.10-7.02 (m, 4.18H); 4.04-3.96 (m, 12H); 3.82-3.71 (m, 13.8H).

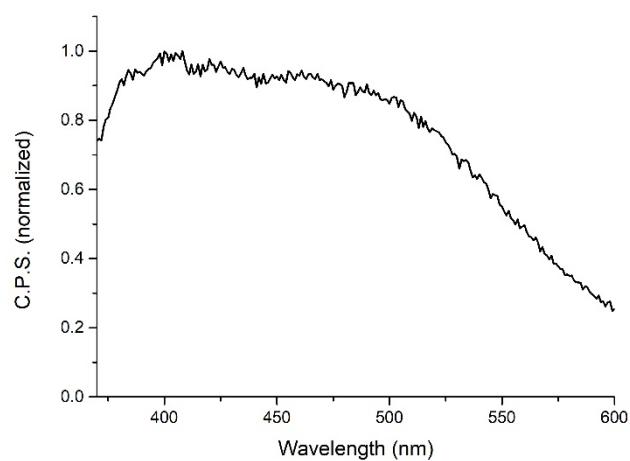
Aspect: pale yellow powder



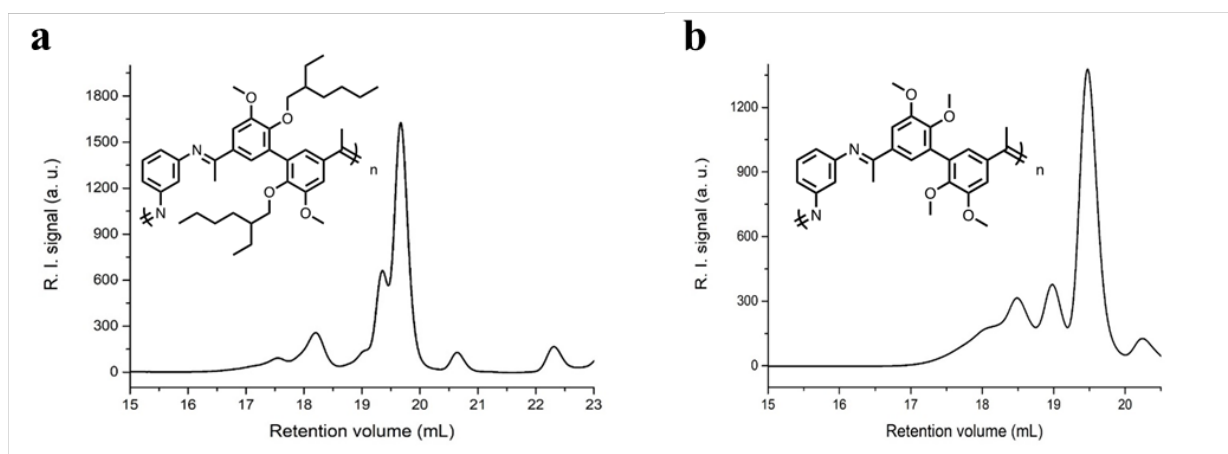
**Figure 81:**  $^1\text{H-NMR}$  spectrum of **P10** (400.20 MHz, in  $\text{CDCl}_3$ , 128 scans)



**Figure 82a:** SEC trace of **P10** in THF, R. I. detection. **b:** TGA curve of **P10** at  $10^\circ\text{C}/\text{min}$  under  $\text{N}_2$



**Figure 83:** Emission spectrum of **P10** in methylene chloride ( $10^{-2}$  g/L)

6.6.12. Characterization of **P11** and **P12**

**Figure 84a:** SEC trace of **P11** in THF, R. I. detection. **b:** SEC trace of **P12** in THF, R. I. detection.

## 6.7. Synthesis and characterization of model compounds and their precursors

6.7.1. Characterization of **VM**

## 3,4-dimethoxy-benzaldehyde

COc1ccc(C=O)cc1OC
<sup>1</sup>H-NMR (400.20 MHz, CDCl<sub>3</sub>, ppm): 9.85 (s, 1H); 7.47-7.45 (dd, J = 2Hz, J = 8Hz, 1H); 7.41 (d, J = 2Hz, 1H); 6.99-6.97 (d, J = 8Hz, 1H); 3.97 (s, 3H); 3.94 (s, 3H). <sup>13</sup>C-NMR (100.70 MHz, CDCl<sub>3</sub>) 190.9; 154.5; 149.6; 130.2; 126.9; 110.4; 108.9; 56.2; 56.0.

Aspect: white crystal

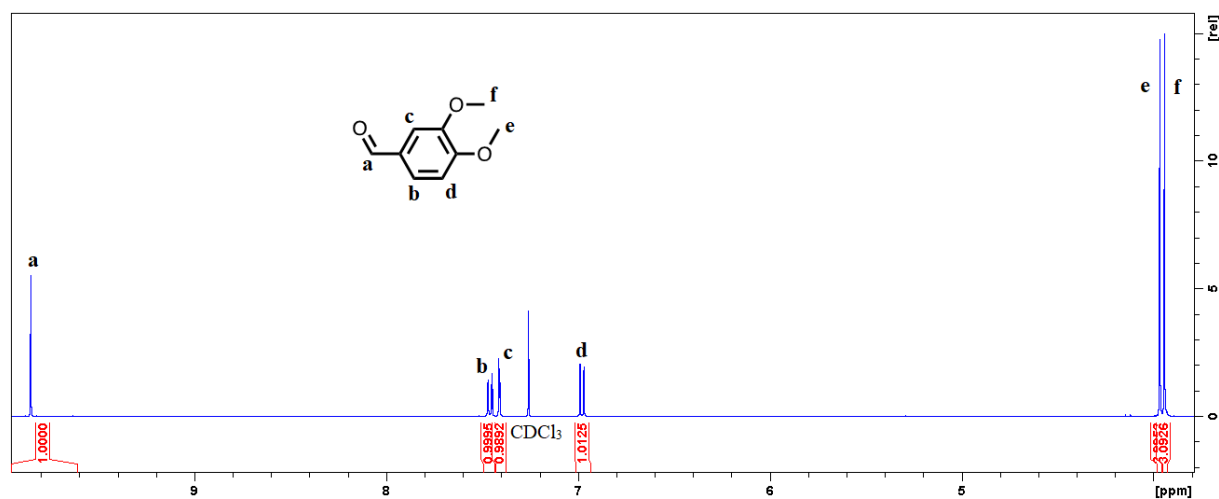


**Figure 85:** <sup>1</sup>H-NMR spectrum of **VM** (400.20 MHz, in CDCl<sub>3</sub>)



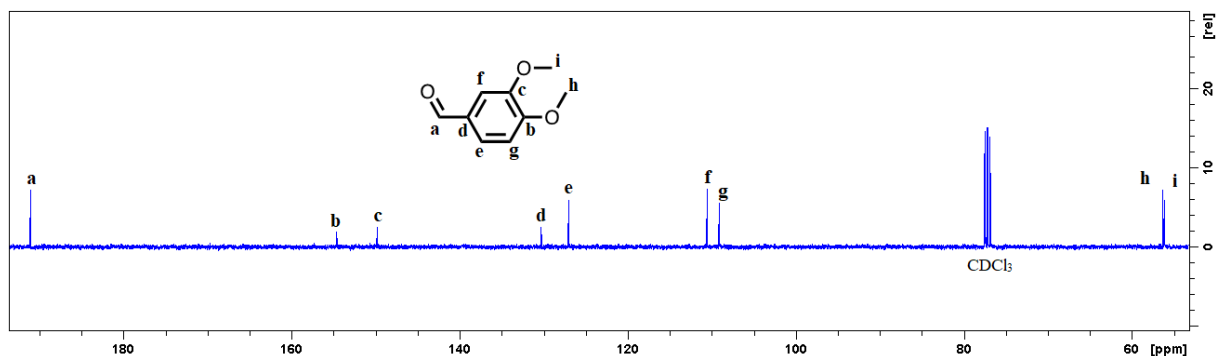
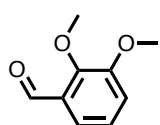


Figure 86: <sup>13</sup>C-NMR spectrum of VM (100.70 MHz, in CDCl<sub>3</sub>)

### 6.7.2. Characterization of oVM

#### 2,3-dimethoxy-benzaldehyde



<sup>1</sup>H-NMR (400.20 MHz, CDCl<sub>3</sub>, ppm): 10.43 (s, 1H); 7.43-7.41 (dd, J = 4Hz, J = 7Hz, 1H); 7.16-7.13 (m, 2H); 3.99 (s, 3H); 3.91 (s, 3H). <sup>13</sup>C-NMR (100.70 MHz, CDCl<sub>3</sub>, ppm): 190.3; 153.1; 152.8; 129.9; 124.3; 119.3; 118.2; 62.5; 56.2.

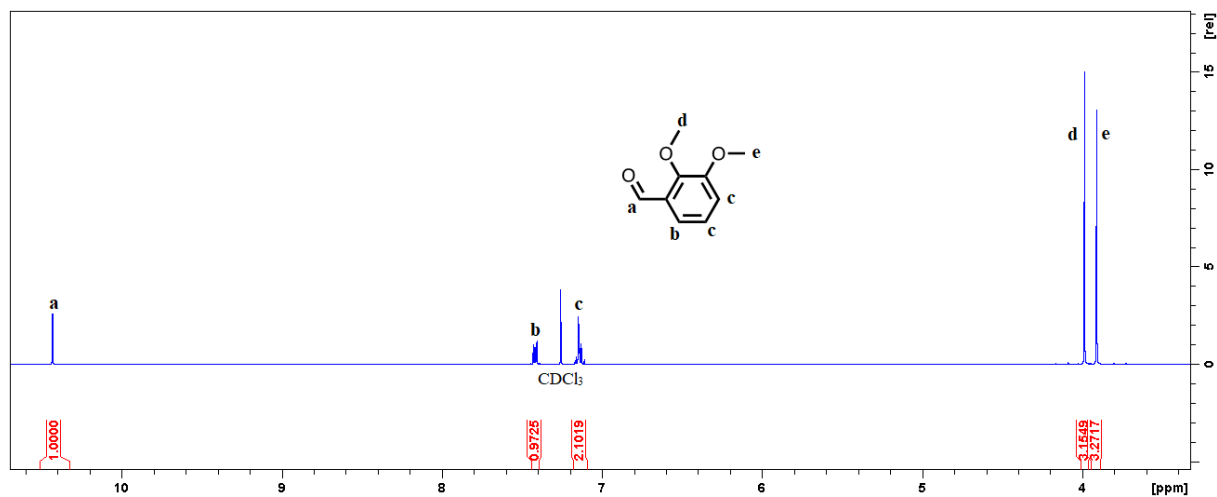


Figure 87: <sup>1</sup>H-NMR spectrum of oVM (400.20 MHz, in CDCl<sub>3</sub>)

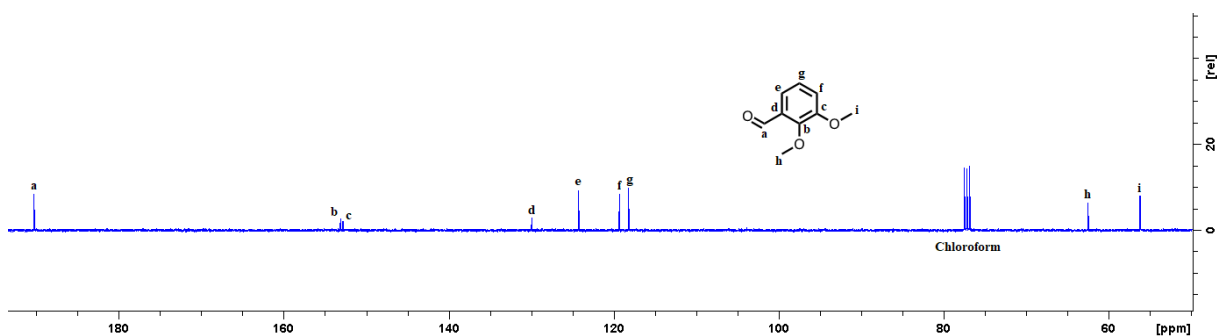


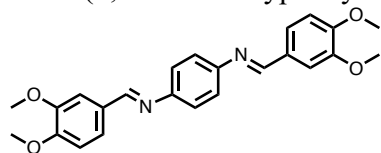
Figure 88: <sup>13</sup>C-NMR spectrum of oVM (100.70 MHz, in CDCl<sub>3</sub>)

## 6.8. General protocol for the synthesis of model compounds

In a flame-dried flask equipped with stirrer and condenser, 2 eq. of (di)aldehyde (or 1 eq.) was dissolved with the (di)amine (1 or 2 eq.) in methanol, under inert atmosphere. The resulting solution was heated at the reflux using conventional heating for 30 minutes, and then filtrated on 0.45 $\mu$ m PTFE filter, and the solvent evaporated under vacuum. The solvents used for purification are indicated for each molecule.

### 6.8.1. Synthesis and purification of M1

#### Di(3,4-dimethoxyphenylmethylidene)-(1,4-diamine benzene)



**Reactants:** methylated vanillin (2 eq.) + para-phenylene-diamine (1 eq.) using general protocol. The obtained product was recrystallized from a warm mixture of methylene chloride and methanol. E/Z in the crude material: 92/8. Conversion: 95 %.

$^1\text{H-NMR}$  (400 MHz,  $\text{CD}_2\text{Cl}_2$ )  $\delta$  (ppm): 8.43 (s, 2H); 7.61 (m, 2H); 7.36-7.33 (d,  $J = 12\text{Hz}$ , 2H); 7.26 (s, 4H); 6.95 (m, 2H); 3.94 (s, 6H); 3.91 (s, 6H).  $^{13}\text{C-NMR}$  (400 MHz,  $\text{CD}_2\text{Cl}_2$ )  $\delta$  (ppm): 159.3; 152.6; 150.2; 150; 130.1; 124.5; 122.1; 111.1; 109.5; 56.2.

**Aspect:** dark orange crystal

#### X-Ray Diffraction data

Space group:  $P\bar{1}$  (triclinic)

Cell length ( $\text{\AA}$ ): **a** 6.7944; **b** 6.961; **c** 11.7543.

Cell angles:  $\alpha$  77.347;  $\beta$  81.596;  $\gamma$  65.069.

Cell volume ( $\text{\AA}^3$ ): 490.993

R factor: 3.6 %

Symmetry: -x, -y, -z.

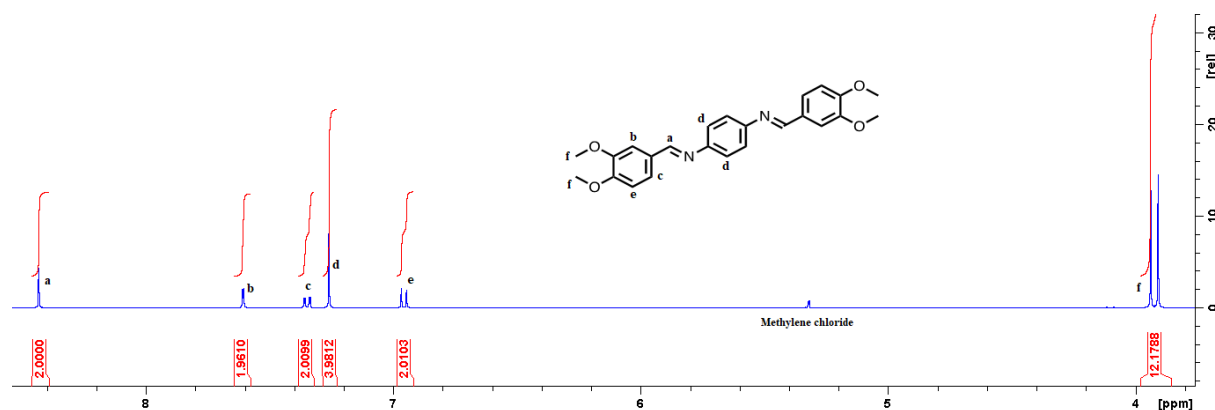


Figure 89:  $^1\text{H-NMR}$  spectrum of M1 (400.20 MHz, in  $\text{CD}_2\text{Cl}_2$ )

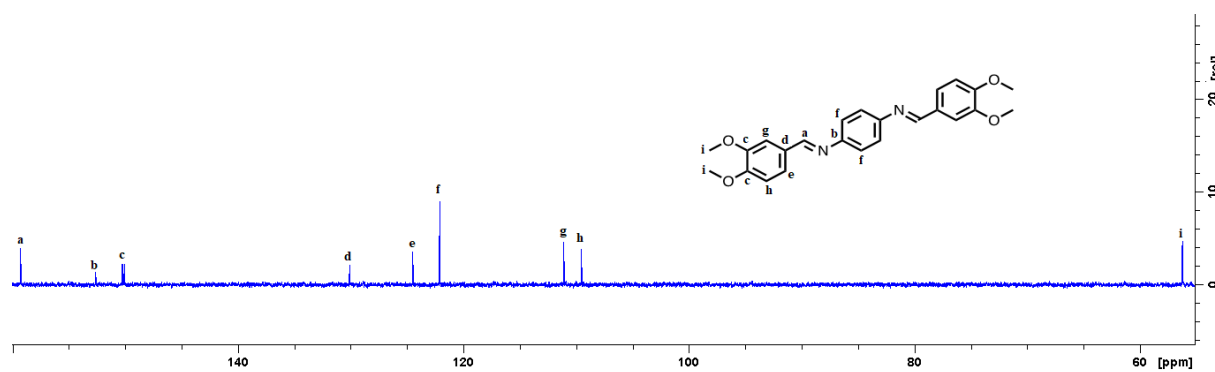
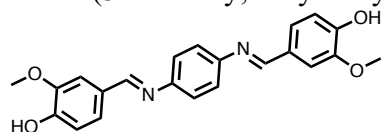


Figure 90:  $^{13}\text{C}$ -NMR spectrum of **M1** (100.70 MHz, in  $\text{CD}_2\text{Cl}_2$ )

### 6.8.2. Synthesis and purification of **M1'**

#### Di (3-methoxy, 4-hydroxyphenylmethylidene)-1,4-diaminobenzene



**Reactants:** vanillin (2 eq.) + para-phenylene-diamine (1 eq.) using general protocol. The final product was obtained after recrystallization from warm methylene chloride/methanol. E/Z in the crude material: 85/15. Conversion: 85 %.

$^1\text{H}$ -NMR (400 MHz,  $\text{DMSO-d}_6$ )  $\delta$  (ppm): 9.74 (s, 2H); 8.51 (s, 2H); 7.55-7.54 (d,  $J = 4\text{Hz}$ , 2H); 7.36-7.34 (d,  $J = 8\text{Hz}$ , 2H); 7.28 (s, 4H); 6.92-6.90 (d,  $J = 8\text{Hz}$ , 2H); 3.86 (s, 6H).  $^{13}\text{C}$ -NMR (400 MHz,  $\text{DMSO-d}_6$ )  $\delta$  (ppm): 159.4; 150.2; 148.0; 128.1; 124.1; 121.8; 115.4; 110.4; 55.6.

#### X-Ray Diffraction data

Space group:  $\text{P2}_1/\text{n}$

Cell length ( $\text{\AA}$ ): **a** 8.4611; **b** 7.6710; **c** 17.4975.

Cell angles:  $\alpha$  90;  $\beta$  101.566;  $\gamma$  90.

Cell volume ( $\text{\AA}^3$ ): 1112.62

R factor: 5.37 %

Symmetry:  $\frac{1}{2}-x, \frac{1}{2}+y, \frac{1}{2}-z$ ;  $-x, -y, -z$ ;  $\frac{1}{2}+x, \frac{1}{2}-y, \frac{1}{2}+z$ .

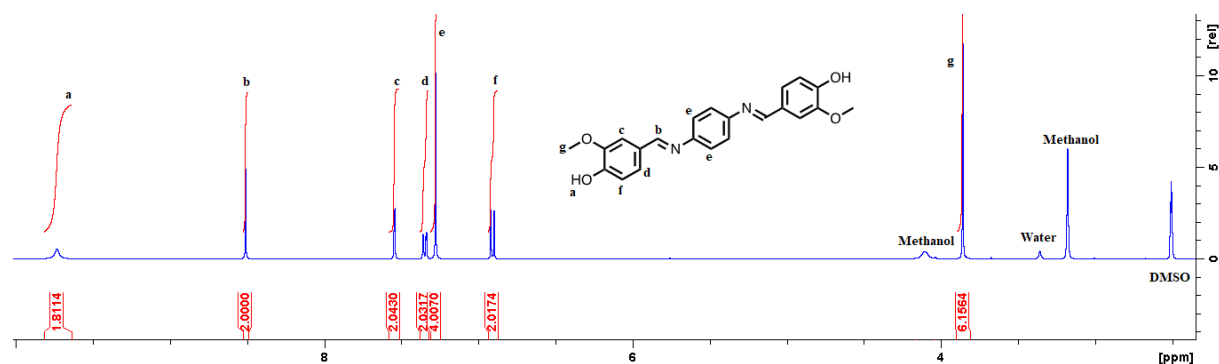


Figure 91:  $^1\text{H}$ -NMR spectrum of **M1'** (400.20 MHz, in  $\text{DMSO-d}_6$ )

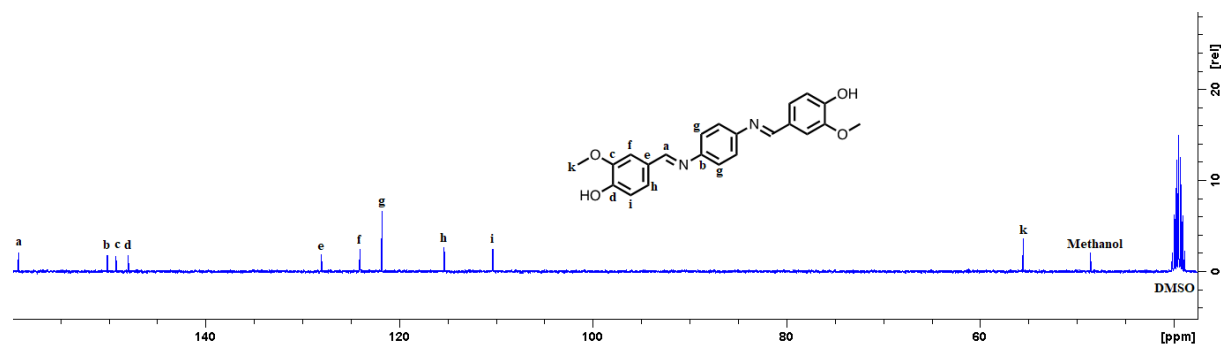
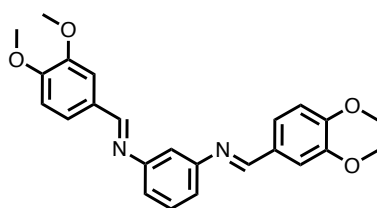


Figure 92:  $^{13}\text{C}$ -NMR spectrum of **M1'** (100.70 MHz, in DMSO- $d_6$ )

### 6.8.3. Synthesis and purification of **M2**



Di(3,4-dimethoxyphenylmethylidene)-1,3-diaminobenzene  
**Reactants:** methylated vanillin (2 eq.) + meta-phenylenediamine (1 eq.) using general protocol. The obtained product was dissolved again in methanol and filtrated on  $0.45\mu\text{m}$  PTFE. The crystallization starts spontaneously to give the final product. E/Z in the crude material: 75/25. Conversion: 80 %.

$^1\text{H}$ -NMR (400 MHz,  $\text{CD}_2\text{Cl}_2$ )  $\delta$  (ppm): 8.43 (s, 2H); 7.61-7.60 (d,  $J = 3\text{Hz}$ , 2H); 7.42-7.34 (m, 3H); 7.07-7.01 (m, 3H); 6.97-6.95 (m, 2H); 3.94 (s, 6H); 3.91 (s, 6H).  $^{13}\text{C}$ -NMR (400 MHz,  $\text{CD}_2\text{Cl}_2$ )  $\delta$  (ppm): 160.4; 153.7; 152.7; 150.0; 129.9; 124.6; 118.6; 113.2; 111.1; 109.5; 56.3.

#### X-Ray Diffraction data

Space group:  $\text{P2}_1/\text{c}$  (monoclinic)

Cell length ( $\text{\AA}$ ): **a** 6.94400; **b** 22.3804; **c** 6.55780.

Cell angles:  $\alpha$  90;  $\beta$  95.903;  $\gamma$  90.

Cell volume ( $\text{\AA}^3$ ): 1013.74

R factor: 3.62 %

Symmetry:  $-x, \frac{1}{2}+y, \frac{1}{2}-z$ ;  $-x, -y, -z$ ;  $x, \frac{1}{2}-y, \frac{1}{2}+z$ .

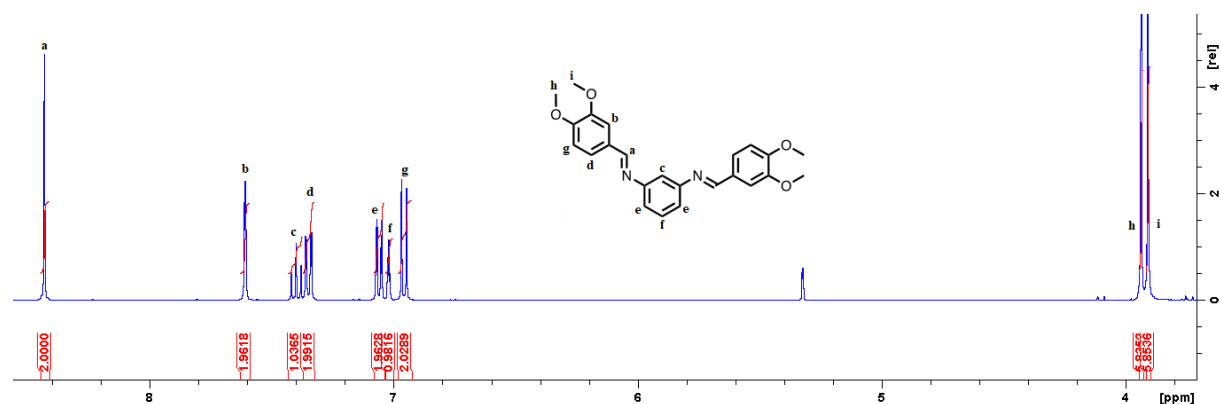


Figure 93:  $^1\text{H}$ -NMR spectrum of **M2** (400.20 MHz, in  $\text{CD}_2\text{Cl}_2$ )

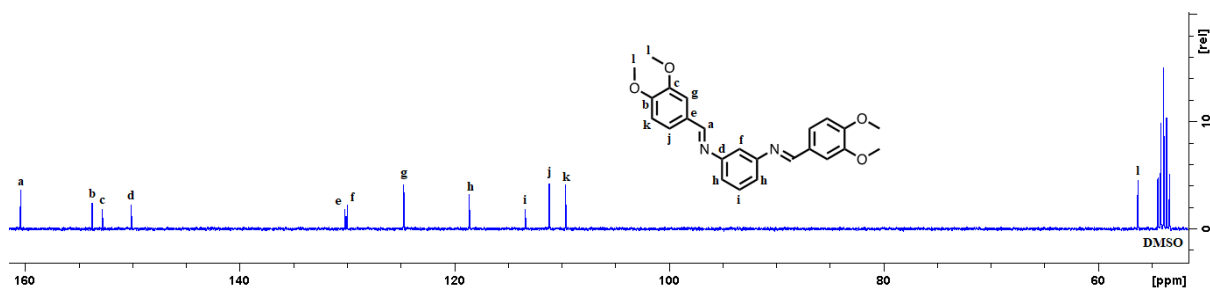
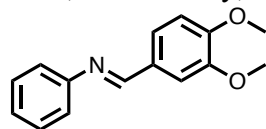


Figure 94:  $^{13}\text{C}$ -NMR spectrum of **M2** (100.70 MHz, in  $\text{CD}_2\text{Cl}_2$ )

#### 6.8.4. Synthesis and purification of **M3**

1,2-dimethoxy, 4-(phenylimino)methyl)benzene



**Reactants:** methylated vanillin (1 eq.) + aniline (1 eq.) using general protocol. The obtained product was recrystallized from a warm mixture of methylene chloride and methanol. E/Z in the crude material: 100/0. Conversion: 94 %.

$^1\text{H}$ -NMR (400 MHz,  $\text{CD}_2\text{Cl}_2$ )  $\delta$  (ppm): 8.37 (s, 1H); 7.59 (d,  $J = 2\text{Hz}$ , 1H); 7.41-7.37 (m, 2H); 7.35-7.32 (d,  $J = 12\text{Hz}$ , 1H); 7.24-7.18 (m, 3H); 6.96-6.94 (d,  $J = 8\text{Hz}$ , 1H); 3.93 (s, 3H); 3.90 (s, 3H).  $^{13}\text{C}$ -NMR (400 MHz,  $\text{CD}_2\text{Cl}_2$ )  $\delta$  (ppm): 159.7; 152.3; 129.5; 129.1; 125.5; 124.1; 120.8; 110.7; 109.2; 55.8.

#### X-Ray Diffraction data

Space group: Pbc<sub>a</sub> (orthorhombic)

Cell length (Å): **a** 15.8744; **b** 6.14640; **c** 25.5742.

Cell angles:  $\alpha$  90;  $\beta$  90;  $\gamma$  90.

Cell volume (Å<sup>3</sup>): 2495.33

R factor: 3.9%

Symmetry:  $\frac{1}{2}-x, -y, \frac{1}{2}+z$ ;  $-x, \frac{1}{2}+y, \frac{1}{2}-z$ ;  $\frac{1}{2}+x, \frac{1}{2}-y, -z$ ;  $-x, -y, -z$ ;  $\frac{1}{2}+x, y, \frac{1}{2}-z$ ;  $x, \frac{1}{2}-y, \frac{1}{2}+z$ ;  $\frac{1}{2}-x, \frac{1}{2}+y, z$ .

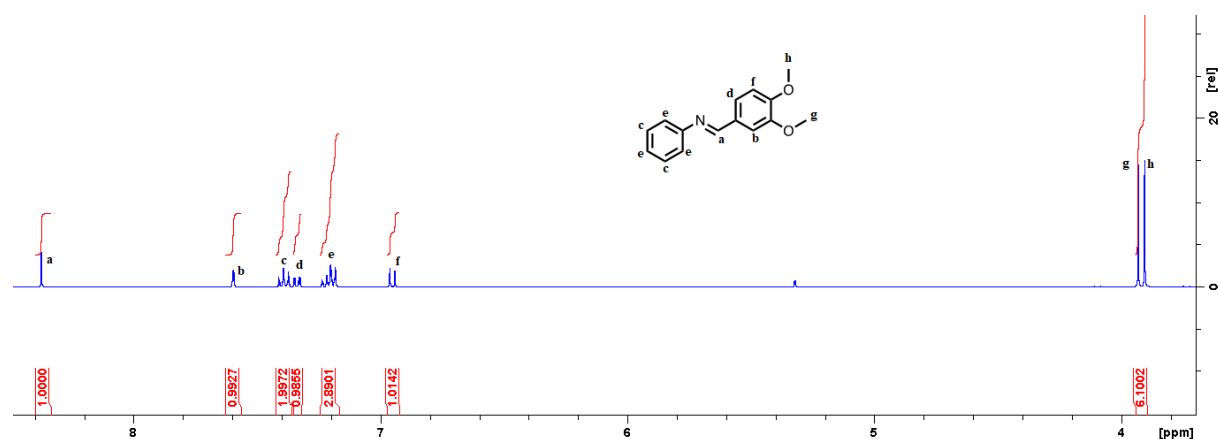


Figure 95:  $^1\text{H}$ -NMR spectrum of **M3** (400.20 MHz, in  $\text{CD}_2\text{Cl}_2$ )

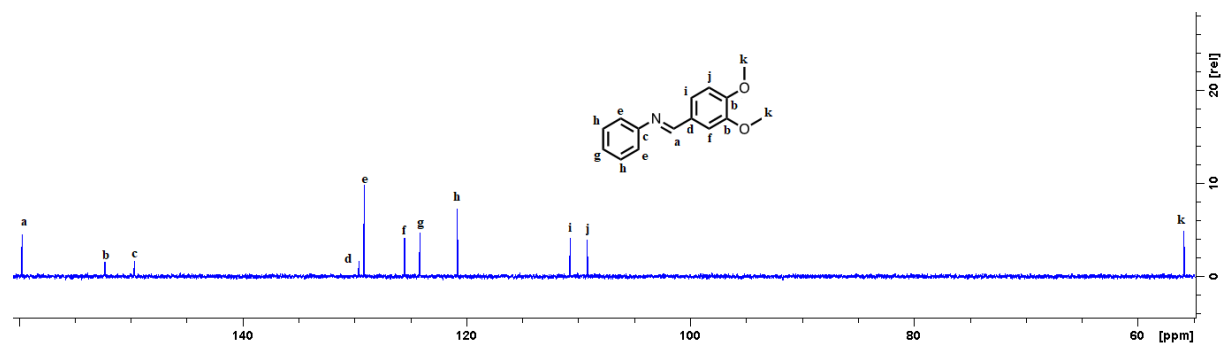
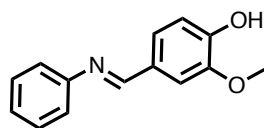


Figure 96:  $^{13}\text{C}$ -NMR spectrum of **M3** (100.70 MHz, in  $\text{CD}_2\text{Cl}_2$ )

### 6.8.5. Synthesis and purification of **M3'**

#### 2-methoxy, 4-(phenylimino)methylphenol



Reactants: vanillin (1 eq.) + aniline (1 eq.) using general protocol.

The final product was obtained after recrystallization from warm cyclohexane/methylene chloride. E/Z in the crude material: 100/0.

Conversion: 95 %.

$^1\text{H}$ -NMR (400 MHz,  $\text{DMSO-d}_6$ )  $\delta$  (ppm): 9.74 (s, 1H); 8.44 (s, 1H); 7.54-7.53 (d,  $J = 4\text{ Hz}$ , 1H); 7.41-7.36 (m, 2H); 7.35-7.33 (d,  $J = 8\text{ Hz}$ , 1H); 7.21-7.19 (m, 3H); 6.91-6.89 (d,  $J = 8\text{ Hz}$ , 1H); 3.85 (s, 3H).  $^{13}\text{C}$ -NMR (400 MHz,  $\text{DMSO-d}_6$ )  $\delta$  (ppm): 160.2; 152.1; 150.3; 148.2; 129.2; 128.0; 125.5; 124.4; 120.9; 115.3; 110.4; 55.6.

#### X-Ray Diffraction data

Space group:  $\text{C}222_1$  (orthorhombic)

Cell length ( $\text{\AA}$ ): **a** 16.7830; **b** 18.1688; **c** 15.2042.

Cell angles:  $\alpha$  90;  $\beta$  90;  $\gamma$  90.

Cell volume ( $\text{\AA}^3$ ): 4636.17

R factor: 6.8%

Symmetry:  $-x, -y, \frac{1}{2}+z$ ;  $-x, y, \frac{1}{2}-z$ ;  $x, -y, -z$ ;  $\frac{1}{2}+x, \frac{1}{2}+y, z$ ;  $\frac{1}{2}-x, \frac{1}{2}-y, \frac{1}{2}+z$ ;  $\frac{1}{2}-x, \frac{1}{2}+y, \frac{1}{2}-z$ ;  $\frac{1}{2}+x, \frac{1}{2}-y, -z$ .

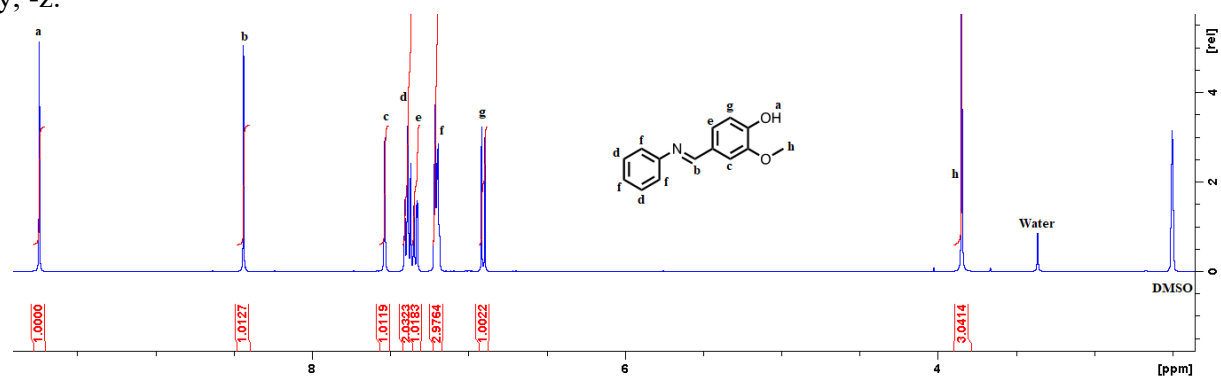


Figure 97:  $^1\text{H}$ -NMR spectrum of **M3'** (400.20 MHz, in  $\text{DMSO-d}_6$ )

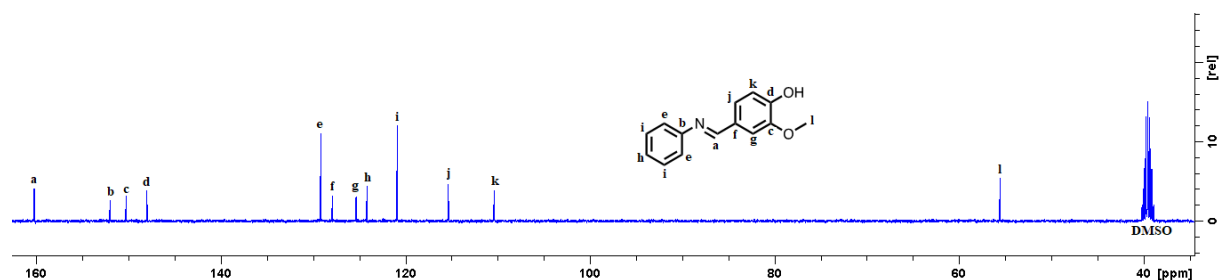
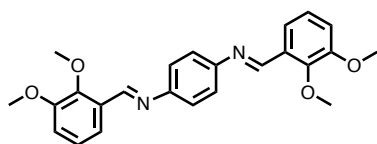


Figure 98:  $^{13}\text{C}$ -NMR spectrum of **M3'** (100.70 MHz, in  $\text{DMSO-d}_6$ )

6.8.6. Synthesis and purification of **M4**

Di(2,3-dimethoxyphenylmethylidene)-1,4-diaminobenzene

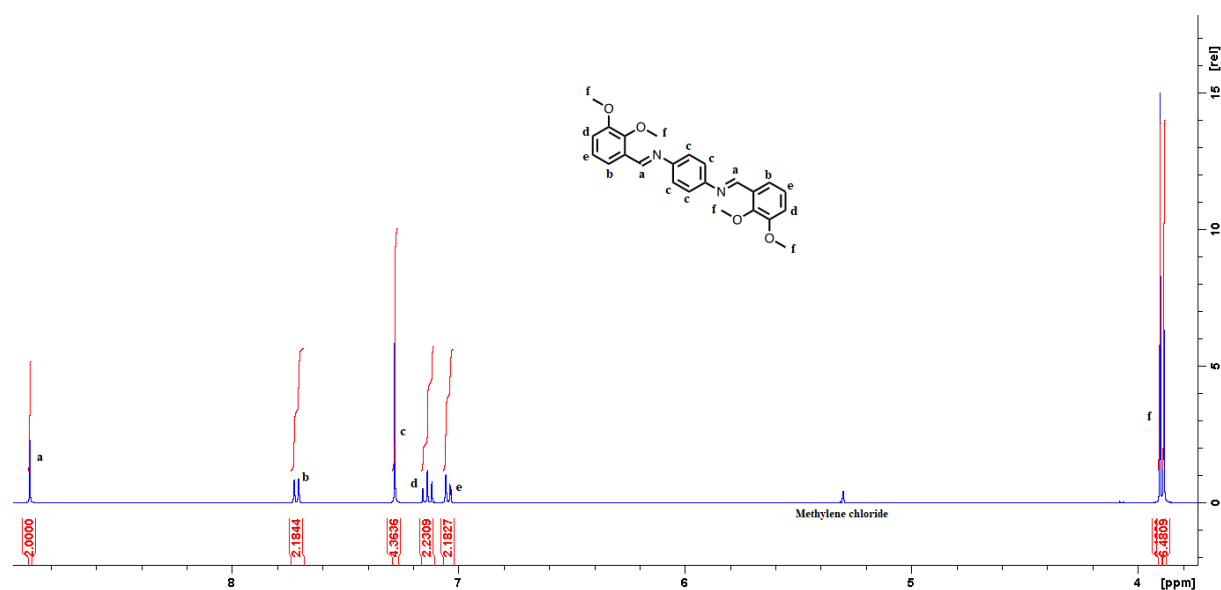
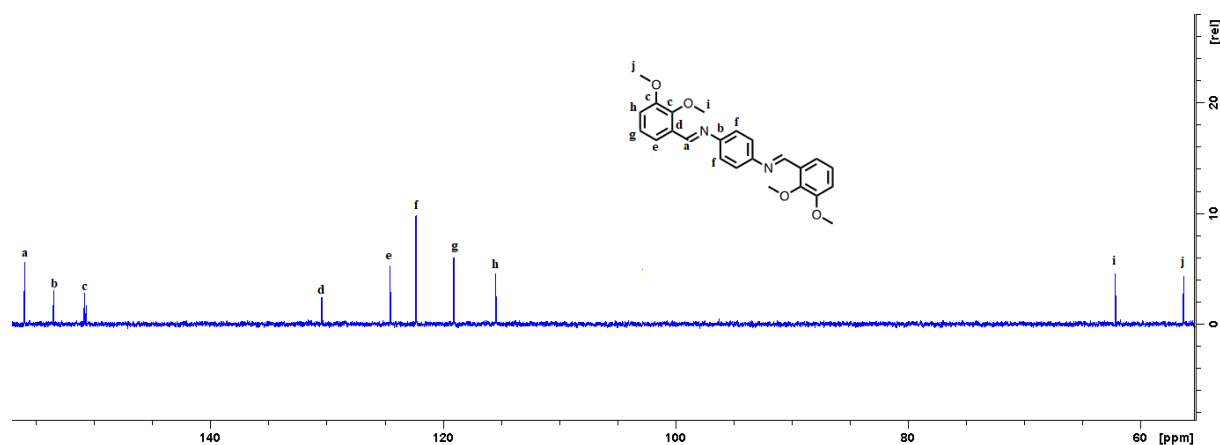


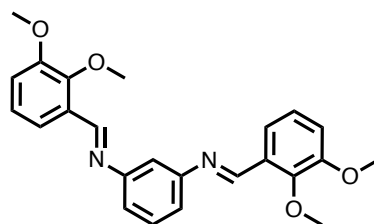
**Reactants:** methylated ortho-vanillin (2 eq.) + para-phenylene diamine (1 eq.) using general protocol. The obtained product was recrystallized from a warm mixture of methylene chloride and methanol. E/Z in the crude material: 95/5. Conversion: 96 %.

$^1\text{H-NMR}$  (400 MHz,  $\text{CD}_2\text{Cl}_2$ )  $\delta$  (ppm): 8.90 (s, 1H); 7.72-7.70 (d,  $J = 8\text{Hz}$ , 2H); 7.28 (s, 4H); 7.15-7.03 (m, 4H); 3.90 (s, 6H); 3.88 (s, 6H).  $^{13}\text{C-NMR}$  (400 MHz,  $\text{CD}_2\text{Cl}_2$ )  $\delta$  (ppm): 155.9; 153.4; 150.8; 150.6; 130.7; 124.5; 122.3; 119; 115.4; 62.1; 56.2.

**X-Ray Diffraction data**Space group:  $P2_1/c$  (monoclinic)Cell length ( $\text{\AA}$ ): **a** 6.94400; **b** 22.3804; **c** 6.55780.Cell angles:  $\alpha$  90;  $\beta$  95.903;  $\gamma$  90.Cell volume ( $\text{\AA}^3$ ): 1013.74

R factor: 3.62 %

Symmetry:  $-x, \frac{1}{2}+y, \frac{1}{2}-z$ ;  $-x, -y, -z$ ;  $x, \frac{1}{2}-y, \frac{1}{2}+z$ .Figure 99:  $^1\text{H-NMR}$  spectrum of **M4** (400.20 MHz, in  $\text{CD}_2\text{Cl}_2$ )Figure 100:  $^{13}\text{C-NMR}$  spectrum of **M4** (100.70 MHz, in  $\text{CD}_2\text{Cl}_2$ )

6.8.7. Synthesis and purification of **M5**

## Di(2,3-dimethoxyphenyl)benzene-1,3-diaminobenzene

**Reactants:** methylated ortho-vanillin (2 eq.) + meta-phenylene diamine (1 eq.) using general protocol. The obtained product was dissolved again in methanol and filtrated on 0.45 $\mu$ m PTFE. The crystallization starts spontaneously to give the final product. E/Z in the crude material: 90/10. Conversion: 95 %.

$^1\text{H-NMR}$  (400 MHz,  $\text{CD}_2\text{Cl}_2$ )  $\delta$  (ppm): 8.91 (s, 2H); 7.74-7.72 (d,  $J = 8\text{Hz}$ , 2H); 7.44-7.40 (t,  $J = 16\text{Hz}$ , 1H); 7.18-7.13 (t, 20Hz, 2H); 7.12-7.11 (m, 1H); 7.09-7.05 (m, 4H); 3.91 (s, 6H); 3.90 (s, 6H).  $^{13}\text{C-NMR}$  (400 MHz,  $\text{CD}_2\text{Cl}_2$ )  $\delta$  (ppm): 157.1; 153.9; 153.4; 150.7; 130.2; 130.0; 124.5; 119.0; 118.9; 115.5; 113.6; 62.1; 56.2.

**X-Ray Diffraction data**

Space group: Fdd2 (orthorhombic)

Cell length ( $\text{\AA}$ ): **a** 9.0852; **b** 44.1903; **c** 10.1773.

Cell angles:  $\alpha$  90;  $\beta$  90;  $\gamma$  90.

Cell volume ( $\text{\AA}^3$ ): 4085.96

R factor: 2.61 %

Symmetry:  $-x, -y, z$ ;  $1/4+x, 1/4-y, 1/4+z$ ;  $1/4-x, 1/4+y, 1/4+z$ ;  $x, 1/2+y, 1/2+z$ ;  $-x, 1/2-y, 1/2+z$ ;  $1/4+x, 3/4-y, 3/4+z$ ;  $1/4-x, 3/4+y, 3/4+z$ ;  $1/2+x, y, 1/2+z$ ;  $1/2-x, -y, 1/2+z$ ;  $3/4+x, 1/4-y, 3/4+z$ ;  $3/4-x, 1/4+y, 3/4+z$ ;  $1/2+x, 1/2+y, z$ ;  $1/2-x, 1/2-y, z$ ;  $3/4+x, 3/4-y, 1/4+z$ ;  $3/4-x, 3/4+y, 1/4+z$ .

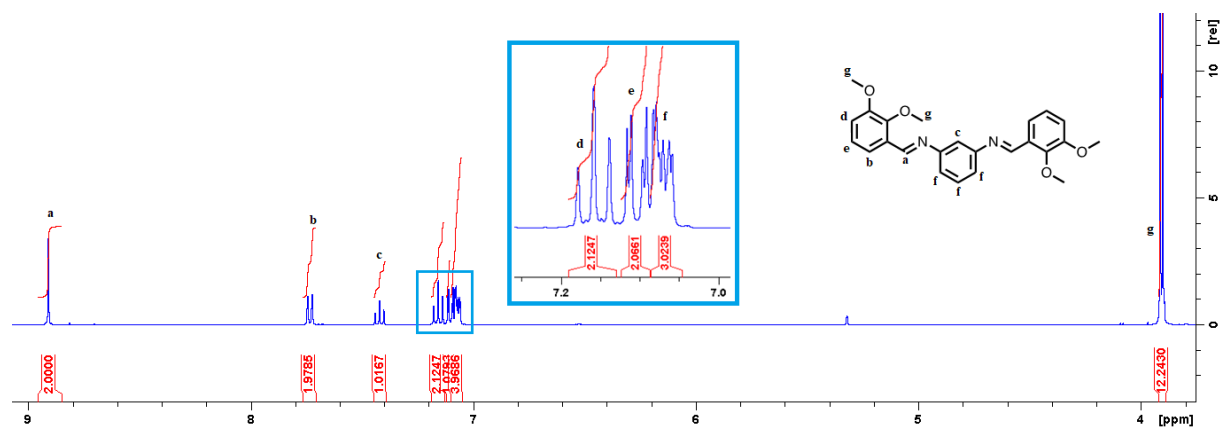


**Figure 101:**  $^1\text{H-NMR}$  spectrum of **M5** (400.20 MHz, in  $\text{CD}_2\text{Cl}_2$ )

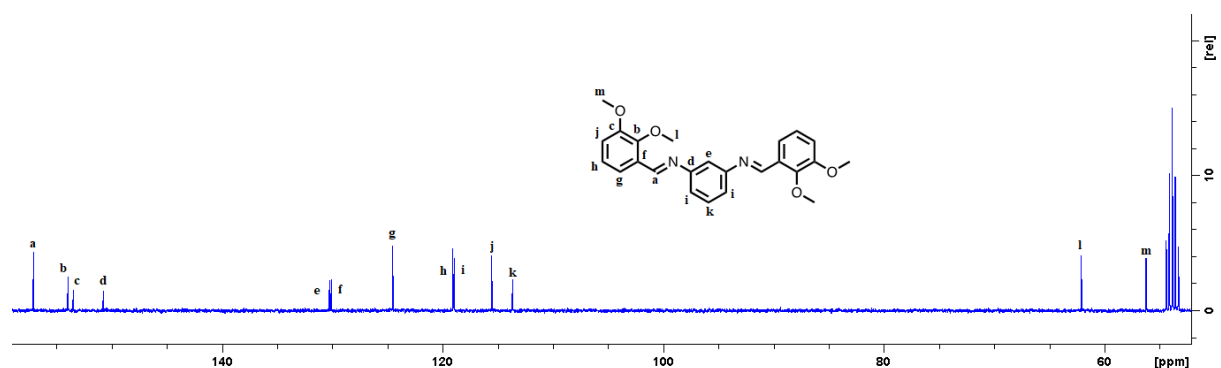
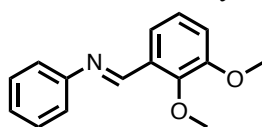


**Figure 102:**  $^{13}\text{C-NMR}$  spectrum of **M5** (100.70 MHz, in  $\text{CD}_2\text{Cl}_2$ )



6.8.8. Synthesis and purification of **M6**

## 1,2-dimethoxy, 3-(phenylimino)methylbenzene



**Reactants:** methylated ortho-vanillin (1 eq.) + aniline (1 eq.) using general protocol. The obtained product was recrystallized from a warm mixture of methylene chloride and methanol. E/Z in the crude material: 100/0. Conversion: 84 %.

$^1\text{H-NMR}$  (400 MHz,  $\text{CD}_2\text{Cl}_2$ )  $\delta$  (ppm): 8.85 (s, 1H); 7.73-7.70 (d,  $J = 12\text{Hz}$ , 1H); 7.42-7.38 (m, 2H); 7.26-7.21 (m, 3H); 7.17-7.13 (t,  $J = 8\text{Hz}$ , 1H); 7.07-7.05, m, 1H); 3.91 (s, 3H); 3.90 (s, 3H).  $^{13}\text{C-NMR}$  (400 MHz,  $\text{CD}_2\text{Cl}_2$ )  $\delta$  (ppm): 156.7; 153.4; 153.0; 150.7; 130.3; 129.5; 126.2; 124.5; 121.3; 119; 115.5; 62.1; 56.2.

**X-Ray Diffraction data**

Space group:  $\text{P2}_1\text{2}_1\text{2}_1$  (orthorhombic)

Cell length ( $\text{\AA}$ ): **a** 6.74160; **b** 9.92130; **c** 18.5760.

Cell angles:  $\alpha$  90;  $\beta$  90;  $\gamma$  90.

Cell volume ( $\text{\AA}^3$ ): 1242.46

R factor: 2.75 %

Symmetry:  $\frac{1}{2}-x, -y, \frac{1}{2}+z; -x, \frac{1}{2}+y, \frac{1}{2}-z; \frac{1}{2}+x, \frac{1}{2}-y, -z$ .

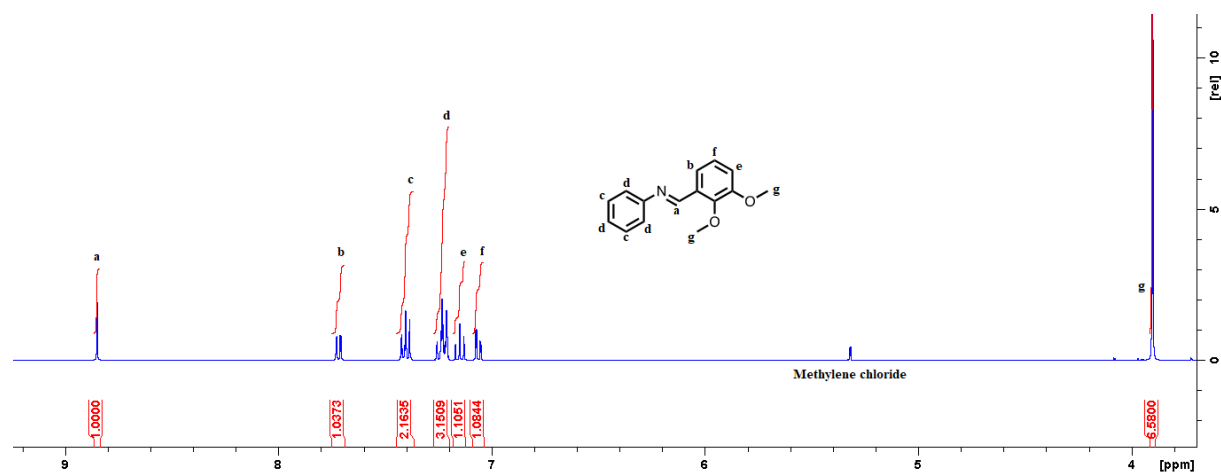


**Figure 103:**  $^1\text{H-NMR}$  spectrum of **M6** (400.20 MHz, in  $\text{CD}_2\text{Cl}_2$ )

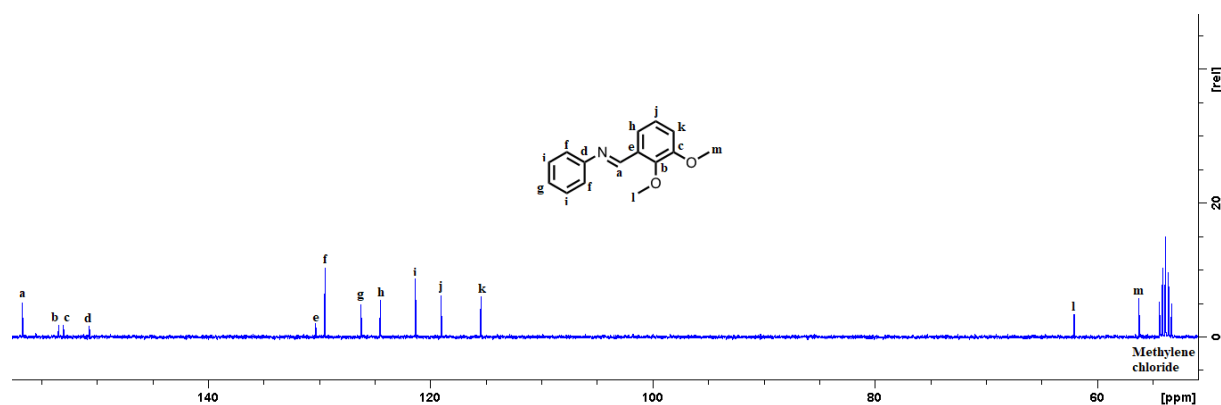
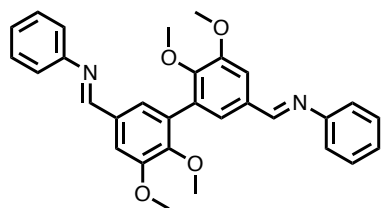


**Figure 104:**  $^{13}\text{C-NMR}$  spectrum of **M6** (100.70 MHz, in  $\text{CD}_2\text{Cl}_2$ )

6.8.9. Synthesis and purification of **M7**

## 6,6'-Methoxy-5,5'-dimethoxy-[1,1'-biphenyl]-3,3'-di(phenylimino)methyl



**Reactants:** methylated divanillin (1 eq.) + aniline (2 eq.) using general protocol. The obtained product was recrystallized from a warm mixture of methylene chloride and methanol. E/Z in the crude material: cannot be determined clearly. Conversion: 98 %.

$^1\text{H-NMR}$  (400 MHz,  $\text{CD}_2\text{Cl}_2$ )  $\delta$  (ppm): 8.42 (s, 2H); 7.67 (d,  $J = 2\text{Hz}$ , 2H); 7.42-7.38 (m, 4H); 7.32 (d,  $J = 2\text{Hz}$ , 2H); 4.01 (s, 6H); 3.74 (s, 6H).  $^{13}\text{C-NMR}$  (400 MHz,  $\text{CD}_2\text{Cl}_2$ )  $\delta$  (ppm): 159.9; 153.7; 152.5; 150.3; 132.7; 132.3; 129.6; 126.2; 125.8; 121.2; 110.5; 61.0; 56.3.

**X-Ray Diffraction data**

Space group: monoclinic  $P2_1/c$

Cell length ( $\text{\AA}$ ): **a** 7.44380; **b** 17.1323; **c** 19.4003.

Cell angles:  $\alpha$  90;  $\beta$  93.7320;  $\gamma$  90.

Cell volume ( $\text{\AA}^3$ ): 2468.86

R factor: 3.89 %

Symmetry:  $x, \frac{1}{2}+y, \frac{1}{2}+z; -x, \frac{1}{2}+y, \frac{1}{2}-z; -x, -y, -z.$

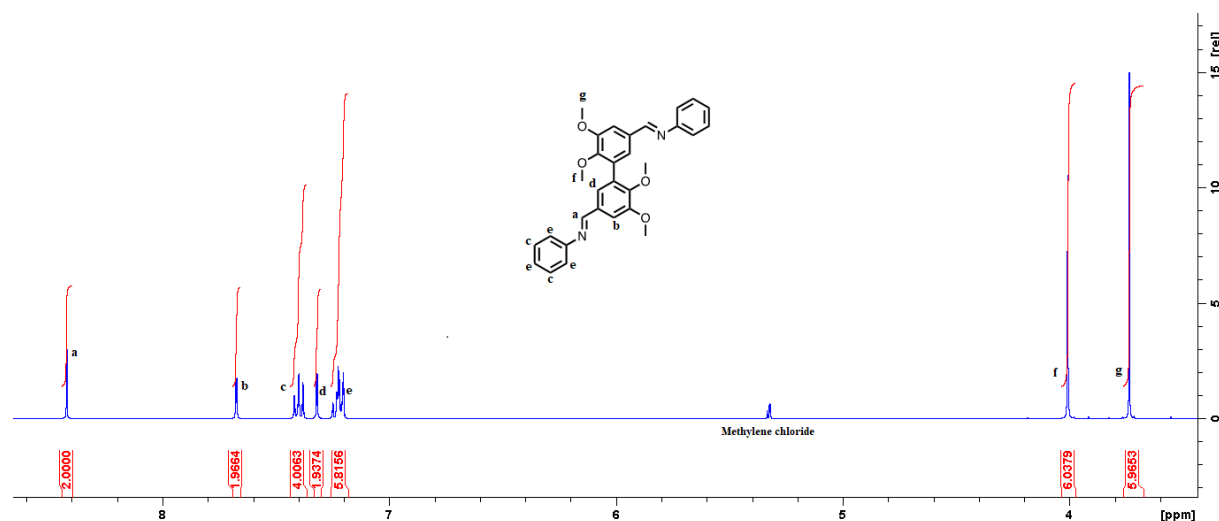


**Figure 105:**  $^1\text{H-NMR}$  spectrum of **M7** (400.20 MHz, in  $\text{CD}_2\text{Cl}_2$ )



**Figure 106:**  $^{13}\text{C-NMR}$  spectrum of **M7** (100.70 MHz, in  $\text{CD}_2\text{Cl}_2$ )



## **Chapter 3: Towards fully conjugated polyazomethines**



---

## Table of contents

|   |     |
|---|-----|
| <b>1. Introduction</b> .....  | 139 |
| <b>2. Synthesis of new bio-based monomers by enzymatic coupling</b> .....   | 140 |
| 2.1. Enzymatic coupling of ortho-vanillin .....   | 140 |
| 2.2. Enzymatic coupling of iso-vanillin .....   | 142 |
| 2.3. Conclusion .....   | 144 |
| <b>3.2. Synthesis and characterization of para-divanillin monomer</b> .....   | 145 |
| 3.2.1. Literature overview of metalation.....   | 145 |
| 3.2.2. Synthesis of para-divanillin monomer <i>via</i> formylation by metalation .....                              | 146 |
| 3.2.3. Conclusion .....   | 149 |
| <b>4. Polyazomethines with para-divanillin-based monomer</b> .....  | 150 |
| 4.1. Polyazomethine synthesis, physical characterizations and comparison with divanillin-based polyazomethines..... | 150 |
| 4.2. Conclusion on the synthesis and thermal characterizations of polyazomethines from para-divanillin .....        | 152 |
| 4.3. Optical properties of polyazomethines from para-divanillin .....   | 152 |
| 4.4. Conclusion on optical properties.....  | 154 |
| <b>5. Model compounds of para-divanillin-based polyazomethines</b> .....  | 155 |
| 5.1. Synthesis and purification of model compounds .....  | 155 |
| 5.2. X-Ray Diffraction analysis .....   | 157 |
| 5.3. Brief conclusion on synthesis and X-Ray Diffraction characterization.....                                      | 158 |
| 5.4. Optical characterization .....   | 159 |
| 5.5. General conclusion on para-divanillin-based model compounds .....  | 163 |
| <b>6. General conclusion</b> .....  | 164 |
| <b>7. References</b> .....  | 166 |
| <b>8. Experimental part</b> .....   | 168 |



## 1. Introduction

As described in the previous chapter, divanillin-based polyazomethines have a limited conjugation pathway. Indeed, the two aromatic rings of divanillin are linked in meta position with respect to the aldehyde functions, which breaks conjugation along the divanillin-based polyazomethines backbone. To improve the opto-electronic properties, new biphenyl monomers were designed. As the objective of this PhD work is to obtain bio-based conjugated polymers, ortho-vanillin and iso-vanillin were used, as these two vanillin derivatives are naturally occurring in plants.<sup>1,2</sup> These latter were reacted with Laccase from *Trametes Versicolor* in order to obtain new biphenyl monomers. The enzymatic coupling of ortho-vanillin could yield a biphenyl compound with different substituent positions than divanillin, which could give some insights on the influence of the substituents position on opto-electronics properties (cf. **Figure 1**). To improve the conjugation pathway, another strategy was to target a biphenyl compound with its two aromatic rings linked either in ortho or para position with respect to the aldehyde functions. The “ortho-divanillin” could be obtained by enzymatic coupling of iso-vanillin (cf. **Figure 1**).

Another strategy was used to obtain a para-divanillin-based monomer. As the para positions are available on the divanillin, an original approach was to add new aldehyde functions in these positions to obtain a “para-divanillin”. The formylation reaction can be achieved through various reactions, like the Vilsmeier-Haack<sup>3,4</sup> or the Rieche reaction.<sup>5</sup> In our case, the formylation reaction was performed by metalation. The desired bis-vanillin compounds are represented in **Figure 1**.

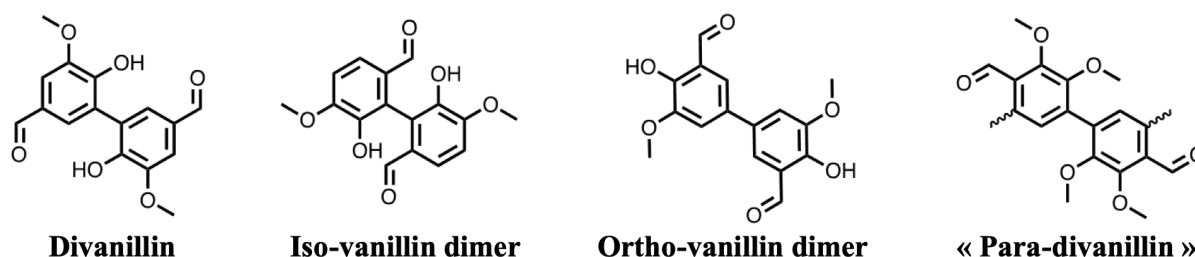


**Figure 1:** Structures of different vanillin-based monomers

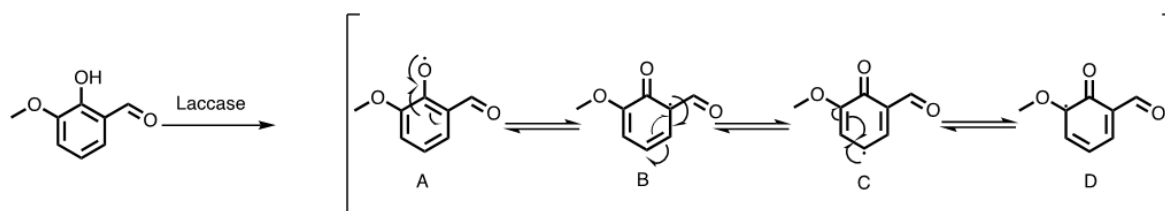
This first section of this chapter is therefore dedicated to the synthesis of these vanillin-based monomers. The obtained derivative was then used in the course of the polymerization with various diamines. The polyazomethines so formed were characterized in terms of physical and optical properties. In order to better analyze the structure and properties of these novel polyazomethines, model compounds were synthesized and characterized optically and by X-Ray Diffraction. A general discussion is presented at the end of this chapter.



## 2. Synthesis of new bio-based monomers by enzymatic coupling

### 2.1. Enzymatic coupling of ortho-vanillin

Ortho-vanillin is a vanillin derivative, bearing its phenol function on the ortho position of the aldehyde. In **Scheme 1**, the different mesomeric structures obtained after oxidation by Laccase are represented.



**Scheme 1:** Different mesomeric structures obtained by Laccase on ortho-vanillin

According to the different mesomeric structures, the radical sites **A** and **C** are the most reactive because less sterically hindered. The same experimental conditions as the ones developed with vanillin were performed. After filtration, a brown powder was recovered with only 35% yield. The reaction medium was extracted with dichloromethane and then ethyl acetate. Three different fractions were obtained (**Figure 2**).

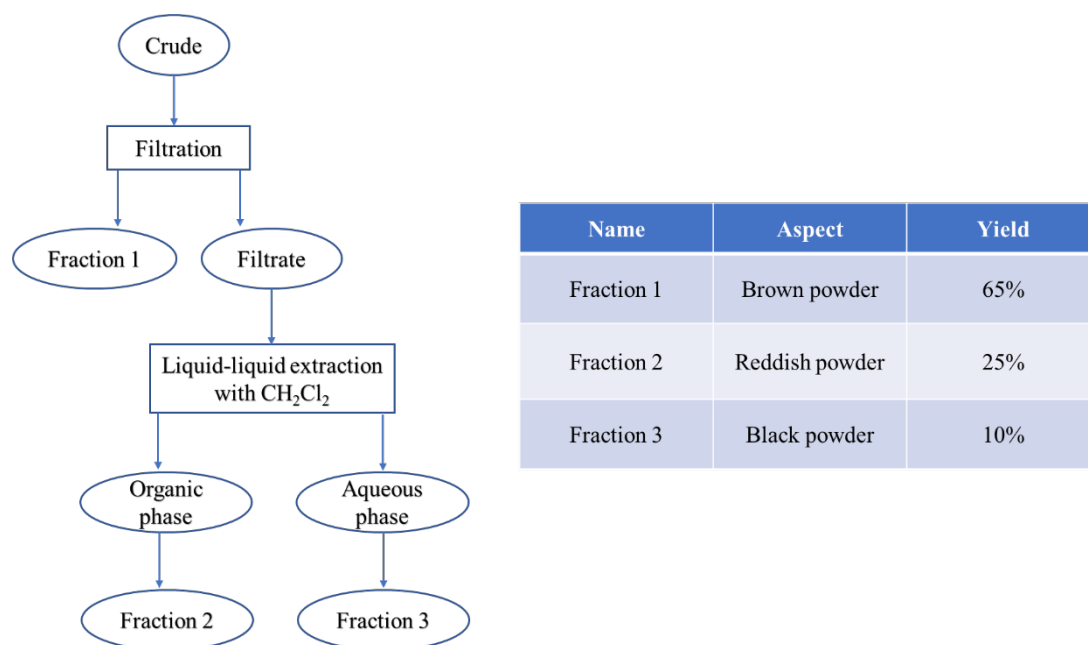
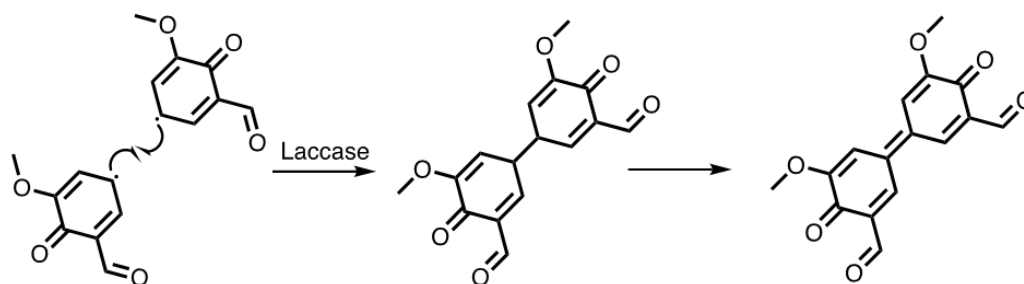


**Figure 2:** Sum up of the different fractions obtained after reaction of ortho-vanillin with Laccase

The reddish solid (**Fraction 2**) analyzed *via* <sup>1</sup>H-NMR spectroscopy is ortho-vanillin left with some impurities. The black powder (**Fraction 3**) is poorly soluble in the different solvents tested (THF, water, methylene chloride, chloroform, trichlorobenzene), and therefore could not be characterized *via* NMR spectroscopy. However, its color (black) and its very poor solubility indicates that this could be a quinone, given by the reaction between two radical sites **C**, as shown in **Schemes 1** and **2**.



**Scheme 2:** Possible pathway toward the formation of a quinone, by the recombination of two radicals from ortho-vanillin

Similar result was obtained by performing the reaction with 2,6-dimethoxyphenol and a quantitative coupling was obtained.<sup>6</sup>

For the brown powder, the <sup>1</sup>H-NMR spectrum is given in **Figure 3**, with the spectrum of ortho-vanillin:

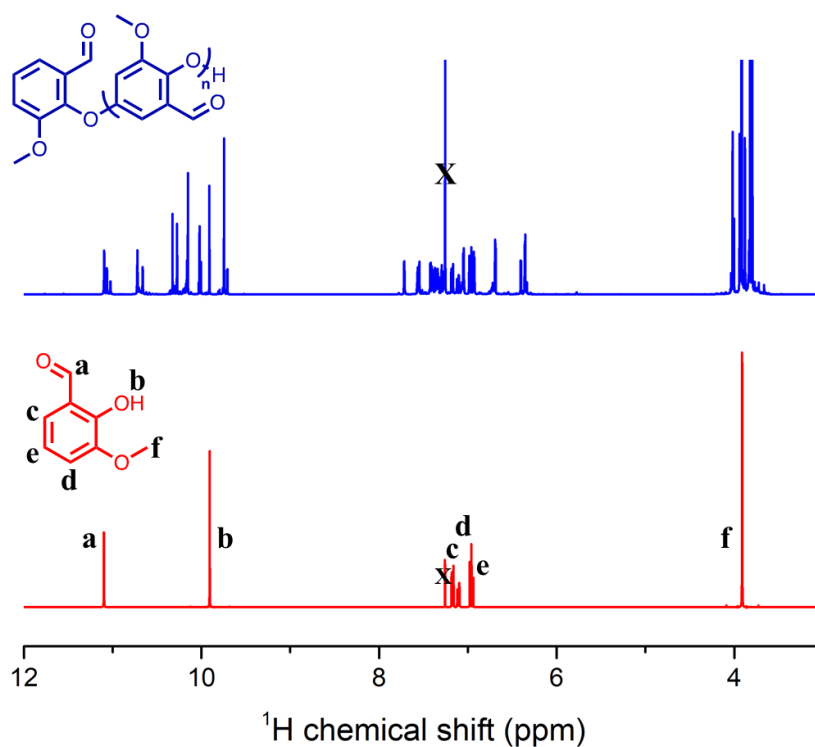


**Figure 3:** Comparison of <sup>1</sup>H-NMR spectra of **Fraction 1** and its potential structure (blue) and ortho-vanillin (red) (both in CDCl<sub>3</sub>, 128 scans)

The peaks of ortho-vanillin can be identified, but with numerous other peaks, suggesting the formation of oligomers. SEC in THF confirmed this assertion (**Figure 4**), as a series of oligomers are detectable. The formation of these oligomers could be due to the reactions between radical sites **A** and **C** on ortho-vanillin (cf. **Scheme 1**).

Even if the dimer is the main product formed, higher molar mass oligomers up to seven units were formed.

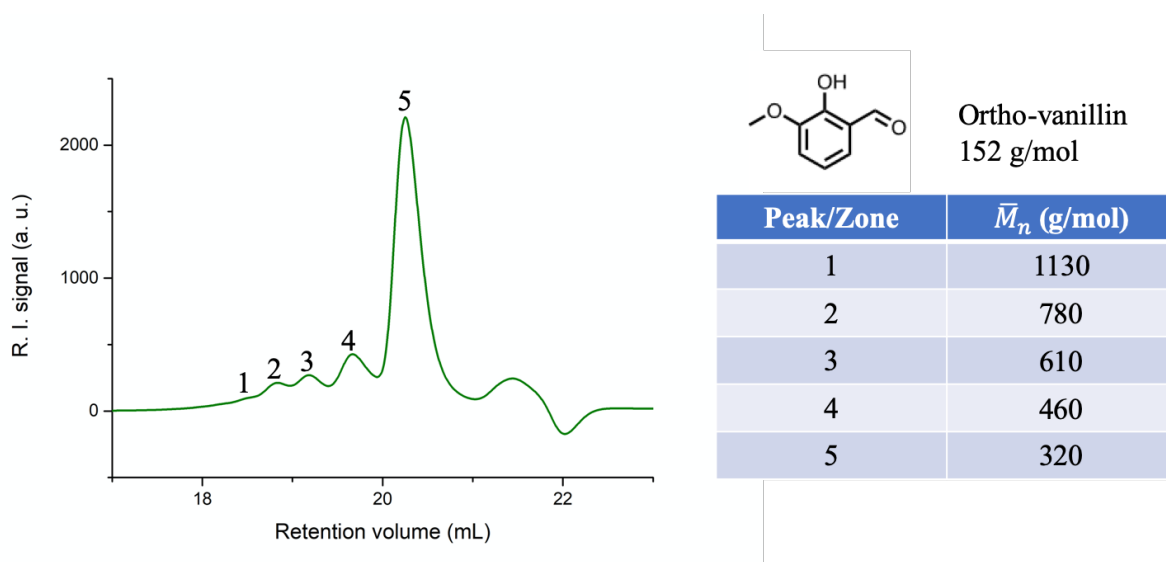
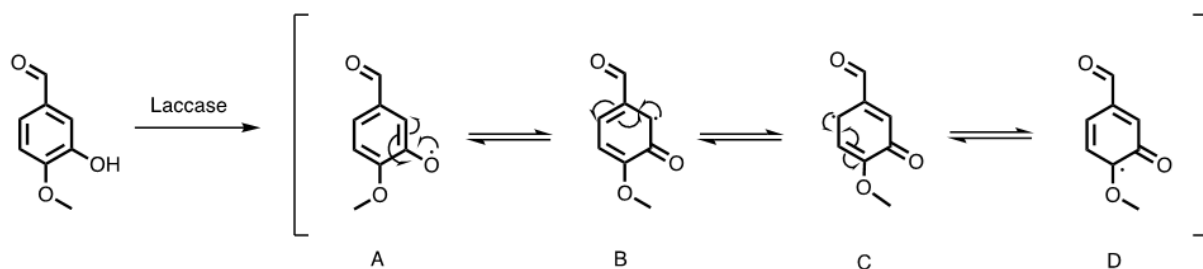


**Figure 4:** SEC trace of **Fraction 1** in THF and the corresponding molar masses (in reference to PS standards)

As a conclusion of this part, the enzymatic coupling between ortho-vanillin molecules is not regio-selective, as it does not yield a simple dimer but rather a mixture of oligomers.

## 2.2. Enzymatic coupling of iso-vanillin

Iso-vanillin is another vanillin derivative, with its phenol function in meta position of the aldehyde. The different possible mesomeric forms after oxidation with Laccase from *Trametes Versicolor* are represented in **Scheme 3**:



**Scheme 3:** Different mesomeric formulas obtained by Laccase on iso-vanillin

Isovanillin was reacted with Laccase from *Trametes Versicolor*, in the same conditions as the ones for divanillin. Two fractions were obtained, a beige powder after filtration (90% yield), **Fraction 1'** and a reddish oil after liquid-liquid extraction of the filtrate with chloroform (7% yield), **Fraction 2'**.

The  $^1\text{H-NMR}$  spectra of **Fraction 1'**, **Fraction 2'** and **iso-vanillin** in chloroform are given in **Figure 5**.

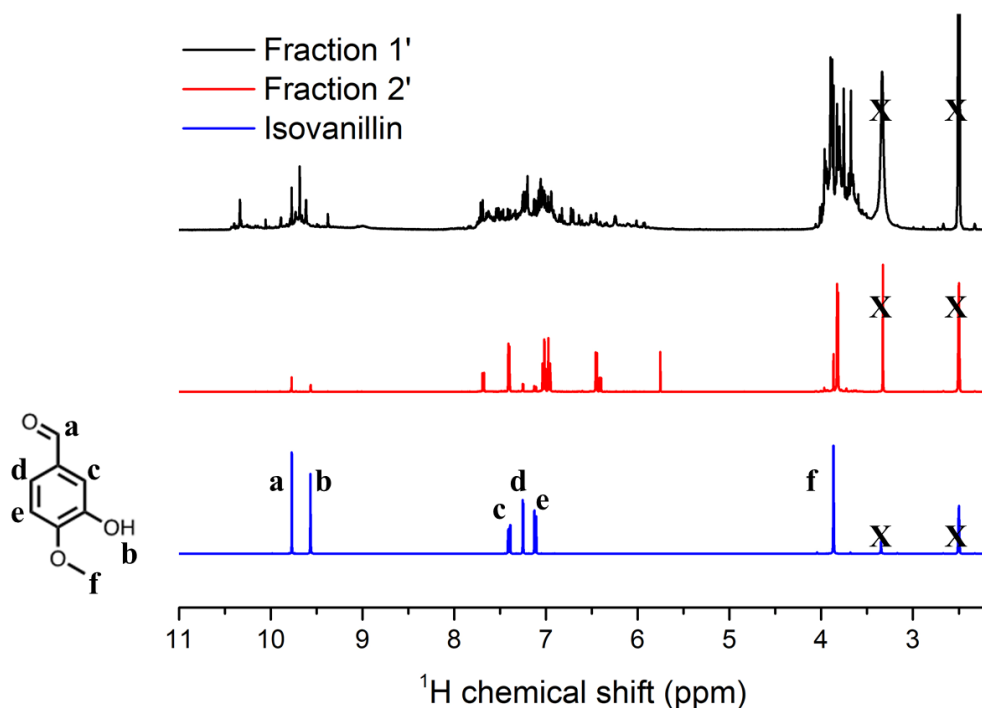


**Figure 5:**  $^1\text{H}$ -NMR spectra of **Fraction 1'**, **Fraction 2'** and iso-vanillin (from top to bottom) (in  $\text{DMSO-d}_6$ , 128 scans)

On the spectrum of **Fraction 1'**, various peaks can be observed, suggesting the presence of oligomers, in reference to the simplicity of the spectrum of iso-vanillin. The spectrum of **Fraction 2'** is simpler than the one of **Fraction 1'** but still suggests the presence of oligomers

The SEC trace of **Fraction 1'** in THF can be found in **Figure 6**. Indeed, two main populations are detectable, one corresponding to the dimer and the second to oligomers.

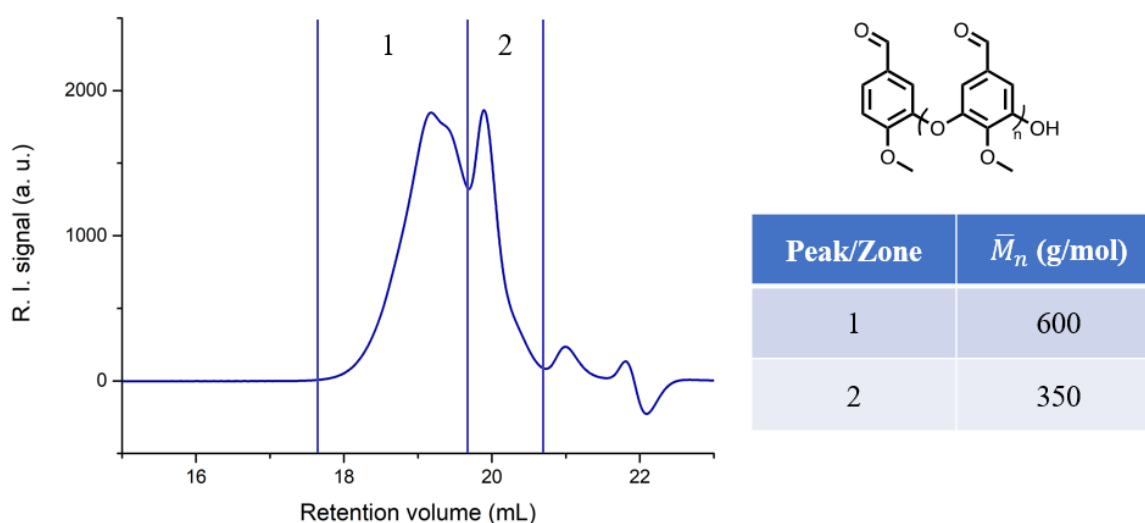


**Figure 6:** SEC trace of **Fraction 1'** in THF (RI detection), corresponding molar masses (in reference to PS standards), and potential structure

The SEC chromatogram of **Fraction 2'** is given in **Figure 7**, which shows again the formation of various oligomers. **Peak 5** most likely corresponds to the dimer – it does not have an exact molar mass of 300 g/mol, because these low molar masses correspond to the limit of the SEC detection.

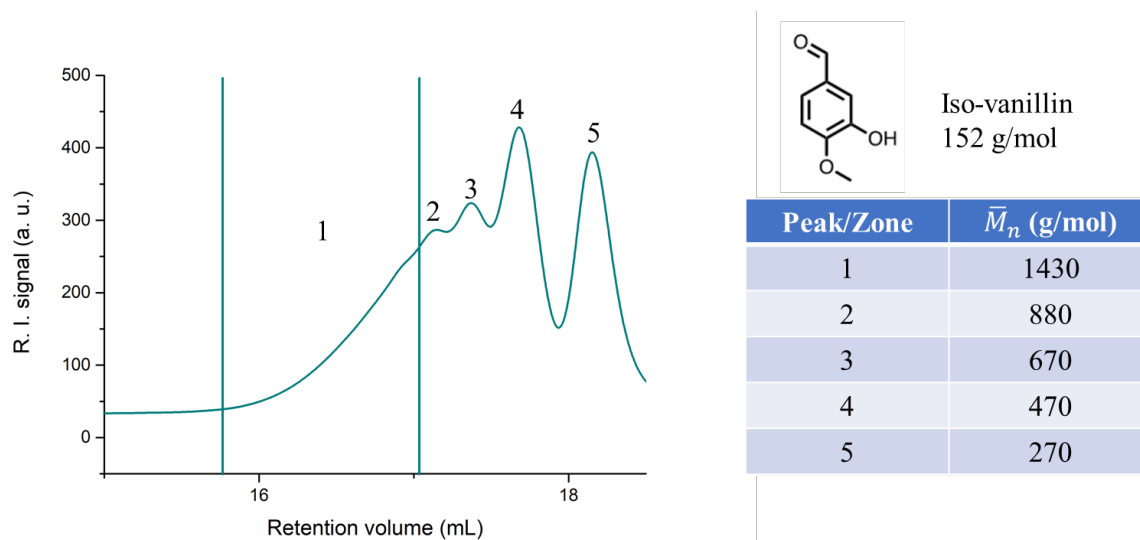


**Figure 7:** SEC trace of **Fraction 1'** in THF (RI detection), the corresponding molar masses (in reference to PS standards) and potential structure

Again, the dimerization of iso-vanillin produces oligomers, mostly dimers and oligomers. The molar masses of these latter depend on the work up method, either filtration or liquid-liquid extraction.

### 2.3. Conclusion

The enzymatic coupling of iso-vanillin and ortho-vanillin did not yield pure dimer structures but rather a mixture of oligomers. Indeed, the enzymatic coupling of ortho-vanillin yields a quinone-like compound and a mixture of oligomers. In the case of iso-vanillin, the enzymatic coupling is not regio-selective and produces a mixture of oligomers; the structure of all these products is given in **Figure 8**.

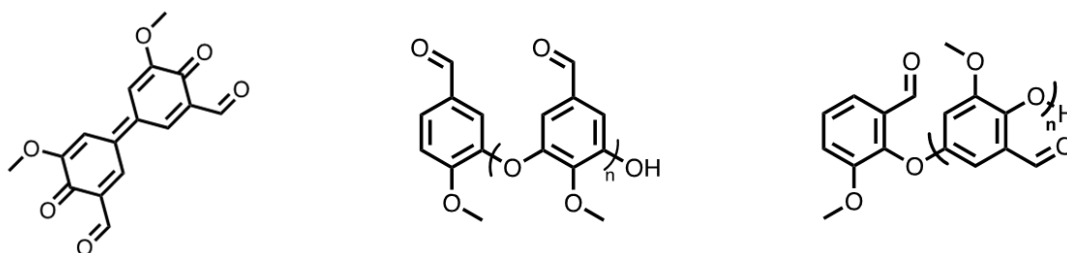


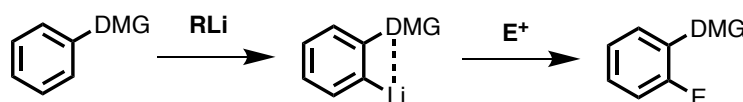
**Figure 8:** Structures of products obtained by enzymatic coupling of ortho-vanillin (left and middle) and iso-vanillin (right)

Another strategy was thus performed which deals with the formylation reaction by metalation. This methodology enables to add an aldehyde function on an aromatic ring; it is discussed in the next section.

### 3.2. Synthesis and characterization of para-divanillin monomer

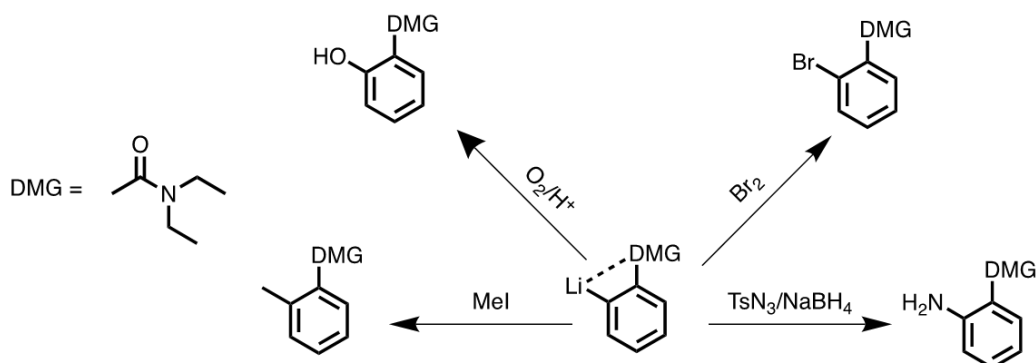
#### 3.2.1. Literature overview of metalation

Gilman and Wittig discovered independently the directed ortho-metalation reaction (DOM) in 1939 and 1940 respectively.<sup>7,8</sup> In this reaction, an aromatic ring bearing a substituent (called Directed Metalation Group or DMG) interacts with an alkyllithium. As the alkyllithium derivative is a strong base, it deprotonates the position in ortho position of the DMG, thus forming an aryllithium intermediate. This intermediate can then react with an electrophile ( $E^+$ ) through an electrophilic aromatic substitution (**Scheme 4**).



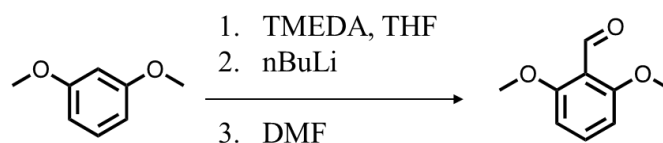
**Scheme 4:** General reaction scheme of directed ortho-metalation

This reaction is regioselective, as the DMG strongly orients the addition of lithium in ortho position. If the aromatic ring bears more than one DMG, then the stronger one will dictate the position of the lithium atom.<sup>9</sup> The DOM reaction can be performed with multiple electrophiles, leading to the addition of various chemical functions, as exemplified in **Scheme 5**: methyl,<sup>10</sup> alcohol,<sup>11</sup> bromide,<sup>12</sup> amine,<sup>13</sup> etc.



**Scheme 5:** Examples of molecules obtained after metalation, using various electrophiles

The DOM reaction can also be used to add aldehyde function onto aromatic bearing methoxy group as DMG.<sup>14,15</sup> This reaction gives the desired product with good yield and purity (89% yield by Collins *et al.*<sup>15</sup>). This formylation reaction was scaled up by Haight *et al.*<sup>14</sup>, to produce 68kg of final product with a 68% yield. The experimental conditions are given in **Scheme 6**:

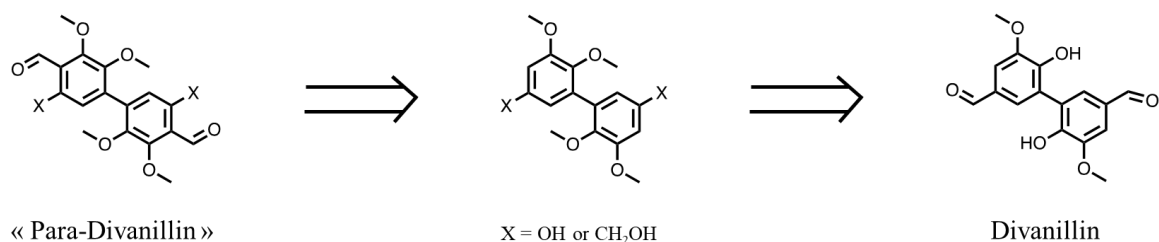


**Scheme 6:** Formylation reaction of 1,3-dimethoxybenzene (Adapted from <sup>15,14</sup>)

In THF, it is well-known that nBuLi is aggregated. The addition of TMEDA enables to break down these aggregates, thus increasing the reactivity of nBuLi.<sup>9</sup> TMEDA also stabilizes the aryllithium intermediates.<sup>14</sup> As there are two identical DMG on the aromatic ring, the formylation occurs on the carbon corresponding to the ortho position of both DMG (**Scheme 6**). This experimental protocol was used as such on the divanillin derivative, as discussed in the next section.

3.2.2. Synthesis of para-divanillin monomer *via* formylation by metalation

As already stated, the objective is to form a divanillin derivative exhibiting aldehyde functions in para position instead of meta with respect to the aldehyde functions, to increase the conjugation length of the corresponding polymers. For this purpose, the strategy was first to remove the already present aldehyde functions and then to add the new aldehyde functions in para position, as described in **Scheme 7**:



**Scheme 7:** General strategy followed to obtain para-divanillin from divanillin

A first protocol was tested, which starts by the reduction of divanillin with sodium borohydride. The disappearance of the aldehyde function was assessed by  $^1\text{H-NMR}$  analysis, as shown in **Figure 9**:

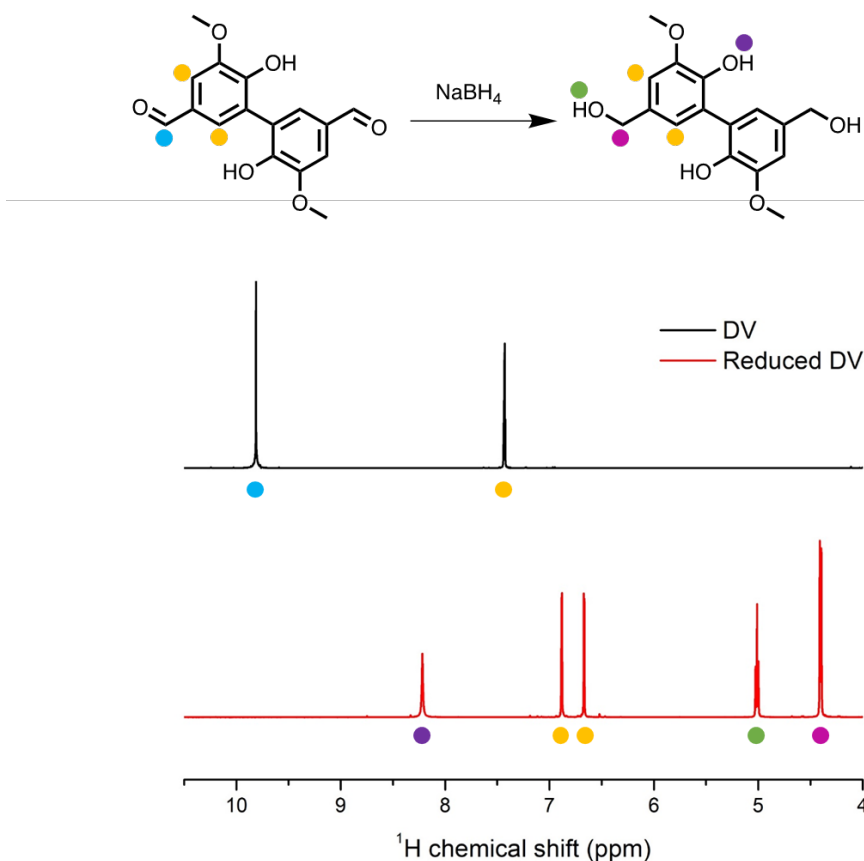
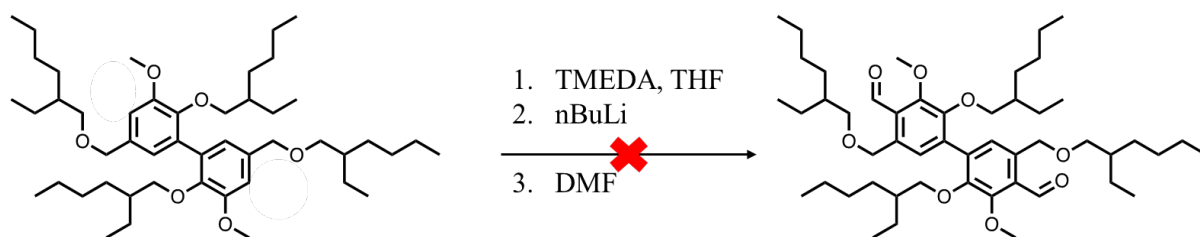


**Figure 9:** Reduction of divanillin by sodium borohydride and  $^1\text{H-NMR}$  spectra of reactant and product (in  $\text{DMSO-d}_6$ )

The peak of the aldehyde proton disappeared, and the one of the aromatics shifted as two doublets (6.88 and 6.67 ppm,  $J = 2$  Hz for both). Two new peaks appeared at 5 ppm and 4.2 ppm, which correspond to the methylene and the OH groups of the  $\text{CH}_2\text{OH}$  moiety, respectively. The peak at 8.2 ppm corresponds to the alcohol proton already present in DiVanillin (**DV**). The reduced **DV** was then alkylated with 2-ethylhexyl bromide to improve the solubility of the final polymers but also to prevent any side reactions from the phenol functions during the formylation reaction. This alkylation step was performed following

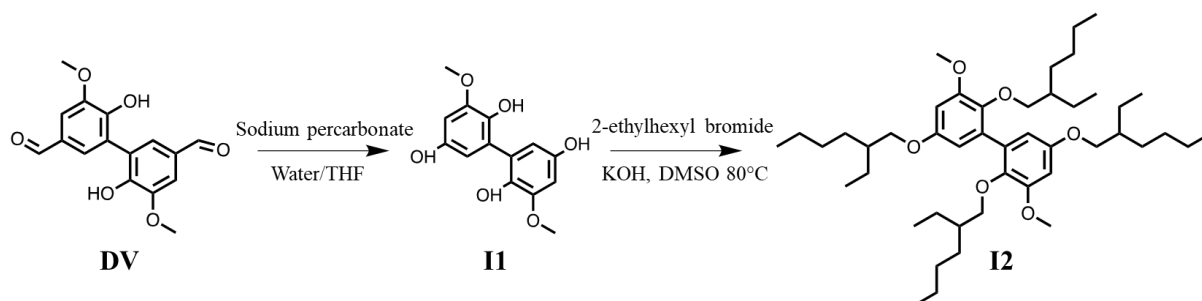
a protocol previously described,<sup>16</sup> to give fully alkylated compound after derivatization of alcohol and phenol functions. However, the yield was relatively low (20%) as the product was degraded during the purification work up by flash chromatography over silica. This reduced divanillin then underwent a formylation reaction, as can be seen in **Scheme 8**:



**Scheme 8:** Formylation of alkylated reduced divanillin

However, no sign of formylation was observed after <sup>1</sup>H- and <sup>13</sup>C-NMR analyses of the reaction product. This failed reaction could be due to the presence of the methoxy(2-ethylhexane) moiety that is not a good DMG due to the spacer between aromatic rings and oxygen atom and cannot favor the aryllithium intermediate formation. Moreover, this alkyl moiety also brings steric hindrance. Consequently, a new synthetic methodology towards para-divanillin was undertaken.

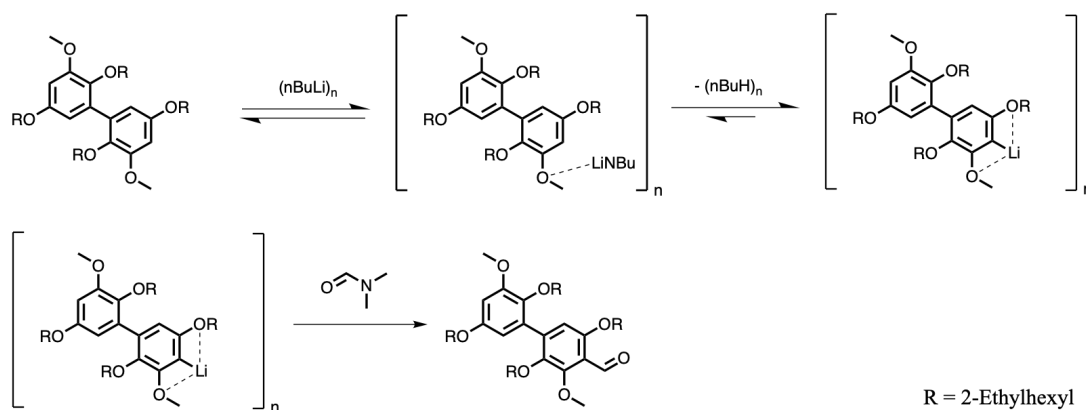
To avoid having a spacer between the aromatic ring and the 2-ethylhexoxy moiety, divanillin was oxidized through Dakin reaction. This reaction consists in the derivatization of the aldehyde functions into phenols, as can be seen in **Scheme 9**. Interestingly, the Dakin oxidation is performed in water, at RT and with an environmentally benign oxidizing agent, i.e. sodium percarbonate.<sup>17</sup>



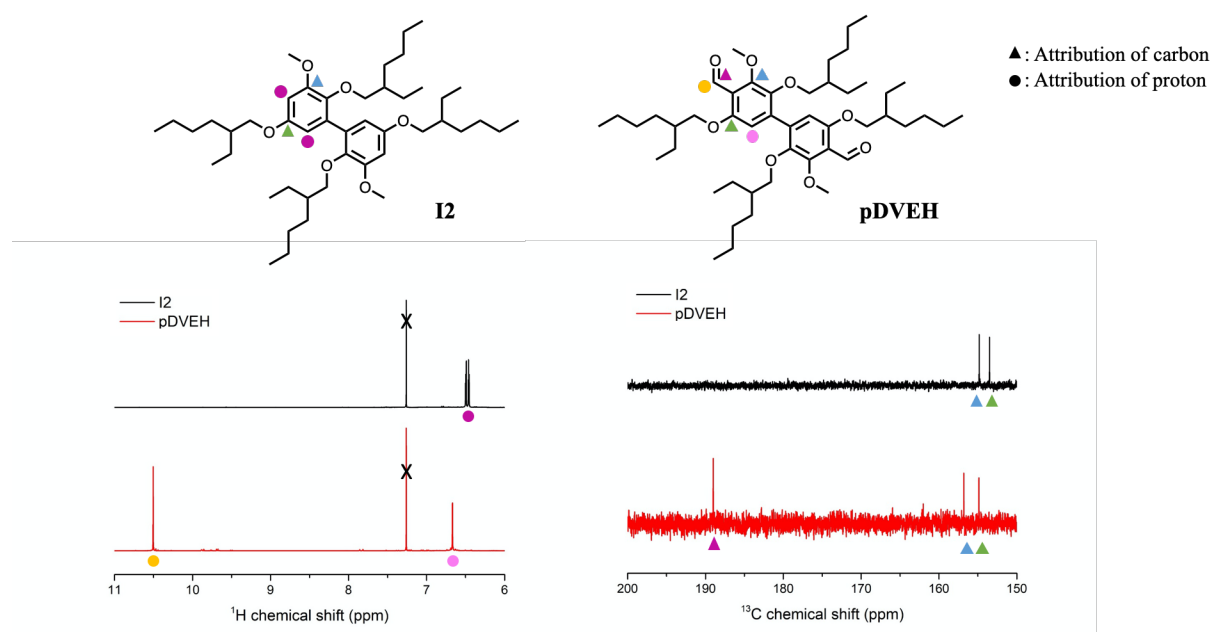
**Scheme 9:** Successive reactions performed on divanillin: first Dakin oxidation, then alkylation

Compound **I1** is not stable and can form a quinone. For this reason, it was not isolated and **I2** was recovered after purification using flash chromatography over silica, with an overall yield of 56%. **I2** then underwent a formylation reaction by metalation using the same conditions as shown in **Scheme 8**. The mechanism is given in **Scheme 10**:



Scheme 10: Mechanism of formylation by metalation of **12**

The formylation on one position is represented in **Scheme 10**. Indeed, this formylation reaction onto **12** may happen on the two para positions at the same time, or successively. Both  $^1\text{H}$ - and  $^{13}\text{C}$ -NMR analyses confirmed that the formylation occurred, as illustrated in **Figure 10**:

Figure 10: Structures of **12** and **pDVEH** and their  $^1\text{H}$ - and  $^{13}\text{C}$ -NMR spectra, with peak attributions (in  $\text{CDCl}_3$ )

Indeed, a new peak appeared at 10.5 ppm on the  $^1\text{H}$ -NMR spectrum, which corresponds to the proton of the newly formed aldehyde functions. The signal of the aromatic changes, from two peaks to a singlet. These aldehyde functions can also be observed by  $^{13}\text{C}$ -NMR analysis, with the apparition of a new peak at 188 ppm. The peak integrations confirmed that the formylation occurred on both sides of **12** (see **Experimental part** for full spectra and integrations) demonstrating that the methoxy group is a better DMG than the other substituents and thus dictate the formylation position in ortho position. The formylation was also confirmed by mass spectroscopy (**Figure 11**).

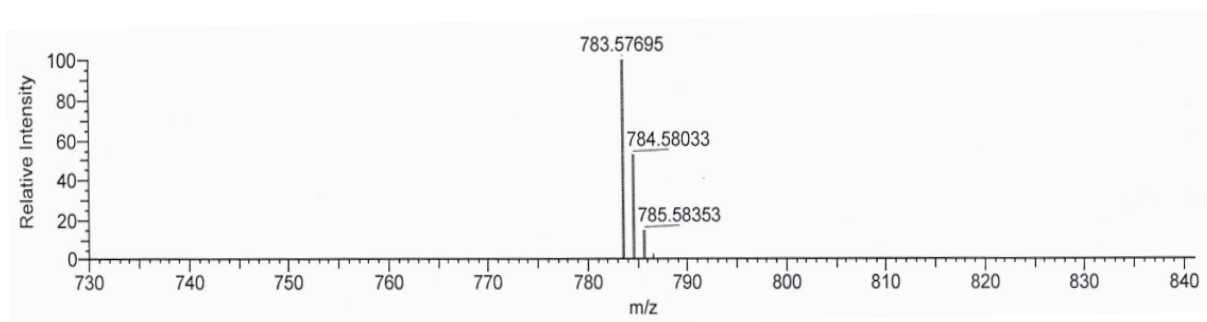
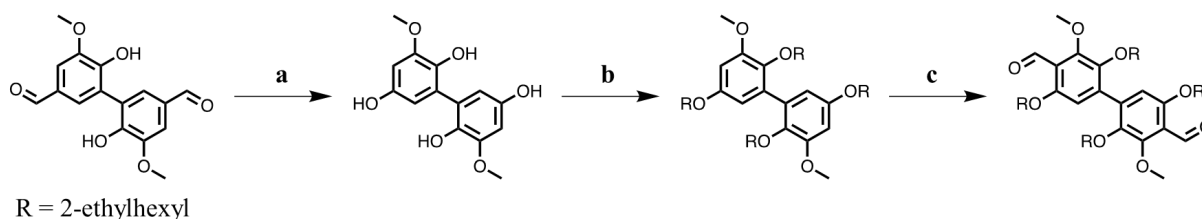


**Figure 11:** High-resolution mass spectrum of **pDVEH** (molecular peak, ESI, positive mode)

### 3.2.3. Conclusion

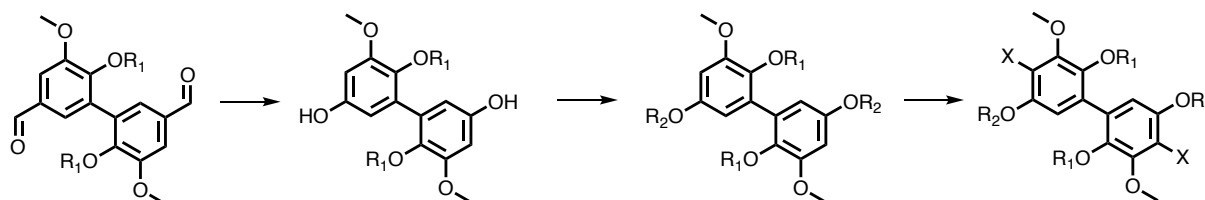
A divanillin-based compound was synthesized, with aldehyde functions in para positions on both aromatic rings. This derivative was obtained in three steps, (i) a Dakin oxidation, using an environmentally benign oxidizing agent at RT, (ii) followed by an alkylation, without any purification step and (iii) a formylation reaction by metalation, to give the new para-divanillin with an overall yield of 44% (**Scheme 11**).



**Scheme 11:** General scheme to obtain the para-divanillin monomer (a: Dakin oxidation b: alkylation using 2-ethylhexyl bromide c: formylation by metalation)

To the best of our knowledge, such para-divanillin was never reported before. Its structure was confirmed by  $^1\text{H}$ - and  $^{13}\text{C}$ -NMR analyses and mass spectroscopy. The latter, named **pDVEH**, for para-DiVanillin 2-EthylHexyl, was tested as co-monomer in the course of polyazomethines, as discussed in the next section.

In addition, a new platform of **pDVEH'** derivatives can be created, as exemplified in **Scheme 12**.



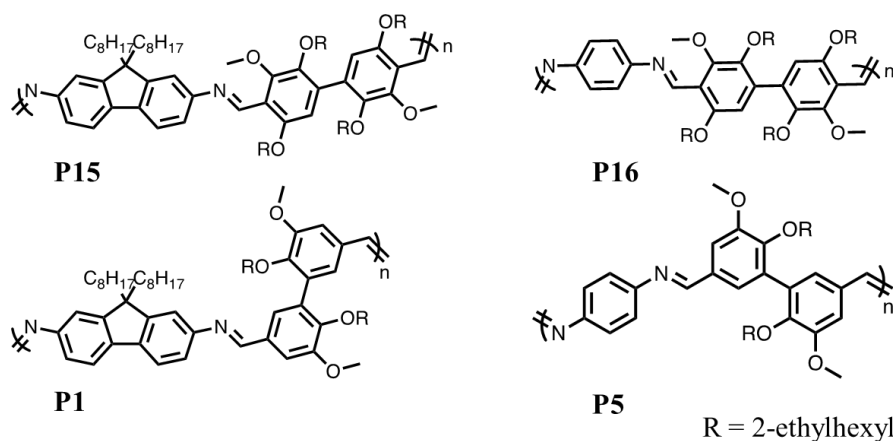
**Scheme 12:** General equation to obtain platform of divanillin based molecules

By starting from alkylated divanillin and then performing a Dakin oxidation, it is possible to have  $\mathbf{R}_1$  different from  $\mathbf{R}_2$ . For example,  $\mathbf{R}_1$  could be a long alkyl moiety to improve solubility, and  $\mathbf{R}_2$  a short one to avoid hindrance during the formylation reaction. Additionally, various chemical functions can be added in para positions of the aromatic ring such as amine, phenol, carboxylic acid, etc.<sup>9</sup>

#### 4. Polyazomethines with para-divanillin-based monomer

##### 4.1. Polyazomethine synthesis, physical characterizations and comparison with divanillin-based polyazomethines

Polyazomethines were synthesized using **pDVEH** and two diamines, para-phenylene diamine and fluorene diamine (**P15** and **P16**). The polymerization was performed using the optimized protocol discussed previously: five minutes of microwave irradiation at 130°C, then a recovery step by evaporating methanol using a rotary evaporator. **P15** is soluble in common solvents (chloroform, THF, methylene chloride), unlike **P16** which is only partially soluble in these latter (~50% of soluble fraction in THF). The polymerization was assessed by <sup>1</sup>H-NMR and SEC analyses on the soluble fractions and the characteristics of the polyazomethines are gathered in **Table 1** with their structures together with the ones of their equivalent with **DVEH**.



| Name       | $\bar{M}_n^a$ (g/mol) | $\bar{M}_w^a$ (g/mol) | $\bar{D}^a$ | $\overline{DP}_n^a$ | Solubility In THF <sup>b</sup> | $T_d^c$ (°C) |
|------------|-----------------------|-----------------------|-------------|---------------------|--------------------------------|--------------|
| <b>P15</b> | 7 000                 | 23 500                | 3.3         | 6                   | 100%                           | 320          |
| <b>P1</b>  | 21 100                | 45 500                | 2.2         | 23                  | 100%                           | 387          |
| <b>P16</b> | 3 800                 | 11 400                | 3.0         | 4                   | 50%                            | 327          |
| <b>P5</b>  | 10 600                | 21 900                | 2.1         | 18                  | 100%                           | 374          |

**Table 1:** Structures of **DVEH**- and **pDVEH**-based polyazomethines and table summing up their properties.

<sup>a</sup> Determined by SEC relative to polystyrene standards in THF at 30°C. <sup>b</sup> % of soluble fraction, targeted concentration: 5 mg/mL. <sup>c</sup> Decomposition temperature at 10% weight loss, evaluated under N<sub>2</sub> at a heating rate of 10 °C/min by TGA.

**P15** and **P16** are comparatively less stable thermally than their homologues with divanillin. Indeed, **P15** has a degradation temperature 67°C lower than its **DVEH**-bearing counterpart. With respect to the SEC results, the soluble polymer chains of **P15** and **P16** are much shorter than for the corresponding polyazomethines with **DVEH**: **P15** is only 6-unit long and **P16** 4-unit long. In the case of **P15**, these shorter chains could be due to a lower reactivity of the new **pDVEH** or to some steric hindrance around

the aldehyde function. It is not possible to conclude for **P16**, as it is not fully soluble. The dispersity is rather high, as it corresponds to broad distribution as shown in **Figure 12**:

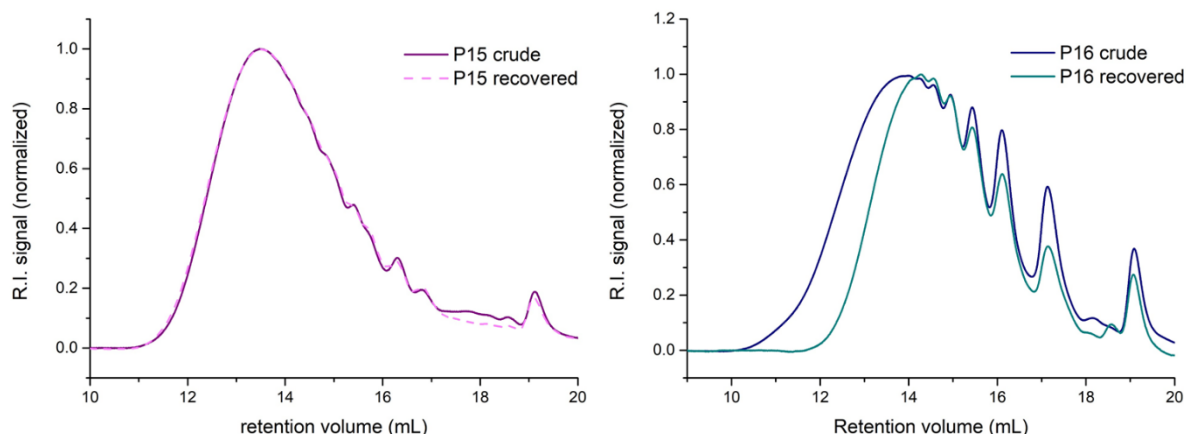


**Figure 12:** SEC traces of **P15** (left) and **P16** (right) in THF, crude and after recovery (R.I. detection)

In the previous chapter, the polyazomethines molar masses were increased during the recovery step. This step is performed by dissolving the sample in a minimum amount of methylene chloride, adding methanol and then evaporating both solvents using a rotary evaporator. The powder obtained is then rinsed with methanol to give the recovered polymer. In the case of **P15** the SEC traces before and after recovery are identical. Whereas for **P16**, the recovery seems to have quite a negative effect, as the molar masses do not increase but rather decrease. For **P16** this decrease could be explained by the poor solubility of the polymer. The recovery might create longer and thus less soluble chains, leading to a SEC trace of lower molar masses. Indeed, the crude of **P16** is soluble at ~65% while the purified fraction is soluble at ~50% in THF. This solubility issue might also explain why **P15** is not affected by the recovery: maybe some limitations in terms of molar mass and/or solubility have been reached, and therefore molar masses cannot evolve anymore.

The  $^1\text{H-NMR}$  spectra of the soluble fraction of **P15**, **P16** and their divanillin bearing counterparts are given in **Figure 13**.

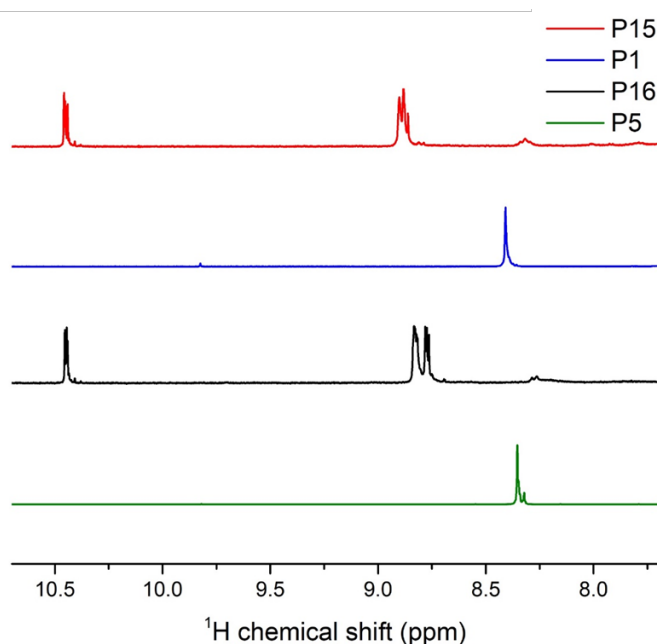


**Figure 13:**  $^1\text{H-NMR}$  spectra of pDVEH- and DVEH-bearing polyazomethines (128 scans, in  $\text{CDCl}_3$ )

Only a fraction of **P15** and **P16** was analyzed, as they are partially soluble in chloroform (80% for **P15** and 40% for **P16**). The azomethine peaks of **P15** and **P16** are shifted towards higher chemical shift compared to **P1** and **P5** (8.8 ppm vs 8.4 ppm). This shift is expected, as the azomethine bond of **P15** and **P16** is more shielded due the presence of an additional OR group linked to the aromatic rings of **pDVEH** in comparison to **DVEH**. However, some residual aldehyde is detectable for **P15** and **P16**, with intense peaks at 10.4 ppm. This might be due to the samples' poor solubility, and therefore is not representative of the whole samples.

4.2. Conclusion on the synthesis and thermal characterizations of polyazomethines from para-divanillin

New polyazomethines were synthesized from **pDVEH**, either with fluorene diamine or para-phenylene diamine. These polyazomethines have molar masses and degradation temperature a bit lower than the ones of **DVEH**-based polyazomethines. However, the **pDVEH**-based polyazomethines are partially soluble in common solvents, which prevents from drawing a clear conclusion. The **pDVEH**-based polyazomethines were then characterized in terms of optical properties, as is discussed in the next section.

#### 4.3. Optical properties of polyazomethines from para-divanillin

The previously synthesized polyazomethines were characterized by UV-Vis spectroscopy; their spectra are displayed in **Figure 14** and compared to the ones of polyazomethines from **DVEH**.

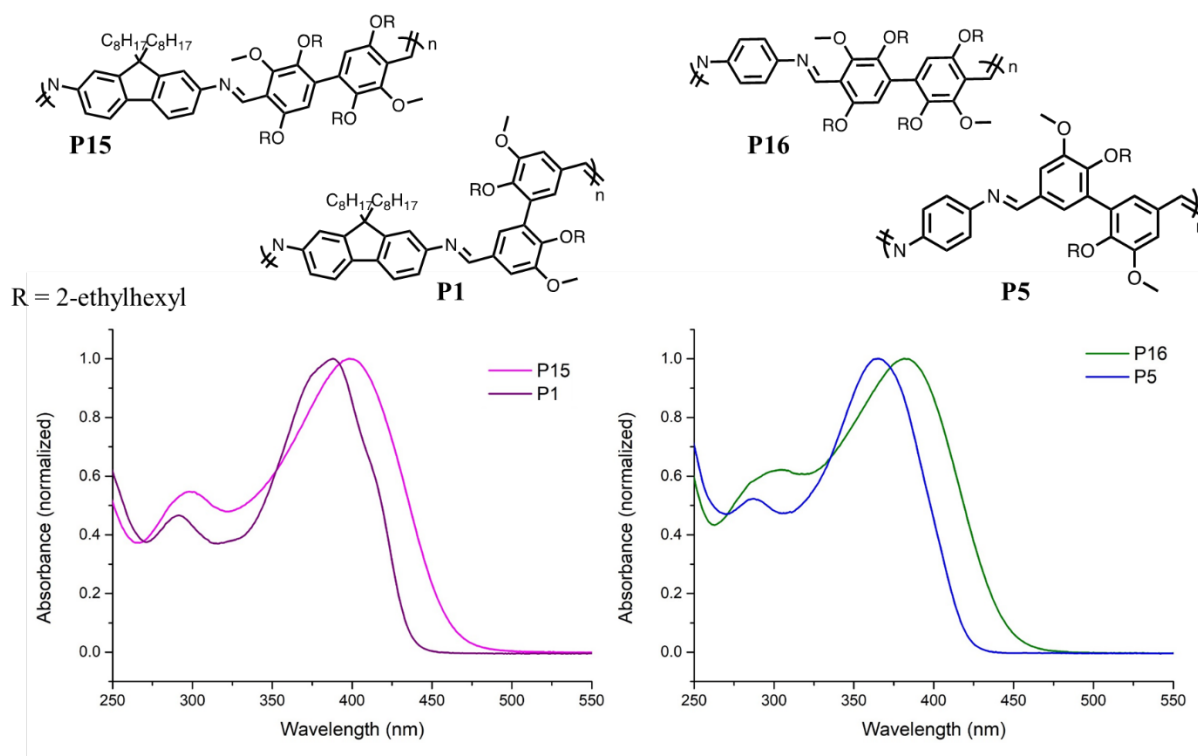


**Figure 14:** Absorbance spectra of **pDVEH**- and **DVEH**-based polyazomethines in methylene chloride ( $10^{-2}$  g/L, soluble fraction for **P16**)

The absorbance spectrum of **P15** is composed of two peaks, a main one towards higher wavelengths, which corresponds to  $\pi$ - $\pi^*$  transitions and another one around 300 nm, which could correspond to  $n$ - $\sigma^*$  transitions. Compared to **P1**, the spectrum of **P15** does not exhibit any shoulder at 410 nm. This could be due to the absence of aggregates, or to the absence of  $n$ - $\pi^*$  interactions for this polyazomethine. **P16** has the same two-peak shaped absorbance spectrum. What is worth noticing is that both **pDVEH**-based polyazomethines are more red-shifted than their homologues with **DVEH** are. **P15** is red-shifted by

11 nm in comparison to **P1** and **P16** by 18 nm with respect to **P5**. This red shift could mean an improvement of the conjugation pathway, either because the latter is more planar or longer.

The emission spectra of **pDVEH**-based polyazomethines and their counterparts with **DVEH** are given in **Figure 15**:

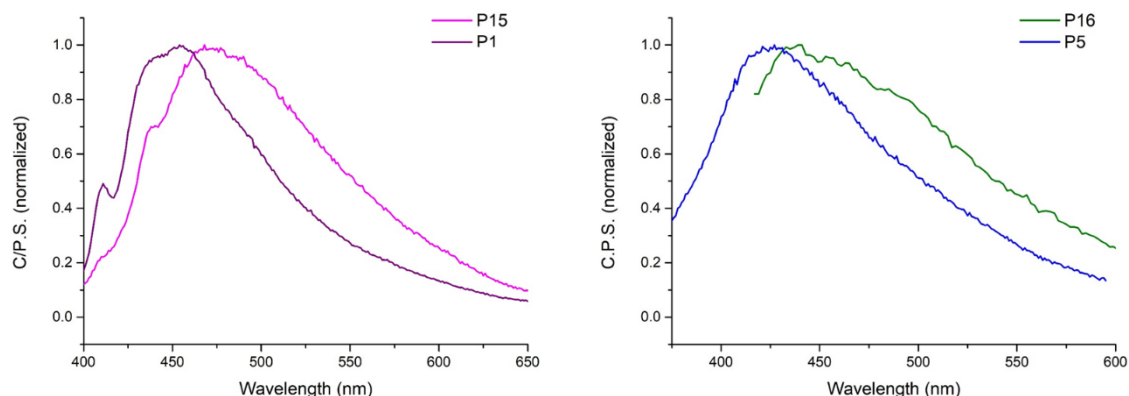
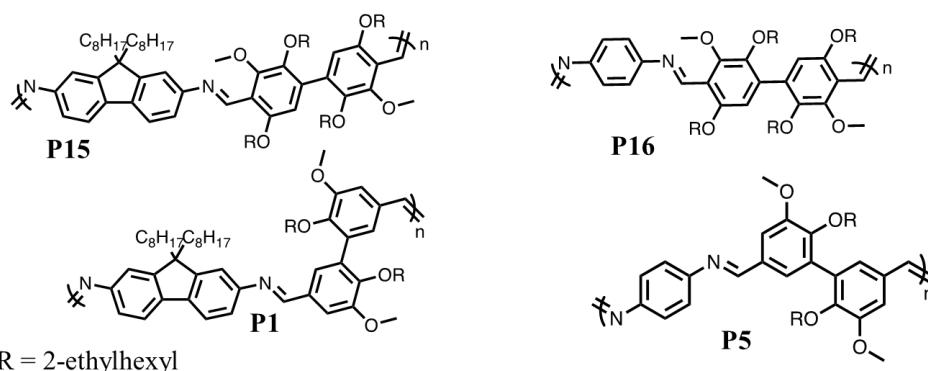


**Figure 15:** Emission spectra of polyazomethines in methylene chloride ( $10^{-2}$  g/L, soluble fraction for **P16**, integration time: 0.5 s, excitation wavelength: 15 nm below the absorbance maximum)

The experimental conditions to record the emission spectra are the same as the ones used in the previous chapter. The integration time was set at 0.5 s and relatively concentrated solutions ( $10^{-2}$  g/L, absorbance at 1) were used to obtain a more intense signal. Moreover, the polyazomethines were excited at lower wavelengths than their absorbance maximum: this enables shifting the solvent Raman peak and therefore obtaining the polyazomethines' spectra without any parasitic peak.

The emission spectra of **P15** and **P16** are both red-shifted compared to their **DVEH**-based counterparts. This is once more a sign of improvement of the conjugation pathway. No charge transfer like behavior was observed for these polyazomethines in solution. In **Table 2**, the optical properties of **pDVEH**- and **DVEH**-based polymers are indicated both in films and in solution.



| Name       | Absorbance                      |                                  | Emission                        |                                  |
|------------|---------------------------------|----------------------------------|---------------------------------|----------------------------------|
|            | $\lambda_{\max}^{\text{sol a}}$ | $\lambda_{\max}^{\text{film b}}$ | $\lambda_{\max}^{\text{sol a}}$ | $\lambda_{\max}^{\text{film b}}$ |
| <b>P15</b> | 399                             | 399                              | 475                             | 550                              |
| <b>P1</b>  | 388                             | 392                              | 455                             | 470 - 560                        |
| <b>P16</b> | 383                             | 385                              | 440                             | 465 - 555                        |
| <b>P5</b>  | 365                             | 371                              | 432                             | 460 - 510                        |

**Table 2:** Sum up of the polyazomethine optical properties, in solution and in film <sup>a</sup> In methylene chloride,  $10^{-2}$  g/L <sup>b</sup> Films prepared by drop-casting on quartz plate

As a general trend, polyazomethines bearing a **pDVEH** moiety are more red-shifted than their homologues with **DVEH**. **P15** is more red-shifted than **P16**, which is expected as **P15** bears a fluorene diamine group. Indeed, fluorene is composed of three attached rings, bringing more planarity and therefore a red shift compared to a phenyl. All polyazomethines present a charge transfer like behavior in films. In the case of **P15**, it is so potent that it overcomes the locally excited state emission. In films, **DVEH**-bearing polyazomethines are more red-shifted than in solution, with a shift up to 6 nm for **P5**. However, in the case of **pDVEH**-bearing polyazomethines, this shift is much lower, only 2 nm for **P16** and none for **P15**. This is due to the shape of the absorbance spectra, as it is illustrated in **Figure 16**. Indeed, even if the spectrum maxima are not shifted, the spectra are broader. The bathochromic shift is due to the reorganization of the polymer chains in films, as they can organize themselves better and therefore get more planar. However, the broader signal could be due to a less defined structure in the sample, maybe because the latter is composed of multiple populations.

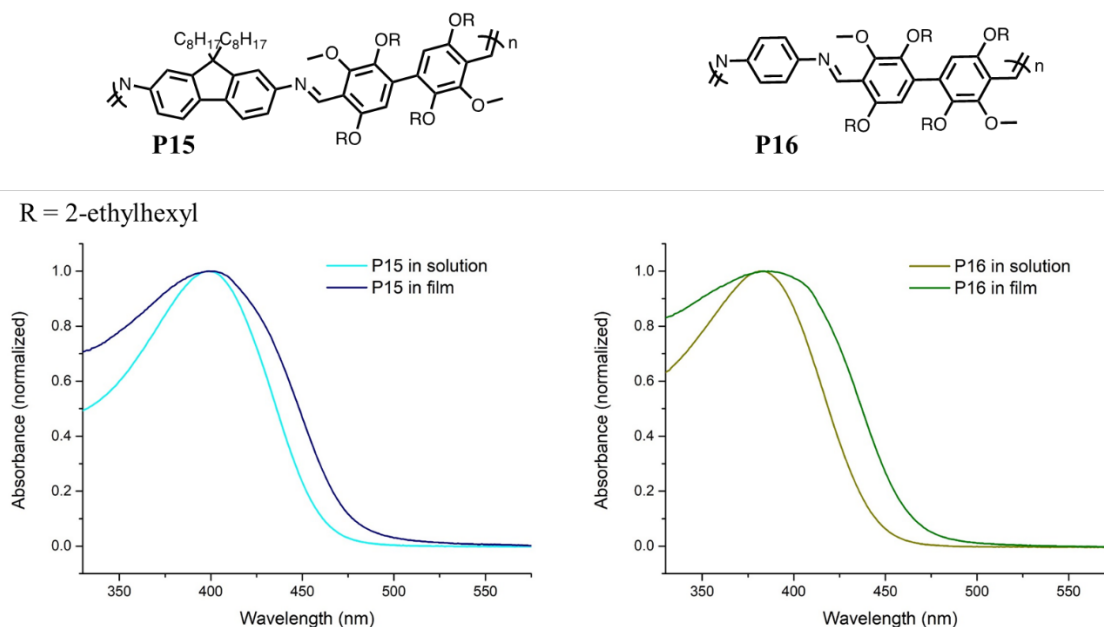


**Figure 16:** Absorbance spectra of polyazomethines in solution in methylene chloride ( $10^{-2}$  g/L) and drop-casted on quartz plate

#### 4.4. Conclusion on optical properties

Polyazomethines with **pDVEH** were characterized in terms of absorbance and emission. These latter have interesting optical properties, with absorbance maxima up to 399 nm and emission in the visible range. However, their emission in solution is very weak, in agreement with literature data.<sup>18</sup> These polyazomethines have a charge transfer-like behavior in films, and are more red-shifted in films than in solution, both in terms of absorbance and emission.

Compared to their **DVEH**-based counterparts, the **pDVEH**-based polyazomethines are more red-shifted, up to 18 nm in absorbance in solution. This red shift could be a sign of a longer or more planar conjugation pathway. However, this value is under what was expected. Indeed, by going from a **DVEH**-based polyazomethine with a short conjugation pathway to a fully conjugated **pDVEH**-based polyazomethine, one would expect more than a 18 nm bathochromic shift. Skene *et al.*<sup>19</sup> synthesized model compounds of azomethines with various number of units as exemplified in **Figure 17**.

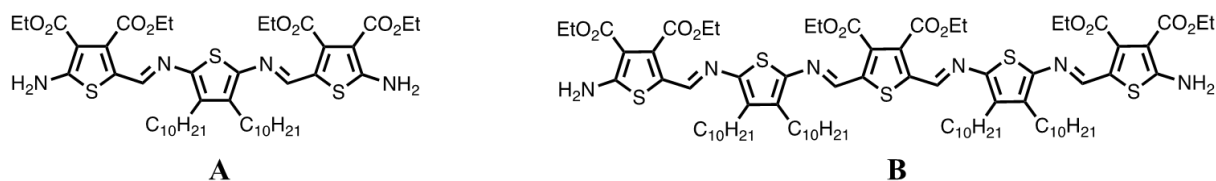


Figure 17: Thiophene-based azomethines (adapted from <sup>19</sup>)

By adding one motive (going from **A** to **B**), a 72 nm bathochromic shift was observed, induced by the lengthening of the conjugation pathway.<sup>20</sup> To better understand the small bathochromic shift obtained for **pDVEH**-based polyazomethines, some model compounds were designed and synthesized for structure-properties studies.

## 5. Model compounds of para-divanillin-based polyazomethines

### 5.1. Synthesis and purification of model compounds

Model compounds were synthesized in order to better understand the properties of **pDVEH** and **pDVEH**-based polymers. As discussed in the previous chapter, azomethines cannot be purified by flash chromatography over silica as it degrades them. Therefore, these latter compounds were purified by recrystallization. Model compounds bearing methyl groups were chosen, as they recrystallize more easily than their 2-ethylhexyl bearing homologues. **Figure 18** details the model compounds synthesized and their names.

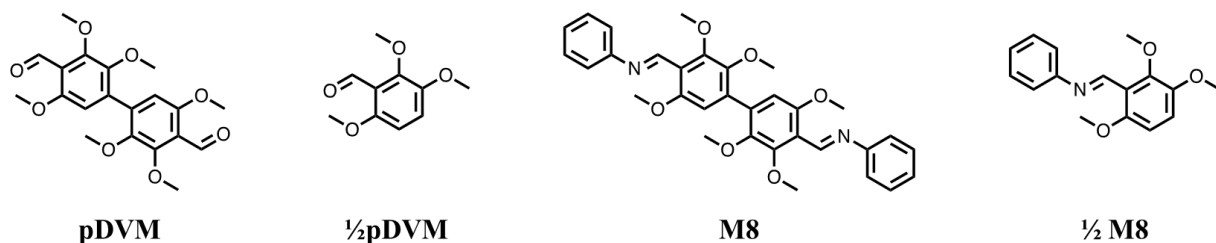
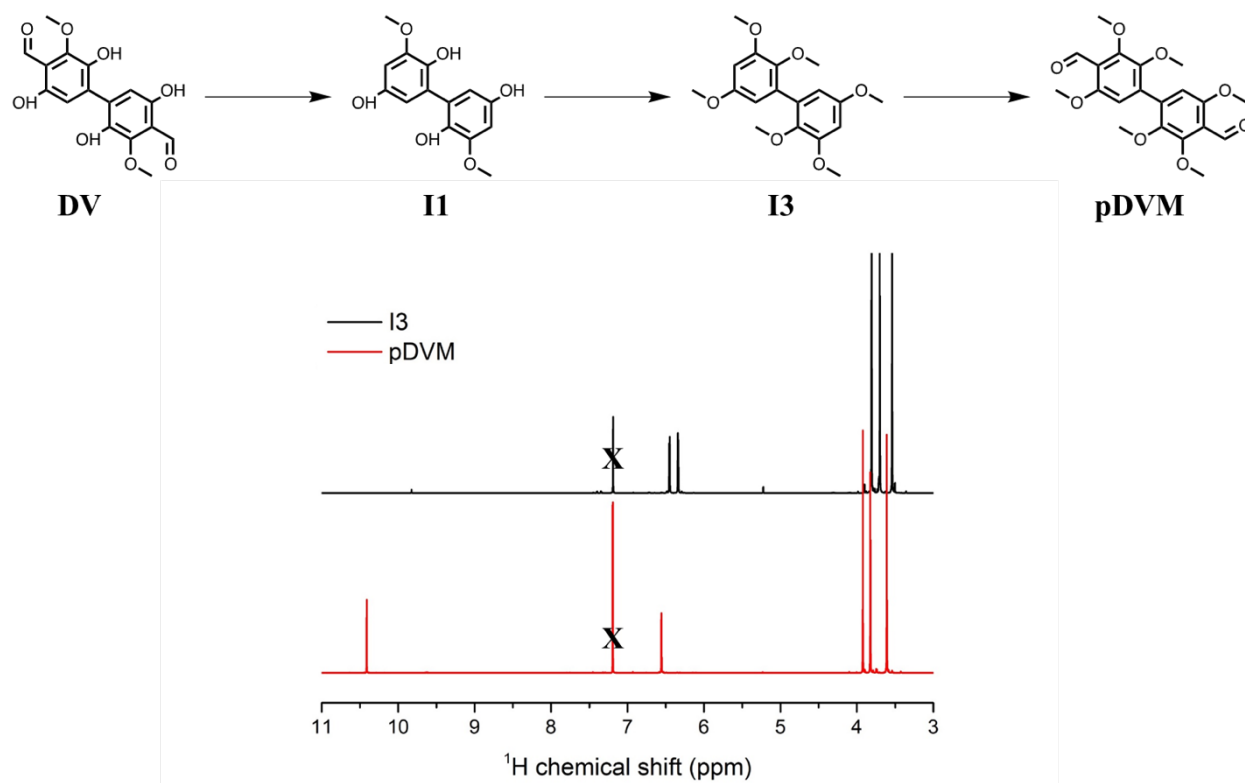


Figure 18: Sum up of the model compounds synthesized based on **pDVEH**

**pDVM** (para-DiVanillin Methylated) was obtained using the same steps as **pDVEH**, as illustrated in **Figure 19**: (i) Dakin oxidation, then (ii) alkylation and finally (iii) formylation reaction by metalation. However, a new methylation protocol<sup>21</sup> had to be used, to improve the otherwise very low yield. The intermediate **I3** was purified by flash chromatography over silica, using methylene chloride as the eluent.





**Figure 19:** General scheme of the synthesis of **pDVM** and  $^1\text{H}$ -NMR spectra of **pDVM** and its intermediate (in  $\text{CDCl}_3$ )

The  $^1\text{H}$ -NMR spectra of **I3** illustrates the Dakin oxidation, as the aldehyde peak disappeared. The formylation of **I3** was assessed by  $^1\text{H}$ -NMR analysis, as is shown in **Figure 19** with the apparition of a new peak at 10.4 ppm.  $^{13}\text{C}$ -NMR analysis, mass spectroscopy and X-RD also confirmed the structure of **pDVM**.

$\frac{1}{2}\text{pDVM}$  was obtained by formylating the commercially available 1,2,4 trimethoxyphenyl. However,  $\frac{1}{2}\text{pDVM}$  could not be recrystallized, and thus analyzed by X-RD this molecule, as it is oily at room temperature. Nonetheless,  $\frac{1}{2}\text{pDVM}$  was purified by flash chromatography over silica and characterized by  $^1\text{H}$ - and  $^{13}\text{C}$ -NMR spectroscopy.

**M8** was obtained by reacting **pDVM** and aniline in methanol, at the reflux for 30 minutes. It was then recrystallized as described in the previous chapter, to isolate the main isomer. The reaction was assessed by  $^1\text{H}$ -NMR spectroscopy, with the disappearance of the aldehyde peak and apparition of new peaks, such as azomethine bond and phenyl proton, as is illustrated in **Figure 20**.

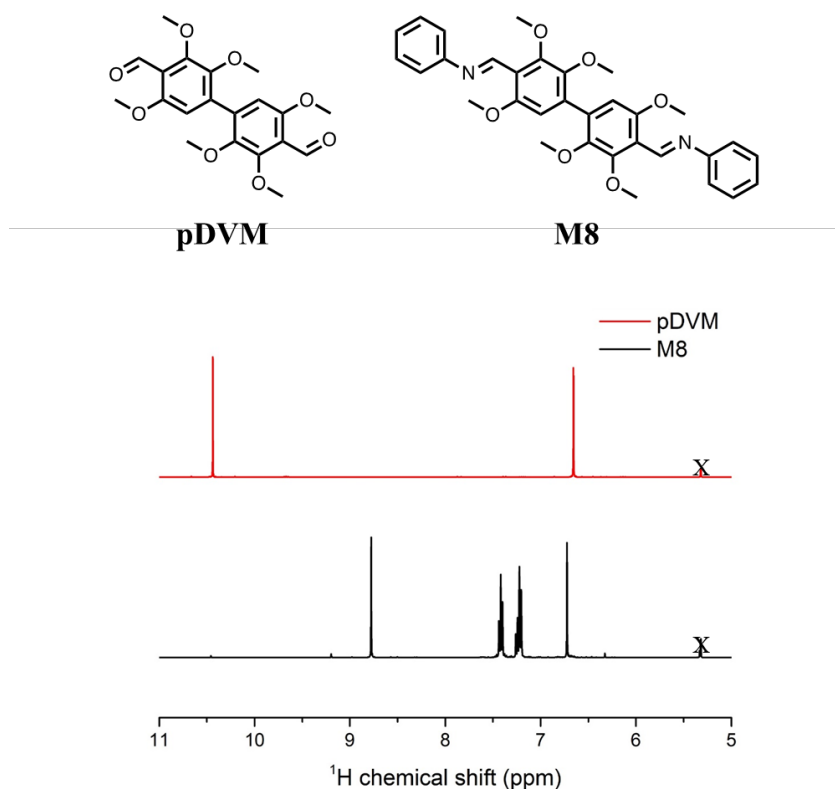


**Figure 20:** Structure and  $^1\text{H}$ -NMR spectra of **M8** and its precursor **pDVM** (in  $\text{CD}_2\text{Cl}_2$ )

$\frac{1}{2}\text{M8}$  was synthesized and the formation of the azomethine bond assessed by  $^1\text{H}$ -NMR spectroscopy. The E/Z ratio is 85/15 for **M8**, and 100/0 for its half  $\frac{1}{2}\text{M8}$ .  $\frac{1}{2}\text{M8}$  is an oil at RT, and therefore could not be recrystallized. It could not be purified by flash chromatography over silica and was set aside.

## 5.2. X-Ray Diffraction analysis

**pDVM** was resolved by X-RD, and its structure is shown in **Figure 21**:

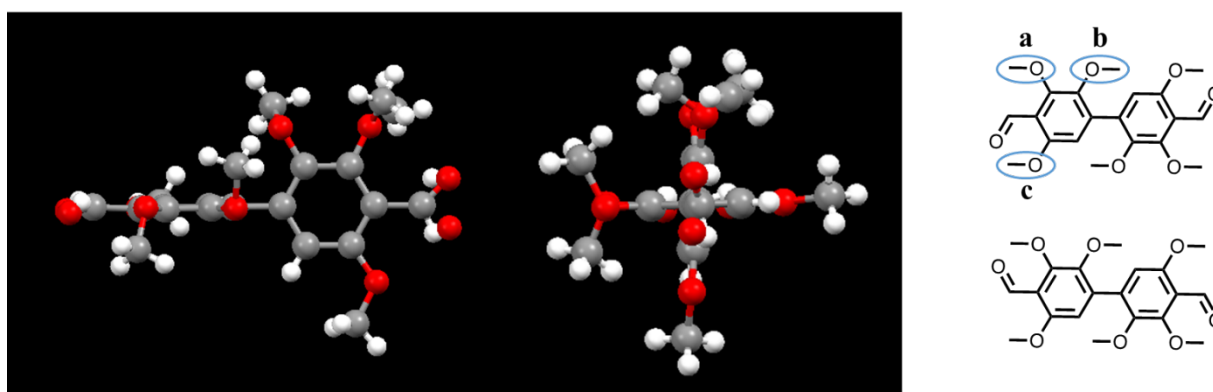


**Figure 21:** Face and side view of X-RD structure of **pDVM**

The aldehyde functions can have two different orientations, as represented in **Figure 21**. This is why the X-RD structure has two aldehyde functions shown on both sides of the molecule, as the two are equiprobable. The most remarkable observation to emerge from this X-RD structure is the angle between the two aromatic rings. This torsion angle is  $86.4^\circ$  and is most likely due to steric hindrance between the methoxy functions **b** (see **Figure 21**) in ortho position of the aromatic rings. Steric hindrance also governs the position of the methoxy functions: **c** is in the plan of the aromatic ring while **a** and **b** are not.

The structure of **M8** was also resolved by X-RD and its structure given in **Figure 22**.

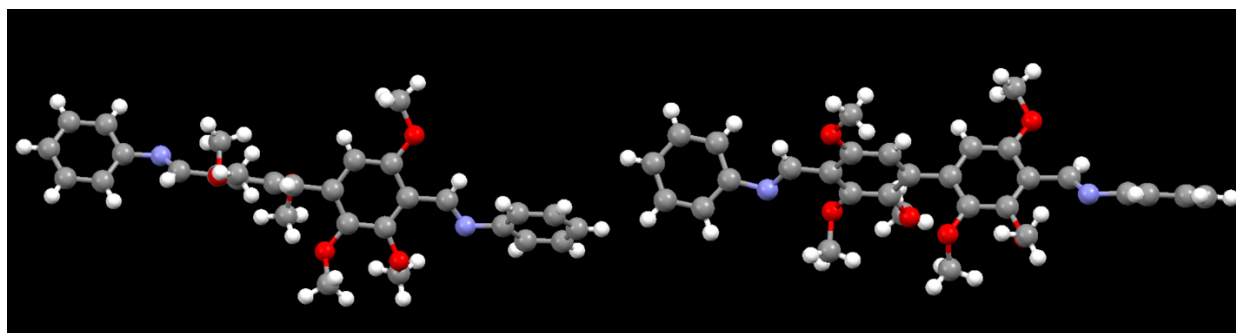


**Figure 22:** Face and side view of X-RD structure of **M8**

The torsion angle between the two aromatic rings is now  $98.9^\circ$ , therefore more planar than **pDVM**. By comparison, the equivalent model compound with **DVM** (noted **M7**) has a torsion angle between aromatic rings of  $126.9^\circ$ . The azomethine bonds have both E configuration, in agreement with literature data.<sup>22</sup> The angle between the two planes created by the aromatic rings on each side of the azomethine bond (noted  $\theta_1$ ) is  $61^\circ$ , which is larger than the one of **M7** ( $54.7^\circ$ ). This higher value is most likely due to steric hindrance, even if there are interactions between the oxygen of the methoxy function and the nitrogen of the azomethine bond, as is represented in **Figure 23**.

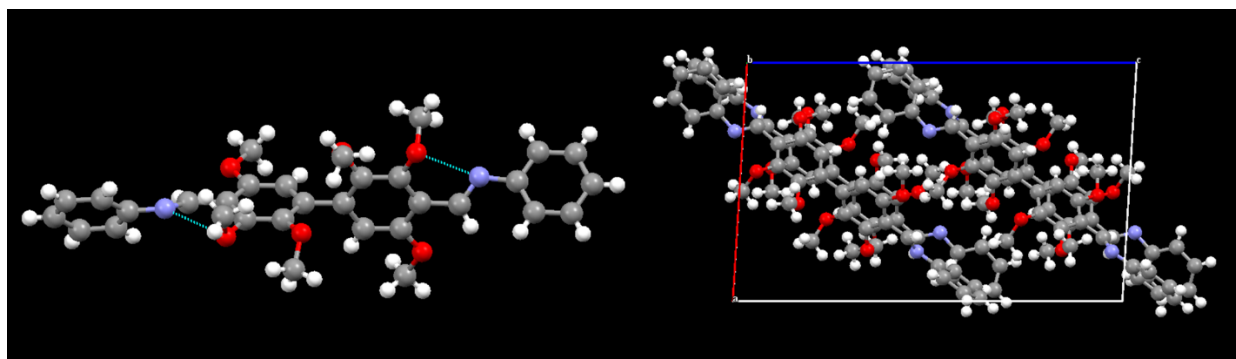


**Figure 23:** X-RD structure of **M8** and view along the b axis (right)

Given the packing of the molecules in **Figure 23** (right),  $\pi$  stacking could be possible. Indeed, it seems that **pDVM** moieties are packed on top of each other. However, the steric hindrance from the two aniline moieties and the angle between the aromatic rings prevent them from getting too close.

### 5.3. Brief conclusion on synthesis and X-Ray Diffraction characterization

Model compounds of para-divanillin-based polyazomethines were synthesized and purified by recrystallization when possible. Indeed, some of them were oily at RT, preventing effective recrystallization. Their structure was confirmed by  $^1\text{H}$ - and  $^{13}\text{C}$ -NMR spectroscopy and two model compounds were solved by X-RD. The E isomer was solved for the azomethine model compound. Interestingly, the two aromatic rings of **pDVM** are nearly perpendicular, with a torsion angle between the two aromatic rings of  $86.4^\circ$ . This torsion is due to steric hindrance between the methoxy functions in ortho position of the two aromatic rings. Concerning the **pDVM**-based azomethine (**M8**), the torsion angle between the two aromatic rings of the **pDVM** moiety is slightly lessened compared to **pDVM**. Moreover, there are interactions between the nitrogen of the azomethine bond and the oxygen atom of the methoxy function in **M8**. The effect of the twist on the optical properties will be discussed in the next section.

## 5.4. Optical characterization

**Figure 24** compares the absorbance spectra of two molecules synthesized previously: **pDVM** and its half  $\frac{1}{2}$ **pDVM**.

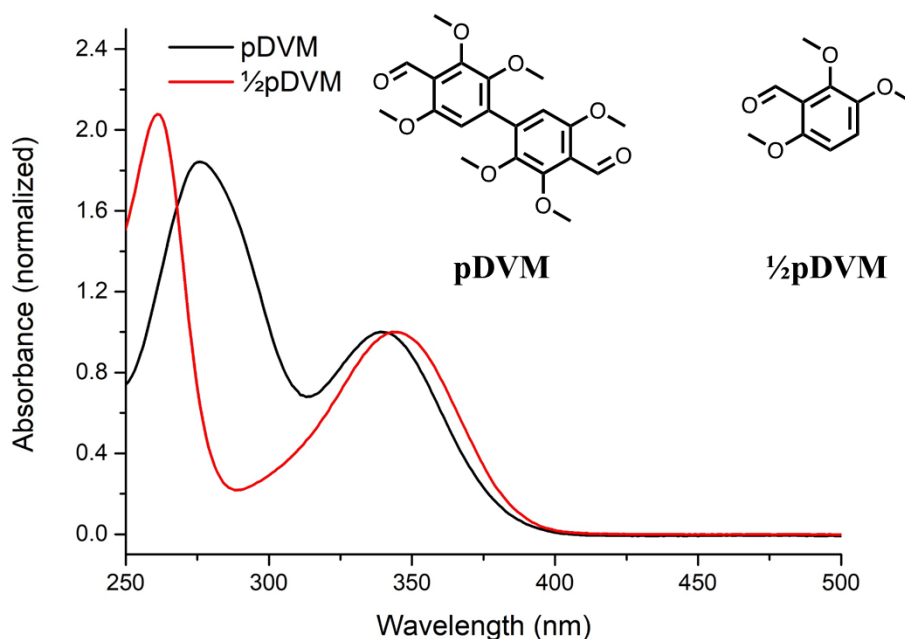


**Figure 24:** Absorbance spectra of **pDVM** and  $\frac{1}{2}$ **pDVM** in methylene chloride ( $10^{-2}$  g/L)

Both spectra have the same shape: a more intense peak towards 270 nm, which could correspond to  $n-\sigma^*$  transitions, and another one towards 340 nm that could correspond to  $\pi-\pi^*$  transitions. Remarkably,  $\frac{1}{2}$ **pDVM** is red shifted compared to **pDVM**. Indeed, there is a bathochromic shift of 5 nm between the two absorbance maxima. This means that there is no conjugation between the two aromatic rings of **pDVM**. This is in agreement with the previously discussed X-RD data, as the two phenyls of **pDVM** are nearly perpendicular to each other. This near right angle prevents orbital overlaps between the two rings, but also hinders it within the aromatic ring. Indeed, the peak corresponding to  $\pi-\pi^*$  transitions in **pDVM** is blue-shifted compared to the one of  $\frac{1}{2}$ **pDVM**. This hypsochromic shift means that more energy is needed to realize this transition in **pDVM** than in  $\frac{1}{2}$ **pDVM**. However, the  $n-\sigma^*$  transition peak is more red-shifted for **pDVM** than for  $\frac{1}{2}$ **pDVM**. This implies that transitions between non-bonding oxygen orbitals and sigma bond are promoted, possibly because of the presence of the additional aromatic ring that acts as an electron withdrawing substituent.

In **Figure 25** the absorbance spectra of **P16** and model compounds of its backbone are represented.

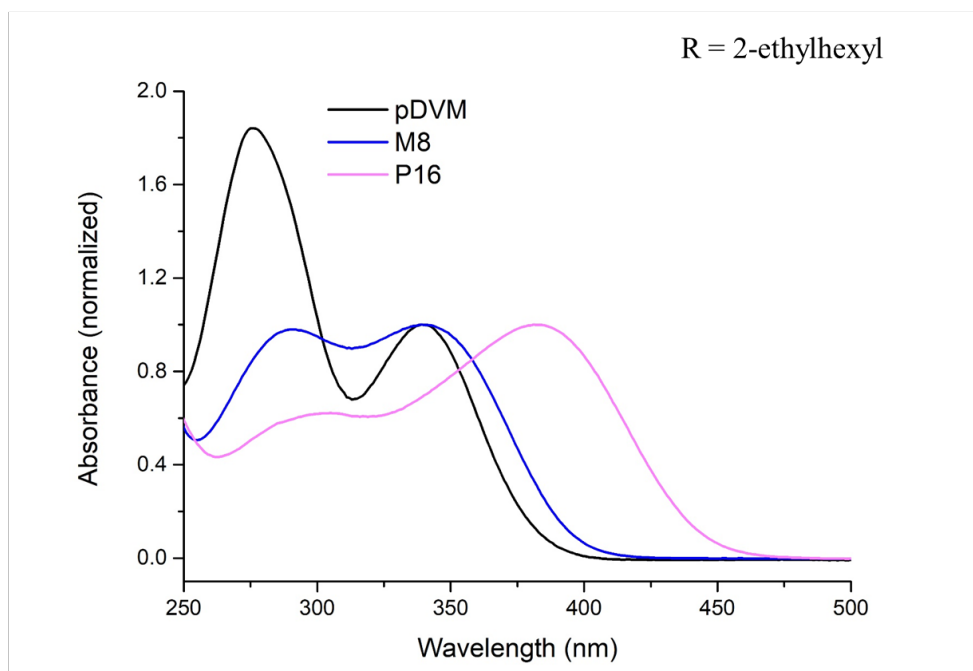
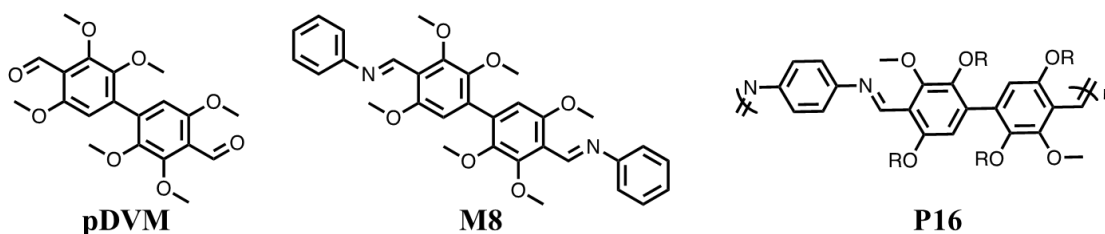


**Figure 25:** Absorbance spectra of **pDVM**, **M8** and **P16** in methylene chloride ( $10^{-2}$  g/L) and their structure

A clear bathochromic shift was expected between **pDVM** and **M8**, as **M8** has a longer conjugation pathway thanks to the addition of aniline moiety. However, this is not the case as **pDVM** and **M8** have the same absorbance maxima, even if **M8** spectrum is broader. In contrast, the peak corresponding to  $n-\sigma^*$  transitions is strongly affected by the addition of aniline moiety, as it gets red-shifted and less intense. **P16** is red shifted by nearly 40 nm compared to the two others. This bathochromic shift is due to **P16**'s longer conjugation pathway. Indeed, the longer pathway without being interrupted by the near right angle of **pDVM** is illustrated in **Figure 26**.

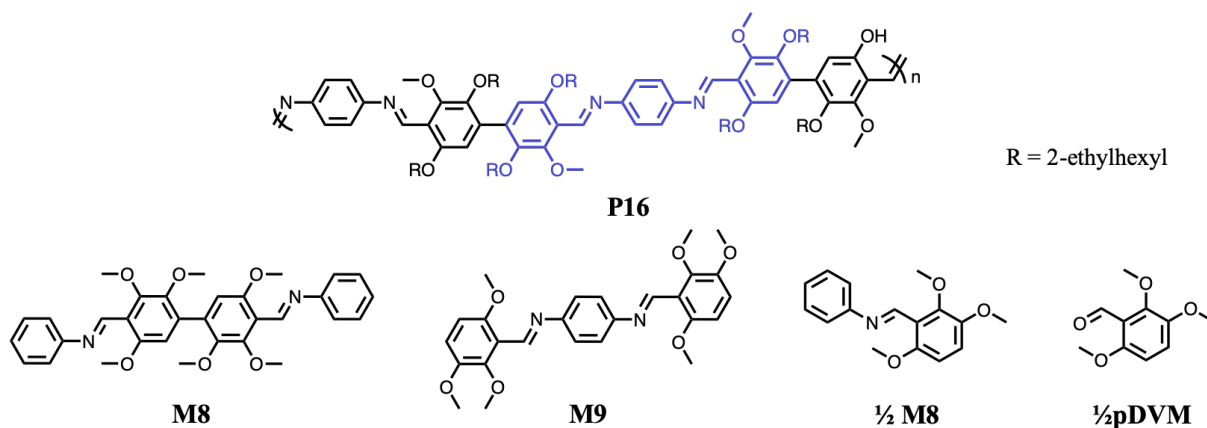


**Figure 26:** Structure of **P16** and model compounds of its backbone

There is a strong probability that **M9** has the same absorbance maximum as **P16**, as it mimics its backbone, even if there might be some differences due to the presence of 2-ethylhexyl moieties on **P16**. **M9** was not synthesized, as it is most likely an oily azomethine and therefore cannot be recrystallized or be purified by flash chromatography over silica. Indeed, both  $\frac{1}{2}$ **M8** and  $\frac{1}{2}$ **pDVM** are oily at RT, heralding the same behavior for **M9**.

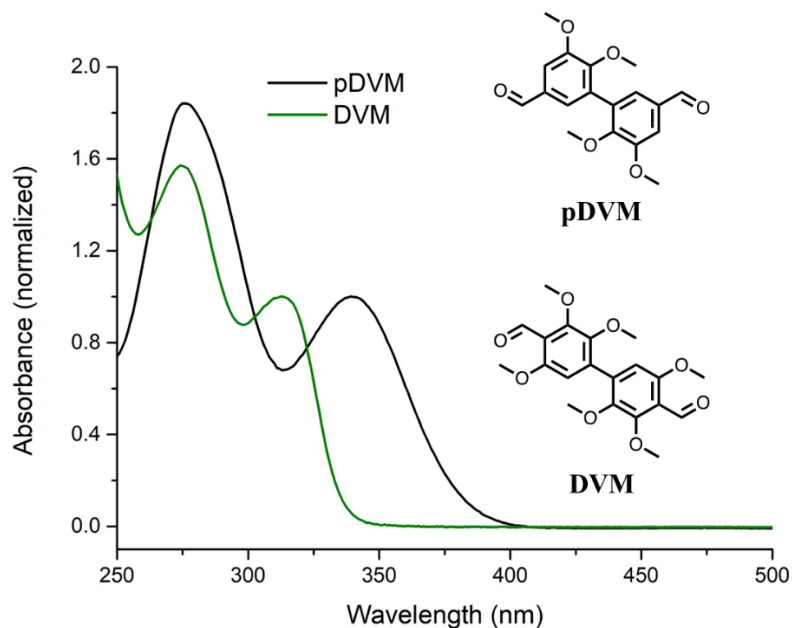


Figure 27: Absorbance spectra of **pDVM** and **DVM** in methylene chloride ( $10^{-2}$  g/L)

Interestingly, **pDVM** is red-shifted compared to **DVM**, as illustrated in **Figure 27**. Indeed, there is a 27 nm bathochromic shift between the two local maxima. This red shift is due to the additional electron donating methoxy function on **pDVM**, and is consistent with literature data.<sup>23</sup>

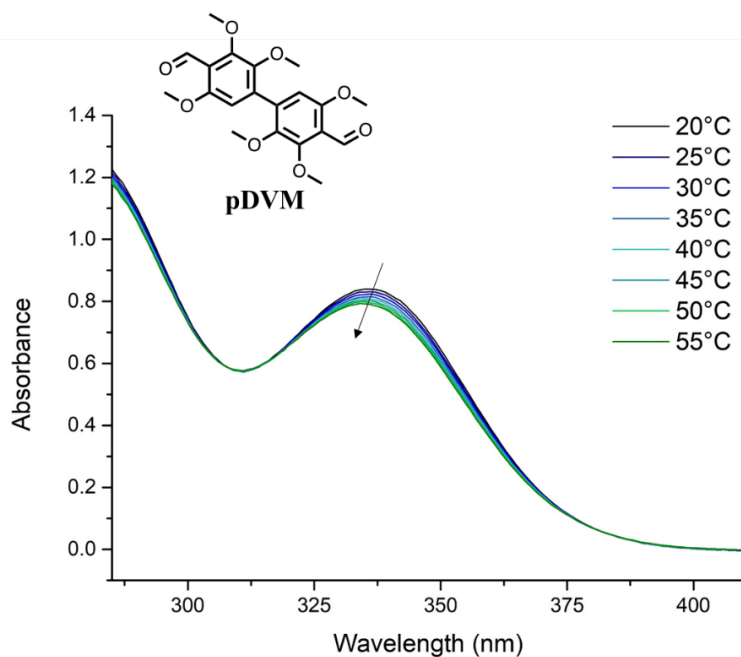
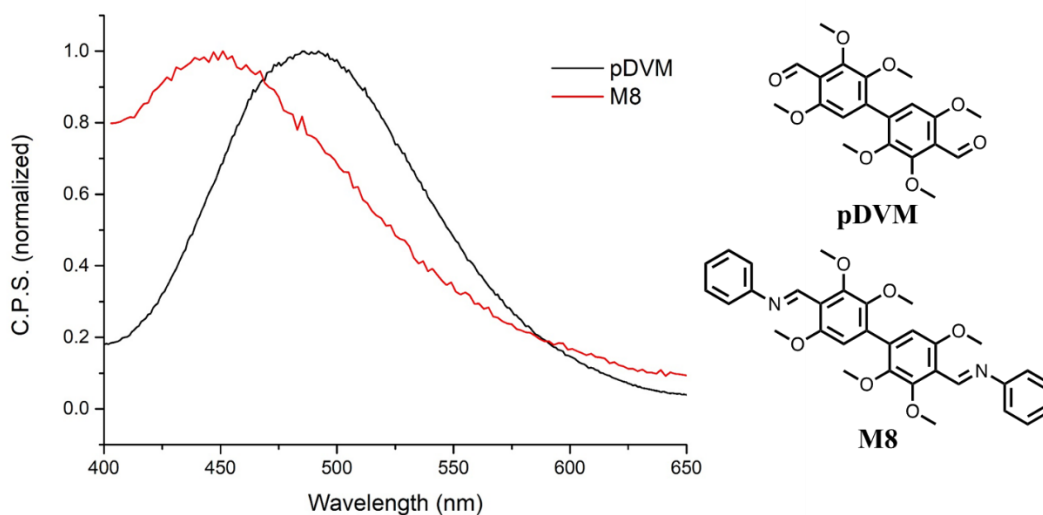


Figure 28: Absorbance of **pDVM** in toluene at increasing temperatures (from 20°C to 55°C,  $10^{-2}$  g/L)

In order to see the influence of temperature on **pDVM**, its absorbance was measured at different temperatures, from 20°C to 55°C in toluene (see **Figure 28**). When the temperature increases, the absorbance gets less intense and the maximum is slightly blue-shifted. This means that there is no improvement of planarity with increasing temperatures. This lowered intensity was observed for the  $\pi$ - $\pi^*$  transitions band at 334 nm, but also for the  $n$ - $\sigma^*$  transitions band. However, this last observation should be treated with caution, as the entire band is not detectable due to the solvent cut-off wavelength (285 nm for toluene).

Emission spectra were also measured for **pDVM** and **M8**, as represented in **Figure 29**.



**Figure 29:** Emission spectra and structure of **pDVM** and **M8**

**DVM**-based azomethines were so weakly fluorescent that relatively concentrated solutions had to be used to improve the emission signal. This is not the case for **M8**, as fluorescence could be observed even with relatively diluted solution (absorbance at 0.1). However, the fluorescence was still too weak to measure properly a quantum yield. **pDVM** is more red-shifted than **M8**, even if **M8** has a longer conjugation pathway most likely because the spectrum of **pDVM** corresponds to a potential charge transfer behavior while CT behavior was not observed for **M8**.

## 5.5. General conclusion on para-divanillin-based model compounds

Model compounds mimicking **pDVEH**- and **pDVEH**-based polymers backbone were designed for structure-properties studies. **Figure 30** sums up the model compounds synthesized.

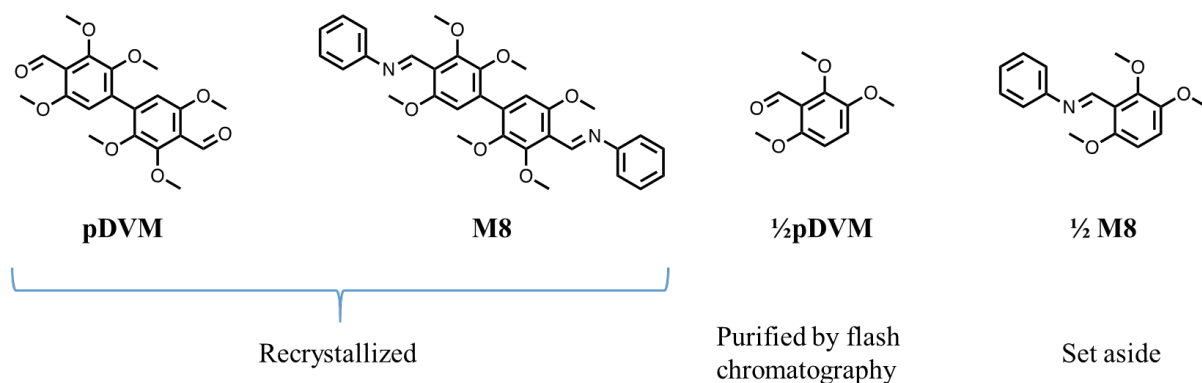


**Figure 30:** Structures of para-divanillin-based model compounds synthesized

These model compounds were purified by recrystallization when possible. However, some of them are oily at RT (**1/2pDVM** and **1/2M8**), which prevents effective recrystallization. The most remarkable result to emerge from X-RD characterization is the strong torsion between aromatic rings of **pDVM**, which are nearly perpendicular ( $86.4^\circ$ ). This near right angle has an effect on absorbance spectra, as **1/2pDVM** is more red-shifted than **pDVM**. This bathochromic shift is due to poor electron orbital overlap. **M8** has a broader absorbance spectrum than **pDVM** as it has a longer conjugation pathway than the latter, however they have the same absorbance maximum.

Some azomethine model compounds had to be set aside because they were oily at RT (**1/2M8**, **M9**). They cannot be recrystallized, and flash chromatography over silica degrades them. Yet it would be interesting to obtain them to complete the study. Potential purification methods are thermal evaporation or flash chromatography using alumina columns instead of silica for example, to prevent degradation.



## 6. General conclusion

To obtain new biphenyl compounds, ortho- and iso-vanillin were reacted with Laccase from *Trametes Versicolor*. However, no dimers were obtained but rather mixture of oligomers, as this reaction is not regioselective. Another strategy to obtain vanillin-based biphenyl compound was adopted, by performing a formylation by metalation on the two available para positions of divanillin. The molecule obtained is called **pDVEH** when alkylated with 2-ethylhexyl and **pDVM** when it is alkylated with a methyl, as represented in **Figure 31** – to the best of our knowledge, both molecules were never reported before. As the aldehyde functions are in para position with respect to the aldehyde functions, they are expected to give a longer conjugation pathway than divanillin.

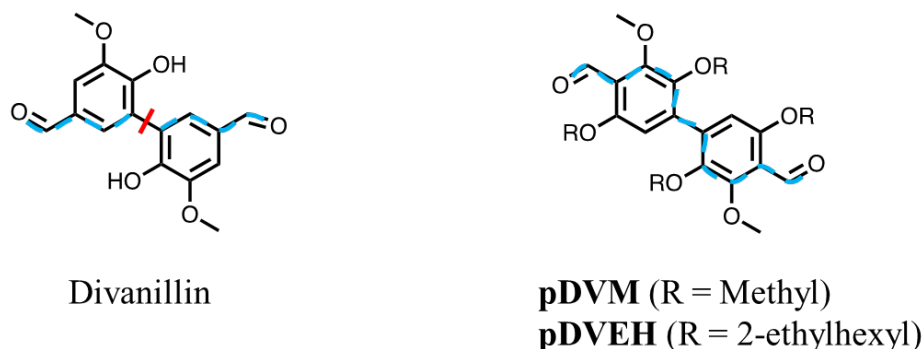


**Figure 31:** Structures of divanillin and “para-divanillin” and schematic conjugation pathway represented

NMR and mass spectroscopy confirmed these molecules’ structures. **pDVEH** was then used as a monomer in the course of polymerization with either fluorene diamine or para-phenylene diamine (see **Figure 32**). The obtained polyazomethines have solubility issues and their soluble fractions have smaller molar masses in comparison to their homologues with divanillin. The **pDVEH**-based polyazomethines are also less stable thermally than their counterparts with divanillin, with lower degradation temperature.

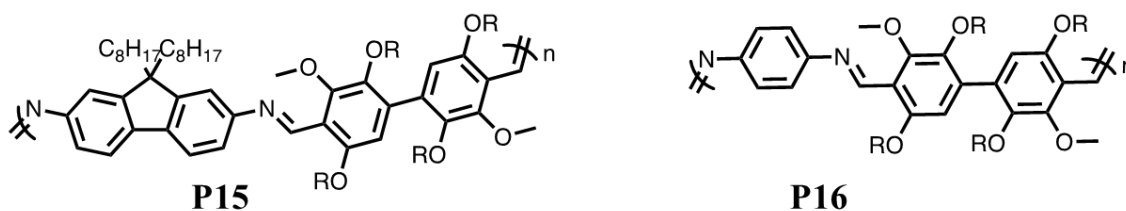


**Figure 32:** Structures of **pDVEH**-based polyazomethines

However, the **pDVEH**-based polyazomethines exhibit a bathochromic shift (up to 18 nm) compared to the **DVEH**-based ones, with absorbance maximum up to 399 nm for **P15**. Contrary to expectations, this red shift is not due to a longer conjugation pathway but rather to the influence of the additional alkoxy group on **pDVEH** compared to **DVEH**. In fact, investigations on model compounds revealed that **pDVEH** also has a short conjugation pathway, like **DVEH**. This result was obtained by studying the absorbance of model compounds mimicking **pDVM**.

The short conjugation pathway of **pDVM** and **pDVEH** is most likely due to steric hindrance. Indeed, X-RD analysis showed that the angle between the two aromatic rings of **pDVM** is 86.4°, as illustrated in **Figure 33**.

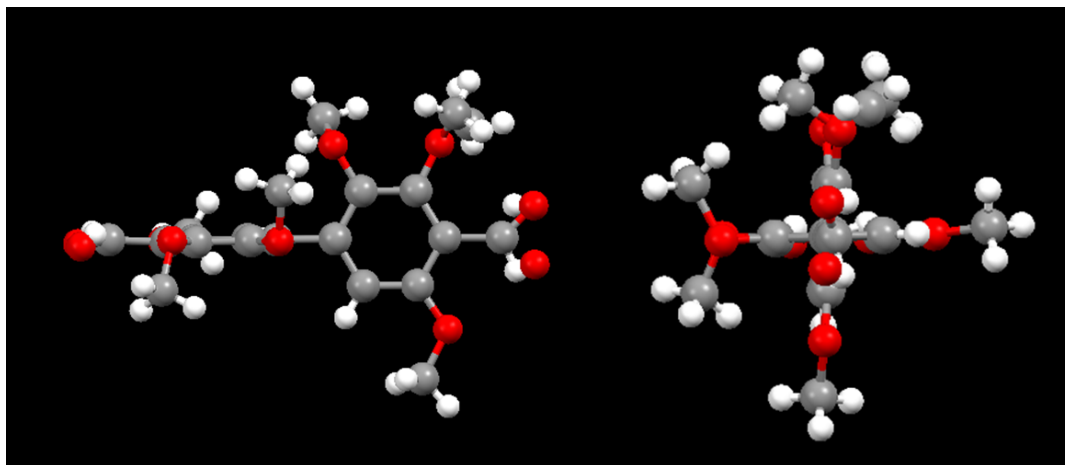
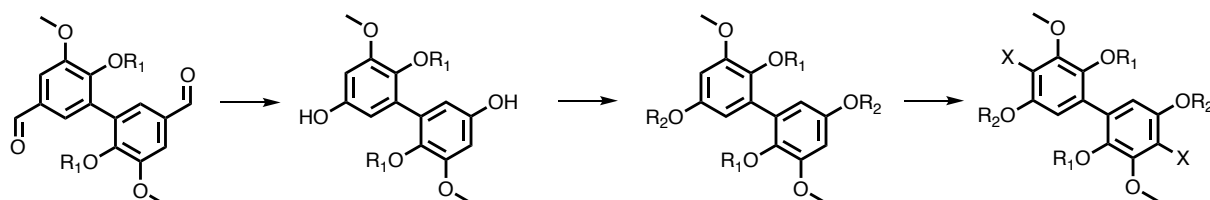


**Figure 33:** Structure of **pDVM** solved by X-RD analysis

This near perpendicular angle leads to poor orbitals overlap and therefore short conjugation pathway. Further works need to be carried out to synthesize and isolate more model compounds to mimic the longest conjugation pathway and better understand this type of polyazomethines backbone.

Following the strategy to obtain **pDVEH** and **pDVM**, a new platform of molecule is accessible, with various functions instead of the aldehyde group: bromide, amine, etc. as exemplified in **Scheme 13**. These molecules could be used to break the conjugation pathway at specific positions.



**Scheme 13:** General reaction to obtain new platform of para-divanillin based building blocks

## 7. References

1. Tiemann, F. Ueber die der Coniferyl- und Vanillinreihe angehörigen Verbindungen. *Berichte der Dtsch. Chem. Gesellschaft* **9**, 409–423 (1876).
2. Yi, B. *et al.* Antioxidant phenolic compounds of cassava (*Manihot esculenta*) from Hainan. *Molecules* **16**, 10157–10167 (2011).
3. Mallegol, T., Gmouh, S., Meziane, M. A. A., Blanchard-Desce, M. & Mongin, O. Practical and efficient synthesis of tris(4-formylphenyl)amine, a key building block in materials chemistry. *Synthesis (Stuttg)*. 1771–1774 (2005). doi:10.1055/s-2005-865336
4. Vilsmeier, A. & Haack, A. Über die Einwirkung von Halogenphosphor auf Alkyl-formanilide. Eine neue Methode zur Darstellung sekundärer und tertiärer p -Alkylamino-benzaldehyde . *Berichte der Dtsch. Chem. Gesellschaft (A B Ser.* **60**, 119–122 (1927).
5. Rieche, A., Gross, H. & Höft, E. Aromatic Aldehydes. Mesitaldehyde. *Org. Synth.* 49–49 (2003). doi:10.1002/0471264180.os900.15
6. Llevot, A. Resinic acid and lignin derivative dimers: new precursors for the synthesis of biobased polymers. (Université de Bordeaux, 2014).
7. Wittig, G., Pieper, G. & Fuhrman, G. Über die Bildung von Diphenyl aus Fluorbenzol und Phenyl-lithium (IV. Mitteil. über Austauschreaktionen mit Phenyl-lithium. *Berichte der Dtsch. Chem. Gesellschaft (A B Ser.* **73**, 1193–1197 (1940).
8. Gilman, H. & Bebb, R. L. Relative Reactivities of Organometallic Compounds. XX. Metalation. *J. Am. Chem. Soc.* **61**, 109–112 (1939).
9. Snieckus, V. Directed Ortho Metalation. Tertiary Amide and O-Carbamate Directors in Synthetic Strategies for Polysubstituted Aromatics. *Chem. Rev.* **90**, 879–933 (1990).
10. Beak, P. & Snieckus, V. Directed Lithiation of Aromatic Tertiary Amides: An Evolving Synthetic Methodology for Polysubstituted Aromatics. *Acc. Chem. Res.* **15**, 306–312 (1982).
11. Parker, K. A. & Koziski, K. A. Directed Hydroxylation of Aromatics. *J. Org. Chem.* **52**, 674–676 (1987).
12. Eaton, P. E. & Martin, R. M. Transmetalation and Reverse Transmetalation on Ortho-Activated Aromatic Compounds: A Direct Route to o,o'-Disubstituted Benzenes. *J. Org. Chem.* **53**, 2728–2732 (1988).
13. Reed, J. N. & Snieckus, V. Ortho-amination of lithiated tertiary benzamides. Short route to polysubstituted anthranilamides. *Tetrahedron Lett.* **24**, 3795–3798 (1983).
14. Haight, A. R. *et al.* A scaleable synthesis of fiduxosin. *Org. Process Res. Dev.* **8**, 897–902 (2004).
15. Collins, R. C., Paley, M. N., Tozer, G. M. & Jones, S. Synthesis of [3-13C]-2,3-dihydroxy-4-methoxybenzaldehyde. *Tetrahedron Lett.* **57**, 563–565 (2016).
16. Garbay, G. Original metal-free synthesis routes of semi-conducting oligomers and (co)polymers for organic electronics. (Université de Bordeaux, 2016).
17. Fache, M. *et al.* Vanillin, a promising biobased building-block for monomer synthesis. *Green Chem.* **16**, 1987–1998 (2014).
18. Mallet, C., Bolduc, A., Bishop, S., Gautier, Y. & Skene, W. G. Unusually high fluorescence quantum yield of a homopolyfluorenylazomethine – towards a universal fluorophore. *Phys.*

- Chem. Chem. Phys.* **16**, 24382–24390 (2014).
19. Bolduc, A., Mallet, C. & Skene, W. G. Survey of recent advances of in the field of  $\pi$ -conjugated heterocyclic azomethines as materials with tuneable properties. *Sci. China Chem.* **56**, 3–23 (2013).
  20. Milad, R. *et al.* Effective conjugation in conjugated polymers with strongly twisted backbones: A case study on fluorinated MEHPPV. *J. Mater. Chem. C* **4**, 6900–6906 (2016).
  21. Abrams, M. L., Foarta, F. & Landis, C. R. Asymmetric hydroformylation of Z -Enamides and enol esters with rhodium-bisdiazaphos catalysts. *J. Am. Chem. Soc.* **136**, 14583–14588 (2014).
  22. E. A. Dikumar, V. I. P. N. G. K. and A. P. Y. Synthesis of N,N'-bis-[3-alkoxy-4-(hydroxy, alkoxy, acyloxy)- phenylmethylene- and -Phenylmethyl]-1,3-phenylenediamines. *J. Pept. Sci.* **60**, 58–60 (2001).
  23. Mustroph, H. Studies on UV/VIS absorption spectra of azo dyes. Part 26.\* Electronic Absorption Spectra of 4, 4'- Diaminoazobenzene. *Dye. Pigment.* **16**, 223–230 (1991).

## 8. Experimental part

|  |     |
|--|-----|
| <b>8.1. General</b> .....  | 169 |
| <b>8.2. Characterization</b> .....   | 169 |
| <b>8.3. Synthesis and characterization of monomers</b> .....                     | 170 |
| 8.3.1. Protocol for reduction of <b>DV</b> .....                                 | 170 |
| 8.3.2. Characterization of reduced divanillin.....                               | 170 |
| 8.3.3. Characterization of alkylated reduced divanillin .....                    | 171 |
| 8.3.4. Protocol for formylation reaction by metalation <sup>15</sup> .....       | 172 |
| 8.3.5. Protocol for Dakin oxidation and alkylation with 2-ethylhexyl group ..... | 172 |
| 8.3.6. Characterization of <b>I2</b> .....                                       | 172 |
| 8.3.7. Characterization of <b>pDVEH</b> .....                                    | 173 |
| <b>8.4. Synthesis and characterization of polymers</b> .....                     | 174 |
| 8.4.1. General procedure for polymerization .....                                | 174 |
| 8.4.2. Characterization of <b>P15</b> .....                                      | 175 |
| 8.4.3. Characterization of <b>P16</b> .....                                      | 176 |
| <b>8.5. Synthesis and characterization of model compounds</b> .....              | 177 |
| 8.5.1. Synthesis of <b>I3</b> .....  | 177 |
| 8.5.2. Characterization of <b>I3</b> .....                                       | 177 |
| 8.5.3. Synthesis and characterization of <b>pDVM</b> .....                       | 178 |
| <b>8.6. General protocol for synthesis of model compounds</b> .....              | 179 |
| 8.6.1. Characterization of <b>M8</b> .....                                       | 180 |
| 8.6.2. Characterization of $\frac{1}{2}$ <b>pDVM</b> .....                       | 181 |

### 8.1. General

Iso-vanillin and ortho-vanillin were graciously provided by Solvay. Vanillin (>97%), 2-ethylhexyl bromide (95%), potassium carbonate, para-phenylene diamine, n-Buthyl lithium (2.5M in hexane), dimethyl sulfate, sodium borohydrate and sodium bisulfite were obtained from Sigma-Aldrich. Paratoluene sulfonic acid (PTSA, 99%), 2, 7-diamino-9, 9-di-n-octylfluorene and 1, 2, 4 trimethoxybenzene were purchased from TCI. Potassium hydroxide, iodomethane, fuming hydrochloric acid and sodium hydroxide were obtained from Fischer. Aniline and sodium percarbonate were obtained from Acros Organics. TMEDA was obtained from Alfa Aesar. All products and solvents (reagent grade) were used as received except otherwise mentioned. The solvents were of reagent grade quality and were purified whenever necessary according to the methods reported in the literature. For the emission and absorbance measurements, methylene chloride with spectroscopy grade from Sigma was used. Flash chromatography was performed on a Grace Reveleris apparatus, employing silica cartridges from Grace. Cyclohexane: ethyl acetate gradients and methylene chloride were used as eluents. The detection was performed through ELSD and UV detectors at 254 nm and 280 nm. The reactions under microwave irradiation were performed on a Discover-SP from CEM, with the temperature measured by infrared; the power of the apparatus is constantly adjusted to reach and then stay at the set temperature.

### 8.2. Characterization

$^1\text{H}$ ,  $^{13}\text{C}$  and  $^1\text{H}$ - $^{13}\text{C}$  HSQC NMR measurements were performed with a Bruker Avance 400 spectrometer (400.20 MHz and 100.7 MHz for  $^1\text{H}$  and  $^{13}\text{C}$ , respectively) at room temperature using deuterated solvent.

IR spectra were recorded with Bruker Tensor 27 spectrometer using a 0.6 mm-diameter beam. Samples were analyzed with the attenuated total reflection (ATR) method.

Mass spectra were performed by the CESAMO (Bordeaux, France) on a Qexactive mass spectrometer (Thermo). The instrument is equipped with an ESI source and spectra were recorded in the positive mode. The spray voltage was maintained at 3200 V and capillary temperature set at 320°C. Samples were introduced by injection through a 20  $\mu\text{L}$  sample loop into a 300  $\mu\text{L}/\text{min}$  flow of methanol from the LC pump.

Optical absorption spectra were obtained with a UV-visible spectrophotometer (UV-3600, Shimadzu). Photoluminescence spectra were obtained from a spectrofluorometer (Fluoromax-4, Horiba Scientific). In both cases, solvents of spectroscopic grade were used (from Sigma).

Molar masses of polymers were determined by size exclusion chromatography (SEC) using a three-column set of Resipore Agilent: one guard column Resipore -Agilent PL1113-1300, then two column Resipore Agilent PL1113-6300, connected in series, and calibrated with narrow polystyrene standards from polymer Laboratories using both refractometric (GPS 2155) and UV detectors (Viscotek). THF was used as eluent (0.8 mL/min) and trichlorobenzene as a flow marker (0.15%) at 30°C.

TGA were performed on a TA-Q50, from 25°C to 750°C with a heating of 10°C/min under nitrogen flow.

Diffraction data from a single crystal of the different model compounds were measured by the IECB (Bordeaux, France) on a 3 kW microfocus Rigaku FRX rotating anode. The source is equipped with high flux Osmic Varimax HF mirrors and a hybrid Dectris Pilatus 200 K detector. The source is operating at the copper  $k\alpha$  wavelength with a partial chi goniometer that decreases blind areas and enables automatic axial adjustment. Data were processed with the CrysAlisPro suite version 1.171.38.43.<sup>1</sup> Empirical absorption correction using spherical harmonics, implemented in SCALE3 ABSPACK scaling algorithm was used.

The structure was solved with Shelxt<sup>2</sup> and refined by full-matrix least-squares method on F2 with Shelxl-2014<sup>2</sup> within Olex2.<sup>3</sup> For all atoms, anisotropic atomic parameters were used. Hydrogen atoms were placed at idealized positions and refined as riding on their carriers with Uiso(H) = 1.2 Ueq (CH, CH<sub>2</sub>, NH) and Uiso(H) = 1.5 Ueq (CH<sub>3</sub>). DFIX and AFIX instructions were used to improve the geometry of molecules and RIGU to model atomic displacement parameters. Disordered solvent molecules were removed using the SQUEEZE procedure from the PLATON suite.<sup>4</sup> For search and analysis of solvent accessible voids in the structures default parameters were utilized: grid 0.20 Å, probe radius 1.2 Å and NStep 6. Calculated total potential solvent accessible void volumes and electron counts per unit cell are given in the CIF files that were checked using IUCR's checkcif algorithm. Due to the characteristics of some of the crystals, i.e. large volume fractions of disordered solvent molecules, weak diffraction intensity and moderate resolution, few A-level and B-level alerts remain in the check cif file. These alerts are inherent to the data and refinement procedures and do not reflect errors on the model refined.

<sup>1</sup> CrysAlisPRO : CrysAlisPRO, Oxford Diffraction /Agilent Technologies UK Ltd, Yarnton, England.

<sup>2</sup> Sheldrick, G. M. (2015). Acta Cryst. A71, 3-8.

<sup>3</sup> OLEX2: O. V. Dolomanov, L. J. Bourhis, R. J. Gildea, J. A. K. Howard and H. Puschmann. J. Appl. Cryst. (2009). 42, 339-341.

<sup>4</sup> Spek, A. L. (2009). Acta Cryst. D65, 148-155.

### 8.3. Synthesis and characterization of monomers

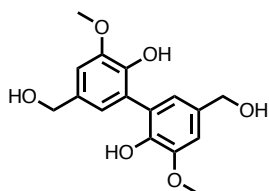
#### 8.3.1. Protocol for reduction of DV

2 g of DV (6.6 mmol) were dispersed in 40 mL of a solution of 0.5 M of NaOH, in a two-neck flask equipped with a condenser. The flask was set in an ice bath, and 1.2 g of NaBH<sub>4</sub> (14 mmol) were added slowly. The reaction mixture was then left at RT for 30 minutes. Then the flask was once more put into an ice bath, and the pH of the reaction mixture was lowered to 7 using molar HCl. With the drop of pH, the reduced divanillin precipitates readily and can be recovered by filtration. It was then rinsed with water and dried under vacuum for 24 hours.

Yield: 80%

Aspect: fine white powder

#### 8.3.2. Characterization of reduced divanillin



6,6'- dihydroxy-5,5'-dimethoxy- 3,3' dimethanol -[1,1'-biphenyl]

<sup>1</sup>H-NMR (400.20 MHz, (CD<sub>3</sub>)<sub>2</sub>SO) δ (ppm): 9.22 (s, 2H); 6.88 (d, J = 2Hz, 2H); 6.67 (d, J = 2Hz, 2H); 5.01 (t, J = 4Hz, 2H); 4.41 – 4.39 (d, J = 8Hz, 4H); 3.81 (s, 6H).

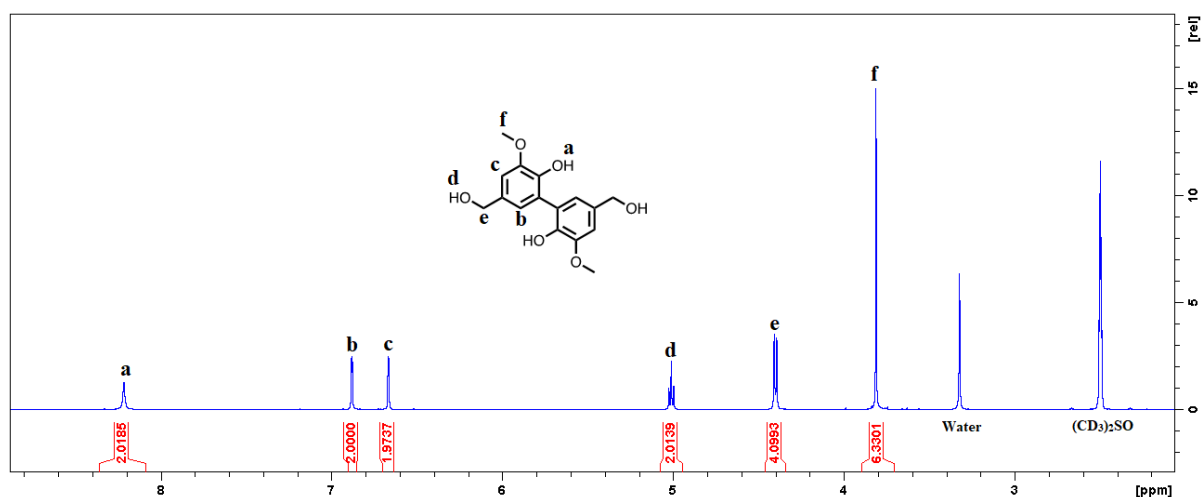


Figure 34: <sup>1</sup>H-NMR spectrum of reduced vanillin (400.20 MHz, in DMSO-d<sub>6</sub>)

### 8.3.3. Characterization of alkylated reduced divanillin

6,6'- diethylhexoxy -5,5'-dimethoxy- 3,3' dimethoxyethylhexoxane -[1,1'-biphenyl]

<sup>1</sup>H-NMR (400.20 MHz, CDCl<sub>3</sub>) δ (ppm): 6.91 (d, J = 2Hz, 2H); 6.82 (d, J = 2Hz, 2H); 4.43 (s, 2H); 3.86 (s, 3H); 3.63 (m, 2H); 3.33-3.31 (d, J = 8Hz, 2H); 1.6-0.6 (m, 60H).  
<sup>13</sup>C-NMR (100.70 MHz, CDCl<sub>3</sub>) δ (ppm): 153.1; 145.7; 133.5; 132.7; 123.1; 110.7; 75.0; 73.1; 73.0; 55.9; 40.4; 39.9; 30.8; 30.4; 29.3; 29.2; 24.0; 23.7; 23.2; 23.1; 14.3; 14.2; 11.2; 11.0.

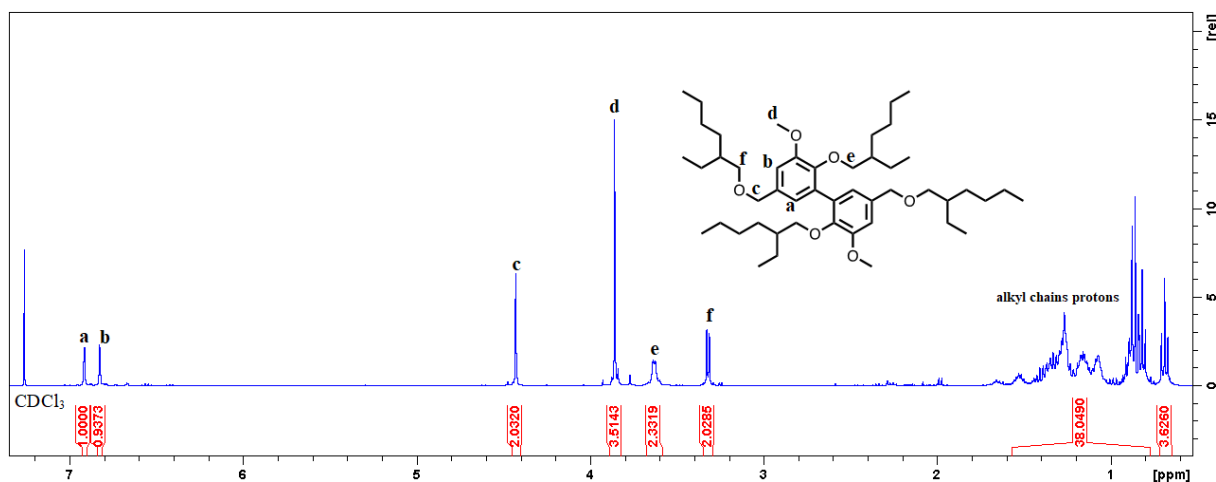
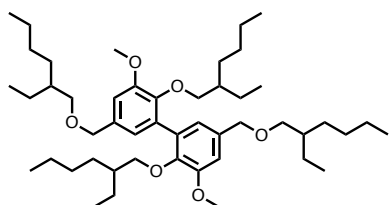


Figure 35: <sup>1</sup>H-NMR spectrum of alkylated reduced vanillin (400.20 MHz, in CDCl<sub>3</sub>)



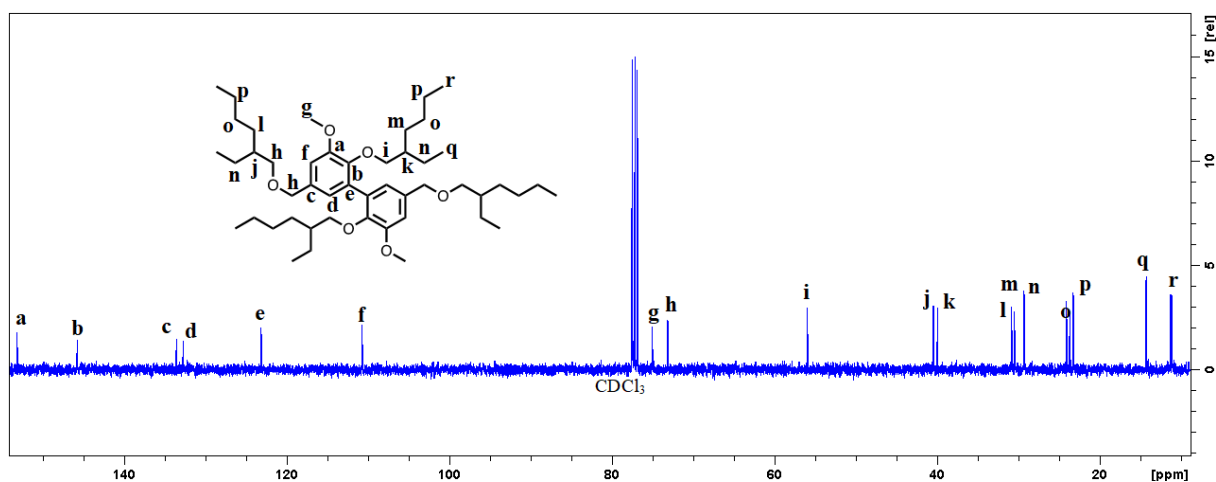


Figure 36:  $^{13}\text{C}$ -NMR spectrum of alkylated reduced vanillin (100.70 MHz, in  $\text{CDCl}_3$ )

### 8.3.4. Protocol for formylation reaction by metalation<sup>15</sup>

A two-neck flask was fitted with an adapter; both were flamed and put under inert atmosphere. The compound that will undergo the formylation reaction (2 mmol) was then inserted in the flask with benzene, and freeze-dried. It was left under vacuum for 16 h to remove water completely. Then THF (20 mL, freshly distilled with sodium) was added to the flask using a burette and the adapter. 4.4 mmol of TMEDA were also added. The flask was set in an ice bath, and 4.8 mmol of *n*BuLi as a 2.5 M solution in hexane were added. The flask was then left at RT for 4 hours. Afterwards, the ice bath was set again and 6 mmol of DMF (distilled with  $\text{CaH}_2$ ) were added slowly. The flask was then left at RT for two more hours. Afterwards a bubbler was added to the set-up and the reaction was quenched with 20 mL of molar HCl. The crude mixture was extracted with diethyl ether three times, and the organic phase rinsed with brine. The final product is obtained without further purification unless specified otherwise.

Yield: 78%

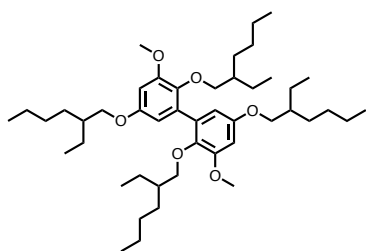
### 8.3.5. Protocol for Dakin oxidation and alkylation with 2-ethylhexyl group

In a two-neck flask, 4 g of divanillin (13.2 mmol) were dispersed in 100 mL of THF and 40 mL of mQ water. The dispersion was degassed for 30 min, then 4.3 g of sodium percarbonate (27 mmol) were added slowly. The reaction mixture was left at RT for 3 hours, then quenched with molar HCl. The crude was extracted three times with ethyl acetate, and the organic phase rinsed with brine and the solvents evaporated. The obtained compound is viscous and red. It was put in a two-neck flask to undergo alkylation with 2-ethylhexyl bromide, as was described in **Chapter 2**. It was finally purified by flash chromatography, with ethyl acetate/cyclohexane (5/95).

Yield: 56%

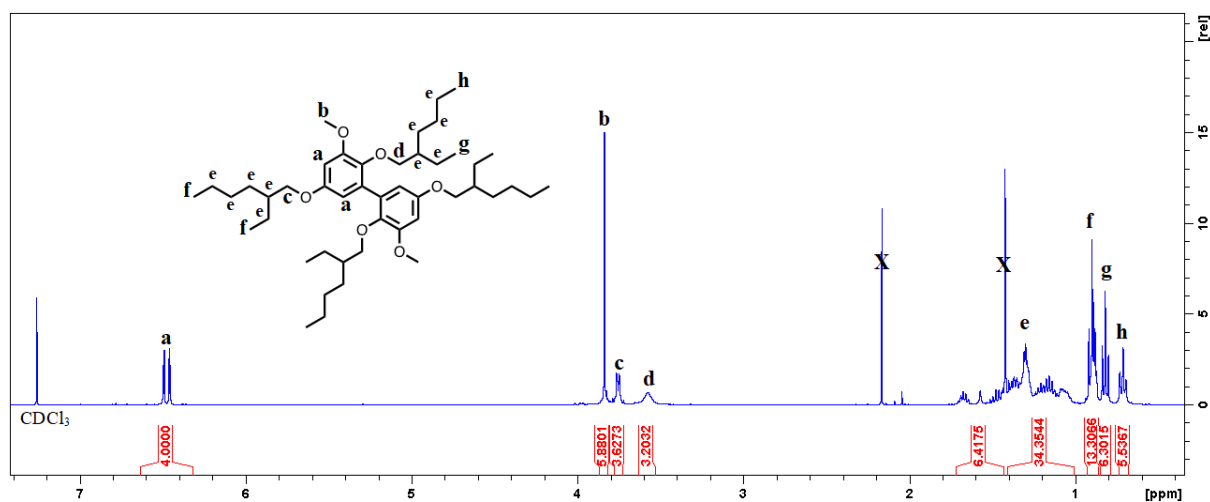
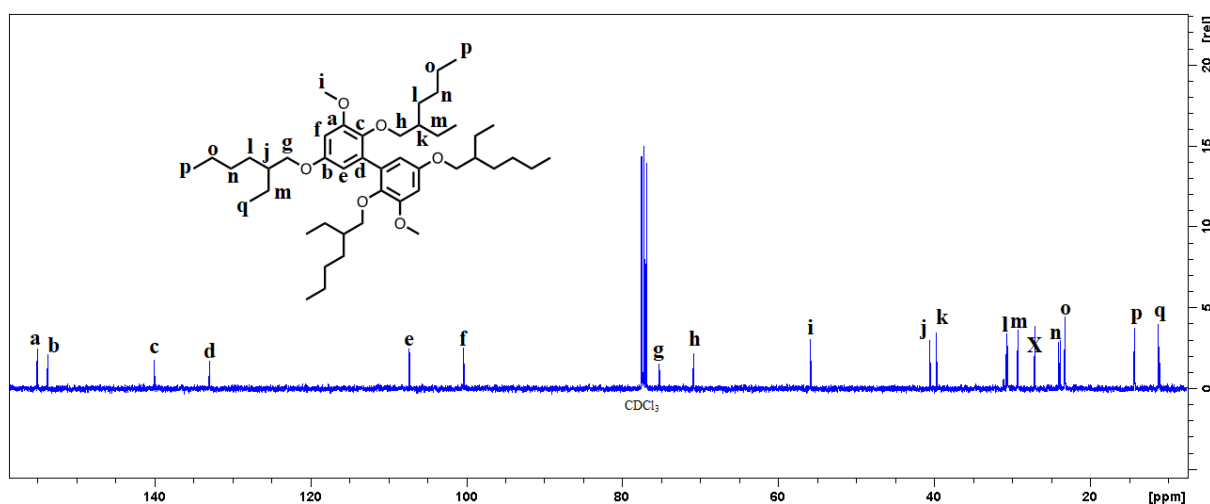
### 8.3.6. Characterization of **I2**

3,3'-6,6'- tetraethylhexoxy -5,5'-dimethoxy -[1,1'-biphenyl]

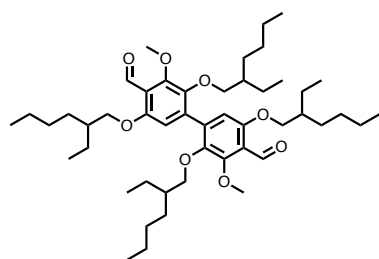


$^1\text{H}$ -NMR (400.20 MHz,  $\text{CDCl}_3$ )  $\delta$  (ppm): 6.49-6.46 (dd,  $J = 4\text{Hz}$ ,  $J = 12\text{Hz}$ , 4H); 3.84 (s, 6H); 3.77-3.75 (m, 4H); 3.58 (s, 4H); 1.7-1.03 (m, 36H); 0.93-0.87 (m, 12H); 0.82 (t,  $J = 8\text{Hz}$ ; 6H); 0.71 (t,  $J = 8\text{Hz}$ , 6H).  
 $^{13}\text{C}$ -NMR (100.70 MHz,  $\text{CDCl}_3$ )  $\delta$  (ppm): 155.0; 153.7; 140.0; 132.9; 107.3; 100.3; 75.2; 70.8; 55.8; 40.5; 39.6; 30.7; 30.5; 29.2; 24.0; 23.8; 23.2; 14.3; 14.2; 11.2; 11.1.

Aspect: yellow oil

Figure 37:  $^1\text{H}$ -NMR spectrum of **I2** (400.20 MHz, in  $\text{CDCl}_3$ )Figure 38:  $^{13}\text{C}$ -NMR spectrum of **I2** (100.70 MHz, in  $\text{CDCl}_3$ )

### 8.3.7. Characterization of pDVEH

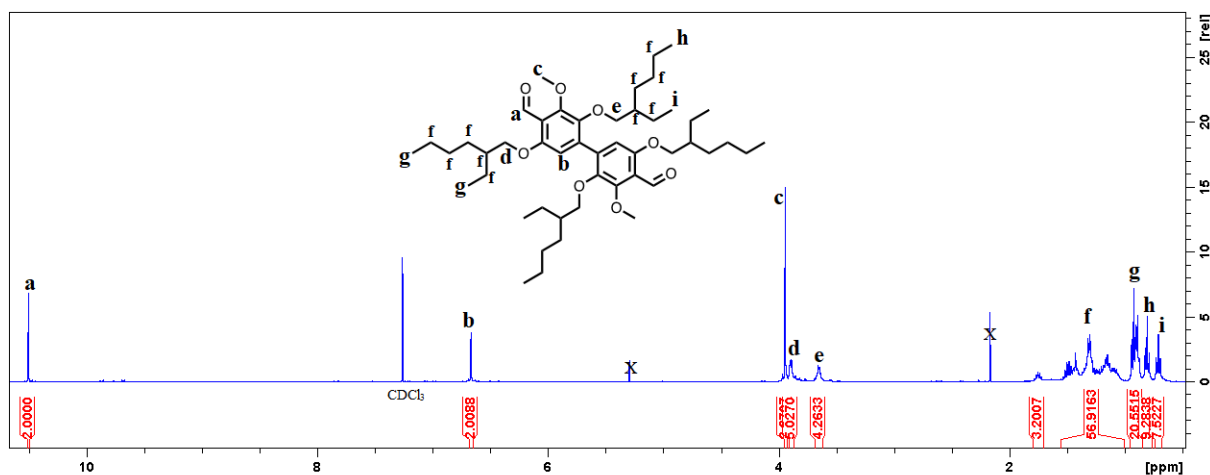
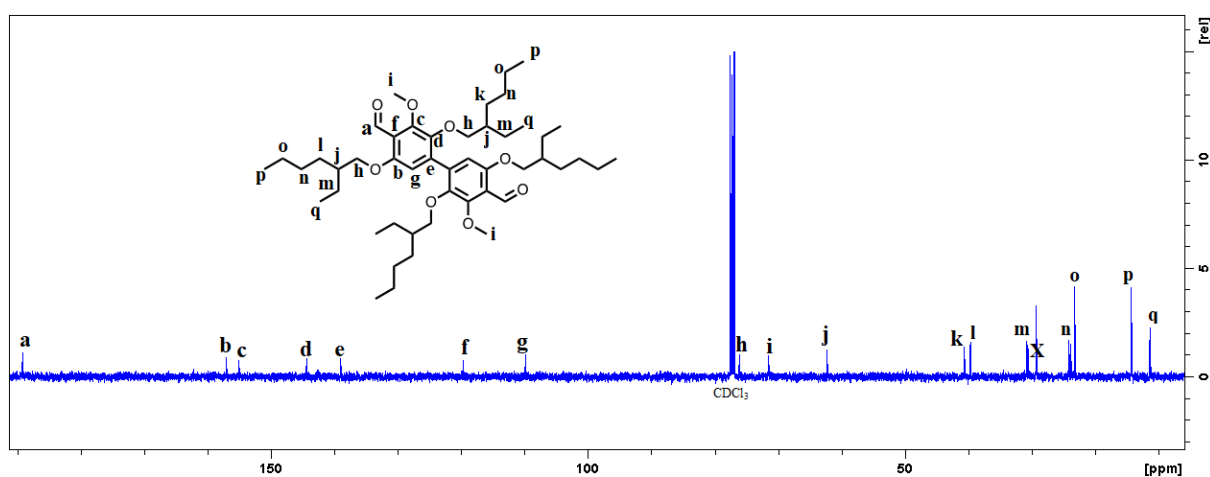
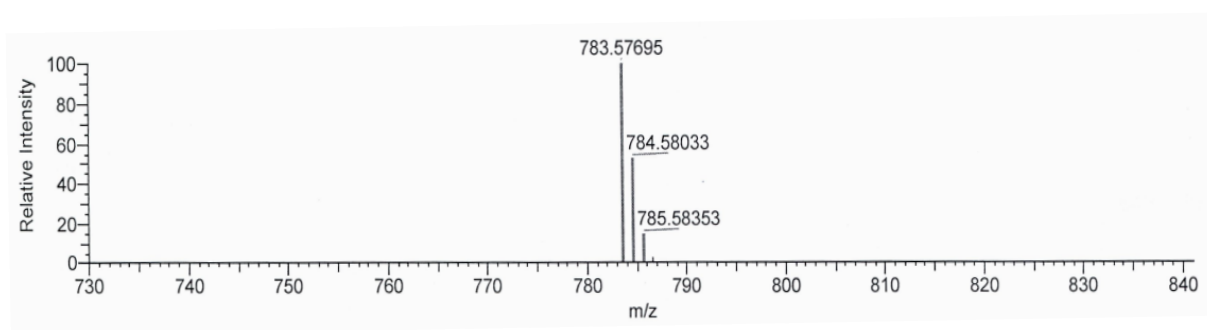


3, 3'-6,6'- tetraethylhexoxy -5,5'-dimethoxy -[1,1'-biphenyl] -4,4' dicarboxaldehyde

$^1\text{H}$ -NMR (400.20 MHz,  $\text{CDCl}_3$ )  $\delta$  (ppm): 10.50 (s, 2H); 6.67 (s, 2H); 3.94 (s, 6H); 3.91-3.88 (m, 4H); 3.67-3.64 (m, 4H); 1.79-1.01 (m, 36H); 0.95-0.85 (m, 12H); 0.80 (t,  $J = 8\text{Hz}$ , 6H); 0.71 (t,  $J = 8\text{Hz}$ , 6H).  $^{13}\text{C}$ -NMR (100.70 MHz,  $\text{CDCl}_3$ )  $\delta$  (ppm): 189.2; 156.9; 155.0; 144.3; 138.9; 119.6; 109.8; 76.0; 71.4; 62.2; 40.5; 39.6; 30.7; 30.5;

29.2; 24.1; 23.8; 23.1; 14.2; 11.3; 11.2.

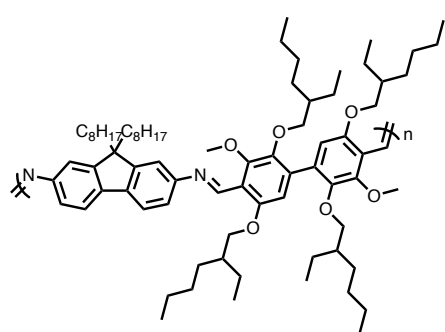
Aspect: yellow/orange oil

Figure 39:  $^1\text{H}$ -NMR spectrum of **pDVEH** (400.20 MHz, in  $\text{CDCl}_3$ )Figure 40:  $^{13}\text{C}$ -NMR spectrum of **pDVEH** (100.70 MHz, in  $\text{CDCl}_3$ )Figure 41: Mass spectrum of **pDVEH**, obtained by ESI, positive mode

## 8.4. Synthesis and characterization of polymers

### 8.4.1. General procedure for polymerization

In a vial fitted for microwave irradiation, stoichiometric quantities of **pDVEH** and diamine were dispersed in 5 mL of toluene, with a catalytic amount of PTSA. The mixture was heated up to  $130^\circ\text{C}$ , for 5 minutes. The tube was then rinsed with THF and methylene chloride and the solvents evaporated by rotary evaporator. The crude was then recovered by dissolving it in a minimum amount of methylene chloride, and then by adding 100 mL of methanol. The solvents were then evaporated using rotary evaporator, to give a yellow/orange powder that was rinsed with methanol.

8.4.2. Characterization of **P15**

Poly (3,3' - 6,6' - tetraethylhexoxy - 5,5' - dimethoxy - [1,1'-biphenyl] - 4,4' - methylidene - (9,9 dioctyl 1- n, n, fluorenylamine))

$^1\text{H-NMR}$  (400.20 MHz,  $\text{CDCl}_3$ )  $\delta$  (ppm): 10.53-10.51 (m, 1H); 8.97-8.93 (m, 2.8H); 7.71-7.46 (m, 5.8H); 6.76-6.62 (m, 7.8H); 4.05-3.66 (m, 38.7H); 2.07-0.72 (m, 292H - **distorted value because of solvent peak**).

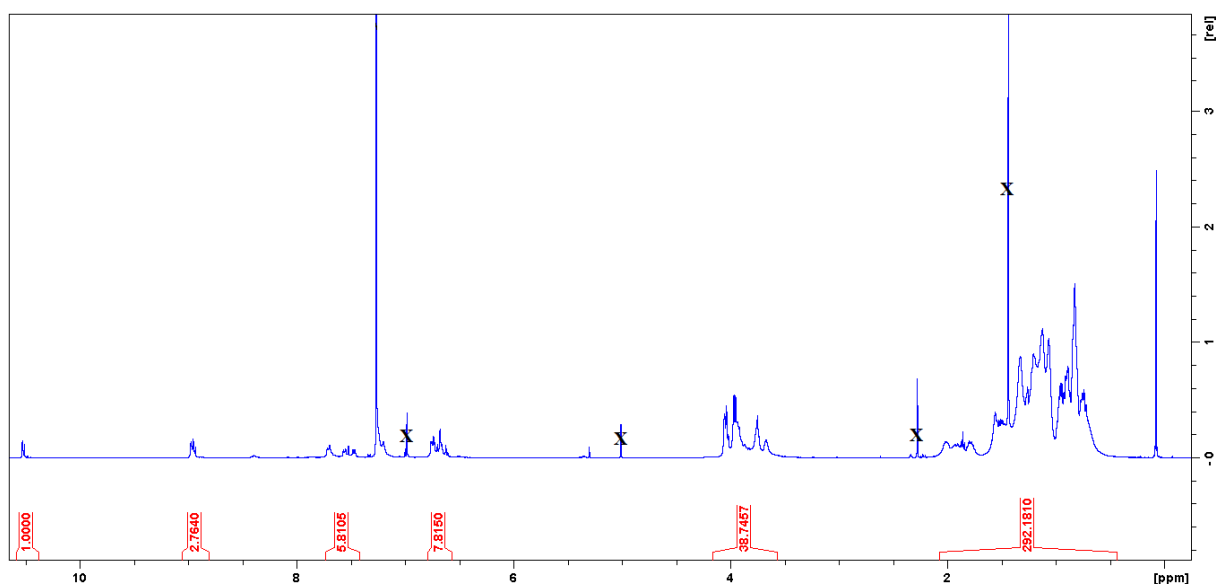


Figure 42:  $^1\text{H-NMR}$  spectrum of **P15** in  $\text{CDCl}_3$  (128 scans)

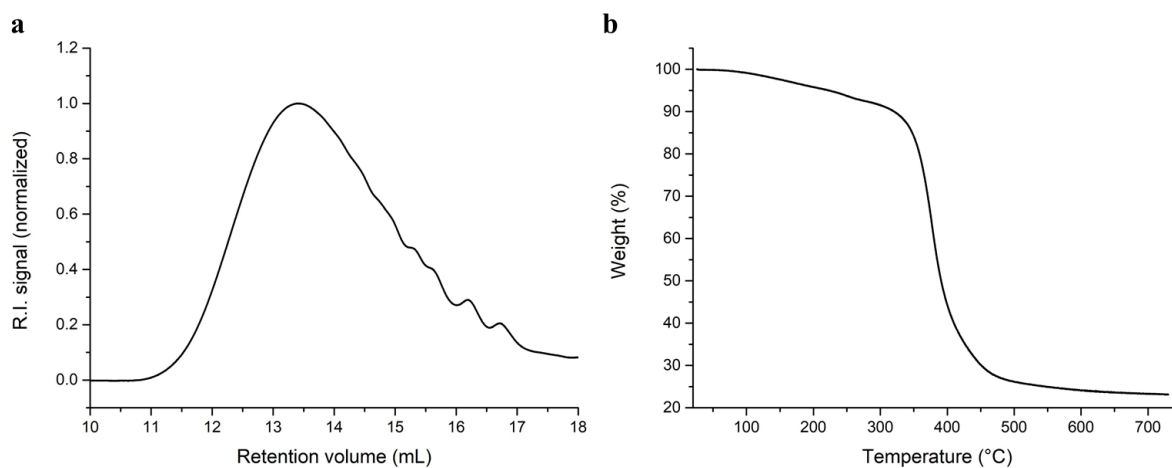
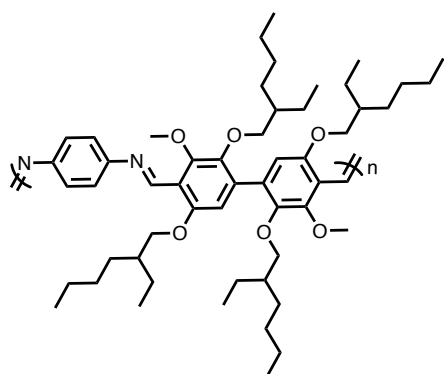
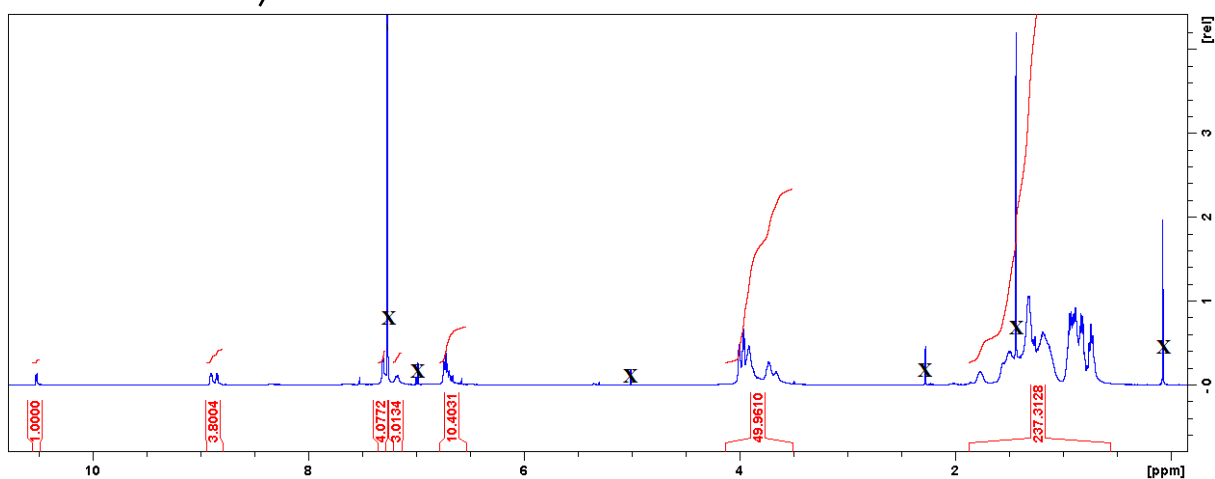


Figure 43a: SEC trace of **P15** in THF, R. I. detection. **b**: TGA curve of **P15** at  $10^\circ\text{C}/\text{min}$  under  $\text{N}_2$

8.4.3. Characterization of **P16**

Poly (3,3' - 6,6' - tetraethylhexoxy - 5,5' - dimethoxy - [1,1'biphenyl] - 4,4' - methylidene - (1,4 benzene amine))

$^1\text{H-NMR}$  (400.20 MHz,  $\text{CDCl}_3$ )  $\delta$  (ppm): 10.52-10.50 (m, 1H); 8.90-8.83 (m, 3.8H); 7.32-7.27 (m, 4H); 7.21-7.14 (m, 3H); 6.75-6.65 (10H); 4.00-3.62 (m, 50H); 1.82-0.71 (m, 237H – distorted value because of solvent peak).



**Figure 44:**  $^1\text{H-NMR}$  spectrum of **P16** in  $\text{CDCl}_3$  (128 scans)

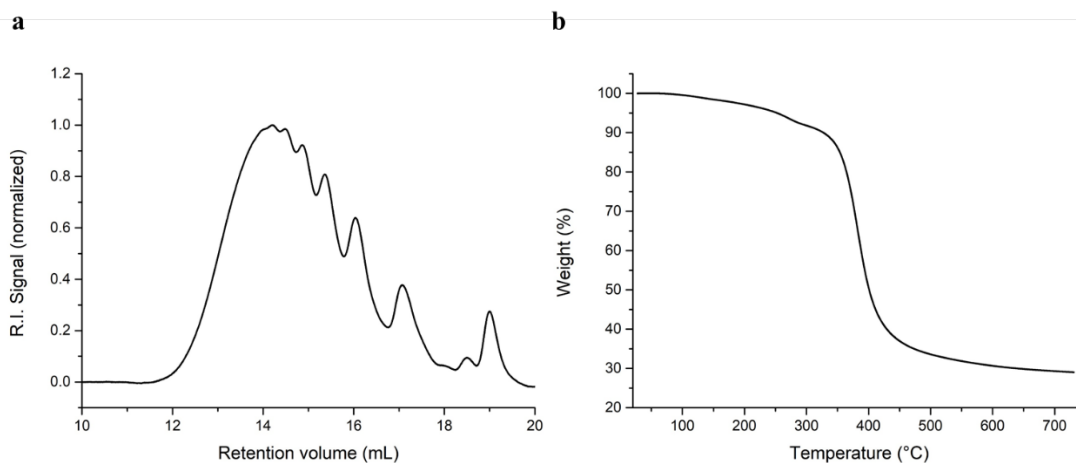


**Figure 45a:** SEC trace of **P16** in THF, R. I. detection. **b:** TGA curve of **P16** at  $10^\circ\text{C}/\text{min}$  under  $\text{N}_2$

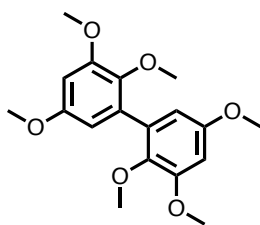
## 8.5. Synthesis and characterization of model compounds

8.5.1. Synthesis of **I3**

8g of **DV** (27 mmol) were dispersed in 100 mL of THF, and degassed for 30 minutes. 9.5 g of sodium percarbonate (30.3 mmol) were dissolved in 60 mL of mQ water and added to the **DV** + THF mixture. It was left overnight at 30°C, under argon. Afterwards molar HCl was added until pH 1. THF was evaporated, and the crude mixture filtrated to remove solid impurities which were rinsed with ethyl acetate. It was then extracted with ethyl acetate three times and rinsed with brine and the solvents were evaporated to give pinkish pellets

In a two-neck flask equipped with condenser, dried and under inert atmosphere, 7 g of the previously obtained product were dissolved in 60 mL of ethanol, and 24 mL of dimethyl sulfate (25.3 mmol) were added. The flask was set in an ice bath and 1.6 g of NaHSO<sub>3</sub> were added, followed by 16.6 g of NaOH dissolved in 32 mL of water. **This step is exothermic.** The flask was left in the ice bath for 45 minutes, and then heated up to 80°C overnight. It was then extracted three times with ethyl acetate, and the solvents evaporated using rotary evaporator. The crude was purified by flash chromatography, using methylene chloride as the only eluent, to give the final product as pale yellow crystals.

Yield: 60%

8.5.2. Characterization of **I3**

2, 2'-3,3'-5,5'- hexamethoxy -[1,1'-biphenyl]

<sup>1</sup>H-NMR (400.20 MHz, CDCl<sub>3</sub>) δ (ppm): 6.52-6.41 (dd, J = 4Hz, J = 40Hz, 4H); 3.88 (s, 6H); 3.77 (s, 6H); 3.61 (s, 6H). <sup>13</sup>C-NMR (100.70 MHz, CDCl<sub>3</sub>) δ (ppm): 155.5; 153.5; 140.9; 132.9; 106.0; 99.9; 60.9; 55.9; 55.7.

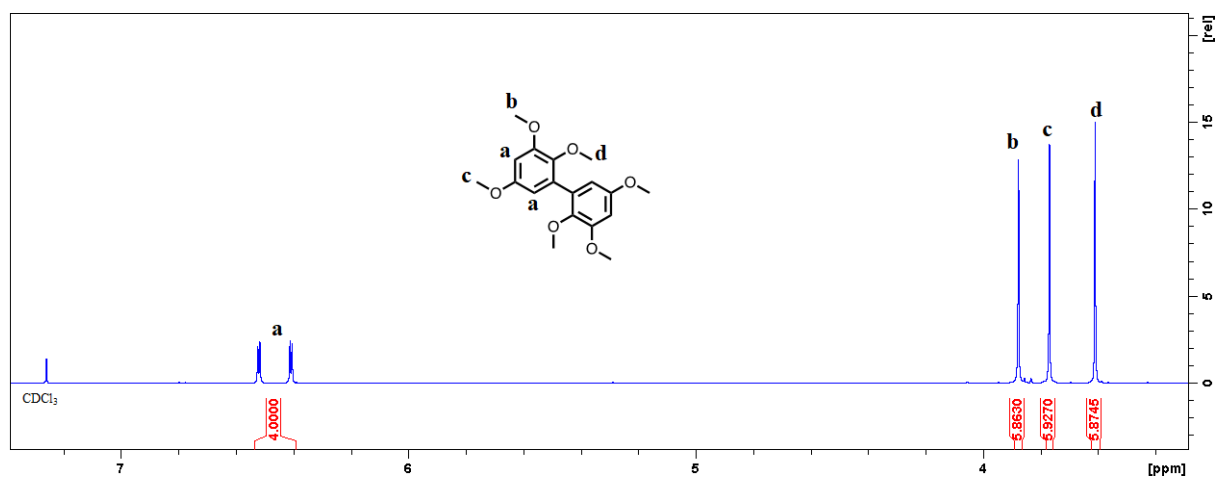


Figure 46: <sup>1</sup>H-NMR spectrum of **I3** (400.20 MHz, in CDCl<sub>3</sub>)

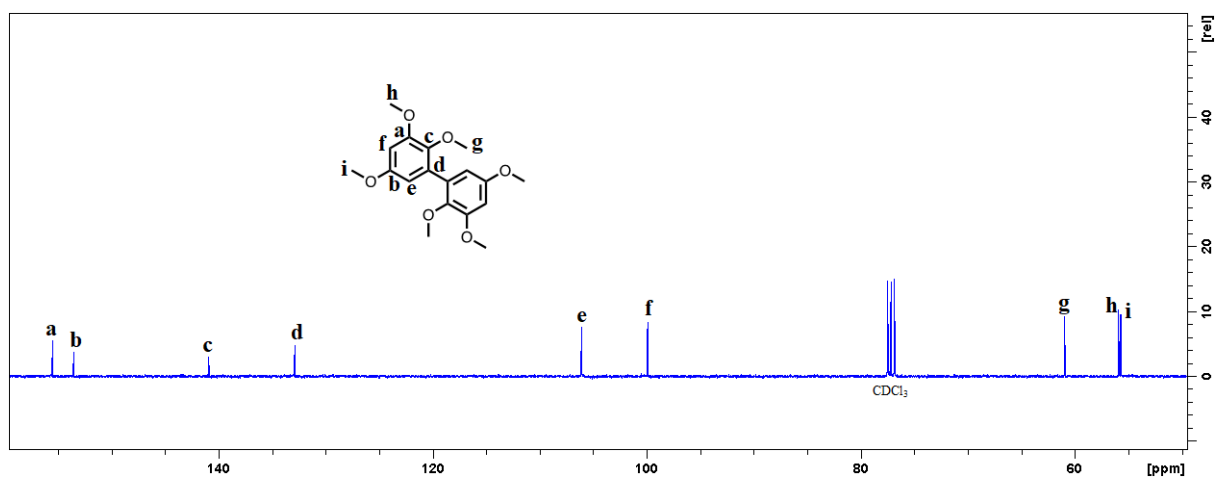
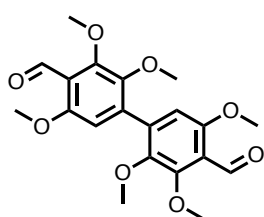


Figure 47:  $^{13}\text{C}$ -NMR spectrum of **13** (100.70 MHz, in  $\text{CDCl}_3$ )

### 8.5.3. Synthesis and characterization of pDVM



3,3'-6,6'-5,5'-hexamethoxy-[1,1'-biphenyl]-4,4'-dicarboxaldehyde

#### Synthesis

pDVM was obtained by formylating **13**, using the experimental protocol described previously. The crude mixture obtained after the formylation reaction spontaneously crystallized after a few days at  $+3^\circ\text{C}$ . These latter crystals were recrystallized using warm cyclohexane and ethyl acetate.

Yield: 40%

#### Characterization

$^1\text{H}$ -NMR (400.20 MHz,  $\text{CD}_2\text{Cl}_2$ )  $\delta$  (ppm): 10.44 (s, 2H); 6.66 (s, 2H); 3.95 (s, 6H); 3.87 (s, 6H); 3.65 (s, 6H).  $^{13}\text{C}$ -NMR (100.70 MHz,  $\text{CD}_2\text{Cl}_2$ )  $\delta$  (ppm): 189.0; 157.0; 155.8; 145.0; 138.8; 119.9; 108.9; 62.2; 61.3; 56.7.

#### X-Ray Diffraction data

Space group:  $\text{P2}_1/\text{n}$

Cell length ( $\text{\AA}$ ): **a** 13.3287; **b** 10.4485; **c** 14.9512.

Cell angles:  $\alpha$  90;  $\beta$  116.412;  $\gamma$  90.

Cell volume ( $\text{\AA}^3$ ): 1864.84

R factor: 7.74%

Symmetry:  $\frac{1}{2}-x, \frac{1}{2}+y, \frac{1}{2}-z; -x, -y, -z; \frac{1}{2}+x, \frac{1}{2}-y, \frac{1}{2}+z$ .

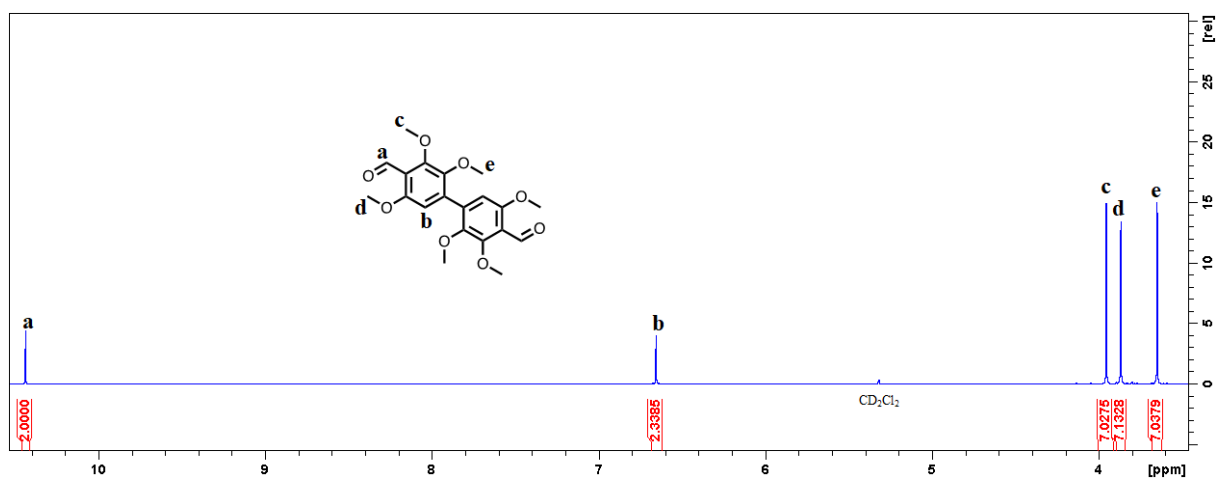
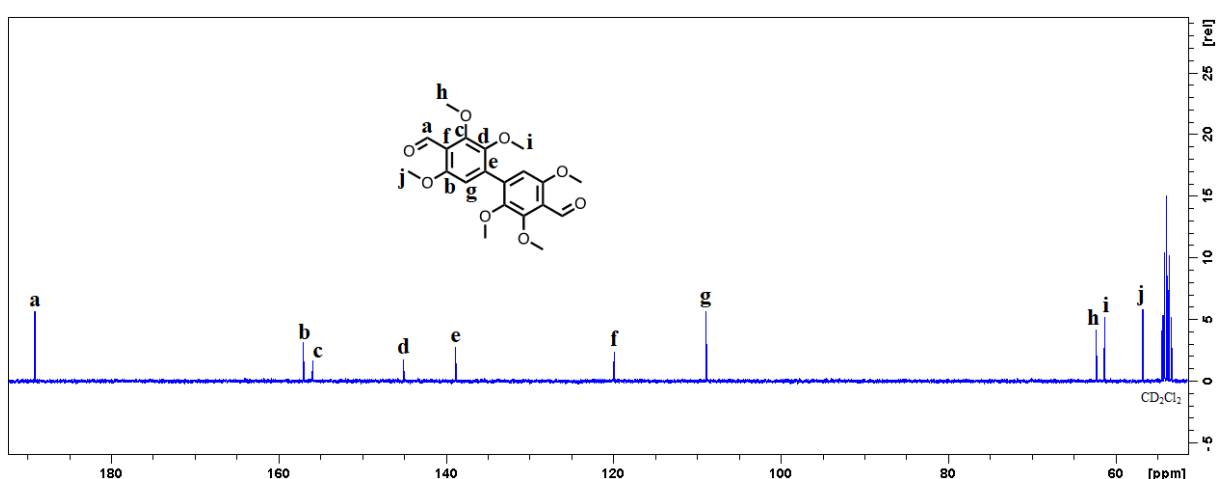
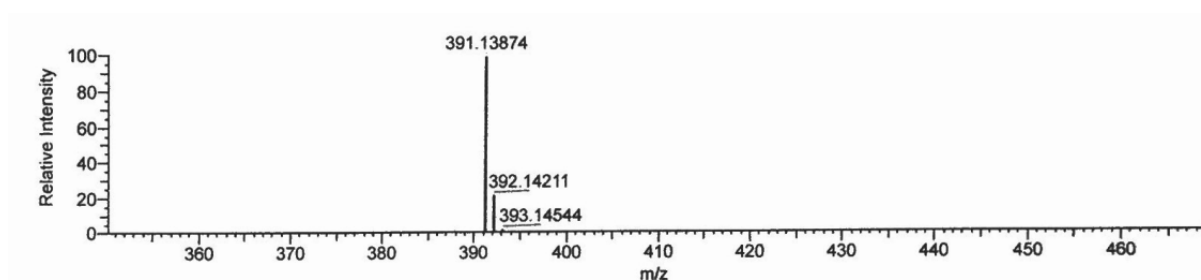
Figure 48:  $^1\text{H-NMR}$  spectrum of pDVM (400.20 MHz, in  $\text{CD}_2\text{Cl}_2$ )Figure 49:  $^{13}\text{C-NMR}$  spectrum of pDVM (100.70 MHz, in  $\text{CD}_2\text{Cl}_2$ )

Figure 50: High-resolution mass spectrum of pDVM obtained by ESI, positive mode (molecular peak)

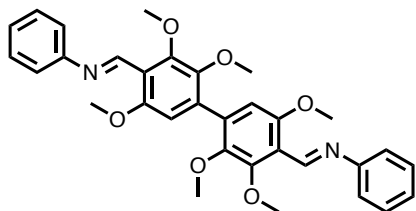
### 8.6. General protocol for synthesis of model compounds

In a flame-dried flask equipped with stirrer and condenser, 2 eq. of (di)aldehyde (or 1 eq.) was dissolved with the (di)amine (1 or 2 eq.) in methanol, under inert atmosphere. The resulting solution was heated at the reflux using conventional heating for 30 minutes, and then filtrated on 0.45  $\mu\text{m}$  PTFE filter and the solvent evaporated under vacuum. The solvents used for purification are given for each molecule.



8.6.1. Characterization of **M8**

2,2'-dimethoxy-3,3'-dimethoxy-5,5'-dimethoxy-[1,1'-biphenyl]-4,4'-di(phenylimino)methyl

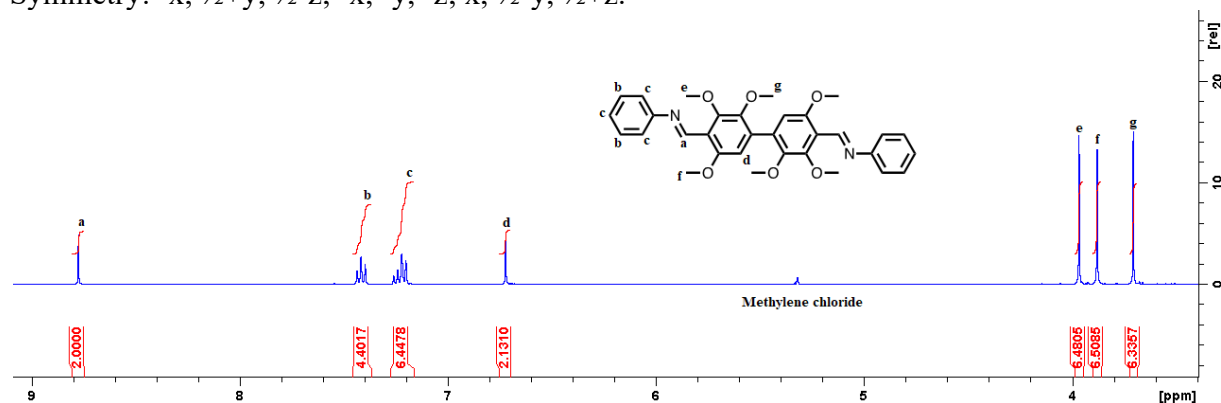
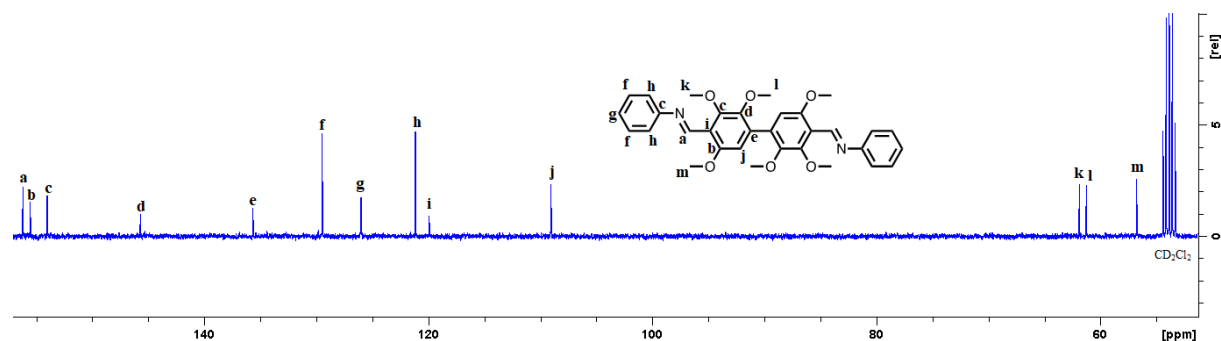


**Reactants:** **pDVM** (1 eq.) + aniline (2 eq.) using general protocol. The final product was obtained after recrystallization from warm n-heptane/methylene chloride. E/Z in the crude material: 85/15. Conversion: 92%

$^1\text{H-NMR}$  (400 MHz,  $\text{CD}_2\text{Cl}_2$ )  $\delta$  (ppm): 8.78 (s, 2H); 7.44-7.20 (m, 10H); 6.72 (s, 2H); 3.97 (s, 3H); 3.88 (s, 3H); 3.71 (s, 3H).  $^{13}\text{C-NMR}$  (400 MHz,  $\text{CD}_2\text{Cl}_2$ )  $\delta$  (ppm): 156.2; 155.5; 154.0; 145.7; 135.7; 129.5; 126.0; 121.2; 119.9; 109.1; 61.9; 61.2; 56.8.

**X-Ray Diffraction data**Space group:  $P2_1/c$ Cell length ( $\text{\AA}$ ): **a** 12.75200; **b** 10.51860; **c** 20.8426.Cell angles:  $\alpha$  90;  $\beta$  93.4460;  $\gamma$  90.Cell volume ( $\text{\AA}^3$ ): 2790.63

R factor: 4.22%

Symmetry:  $-x, \frac{1}{2}+y, \frac{1}{2}-z; -x, -y, -z; x, \frac{1}{2}-y, \frac{1}{2}+z$ .Figure 51:  $^1\text{H-NMR}$  spectrum of **M8** (400.20 MHz, in  $\text{CD}_2\text{Cl}_2$ )Figure 52:  $^{13}\text{C-NMR}$  spectrum of **M8** (100.70 MHz, in  $\text{CD}_2\text{Cl}_2$ )

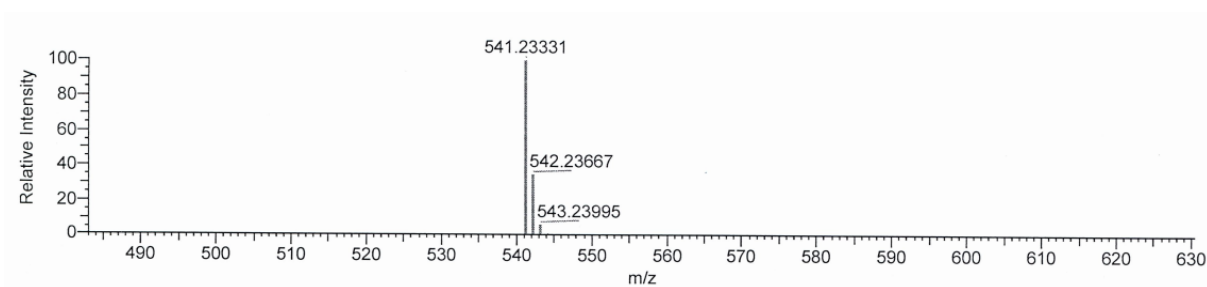
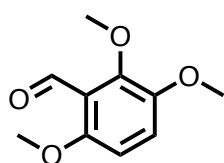


**Figure 53:** High-resolution mass spectrum of **M8** obtained by ESI, positive mode (molecular peak)

### 8.6.2. Characterization of $\frac{1}{2}$ pDVM



#### 2, 3, 6 – trimethoxy benzaldehyde

The general formylation protocol was applied to 1,2,4 trimethoxybenzene, the crude was purified by flash chromatography using methylene chloride as an eluent.

$^1\text{H-NMR}$  (400 MHz,  $\text{CD}_2\text{Cl}_2$ )  $\delta$  (ppm): 10.40 (s, 1H); 7.09-7.68 (dd,  $J = 8\text{Hz}$ ,  $J = 40\text{Hz}$ , 2H); 3.87 (s, 3H); 3.83-3.82 (m, 6H).  $^{13}\text{C-NMR}$  (400 MHz,  $\text{CD}_2\text{Cl}_2$ )  $\delta$  (ppm) : 189.7; 155.3; 152.1; 147.3; 120.2; 119.2; 106.9; 62.1; 56.9; 56.5.

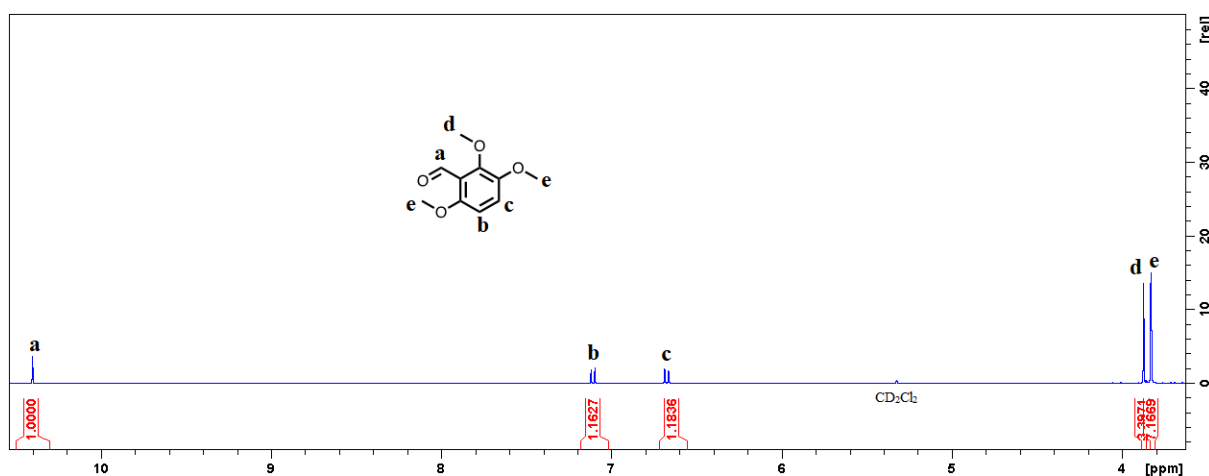


**Figure 54:**  $^1\text{H-NMR}$  spectrum of  $\frac{1}{2}$ pDVM (400.20 MHz, in  $\text{CD}_2\text{Cl}_2$ )

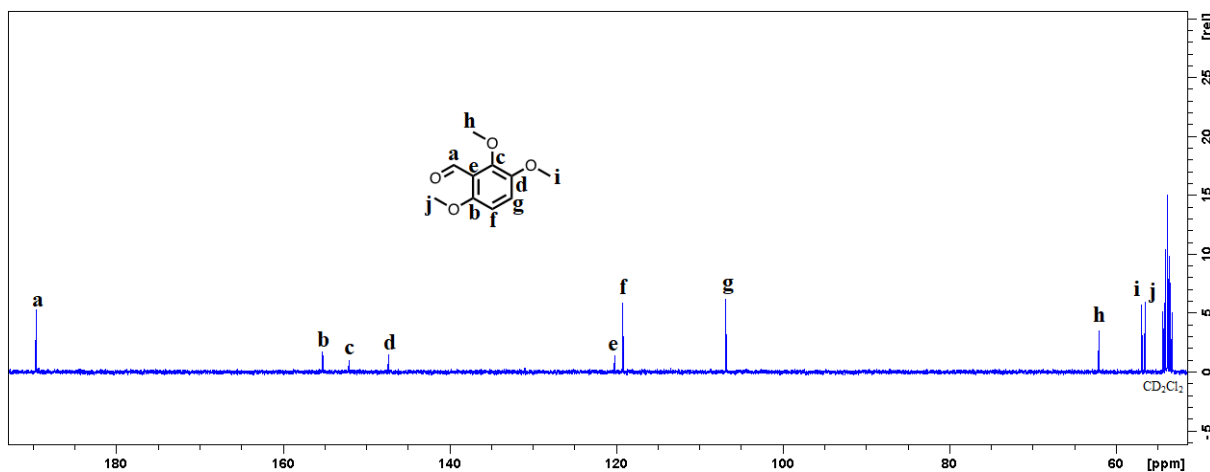


**Figure 55:**  $^{13}\text{C-NMR}$  spectrum of  $\frac{1}{2}$ pDVM (100.70 MHz, in  $\text{CD}_2\text{Cl}_2$ )

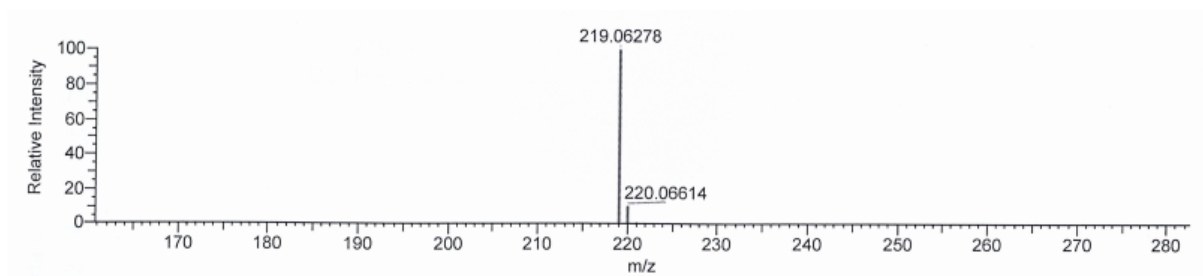


**Figure 56:** High-resolution mass spectrum of  $\frac{1}{2}\text{pDVM}$  obtained by ESI, positive mode. Peaks correspond to  $[\text{M} + {}^{23}\text{Na}]$

**Chapter 4: Divanillin-based polymers with  
benzobisthiazole and  
thiazolothiazole moieties**



## Table of Contents

|   |     |
|---|-----|
| <b>1. Introduction</b> .....  | 187 |
| <b>2. Literature overview of polybenzobisthiazoles and polythiazolothiazoles</b> .....                | 188 |
| <b>3. Synthesis and characterization of polymers with benzobisthiazole and thiazolothiazole</b> ..... | 190 |
| 3.1. Synthesis and physical characterization.....   | 190 |
| 3.2. Optical characterization .....   | 194 |
| 3.3. Divanillin-based polybenzobisthiazoles and polythiazolothiazoles: conclusion.....                | 196 |
| <b>4. Model compounds of divanillin-based polybenzobisthiazoles</b> .....                             | 197 |
| 4.1. Synthesis and purification of model compounds .....  | 197 |
| 4.2. X-Ray Diffraction characterization of model compounds.....                                       | 199 |
| 4.2. Optical properties of model compounds .....  | 201 |
| 4.3. Model compounds with benzothiazole and benzobisthiazole: conclusion .....                        | 206 |
| <b>5. Toward Organic Light Emitting Diode</b> .....   | 206 |
| <b>6. General conclusion</b> .....  | 209 |
| <b>7. References</b> .....  | 211 |
| <b>8. Experimental part</b> .....   | 213 |



## 1. Introduction

Initially in this PhD work, divanillin-based polyazomethines were designed and characterized. These latter have relatively high molar masses, good thermal stability and are soluble in common solvents. They also exhibit interesting optical properties, such as absorbance in the near UV region and emission in the visible range. However, they have a short conjugation pathway due to the nature of the link between aromatic rings of divanillin, which is in meta position with respect to the aldehyde functions, as it is represented in **Figure 1**. To improve the conjugation pathway, a para-divanillin monomer was designed with aldehyde functions in para position. Despite its para link with respect to the aldehyde functions, this divanillin-based monomer also has a short conjugation pathway due to steric hindrance, as illustrated in **Figure 1**. Moreover, solubility issues arose, most likely due to the strongly twisted backbone of these polyazomethines. These latter were also less stable thermally than the divanillin-based polyazomethines.

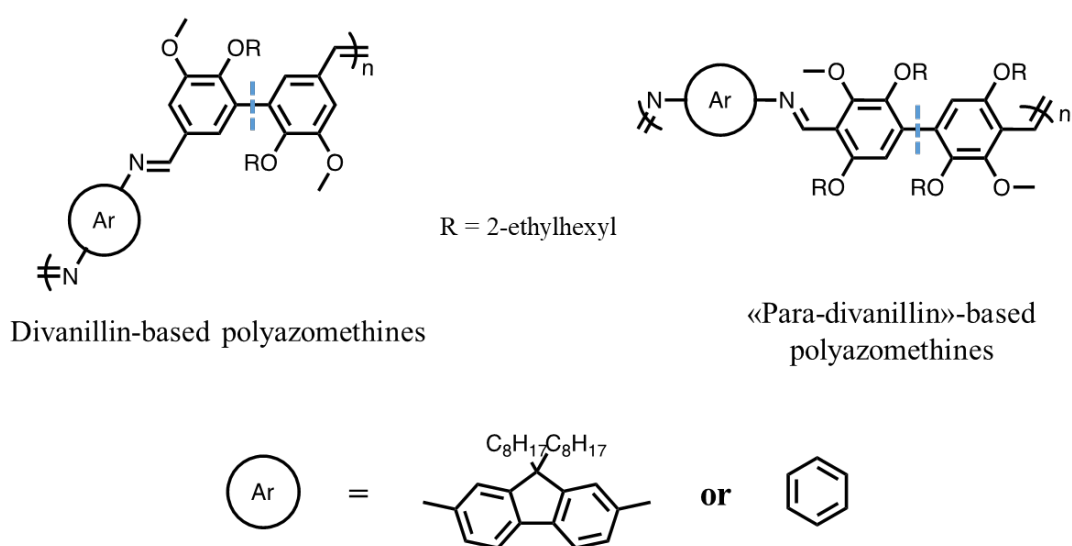


**Figure 1:** General structure of polyazomethines synthesized previously and break of conjugation represented

Consequently, a new strategy was adopted, using divanillin as a monomer. Indeed, its short conjugation pathway could be beneficial to polymers with rigid backbones. Divanillin was thus integrated in polymers bearing benzobisthiazole or thiazolothiazole moieties (see **Figure 2**). These polymers have excellent optical properties as will be discussed in the next section, but also solubility issues due to their rigid backbone. They are also electron deficient, and thus pairing them with the electron-rich divanillin could yield donor-acceptor polymers.

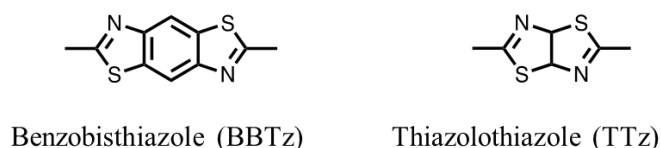


**Figure 2:** Structure of benzobisthiazole and thiazolothiazole moieties

This chapter begins by a brief literature overview on polybenzobisthiazoles and polythiazolothiazoles. The second section describes the synthesis and characterization of divanillin-based polybenzobisthiazoles (**PBBTz**) and polythiazolothiazoles (**PTTz**). Model compounds of these polymers were also synthesized and characterized, and finally the polymers were integrated in OLED.



## 2. Literature overview of polybenzobisthiazoles and polythiazolothiazoles

Polybenzobisthiazoles are characterized by the presence in their backbone of a benzobisthiazole moiety, as is represented in **Figure 2**. These fused rings bring the polybenzobisthiazoles thermal stability and high modulus.<sup>1</sup> Hence they were used as high-strength organic fibres,<sup>2</sup> notably for aeronautical applications (see polymer **A** in **Figure 3**).<sup>3</sup> Their rigid-rod backbone was also exploited for optoelectronic applications. Indeed, the three attached heterocyclic rings bring planarity, efficient  $\pi$  stacking and crystallinity.<sup>4</sup> Jenekhe *et al.* designed the polymers **B** and **C** represented in **Figure 3**.<sup>5</sup>

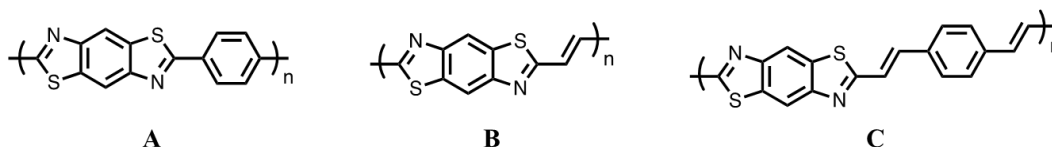
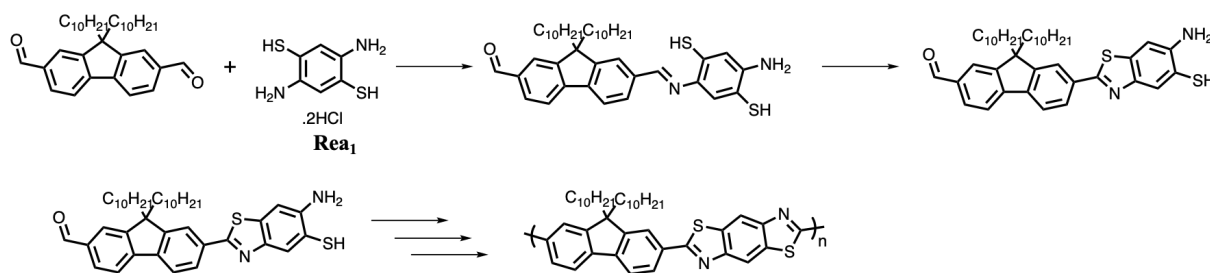


**Figure 3:** Structure of polybenzobisthiazoles for various applications (adapted from <sup>1,6</sup>)

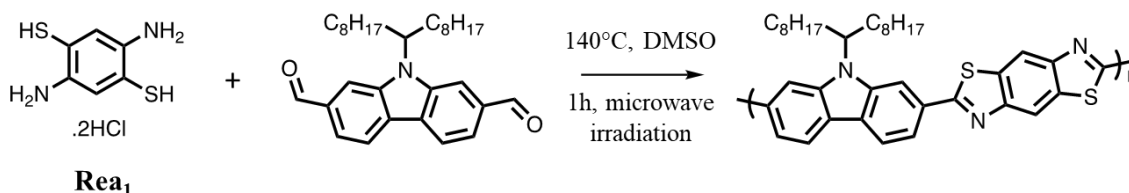
The latter emit in the red region of the visible spectrum with high efficiency (quantum yield up to 100%). Nonetheless, solubility was an issue for these polybenzobisthiazoles. Indeed, they had to be either complexed or dissolved in acids such as methane sulfonic acid to obtain a soluble fraction.<sup>5</sup> Solubility can be improved by adding alkyl moieties on the available positions on the aromatic ring of polybenzobisthiazoles, or by using a co-monomer that will enhance the solubility.

There are two ways of synthesizing polybenzobisthiazoles: either the rings are formed during polymerization, or a monomer already bearing this moiety is reacted with another monomer. The first method is much less used, as it gives less choice for the co-monomer.<sup>7</sup> The BBTz moiety is obtained by reacting a dialdehyde or a diketone with 2,5-diamino-1,4-benzenethiol dihydrochloride (noted **Rea<sub>1</sub>**). A mechanism for this reaction is proposed in **Scheme 1**.



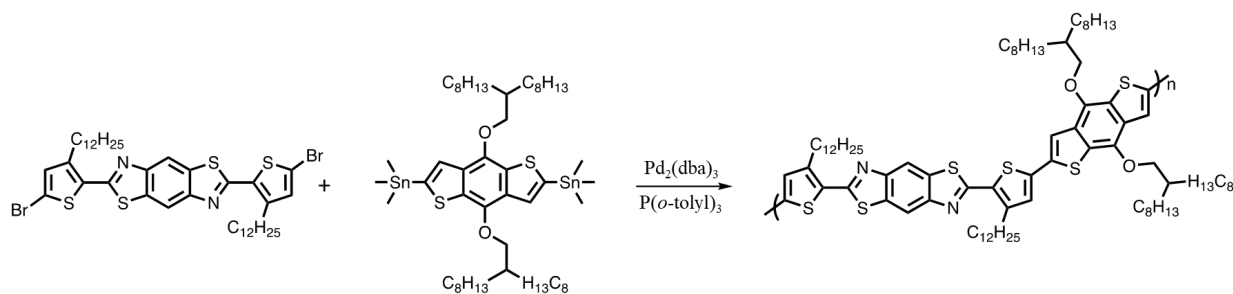
**Scheme 1:** Mechanism of BBTz-moiety formation and ensuing polymerization (adapted from <sup>7</sup>)

This reaction is three-step long, as there is (i) first dehydrochlorination of **Rea<sub>1</sub>** to remove HCl, (ii) then formation of imine and (iii) cyclisation. Belfied *et al.* reported a two-day long synthesis using phosphorus acid as a catalyst, to obtain the polymer presented in **Scheme 1**.<sup>7</sup> In contrast, a synthesis of polybenzobisthiazoles in only one hour using microwave irradiation was reported, as shown in **Scheme 2**. However, the polymer could not be fully characterized as it was poorly soluble.



**Scheme 2:** Synthesis of carbazole-based PBBTz (adapted from <sup>8</sup>)

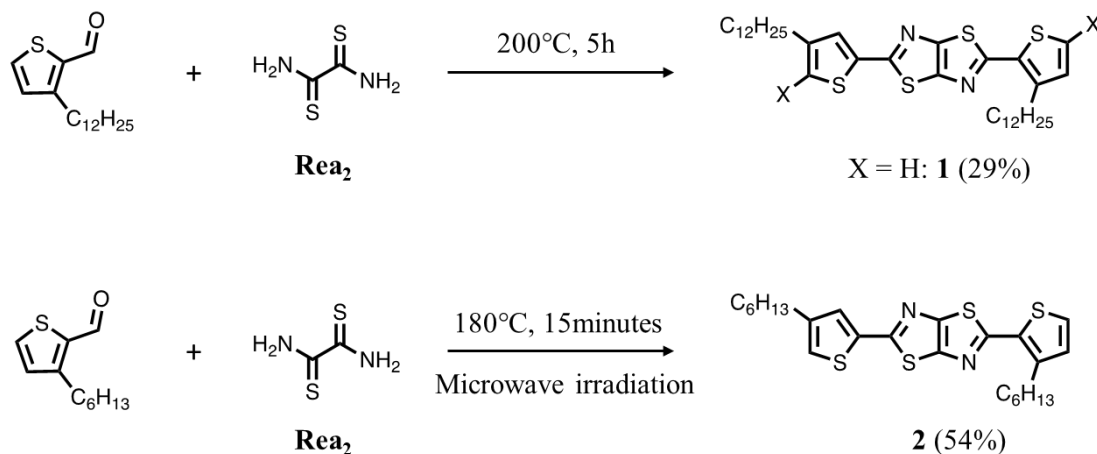
The second method of synthesis can be done using various transition metal couplings, as illustrated in **Scheme 3** with Stille coupling.



**Scheme 3:** Synthesis of PBBTz *via* Stille coupling (adapted from <sup>9</sup>)

By changing the bromide function on the BBTz-bearing moiety, other couplings are accessible, such as Suzuki or Kumada coupling. With various co-monomers a large palette of polybenzobisthiazoles was obtained, with absorbance maxima ranging from 490 to 574 nm, and fluorescence maximum between 573 and 650 nm. This family of polymers was integrated in photovoltaic cells and high stability field effect transistors. Indeed, these latter remained stable under ambient air during two years.<sup>9</sup> McCullough *et al.* also integrated polybenzobisthiazoles into OFET showing high stability even in highly humid air.<sup>10</sup> Polybenzobisthiazoles were integrated into Polymer Light Emitting Diodes (PLED), leading once more to efficient and stable devices.<sup>11</sup>

Another type of polymers bearing hetero aromatic rings are polythiazolothiazoles (PTTz). These latter have two fused heteroatom rings, which improve their solubility compared to polybenzobisthiazoles. They are also planar, with interesting opto-electronic properties such as bright fluorescence. Indeed, they were integrated in PLED, with promising properties such as stability in air, relatively low turn-on voltage and good External Quantum Efficiency (EQE). However, the co-monomer choice is crucial to get the optimum properties.<sup>12,13,14</sup> Polythiazolothiazoles were also integrated into stable OFET.<sup>15,4,16</sup> The synthesis of the thiazolothiazole (TTz) moiety is exemplified in **Scheme 4**.



**Scheme 4:** Syntheses of TTz-moiety, both in bulk (adapted from <sup>15,17</sup>)

Both syntheses are done in bulk, without any solvents. The first one, using conventional heating, has a yield of 29%.<sup>15</sup> Whereas the second, under microwave irradiation, has a yield of 54% – however, this second experimental protocol requires an excess of aldehyde compound ( $[\text{CHO}]/[\text{Rea}_2]=4$ ).<sup>17</sup>

Compound **1** was further derivatized to obtain  $X = \text{Br}$  or  $X = \text{Sn}(\text{Me})_3$ , to be used in polymerization reaction *via* Stille coupling for example. Compound **2** was also derivatized and integrated in solar cells.

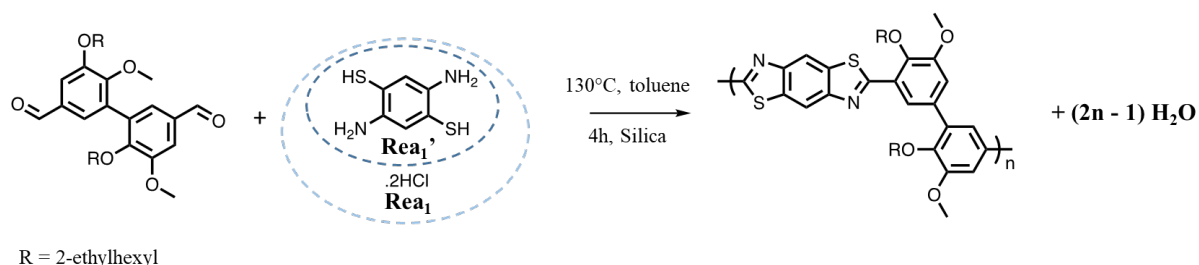
In conclusion, PBBTz have interesting opto-electronic properties such as planarity, efficient  $\pi$  stacking and intense fluorescence but they exhibit solubility issues. Another type of heteroaromatic polymers is PTTz. These latter are usually more soluble than PBBTz and have good opto-electronic properties like bright and strong fluorescence. Both types of polymers are synthesized by first designing a TTz- or BBTz-based monomer, followed by a polymerization using transition metal coupling. There are some reports of ring formation during polymerization for PBBTz, but not for PTTz. Therefore most syntheses require hazardous monomer and produces dangerous by-products, even if they were some tries to use less hazardous monomers, for example *via* direct arylation.<sup>18</sup>

In the next section, synthesis of **DVEH**-based PTTz and PBBTz will be discussed, by cyclisation during polymerization to avoid the use of transition metal.

### 3. Synthesis and characterization of polymers with benzobisthiazole and thiazolothiazole

#### 3.1. Synthesis and physical characterization

The synthesis of **DVEH**-based polybenzobisthiazoles (PBBTz) was performed at 130°C under microwave irradiation, as described in **Scheme 5**. Silica acts as a desiccant and as an acidic catalyst – as PBBTz are less sensitive than polyazomethines, silica should not affect the final polymers' opto-electronic properties.



**Scheme 5:** Synthesis of **DVEH**-based PBBTz under microwave irradiation

**Rea<sub>1</sub>'** corresponds to **Rea<sub>1</sub>** after dehydrochlorination, meaning after removal of the two HCl. Two monomers ratios were tested:  $[\text{DVEH}]/[\text{Rea}_1] = 1$  (**P17**) and  $[\text{DVEH}]/[\text{Rea}_1'] = 1$  (**P18**). The polymers were recovered by filtration to remove silica, without any purification work up. These latter are soluble in common solvents such as chloroform, THF, methylene chloride, but also methanol, heralding low average molar mass. This was confirmed by SEC (**Figure 4a**).

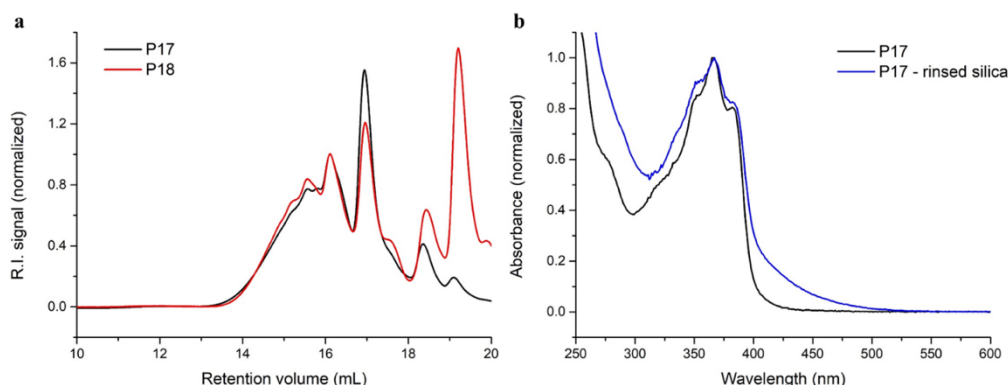


**Figure 4a:** SEC profiles of **P17** and **P18** in THF (R.I. detection). **b:** Absorbance spectra of **P17** and fraction obtained after rinsing silica ( $10^{-2}$  g/L, in methylene chloride)

Both polymers have low apparent molar masses, with the presence of short oligomers. In the case of  $[\text{DVEH}]/[\text{Rea}] = 1$  (**P18**), there is also some remaining monomer detectable (**DVEH**). The yield was only 45%, as the rest precipitated on silica. This could be due to solubility issues during the polymerization reaction, as longer chains tend to precipitate on silica. The latter was rinsed with chloroform and triethylamine (TEA), to recover a partially soluble fraction that could not be analyzed by SEC (solubility under 0.1 mg/mL). However, the latter was analyzed by UV-Vis spectroscopy and compared with the corresponding polymer (**Figure 4b**). Both spectra have the same shape with the characteristic three peaks of benzobisthiazole, as will be discussed in the next section. However, the fraction on silica has a shoulder towards higher wavelength, which could be a sign of aggregates or longer molar masses, which would explain the poor solubility of this fraction.

PBBTz with methylated divanillin (**DVM**) was also synthesized using the same experimental protocol. A soluble fraction was recovered after filtration of silica (**P19**), with low yield (13%). **P19** is soluble in THF, and its SEC profile is given in **Figure 5a**, showing low molar masses. The remaining 87% precipitated on silica, and a fraction could be recovered by rinsing it with chloroform and TEA. The latter fraction was analyzed by SEC as it was partially soluble in THF (around 60% of the fraction recovered from silica was dissolved). This soluble fraction corresponds to shorter chains than **P19**, and both have remaining monomer (**DVM**, peak at 20 mL), as is shown in **Figure 5a**.

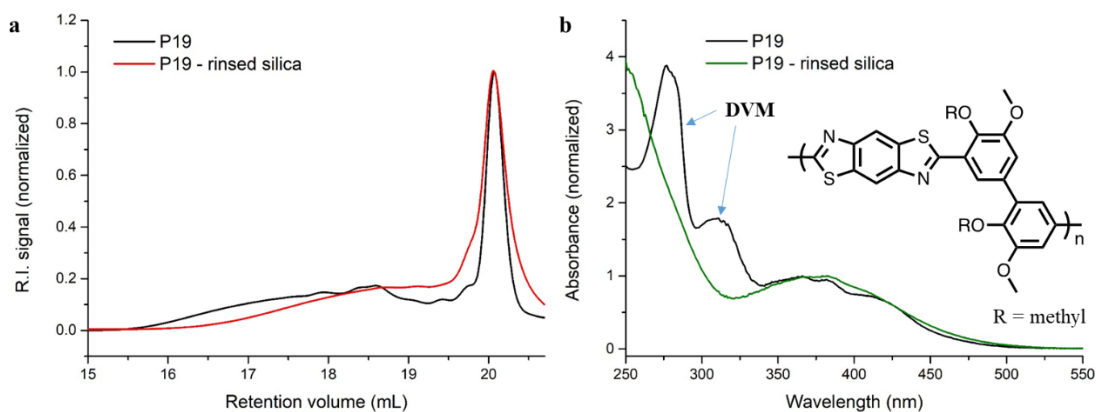


**Figure 5a:** SEC profile of **P19** and its silica fraction in THF (R.I. detection). **b:** Absorbance spectra of **P19** and its silica fraction in methylene chloride ( $10^{-2}$  g/L)

Both **P19** and its silica fraction (soluble at 80% in methylene chloride) were analyzed by UV-Vis spectroscopy. Interestingly, **DVM** was not detectable by UV-VIS spectroscopy in the silica fraction,

contrary to **P19** (**Figure 5b**). It is however not possible to conclude clearly as the fractions are not fully soluble.

Other experimental protocols were tested, with different ratio and catalyst such as Eaton's reagent or polyphosphoric acid, but they produced a mixture of short oligomers in low yield. The most promising protocol is to use microwave irradiation for 30 minutes, without silica (**Figure 6**). The yield is low and a large fraction could not be solubilized in THF (60% of the crude remained insoluble), but the soluble fraction in THF corresponds to polymer chains with higher molar mass than those of polymers synthesized previously (~2 500 g/mol). However, there are some remaining monomer (peak at 19.5 mL).

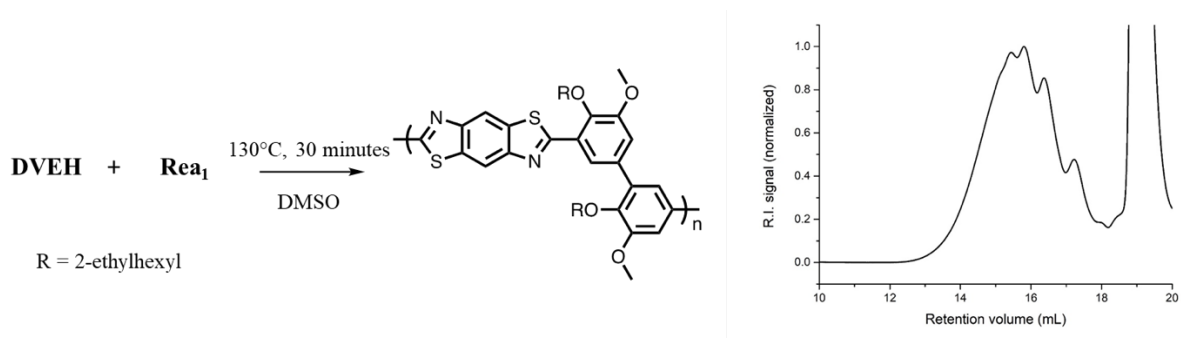
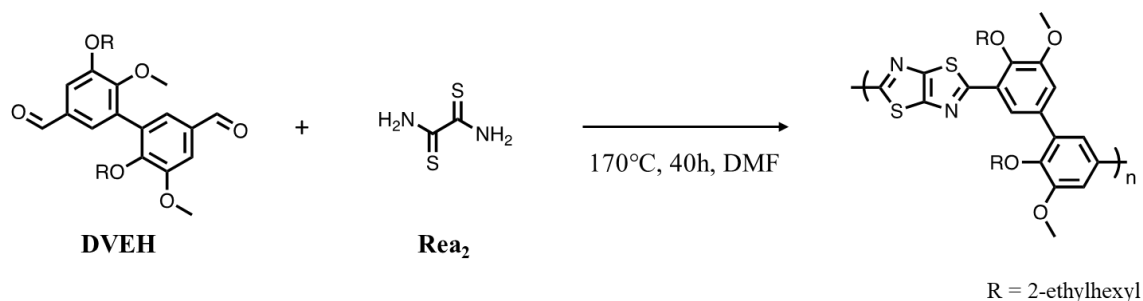


**Figure 6:** Synthesis of **DVEH**-based PBBTz and SEC profile in THF (R.I. detection)

To conclude, the divanillin-based PBBTz previously synthesized have low molar masses and tend to precipitate on silica, leading to poor yield. There may be longer polymer chains on silica, but they either could not be dissolved or detached from it. Other experimental protocols were tested, but produced either short oligomers or insoluble fractions, with low yield in both cases. Therefore, PBBTz were set aside to focus on **DVEH**-based PTTz.

The synthesis of model compounds gave some insights on PTTz synthesis, as will be discussed in the Section 4.1. Indeed, no quantitative TTz-moiety formation could be achieved in 4 hours using microwave irradiation at 130°C. Therefore, the experimental conditions were adapted: the polymers were obtained after 40 hours in DMF at 170°C without any catalyst, as illustrated in **Scheme 6**:



**Scheme 6:** Synthesis of **DVEH**-based PTTz

The purification work up was done by precipitation in methanol, producing PTTz with a 30% yield. The synthesis was done twice with a 1:1 monomer ratio at different reaction times: 16 hours (**P20**) and 40 hours (**P21**) and once with a monomer ratio  $[\text{DVEH}]/[\text{Rea}_2] = 0.9$  for 40 hours (**P22**). These latter polymers are soluble in common solvents (THF, methylene chloride, chloroform) and their SEC profiles are given in **Figure 7**.

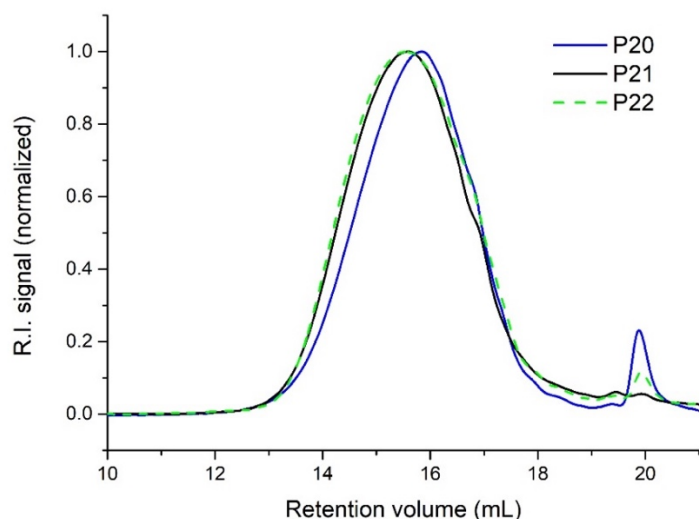
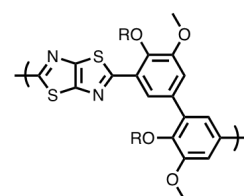


**Figure 7:** SEC profiles of **P20**, **P21**, and **P22** in THF (R.I. detection)

By increasing the reaction time from 16 to 40 hours, higher molar masses can be obtained (**P20** and **P21**). Interestingly the SEC profiles of **P21** and **P22** are identical, implying that the monomer ratio did not affect the molar masses. The polymers may have reached a limit in terms of molar mass and solubility during the reaction. At monomer ratios of 0.8 and 1.2, polymers were not obtained but rather small oligomers that could not be precipitated in methanol. **Table 1** sums up the features of **DVEH**-based PTTz.

| Name       | [DVEH]/[Rea <sub>2</sub> ] | Reaction time | $\bar{M}_n^a$ (g/mol) | $\bar{M}_w^a$ (g/mol) | $\bar{D}^a$ | $\bar{DP}_n^a$ | $T_d^b$ (°C) |
|------------|----------------------------|---------------|-----------------------|-----------------------|-------------|----------------|--------------|
| <b>P20</b> | 1/1                        | 16h           | 3 900                 | 7 600                 | 1.9         | 6              | ND           |
| <b>P21</b> | 1/1                        | 40h           | 4 700                 | 9 900                 | 2.1         | 8              | 310          |
| <b>P22</b> | 0.9                        | 40h           | 4 700                 | 9 500                 | 2.0         | 8              | ND           |



R = 2-ethylhexyl

**Table 1:** Structure of **DVEH**-based PTTz and table summing up their properties. <sup>a</sup> Determined by SEC relative to PS standards in THF at 30°C. <sup>b</sup> Decomposition temperature at 10% weight loss, evaluated under N<sub>2</sub> at a heating rate of 10 °C/min by TGA.

The molar masses go up to 4 700 g/mol, which corresponds to 8 units. The dispersity is around 2, which is expected for a polycondensation reaction. The degradation temperature is quite low compared to the one of **DVEH**-based polyazomethine (387°C for fluorene and **DVEH**-based polyazomethine **P1**). This may be explained by remaining solvents in the sample, as the degradation temperature at 20 wt% loss is 390°C for **P21**.

To conclude this section, **DVEH**-based PBBTz and PTTz were designed. The synthesis of PBBTz did not yield any polymers but rather a mixture of oligomers. Therefore, we chose to focus on **DVEH**-based PTTz. These latter are soluble in common solvents and molar masses of 4 700 g/mol were obtained. The synthesis is done without any catalyst, at the reflux of DMF. **DVEH**-based PTTz were then characterized optically, as will be discussed in the next section.

## 3.2. Optical characterization

The previously synthesized PTTZ (**P21**) was characterized by UV-Vis spectroscopy, its spectrum is given in **Figure 8**.

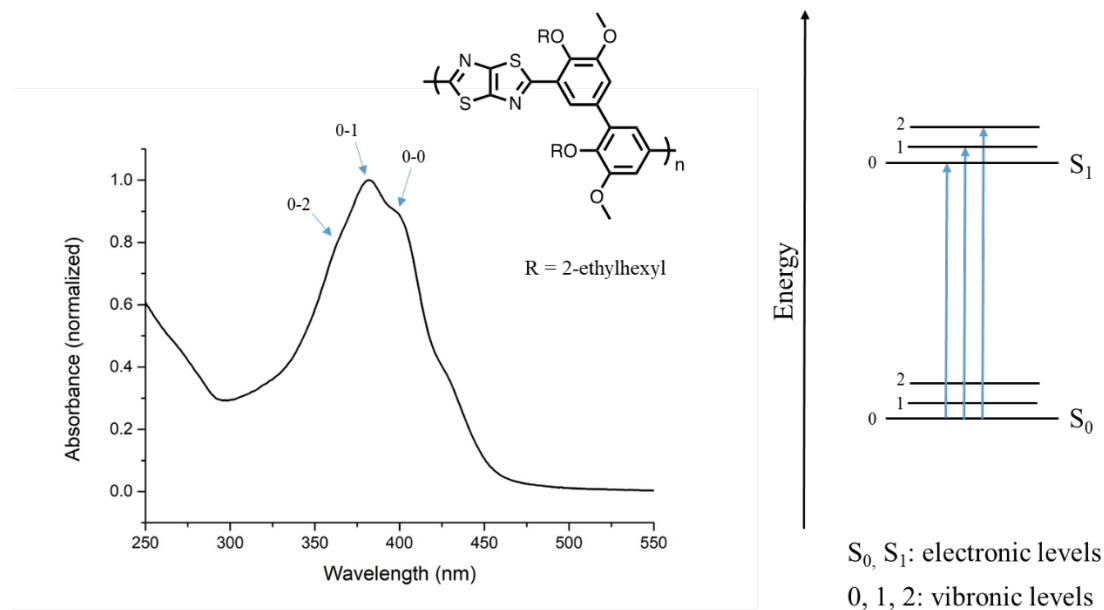


**Figure 8:** Absorbance spectrum of **P21** in methylene chloride ( $10^{-2}$  g/L) and typical energy levels scheme

**P21** has well-defined vibronic structures, as highlighted in **Figure 8**. These peaks correspond to transitions from the electronic ground level ( $S_0$ ) towards vibrational levels of the excited electronic level ( $S_1$ ), the latter corresponding most likely to  $(\pi, \pi)^*$  state. Well-defined vibrational structures indicate that the polymers has a rigid and well-defined structure, and is a phenomenon well-known for PTTz and PBBTz.<sup>14,19,20,21</sup> The shoulder towards higher wavelengths could be due to  $n-\pi^*$  transitions or aggregates.

**Figure 9** compares the absorbance and emission spectrum of **P21** in solution and in films.

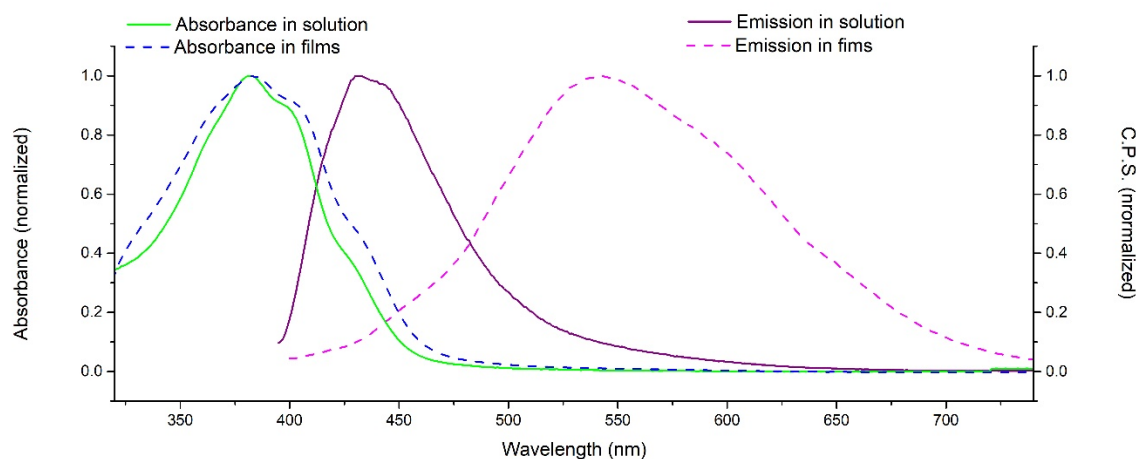


**Figure 9:** Absorbance and emission spectra of **P21** in solution ( $10^{-2}$  g/L for absorbance,  $10^{-5}$  g/L for emission) and in films (drop-casted on quartz plate)

**P21** exhibits a narrow emission spectrum in solution with a vibronic structure detectable. This emission spectrum corresponds to the blue light in the visible range. In films, the absorbance maximum does not shift, however the spectrum gets broader, with vibronic structure still detectable. Interestingly, the

emission in films is strongly shifted towards higher wavelength compared to the emission in solution. Indeed, there is a 90 nm bathochromic shift between maxima of emission in solution and in films. The Stokes shift between absorbance and emission, both in films, is 157 nm, heralding low reabsorption and promising properties for OLED. The emission spectrum in films is broad and structure-less, which could be a sign of charge-transfer behavior. **Figure 10** highlights the bathochromic shift and broadening of **P21** in films compared to its behavior in solution.

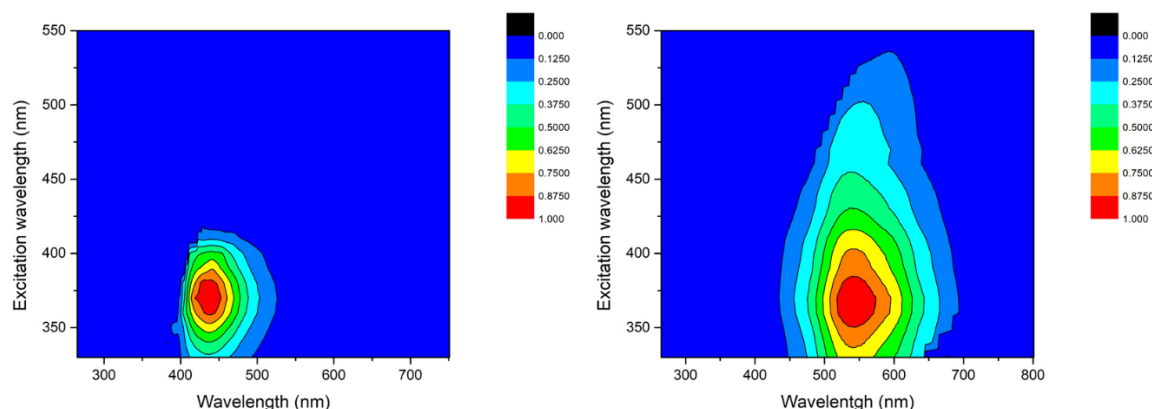
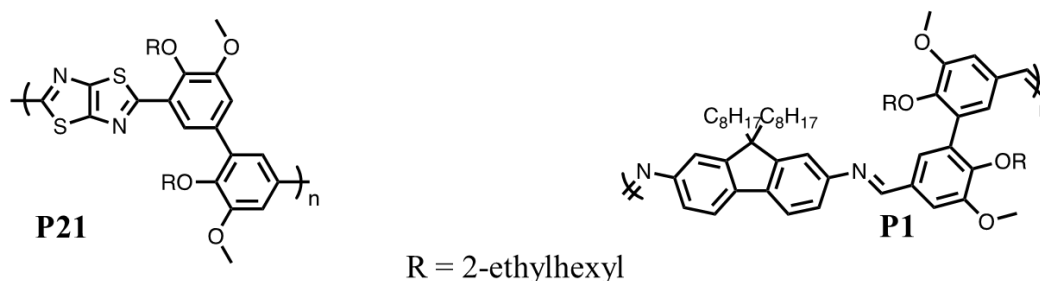


**Figure 10:** 3D emission spectra of **P21** in solution (left,  $10^{-5}$  g/L in methylene chloride) and in films (right, drop-casted on quartz), both normalized.

The optical properties of **P21** are summed up in **Table 2**, along with the characteristics of **P1**, the **DVEH**- and fluorene-based polyazomethine (see **Chapter 2**).



| Name       | Absorbance                      |                                  | Emission                        |                                  |
|------------|---------------------------------|----------------------------------|---------------------------------|----------------------------------|
|            | $\lambda_{\max}^{\text{sol a}}$ | $\lambda_{\max}^{\text{film b}}$ | $\lambda_{\max}^{\text{sol c}}$ | $\lambda_{\max}^{\text{film b}}$ |
| <b>P21</b> | 361-383-400                     | 363-383-405                      | 431                             | 540                              |
| <b>P1</b>  | 388                             | 392                              | 455                             | 470 - 560                        |

**Table 2:** Optical properties of **DVEH**-based polyazomethine **P1** and **DVEH**-based PTTz (**P21**). <sup>a</sup> Measured in methylene chloride,  $10^{-2}$  g/L. <sup>b</sup> Measured in films made by drop-casting on quartz. <sup>c</sup> Measured in methylene chloride,  $10^{-5}$  g/L for **P21** and  $10^{-2}$  g/L for **P1**

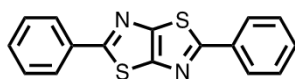
**P1** is more red-shifted than **P21**, with respect to both emission and absorbance. This could be due to the longer conjugation pathway of **P1**. Indeed the fluorene moiety has three fused rings while the TTz moiety has two. However, **P1** has a weak fluorescence that could not be measured, contrary to **P21**. Its quantum yield (QY) was measured using quinine sulfate as a secondary standard and a well-known protocol, with uncertainties of  $\pm 10\%$ .<sup>22</sup> Solutions of the compounds of interest (sample and standard) were prepared with absorbance ranging from 0.1 to 0.01, and their fluorescence measured. The QY was then calculated using the **Equation 1**:



$$QY(x) = QY(st) * \frac{Grad(x)}{Grad(st)} * \frac{n(x)^2}{n(st)^2}$$

**Equation 1:** Determination of quantum yield using a secondary standard (*st* refers to the standard and *x* to the sample)

Where *Grad* is the gradient of the straight line obtained when plotting the area under the emission curve against the absorbance of the solution. Contrary to expectations, **P21** has a quantum yield of 2%, which is quite low. Indeed, the small molecule represented in **Figure 11** has a quantum yield of 16% in chloroform. The authors suggest that this relatively low value in chloroform with respect to other solvents is due to poor solubility that would lead to aggregates and therefore self-quenching.<sup>23</sup> The latter phenomenon is one of the reason given to explain why polymers usually have lower QY than corresponding small molecules.<sup>7</sup>



| Solvent      | QY   |
|--------------|------|
| Cyclohexane  | 0.25 |
| Chloroform   | 0.16 |
| Acetonitrile | 0.23 |
| Methanol     | 0.22 |
| DMSO         | 0.16 |

**Figure 11:** Structure and table of QY for various solvents of TTz-based molecule (adapted from <sup>23</sup>)

### 3.3. Divanillin-based polybenzobisthiazoles and polythiazolothiazoles: conclusion

**DVEH**-based polybenzobisthiazoles (PBBTz) were designed. However, no satisfactory PBBTz could be obtained with the various experimental protocols tested. Therefore another type of fused-ring polymers was synthesized, polythiazolothiazoles. These latter are soluble in common solvents and are synthesized in DMF, without any catalyst. The polymers have molar masses up to 4 700 g/mol, which corresponds to 8 units.

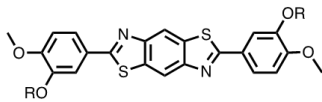
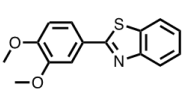
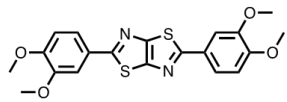
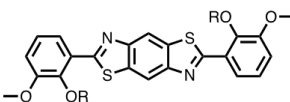
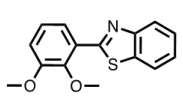
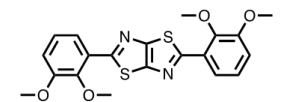
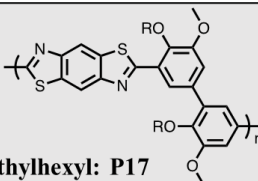
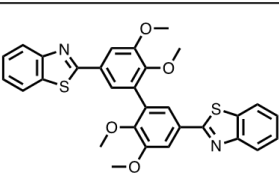
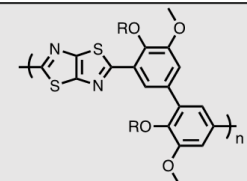
The **DVEH**-based PTTz named **P21** has an absorbance maximum at 383 nm, with vibronic structures detectable. These latter are a sign of well-defined and rigid structure. **P21** has a narrow emission in the visible range, in the blue region. Interestingly it has a Stock shift of 157 nm between absorbance and emission maxima in films, heralding low reabsorption and promising properties for the integration in a device, even if the QY in solution is low (2%).

This low QY could be a sign of aggregates and therefore be due to self-quenching. Indeed, a small molecule with a TTz moiety and two aromatic rings has a QY of 16% – therefore a QY of this order of magnitude was expected for **P21**. The low QY of **P21** could be improved by protonation using an acid.<sup>24</sup>

## 4. Model compounds of divanillin-based polybenzobisthiazoles

## 4.1. Synthesis and purification of model compounds

Model compounds were designed for structure-properties studies and are represented in **Table 3**.

|                       | Benzobisthiazole  | Benzothiazole  | Thiazolothiazole  |
|-----------------------|---|--|---|
| <b>Vanillin</b>       |  <p>R= 2-ethylhexyl: <b>M10</b><br/>R= methyl: <b>M11</b></p>  |  <p><b>M12</b></p>  |  <p><b>M13</b></p>                   |
| <b>Ortho-Vanillin</b> |  <p>R= 2-ethylhexyl: <b>M14</b><br/>R= methyl: <b>M15</b></p>  |  <p><b>M16</b></p>  |  <p><b>M17</b></p>                   |
| <b>DiVanillin</b>     |  <p>R= 2-ethylhexyl: <b>P17</b><br/>R= methyl: <b>P19</b></p> |  <p><b>M18</b></p> |  <p>R= 2-ethylhexyl: <b>P21</b></p> |

**Table 3:** Sum up of model compounds synthesized

Initially these syntheses were performed using microwave irradiation at 130°C with silica, and the reaction was monitored by measuring the absorbance as exemplified in **Figure 12**.

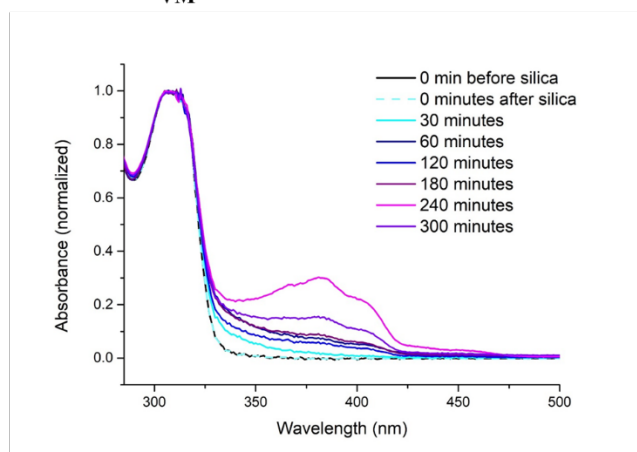
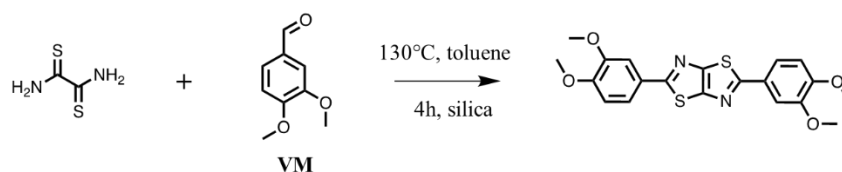


**Figure 12:** Synthesis of **M13** and follow-up by absorbance (in toluene,  $\sim 10^{-2}$  g/L)

UV-Vis spectroscopy assessed the formation of a red-shifted compound with the same vibronic structure as the corresponding polymer **P21**, heralding similar structure and therefore the formation of the desired TTZ group. However, the chemical structure could not be confirmed by NMR spectroscopy as the model compound was not soluble enough (solubility below 0.1 mg/mL). Moreover, the yield is low and the reaction relatively slow, as can be observed by comparing the intensity of the peak of the remaining monomer (**VM**, peak at 308 nm) and of the peaks of the model compound.

Only **M12** was obtained using the experimental protocol described previously. The latter was then recrystallized and its structure was confirmed by NMR spectroscopy. For the other model compounds, the experimental protocol using microwave irradiation and silica did not produce pure model compounds. Other protocols were tested to synthesize these latter compounds, using catalysts such as lemon juice<sup>25</sup> or polyphosphoric acid,<sup>7</sup> but also using microwave irradiation in bulk.<sup>26</sup> None of these experimental protocols yielded the desired model compounds in sufficient yield and/or purity to perform a purification (either by recrystallization or by flash chromatography).

**M18** was obtained by mixing the two reactants in DMSO at the reflux for 4 hours. The latter crystallized during the cool-down of the crude mixture, without any additional purification step required. Two experimental protocols are compared in **Figure 13**.

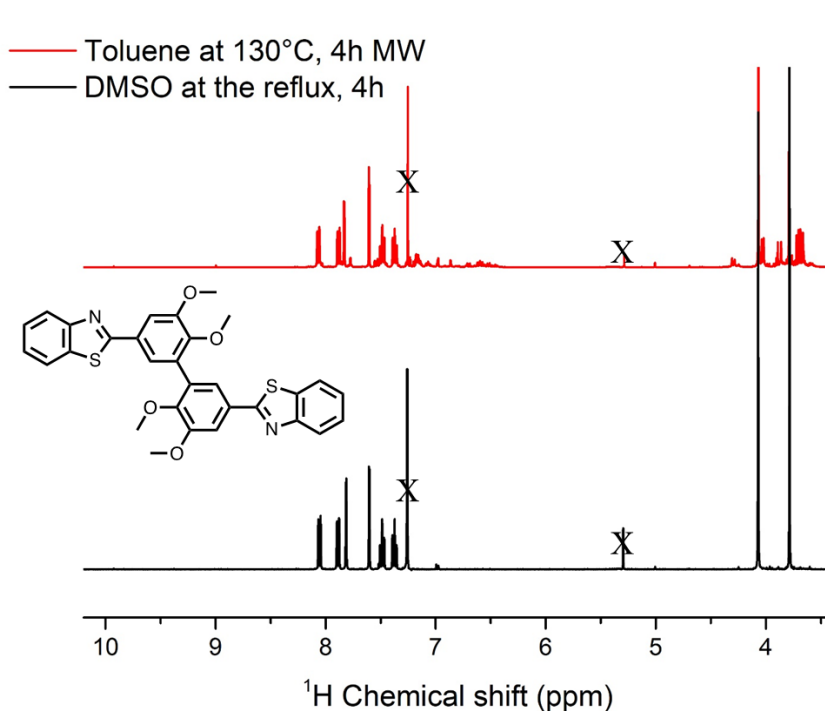


**Figure 13:** <sup>1</sup>H-NMR spectra of **M18** using different experimental protocols (in CDCl<sub>3</sub>)

The <sup>1</sup>H-NMR spectrum confirms the formation of the desired product, without remaining impurities. The crystals obtained after the cool-down were used as such for X-RD analysis.

To conclude, two model compounds were synthesized and purified as crystals to be analyzed by X-RD, as will be discussed in the next section. Both bear a benzothiazole moiety with either a vanillin or a divanillin moiety (see **Figure 14**). However, due to the low yield and/or solubility issue the other model compounds were not isolated after synthesis. The absorbance of their crude mixture was recorded, as will be discussed in **Section 4.2**.

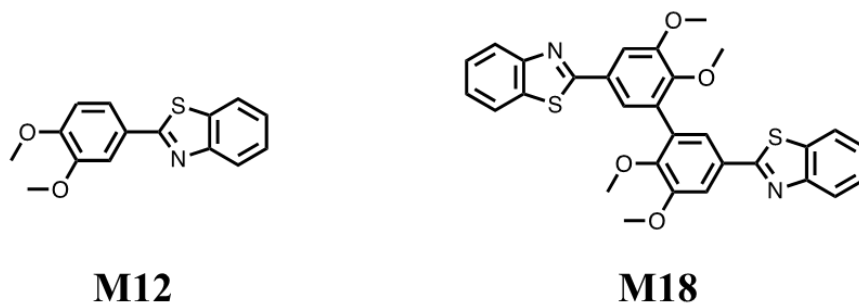


**Figure 14:** Structure of benzothiazole-based model compounds that were isolated and recrystallized

#### 4.2. X-Ray Diffraction characterization of model compounds

**M12** was solved by X-RD diffraction, and its structure is represented in **Figure 15**.

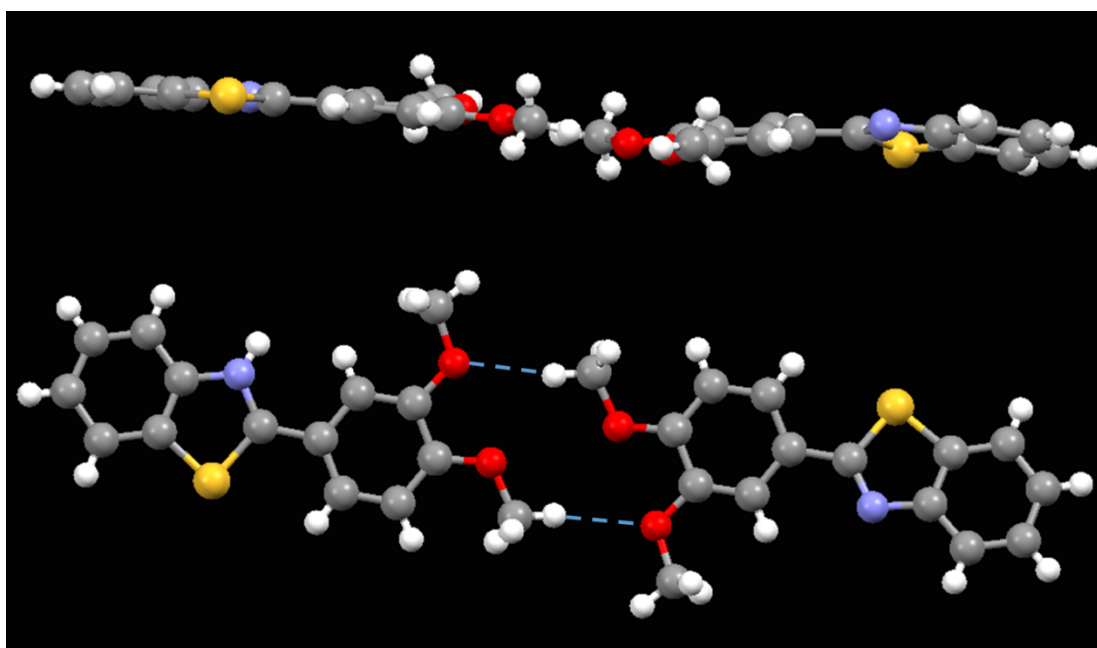


**Figure 15:** X-RD structure of **M12**, side view and front view

There are two types of molecules in the lattice, linked together by hydrogen bonds. One type of **M12** molecule is planar, while the other one has an angle of  $20^\circ$  between the vanillin aromatic ring and the benzothiazole group. As a comparison, the molecule with vanillin and benzene linked by an azomethine (**M3**) bond has a  $69.1^\circ$  angle between its two aromatic rings.

No  $\pi$  stacking was observed, as can be seen in the packing in **Figure 16**.

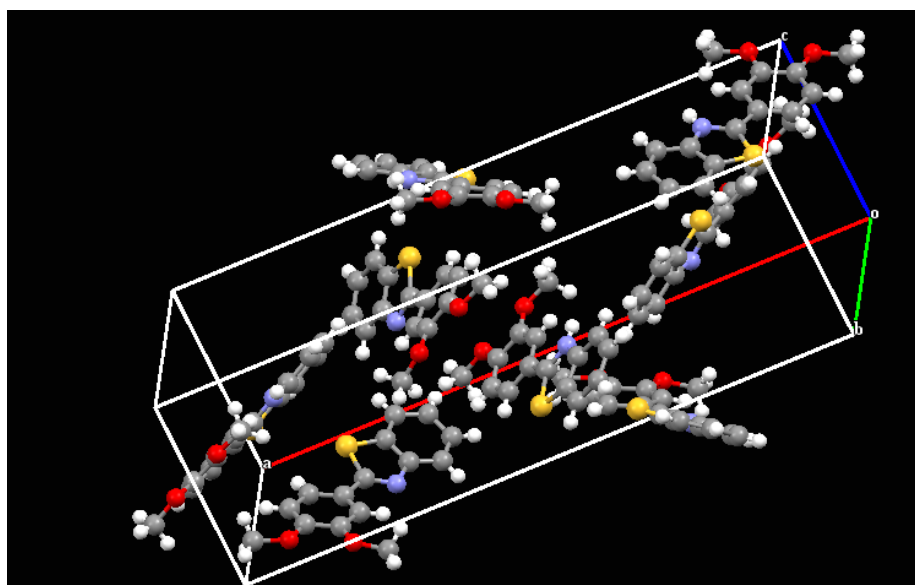


Figure 16: Packing of M12

M18 was also resolved by X-RD, and its structure is given in Figure 17.

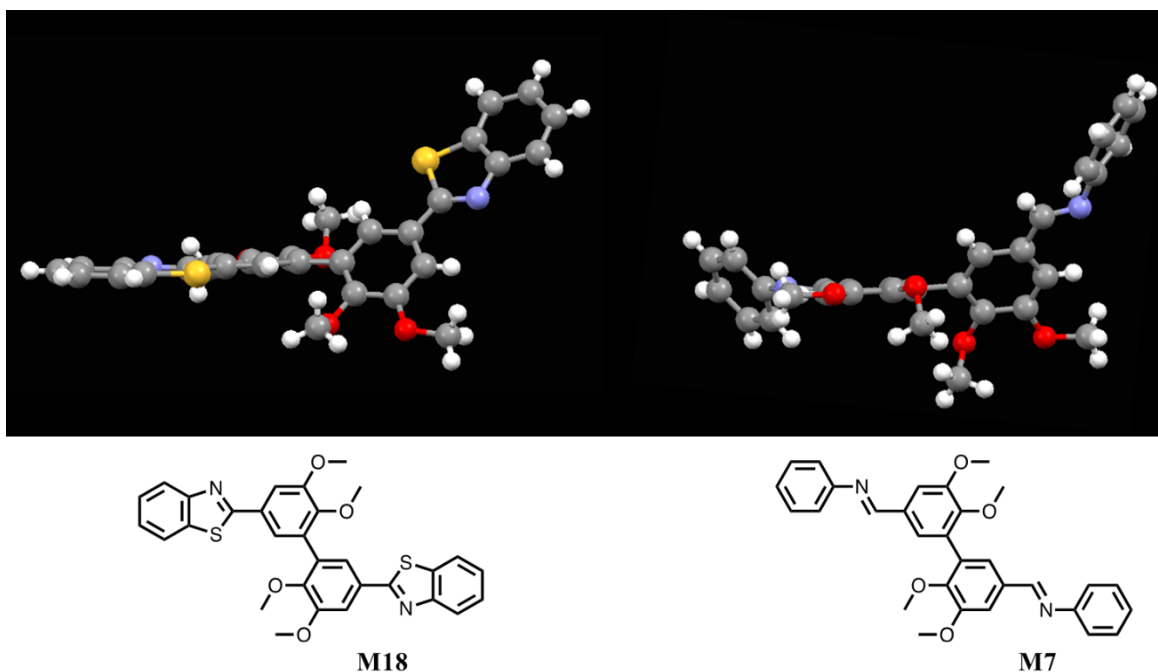
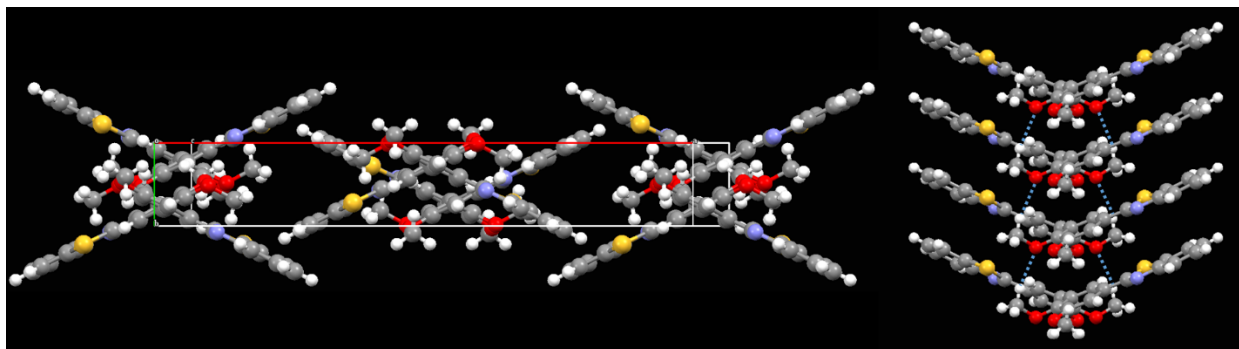


Figure 17: Side view of X-RD structure of M18 (left) and M7 (right)

The torsion angle between the aromatic rings of divanillin is  $126.3^\circ$  for M18, which is close to the value for M7, the azomethine corresponding model compound ( $126.9^\circ$ ). In M18, the aromatic rings of the divanillin moiety are both coplanar with the adjacent benzothiazole group, heralding an improved conjugation pathway compared to M7.

Efficient  $\pi$  stacking was observed for M18 in the lattice, as can be observed in Figure 18.



**Figure 18:** X-RD structure of **M18**, packing in lattice along b axis (left, six molecules represented) and four **M18** molecules linked by H bonding (right)

Due to the enhanced planarity of **M18**, the benzothiazole and vanillin moieties can stack neatly on top of each other, linked by hydrogen bonding between divanillin moieties. The  $\pi$  stacking distance is 3.92 Å, with a herringbone pattern. The torsion angle between the divanillin rings prevents a fully planar  $\pi$  stacking, giving the molecule a butterfly shape – the angle between the two planes is 53.5°.

#### 4.2. Optical properties of model compounds

The previously synthesized and purified model compounds were characterized by UV-Vis spectroscopy, and their spectra are given in **Figure 19**.

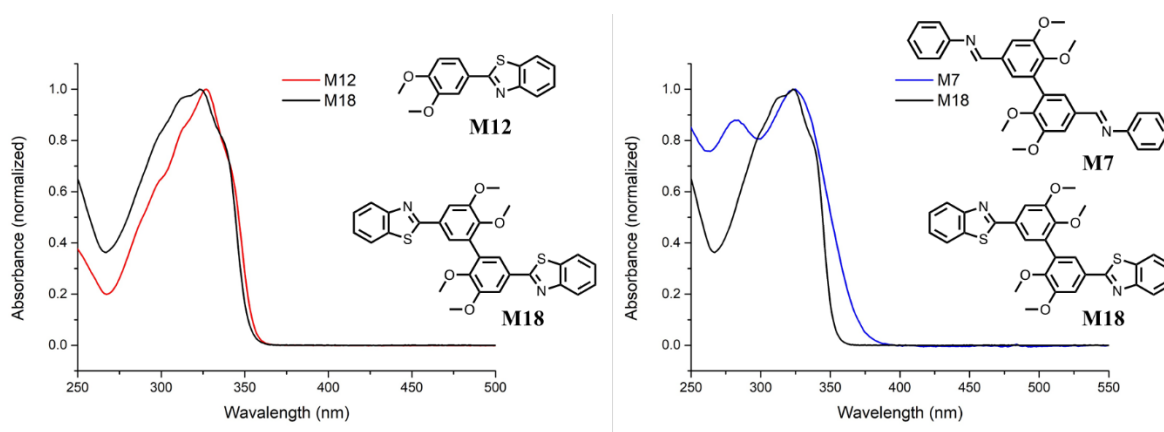


**Figure 19:** Absorbance spectra of **M12**, **M18** and **M17**, in methylene chloride ( $10^{-2}$  g/L)

Both **M12** and **M18** have well-defined vibronic structure, as expected from benzothiazole-based compounds. Identical absorbance maxima were expected, as the bond linking the two rings of divanillin is in meta position with respect to the benzothiazole moiety. Interestingly this is not the case, as **M12** is more red-shifted than **M18** by 4 nm. This could be due to steric hindrance or the effect of the additional aromatic ring that acts as a substituent in **M18** compared to **M12**. As seen in the previous section, **M18** is more planar than **M7**; consequently, a bathochromic shift was expected. However, this is not the case as **M7** and **M18** have the same absorbance maxima. The electron withdrawing behavior of the benzothiazole moiety might limit the absorbance improvement.

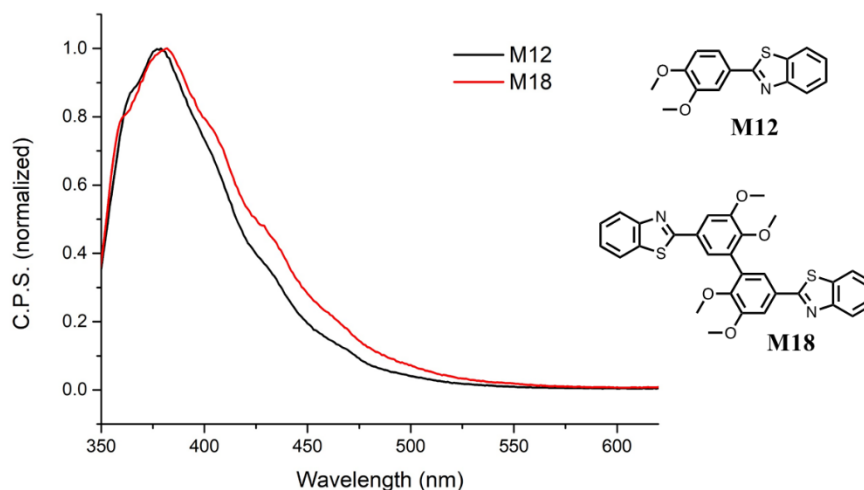
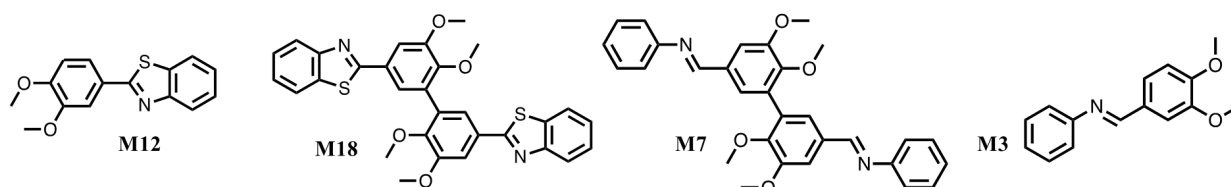


**Figure 20:** Emission spectra of **M12** and **M18** in methylene chloride ( $10^{-5}$  g/L, excitation wavelength: 325 nm)

**Figure 20** compares the absorbance spectra of **M12** and **M18**. Both spectra are well structured, with vibronic structures detectable. Remarkably, **M18** is slightly red-shifted compared to **M12** by 3 nm – the opposite was observed for the absorbance spectra. The differences between the vibronic or electronic levels of **M12** and **M18** could explain this feature. Further work such as computational analysis needs to be carried out before drawing any conclusion. The optical properties of azomethine and benzothiazole vanillin-based model compounds are summed up in **Table 4**.



| Name       | Absorbance                      |   |   | Emission                        |                            |
|------------|---------------------------------|---|---|---------------------------------|----------------------------|
|            | $\lambda_{\max}^{\text{sol a}}$ | $\epsilon^{\text{toluene b}}$<br>( $\text{cm}^{-1} \cdot \text{mol}^{-1} \cdot \text{L}^{-1}$ ) | $\epsilon^{\text{dichloromethane c}}$<br>( $\text{cm}^{-1} \cdot \text{mol}^{-1} \cdot \text{L}^{-1}$ ) | $\lambda_{\max}^{\text{sol d}}$ | Quantum yield <sup>e</sup> |
| <b>M12</b> | 311 - 327 - 343                 | 22 000  | 26 700  | 364 - 379 - 404                 | 0.20                       |
| <b>M18</b> | 311 - 323 - 339                 | 39 400  | 40 300  | 360 - 374 - 382 -<br>405        | 0.19                       |
| <b>M3</b>  | 323 - 283                       | 18 800  | 22 700  | 380                             | ND                         |
| <b>M7</b>  | 323 - 281                       | 30 600  | 44 000  | 380                             | ND                         |

**Table 4:** Sum up of optical properties of **DVM**-based azomethine and benzothiazole model compounds. <sup>a</sup> In methylene chloride,  $10^{-2}$  g/L. <sup>b</sup> In toluene, using a range of concentration from  $10^{-2}$  to  $10^{-3}$  g/L. <sup>c</sup> In methylene chloride, using a range of concentration from  $10^{-2}$  to  $10^{-3}$  g/L. <sup>d</sup> In methylene chloride,  $10^{-5}$  g/L for **M12** and **M18**,  $10^{-2}$  g/l for **M3** and **M7**. <sup>e</sup> Determined using quinine sulfate as a secondary standard.

As a general trend, the molar extinction coefficients are similar between azomethine- and benzothiazole-based model compounds, with higher values in methylene chloride compared to the ones measured in toluene. Remarkably, **M12** and **M18** have QY around 20% – the slight difference between the two values could be due to uncertainties during measurement. **M12** was reported previously, but for health-related applications, such as anti-inflammatory derivative – its opto-electronic properties were not discussed.<sup>27,28</sup> As for **M18**, it was never reported to the best of our knowledge.

**M12** and **M18** were the only model compounds that could be isolated and purified after synthesis. **Figure 21** compares the absorbance spectra of crude and purified compounds.

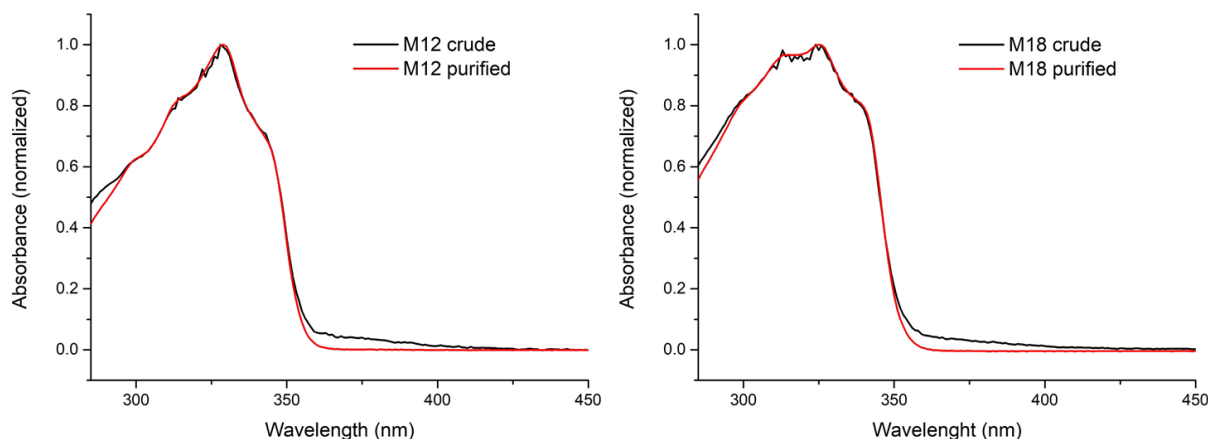


**Figure 21:** Absorbance spectra of **M12** and **M19**, crude and purified, in toluene ( $10^{-2}$  g/L)

For both **M12** and **M18**, the absorbance of the crude and purified compound is similar, with identical local maxima of the vibronic structure – the noisy signal of the crude compounds is due to artefacts from the spectrometer, and does not reflect the sample's behavior. There is a slight shoulder toward higher wavelengths (between 360 and 400 nm) for the crude compound that is not observed for the purified ones. This shoulder could be a sign of aggregates, as it disappears after purification. As the spectra of the purified and crude forms of the molecules have identical local maxima, we can assume that maxima observed in the crude forms are due to the desired model compounds. Therefore, we can compare and use the absorbance spectra of the crude compounds synthesized previously (see **Table 3**) even if it is not possible to conclude definitely as the molecules were not isolated.

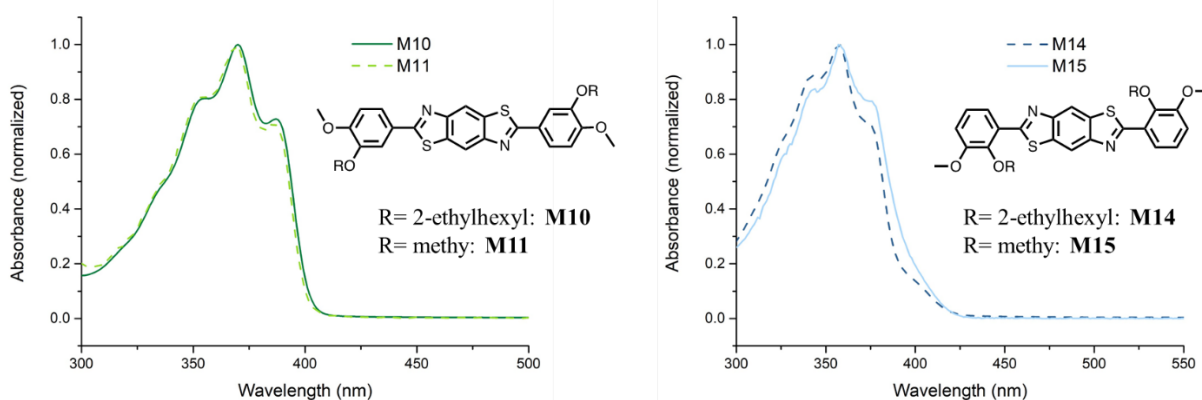


**Figure 22:** Absorbance spectra of BBTz-based model compounds with different alkyl chains (in toluene,  $10^{-2}$  g/L, crude compounds)



**Figure 22** illustrates the effect of the alkyl group on the absorbance of BBTz-based model compounds. The alkyl moiety does not influence the absorbance maxima, for both vanillin and ortho-vanillin based molecules. However, the shape of the absorbance can be impacted. Indeed, the vibronic structure of **M14** at 375 nm does not have the same intensity as the ones of **M15**, whereas there is no difference between the spectra of **M10** and **M11**. These observations are coherent, as the alkyl group is closer to the BBTz moiety in **M14** and **M15**. Therefore, the nature of the alkyl group can affect the vibronic level, as the concerned orbitals are mostly on the BBTz moiety. Meanwhile for **M10** and **M11**, the alkyl group is distant enough that it does not affect the vibronic levels.

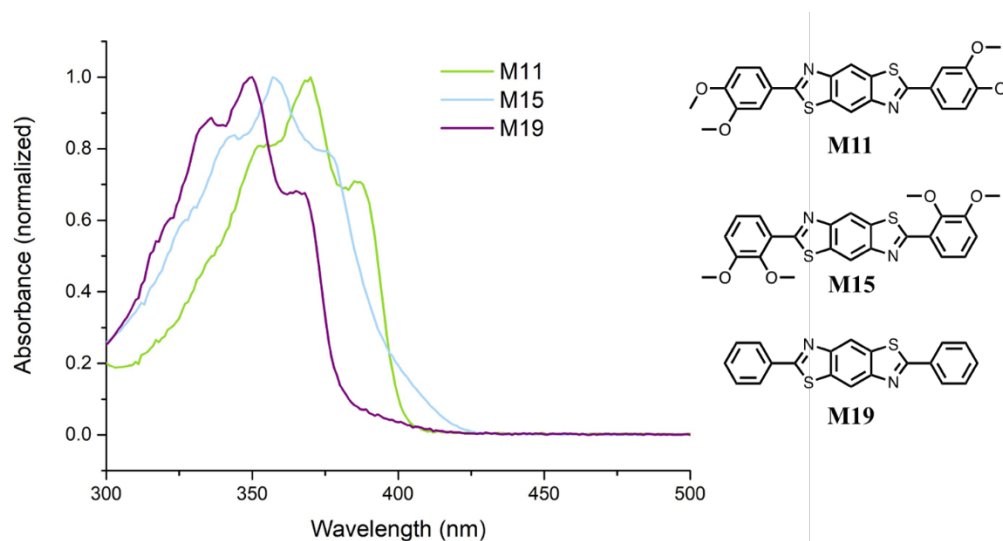


**Figure 23:** Absorbance spectra of crude BBTz-based compounds in toluene ( $10^{-2}$  g/L)

**Figure 23** highlights the impact of the substituent on the absorbance spectra. **M19** has a BBTz moiety and two bare rings, while **M11** and **M15** have additional methoxy functions. As expected, **M19** is the most blue-shifted. Indeed, adding electron donating moiety such as methoxy group is reported to induce bathochromic shift.<sup>29</sup> Interestingly, **M11** is blue shifted compared to **M15**. This bathochromic shift is most likely due to the position of the methoxy group – in **M11** it is in para position with respect to the BBTz moiety and in **M15** it is in ortho position. This effect was also observed for azomethine model compounds.

The absorbance of the BBTz and TTz moieties are compared in **Figure 24**.

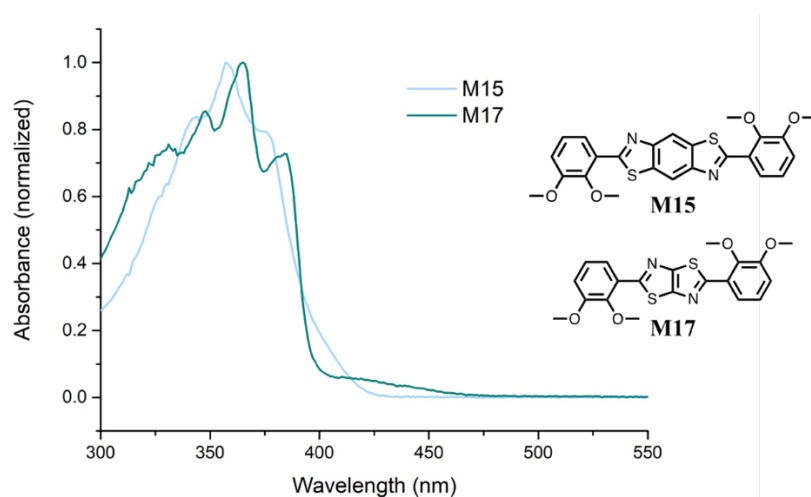


**Figure 24:** Absorbance spectra of crude ortho-Vanillin-based compounds with either BBTz or TTz moiety (in toluene,  $10^{-2}$  g/L)

Interestingly, **M17** is more red-shifted than **M15**, even if it has a smaller conjugation pathway (only two fused rings while **M15** has three). This bathochromic shift is due to the presence of the benzene ring in the BBTz that makes it a weak electron acceptor, while the TTz group is a medium one. The ensuing bathochromic shift is exemplified with polymers represented in **Figure 25**.

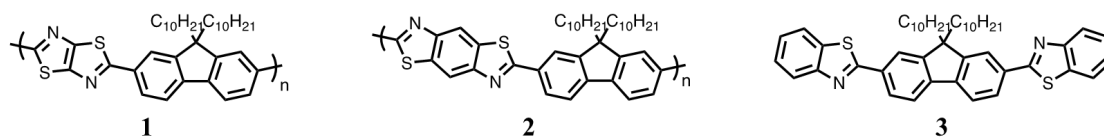


**Figure 25:** TTz- and BBTz-based polymers and model compound (adapted from <sup>7</sup>)

Polymer **1** is red-shifted by 29 nm compared to polymer **2** in solution with respect to the absorbance spectra. As for the fluorescence spectra, there is also a bathochromic shift of 28 nm between **2** and **1**. Interestingly, **1**, **2** have QY around 60% and **3** has a QY of 74%.<sup>7</sup>

The absorbance maxima of the crude compounds in toluene are summarized in **Table 5**.

|                       | Benzobisthiazole   | Benzothiazole                                     | Thiazolothiazole                 |
|-----------------------|--|---|----------------------------------|
| <b>Vanillin</b>       | <br>R= 2-ethylhexyl: <b>M10</b> : 353 - 370 - 386<br>R= methyl: <b>M11</b> : 353 - 370 - 386 | <br><b>M12</b> : 313 - 327 - 343                  | <br><b>M13</b> : ND              |
| <b>Ortho-Vanillin</b> | <br>R= 2-ethylhexyl: <b>M14</b> : 344 - 358 - 376<br>R= methyl: <b>M15</b> : 344 - 358 - 376 | <br><b>M16</b> : 302 - 313 - 328                  | <br><b>M17</b> : 348 - 365 - 385 |
| <b>DiVanillin</b>     | <br>R= 2-ethylhexyl: <b>P17</b><br>R= methyl: <b>P19</b>                                     | <br><b>M18</b> : 313 - 323 - 339                  | <br>R= 2-ethylhexyl: <b>P21</b>  |
|                       | <br><b>M19</b> : 336 - 350 - 366   | <br>R= 2-ethylhexyl: <b>M20</b> : 344 - 358 - 376 |                                  |

**Table 5:** Sum up of the model compounds synthesized with their local absorbance maxima in toluene (in nm), for the crude products ( $10^{-2}$  g/L)

The molecule **M20**, with benzobisoxazole, is blue shifted with respect to its counterpart with a BBTz group, as shown in **Figure 26**. As the oxygen atom is more electronegative than the sulphur one, the  $\pi$  orbitals are more delocalized along the BBTz moiety than along the benzobisoxazole one, leading to a bathochromic shift.

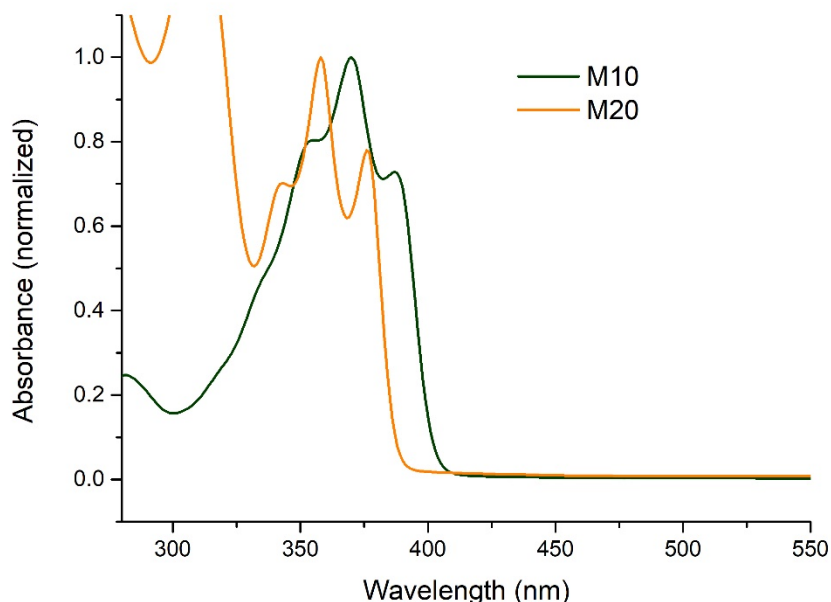


**Figure 26:** Absorbance spectra of crude BBtz and benzobisoxazole compounds in toluene ( $10^{-2}$  g/L)

#### 4.3. Model compounds with benzothiazole and benzobisthiazole: conclusion

A series of BBTz- and TTz-based model compounds were synthesized, using various protocols. However only two could be recrystallized and analyzed by single crystal X-RD. These latter molecules are based on benzothiazole with either vanillin (**M12**) or divanillin (**M18**). The one with divanillin and benzothiazole (**M18**) exhibits efficient  $\pi$  stacking.  $\pi$  stacking can bring interesting properties depending on the applications targeted. Indeed, these strong interactions between molecules or polymer chains can lead to better charge transport, which is fundamental for OFET. However, in the case of OLED  $\pi$  stacking is not desired. Indeed, if the charge transport is too efficient, this phenomenon will be favored instead of production of photons, thus leading to poor fluorescence.<sup>4</sup> In the case of divanillin-based model compounds, this stacking is not along the whole molecule as the bond between the rings of divanillin induces a twist.

Both **M12** and **M18** have a quantum yield of fluorescence in solution around 20%. These relatively high values comfort the idea that the low QY of the TTz-based polymers **P21** (2%) is due to aggregates. The absorbance maxima of the synthesized molecules were compared, as local maxima were identical between pure and purified fractions for **M12** and **M18**.

### 5. Toward Organic Light Emitting Diode

To calculate the HOMO and LUMO energy values of **P21**, the latter underwent cyclic voltammetry analysis. The characterization of HOMO and LUMO is fundamental before integration into OLED, as it drives the choice of the layers' nature for the OLED. The voltammograms of **P21** (oxidation and reduction) are displayed in **Figure 27**.

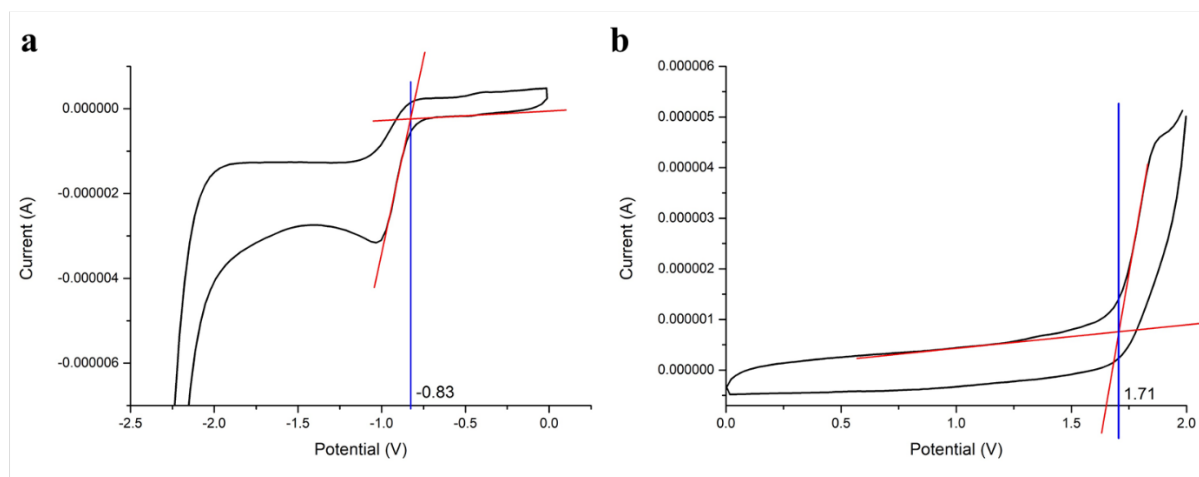


**Figure 27:** Voltammograms of **P21** in solution ( $10^{-2}$  g/L) in methylene chloride with  $\text{TBAPF}_6$  as an electrolyte. **a:** Reduction. **b:** Oxidation.

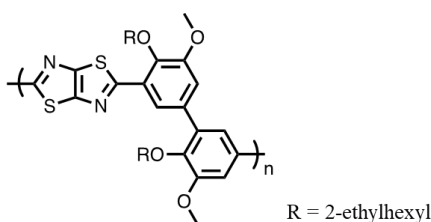
The HOMO and LUMO were then calculated using the **Equations 2 and 3**.

$$E_{HOMO} = -(E_{Onset}(Ox) + 4.8 - E_{Ferrocene})$$

$$E_{LUMO} = -(E_{Onset}(Red) + 4.8 - E_{Ferrocene})$$

**Equations 2 and 3:** Determination of HOMO and LUMO energy using onset of oxidation (ox) and reduction (red) voltammograms.

In the previous equations,  $E_{Onset}$  corresponds to the value obtained in **Figure 27**, by graphically determining the onset of both oxidation and reduction voltammograms. The value of 4.8 eV corresponds to the energy level of ferrocene<sup>30</sup> (in vacuum) – this value is corrected by  $E_{ferrocene}$ , which is the potential of the couple Ferrocene/Ferrocene<sup>+</sup> (0.455 eV) measured using the same conditions as the ones used to analyze **P21**. The HOMO/LUMO levels energy are given in **Table 6**, determined either by cyclic voltammetry or by using the onset of absorbance spectra.



| HOMO (eV) <sup>a</sup> | LUMO (eV) <sup>a</sup> | $E_g^{\text{elec}}$ (eV) <sup>a</sup> | $E_g^{\text{opt. sol}}$ (eV) <sup>b</sup> | $E_g^{\text{opt. Film}}$ (eV) <sup>c</sup> |
|------------------------|------------------------|---------------------------------------|---|--|
| -6.1                   | -3.52                  | 2.54                                  | 2.68                                      | 2.64                                       |

**Table 6:** Electronic and optic determination of HOMO and LUMO values for **P21**. <sup>a</sup> Determined by cyclic voltammetry in solution in methylene chloride with  $\text{TBAPF}_6$  as an electrolyte ( $10^{-2}$  g/L). <sup>b</sup> Determined by using the onset of the absorbance spectrum of **P21** in solution ( $10^{-2}$  g/L). <sup>c</sup> Determined by using the onset of the absorbance spectrum of **P21** in films (drop-casted on quartz)

Cyclic voltammetry and absorbance spectroscopy give similar values for the electronic gaps – the HOMO is at -6.1 eV and the LUMO at -3.52 eV. The slight difference between optical and electrical characterization could be due to experimental uncertainties.<sup>30,31</sup> These values determine the choice of material for the cathode, as schematized in **Figure 28**.

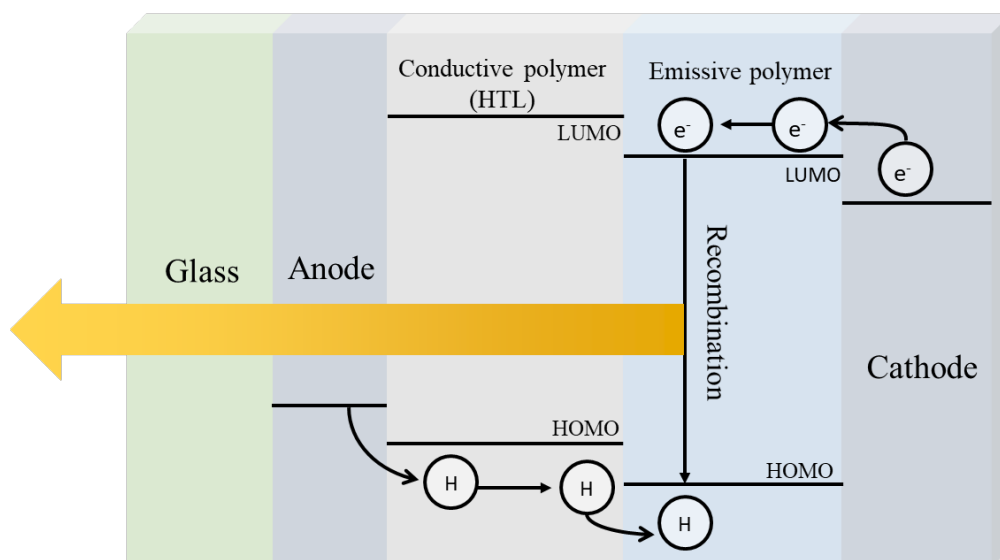


**Figure 28:** General scheme of the working principle of an OLED (HTL: Hole Transport Layer)

The production of light in an OLED is due to the succession of various steps: (i) an electron is injected by the cathode in the emissive polymer – in the meantime a hole is also injected; (ii) both holes and electrons move through the device and (iii) holes and electrons recombine in the emissive polymer layer, giving it energy that is used to produce photons. The hole transport layer enables the transport of holes further from the anode to avoid recombination outside of the emissive polymer layer. The HOMO and LUMO of the various layers have to be close enough to each other to allow efficient travel of holes and electrons. A first structure was tested and is represented in **Figure 29**.

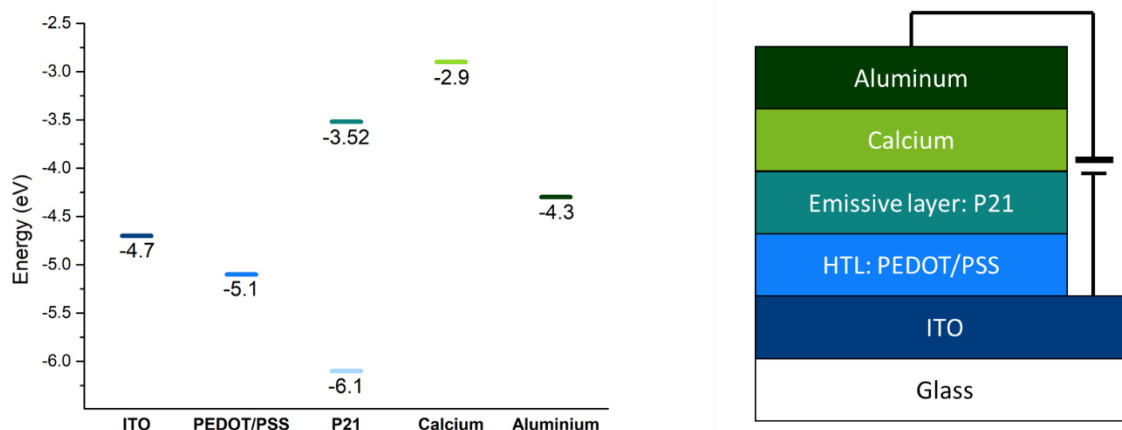


**Figure 29:** Energy levels and structure of the device

Various thicknesses were tested for the layer of **P21**, unfortunately none of the OLED turned on, even at high voltage ( $>15$  V). There are multiple reasons to explain this fail: first, the calcium layer may not be adapted in this case; it is usually used to help electrons to move from the cathode towards the emissive layer, but the work function of calcium may be too high for this structure. Secondly the thickness of the layers is not optimized, and they may be too thin, enhancing the risk of short circuits. Finally, the QY of **P21** is really low. Further tests are needed to improve the thickness and try out new electrodes (with only aluminum for example).

## 6. General conclusion

Divanillin-based polybenzobisthiazoles and polythiazolothiazoles were synthesized and characterized. These former were actually a mixture of oligomers and were therefore set aside – these latter had molar masses up to 4 700 g/mol. Polythiazolothiazoles were synthesized without any catalyst; the synthesis appears to be quite robust and reproducible. The divanillin-based polythiazolothiazole **P21** has an absorbance maximum at 388 nm in solution and, interestingly, a broad emission in films, as illustrated in **Figure 30**.

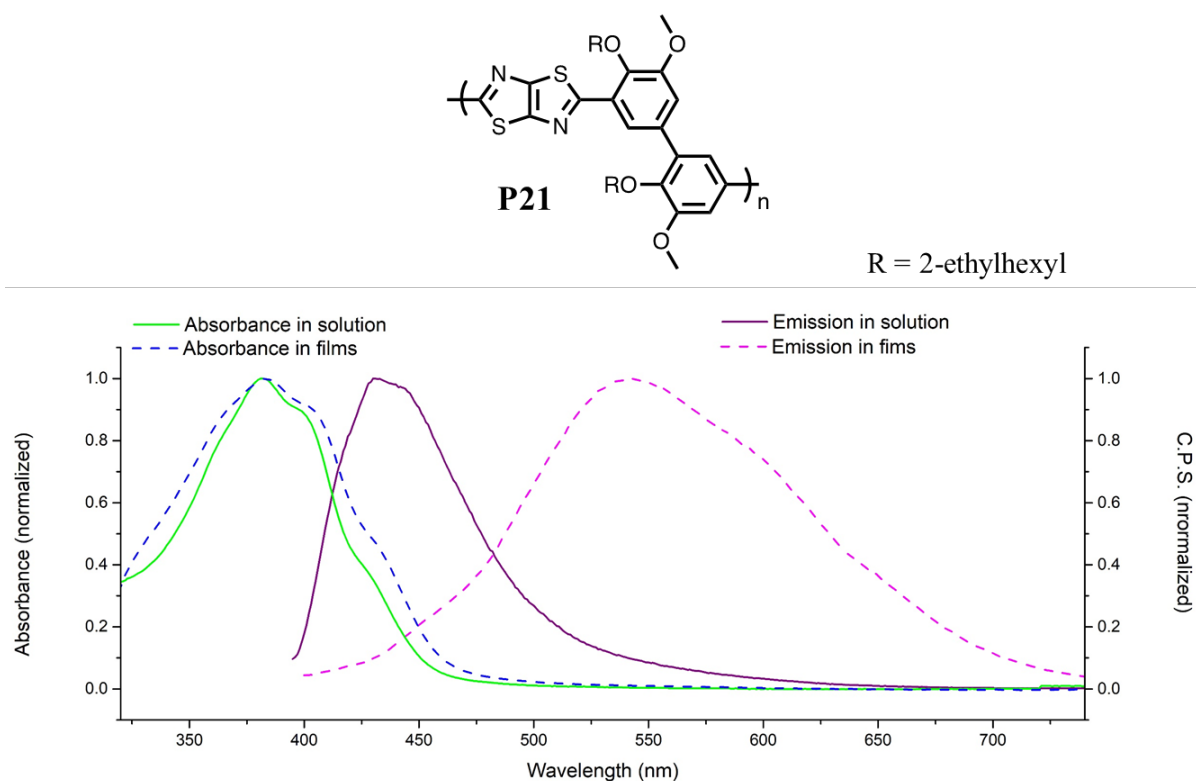


**Figure 30:** Structure and absorbance and emission spectra of **P21** in solution ( $10^{-2}$  g/L for absorbance,  $10^{-4}$  g/L for emission) and in films (drop-casted on quartz plate)

However, **P21** has a poor quantum yield (QY): only 2%, while a QY around 10-20% was expected.<sup>23</sup> This low QY could be due to self-quenching in aggregates, a phenomenon frequently reported.<sup>7</sup> Tests were performed to integrate **P21** in an OLED, but none lit up, possibly because of an unsuitable structure of the layers or because of the too low QY of **P21**.

Model compounds mimicking the backbone of divanillin-based polybenzobisthiazoles and polythiazolothiazoles were synthesized. The analysis of the crude compounds by UV-Vis spectroscopy gave some insights on the impact of the substituents' position, even if it is not possible to conclude clearly as they were not purified. Due to solubility issues, only two of the model compounds were recrystallized and analyzed by X-RD as are represented in **Figure 31**.

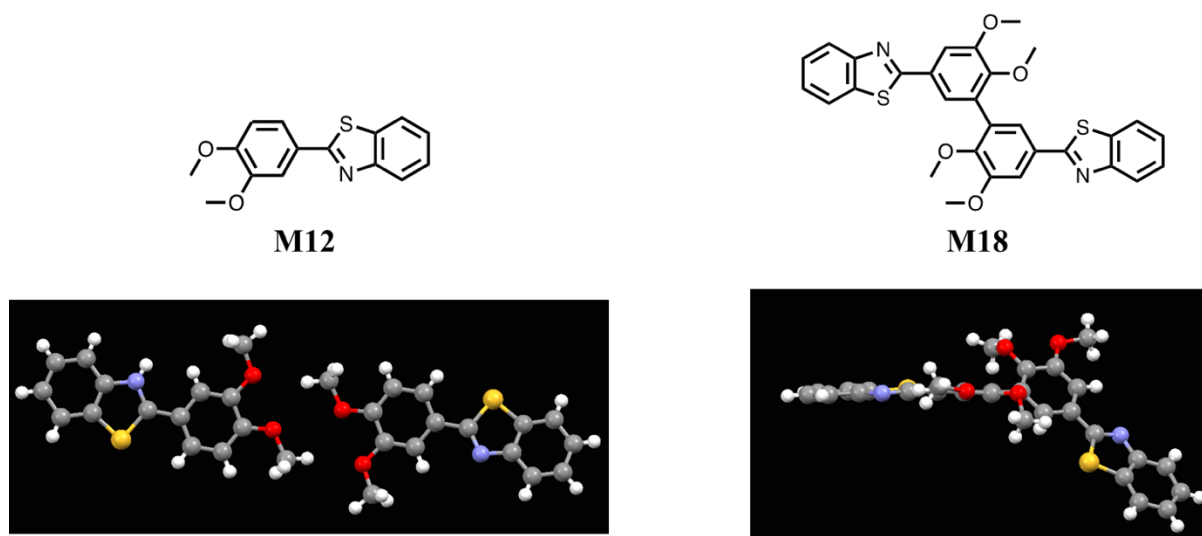


Figure 31: Structures of **M12** and **M18**, solved by X-RD

Both model compounds exhibit a QY of 20% and molecules of **M18** can neatly stack on top of each other. This  $\pi$  stacking is not fully planar, as the torsion angle between aromatics of divanillin induces a twist, as represented in **Figure 32**.

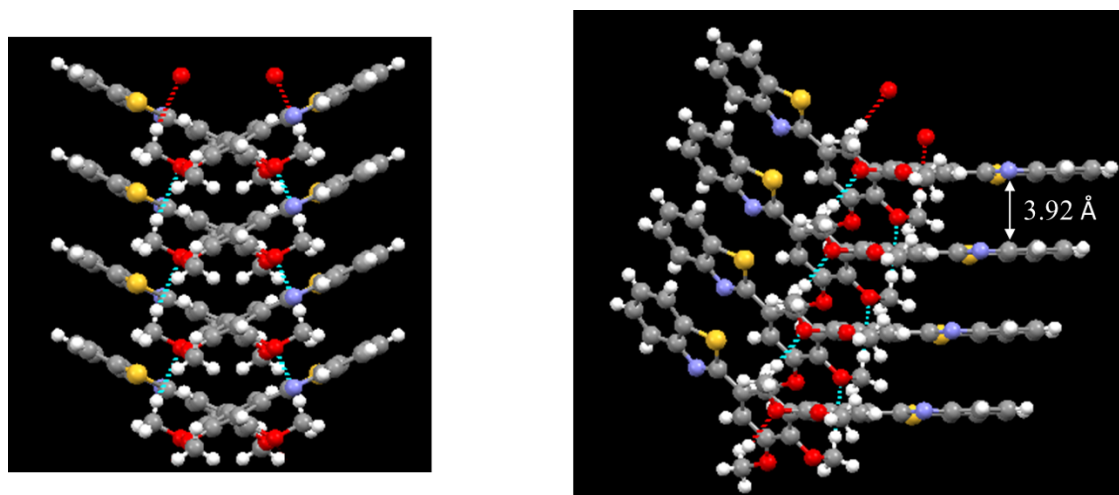


Figure 32: Structure of packed molecules of **M18**, solved by X-RD

These molecules could be used for OLED or OFET devices but first, they need to be synthesized with a longer alkyl moiety to improve their processability.

## 7. References

1. Wolfe, J. F., Loo, B. H. & Arnold, F. E. Rigid-Rod Polymers. 2. Synthesis and Thermal Properties of Para-Aromatic Polymers with 2,6-Benzobisthiazole Units in the Main Chain. *Macromolecules* **14**, 915–920 (1981).
2. Hu, X., Polk, M. B. & Kumar, S. Tetramethylbiphenyl poly(benzobisthiazole): Synthesis, characterization, fiber spinning, and properties. *Macromolecules* **33**, 3342–3348 (2000).
3. Wolfe, J. F. & Arnold, F. E. *Synthesis and Properties of Rodlike Condensation Polymers*. Air Force Wright Aeronautical Laboratories (1978). doi:10.1016/b978-0-12-108650-3.50010-0
4. Lin, Y., Fan, H., Li, Y. & Zhan, X. Thiazole-based organic semiconductors for organic electronics. *Adv. Mater.* **24**, 3087–3106 (2012).
5. Osaheni, J. A. & Jenekhe, S. A. Synthesis and Processing of Heterocyclic Polymers as Electronic, Optoelectronic, and Nonlinear Optical Materials. 1. New Conjugated Rigid-Rod Benzobisthiazole Polymers. *Chem. Mater.* **4**, 1282–1290 (1992).
6. Osaheni, J. A. & Jenekhe, S. A. New Red Light-Emitting Conjugated Rigid-Rod Polymer: Poly (benzobisthiazole-1,4-phenylenebisvinylene). *Macromolecules* **26**, 4726–4728 (1993).
7. Belfield, K. D. *et al.* Synthesis and characterization of novel rigid two-photon absorbing polymers. *Polym. Adv. Technol.* **16**, 150–155 (2005).
8. Garbay, G. Original metal-free synthesis routes of semi-conducting oligomers and (co)polymers for organic electronics. (Université de Bordeaux, 2016).
9. Ahmed, E., Subramaniyan, S., Kim, F. S., Xin, H. & Jenekhe, S. A. Benzobisthiazole-based donor-acceptor copolymer semiconductors for photovoltaic cells and highly stable field-effect transistors. *Macromolecules* **44**, 7207–7219 (2011).
10. Osaka, I., Takimiya, K. & McCullough, R. D. Benzobisthiazole-based semiconducting copolymers showing excellent environmental stability in high-humidity air. *Adv. Mater.* **22**, 4993–4997 (2010).
11. Alam, M. M. & Jenekhe, S. A. Polybenzobisazoles are efficient electron transport materials for improving the performance and stability of polymer light-emitting diodes. *Chem. Mater.* **14**, 4775–4780 (2002).
12. In Hwan Jung, Young Kwan Jung, Jonghee Lee, Jong-Hwa Park, Han Young Woo, Jeong-Ik Lee, Hye Yong Chu, H.-K. S. Synthesis and Electroluminescent Properties of Fluorene-Based Copolymers Containing Electron-Withdrawing Thiazole Derivatives. *J. Polym. Sci.* **46**, 7148–7161 (2008).
13. Mishra, S. P. *et al.* Highly air-stable thieno[3,2-b]thiophene-Thiophene-Thiazolo[5,4-d]thiazole-based polymers for light-emitting diodes. *Macromol. Chem. Phys.* **211**, 1890–1899 (2010).
14. Peng, Q., Peng, J. B., Kang, E. T., Neoh, K. G. & Cao, Y. Synthesis and electroluminescent properties of copolymers based on fluorene and 2,5-Di(2-hexyloxyphenyl)thiazolothiazole. *Macromolecules* **38**, 7292–7298 (2005).
15. Osaka, I., Sauv e, G., Zhang, R., Kowalewski, T. & McCullough, R. D. Novel thiophene-thiazolothiazole copolymers for organic field-effect transistors. *Adv. Mater.* **19**, 4160–4165 (2007).
16. Bujak, P. *et al.* Polymers for electronics and spintronics. *Chem. Soc. Rev.* **42**, 8895 (2013).
17. Dessi, A. *et al.* Organic Chromophores Based on a Fused Bis-Thiazole Core and Their



- Application in Dye-Sensitized Solar Cells. 1916–1928 (2013). doi:10.1002/ejoc.201201629
18. Wakioka, M., Ishiki, S. & Ozawa, F. Synthesis of Donor-Acceptor Polymers Containing Thiazolo[5,4-d]thiazole Units via Palladium-Catalyzed Direct Arylation Polymerization. *Macromolecules* **48**, 8382–8388 (2015).
  19. Zhang, Z. *et al.* Control of the Reversibility of Excited-State Intramolecular Proton Transfer (ESIPT) Reaction: Host-Polarity Tuning White Organic Light Emitting Diode on a New Thiazolo[5,4-d]thiazole ESIPT System. *Chem. Mater.* **28**, 8815–8824 (2016).
  20. Ahmed, E., Kim, F. S., Xin, H. & Jenekhe, S. A. Benzobisthiazole - Thiophene copolymer semiconductors: synthesis, enhanced stability, field-effect transistors, and efficient solar cells. *Macromolecules* **42**, 8615–8618 (2009).
  21. Subramaniyan, S. *et al.* Thiazolothiazole donor-acceptor conjugated polymer semiconductors for photovoltaic applications. *Macromolecules* **47**, 4199–4209 (2014).
  22. Würth, C., Grabolle, M., Pauli, J., Spieles, M. & Resch-Genger, U. Relative and absolute determination of fluorescence quantum yields of transparent samples. *Nat. Protoc.* **8**, 1535–1550 (2013).
  23. Pinto, M. R., Takahata, Y. & Atvars, T. D. Z. Photophysical properties of 2,5-diphenylthiazolo[5,4-d]thiazole. *J. Photochem. Photobiol. A Chem.* **143**, 119–127 (2001).
  24. Wang, K. *et al.* Multicolor fluorescence and electroluminescence of an ICT-type organic solid tuned by modulating the accepting nature of the central core. *Chem. Sci.* **4**, 3288–3293 (2013).
  25. Patil, M. A., Ubale, P. A., Karhale, S. S. & Helavi, V. B. Lemon Juice : An Environmentally Benign Catalyst for Synthesis of Benzothiazoles and Benzoxazole Derivatives in Aqueous Medium. **8**, 198–205 (2017).
  26. Dessì, A. *et al.* Microwave-activated synthesis of thiazolo[5,4-d]thiazoles by a condensation/oxidation sequence. *RSC Adv.* **4**, 1322–1328 (2014).
  27. Mortimer, C. G. *et al.* Antitumor benzothiazoles. 26.1 2-(3,4-dimethoxyphenyl)-5-fluorobenzothiazole (GW 610, NSC 721648), a simple fluorinated 2-arylbenzothiazole, shows potent and selective inhibitory activity against lung, colon, and breast cancer cell lines. *J. Med. Chem.* **49**, 179–185 (2006).
  28. Kim, Y. M., Kim, H., You, S. & Yim, D. IMMUNOSUPPRESSIVE COMPOUNDS. (2014).
  29. Muroph, H. Studies on UV/VIS absorption spectra of azo dyes. Part 26.\* Electronic Absorption Spectra of 4, 4'- Diaminoazobenzene. *Dye. Pigment.* **16**, 223–230 (1991).
  30. Cardona, C. M., Li, W., Kaifer, A. E., Stockdale, D. & Bazan, G. C. Electrochemical considerations for determining absolute frontier orbital energy levels of conjugated polymers for solar cell applications. *Adv. Mater.* **23**, 2367–2371 (2011).
  31. Viezbicke, B. D., Patel, S., Davis, B. E. & Birnie, D. P. Evaluation of the Tauc method for optical absorption edge determination: ZnO thin films as a model system. *Phys. Status Solidi Basic Res.* **252**, 1700–1710 (2015).

## 8. Experimental part

|   |     |
|---|-----|
| <b>8.1. General</b> .....   | 213 |
| <b>8.2. Characterization</b> .....                                | 213 |
| <b>8.3. Synthesis and characterization of polymers</b> .....      | 215 |
| 8.3.1. Characterization of <b>P21</b> .....                       | 215 |
| <b>8.4. Synthesis of model compounds</b> .....                    | 216 |
| 8.4.1. General protocol for the synthesis of model compounds..... | 216 |
| 8.4.2. Synthesis and characterization of <b>M12</b> .....         | 217 |
| 8.4.3. Synthesis and characterization of <b>M18</b> .....         | 218 |

### 8.1. General

Ortho-vanillin was graciously provided by Solvay. Vanillin (>97%), 2-aminothiophenol (>99%), polyphosphoric acid, Eaton's reagent and 4,6-diaminoresorcinol dihydrochloride were obtained from Sigma-Aldrich. 2,5-diamino-1,4-benzenedithiol dihydrochloride (>97%) was purchased from TCI. Silica gel (pore size 60 Å, 230-400 mesh particle size, particle size 40-63 µm) was obtained from Honeywell Fluka. Dithiooxamide was obtained from Acros Organics. All products and solvents (reagent grade) were used as received except otherwise mentioned. The solvents were of reagent grade quality and were purified whenever necessary according to the methods reported in the literature. For the emission and absorbance measurements, methylene chloride with spectroscopy grade from Sigma was used. Flash chromatography was performed on a Grace Reveleris apparatus, employing silica cartridges from Grace. Cyclohexane: ethyl acetate gradients and methylene chloride were used as eluents. The detection was performed through ELSD and UV detectors at 254 nm and 280 nm. The reactions under microwave irradiation were performed on a Discover-SP from CEM, with the temperature measured by infrared; the power of the apparatus is constantly adjusted to reach and then stay at the set temperature.

### 8.2. Characterization

$^1\text{H}$ ,  $^{13}\text{C}$  and  $^1\text{H}$ - $^{13}\text{C}$  HSQC NMR measurements were performed with a Bruker Avance 400 spectrometer (400.20 MHz and 100.7 MHz for  $^1\text{H}$  and  $^{13}\text{C}$ , respectively) at room temperature using deuterated solvent.

IR spectra were recorded with Bruker Tensor 27 spectrometer using a 0.6 mm-diameter beam. Samples were analyzed with the attenuated total reflection (ATR) method.

Mass spectra were performed by the CESAMO (Bordeaux, France) on a Qexactive mass spectrometer (Thermo). The instrument is equipped with an ESI source and spectra were recorded in the positive mode. The spray voltage was maintained at 3200 V and capillary temperature set at 320°C. Samples were introduced by injection through a 20 µL sample loop into a 300 µL/min flow of methanol from the LC pump.

Optical absorption spectra were obtained with a UV-visible spectrophotometer (UV-3600, Shimadzu). Photoluminescence spectra were obtained from a spectrofluorometer (Fluoromax-4, Horiba Scientific). In both cases, solvent of spectroscopic grade were used (from Sigma).

Quantum yield measurements were done by using the previously named spectrofluorometer and quinine sulfate as a secondary standard. A solution of quinine in 0.1M sulphuric acid was prepared and its

absorbance measured. The sample to be analyzed was dissolved in spectroscopic grade methylene chloride, and its absorbance measured too. The intersection of the two spectra was used as excitation wavelength, as is illustrated in **Figure 33**.

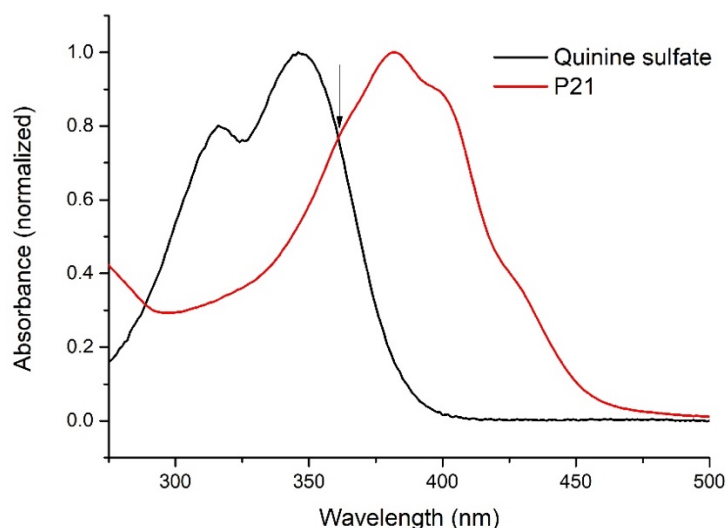


**Figure 33:** Absorbance spectra of **P21** (in methylene chloride) and quinine sulfate (in 0.1M sulphuric acid) (both at  $10^{-2}$  g/L)

Various solutions of the standard and the sample were then prepared with absorbance ranging from 0.1 to 0.01 and their emission spectrum measured at the excitation wavelength determined previously. Both slits were set appropriately to avoid saturation of the detector. The area under the emission curve was calculated for all spectra and it was plotted against the absorbance. The straight line obtained has a gradient noted  $Grad(x)$  for the sample and  $Grad(st)$  for the standard – with respect to notation in this section, “x” refers to the sample and “st” to the standard. Finally, the following equation was applied:

$$QY(x) = QY(st) * \frac{Grad(x)}{Grad(st)} * \frac{n(x)^2}{n(st)^2}$$

Where QY is the quantum yield and n is the refractive index of the solvents used.

Molar masses of polymers were determined by size exclusion chromatography (SEC) using a three-column set of Resipore Agilent: one guard column Resipore Agilent PL1113-1300, then two columns Resipore Agilent PL1113-6300, connected in series, and calibrated with narrow polystyrene standards from polymer Laboratories using both refractometric (GPS 2155) and UV detectors (Viscotek). THF was used as eluent (0.8 mL/min) and trichlorobenzene as a flow marker (0.15 %) at 30°C.

TGA have been performed on a TA-Q50, from 25°C to 750°C with a heating of 10°C/min under nitrogen flow.

Electrochemical measurements and HOMO-LUMO calculation were performed in solution. A solution of 0.1 g.L<sup>-1</sup> of the investigated polymer in CH<sub>2</sub>Cl<sub>2</sub> with 0.1 M tetrabutylammonium hexafluorophosphate (TBAPF<sub>6</sub>) as electrolyte was prepared. Cyclic voltammetry measurements were then performed on the solution using silver wire as reference electrode and platinum for the working and counter electrodes. A solution of ferrocene (1 mM in the same solvent) was prepared in the same conditions and the redox potential of Fc/Fc<sup>+</sup> vs Ag (EFc/Fc<sup>+</sup> Ag) was measured, to be used as a reference for calibration. All solutions were bubbled with nitrogen before analysis.

Diffraction data from a single crystal of the different model compounds were measured at the IECB (Bordeaux, France) on a 3 kW microfocus Rigaku FRX rotating anode. The source is equipped with

high flux Osmic Varimax HF mirrors and a hybrid Dectris Pilatus 200 K detector. The source is operating at the copper  $\kappa\alpha$  wavelength with a partial chi goniometer that decreases blind areas and enables automatic axial adjustment. Data were processed with the CrysAlisPro suite version 1.171.38.43.<sup>1</sup> Empirical absorption correction using spherical harmonics, implemented in SCALE3 ABSPACK scaling algorithm was used.

The structure was solved with Shelxt<sup>2</sup> and refined by full-matrix least-squares method on F<sup>2</sup> with Shelxl-2014<sup>2</sup> within Olex2.<sup>3</sup> For all atoms, anisotropic atomic parameters were used. Hydrogen atoms were placed at idealized positions and refined as riding on their carriers with Uiso(H) = 1.2 Ueq (CH, CH<sub>2</sub>, NH) and Uiso(H) = 1.5 Ueq(CH<sub>3</sub>). DFIX and AFIX instructions were used to improve the geometry of molecules and RIGU to model atomic displacement parameters. Disordered solvent molecules were removed using the SQUEEZE procedure from the PLATON suite.<sup>4</sup> For search and analysis of solvent accessible voids in the structures default parameters were utilized: grid 0.20 Å, probe radius 1.2 Å and NStep 6. Calculated total potential solvent accessible void volumes and electron counts per unit cell are given in the CIF files that were checked using IUCR's checkcif algorithm. Due to the characteristics of the crystals, i.e. large volume fractions of disordered solvent molecules, weak diffraction intensity and moderate resolution, few A-level and B-level alerts remain in the check cif file. These alerts are inherent to the data and refinement procedures and do not reflect errors on the model refined.

<sup>1</sup> CrysAlisPRO : CrysAlisPRO, Oxford Diffraction /Agilent Technologies UK Ltd, Yarnton, England.

<sup>2</sup> Sheldrick, G. M. (2015). *Acta Cryst.* A71, 3-8.

<sup>3</sup> OLEX2: O. V. Dolomanov, L. J. Bourhis, R. J. Gildea, J. A. K. Howard and H. Puschmann. *J. Appl. Cryst.* (2009). 42, 339-341.

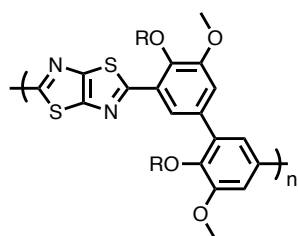
<sup>4</sup> Spek, A. L. (2009). *Acta Cryst.* D65, 148-155.

The OLED were characterized using an External Quantum Efficiency Measurement System C9920-12 from Hamamatsu Photonics.

### 8.3. Synthesis and characterization of polymers

#### 8.3.1. Characterization of P21

Poly(6,6'-(2-ethylhexoxy)-5,5'-dimethoxy-[1,1'-biphenyl]-3,3'-[1,3]Thiazolo[4,5-d][1,3]thiazole)



In a flamed and dried flask, stoichiometric amount of **DVEH** (see Experimental part of Chapter II/ for the synthesis of **DVEH**) and dithiooxamide were dispersed in 30 mL of dry DMSO. The mixture was then heated at the reflux for 40 hours. The crude mixture was then cooled down and poured in methanol, where it precipitates. The brownish powder obtained was then rinsed with methanol and extensively dried.

<sup>1</sup>H-NMR (400.2 Hz, CDCl<sub>3</sub>): 9.89 (s, 1H); 7.68-7.44 (m, 18H); 4.01 – 3.93 (m, 28H); 3.85 – 3.54 (m, 56H); 1.66 – 1.52 (broad s, 10H); 1.41 – 0.48 (m, 182H).

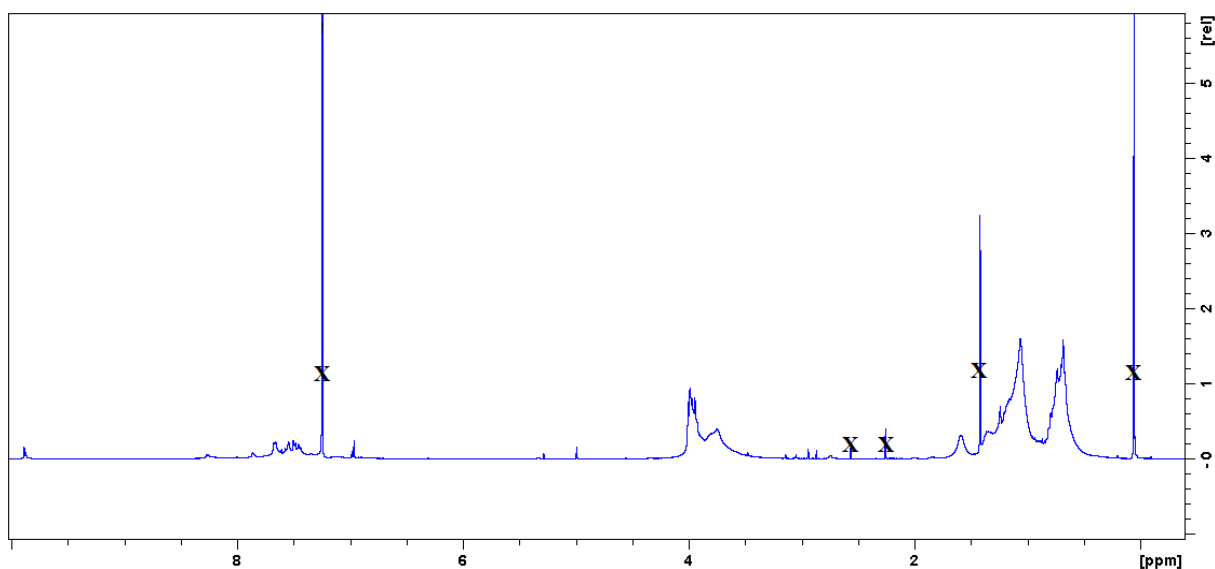


Figure 34:  $^1\text{H-NMR}$  spectrum of **P21** (400.20 MHz, in  $\text{CDCl}_3$ , 128 scans)

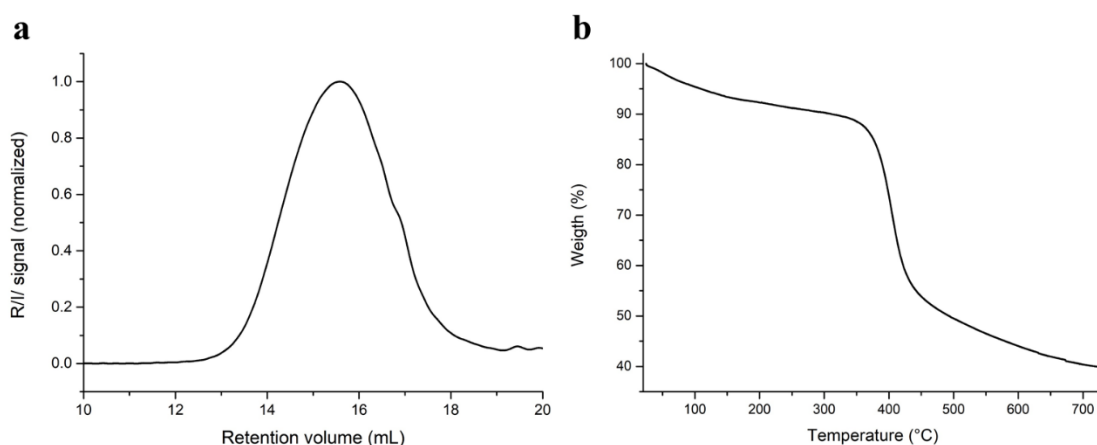


Figure 35a: SEC trace of **P21** in THF, R. I. detection. **b**: TGA curve of **P21** at  $10^\circ\text{C}/\text{min}$  under  $\text{N}_2$

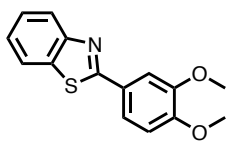
## 8.4. Synthesis of model compounds

### 8.4.1. General protocol for the synthesis of model compounds

In a microwave vial equipped with stirrer, the vanillin or divanillin derivative (2 or 1 eq.) was dissolved with either 2-aminothiophenol (1 eq.), or dithioamide (1 eq.), or 2, 5 diamino-1, 4- benzenedithiol dihydrochloride (1 eq.) in toluene, with silica. The reaction was performed under microwave irradiation, at  $130^\circ\text{C}$  for 4 h, the reaction was monitored by absorbance spectroscopy. The crude product was filtered to remove silica. The final product was obtained after recrystallization from warm methanol/methylene chloride.

8.4.2. Synthesis and characterization of **M12**

## 2-(3, 4-dimethoxyphenyl)benzo[d]thiazole



In a microwave vial equipped with stirrer, methylated vanillin (1 eq.) was dissolved with 2-aminothiophenol (1 eq.) in toluene, with silica. The reaction was performed under microwave irradiation, at 130°C for 4 h. The crude product was filtered to remove silica. The final product was obtained after recrystallization from warm methanol/methylene chloride. Yield : 70%

$^1\text{H-NMR}$  (400.20 MHz,  $\text{CD}_2\text{Cl}_2$ )  $\delta$  (ppm): 8-7.98 (m, 1H); 7.91-1.89 (m, 1H); 7.70-7.69 (m, 1H); 7.62-7.60 (m, 1H); 7.50-7.46 (m, 1H); 7.39-7.35 (m, 1H); 6.96-6.94 (m, 1H); 3.96 (s, 3H); 3.90 (s, 3H).  $^{13}\text{C-NMR}$  (400 MHz,  $\text{CD}_2\text{Cl}_2$ )  $\delta$  (ppm): 168.2; 154.6; 152.2; 149.9; 135.4; 126.9; 126.6; 111.6; 110.3; 56.4; 56.3.

**X-Ray Diffraction data**

Space group:  $\text{Pna}2_1$  (orthorhombic)

Cell length ( $\text{\AA}$ ): **a** 26.7728; **b** 11.7154; **c** 8.40190.

Cell angles:  $\alpha$  90;  $\beta$  90;  $\gamma$  90.

Cell volume ( $\text{\AA}^3$ ): 2635.29

R factor: 4.44 %

Symmetry:  $-x, -y, \frac{1}{2}+z$ ;  $\frac{1}{2}+x, \frac{1}{2}-y, z$ ;  $\frac{1}{2}-x, \frac{1}{2}+y, \frac{1}{2}+z$ .

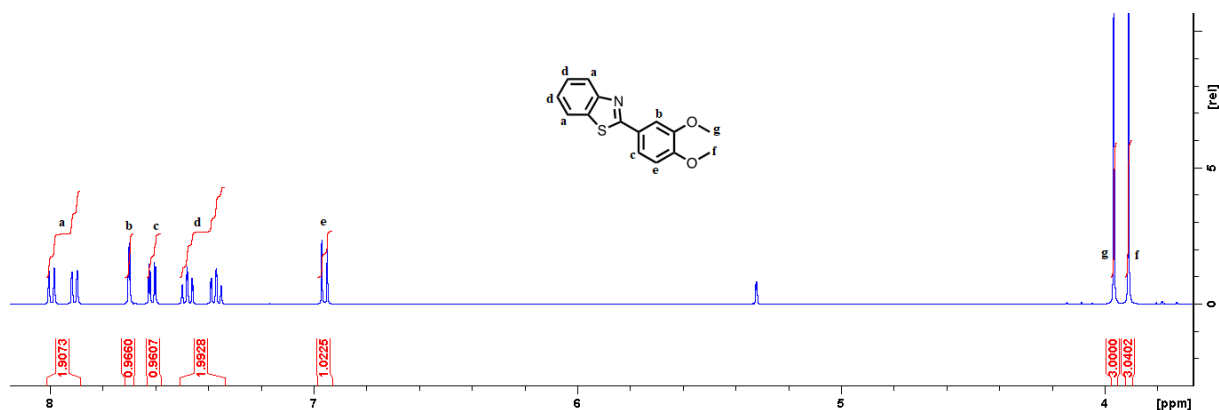


Figure 36:  $^1\text{H-NMR}$  spectrum of **M12** (400.20 MHz, in  $\text{CD}_2\text{Cl}_2$ )

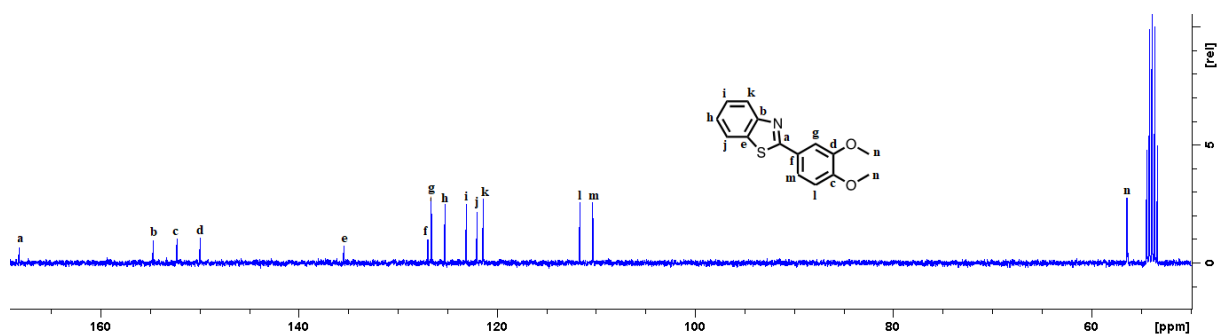
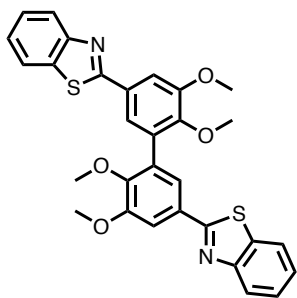


Figure 37:  $^{13}\text{C-NMR}$  spectrum of **M12** (100.70 MHz, in  $\text{CD}_2\text{Cl}_2$ )

8.4.3. Synthesis and characterization of **M18**

## 2, 2', 3, 3'-(tetramethoxy)[1,1'-biphenyl]-5,5'-bis(benzothiazole)

In a flame-dried flask equipped with stirrer and condenser, methylated divanillin (1 eq.) was dissolved with 2-aminothiophenol (2 eq.) in DMSO, under inert atmosphere. The resulting solution was heated at the reflux using conventional heating for 4 h and left to cool back to room temperature. The product precipitated and was recovered by filtration. It was dissolved in hot DMSO, then cooled down with a plateau at 60°C - if the cooling is too harsh, the product will precipitate. Yield: 80%

$^1\text{H-NMR}$  (400.20 MHz,  $\text{CD}_2\text{Cl}_2$ )  $\delta$  (ppm): 8.03-8.02 (m, 2H); 7.93-7.91 (m, 2H); 7.82 (m, 2H); 7.60 (m, 2H); 7.52-7.48 (t,  $J = 8\text{Hz}$ , 2H); 7.41-7.37 (t,  $J = 8\text{Hz}$ , 2H); 4.06 (s, 6H); 3.78 (s, 6H).  $^{13}\text{C-NMR}$  (400 MHz,  $\text{CD}_2\text{Cl}_2$ )  $\delta$  (ppm): 167.8; 154.6; 153.6; 149.9; 135.6; 132.9; 129.4; 126.7; 125.5; 123.3; 123.0; 122.1; 111.0; 61.1; 56.5.

**X-Ray Diffraction data**

Space group:  $C2/c$  (monoclinic)

Cell length ( $\text{\AA}$ ): **a** 26.9192; **b** 3.9227; **c** 24.4235.

Cell angles:  $\alpha$  90;  $\beta$  105.54;  $\gamma$  90.

Cell volume ( $\text{\AA}^3$ ): 2484.75

R factor: 6.41 %

Symmetry:  $-x, y, \frac{1}{2}-z; \frac{1}{2}+x, \frac{1}{2}+y, z; \frac{1}{2}-x, \frac{1}{2}+y, \frac{1}{2}-z; -x, -y, -z; x, -y, \frac{1}{2}+z; \frac{1}{2}-x, \frac{1}{2}-y, -z; \frac{1}{2}+x, \frac{1}{2}-y, \frac{1}{2}+z.$

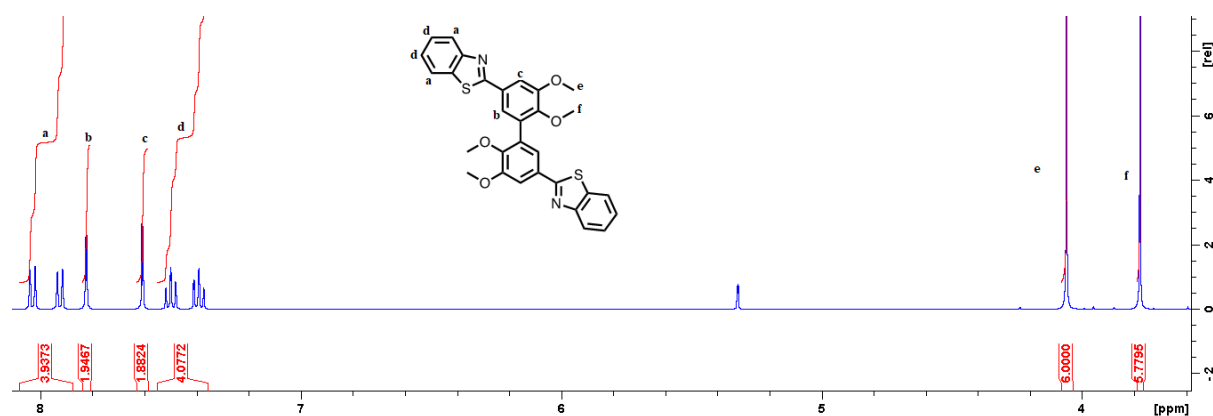


**Figure 38:**  $^1\text{H-NMR}$  spectrum of **M18** (400.20 MHz, in  $\text{CD}_2\text{Cl}_2$ )

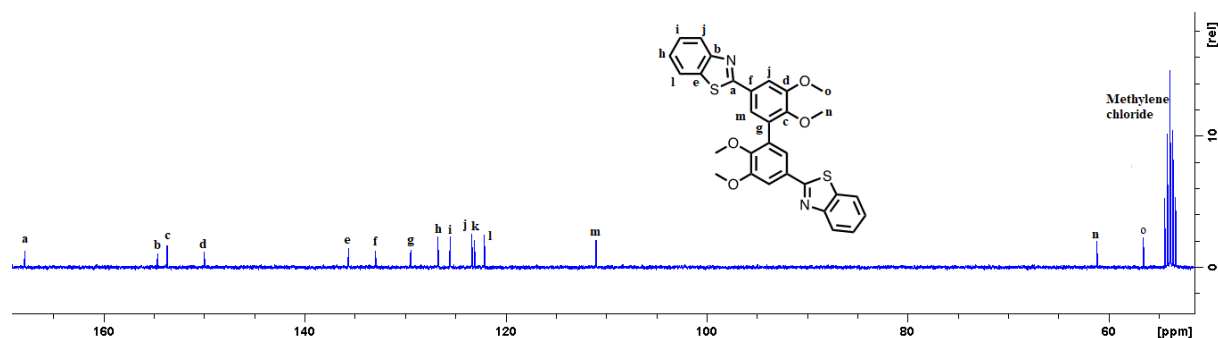


**Figure 39:**  $^{13}\text{C-NMR}$  spectrum of **M18** (100.70 MHz, in  $\text{CD}_2\text{Cl}_2$ )

### 8.5. Fabrication of OLED

A 15mm\*15mm slide of ITO-coated glass was treated with UV-ozone for 5 minutes, and immediately spin-coated with a solution of PEDOT/PSS Clevios 1000 (5% DMSO, 0.04% zonyl) at 1500 rpm during 30 seconds and annealed 10 minutes at 120°C. Solutions of **P21** in chloroform were then spin-coated with various thicknesses, and annealed at 120°C for 10 minutes. 50 nm of calcium and 100 nm of aluminum were then deposited by thermal evaporation, using the mask represented in **Figure 40**.

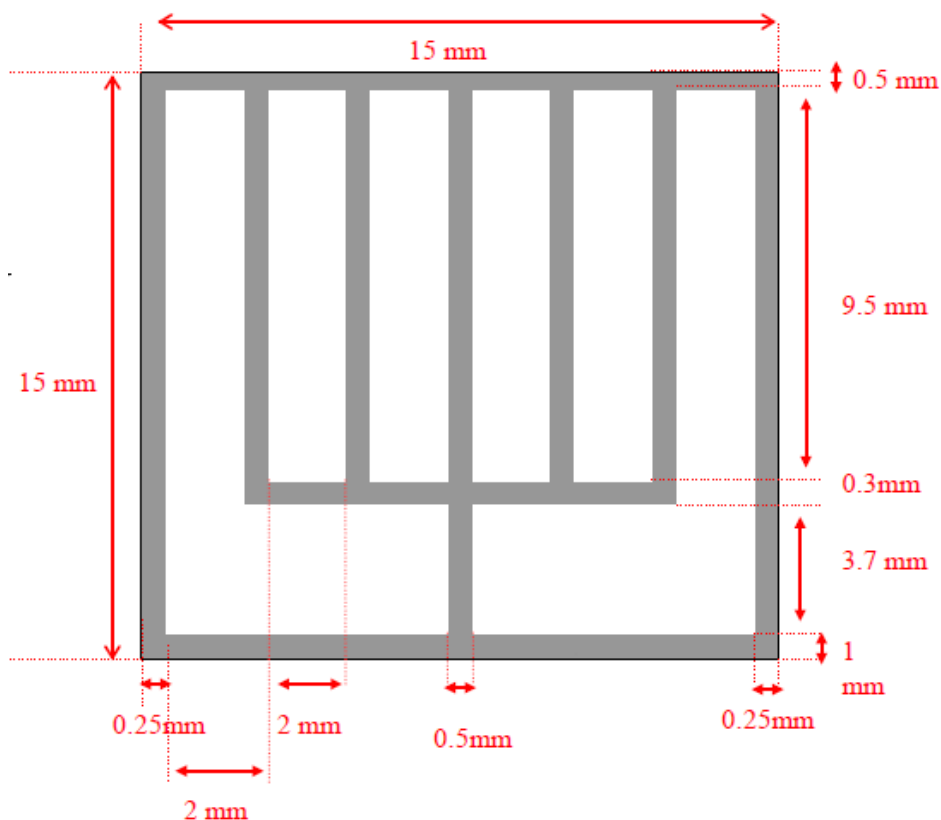


**Figure 40:** Lay-out of the mask used for thermal evaporation





## General Conclusion and Perspectives

The aim of this PhD was to investigate the synthesis of bio-based conjugated polymers with physico-chemical properties valuable for organic electronic applications. The selected building block of the targeted polymers was vanillin. Indeed, not only the latter can be industrially produced from lignocellulosic biomass but it can also be easily and efficiently dimerized, yielding a bis-aldehyde and biphenyl substrate prone to polymerization.<sup>1</sup>

First, divanillin-based polyazomethines were synthesized, *via* polycondensation of divanillin and various diamines. The only by-product is water and no metallic catalysts are required. The experimental protocol was improved: from 4 hours using micro-wave irradiation and silica as a desiccant to only 5 minutes, without silica. Interestingly, the key step is actually the recovery step during which solvents are removed using a rotary evaporator, leading to a dramatic increase of the polyazomethines molar masses. As for the optical properties, the absorbance maximum can be tuned from 325 to 388 nm by changing the diamine. However, the polyazomethines were weakly fluorescent (so much so that no quantum yield could be measured). Indeed, azomethine bond are known to quench fluorescence.<sup>2</sup> Therefore, a perspective for this family of polyazomethines would be to investigate their fluorescence after doping, either by using an acid or by lowering the temperature.<sup>3</sup> If the polyazomethines' fluorescence is sensitive enough to acids, the former could be used as sensors.<sup>4</sup> Investigation on model compounds gave some insights on the structural behavior of vanillin- and ortho-vanillin-based azomethines, namely the angle between the azomethine bond and the aromatic ring together with the torsion angle between the two aromatic rings of divanillin. The absorbance spectra of model compounds also showed that divanillin-based polyazomethines are not fully conjugated due to the meta bond between aromatic rings of divanillin, as illustrated in **Figure 1**.

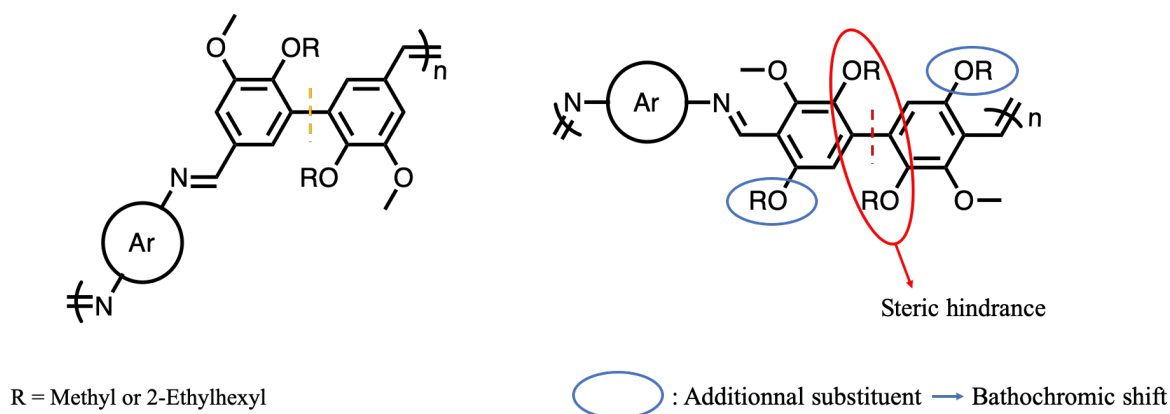


**Figure 1:** General structure of divanillin- (left) and paradivanillin-based (right) polyazomethines, with the break of conjugation represented.

To improve the conjugated pathway of divanillin, the latter was derivatized to obtain a compound with aldehyde in para positions with respect to the link between aromatics, as represented in **Figure 1** – to the best of our knowledge, this molecule was never reported previously. This “para-divanillin” was obtained in three steps: i) a Dakin oxidation, followed by ii) alkylation of the hydroxy functions and finally iii) formylation by metalation. This strategy could be applied to obtain various compounds starting from divanillin, by simply changing the function added at the end: diamines could be obtained for example. This “para-divanillin” then underwent polymerization to yield polyazomethines. The polyazomethines obtained were red shifted in comparison to their homologues with divanillin. However, this bathochromic shift was actually due to the presence of an additional alkoxy group, as is highlighted in **Figure 1**. Investigations on model compounds of paradivanillin revealed that the latter is actually extremely twisted, due to steric hindrance: the two aromatic rings are nearly perpendicular to each other, preventing orbitals overlap and therefore effective conjugation. Moreover, para-divanillin-based

polyazomethines were less soluble than their divanillin-based homologues, possibly because of the aforementioned twisting. Para-divanillin could be used to stop conjugation at definite position – however the comonomer should be chosen carefully to prevent solubility issues.

Finally, a new strategy was chosen to synthesize polymers with better opto-electronics properties, notably fluorescence. Divanillin was integrated in polythiazolothiazoles, as the former's short conjugated pathway could be beneficial to the latter: polythiazolothiazoles tend to be insoluble, something that could be prevented with divanillin. Indeed, the divanillin-based polythiazolothiazole (**Figure 2**) synthesized was soluble in common solvents.

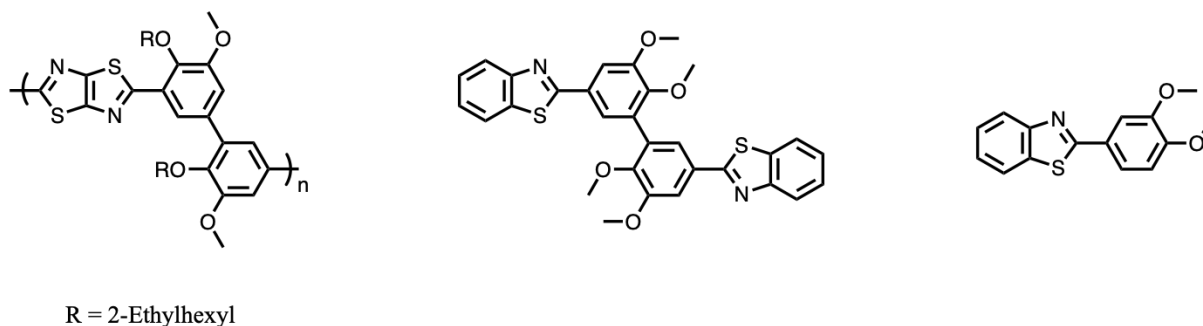


**Figure 2:** Structures of divanillin-based polythiazolothiazole and benzothiazole-based model compounds

The divanillin-based polythiazolothiazole has a maximum of absorbance at 383 nm in solution, with well-defined vibronic structure. Interestingly this polymer has a narrow emission in the blue range in solution, and a larger one in the yellow range in films. However, it has a low quantum yield (2% in solution), possibly due to self-quenching in aggregates. Still, by a careful choice of the structure of the device, it could be incorporated in OLED for example. Benzothiazole-based model compounds were also synthesized and characterized (**Figure 2**). The latter both exhibit a quantum yield of 20% and the divanillin-based one exhibited some  $\pi$  stacking. This  $\pi$  stacking is not along the whole molecule, due to the torsion of divanillin. The  $\pi$  stacking could be used in devices requiring charge transfer such as OFET or OPV. Both model compounds could be alkylated to make them more processable and lessen the  $\pi$  stacking, to integrate them in OLED for example.

**References:**

1. Llevot, A., Grau, E., Carlotti, S., Grelier, S. & Cramail, H. Selective laccase-catalyzed dimerization of phenolic compounds derived from lignin: Towards original symmetrical bio-based (bis) aromatic monomers. *J. Mol. Catal. B Enzym.* **125**, 34–41 (2016).
2. Mallet, C., Bolduc, A., Bishop, S., Gautier, Y. & Skene, W. G. Unusually high fluorescence quantum yield of a homopolyfluorenylazomethine – towards a universal fluorophore. *Phys. Chem. Chem. Phys.* **16**, 24382–24390 (2014).
3. Barik, S., Bletzacker, T. & Skene, W. G.  $\pi$ -Conjugated fluorescent azomethine copolymers: Opto-electronic, halochromic, and doping properties. *Macromolecules* **45**, 1165–1173 (2012).
4. Mallet, C., Le Borgne, M., Starck, M. & Skene, W. G. Unparalleled fluorescence of a polyazomethine prepared from the self-condensation of an automer and its potential use as a fluorimetric sensor for explosive detection. *Polym. Chem.* **4**, 250–254 (2013).

## Dérivés de la vanilline pour la synthèse de polymères $\pi$ -conjugués biosourcés : application en électronique organique

### Résumé :

Ces travaux de thèse portent sur la synthèse de polymères  $\pi$ -conjugués biosourcés issus de la vanilline, visant des applications potentielles en électronique organique (photovoltaïque ou Organic Light Emitting Diode, OLED). Des polyazométhines de masses molaires élevées, issus de la copolymérisation entre la divanilline et différentes diamines, ont été obtenus par polymérisation sous irradiation micro-onde durant 5 minutes puis séchage à l'évaporateur rotatif. Ces derniers ont une absorbance dans le proche UV mais un chemin de conjugaison très court, comme l'a révélé l'analyse de molécules modèles. Pour améliorer ce chemin de conjugaison, une molécule à base de divanilline a été synthétisée avec les fonctions aldéhyde en position para par rapport à la liaison entre les deux cycles aromatiques. Cette para-divanilline, encore jamais décrite, a été utilisée pour la synthèse de polyazométhines. Ces derniers présentent également un court chemin de conjugaison en raison de l'encombrement stérique entre les deux groupes phényle. Une dernière famille de polymère a alors été étudiée : les polythiazolothiazoles à base de divanilline. Ces polymères présentent des propriétés d'émission qui se caractérisent par une émission dans le bleu en solution et dans le jaune à l'état de film. Des molécules modèles à base de benzothiazole ont également été synthétisées et présentent un rendement quantique de fluorescence de 20% ainsi qu'un empilement  $\pi$  en « chevrons », leur conférant un fort potentiel pour diverses applications en électronique organique.

**Mots-clés :** Polymères, électronique organique, biosourcés, divanilline, polyazométhines, polythiazolothiazoles

---

### Bis-vanillin substrates as source of $\pi$ -conjugated polymers for organic electronic

### Abstract:

The objective of this PhD is to synthesize  $\pi$ -conjugated bio-based polymers from vanillin, with potential applications in the field of organic electronic (photovoltaic, Organic Light Emitting Diode, OLED). Polyazomethines with high molar masses were obtained *via* the copolymerization of divanillin with various diamines. This polycondensation was performed in 5 minutes under microwave irradiation, followed by solvent removal using a rotary evaporator. Divanillin-based polyazomethines absorb in the near-UV range but have a short conjugation pathway, as revealed investigations on model compounds. To improve this conjugated pathway, a divanillin-based molecule bearing aldehyde functions in para positions with respect to the link between the rings, was designed. This so-called para-divanillin, never reported before, was copolymerized to yield polyazomethines. These latter polymers also have a short conjugation pathway due to steric hindrance between the two aromatic rings of the para-divanillin skeleton. A last family of divanillin-based polymers was thus investigated: polythiazolothiazoles. The latter exhibit specific emission properties as they emit in the blue range in solution and in the yellow range in films. Benzothiazole-based model compounds were also synthesized and exhibited a fluorescence quantum yield of 20% and "herringbone-like"  $\pi$ -stacking, giving them a strong potential for various organic electronic applications.

**Keywords:** Polymers, organic electronic, bio-based, divanillin, polyazomethines, polythiazolothiazoles.

---

### Unité de recherche

Laboratoire de Chimie des Polymères Organiques, UMR5629, Allée Geoffroy St Hilaire 33600 Pessac et 16 avenue Pey-Berland, 33600 Pessac